CENTRAL NERVOUS SYSTEM ACTING DRUGS – MOLECULAR MECHANISMS OF NEUROPROTECTION AND NEURODEGENERATION

EDITED BY: Nesrine Salah El Dine El Sayed, Riham Salah El Dine, Jolanta Kotlinska, Barbara Budzynska and Anna Boguszewska-Czubara

PUBLISHED IN: Frontiers in Pharmacology and Frontiers in Neuroscience

frontiers Research Topics

ISSN 1664-8714
ISBN 978-2-83250-661-5
DOI 10.3389/978-2-83250-661-5

About Frontiers

Frontiers is more than just an open-access publisher of scholarly articles: it is a pioneering approach to the world of academia, radically improving the way scholarly research is managed. The grand vision of Frontiers is a world where all people have an equal opportunity to seek, share and generate knowledge. Frontiers provides immediate and permanent online open access to all its publications, but this alone is not enough to realize our grand goals.

Frontiers Journal Series

The Frontiers Journal Series is a multi-tier and interdisciplinary set of open-access, online journals, promising a paradigm shift from the current review, selection and dissemination processes in academic publishing. All Frontiers journals are driven by researchers for researchers; therefore, they constitute a service to the scholarly community. At the same time, the Frontiers Journal Series operates on a revolutionary invention, the tiered publishing system, initially addressing specific communities of scholars, and gradually climbing up to broader public understanding, thus serving the interests of the lay society, too.

Dedication to Quality

Each Frontiers article is a landmark of the highest quality, thanks to genuinely collaborative interactions between authors and review editors, who include some of the world's best academicians. Research must be certified by peers before entering a stream of knowledge that may eventually reach the public - and shape society; therefore, Frontiers only applies the most rigorous and unbiased reviews.
Frontiers revolutionizes research publishing by freely delivering the most outstanding research, evaluated with no bias from both the academic and social point of view. By applying the most advanced information technologies, Frontiers is catapulting scholarly publishing into a new generation.

What are Frontiers Research Topics?

Frontiers Research Topics are very popular trademarks of the Frontiers Journals Series: they are collections of at least ten articles, all centered on a particular subject. With their unique mix of varied contributions from Original Research to Review Articles, Frontiers Research Topics unify the most influential researchers, the latest key findings and historical advances in a hot research area! Find out more on how to host your own Frontiers Research Topic or contribute to one as an author by contacting the Frontiers Editorial Office: frontiersin.org/about/contact

CENTRAL NERVOUS SYSTEM ACTING DRUGS – MOLECULAR MECHANISMS OF NEUROPROTECTION AND NEURODEGENERATION

Topic Editors:
Nesrine Salah El Dine El Sayed, Cairo University, Egypt
Riham Salah El Dine, Cairo University, Egypt
Jolanta Kotlinska, Medical University of Lublin, Poland
Barbara Budzynska, Medical University of Lublin, Poland
Anna Boguszewska-Czubara, Medical University of Lublin, Poland

Citation: El Dine El Sayed, N. S., El Dine, R. S., Kotlinska, J., Budzynska, B., Boguszewska-Czubara, A., eds. (2023). Central Nervous System Acting Drugs – Molecular Mechanisms of Neuroprotection and Neurodegeneration. Lausanne: Frontiers Media SA. doi: 10.3389/978-2-83250-661-5

Table of Contents

frontiers | Frontiers in Neuroscience

TYPE Editorial
PUBLISHED 18 October 2022
DOI 10.3389/fnins.2022.1060515

OPEN ACCESS

EDITED AND REVIEWED BY
Nicholas M. Barnes,
University of Birmingham,
United Kingdom

*CORRESPONDENCE
Nesrine S. El Sayed
nesrine.salah@pharma.cu.edu.eg
Riham Salah El Dine
Riham.salaheldine@pharma.cu.edu.eg

SPECIALTY SECTION
This article was submitted to Neuropharmacology, a section of the journal Frontiers in Neuroscience

RECEIVED 03 October 2022
ACCEPTED 05 October 2022
PUBLISHED 18 October 2022

CITATION
El Sayed NS, Salah El Dine R, Budzyńska B, Boguszewska-Czubara A and Kotlińska J (2022) Editorial: Central nervous system acting drugs-molecular mechanisms of neuroprotection and neurodegeneration.
Front. Neurosci. 16:1060515.
doi: 10.3389/fnins.2022.1060515

Editorial: Central nervous system acting drugs-molecular mechanisms of neuroprotection and neurodegeneration

Nesrine S. El Sayed[1]*, Riham Salah El Dine[2]*, Barbara Budzyńska[3], Anna Boguszewska-Czubara[4] and Jolanta Kotlińska[5]

[1]Department of Pharmacology and Toxicology, Faculty of Pharmacy, Cairo University, Cairo, Egypt, [2]Department of Pharmacognosy, Faculty of Pharmacy, Cairo University, Cairo, Egypt, [3]Independent Laboratory of Behavioral Studies, Medical University of Lublin, Lublin, Poland, [4]Department of Medical Chemistry, Medical University of Lublin, Lublin, Poland, [5]Department of Pharmacology and Pharmacodynamics, Medical University of Lublin, Lublin, Poland

KEYWORDS

neurodegeneration, oxidative stress, neuroinflammation, neuroprotection, molecular mechanisms

Editorial on the Research Topic
Central nervous system acting drugs-molecular mechanisms of neuroprotection and neurodegeneration

In the current world, humans are continuously exposed to different compounds that can exert deleterious effects within their bodies, notably, by changing the activity of their brains through neurodegeneration and neuroprotection. Neurodegenerative diseases are an increasingly important issue in our society. There are, however, still many obstacles in the way of finding methods for their cure. Various types of biological mechanisms have been associated with neurodegeneration, including oxidative stress, neuroinflammation, insulin signaling, mitochondrial function, iron homeostasis, and excitotoxicity. Activation of these mechanisms leads to long-term programmed cell death, whereas their blockade may improve central nervous system function, i.e., neuroprotection.

As there is currently no effective treatment for neurodegeneration resulting from both abuse of psychoactive drugs and age-dependent brain diseases, a significant part of current research effort has shifted toward finding preventive, as well as remediation treatments for neurodegeneration.

The need for effective and well-tolerated remedies for neurodegeneration has led scientists to analyze thoroughly the mechanisms of neurodegeneration and the possibility of using new drugs for the treatment of neurodegenerative diseases.

In this Research Topic, we aimed to discuss the molecular mechanisms of neurodegeneration and neuroprotection. The intention of creating this missive is to provide a thorough look into neurotoxicity induced by drug abuse, as well as

the pharmacological and chemical properties, safety aspects, and interactions of new medicines for neurodegeneration treatment. We welcomed original research, and systematic reviews covering, but not limited to, the following themes:

- Overview of neuroprotective drugs that are currently in research and development to give readers ideas about the complexity of drug discovery in this field;
- Neurodegenerative mechanisms of synthetic substances, including illicit drugs;
- Molecular mechanisms of action for neuroprotective agents.

A brief discussion of the submitted papers follows.

On seizure score, as well as numerous biochemical markers, temozolomide (TMZ) has demonstrated a promising anti-seizure capability. El Shorbagy et al. have revealed that the curative effects of TMZ might be related to its capacity to reduce glutamate buildup and mitochondrial oxidative damage, in addition to a favorable regulation of p-ERK1/2/p-AMPK signaling. Moreover, TMZ administration was successful in minimizing astrocyte activation and ATP-dependent energy disturbances. All of this was demonstrated by a decrease in neuronal apoptosis and the preservation of cellular integrity.

In a ground-breaking hypothesis, Wu et al. suggest that demyelination occurs during the pathogenic Perioperative Neurocognitive Disorder (PND) phase. By inhibiting the overactivation of the WNT/-catenin signaling pathway through anti-neuroinflammation to promote oligodendrocytes (OLs) development and remyelination, the study was capable of pinpointing the ameliorative impact of clemastine on PND. At the same time, mature hippocampus neuron survival and synaptic plasticity both significantly increased. The findings may have practical ramifications and offer fresh insights and suggestions for the therapeutic management of PND.

The behavioral, histological, cellular, as well as neurochemical outcomes of the current investigation by Mustafa et al. provide evidence for the potential role of inhibition of brain GTP cyclohydrolase I in Huntington's Disease, by confirming the activation of the MasR/PI3K/Akt/CREB/BDNF/TrKB pathway and suppression of iNOS in the neuroprotective effect of 2,4-diamino-6-hydroxypyrimidine against neurotoxicity and mitochondrial dysfunction induced by 3-nitropropinic acid.

Lee et al. demonstrated the effect of HEXA-018, a novel compound containing a catechol derivative structure, as an inducer of autophagy. HEXA-018 suppressed neuronal toxicity in cell and *Drosophila* models observed as neuronal damage and behavioral impairment. These findings raise the prospect that HEXA-018-mediated amyotrophic lateral sclerosis activation might represent a cutting-edge therapeutic approach for treating neurodegenerative disorders with TDP-43 proteinopathy.

Ge et al. found that asaronol, a major compound isolated from the Chinese medicinal herb *Acorus gramineus,* promoted oligodendrocyte precursor cell (OPC) differentiation and myelination in the corpus callosum of preterm white matter injury (PWMI) rats induced by hypoxia-ischemia. They revealed that glutamate was significantly decreased, and the levels of PPARγ and glutamate transporter 1 (GLT-1) were increased by asaronol treatment. Thus they suggested that PPAR-GLT-1 mechanism mediates the effect of asaronol on OPC differentiation and myelination. Moreover, Ge et al. concluded that as asaronol could control PPAR-GLT-1 signaling it can be applied to treat myelin-related diseases.

Fluoxetine, an anti-depressive drug, has regulatory effects on autophagy and phagocytosis, which are necessary functions for microglia. Park et al., found that fluoxetine treatment causes autophagic activation, as seen by increased LC3-II and LC3 punctate distribution and autophagosome accumulation. Furthermore, the fluoxetine-mediated increase in phagocytosis was blocked by the autophagy inhibitor Baf in microglia. These findings imply that fluoxetine acts as an anti-inflammatory and neuroprotective agent in the brain *via* microglia and that altering the autophagy-lysosomal pathway may be a viable treatment for the removal of amyloid plaques in Alzheimer's disease.

A research article by Zheng et al. reported that daidzein has therapeutic potential for brain damage brought on by ischemia/reperfusion. The findings show that daidzein stimulates neural regeneration after ischemic stroke by upregulating Akt/CREB and boosting BDNF expression, albeit the potential mechanism and viability of long-term usage need to be verified. Daidzein is thought to have the potential to be a novel drug utilized in the treatment of localized cerebral ischemia.

Zhang et al.'s review provided an overview on lipoxins neuroprotective effect. When it comes to neurological conditions including ischemic or hemorrhagic stroke, newborn hypoxia-ischemia encephalopathy, brain, spinal cord injuries, Alzheimer's disease, multiple sclerosis, chronic cerebral hypoperfusion, as well as neuropathic pain; lipoxins can have a variety of protective and beneficial effects. They also have considerable therapeutic promise for neuroinflammatory and neurodegenerative ailments.

The active ingredients of bee venom have the ability to pass through the blood brain barrier and can therefore be used in the treatment of diseases of the central nervous system. Unfractionated bee venom has a dose- and time-dependent impact on glial cancer cell ability to survive. Additionally, Malek et al. revealed that the secretion of metalloproteinases MMP-2 and MMP-9 is inhibited, which could have an effect on how quickly a tumor spreads.

The development of innovative therapies for methamphetamine addiction, based on enhancing the functioning of dopamine D2-type receptors, was described by Okita et al. They revealed that upregulation of D2-type

receptor and/or attenuation of neuroinflammation may provide a therapeutic effect for this disorder. *In vitro* studies have shown that blockage of adenosine 2A (A2A) receptors may prevent D2-receptor downregulation and neuroinflammation-related brain damage.

The study of Aldabbagh et al. supports the idea that Alzheimer's disease pathogenesis in the hippocampus is linked to an increased GABA content in reactive astrocytes. Astrocyte-specific GABA transporter 3/4 (GAT3/4) and expression of GAD67, an enzyme that catalyzes GABA production is altered in *APP* knock-in mouse model of Alzheimer's disease, which, may lead to an intensified tonic inhibition in the hippocampus. The mechanisms by which GAT3/4 contributes to modulating tonic inhibition are complex. Since bath-application of SNAP-5114, GAT3/4 inhibitor worsened AD-related synaptic hyperactivity. Thus, further studies are required.

Compelling evidence presented by Frank et al. confirmed that the pyruvate-induced blood glutamate scavenging mechanism results in the induction of antidepressant effects. These mechanisms prevent or treat anhedonia and hyperlocomotion, which are brought on by glutamate dysregulation following traumatic brain injury in rats. The work by Frank et al. confirmed that blood glutamate scavengers should be considered a possible therapeutic option for post-traumatic brain injury depression.

Through the research article of Liu et al., dexmedetomidine delivered in a loading dose can significantly inhibit intraoperative neuromonitoring parameters in thoracic spinal decompression surgery. Special attention should be paid to the timing of a bolus dose of dexmedetomidine under intraoperative neuromonitoring. However, dexmedetomidine delivered at a constant speed does not exert inhibitory effects.

Leite et al., in their review, deduced that cardiotonic steroids like ouabain have the ability to mobilize Ca^{2+}. In their work, an increase in Ca^{2+} was described in all models that were investigated, including synaptosomes, brain slices, and cell cultures. Other effects were also observed, as Ca^{2+} may be involved in significant cellular impacts, mostly *via* activating signaling pathways. In addition to the well-known cytotoxic effects of ouabain, which occur from activation of the Na^{+}/Ca^{2+} exchanger reverse mode and elevated Ca^{2+}, cholinergic, noradrenergic, and glutamatergic neurotransmission might all be increased by oubabin-induced Ca^{2+} signaling. Authors suggest that ouabain therapy can dramatically enhance biological second messengers, among other biological processes. The actions and signals that cardiotonic steroids (ouabain) mediate in the nervous system (which has been demonstrated to be concentration-dependent) are more understood after the lecture of this review. The paper concludes that the development of novel, less toxic drugs with neuroprotective properties may benefit from structural alterations of the cardiotonic steroids.

Wang et al. revealed that the neuroprotective effects of epigallocatechin-3-gallate (EGCG), a bioactive ingredient in green tea, against cerebral ischemia/reperfusion injury (CIRI) are related to its ability to inhibit autophagy *via* phosphorylating AKT/AMPK/mTOR. Moreover, the research offers a fresh understanding of the possible processes underlying EGCG's influence on autophagy and cerebral ischemia damage, and it may be used to develop more effective stroke treatment plans.

Liu et al. demonstrate conclusively that akebia saponin D (ASD) enhances neural stem/precursor cells proliferation, survival, and neuronal development *via* activating the PI3K-Akt pathway and shielding them from the microglia-mediated inflammatory microenvironment. The findings suggest the need for additional research into ASD's potential as a therapeutic option for illnesses such as Alzheimer's disease, major depressive disorder, and other disorders with reduced neurogenesis.

Zhou et al. confirmed through the published review that antipsychotic medications, especially olanzapine, cause hypothalamic endoplasmic reticulum (ER) stress that is linked to inflammation and weight gain. According to the paper, antipsychotics appear to cause hypothalamic (ER) stress through the following mechanisms: (1) blocking proopiomelanocortin processing, attenuating leptin signaling, and upregulating neuropeptide Y and agouti-related protein expression, which results in hyperphagia; (2) reducing white adipose tissue browning and brown adipose tissue thermogenesis, which minimize energy expenditure; and (3) activating the MyD88-independent and MyD88-dependent pathways in astrocytes, which increases the release of pro-inflammatory cytokines. According to the review published by Zhou et al., antipsychotic-induced ER stress and the ensuing inflammation may be connected to the antagonistic interactions between histamine H1 receptor and dopamine D2 receptor and antipsychotics. When taken as a whole, hypothalamic ER stress may be a useful target for reducing the metabolic adverse effects of schizophrenia and antipsychotics, such as obesity and weight gain.

In the work of Deng et al., in rat and mouse models of traumatic spinal cord injury, high mobility group box-1 (HMGB1)-targeted treatment was found to enhance locomotor function recovery, lower inflammation attenuate edema, and lower apoptosis. The best therapy suggested by Deng et al. may be an intrathecal injection of anti-HMGB1 Ab 0–3 h after spinal cord injury. However, the low methodological caliber of the included studies severely restricted the applicability of this meta-analysis.

The presented research shows a great interest of scientists in an interdisciplinary approach of broadly understood neurodegeneration, aimed at both the discovery of molecular, cellular and biochemical mechanisms of emerging changes as well as the development of innovative therapies based on new synthetic substances and naturally obtained from the environment (from plants, bacteria, animals, etc.).

Author contributions

All authors listed have made a substantial, direct, and intellectual contribution to the work and approved it for publication.

Conflict of interest

The authors declare that the research was conducted in the absence of any commercial or financial relationships that could be construed as a potential conflict of interest.

Publisher's note

frontiers in Pharmacology

ORIGINAL RESEARCH
published: 23 August 2021
doi: 10.3389/fphar.2021.738590

Clemastine Ameliorates Perioperative Neurocognitive Disorder in Aged Mice Caused by Anesthesia and Surgery

*Wensi Wu[1†], Xiaojun Zhang[1†], Jiaxin Zhou[1], Hongmei Yang[1], Junjun Chen[1], Le Zhao[1], Junying Zhong[1], Wei-jye Lin[2,3] and Zhi Wang[1]**

[1]Department of Anesthesiology, Sun Yat-Sen Memorial Hospital, Guangzhou, China, [2]Guangdong Provincial Key Laboratory of Malignant Tumor Epigenetics and Gene Regulation, Sun Yat-Sen Memorial Hospital, Sun Yat-Sen University, Guangzhou, China, [3]Medical Research Center of Sun Yat-Sen Memorial Hospital, Sun Yat-Sen University, Guangzhou, China

Perioperative neurocognitive disorder (PND) leads to progressive deterioration of cognitive function, especially in aged patients. Demyelination is closely associated with cognitive dysfunction. However, the relationship between PND and demyelination remains unclear. Here we showed that demyelination was related to the pathogenesis of PND. Clemastine, an antihistamine with potency in remyelination, was predicted to have a potential therapeutic effect on PND by next-generation sequencing and bioinformatics in our previous study. In the present study, it was given at 10 mg/kg per day for 2 weeks to evaluate the effects on PND in aged mice. We found that clemastine ameliorated PND and reduced the expression levels of inflammatory factors such as tumor necrosis factor alpha (TNF-α) and interleukin-1 beta (IL-1β). Further investigation suggested clemastine increased the expression of oligodendrocyte transcription factor 2 (OLIG2) and myelin basic protein (MBP) to enhance remyelination by inhibiting the overactivation of the WNT/β-catenin pathway. At the same time, the expression of post-synaptic density protein 95 (PSD95, or DLG4), brain-derived neurotrophic factor (BDNF), synaptosomal-associated protein 25 (SNAP25) and neuronal nuclei (NEUN) were also improved. Our results suggested that clemastine might be a therapy for PND caused by anesthetic and surgical factors in aged patients.

Keywords: perioperative neurocognitive disorder, clemastine, neuroinflammation, wnt/β-catenin signaling, remyelination, synaptic plasticity

OPEN ACCESS

Edited by:
Nesrine Salah El Dine El Sayed, Cairo University, Egypt

Reviewed by:
Junhui Wang, University of Toronto, Canada
Lamiaa A. Ahmed, Cairo University, Egypt
Dalia El-Tanbouly, Cairo University, Egypt

****Correspondence:***
Zhi Wang
wangzhi@mail.sysu.edu.cn

†These authors have contributed equally to this work

Specialty section:
This article was submitted to Neuropharmacology, a section of the journal Frontiers in Pharmacology

Received: *09 July 2021*
Accepted: *10 August 2021*
Published: *23 August 2021*

Citation:
Wu W, Zhang X, Zhou J, Yang H, Chen J, Zhao L, Zhong J, Lin W and Wang Z (2021) Clemastine Ameliorates Perioperative Neurocognitive Disorder in Aged Mice Caused by Anesthesia and Surgery. Front. Pharmacol. 12:738590. doi: 10.3389/fphar.2021.738590

INTRODUCTION

Perioperative neurocognitive disorder (PND) is one of the most common perioperative central nervous system complications in aged patients, which can cause changes in personality, social ability and cognitive function (Evered et al., 2018). Advanced age is considered as an independent risk factor of PND (Luo et al., 2019). The incidence of PND is about 10–54%, which is higher in patients over age of 65. Some of them even developed into dementia in 3–5 years after suffering PND (Punjasawadwong et al., 2018). Poor perioperative cognitive function seriously affects patient's life quality and increases perioperative complications and mortalities (Jiang et al., 2019). At present, the exact pathogenesis of PND remains unclear. Neuroinflammation is primarily involved in the mechanism and there is a lack of effective treatment.

The maintenance of cognitive function mainly depends on the normal physiological status of neurons. Myelin sheath, the tubular membrane surrounding the axon, playing an important

role in maintaining the normal physiological condition of neuron (Del Giovane and Ragnini-Wilson, 2018). First, myelin sheath isolates the axon from the surrounding tissues to avoid interference between nerve impulses (Ravera et al., 2016; Huntemer-Silveira et al., 2020). Second, it increases the conduction speed of nerve impulses (Saab and Nave, 2017). More importantly, myelin sheath has a protective effect on inducing the regeneration of the axon when it comes to injury (Grove et al., 2020). The correct formation of myelin sheath requires the differentiation and maturation of oligodendrocytes (OLs), which is regulated by various signaling pathways, particularly the WNT/β-catenin (Tandon et al., 2020). It suppresses oligodendrogenesis via direct inhibition of OLIG2 expression (Jiang et al., 2020). Meanwhile, neuroinflammation induces axonal hypomyelination through the overactivation of WNT/β-catenin signal pathway (Huang et al., 2020). In other words, neuroinflammation is one of the main factors leading to demyelination (Huang et al., 2020; das Neves et al., 2020; Borgonetti et al., 2020). Demyelination pathological changes widely exist in many kinds of neurodegenerative, brain injury and cognitive impairment diseases, such as Alzheimer's disease, multiple sclerosis, stroke, traumatic brain injury and spinal cord injury (Mayne et al., 2020). It is worth noting that no studies have been conducted on the relationship between PND and demyelination. On the contrary, remyelination contributes to the improvement of cognitive function (Del Giovane and Ragnini-Wilson, 2018; Chen et al., 2021a), which might be helpful in the treatment of PND. Besides, neuronal function can also benefit from remyelination and mainly manifested by synaptic function (Del Giovane and Ragnini-Wilson, 2018). Synaptic plasticity is one of the criterions for evaluating synaptic function. Previous studies have confirmed that PND is closely related to the impairment of synaptic plasticity (Gao et al., 2021).

The antihistamine clemastine, an FDA-approved drug with high potency in enhancing remyelination, anti-neuroinflammatory and brain function improvement in a variety of diseases including hypoxic-ischemic encephalopathy, aging, multiple sclerosis and depression (Liu et al., 2016; Green et al., 2017; Cree et al., 2018; Su et al., 2018; Wang et al., 2020a; Xie et al., 2020). Meanwhile, clemastine ameliorates cognitive impairment in mice caused by early postnatal exposure to isoflurane through enhancing remyelination (Li et al., 2019). However, the effect of clemastine on PND is unknown. In our previous study, clematine was predicted to have a potential therapeutic effect on PND through next-generation sequencing combined with bioinformatics analysis (Wu et al., 2021).

Thus, we hypothesized that clemastine ameliorated the impairment of learning and memory induced by anesthesia and surgery in aged mice. To test these hypotheses, we performed surgery and anesthesia on aged (18-month-old) male C57BL/6 mice and explored the effect of clemastine on PND.

MATERIALS AND METHODS

Animals

Male C57BL/6 mice at 18 months and weighing 45–50 g were supplied by Sun Yat-sen University (Guangzhou, China). These mice were housed in specific pathogen free environment kept at 19–23°C and 40–60% humidity with a 12-h light/12-h dark cycle (light from 07:00 to 19:00). The mice were grouped into four categories in a random manner: control (CON), control plus clemastine group (CON + CLE), PND alone (PND), and PND plus clemastine group (PND + CLE) (n = 20, each group). Five animals were kept in each cage and allowed to have food and water ad libitum. The experiment started until all animals had adapted to the environment for 2 weeks. All the animal experiments in the present study were approved by the Institutional Animal Care and Use Committee (Approval No: SYSU-IACUC-2020-000326) and the Laboratory Animal Ethics Committee of Sun Yat-sen University. All procedures were performed in accordance with the approved guidelines. The schematic timeline of the experimental process is shown in **Figure 1**.

Animal Model

Isoflurane anesthesia plus exploratory laparotomy has been proved to be an effective method to construct PND model (Qiu et al., 2020). Before exploratory laparotomy, the mice were anesthetized by exposing to an oxygen chamber prefilled with 1.5% isoflurane for 30 min. A median incision approximately 2 cm in the abdomen was made to enter the abdominal cavity and explore the abdominal organs such as the liver, spleen, and intestine. Sterile 5–0 surgery sutures were used to suture the peritoneum and skin. Surgery was also performed with isoflurane inhalation anesthesia and lasted 30 min. As shown in our previous study, mice received this surgery with isoflurane inhalation anesthesia had no hypoxia, heart rates and respiratory rates were kept within the normal ranges (Wu et al., 2021). During the whole process, an anesthesia monitor (B450, GE, United States) was used to dynamically monitor the depth of anesthesia and maintain the anesthesia level when toe pinch and surgery did not respond. Meanwhile, the rectal temperature was monitored and maintained at 37°C with the aid of a heating blanket (69,020, RWD, CHN). At the end of surgery and every day within 3 days after surgery, 2.5% lidocaine cream was applied to the incision to alleviate the postoperative pain, and povidone iodine solution was applied to prevent infection. For the mice that served as controls, neither anesthesia nor surgery was performed.

Drug

From the first day after anesthesia and surgery, aged mice in CON + CLE group and PND + CLE group were intraperitoneally injected with clemastine (C129211, Aladdin, CHN) at 10 mg/kg per day for 2 weeks. Clemastine was prepared freshly each day by dissolving the powder in normal saline. The selected dose is based on previous studies, which proves that clemastine has the effect of enhancing cognition and remyelination (Li et al., 2019; Chen et al., 2021b; Li et al., 2021). Aged mice in the CON

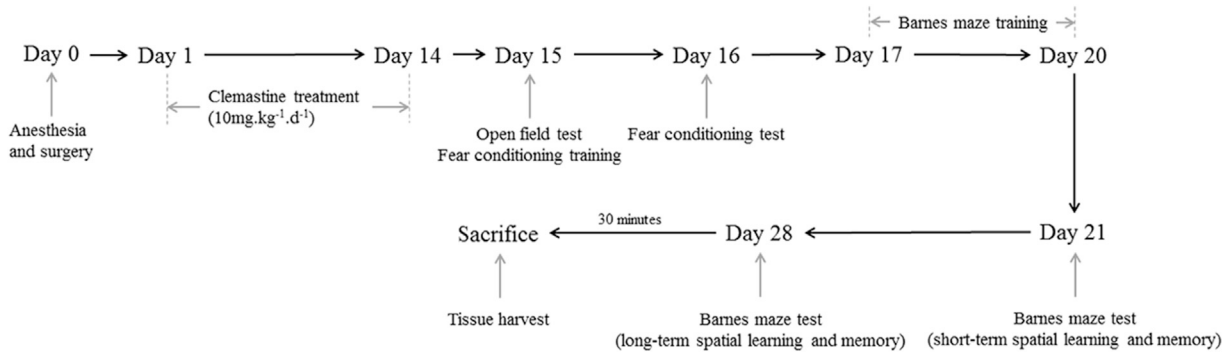

FIGURE 1 | Diagram of timeline of experimental procedures.

and PND group received an intraperitoneal injection of the same amount of normal saline every day to ensure the consistency of the experiment.

Behavioral Studies

All behavior tests were performed in a sound-isolated room between 12:00 and 18:00. All behavioral data was recorded by the same two researchers who were blinded to the animal grouping.

Open Field

A black opaque plastic chamber (60 × 60 × 50 cm, ZH-ZFT, Anhui Zhenghua Biological Instrument equipments Co., Ltd., Anhui, China) was used as the open field arena. On the first day after 2 weeks of clemastine treatment, the open field test was performed to evaluate the locomotor activity and postoperative anxiety of the mice (Qiu et al., 2020). Each mouse was placed in the center of the field and allowed to explore freely for 5 min with a video tracking system (Smart v3.0.06, Panlab Harvard Apparatus, Barcelona, ES) automatically recorded its movements, analyzed the total distance in the whole area and the time spent in the center area. During each test interval, the field was cleaned with 75% ethanol to eliminate feces and odors.

Fear Conditioning

Two hours after the open field test, each mouse was placed into the conditioning chamber (Freeze Monitor, San Diego Instruments, San Diego, CA) and allowed to explore the room freely for 180 s. Then they were given a 30 s tone (70 db), followed by a 2 s foot shock (0.7 mA), and the next tone-shock stimulation cycle was entered at an interval of 60 s. A total of 3 cycles were performed as training. One day later, each mouse was placed into the conditioning chamber without any tone or electrical stimulation for 360 s and the environment was identical with that before, the time of freezing behavior was recorded to test the context-related memory (hippocampus-dependent memory). 2 hours later, they were placed into a new environment completely different from that before and explored room freely for 180 s. Then they were given the same tone stimulation as before (without electrical stimulation), the time of freezing behavior was recorded to test the tone-related memory (hippocampus-independent memory). Freezing behavior means there is no visible movement other than breathing (Qiu et al., 2016). During each test interval, the conditioning chamber was cleaned with 75% ethanol to eliminate feces and odors.

Barnes Maze

2 hours after the fear conditioning test, each mouse was placed in a small dark recessed chamber to acclimate for 5 minutes. Over the next 12 days, we performed Barnes maze to evaluate the spatial learning and memory of mice (Zheng et al., 2017). In the first 4 days, each mouse was placed in the center of a circular platform (Anhui Zhenghua Biological Instrument equipments Co., Ltd., Anhui, China) with a diameter of 92 cm, which had 20 equally spaced holes. Among all the holes, only one was linked to the dark chamber. The mice were expected to find the hole and enter the dark chamber under the bright light (200 W). The mice were trained for 4 days with 3 trials per day, with each trial lasting 3 min, and an interval of 15 min between each trial. If the mice could not find the correct hole and enter the dark chamber over 3 min, they would be guided to the correct location. During each test interval, the platform and dark chamber were cleaned with 75% ethanol to eliminate feces and odors. On the 5th day, the escape latency and the number of wrong holes explored were recorded and measured by a video tracking system (Smart v3.0.06, Panlab Harvard Apparatus, Barcelona, ES), which was used to evaluate the short-term spatial learning and memory of mice. The escape latency is the time a mouse used to enter the dark chamber. A week later, the mice were tested for long-term spatial learning and memory in the same way.

Sequencing Data and Identification of Differentially Expressed Genes

The gene expression profile data (accession number GSE174413) which we previously obtained through next-

generation sequencing was downloaded from the Gene Expression Omnibus (GEO) database. It contains the gene expression profiles of the brain tissues of three aged male C57BL/6 mice in the PND group and the CON group, respectively (Wu et al., 2021). Limma package in R software was applied to screen differentially expressed genes of PND with p-value < 0.05, | log2 (Fold Change) | ≥ 1. By processing the ggpubr and ggthemes package of R software, we accomplished the visualization of differentially expressed genes.

Identification of Protein-Protein Interactions

The Search Tool for the Retrieval of Interacting Genes (STRING, version 11.0, https://www.string-db.org/) database was used to identify protein-protein interactions between genes. The protein-protein minimum required interaction score was set to 0.4, indicating medium confidence.

Harvesting of Brain Tissue

Mice were deeply anesthetized with isoflurane 30 min after the Barnes maze test (long-term spatial learning and memory test), and perfused transcardially with normal saline (n = 10, each group). The brain was dissected in 4°C environment and stored at 80°C before use. The hippocampus was isolated for subsequent experiments on genes and proteins levels. Other mice were perfused transcardially with normal saline and 4% paraformaldehyde, and further fixed with 4% paraformaldehyde for 24 h (n = 10, each group). Then dehydrated with a gradient of 10, 20, and 30% sucrose for 1 day each until the brain was completely sunk to the bottom. Absorbed the moisture on the surface and used optimum cutting temperature (OCT) compound (4583, SAKURA, JP) for embedding in subsequent immunofluorescence staining.

Reverse Transcription-Quantitative Polymerase Chain Reaction

Hippocampus was lysed and total RNA was extracted using RNA Quick Purification kit (RN001, ESscience, CHN). The concentrations of the RNA samples were determined spectrophotometrically at 260, 280, and 230 nm by using a NanoDrop ND-2000 (Thermo, United States) instrument. Total RNA was subsequently reverse transcribed into cDNA using Hifair® III 1st Strand cDNA Synthesis SuperMix for qPCR (11141ES60, Yeasen, CHN). The reverse transcription conditions were as follows: 25°C for 5 min, 55°C for 15 min and 85°C for 5 min. The qPCR was performed using Hieff UNICON® qPCR SYBR® Green Master Mix (11198ES08, Yeasen, CHN) on Roche LightCycler 480 II Real-Time PCR System (Roche, United States). The thermocycling conditions were as follows: Initial denaturation at 95°C for 30 s, followed by 40 cycles at 95°C for 10 s, 60°C for 20 s and 72°C for 20 s. The data were analyzed using the $2-\Delta\Delta Ct$ method. GAPDH was used as an internal control. The sequences of primers are presented in **Supplementary Table S1**.

Western Blot Analysis

Hippocampus was lysed with RIPA buffer (P0013B, Beyotime, CHN) and protein concentration was determined using a BCA protein quantification kit (P0010, Beyotime, CHN). Proteins were separated by SDS-PAGE (P0012A, Beyotime, CHN) using 10% gels and transferred to PVDF membranes (ISEQ00010, Merck Millipore, United States). After blocking with 5% skimmed milk (A600669, Sangon Biotech, CHN) for 1 h at room temperature, PVDF membranes were incubated with primary antibodies at 4°C overnight, followed by incubation with secondary antibodies at room temperature for 1 h. Subsequently, the protein bands were visualized using ECL reagent (WBKLS0100, Merck Millipore, United States), and quantitated with ImageJ software (National Institutes of Health, Bethesda, MD, United States). Rabbit polyclonal anti-mouse TNF-α antibody (1:1,000, AF8208, Beyotime, CHN), rabbit polyclonal anti-mouse IL-1β antibody (1:1,000, AF7209, Beyotime, CHN), rabbit polyclonal anti-mouse WNT10B antibody (1:1,000, DF9038, Affinity, CHN), rabbit polyclonal anti-mouse β-catenin antibody (1:1,000, AF5126, Beyotime, CHN), rabbit monoclonal anti-mouse OLIG2 antibody (1:1,000, AF1312, Beyotime, CHN), rabbit polyclonal anti-mouse MBP antibody (1:1,000, BA0094, Boster, CHN), rabbit polyclonal anti-mouse SNAP25 antibody (1:1,000, AF8016, Beyotime, CHN), rabbit monoclonal anti-mouse PSD95 antibody (1:1,000, AF1096, Beyotime, CHN), rabbit monoclonal anti-mouse BDNF antibody (1:1,000, AF1423, Beyotime, CHN) and rabbit monoclonal anti-mouse β-tubulin antibody (1:1,500, AF1216, Beyotime, CHN) were the primary antibodies used. The secondary antibodies used were horseradish peroxidase (HRP) - conjugated goat anti-rabbit lgG (1:1,500, A0208, Beyotime, CHN).

Immunofluorescence Assay

Brain tissues were embedded with OCT and sliced into 10 μm. The sections were washed three times with phosphate buffer solution (PBS) to remove OCT from the surface. After blocking with goat serum (16210072, Gibco, United States) for 1 h at room temperature, tissue sections were incubated with mouse monoclonal anti-mouse NEUN antibody (1:100, MAB377, Merck millipore, GER) and rabbit polyclonal anti-mouse MBP antibody (1:100, BA0094, Boster, CHN) at 4°C overnight. After rewarming for 1 h, tissue sections were washed three times with PBS, incubated with donkey anti-mouse IgG (H + L) highly cross-adsorbed secondary antibody, alexa fluor 647 (1:1,000, A-31571, Invitrogen, United States) and CY3-labeled goat anti-mouse IgG (1:500, A0562, Beyotime, CHN) at room temperature for 2 h, and incubated with DAPI (G1012, Servicebio, CHN) at room temperature for 10 min. Tissue sections were sealed with anti-fluorescence quenching reagent (P0128M, Beyotime, CHN) and

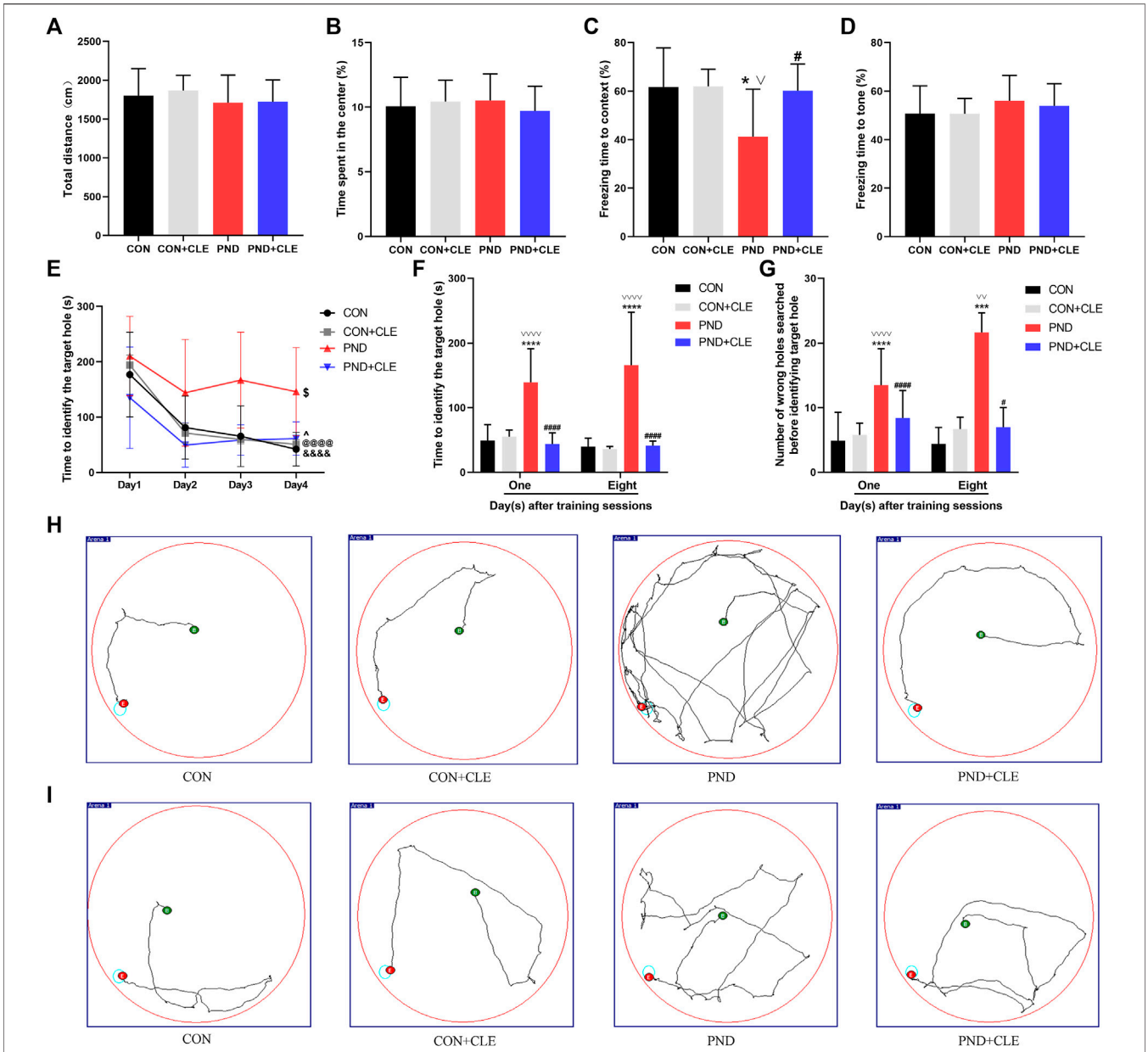

FIGURE 2 | Anesthesia and surgery-induced cognitive impairments were ameliorated by clemastine treatment. (**A**) Total distance in the open field test among four groups. (**B**) Time spent in the center of open field test among four groups. (**C**) Context test in the fear conditioning test among four groups. (**D**) Tone test in the fear conditioning test among four groups. (**E**) Performance during the training phase of the Barnes maze. (**F, G**) Performance during the testing phase of Barnes maze. (**H, I**) Representative movement traces on day 1 and day 8 of the Barnes maze test phase. The data are presented as mean ± S.D. (n = 20 mice per group). $^{*}p < 0.05$ compared with the CON group. $^{***}p < 0.005$ compared with the CON group. $^{****}p < 0.001$ compared with the CON group. $^{\#}p < 0.05$ compared with the PND group. $^{\#\#\#\#}p < 0.001$ compared with the PND group. $^{\vee}p < 0.05$ compared with the CON + CLE group. $^{\vee\vee}p < 0.01$ compared with the CON + CLE group. $^{\vee\vee\vee\vee}p < 0.001$ compared with the CON + CLE group. $^{\&\&\&\&}p < 0.001$ compared with the day 1 in CON group. $^{@@@@}p < 0.001$ compared with the day 1 in CON + CLE group. $^{\$}p < 0.05$ compared with the first day in PND group. $^{\wedge}p < 0.05$ compared with the first day in PND + CLE group.

images were obtained using a laser confocal microscope (×200, magnification) (Zeiss LSM 800 with airyscan, GER).

Statistical Analysis

All data were expressed as mean ± S.D. The statistical analysis of results was performed by using GraphPad Prism version 8.0 (San Diego, CA, United States) and R software. The inter-group comparisons were assessed by one-way repeated measures analysis of variance followed by Tukey test. The data of training sessions in the Barnes maze test was analyzed by two-way repeated measures analysis of variance followed by Tukey test. A p-value < 0.05 was considered statistically significant difference.

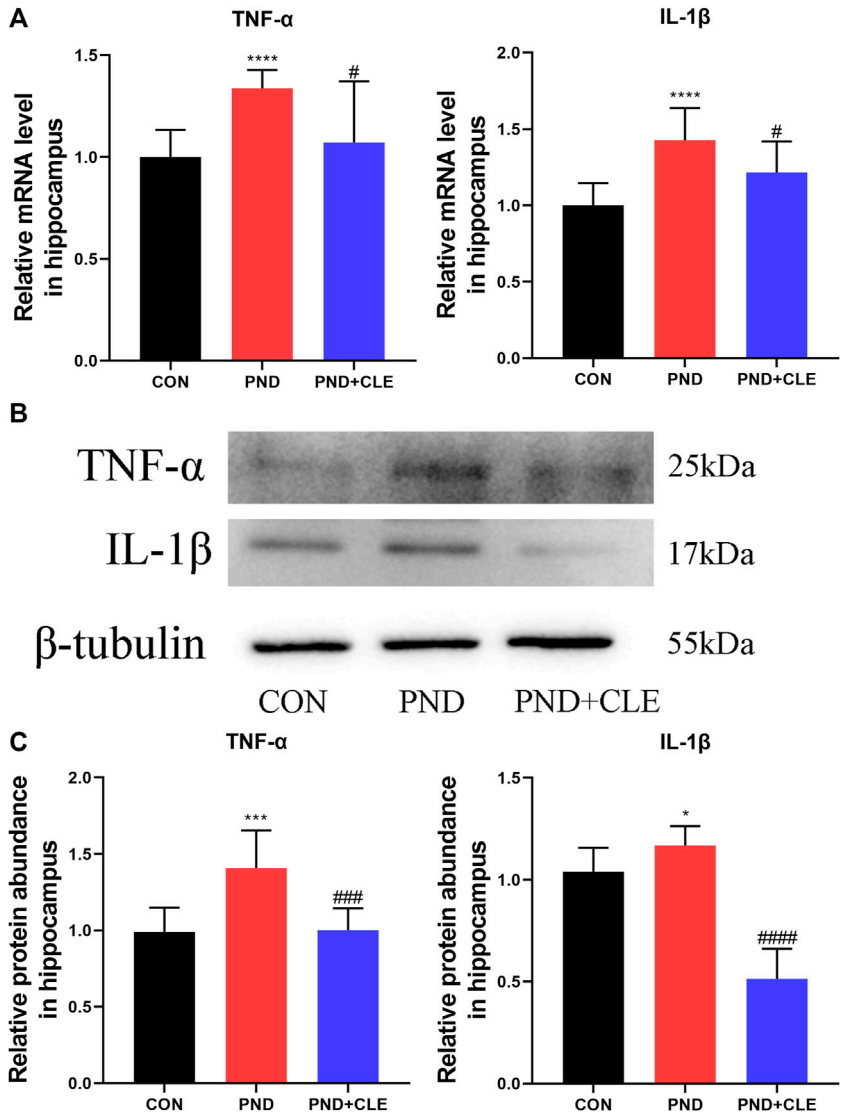

FIGURE 3 | Effects of clemastine on expression levels of inflammatory cytokines in hippocampus of aged mice after anesthesia and surgery. (**A**) Relative mRNA expressions of TNF-α and IL-1β, normalized to that of the GAPDH internal control. (**B**) Representative western blot images of TNF-α and IL-1β. (**C**) Relative protein expressions of TNF-α and IL-1β, normalized to that of the β-tubulin internal control. The data are presented as mean ± S.D. (n = 10 mice per group). $^{*}p < 0.05$ compared with the CON group. $^{***}p < 0.005$ compared with the CON group. $^{****}p < 0.001$ compared with the CON group. $^{\#}p < 0.05$ compared with the PND group. $^{\#\#\#}p < 0.005$ compared with the PND group. $^{\#\#\#\#}p < 0.001$ compared with the PND group.

RESULTS

Clemastine Ameliorated Perioperative Neurocognitive Disorder Caused by Anesthesia and Surgery in Aged Mice

In the behavioral test, we first evaluated the locomotor activity and postoperative anxiety behavior of aged mice in different groups through the open field test. The results showed that anesthesia plus surgery or clemastine had no influence on the locomotor activity of the aged mice, nor did it cause the occurrence of postoperative anxiety behavior (**Figures 2A,B**). Second, we assessed the changes in hippocampal and non-hippocampal memory in aged mice through fear conditioning test. The results showed that anesthesia and surgery-induced hippocampus-dependent memory defects were improved after treatment with clemastine (**Figures 2C,D**). Finally, we estimated the effects of anesthetic and surgical factors on short-term and long-term spatial learning and memory ability of aged mice through Barnes maze test. The time required for all the aged mice to find the target hole on the 4th day of training phase were significantly

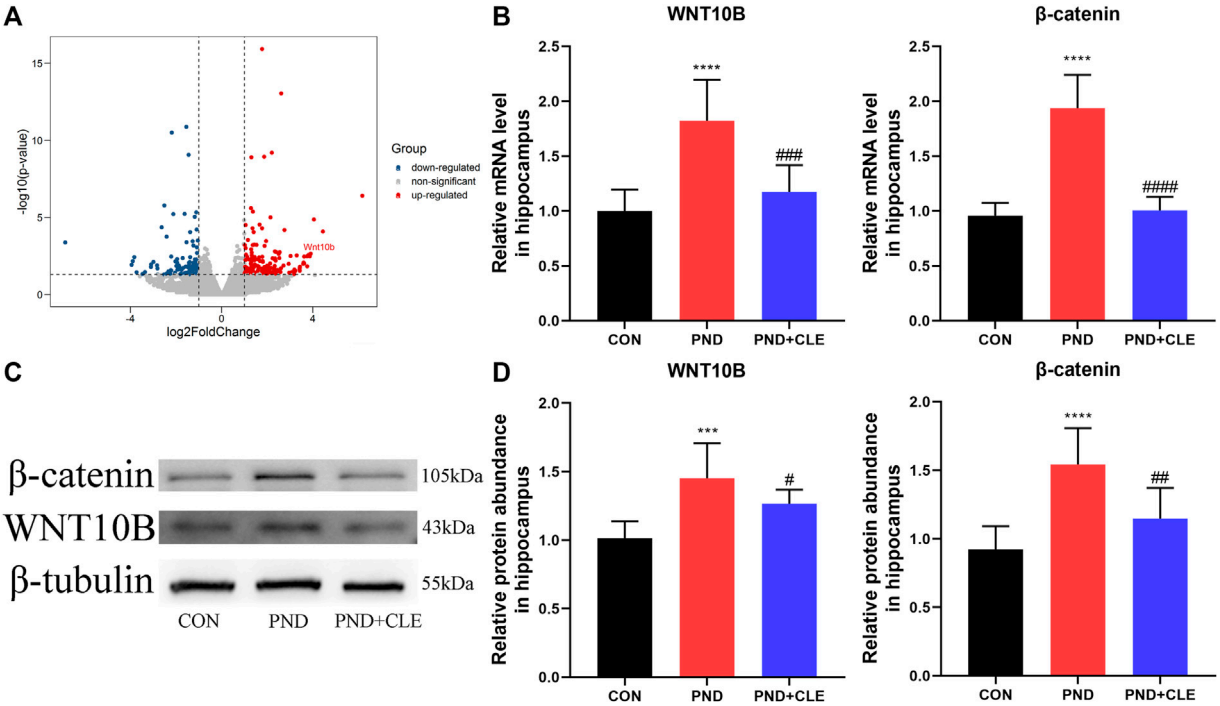

FIGURE 4 | Effects of clemastine on expression levels of WNT/β-catenin signaling pathway. (**A**) The differential expression of WNT10B was labeled in our previous sequencing results. (**B**) Relative mRNA expressions of WNT10B and β-catenin, normalized to that of the GAPDH internal control. (**C**) Representative western blot images of WNT10B and β-catenin. (**D**) Relative protein expressions of WNT10B and β-catenin, normalized to that of the β-tubulin internal control. The data are presented as mean ± S.D. (n = 10 mice per group). $^{***}p < 0.005$ compared with the CON group. $^{****}p < 0.001$ compared with the CON group. $^{\#}p < 0.05$ compared with the PND group. $^{\#\#}p < 0.01$ compared with the PND group. $^{\#\#\#}p < 0.005$ compared with the PND group. $^{\#\#\#\#}p < 0.001$ compared with the PND group.

reduced compared to the first day, indicating that all mice achieved performance development after training (**Figure 2E**). On the first and eighth days of the test phase, we found that the PND group took more time to find the target hole and explored more error holes than the CON group and CON + CLE group. However, the PND + CLE group used shorter time and explored less error holes compared with PND group (**Figures 2F–I**). These results suggested that clemastine could effectively ameliorate PND caused by anesthesia and surgery in aged mice. It is noteworthy that in the above-mentioned tests, clemastine treatment showed no effect on the aged mice of CON group, which was also confirmed in the previous study (Li et al., 2021). In the follow-up studies, brain tissues of aged mice in CON group, PND group and PND + CLE group were harvested to explore the possible mechanism.

Clemastine Exhibited Anti-neuroinflammatory Effects in Aged Mice With Perioperative Neurocognitive Disorder

Neuroinflammation is primarily involved in the pathological mechanism of PND (Liu et al., 2021). In the present study, we measured the expression levels of TNF-α and IL-1β in the hippocampus of aged mice. The results showed the expression of TNF-α and IL-1β were up-regulated in the PND group compared with the CON group. Besides, the expressions were down-regulated in the PND + CLE group compared with the PND group (**Figures 3A–C**). The results showed that clemastine, as a histamine H1 receptor antagonist, effectively reduced neuroinflammatory in aged mice with PND.

Clemastine Inhibited the Overactivation of WNT/β-Catenin Pathway in Aged Mice With Perioperative Neurocognitive Disorder

Neuroinflammation leads to overactivation of the WNT/β-catenin signaling pathway (Huang et al., 2020; Vallée et al., 2018). In our previous sequencing results, the expression of WNT10B (member of the WNT ligand gene family) in aged PND mice was significantly up-regulated (**Figure 4A**) (Wu et al., 2021). It indicated the overactivation of WNT/β-catenin signaling pathway. In the present study, we measured the expression levels of WNT10B and β-catenin in the hippocampus of aged mice. The results showed the expression of WNT10B and β-catenin were up-regulated in the PND group compared with the CON group. Besides, the expressions were down-regulated in the

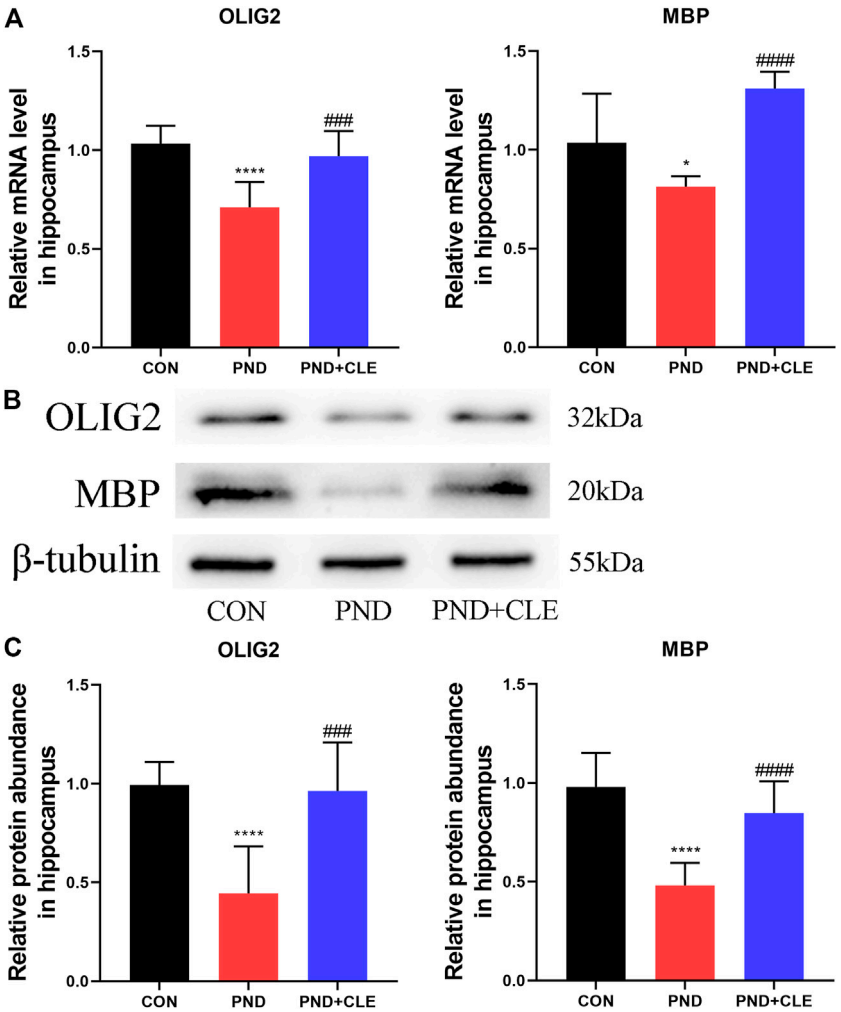

FIGURE 5 | Effects of clemastine on expression levels of OLIG2 and MBP in hippocampus of aged mice after anesthesia and surgery. (**A**) Relative mRNA expressions of OLIG2 and MBP, normalized to that of the GAPDH internal control. (**B**) Representative western blot images of OLIG2 and MBP. (**C**) Relative protein expressions of OLIG2 and MBP, normalized to that of the β-tubulin internal control. The data are presented as mean ± S.D. (n = 10 mice per group). $^{*}p < 0.05$ compared with the CON group. $^{****}p < 0.001$ compared with the CON group. $^{\#\#\#}p < 0.005$ compared with the PND group. $^{\#\#\#\#}p < 0.001$ compared with the PND group.

PND + CLE group compared with the PND group (**Figures 4B–D**). The results showed that clemastine inhibited the overactivation of WNT/β-catenin signaling pathway in aged mice with PND.

Clemastine Enhanced OLs Differentiation and Remyelination in Aged Mice With Perioperative Neurocognitive Disorder

The overactivation of WNT/β-catenin signaling pathway is detrimental to the OLs differentiation and remyelination (Huang et al., 2020; Jiang et al., 2020). The expression of OLIG2 and MBP represent the levels of OLs differentiation and remyelination, respectively. We found that the expression of OLIG2 and MBP were down-regulated in the PND group compared with the CON group, while upregulated in PND + CLE group (**Figures 5A–C**). These results showed that clemastine effectively enhanced OLs differentiation and remyelination in aged mice with PND.

Clemastine Reversed the Dysregulation of Synaptic Plasticity-Related Proteins in Aged Mice With Perioperative Neurocognitive Disorder

Remyelination helps restore the neuronal function and prevents neurodegeneration (Del Giovane and Ragnini-Wilson, 2018). PSD95, BDNF and SNAP25 are the synaptic plasticity-related proteins that closely related to neuronal function, learning and memory (Qiu et al., 2020; Jia et al.,

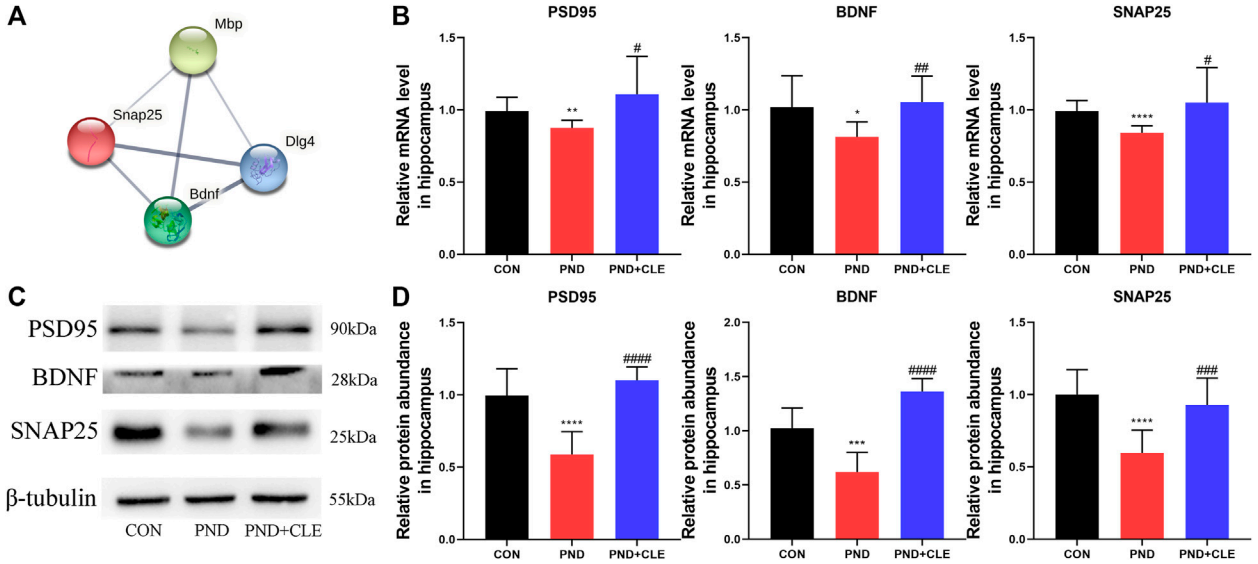

FIGURE 6 | Effects of clemastine on expression levels of synaptic plasticity-related proteins in hippocampus of aged mice after anesthesia and surgery. (**A**) Co-expression relationship of MBP, PSD95 (or DLG4), BDNF and SNAP25 from the STRING database. (**B**) Relative mRNA expressions of PSD95, BDNF and SNAP25, normalized to that of the GAPDH internal control. (**C**) Representative western blot images of synaptic plasticity-related proteins. (**D**) Relative protein expressions of PSD95, BDNF and SNAP25, normalized to that of the β-tubulin internal control. The data are presented as mean ± S.D. (n = 10 mice per group). $^{*}p < 0.05$ compared with the CON group. $^{**}p < 0.01$ compared with the CON group. $^{***}p < 0.005$ compared with the CON group. $^{****}p < 0.001$ compared with the CON group. $^{\#}p < 0.05$ compared with the PND group. $^{\#\#}p < 0.01$ compared with the PND group. $^{\#\#\#}p < 0.005$ compared with the PND group. $^{\#\#\#\#}p < 0.001$ compared with the PND group.

2021; Muscat et al., 2021). Protein-protein interaction analysis results indicated that there were co-expression relationships between MBP, PSD95, BDNF and SNAP25 (**Figure 6A**). The results showed, anesthesia and surgery decreased the expression levels of synaptic plasticity-related proteins, clemastine could reverse the down-regulation (**Figures 6B–D**). These results showed that clemastine could improve synaptic plasticity in aged mice with PND.

Clemastine Prevented the Loss of Hippocampal Mature Neurons in Aged Mice With Perioperative Neurocognitive Disorder

Synaptic plasticity is related to the neuronal survival (Labandeira et al., 2021; Limanaqi et al., 2021). Neuronal loss is also one of the main pathological mechanisms of PND (Zhang et al., 2016). In the present study, similar to the expression level of MBP, immunofluorescence results found that NUEN in the hippocampal dentate gyrus of PND group was significantly decreased compared with the CON group, while clemastine reversed the decrease (**Figures 7A–C**). These results showed that clemastine prevented the loss of hippocampal mature neurons in aged mice with PND.

DISCUSSION

PND is a complication of the central nervous system in elderly patients after surgery, which manifests as psychosis, anxiety, personality changes and impaired memory (Evered et al., 2018). Cardiac surgery and some non-cardiac surgery, such as abdominal and chest surgery, are associated with a high incidence of PND (Newman et al., 2001). In addition, age is an independent risk factor in the occurrence and development of PND (Moller et al., 1998). In elderly patients over 60 years of age, the incidence of PND is 10–62%, which increases the risk of Alzheimer's disease and may related to dementia (Evered et al., 2016; Urits et al., 2019). In this study, we performed exploratory laparotomy plus isoflurane inhalation anesthesia in 18-month-old male C57BL/6 mice to establish the PND model. Behavioral tests suggested that anesthetic and surgical factors impaired the spatial learning memory in aged mice, including short-term and long-term memory related to the hippocampus. But locomotor activity and postoperative anxiety behavior were not affected. In our previous study, the differentially expressed genes in the brain tissues of aged PND mice were identified by next-generation sequencing, and clematine was predicted to have the potential to treat this refractory disease (Wu et al., 2021). In the present study, we found that clemastine treatment ameliorated the impaired hippocampal-related memories caused by surgical and anesthetic factors. At the same time, it did not cause behavioral changes in normal aged mice, which has been confirmed in the previous study (Li et al., 2021). The results indicated that clemastine had a positive effect on PND in aged mice.

Various mechanisms are involved in the pathogenesis of PND, such as neuroinflammation, oxidative stress and neurodegeneration. The pathophysiological changes caused by neuroinflammation of the central nervous system are the main

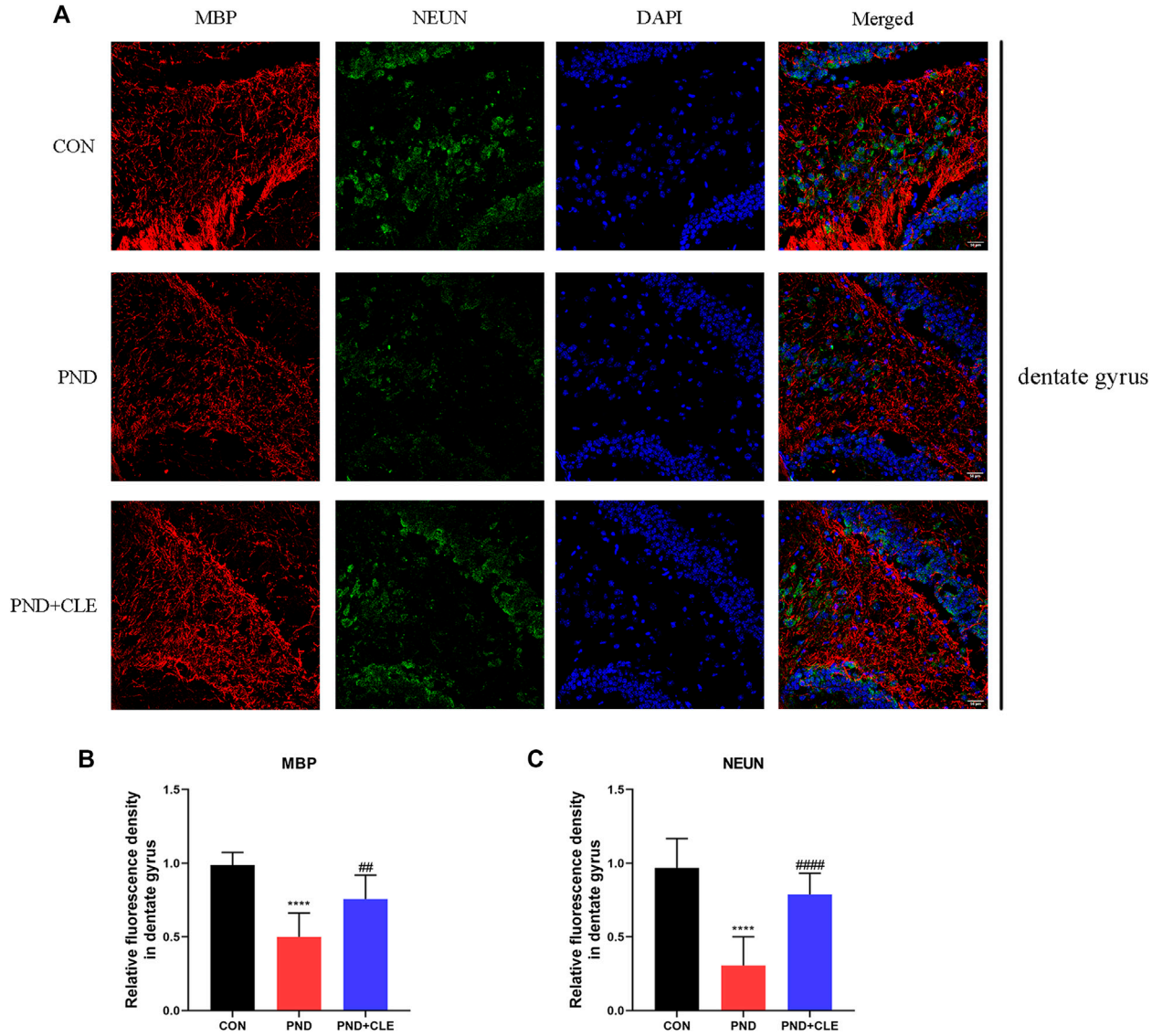

FIGURE 7 | Immunofluorescence analysis detected MBP and NEUN protein levels in hippocampal dentate gyrus (scale bar = 50 μm). (**A**) Representative images of MBP and NEUN in the dentate gyrus. (**B**) Mean fluorescence density of MBP in the dentate gyrus. (**C**) Mean fluorescence density of NEUN in the dentate gyrus. The data are presented as mean ± S.D. (n = 10 mice per group). $^{****}p < 0.001$ compared with the CON group. $^{\#\#}p < 0.01$ compared with the PND group. $^{\#\#\#\#}p < 0.001$ compared with the PND group.

mechanism of PND (Granger and Barnett, 2021; Liu et al., 2021). In the present study, we found that the expression of TNF-α and IL-1β in the hippocampus increased significantly in the PND group compared with the CON group. It was consistent with previous studies, which have confirmed the association between PND and neuroinflammation (Qiu et al., 2020). Anti-neuroinflammatory therapy has shown some positive effects on the treatment of PND. Previous studies have shown that inhibiting neuroinflammatory by reducing the expression of interleukin-6, C-reactive protein and matrix metalloproteinase-9 in serum can significantly alleviate PND in aged patients (Zhang et al., 2018). The activation of microglia is the key factor in aggravating neuroinflammation, especially the M1 type (Lee et al., 2017). Lipopolysaccharide and sevoflurane treatment induced up-regulation of IL-1β and IL-6 expression in microglia *in vitro* (Ye et al., 2013). *In vivo* experiment, isoflurane induced microglial inflammation and cognitive impairment in aged mice through the NLRP3-Caspase-1 pathway (Wang et al., 2018). At the same time, inhibition of NF-kB/MAPKs pathway of microglia by upregulating the expression of interleukin-10 to improve PND through anti-inflammatory effect (Zhang et al., 2019). Clemastine, as an antihistamine, has a positive anti-neuroinflammatory effect, could reduce the activation of microglia and down-regulate the expression of IL-1β and NLRP3 in rats with hypoxic-ischemic brain injury (Xie et al., 2020). Besides, it also reduced the expression of TNF-α and IL-1β

in the hippocampus and serum of depression mice, and inhibited the M1-like activation of microglia (Su et al., 2018). In the present study, we found that clemastine reduced the expression of TNF-α and IL-1β in the hippocampus of aged mice with PND, suggesting the inhibition of neuroinflammation, which is contributed to the treatment of PND.

Neuroinflammation could lead to overactivation of WNT/β-catenin signaling pathway (Xie et al., 2016; Huang et al., 2020). Previous studies have shown that dysregulation of the WNT/β-catenin pathway is closely related to PND (Hu et al., 2016). Our previous sequencing results showed the expression of WNT10B were significantly up-regulated in aged mice with PND (Wu et al., 2021), indicating that PND might induce the overactivation of the WNT/β-catenin pathway. Besides, previous studies demonstrated that the overactivation of WNT/β-catenin pathway leads to the decrease of OLIG2 (Huang et al., 2020; Jiang et al., 2020). The normal expression of OLIG2 contributes to the developmental regulation of oligodendrocytes precursor cells and the early directed differentiation to OLs. OLs are widely distributed in the central nervous system, which contribute to the formation of myelin sheath and could be impaired by neuroinflammation (Xie et al., 2016; Huntemer-Silveira et al., 2020; Joerger-Messerli et al., 2021). In this study, we confirmed PND increased the expression of WNT10B and β-catenin and decreased the expression of OLIG2. Clemastine could reverse the above phenomenon, which contributes to the remyelination (Vallée et al., 2018).

Myelin sheath is formed by OLs and wraps around the outside of axons, accelerating nerve excitatory conduction along nerve fibers and ensuring directional conduction, which is an indispensable process in the development and normal function of nervous system neurons (Ravera et al., 2016; Saab and Nave, 2017; Grove et al., 2020; Huntemer-Silveira et al., 2020). At the same time, myelin sheath regulates the ionic environment and promotes neuron survival through meeting neuronal energy requirements by its metabolites (El Waly et al., 2014; Saab and Nave, 2017). Neuroinflammation is one of the main causes of demyelination. Multiple sclerosis, a chronic inflammatory disease of the central nervous system, characterized by demyelination, can lead to neurodegeneration and neurological function's impairment (das Neves et al., 2020). Besides, demyelination has been found in the frontal cortex in Alzheimer's disease patients (Ferrer and Andrés-Benito, 2020), which leaded to cognitive impairment in population at high risk for dementia in Alzheimer's disease (Kövari et al., 2007; Vanzulli et al., 2020). MBP, as the major component of myelin sheath, its expression level could reflect the level of demyelination. Previous studies have indicated that demyelination, mainly manifested by reduced expression of MBP, was found in aged mice with impaired memory and cognitive ability (Bao et al., 2021). In addition, sevoflurane anesthesia during pregnancy caused the expression of MBP decreased and demyelination in mice, leading to cognitive impairment in the offspring (Zuo et al., 2020). The behavioral function of aged mice was improved when it comes to remyelination, which showed through the up-regulated MBP (Bao et al., 2021). Recent studies have shown that enhanced remyelination reverses cognitive dysfunction in a murine model of Alzheimer's disease (Chen et al., 2021a). This finding was also confirmed in the chronic cerebral hypoperfusion rat model (Li et al., 2020). In this study, the down-regulation of MBP caused by anesthetic and surgical factors in the hippocampus of aged mice suggesting the appearance of demyelination. Clemastine facilitated remyelination in aged mice with PND, indicating it might be an emerging myelin repair agent, which was consistent with the results of previous studies (Wang et al., 2020a; Xie et al., 2020).

Synapses are places for neuronal function connections occurrence and information transmission. The most common is that the axon terminal of one neuron is connected with the dendrites, dendritic spines or cell bodies of another neuron to form axon-dendritic synapses, axon-spindle synapses or axon-body synapses. Myelin sheath is closely related to axons, and the development of axons is pivotal during the formation of synapse (Han et al., 2017). The synapse is composed of presynaptic membrane, synaptic cleft and postsynaptic membrane. SNAP25 and PSD95 are representative synaptic related proteins, which expressed in the presynaptic and postsynaptic membranes, respectively. Previous studies have shown that the expression level of SNAP25 in exosomes and cerebrospinal fluid of Alzheimer's disease patients were significantly down-regulated compared with normal counterparts (Jia et al., 2021). The expression level of SNAP25 in the hippocampus of rats with vascular dementia is closely related to the severity of disease (Ren et al., 2018). Furthermore, the significant down-regulated expression level of PSD95 in hippocampus of PND aged rats suggesting that impaired synaptic structure and/or function might have a key role in this persistent defect (Muscat et al., 2021). BDNF is the most abundant neurotrophic factor in the body, mainly expressed in the cortex and hippocampus. Its expression can promote the survival of neurons, increase synaptic plasticity and neurogenesis (Wang et al., 2020b). Previous studies have shown that the expression level of BDNF was significantly down-regulated in hippocampus of mice with PND, which was associated with the impairment of synapse development (Luo et al., 2020). The up-regulation of BDNF was helpful to prevent the occurrence of PND in aged mice (Chen et al., 2018). The expression of PSD95, BDNF and SNAP25 are associated with synaptic plasticity. Previous studies demonstrated that anesthesia and surgery inhibit synaptic function, PND is closely related to synaptic plasticity impairment (Gao et al., 2021). Rescuing the expression of plasticity-related proteins contributes to improve hippocampal-dependent memory deficits caused by anesthesia and surgery (Xiao et al., 2018). In the present study, we further detected the expression of synaptic plasticity-related proteins. The results showed the expression of PSD95, BDNF and SNAP25 were down-regulated in the hippocampus of aged mice with PND, which were reversed after the treatment with clemastine. These results also demonstrate the role of remyelination in the recovery of neuronal function (Del Giovane and Ragnini-Wilson, 2018). The improvement of synaptic plasticity is one of the cores to ameliorate PND.

As previously mentioned, the expression of BDNF can promote the survival of neurons (Wang et al., 2020b), suggesting that synaptic plasticity is related to the survival of neurons (Labandeira et al., 2021; Limanaqi et al., 2021). Meanwhile, previous studies have shown that anesthesia and surgery caused PND by triggering microglia activation and neuron loss (Zhang et al., 2016). This suggests that neuron loss is also involved in the mechanism of PND. Dentate gyrus is the main region of neurogenesis in the hippocampus. In the present study, we found that surgery and anesthesia decreased the number of mature neurons in the hippocampal dentate gyrus though testing the specific marker of mature neurons NEUN. Clemastine treatment could reverse this phenomenon. It suggested that clemastine prevented the loss of hippocampal mature neurons in aged mice with PND. All the above results indicated that clemastine has a positive therapeutic effect on PND.

However, there were some limitations should be addressed in the present study. First, we treated the mice at a daily dose of 10 mg/kg for 2 weeks without analyzing the effects of other drug doses. Although it has been proved in previous studies that the dose has a good safety and remyelination effects (Li et al., 2015; Chen et al., 2021b; Li et al., 2021). Second, we found that clemastine ameliorated PND in elderly mice through a variety of ways, but the underlying mechanism is still unclear and requires further analysis in subsequent experiments. Finally, we found that clemastine ameliorated PND in aged mice, whether it is effective in human remains unknown, which needs to be further confirmed by follow-up clinical studies.

CONCLUSION

This study innovatively proposed the presence of demyelination in the pathological process of PND. We identified the ameliorative effect of clemastine on PND by blocking the overactivation of WNT/β-catenin signaling pathway through anti-neuroinflammation to promote OLs differentiation and remyelination. At the same time, synaptic plasticity and survival of hippocampal mature neurons were also improved. Our results might have practical implications and provide new clues and ideas for the clinical treatment of PND.

DATA AVAILABILITY STATEMENT

The datasets presented in this study can be found in online repositories. The names of the repository/repositories and accession number(s) can be found below: https://www.ncbi.nlm.nih.gov/geo/.

ETHICS STATEMENT

The animal study was reviewed and approved by Institutional Animal Care and Use Committee (Approval No: SYSU-IACUC-2020-000326) and the Laboratory Animal Ethics Committee of Sun Yat-sen University.

AUTHOR CONTRIBUTIONS

ZW conceived and designed the study and interpreted experiments. WW and XZ performed the experiments, prepared the initial draft of the manuscript. JZ, HY, JC, LZ, JZ and W-jL supervised the project. All authors read and approved the final submission.

FUNDING

This study was supported by grants from the National Natural Science Foundation of China (81571196 to ZW), grants from Guangdong Science and Technology Department (2019A1515012147 and 2021A1515010220 to ZW).

ACKNOWLEDGMENTS

WW wants to thank, in particular, the patience, care, support and love from XZ over the passed years.

SUPPLEMENTARY MATERIAL

The Supplementary Material for this article can be found online at: https://www.frontiersin.org/articles/10.3389/fphar.2021.738590/full#supplementary-material.

REFERENCES

Bao, C., He, C., Shu, B., Meng, T., Cai, Q., Li, B., et al. (2021). Aerobic Exercise Training Decreases Cognitive Impairment Caused by Demyelination by Regulating ROCK Signaling Pathway in Aging Mice. *Brain Res. Bull.* 168, 52–62. doi:10.1016/j.brainresbull.2020.12.010

Borgonetti, V., Sanna, M. D., Lucarini, L., and Galeotti, N. (2020). Targeting the RNA-Binding Protein HuR Alleviates Neuroinflammation in Experimental Autoimmune Encephalomyelitis: Potential Therapy for Multiple Sclerosis. *Neurotherapeutics* 18 (1), 412–429. doi:10.1007/s13311-020-00958-8

Chen, H., Wu, X., Gu, X., Zhou, Y., Ye, L., Zhang, K., et al. (2018). Tacrine(10)-Hupyridone Prevents Post-operative Cognitive Dysfunction via the Activation of BDNF Pathway and the Inhibition of AChE in Aged Mice. *Front Cel Neurosci* 12, 396. doi:10.3389/fncel.2018.00396

Chen, J. F., Liu, K., Hu, B., Li, R. R., Xin, W., Chen, H., et al. (2021a). Enhancing Myelin Renewal Reverses Cognitive Dysfunction in a Murine Model of Alzheimer's Disease. *Neuron* 109 (14), 2292–2307. doi:10.1016/j.neuron.2021.05.012

Chen, L., Ren, S. Y., Li, R. X., Liu, K., Chen, J. F., Yang, Y. J., et al. (2021b). Chronic Exposure to Hypoxia Inhibits Myelinogenesis and Causes Motor Coordination Deficits in Adult Mice. *Neurosci. Bull.*, 1–15. doi:10.1007/s12264-021-00745-1

Cree, B. A. C., Niu, J., Hoi, K. K., Zhao, C., Caganap, S. D., Henry, R. G., et al. (2018). Clemastine Rescues Myelination Defects and Promotes Functional Recovery in Hypoxic Brain Injury. *Brain* 141 (1), 85–98. doi:10.1093/brain/awx312

das Neves, S. P., Sousa, J. C., Sousa, N., Cerqueira, J. J., and Marques, F. (2020). Altered Astrocytic Function in Experimental Neuroinflammation and Multiple Sclerosis. *Glia* 69 (6), 1341–1368. doi:10.1002/glia.23940

Del Giovane, A., and Ragnini-Wilson, A. (2018). Targeting Smoothened as a New Frontier in the Functional Recovery of Central Nervous System Demyelinating Pathologies. *Int. J. Mol. Sci.* 19 (11), 3677. doi:10.3390/ijms19113677

El Waly, B., Macchi, M., Cayre, M., and Durbec, P. (2014). Oligodendrogenesis in the normal and Pathological central Nervous System. *Front. Neurosci.* 8, 145. doi:10.3389/fnins.2014.00145

Evered, L., Silbert, B., Knopman, D. S., Scott, D. A., DeKosky, S. T., Rasmussen, L. S., et al. (2018). Recommendations for the Nomenclature of Cognitive Change Associated with Anaesthesia and Surgery-2018. *Anesth. Analg.* 127 (5), 1189–1195. doi:10.1213/ANE.0000000000003634

Evered, L. A., Silbert, B. S., Scott, D. A., Maruff, P., and Ames, D. (2016). Prevalence of Dementia 7.5 Years after Coronary Artery Bypass Graft Surgery. *Anesthesiology* 125 (1), 62–71. doi:10.1097/ALN.0000000000001143

Ferrer, I., and Andrés-Benito, P. (2020). White Matter Alterations in Alzheimer's Disease without Concomitant Pathologies. *Neuropathol. Appl. Neurobiol.* 46 (7), 654–672. doi:10.1111/nan.12618

Gao, S., Zhang, S., Zhou, H., Tao, X., Ni, Y., Pei, D., et al. (2021). Role of mTOR-Regulated Autophagy in Synaptic Plasticity Related Proteins Downregulation and the Reference Memory Deficits Induced by Anesthesia/Surgery in Aged Mice. *Front. Aging Neurosci.* 13, 628541. doi:10.3389/fnagi.2021.628541

Granger, K. T., and Barnett, J. H. (2021). Postoperative Cognitive Dysfunction: an Acute Approach for the Development of Novel Treatments for Neuroinflammation. *Drug Discov. Today.* 26, 1111–1114. doi:10.1016/j.drudis.2021.01.019

Green, A. J., Gelfand, J. M., Cree, B. A., Bevan, C., Boscardin, W. J., Mei, F., et al. (2017). Clemastine Fumarate as a Remyelinating Therapy for Multiple Sclerosis (ReBUILD): a Randomised, Controlled, Double-Blind, Crossover Trial. *Lancet* 390 (10111), 2481–2489. doi:10.1016/S0140-6736(17)32346-2

Grove, M., Lee, H., Zhao, H., and Son, Y. J. (2020). Axon-dependent Expression of YAP/TAZ Mediates Schwann Cell Remyelination but Not Proliferation after Nerve Injury. *Elife* 9, e50138. doi:10.7554/eLife.50138

Han, Q., Lin, Q., Huang, P., Chen, M., Hu, X., Fu, H., et al. (2017). Microglia-derived IL-1β Contributes to Axon Development Disorders and Synaptic Deficit through P38-MAPK Signal Pathway in Septic Neonatal Rats. *J. Neuroinflammation.* 14 (1), 52. doi:10.1186/s12974-017-0805-x

Hu, N., Wang, C., Zheng, Y., Ao, J., Zhang, C., Xie, K., et al. (2016). The Role of the Wnt/β-Catenin-Annexin A1 Pathway in the Process of Sevoflurane-Induced Cognitive Dysfunction. *J. Neurochem.* 137 (2), 240–252. doi:10.1111/jnc.13569

Huang, P., Zhou, Q., Lin, Q., Lin, L., Wang, H., Chen, X., et al. (2020). Complement C3a Induces Axonal Hypomyelination in the Periventricular white Matter through Activation of WNT/β-catenin Signal Pathway in Septic Neonatal Rats Experimentally Induced by Lipopolysaccharide. *Brain Pathol.* 30 (3), 495–514. doi:10.1111/bpa.12798

Huntemer-Silveira, A., Patil, N., Brickner, M. A., and Parr, A. M. (2020). Strategies for Oligodendrocyte and Myelin Repair in Traumatic CNS Injury. *Front. Cel Neurosci.* 14, 619707. doi:10.3389/fncel.2020.619707

Jia, L., Zhu, M., Kong, C., Pang, Y., Zhang, H., Qiu, Q., et al. (2021). Blood Neuro-Exosomal Synaptic Proteins Predict Alzheimer's Disease at the Asymptomatic Stage. *Alzheimers Dement.* 17 (1), 49–60. doi:10.1002/alz.12166

Jiang, M., Yu, D., Xie, B., Huang, H., Lu, W., Qiu, M., et al. (2020). WNT Signaling Suppresses Oligodendrogenesis via Ngn2-dependent Direct Inhibition of Olig2 Expression. *Mol. Brain.* 13 (1), 155. doi:10.1186/s13041-020-00696-0

Jiang, X. L., Gu, X. Y., Zhou, X. X., Chen, X. M., Zhang, X., Yang, Y. T., et al. (2019). Intestinal Dysbacteriosis Mediates the Reference Memory Deficit Induced by Anaesthesia/surgery in Aged Mice. *Brain Behav. Immun.* 80, 605–615. doi:10.1016/j.bbi.2019.05.006

Joerger-Messerli, M. S., Thomi, G., Haesler, V., Keller, I., Renz, P., Surbek, D. V., et al. (2021). Human Wharton's Jelly Mesenchymal Stromal Cell-Derived Small Extracellular Vesicles Drive Oligodendroglial Maturation by Restraining MAPK/ERK and Notch Signaling Pathways. *Front Cel Dev Biol.* 9, 622539. doi:10.3389/fcell.2021.622539

Kövari, E., Gold, G., Herrmann, F. R., Canuto, A., Hof, P. R., Bouras, C., et al. (2007). Cortical Microinfarcts and Demyelination Affect Cognition in Cases at High Risk for Dementia. *Neurology* 68 (12), 927–931. doi:10.1212/01.wnl.0000257094.10655.9a

Labandeira, C. M., Fraga-Bau, A., Arias Ron, D., Muñoz, A., Alonso-Losada, G., Koukoulis, A., et al. (2021). Diabetes, Insulin and New Therapeutic Strategies for Parkinson's Disease: Focus on Glucagon-like Peptide-1 Receptor Agonists. *Front. Neuroendocrinol* 62, 100914. doi:10.1016/j.yfrne.2021.100914

Lee, J. H., Kam, E. H., Kim, S. Y., Cheon, S. Y., Kim, E. J., Chung, S., et al. (2017). Erythropoietin Attenuates Postoperative Cognitive Dysfunction by Shifting Macrophage Activation toward the M2 Phenotype. *Front. Pharmacol.* 8, 839. doi:10.3389/fphar.2017.00839

Li, M., Meng, N., Guo, X., Niu, X., Zhao, Z., Wang, W., et al. (2020). Dl-3-n-Butylphthalide Promotes Remyelination and Suppresses Inflammation by Regulating AMPK/SIRT1 and STAT3/NF-Kb Signaling in Chronic Cerebral Hypoperfusion. *Front. Aging Neurosci.* 12, 137. doi:10.3389/fnagi.2020.00137

Li, Q., Mathena, R. P., Xu, J., Eregha, O. N., Wen, J., and Mintz, C. D. (2019). Early Postnatal Exposure to Isoflurane Disrupts Oligodendrocyte Development and Myelin Formation in the Mouse Hippocampus. *Anesthesiology* 131 (5), 1077–1091. doi:10.1097/ALN.0000000000002904

Li, Z., He, Y., Fan, S., and Sun, B. (2015). Clemastine Rescues Behavioral Changes and Enhances Remyelination in the Cuprizone Mouse Model of Demyelination. *Neurosci. Bull.* 31 (5), 617–625. doi:10.1007/s12264-015-1555-3

Li, Z. Y., Chen, L. H., Zhao, X. Y., Chen, H., Sun, Y. Y., Lu, M. H., et al. (2021). Clemastine Attenuates AD-like Pathology in an AD Model Mouse via Enhancing mTOR-Mediated Autophagy. *Exp. Neurol.* 342, 113742. doi:10.1016/j.expneurol.2021.113742

Limanaqi, F., Busceti, C. L., Celli, R., Biagioni, F., and Fornai, F. (2021). Autophagy as a Gateway for the Effects of Methamphetamine: From Neurotransmitter Release and Synaptic Plasticity to Psychiatric and Neurodegenerative Disorders. *Prog. Neurobiol.* 2021, 102112. doi:10.1016/j.pneurobio.2021.102112

Liu, J., Dupree, J. L., Gacias, M., Frawley, R., Sikder, T., Naik, P., et al. (2016). Clemastine Enhances Myelination in the Prefrontal Cortex and Rescues Behavioral Changes in Socially Isolated Mice. *J. Neurosci.* 36 (3), 957–962. doi:10.1523/JNEUROSCI.3608-15.2016

Liu, Q., Sun, Y. M., Huang, H., Chen, C., Wan, J., Ma, L. H., et al. (2021). Sirtuin 3 Protects against Anesthesia/surgery-Induced Cognitive Decline in Aged Mice by Suppressing Hippocampal Neuroinflammation. *J. Neuroinflammation* 18 (1), 41. doi:10.1186/s12974-021-02089-z

Luo, A., Yan, J., Tang, X., Zhao, Y., Zhou, B., and Li, S. (2019). Postoperative Cognitive Dysfunction in the Aged: the Collision of Neuroinflammaging with Perioperative Neuroinflammation. *Inflammopharmacology* 27 (1), 27–37. doi:10.1007/s10787-018-00559-0

Luo, F., Min, J., Wu, J., and Zuo, Z. (2020). Histone Deacetylases May Mediate Surgery-Induced Impairment of Learning, Memory, and Dendritic Development. *Mol. Neurobiol.* 57 (9), 3702–3711. doi:10.1007/s12035-020-01987-2

Mayne, K., White, J. A., McMurran, C. E., Rivera, F. J., and de la Fuente, A. G. (2020). Aging and Neurodegenerative Disease: Is the Adaptive Immune System a Friend or Foe? *Front. Aging Neurosci.* 12, 572090. doi:10.3389/fnagi.2020.572090

Moller, J. T., Cluitmans, P., Rasmussen, L. S., Houx, P., Rasmussen, H., Canet, J., et al. (1998). Long-term Postoperative Cognitive Dysfunction in the Elderly ISPOCD1 Study. ISPOCD Investigators. International Study of Post-Operative Cognitive Dysfunction. *Lancet* 351 (9106), 857–861. doi:10.1016/s0140-6736(97)07382-0

Muscat, S. M., Deems, N. P., D'Angelo, H., Kitt, M. M., Grace, P. M., Andersen, N. D., et al. (2021). Postoperative Cognitive Dysfunction Is Made Persistent with Morphine Treatment in Aged Rats. *Neurobiol. Aging.* 98, 214–224. doi:10.1016/j.neurobiolaging.2020.11.008

Newman, M. F., Kirchner, J. L., Phillips-Bute, B., Gaver, V., Grocott, H., Jones, R. H., et al. (2001). Longitudinal Assessment of Neurocognitive Function after Coronary-Artery Bypass Surgery. *N. Engl. J. Med.* 344 (6), 395–402. doi:10.1056/NEJM200102083440601

Punjasawadwong, Y., Chau-In, W., Laopaiboon, M., Punjasawadwong, S., and Pin-On, P. (2018). Processed Electroencephalogram and Evoked Potential Techniques for Amelioration of Postoperative Delirium and Cognitive Dysfunction Following Non-cardiac and Non-neurosurgical Procedures in Adults. *Cochrane Database Syst. Rev.* 5, CD011283. doi:10.1002/14651858.CD011283.pub2

Qiu, L. L., Luo, D., Zhang, H., Shi, Y. S., Li, Y. J., Wu, D., et al. (2016). Nox-2-Mediated Phenotype Loss of Hippocampal Parvalbumin Interneurons Might Contribute to Postoperative Cognitive Decline in Aging Mice. *Front. Aging Neurosci.* 8, 234. doi:10.3389/fnagi.2016.00234

Qiu, L. L., Pan, W., Luo, D., Zhang, G. F., Zhou, Z. Q., Sun, X. Y., et al. (2020). Dysregulation of BDNF/TrkB Signaling Mediated by NMDAR/Ca2+/calpain Might Contribute to Postoperative Cognitive Dysfunction in Aging Mice. *J. Neuroinflammation.* 17 (1), 23. doi:10.1186/s12974-019-1695-x

Ravera, S., Bartolucci, M., Adriano, E., Garbati, P., Ferrando, S., Ramoino, P., et al. (2016). Support of Nerve Conduction by Respiring Myelin Sheath: Role of Connexons. *Mol. Neurobiol.* 53 (4), 2468–2479. doi:10.1007/s12035-015-9216-0

Ren, Z., Yu, J., Wu, Z., Si, W., Li, X., Liu, Y., et al. (2018). MicroRNA-210-5p Contributes to Cognitive Impairment in Early Vascular Dementia Rat Model through Targeting Snap25. *Front. Mol. Neurosci.* 11, 388. doi:10.3389/fnmol.2018.00388

Saab, A. S., and Nave, K. A. (2017). Myelin Dynamics: Protecting and Shaping Neuronal Functions. *Curr. Opin. Neurobiol.* 47, 104–112. doi:10.1016/j.conb.2017.09.013

Su, W. J., Zhang, T., Jiang, C. L., and Wang, W. (2018). Clemastine Alleviates Depressive-like Behavior through Reversing the Imbalance of Microglia-Related Pro-inflammatory State in Mouse Hippocampus. *Front. Cel Neurosci* 12, 412. doi:10.3389/fncel.2018.00412

Tandon, A., Singh, S. J., Gupta, M., Singh, N., Shankar, J., Arjaria, N., et al. (2020). Notch Pathway Up-Regulation via Curcumin Mitigates Bisphenol-A (BPA) Induced Alterations in Hippocampal Oligodendrogenesis. *J. Hazard. Mater.* 392, 122052. doi:10.1016/j.jhazmat.2020.122052

Urits, I., Orhurhu, V., Jones, M., Hoyt, D., Seats, A., and Viswanath, O. (2019). Current Perspectives on Postoperative Cognitive Dysfunction in the Ageing Population. *Turk J. Anaesthesiol Reanim.* 47 (6), 439–447. doi:10.5152/TJAR.2019.75299

Vallée, A., Vallée, J. N., Guillevin, R., and Lecarpentier, Y. (2018). Interactions between the Canonical WNT/Beta-Catenin Pathway and PPAR Gamma on Neuroinflammation, Demyelination, and Remyelination in Multiple Sclerosis. *Cell Mol Neurobiol.* 38 (4), 783–795. doi:10.1007/s10571-017-0550-9

Vanzulli, I., Papanikolaou, M., De-La-Rocha, I. C., Pieropan, F., Rivera, A. D., Gomez-Nicola, D., et al. (2020). Disruption of Oligodendrocyte Progenitor Cells Is an Early Sign of Pathology in the Triple Transgenic Mouse Model of Alzheimer's Disease. *Neurobiol. Aging.* 94, 130–139. doi:10.1016/j.neurobiolaging.2020.05.016

Wang, F., Ren, S. Y., Chen, J. F., Liu, K., Li, R. X., Li, Z. F., et al. (2020). Myelin Degeneration and Diminished Myelin Renewal Contribute to Age-Related Deficits in Memory. *Nat. Neurosci.* 23 (4), 481–486. doi:10.1038/s41593-020-0588-8

Wang, W., Liu, X., Yang, Z., Shen, H., Liu, L., Yu, Y., et al. (2020). Levodopa Improves Cognitive Function and the Deficits of Structural Synaptic Plasticity in Hippocampus Induced by Global Cerebral Ischemia/Reperfusion Injury in Rats. *Front. Neurosci.* 14, 586321. doi:10.3389/fnins.2020.586321

Wang, Z., Meng, S., Cao, L., Chen, Y., Zuo, Z., and Peng, S. (2018). Critical Role of NLRP3-Caspase-1 Pathway in Age-dependent Isoflurane-Induced Microglial Inflammatory Response and Cognitive Impairment. *J. Neuroinflammation.* 15 (1), 109. doi:10.1186/s12974-018-1137-1

Wu, W., Peng, Y., Zhou, J., Zhang, X., Cao, L., Lin, W. J., et al. (2021). Identification of the Potential Gene Regulatory Networks and Therapeutics in Aged Mice with Postoperative Neurocognitive Disorder. *Front. Neurosci.* 15, 689188. doi:10.3389/fnins.2021.689188

Xiao, J. Y., Xiong, B. R., Zhang, W., Zhou, W. C., Yang, H., Gao, F., et al. (2018). PGE2-EP3 Signaling Exacerbates Hippocampus-dependent Cognitive Impairment after Laparotomy by Reducing Expression Levels of Hippocampal Synaptic Plasticity-Related Proteins in Aged Mice. *CNS Neurosci. Ther.* 24 (10), 917–929. doi:10.1111/cns.12832

Xie, D., Ge, X., Ma, Y., Tang, J., Wang, Y., Zhu, Y., et al. (2020). Clemastine Improves Hypomyelination in Rats with Hypoxic-Ischemic Brain Injury by Reducing Microglia-Derived IL-1β via P38 Signaling Pathway. *J. Neuroinflammation.* 17 (1), 57. doi:10.1186/s12974-019-1662-6

Xie, D., Shen, F., He, S., Chen, M., Han, Q., Fang, M., et al. (2016). IL-1β Induces Hypomyelination in the Periventricular white Matter through Inhibition of Oligodendrocyte Progenitor Cell Maturation via FYN/MEK/ERK Signaling Pathway in Septic Neonatal Rats. *Glia* 64 (4), 583–602. doi:10.1002/glia.22950

Ye, X., Lian, Q., Eckenhoff, M. F., Eckenhoff, R. G., and Pan, J. Z. (2013). Differential General Anesthetic Effects on Microglial Cytokine Expression. *PLoS One.* 8 (1), e52887. doi:10.1371/journal.pone.0052887

Zhang, D., Li, N., Wang, Y., Lu, W., Zhang, Y., Chen, Y., et al. (2019). Methane Ameliorates post-operative Cognitive Dysfunction by Inhibiting Microglia NF-κB/MAPKs Pathway and Promoting IL-10 Expression in Aged Mice. *Int. Immunopharmacol.* 71, 52–60. doi:10.1016/j.intimp.2019.03.003

Zhang, M., Zhang, Y. H., Fu, H. Q., Zhang, Q. M., and Wang, T. L. (2018). Ulinastatin May Significantly Improve Postoperative Cognitive Function of Elderly Patients Undergoing Spinal Surgery by Reducing the Translocation of Lipopolysaccharide and Systemic Inflammation. *Front. Pharmacol.* 9, 1007. doi:10.3389/fphar.2018.01007

Zhang, X., Dong, H., Li, N., Zhang, S., Sun, J., Zhang, S., et al. (2016). Activated Brain Mast Cells Contribute to Postoperative Cognitive Dysfunction by Evoking Microglia Activation and Neuronal Apoptosis. *J. Neuroinflammation.* 13 (1), 127. doi:10.1186/s12974-016-0592-9

Zheng, B., Lai, R., Li, J., and Zuo, Z. (2017). Critical Role of P2X7 Receptors in the Neuroinflammation and Cognitive Dysfunction after Surgery. *Brain Behav. Immun.* 61, 365–374. doi:10.1016/j.bbi.2017.01.005

Zuo, Y., Li, B., Xie, J., Ma, Z., Thirupathi, A., Yu, P., et al. (2020). Sevoflurane Anesthesia during Pregnancy in Mice Induces Cognitive Impairment in the Offspring by Causing Iron Deficiency and Inhibiting Myelinogenesis. *Neurochem. Int.* 135, 104693. doi:10.1016/j.neuint.2020.104693

Conflict of Interest: The authors declare that the research was conducted in the absence of any commercial or financial relationships that could be construed as a potential conflict of interest.

Publisher's Note: All claims expressed in this article are solely those of the authors and do not necessarily represent those of their affiliated organizations, or those of the publisher, the editors and the reviewers. Any product that may be evaluated in this article, or claim that may be made by its manufacturer, is not guaranteed or endorsed by the publisher.

GLOSSARY

PND perioperative neurocognitive disorder
TNF-α tumor necrosis factor alpha
IL-1β interleukin-1 beta
OLIG2 oligodendrocyte transcription factor 2
MBP myelin basic protein
PSD95 post-synaptic density protein 95
DLG4 disks large homolog 4
BDNF brain-derived neurotrophic factor
SNAP25 synaptosomal-associated protein 25
NEUN neuronal nuclei
OLs oligodendrocytes; FDA; Food and Drug Administration
GEO Gene Expression Omnibus
OCT optimum cutting temperature
PBS phosphate buffer solution
NFκB nuclear factor kappa-B
MAPK mitogen-activated protein kinase

frontiers in Pharmacology

ORIGINAL RESEARCH
published: 08 October 2021
doi: 10.3389/fphar.2021.735165

Trimetazidine Modulates Mitochondrial Redox Status and Disrupted Glutamate Homeostasis in a Rat Model of Epilepsy

Muhammad Y. Al-Shorbagy[1,2], *Walaa Wadie*[1]* *and Dalia M. El-Tanbouly*[1]

[1]Department of Pharmacology and Toxicology, Faculty of Pharmacy, Cairo University, Cairo, Egypt, [2]Department of Pharmaceutical Sciences, College of Pharmacy, Gulf Medical University, Ajman, United Arab Emirates

Mitochondrial oxidative status exerts an important role in modulating glia–neuron interplay during epileptogenesis. Trimetazidine (TMZ), a well-known anti-ischemic drug, has shown promising potential against a wide range of neurodegenerative disorders including epilepsy. Nevertheless, the exact mechanistic rationale behind its anti-seizure potential has not been fully elucidated yet. Herein, the impact of TMZ against mitochondrial oxidative damage as well as glutamate homeostasis disruption in the hippocampus has been investigated in rats with lithium/pilocarpine (Li/PIL) seizures. Animals received 3 mEq/kg i.p. $LiCl_3$ followed by PIL (single i.p.; 150 mg/kg) 20 h later for induction of seizures with or without TMZ pretreatment (25 mg/kg; i.p.) for five consecutive days. Seizure score and seizure latency were observed. Mitochondrial redox status as well as ATP and uncoupling protein 2 was recorded. Moreover, glutamate homeostasis was unveiled. The present findings demonstrate the TMZ-attenuated Li/PIL seizure score and latency. It improved mitochondrial redox status, preserved energy production mechanisms, and decreased reactive astrocytes evidenced as decreased glial fibrillary acidic protein immune-stained areas in hippocampal tissue. In addition, it modulated phosphorylated extracellular signal-regulated kinases (*p*-ERK1/2) and p-AMP–activated protein kinase (*p*-AMPK) signaling pathways to reflect a verified anti-apoptotic effect. Consequently, it upregulated mRNA expression of astroglial glutamate transporters and reduced the elevated glutamate level. The current study demonstrates that TMZ exhibits robust anti-seizure and neuroprotective potentials. These effects are associated with its ability to modulate mitochondrial redox status, boost *p*-ERK1/2 and *p*-AMPK signaling pathways, and restore glutamate homeostasis in hippocampus.

Keywords: trimetazidine, mitochondrial oxidative stress, glutamate transporters, ERK1/2, astrogliosis

OPEN ACCESS

Edited by:
Barbara Budzynska,
Medical University of Lublin, Poland

Reviewed by:
Chin-Wei,
William Huang,
National Cheng Kung University Hospital, Taiwan
Ivana Grković,
University of Belgrade, Serbia

***Correspondence:**
Walaa Wadie
walaa.wadie@pharma.cu.edu.eg

Specialty section:
This article was submitted to Neuropharmacology, a section of the journal Frontiers in Pharmacology

Received: *02 July 2021*
Accepted: *31 August 2021*
Published: *08 October 2021*

Citation:
Al-Shorbagy MY, Wadie W and El-Tanbouly DM (2021) Trimetazidine Modulates Mitochondrial Redox Status and Disrupted Glutamate Homeostasis in a Rat Model of Epilepsy. Front. Pharmacol. 12:735165. doi: 10.3389/fphar.2021.735165

INTRODUCTION

Mitochondrial oxidative stress is the leading cause of age-related degenerative diseases and may contribute profoundly to seizure instigation (Beal, 2005; Waldbaum and Patel, 2010). Oxidative mitochondrial damage accelerates neuronal excitability *via* affecting mitochondrial roles crucial for normal brain functioning (Rowley and Patel, 2013). The deleterious role of mitochondrial dysfunction in epileptogenesis stems from the correlation between epilepsy and the frequent

incidence of inherited mitochondrial disorders such as those occurring with childhood encephalopathies (Waldbaum and Patel, 2010). Parallel to the impediment of sufficient adenosine triphosphate (ATP) production by neurons, the resultant mitochondrial damage affects antioxidant defenses, fatty acid oxidation, neurotransmitter biosynthesis, regulation of cytosolic Ca^{2+}, and synaptic glutamate homeostasis (Waldbaum and Patel, 2010). Mitochondrial dysfunction is, hence, implicated in excessive neuronal excitability and epileptogenesis. It accelerates apoptotic neuronal death following glutamate excitotoxicity, which independently participates in seizure-induced neuronal loss especially in the hippocampus (Nicholls and Ward, 2000; Noh et al., 2006). The inner mitochondrial membrane protein, uncoupling protein 2 (UCP2), could largely preserve mitochondrial membrane potential and hamper mitochondrial oxidative stress through controlling mitochondrial-derived reactive oxygen species (Pierelli et al., 2017).

Glutamate transporters are responsible for preserving synaptic glutamate in non-neurotoxic levels (Todd and Hardingham, 2020). Though they are highly expressed on both neurons and neuroglia, it has been supposed that astroglial transporters, namely, GLT-1 and GLAST, are responsible for the uptake of the majority of glutamate (Danbolt, 2001). Their dysfunction may accordingly contribute to an increase in glutamate beyond the normal levels, promoting seizure development. This was further verified when the use of threo-β-benzyloxyaspartate, a glutamate transport inhibitor, extended epileptiform activity (Shimamoto et al., 1998). GLT-1 knockout mice develop spontaneous seizures (Tanaka et al., 1997), while those lacking GLAST show high susceptibility to seizures (Ueda et al., 2002). GLT-1 and GLAST hypofunction or hypo-expression has been observed with aging and is indeed implicated in several neurodegenerative disorders, including epilepsy (Todd and Hardingham, 2020). The age-related decline in astroglial glutamate transporters in mitochondrial superoxide dismutase knockout mice coincided with epileptic seizure susceptibility (Liang and Patel, 2004). Glutamate transporters are highly vulnerable to oxidative damage resulting in the impairment of glutamate uptake machinery (Trotti et al., 1998). These observations imply that mitochondrial oxidative stress and secondary dysfunction may be sufficient to increase seizure vulnerability through modifications of astroglial glutamate transporters.

Trimetazidine [1-(2,3,4-trimethoxybenzyl) piperazine dihydrochloride] (TMZ) is mostly used as an anti-ischemic drug. It optimizes oxygen demands *via* shifting fatty acid oxidation to glucose oxidation (Peng et al., 2014). Potentiation of glucose oxidation in an ischemic cell preserves cellular ATP, as energy obtained during glucose oxidation requires less oxygen than fatty acid oxidation (Sandhiya, 2015). TMZ was reported to prevent cerebral ischemia-reperfusion injury in experimental animals (Dhote and Balaraman, 2008). It improved brain activity by increasing brain glucose uptake (Nowak et al., 2006), conserving brain mitochondrial membrane, and protecting neuronal cells against intracellular acidosis (Jain et al., 2010). It also augmented the central ATP level (Al-Kuraishy and Al-Gareeb, 2017) and hindered hippocampal oxidative damage *via* the upregulation of antioxidant enzymes and inhibition of lipid peroxidation in an animal model of Alzheimer's disease (Hassanzadeh et al., 2015). TMZ profoundly elevated seizure threshold in the increasing-current electroshock seizure test (Jain et al., 2010) and prevented pentylenetetrazol (PTZ)-induced kindling in mice (Jain et al., 2011). The exact mechanistic rationale behind its anti-seizure potential, however, has not been fully elucidated yet.

The current study was, therefore, conducted to investigate whether TMZ could modulate mitochondrial redox status and glutamate homeostasis in the hippocampi of rats following lithium/pilocarpine (Li/PIL) injection. It also explored the impact of such effects on the incidence and intensity of induced seizures.

MATERIALS AND METHODS

Animals

Adult male Wistar rats each weighing 180 ± 200 g were obtained from the National Research Centre in Cairo and housed at constant temperature and humidity at the animal facility of the Faculty of Pharmacy, Cairo University. Seizure induction was done from 9 am to 12 pm to diminish circadian effects on seizure vulnerability. The investigation fulfilled the Guide for the Care and Use of Laboratory Animals of the Ethical Committee for Animal Experimentation at Faculty of Pharmacy, Cairo University (Permit number: PT2715).

Drugs and Chemicals

Lithium chloride ($LiCl_3$) and pilocarpine (PIL) were purchased from Sigma-Aldrich, MO, United States, while trimetazidine dihydrochloride (TMZ) was purchased from Rameda Pharmaceutical Company, Cairo, Egypt.

Experimental Design

Animals were randomly allocated into four groups each of 15 rats. Group I received saline i.p. to serve as the normal control group. Group II (normal + TMZ) received TMZ (25 mg/kg; i.p.) for five consecutive days. Group III (Li/PIL control) received $LiCl_3$ in a dose of 3 mEq/kg i.p. followed by PIL (single i.p.; 150 mg/kg) 20 h later, for the induction of seizures (Al-Shorbagy et al., 2013; El-Sayed et al., 2021). Group IV (Li/PIL + TMZ) was pretreated with TMZ (25 mg/kg; i.p.) for five consecutive days before receiving Li/PIL at the same regimen as Group III.

Immediately after PIL injection, rats were placed individually in Plexiglas cages and were observed for 30 min. Each rat was assigned a convulsive score from 0 to 5 based on the Racine scale (Racine, 1972), where behavioral arrest, hair-raising excitement, and rapid breathing are denoted by 0; mouth movements (lips and tongue), vibrissae movements, and salivation are denoted by 1; head and eye clonus is denoted by 2; forelimb clonus and "wet dog shakes" are denoted by 3; clonic rearing is denoted by 4; clonic rearing with a loss of postural control and uncontrollable jumping is denoted by 5. Stage 3–5 seizure latency and median seizure stage as well as seizure incidence were recorded. Animals that did not show Stage 3–5 seizure within the observation period

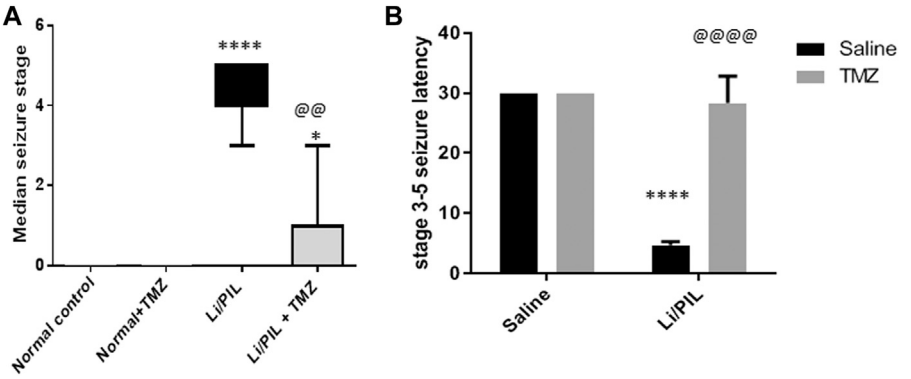

FIGURE 1 | Effect of TMZ on Li/PIL-induced seizures. **(A)** Racine score, data are expressed as box plots of the median of 15 animals. Statistical analysis was done using the Kruskal–Wallis test followed by Dunn's test. **(B)** Seizure latency, data are expressed as mean of 15 animals ± SD. Two-way ANOVA followed by the Tukey–Kramer post-hoc test was used for statistical analyses. *Significantly different from the normal control group (Saline) at $p < 0.05$; ****Significantly different from the normal control group (Saline) at $p < 0.0001$; $^{@@}$Significantly different from the Li/PIL control group at $p < 0.01$; $^{@@@@}$Significantly different from the Li/PIL control group at $p < 0.0001$.

were given a maximum latency of 30 min (Al-Shorbagy et al., 2013; El-Sayed et al., 2021). No mortality was recorded during the observation period.

Four hours after PIL injection, rats were euthanized by decapitation under light anesthesia, and their brains were carefully excised. Brains of three rats from each group were preserved in 10% formalin to be used for histological examinations and immunohistochemical staining. The hippocampi of the remaining rats (n = 12/group) were isolated and divided into two subsets. The hippocampi in the first subset (n = 6/group) were homogenized in cold phosphate buffer saline (PBS; pH = 7.4). In the second subset (n = 6/group), the hippocampi were frozen at −80°C to be used in Western blot and quantitative real-time PCR (qRT-PCR) analyses.

Isolation of Mitochondria-Rich Fraction

The homogenized hippocampal tissues were centrifuged with 0.25 M sucrose at 2,000 × g for 10 min at 4°C. Pellets were discarded, and 0.75 M sucrose in (4-(2-hydroxyethyl)-1-piperazineethanesulfonic acid) HEPES buffer was added to the supernatant and centrifuged at 10,000 × g for 30 min. HEPES buffer was added to the mitochondria pellets after discarding the supernatant and recentrifuged for 10 min at 10,000 × g, then the supernatant was discarded and PBS was added to the final mitochondria-rich fraction pellets (Ahmed and El-Maraghy, 2013; Ahmed et al., 2014). This was stored at −80°C to be used for determination of UCP2 and as oxidative stress biomarkers.

Biochemical Measurements

Mitochondrial Oxidative Stress Biomarkers

The oxidative stress status was estimated in the mitochondria-rich fraction by measuring malondialdehyde (MDA), an end product of lipid peroxidation, using the specific colorimetric kit (Biodiagnostics, Egypt) and expressed as nmol/mg protein. Reduced glutathione (GSH) was measured according to the method of Ellman (1959) and expressed as nmol/mg protein. In addition, the total antioxidant capacity (TAC) was determined colorimetrically, as it considers the cumulative effect of all the antioxidants present in the hippocampal mitochondrial fraction (Biodiagnostics, Egypt) and is expressed as mmol/mg protein.

Adenosine Triphosphate Content

The ATP content was estimated in the total hippocampal homogenate using the BioVision's ATP colorimetric assay kit (BioVision, Milpitas, United States). The assay utilizes the phosphorylation of glycerol to generate a product that is easily quantified colorimetrically at 570 nm and expressed as pg/mg protein.

Enzyme Linked Immunosorbent Assay

The total tissue homogenate was used to determine glutamate and cytochrome c (Cyt c) levels using ELISA assay kits (MyBioSource, San Diego, United States, and Elabscience, Texas, United States, respectively). Their results were expressed as μg/mg protein and pg/mg protein, respectively. In addition, UCP2 was measured in the mitochondrial rich fraction by a specific ELISA kit (Cusabio, Texas, United States) and expressed as pg/mg protein.

Caspase-3 Activity

Caspase-3 activity was estimated in the total hippocampal homogenate using the caspase-3 colorimetric assay kit (Elabscience, Texas, United States). The assay depends on the dissociation of yellow group p-nitroaniline (pNA) from caspase-3 sequence-specific peptides. pNA has an absorption peak which is easily measured colorimetrically at 405 nm and used to express caspase-3 activity as nmol pNA/h/mg protein.

Western Blotting Analysis

Following total hippocampal protein quantification by using the Bradford kit (Bio-Rad Protein Assay Kit, CA, United States), 20 μg protein of each sample was separated by SDS/polyacrylamide gel electrophoresis, then transferred onto polyvinylidene difluoride membranes (Thermo Fischer

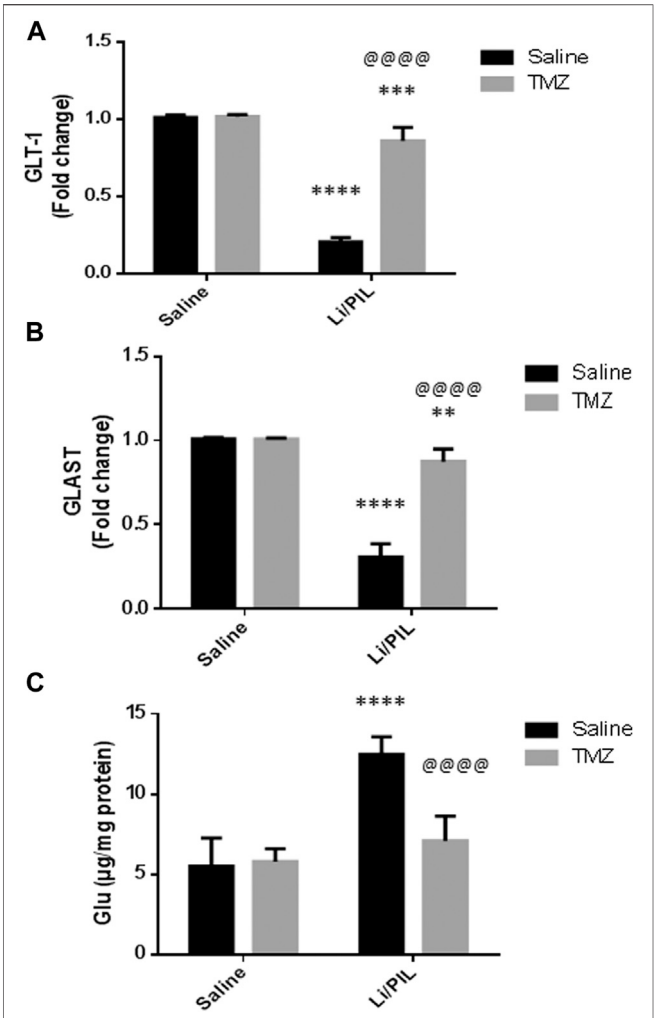

FIGURE 2 | Effect of TMZ on glial glutamate transporters and hippocampal glutamate level in rats with Li/PIL-induced seizures. **(A)** hippocampal mRNA expression of GLT-1 as indicated by qRT-PCR analysis, **(B)** hippocampal mRNA expression of GLAST as indicated by qRT-PCR analysis, **(C)** hippocampal glutamate level. Values are expressed as mean of six animals ± SD. Two-way ANOVA followed by the Tukey–Kramer post-hoc test was used for statistical analyses of data. **Significantly different from the normal control group (Saline) at $p < 0.01$; ***Significantly different from the normal control group (Saline) at $p < 0.001$; ****Significantly different from the normal control group (Saline) at $p < 0.0001$; $^{@@@@}$Significantly different from the Li/PIL control group at $p < 0.0001$.

Scientific, MA, United States). A blocking solution comprising 20 mM Tris-Cl, pH 7.5, 150 mM NaCl, 0.1% Tween 20, and 3% bovine serum albumin (BSA) was then added to the membranes at room temperature for 2 h to avoid nonspecific binding of the antibodies before incubating them overnight at 4°C with one of the following primary antibodies: p-extracellular signal-regulated kinases (p-44/42 ERK1/2) (Thr202/Tyr204), p-AMP-activated protein kinase (*p*-AMPK) (Thy 172), or Beta actin (β-actin) primary antibodies (Thermo Fisher Scientific, MA, United States). Next, the membranes were probed with horseradish peroxidase (HRP)-conjugated secondary antibodies (Thermo Fisher Scientific, MA, United States). Finally, the bands were established with the Chemiluminescence Reagent Kit (Amersham Biosciences, IL, United States), and their intensity was analyzed by Chemi Doc™ Imaging System with Image Lab™ software version 5.1 (Bio-Rad Laboratories Inc., Hercules, CA, United States). All values were normalized to that of β-actin and presented as fold-change.

Quantitative Real-Time PCR Analysis of Glial Glutamate Transporters

An extraction kit (Qiagen, Germantown, MD, United States) was used to extract total RNA from the total hippocampal tissue, which was then measured spectrophotometrically at 260 nm. Equal amounts of the extracted RNA were then reverse transcribed into cDNA using a high-capacity cDNA reverse transcription kit (Thermo Fischer Scientific, MA, United States). To assess the gene expression of glial glutamate transporters, GLAST and GLT-1, qRT-PCR was performed using ABI PRISM 7500 Fast Sequence Detection System (Applied Biosystems, CA, United States). The sequences of the PCR primer pairs used were the following: For GLAST, F:5'- CCA GTGCTGGAACTTTGCCT -3′, R: 5′- TAAAGGG CTGTACCATCCAT -3′, for GLT-1 F:5'- ACAAAAAGCAACGG AGAAGAGCC -3′, R: 5′- TACGGT CGGAGGGCAAATCC -3′, and β-actin (F: 5-TATCCTGGC CTCACTGTCCA-3′, R:5′-A ACGCAGCTCAGTAACAGTC-3′). In brief, 1 µg of the total RNA was mixed with 50 µM oligo (dT) 20, 50 ng/µL random primers, and 10 mM dNTP mix in a total volume of 10 µL in an optical 96-well plate using universal cycling conditions (5 min at 95°C followed by 45 cycles of 5 s at 95°C and 10 s at 60°C). The relative expression of the target genes was obtained using the 2−ΔΔCT formula (Pfaffl, 2001). All values were normalized to that of β-actin and presented as fold-change (Livak and Schmittgen, 2001).

Histopathological Analysis

Brain samples fixed in 10% neutral buffered formalin were trimmed and processed in serial grades of ethanol, cleared in xylene, infiltrated with synthetic wax, and embedded out into Paraplast tissue-embedding media. 3- to 5-µ-thick sagittal sections were cut by a rotatory microtome. The sections were stained with Harris Hematoxylin and Eosin (H&E) as a general tissue examination staining method. Hippocampal neurons were outlined, then the pathological changes in the different hippocampal regions were examined at high power (×400 magnification) in each group. The Lesion scoring system for pathological changes in different hippocampal regions was performed (Al-Sayed et al., 2020). Each animal was given a Lesion score between 0 and 3, for each of the three parameters, viz., neuronal damage, perineuronal edema, and glial cells infiltrates, where, 0 indicates no change, 1 indicates mild change (less than 15% of the examined samples), 2 indicates moderate change (16–35% of examined samples), and 3 indicates severe change (more than 35% of examined samples). Total histology lesion scores, the maximum being 9, were obtained by summing the scores of the three parameters for each animal. In addition, toluidine blue stain was used for the demonstration of intact neurons count with intact subcellular and nuclear details in the different hippocampal zones.

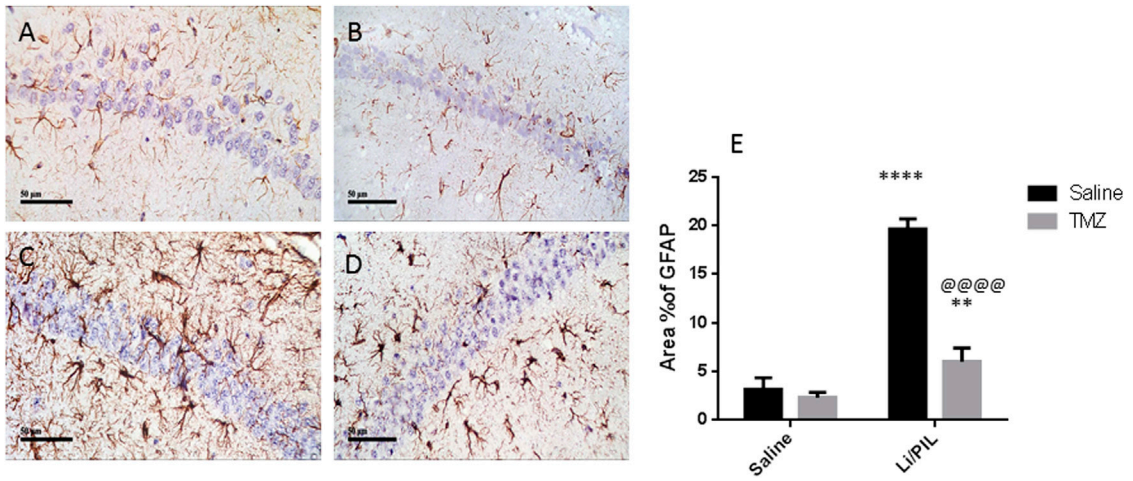

FIGURE 3 | Effect of TMZ on GFAP expression in the hippocampi of rats with Li/PIL-induced seizures as indicated by immunohistochemistry (×400 original magnification). Normal control rats **(A)**, Normal + TMZ rats **(B)**, Li/PIL control rats **(C)**, and TMZ + Li/PIL rats **(D)**. Area % of GFAP **(E)**. Values are expressed as mean of three animals ± SD. Two-way ANOVA followed by the Tukey–Kramer post-hoc test was used for statistical analyses of data. **Significantly different from the normal control group (Saline) at $p < 0.01$; ****Significantly different from the normal control group (Saline) at $p < 0.0001$; $^{@@@@}$Significantly different from the Li/PIL control group at $p < 0.0001$.

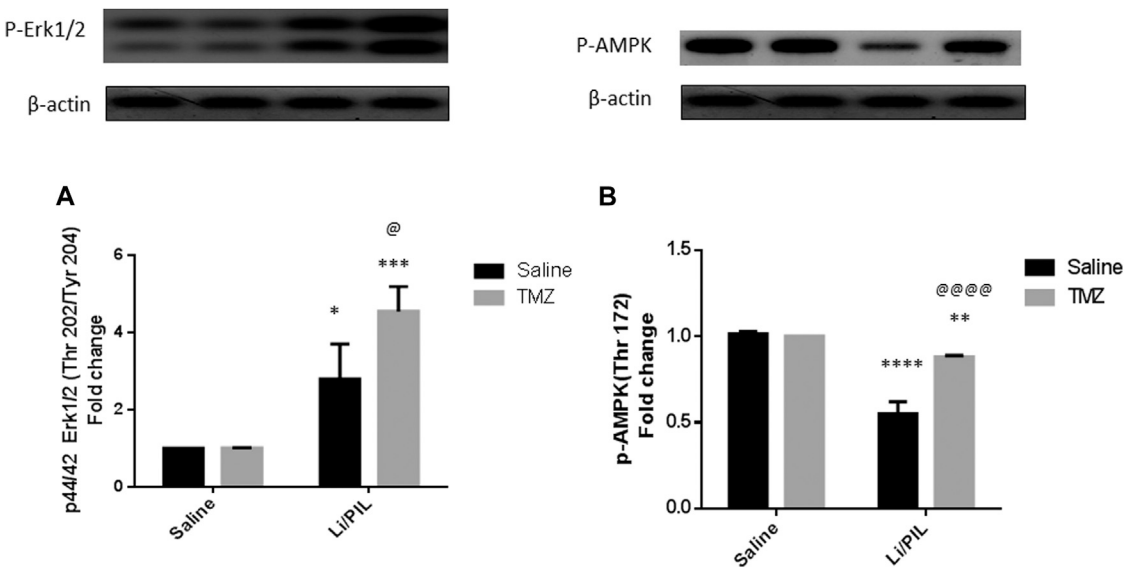

FIGURE 4 | Effect of TMZ on the protein expression of p-44/42 Erk1/2 (Thr202/Tyr204) and *p*-AMPK (Thy172) in the hippocampi of rats with Li/PIL-induced seizures. **(A)** The expression of p-44/42 Erk1/2 (Thr202/Tyr204) as indicated by Western blot analysis; **(B)** the expression of *p*-AMPK (Thy172) as indicated by Western blot analysis. Values are expressed as mean of three animals ± SD. Two-way ANOVA followed by the Tukey–Kramer post-hoc test was used for statistical analyses of data. *Significantly different from the normal control group (Saline) at $p < 0.05$; **Significantly different from the normal control group (Saline) at $p < 0.01$; ***Significantly different from the normal control group (Saline) at $p < 0.001$; ****Significantly different from the normal control group (Saline) at $p < 0.0001$; $^{@}$Significantly different from the Li/PIL control group at $p < 0.05$; $^{@@@@}$Significantly different from the Li/PIL control group at $p < 0.0001$.

Immunohistochemical Assay of Glial Fibrillary Acidic Protein

Deparaffinized 5-μ-thick tissue sections were treated with 3% hydrogen peroxide for 20 min, washed by PBS, then incubated with anti–glial fibrillary acidic protein (GFAP) monoclonal antibody from Thermo Fischer Scientific, MA, United States (1:100) overnight. After that, tissue sections were washed by PBS and incubated with a secondary antibody HRP EnVision kit (DAKO) for 20 min and then with diaminobenzidine for 10 min. Finally, they were counter stained with hematoxylin, dehydrated, and cleared in xylene for microscopic analysis.

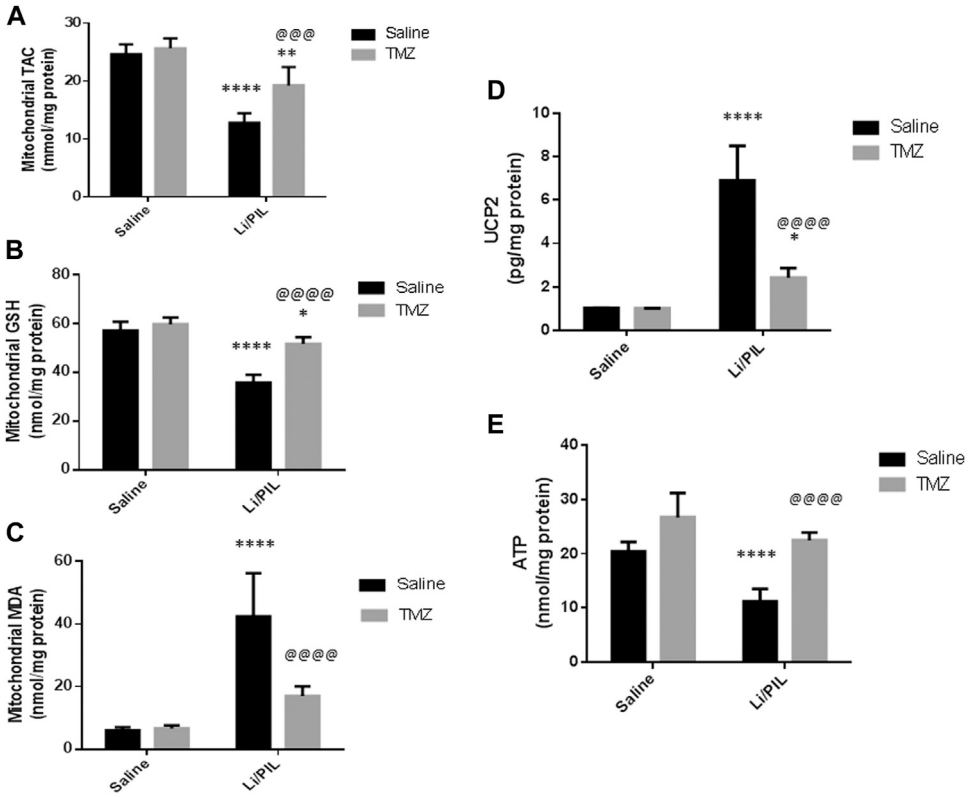

FIGURE 5 | Effect of TMZ on mitochondrial oxidative stress, mitochondrial uncoupling protein 2 (UCP2), and ATP production in the hippocampi of rats with Li/PIL-induced seizures. **(A)** TAC, **(B)** reduced GSH contents, **(C)** MDA levels, **(D)** UCP2, **(E)** ATP. Values are expressed as mean of six animals ± SD. Two-way ANOVA followed by the Tukey–Kramer post-hoc test was used for statistical analyses of data. *Significantly different from the normal control group (Saline) at $p < 0.05$; **Significantly different from the normal control group (Saline) at $p < 0.01$; ****Significantly different from the normal control group at $p < 0.0001$; $^{@@@}$Significantly different from the Li/PIL control group at $p < 0.001$; $^{@@@@}$Significantly different from the Li/PIL control group at $p < 0.0001$.

Microscopic Analysis

Six random nonoverlapping fields from different hippocampal regions per tissue sample were analyzed for determination of average area % of expression of GFAP in immunostained sections, as well as mean intact neurons count in Cornu Ammonis regions (CA1, CA3) and Dentate Gyrus (DG) hilar cells. All micrographs and data were obtained by using a full HD microscope camera operated by the Leica application module for tissue sections analysis (Leica Microsystems GmbH, Wetzlar, Germany)".

Statistical Analyses

All data obtained, except for total histology scores, Racine scores, and seizure incidence, were expressed as mean ± standard deviation (SD). Results were analyzed using the two-way analysis of variance test (ANOVA) followed by the Tukey–Kramer multiple comparison's test as a post-hoc test. Total histology scores and Racine scores were presented as median and analyzed using the Kruskal–Wallis test followed by Dunn's test as a post-hoc test. Incidence of Stage 3–5 seizures was compared using Fisher's exact probability test for all statistical tests, the level of significance was set at $p < 0.05$. GraphPad Prism® software package, version 5 (GraphPad Software, Inc., United States), was used to carry out all statistical tests.

RESULTS

Racine Score and Seizure Latency

As shown in **Figures 1A,B**, Stage 3–5 seizures were reached in all rats subjected to Li/PIL, within nearly 5 min after seizure induction. However, TMZ succeeded in delaying seizure latency to about 28.3 min ($p < 0.0001$) and noticeably reduced seizure incidence ($p < 0.0001$) and severity ($p < 0.01$) by 86.6 and 78.6%, respectively.

Effect of Trimetazidine on Hippocampal mRNA Expression of GLT-1 and GLAST

Hippocampal mRNA expression of GLT-1 and GLAST was prominently reduced reaching 20 and 30%, respectively, as compared to the normal control ($p < 0.0001$). Pretreatment with TZM, however, markedly increased their mRNA

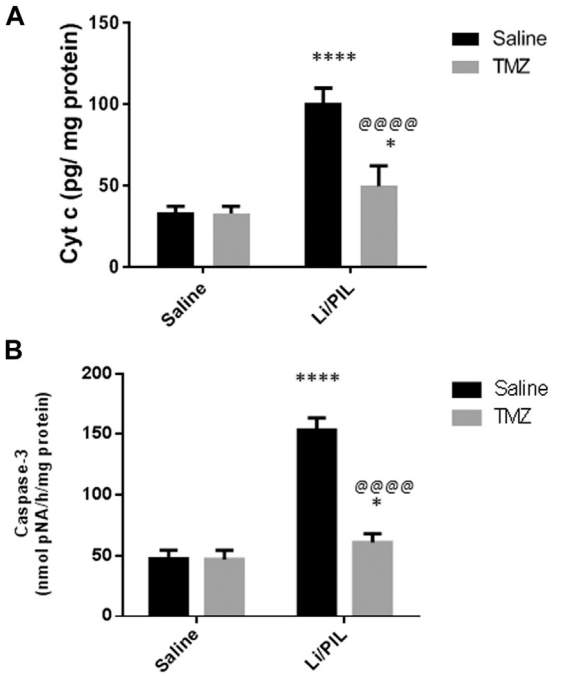

FIGURE 6 | Effect of TMZ on the Cyt c content and caspase-3 activity in rats with Li/PIL-induced seizures. **(A)** Cyt c content, **(B)** caspase-3 activity. Values are expressed as mean of six animals ± SD. Two-way ANOVA followed by the Tukey–Kramer post-hoc test was used for statistical analyses of data. *Significantly different from the normal control group (Saline) at $p < 0.05$; ****Significantly different from the normal control group (Saline) at $p < 0.0001$; @@@@Significantly different from the Li/PIL control group at $p < 0.0001$.

expression to reach 4-fold and 2.8-fold to that in the Li/PIL control group, respectively ($p < 0.0001$) (**Figures 2A,B**).

Effect of Trimetazidine on Hippocampal Glutamate Level

As shown in **Figure 2C**, Li/PIL induced an increase in the hippocampal glutamate level, reaching 2.2-fold to that in the normal control group ($p < 0.0001$ On the contrary, rats pretreated with TMZ exhibited a normal level of glutamate in their hippocampi, $p = 0.21$, recording a decrease of 43.2%, as compared to the Li/PIL control group.

Effect of Trimetazidine on Hippocampal GFAP Expression

Li/PIL induced astrocytes activation as demonstrated by the obvious increase in the immunostaining density of hippocampal GFAP (19.67 ± 1.03 vs 3.2 ± 1.1, respectively), an effect that was largely prevented by TMZ recording a decrease of 69.5%, as compared to the Li/PIL control group (**Figure 3**).

Effect of Trimetazidine on Hippocampal p-44/42 ERK1/2 (Thr202/Tyr204) and *p*-AMPK (Thy172)

Rats subjected to Li/PIL exhibited a marked rise in hippocampal p-44/42 ERK1/2 (2.8 ± 0.9 vs 1 ± 0.0) along with a profound decline in *p*-AMPK (0.55 ± 0.07 vs 1.015 ± 0.01) as compared to that in the normal control ($p < 0.0001$). TMZ induced a further increase in hippocampal *p*-ERK1/2 by 62.5% and prevented the drop in *p*-AMPK reaching 1.6-fold to that in the Li/PIL control group ($p < 0.05$ and $p < 0.0001$, respectively) (**Figures 4A,B**).

Mitochondrial Oxidative Stress in Hippocampus

Induction of seizures was accompanied by a profound disruption in mitochondrial oxidative homeostasis in the hippocampi as manifested by the depletion of the mitochondrial TAC (12.8 ± 1.6 vs 24.7 ± 1.6) and GSH (35.9 ± 1.2 vs 57.1 ± 3.6) content along with the marked increase in mitochondrial MDA (42.5 ± 13.7 vs 6.1 ± 0.97 as compared to that in the normal control group ($p < 0.0001$). Pretreatment with TMZ effectively enhanced the mitochondrial TAC as well as GSH content to reach 1.5-fold and 1.44-fold, respectively, to that in the Li/PIL group ($p < 0.001$ and $p < 0.0001$). Consequently, TMZ reduced mitochondrial MDA production by 60% as compared to Li/PIL rats ($p < 0.0001$), showing a similar level to that in the normal control group $p = 0.065$ (**Figures 5A–C**).

Effect of Trimetazidine on Mitochondrial Uncoupling Protein 2 and ATP Production

Li/PIL increased UCP2 in mitochondria-rich fraction (6.9 ± 1.6 vs 1.02 ± 0.02) with a pronounced reduction in the hippocampal ATP (11.2 ± 2.3 vs 20.5 ± 1.7) content ($p < 0.0001$). However, TMZ was effective in impeding UCP2 expression in mitochondria-rich fraction by 65% as compared with the Li/PIL control group ($p < 0.0001$) and restoring hippocampal ATP, reaching a comparable content to the normal control group, $p = 0.59$, to reach 1.9-fold to that in the Li/PIL control group (**Figures 5D,E**).

Effect of Trimetazidine on Hippocampal Cyt c and Caspase-3 Activity

Injection of Li/PIL was associated with a massive disruption in the mitochondrial inner membrane as revealed by the marked elevation in the hippocampal Cyt c content (100.9 ± 8.9 vs 33.4 ± 3.8) and, sequentially, in caspase-3 activity (153.6 ± 9.8 vs 47.5 ± 7.1), as a marker of apoptotic cell death as compared to the normal control group ($p < 0.0001$). Pretreatment with TMZ largely prevented these mitochondrial derangements recording a decrease by 50.8 and 60.4%, respectively, as compared to that in the Li/PIL control group (**Figures 6A,B**).

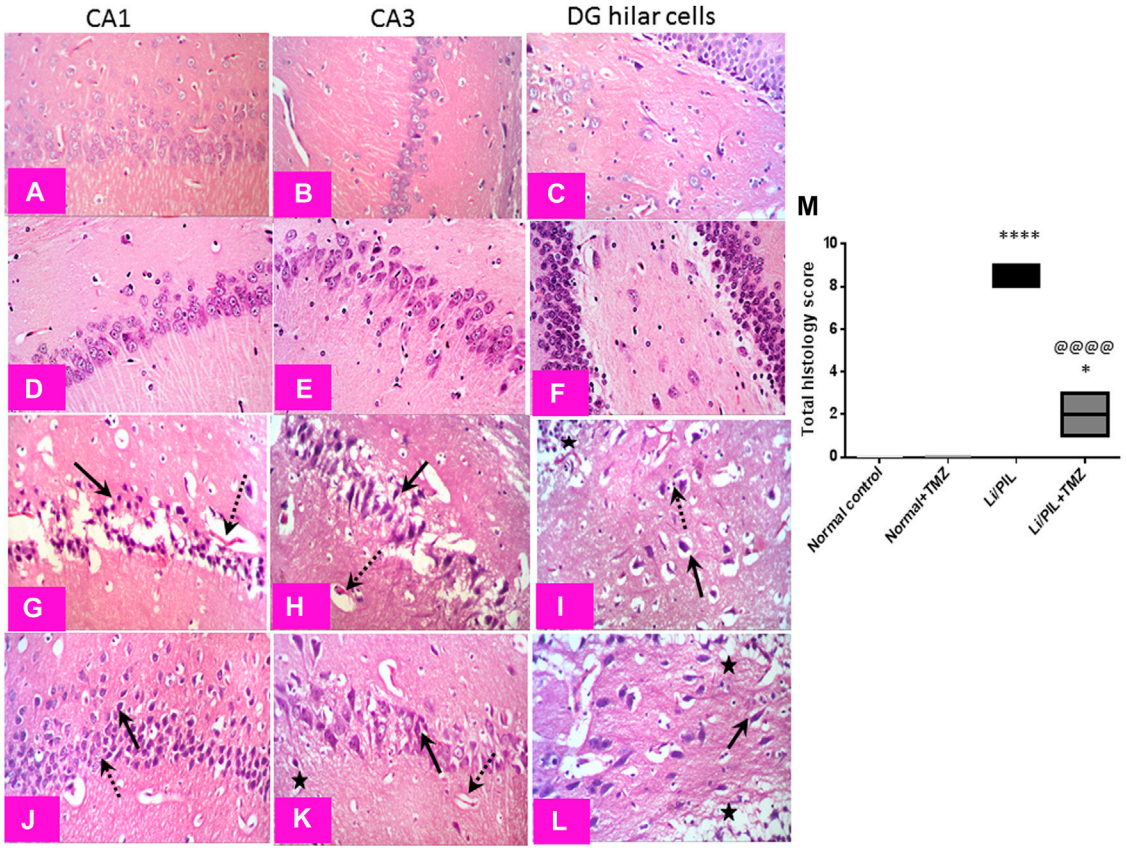

FIGURE 7 | Effect of TMZ on histopathological alterations in the hippocampi of rats with Li/PIL-induced seizures (×400 original magnification). Normal control rats and normal rats treated with TMZ showed normal histology of CA1, CA3, and hilar regions **(A–C)** and **(D–F)**, respectively. Li/PIL control showed a significant loss of pyramidal cells layer (dotted arrows), many apoptotic figures, edema (star), and sloughing of capillary endothelium in CA1 and CA3 regions (arrows); in addition to many degenerated neurons (arrow), pyknotic nuclei, and glial cells infiltration (dotted arrow) **(G,H)**, and edematous fluid effusion and congested blood capillaries in the hilar region **(I)**. TMZ + Li/PIL rats demonstrated partial protection with less edema fluid and congested capillaries (star), more organizing effect on pyramidal cells in CA1 and CA3 regions with mixed arrangement of fewer damaged (arrow) and intact (dotted arrow) neurons **(J,K)**, and lower number of degenerated and apoptotic neurons in the hilar region (arrow) **(L)**. **(M)** Total histology lesion score; data are expressed as box plots of the median of three animals. Statistical analysis was done using the Kruskal–Wallis test followed by Dunn's test. *Significantly different from the normal control group (Saline) at $p < 0.05$; ****Significantly different from the normal control group (Saline) at $p < 0.0001$; $^{@@@@}$Significantly different from the Li/PIL control group at $p < 0.0001$.

Effect of Trimetazidine on Histopathological Alterations and Hippocampal Neuronal Integrity

Microscopical examination of the hippocampi from normal control rats showed the normal architecture of the CA regions (**Figures 7A,B**) and DG region (**Figure 7C**). The mean intact pyramidal neurons count was almost 61 cells/field, 40 cells/field, and 11 cells/field in CA1, CA3, and DG hilar cells, respectively, in toluidine blue-stained tissue sections (**Figures 8,E,I**). Rats subjected to Li/PIL exhibited a significant loss of pyramidal cells layer in CA1 and CA3 regions with many apoptotic figures associated with edema and sloughing of capillary endothelium (**Figures 7G,H**). Examination of the hilar region of DG revealed many degenerated neurons with pyknotic nuclei, glial cells infiltration with edematous fluid effusion, and congested blood capillaries (**Figure 7I**). The mean intact neurons count was almost 7 cells/field, 9 cells/field, and 6 cells/field in CA1, CA3, and DG hilar cells, respectively (**Figure 8C,G,K**). Pretreatment with TMZ demonstrated partial protection with more organizing effect on the pyramidal cells region of CA1 and CA3. Edema fluid and congested capillaries were less evident in all layers than in the Li/PIL group (**Figure 7J,K**). The hilar region examination showed a lower number of degenerated and apoptotic neurons (**Figure 7L**). The mean intact neurons count was almost 36 cells/field, 35 cells/field, and 11 cells/field in CA1, CA3, and DG hilar cells, respectively (**Figure 8D,H,L**).

DISCUSSION

The current investigation emphasizes the efficacy of TMZ in reducing the incidence and severity of seizures in rats subjected to Li/PIL. This anti-seizure potential was associated with a marked reduction in the hippocampal glutamate content along with a

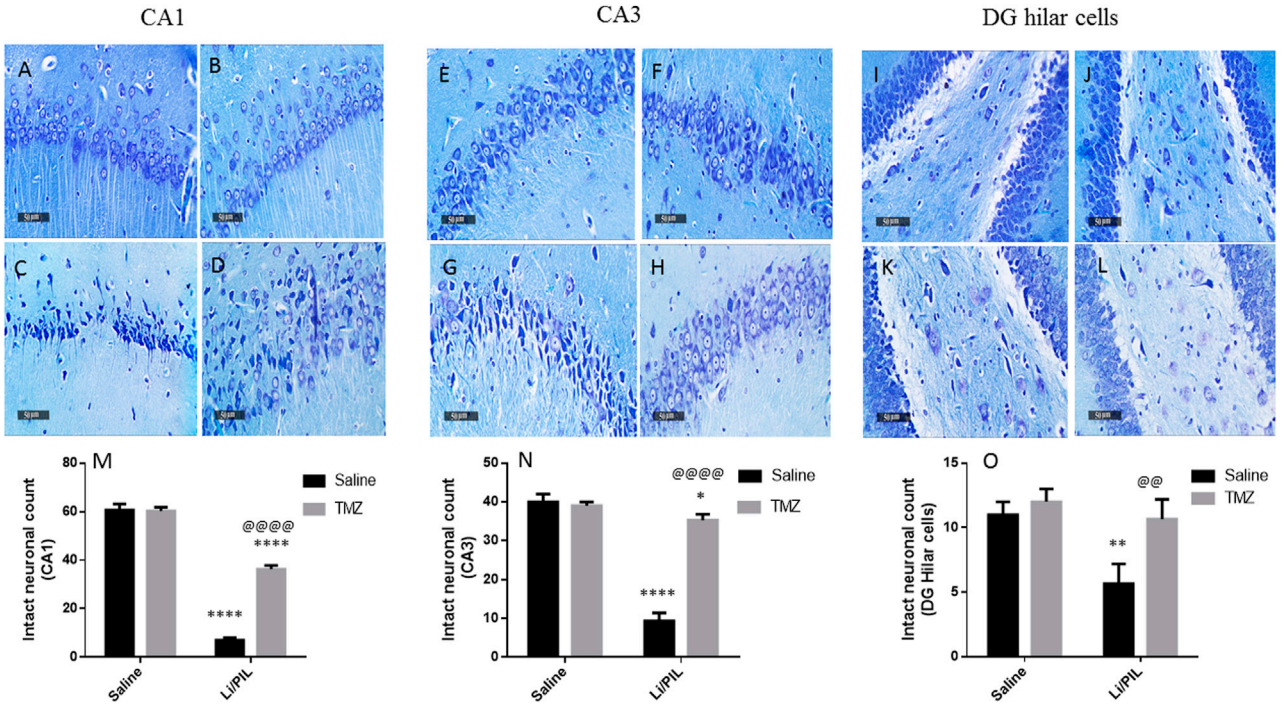

FIGURE 8 | Effect of TMZ on hippocampal neuronal loss of rats with Li/PIL-induced seizures. Photomicrographs demonstrating toluidine blue–stained hippocampal tissue sections of CA1 and CA3 sub regions and DC hilar cells in normal control rats **(A,E,I)**, TMZ control rats **(B,F,J)**, Li/PIL control rats **(C,G,K)**, and TMZ + Li/PIL rats **(D,H,L)**. Intact neurons count in CA1 **(M)**, CA3 **(N)**, and DG hilar cells **(O)**. Values are expressed as mean of three animals ± SD. Two-way ANOVA followed by the Tukey–Kramer post-hoc test was used for statistical analyses of data. *Significantly different from the normal control group (Saline) at $p < 0.05$; **Significantly different from the normal control group (Saline) at $p < 0.01$; ****Significantly different from the normal control group (Saline) at $p < 0.0001$; $^{@@}$Significantly different from the Li/PIL control group at $p < 0.01$; $^{@@@@}$Significantly different from the Li/PIL control group at $p < 0.0001$.

noticeable upregulation of the gene expression of astroglial transporters: GLT-1 and GLAST. These effects were correlated with the ability to preserve the integrity of neurons in the different hippocampal regions.

Disrupting the complex neuroglial circuitry has been shown to robustly contribute to neurological disorders including epilepsy (Diaz Verdugo et al., 2019). Any change in the efficiency of glutamate clearance, especially by astrocytic phenotypes, largely affects synaptic function and accordingly seizures susceptibility (Wallraff et al., 2006). The depletion of astrocytic transporters in various neurodegenerative diseases supports the strong association between the accumulation of neurotoxic levels of glutamate and reactive astrogliosis (Rothstein et al., 2005). Striking morphological and function changes are detected in reactive astrocytes altering neurotransmitter homeostasis to provoke neuronal hyperexcitability (Seifert and Steinhäuser, 2013). Preictal astrocyte activation that shortly begins after a brain insult is likely to be an adaptive response to remove damaged tissues and restore normal function (Sanz and Garcia-Gimeno, 2020). Consistently, initial astrocytes activity is directed to hamper neural activity outbreaks (Diaz Verdugo et al., 2019). During this state, the highly synchronous glial cells activity ensures their homeostatic function. Glial cells networks can efficiently reallocate (Danbolt, 2001) and absorb excessive cations and glutamate by various astrocytes transporters (Pines et al., 1992). Nevertheless, excessive astrogliosis exhausts this homeostatic function and exacerbates inflammatory response, triggering hyperexcitability of neurons and generalized seizures. The mounting efflux of K^+ around astrocytes accompanied with glutamate uptake reverses the working way of transporters and abruptly alters the harmonized glia–neuron interaction (Danbolt, 2001).

In the current study, GFAP was used as a tool to assess astrogliosis during seizures. Rats injected with Li/PIL showed a massive expression of GFAP in the CA1, CA3, and hilar regions of the hippocampi, which were shown to be the same sites of injury by histopathological examination. Our findings harmonize with previous studies that revealed a rapid amplified GFAP expression in various animal models of epilepsy, including PTZ (Torre et al., 1993; Sedky et al., 2017), electrical kindling (Stringer, 1996; Miyazaki et al., 2003), and kainic acid (Bendotti et al., 2000; Choi et al., 2003; Glushakova et al., 2012; Lee et al., 2012). Similarly, Alese and Mabandla (2019) recorded a marked increase in GFAP hippocampal expression 30 min following PIL administration in rats with or without a history of prolonged febrile seizure. Genetically induced extensive astrogliosis in mice disrupted glutamate uptake and triggered spontaneous seizures (Robel et al., 2015). In the same context, a previous study synchronizes with our finding, where the anticonvulsant activity of TMZ in PTZ-treated mice was associated with a

marked decrease in hippocampal GFAP expression (Sedky et al., 2017).

In the current study, enhanced GFAP expression was also accompanied with an increase in the hippocampal glutamate level as well as a marked reduction in mRNA expression of both GLT-1 and GLAST. In agreement with these results, astrocytes activation was coupled with decreased GLT-1 and extracellular glutamate flooding in models of peripheral nerve injury (Cavaliere et al., 2007; Cirillo et al., 2011). Furthermore, the expression of GLAST and GLT-1 has been diminished in the cortices as well as in the hippocampi of rats with genetic absence seizures (Dutuit et al., 2002) and in a mouse model of focal epilepsy (Ingram et al., 2001).

Interestingly, GFAP and *p*-ERK1/2 were found to be co-expressed in the hippocampi of mice subjected to PIL-induced status epilepticus after 6 h. However, GFAP, but not *p*-ERK1/2, was still expressed after 3 days (Li et al., 2009). Similarly, Choi et al. (2003) reported a rapid and transient *p*-ERK1/2 increase in hippocampal neurons and astrocytes following kainic acid–induced seizures. These results go in line with the present study and suggest the possible contribution of *p*-ERK1/2 in the protective effect of astrogliosis in the early stages of epilepsy. In the same context, *p*-ERK1/2 was previously claimed to mediate GLT1 expression in astrocytes (Frizzo et al., 2007); however, its elevated level attained after Li/PIL injection in the present study was probably not enough to increase the gene expression of glutamate transporters. In addition, during astrogliosis, the activated protease, calpain-I, was previously accused of astrocyte transporters degradation (Cavaliere et al., 2007). Coherent with these results, Berkeley et al. (2002) demonstrated that PIL caused initial ERK activation, while its inhibition had not prevented PIL-induced seizures, yet increased its severity. The further increase in *p*-ERK1/2 observed after TMZ may be a partial mechanism through which it could increase mRNA expression of astroglial transporters and, consequently, glutamate uptake.

Simultaneously, mitochondrial dysfunction associated with the obvious alterations in mitochondrial oxidative status exerts an important role in modulating glia–neuron interplay (Jain et al., 1991; Wallace et al., 1992; Lin et al., 2020). Li/PIL injection in the current study provoked a state of mitochondrial oxidative burst as manifested by diminished TAC and GSH along with enhanced lipid peroxidation. In the same context, Waldbaum et al. (2010) reported a persistent perturbation of mitochondrial redox status during acute and chronic phases of Li/PIL-induced epilepsy. Under the condition of ATP deficiency coupled with mitochondrial oxidative damage as demonstrated herein, the expression and function of astroglial transporters are disrupted (Frizzo et al., 2007). Though extracellular ATP release from damaged neurons succeeded in inciting GLT1 expression *via* ERK1/2 activation (Neary et al., 1999, Neary et al., 2003), the reduced ionic gradient following energy failure may refute the driving force essential for glutamate uptake (Kauppinen and Swanson, 2007). Accordingly, synaptic glutamate increase was ascribed to glutamate uptake impairment (Colangelo et al., 2014) paralleled with glutamate efflux by the reversed action of transporters (Seki et al., 1999; Phillis et al., 2000). Additionally, the enhancement of hippocampal large-conductance Ca^{2+}-activated K^+ channels in response to redox status change may pose a plausible mechanism toward increasing hippocampal neuronal excitability after exposure to extracellular glutamate (Waldbaum and Patel, 2010).

TMZ was effective in restoring mitochondrial oxidative homeostasis as evident by the enhanced TAC and restored GSH. Ultimately, it cured lipid peroxidation, an effect that reflected on mitochondrial efficacy in ATP production and, consequentially, function and expression of astroglial glutamate transporters. The activity of TMZ on glial uptake of glutamate was previously documented in an *in vitro* study using rat retinal Müller cell line. It revered glial transporter inhibition and protected the retina from ischemia-induced excitotoxicity (Payet et al., 2004). In agreement with our results, Jain et al. (2011) attributed the anticonvulsant activity of TMZ following PTZ-induced kindling in mice mainly to its robust antioxidant activity. The well-recognized antioxidant properties of TMZ are thought to be mediated indirectly by boosting the anti-oxidant enzymes (Tikhaze et al., 2000). This effect may be linked to the ability of TMZ to increase *p*-AMPK, which largely participates in restoring neuronal energy balance (Ronnett et al., 2009). AMPK activators were reported to induce nuclear retention of antioxidant transcription factors as forkhead box O1 (Yun et al., 2014) and nuclear factor erythroid 2–related factor 2 (Joo et al., 2016). In the same context, TMZ increased the ATP/ADP ratio in the hippocampus of diabetic epileptic rats (Mohamed et al., 2020). In addition, it restored ATP synthesis after cerebral mitochondrial respiration inhibition by cyclosporin (Zini et al., 1996).

Intracellular Ca^{2+} accumulation following excitotoxic insults was reported not only to participate in further mitochondrial ROS production and ATP synthesis inhibition but also inevitability to the activation of membrane transition pores and Cyt c release, leading to apoptotic neuronal death (Sullivan et al., 2005), as demonstrated herein by the increase in caspase-3 activity. The increase in mitochondrial UCP2 observed herein and previously (Diano et al., 2003) is postulated to reduce ROS production and guard against neuronal death. Usually, enhanced UCP2 in response to various neuronal stress is one of the neuroprotective responses, by increasing the number of mitochondria and consequently ATP production. However, these beneficial effects were obviously established after 5 days in a Li/PIL animal model (Dutra et al., 2018). Furthermore, hippocampal neurons employ another survival response *via* boosting ERK expression (Berkeley et al., 2002) to act in a mutual intervention with ERK induced in astrocytes during initial astrogliosis. The implication of ERK1/2 in neuroprotection in response to excitotoxicity was previously attributed to its ability to upregulate the antiapoptotic Bcl2 (Ortuño-Sahagún et al., 2014). In addition, phosphorylation of Kv4.2, fast-inactivating A-type potassium channels present postsynaptically, by activated ERK1/2 enables their localization to areas of hyperactivity in the hippocampus. Consequently, they accelerate repolarization and limit firing of action potential to guard against lethal seizures and neuronal death (Berkeley et al., 2002).

In the present study, the success of TMZ in limiting seizure incidence was associated with a marked reduction in apoptotic neuronal death rate as manifested by the obvious decrease in hippocampal Cyt c and caspase-3 activity. The anti-seizure as well as the antiapoptotic effects of TMZ could be linked to the potentiating effect of ERK phosphorylation in both neurons and glial cells. In addition, the effect of TMZ on AMPK could participate in its antiapoptotic activity *via* endorsing high mitochondrial membrane potential to preserve Ca^{+2} homeostasis (Zhang et al., 2017). In agreement with these results, Liu et al. (2016) reported that TMZ could protect cardiomyocytes against ischemic injury *via* activation of both AMPK and ERK. Intriguingly, purified rat brain mitochondria have been shown to express binding sites for TMZ (Morin et al., 2000). Former *in vitro* studies advocated that TMZ could inhibit mitochondrial permeability transition pores' opening (Rothstein et al., 1992; Argaud et al., 2005) and thus hinder apoptotic neuronal loss following hyperexcitability.

In conclusion, TMZ showed a promising anti-seizure potential that was evident on seizure score as well as on various biochemical indicators. The beneficial actions of TMZ could be attributed to its ability to decrease mitochondrial oxidative damage as well as glutamate accumulation, parallel to a positive modulation of *p*-ERK1/2/p-AMPK signaling. Also, it succeeded in reducing ATP-dependent energy disruptions as well as astrocytes activation. This was all reflected as a reduction in neuronal apoptosis and preserved cellular integrity.

DATA AVAILABILITY STATEMENT

The original contributions presented in the study are included in the article/**Supplementary Material**, further inquiries can be directed to the corresponding author.

ETHICS STATEMENT

The animal study was reviewed and approved by the investigation fulfilled the Guide for the Care and Use of Laboratory Animals of the Ethical Committee for Animal Experimentation at Faculty of Pharmacy, Cairo University (PT2715).

AUTHOR CONTRIBUTIONS

DE and MA: Conceptualization. DE and WW: Data curation, Methodology, Software, Writing—Original draft preparation, Visualization, and Investigation. MA: Analysis, Supervision, Software, Validation. All authors: Writing, Reviewing, and Editing.

SUPPLEMENTARY MATERIAL

The Supplementary Material for this article can be found online at: https://www.frontiersin.org/articles/10.3389/fphar.2021.735165/full#supplementary-material

REFERENCES

Ahmed, L. A., and El-Maraghy, S. A. (2013). Nicorandil Ameliorates Mitochondrial Dysfunction in Doxorubicin-Induced Heart Failure in Rats: Possible Mechanism of Cardioprotection. *Biochem. Pharmacol.* 86 (9), 1301–1310. doi:10.1016/j.bcp.2013.07.005

Ahmed, L. A., Shehata, N. I., Abdelkader, N. F., and Khattab, M. M. (2014). Tempol, a Superoxide Dismutase Mimetic Agent, Ameliorates Cisplatin-Induced Nephrotoxicity Through Alleviation of Mitochondrial Dysfunction in Mice. *PLoS One.* 9 (10), e108889, 2014 . Erratum in: PLoS One. 2014;9(12): e115983. doi:10.1371/journal.pone.0108889

Al-Kuraishy, H. M., and Al-Gareeb, A. I. (2017). Central Beneficial Effects of Trimetazidine on Psychomotor Performance in normal Healthy Volunteers. *Adv. Biomed. Res.* 6, 69. doi:10.4103/2277-9175.190994

Al-Sayed, E., Michel, H. E., Khattab, M. A., El-Shazly, M., and Singab, A. N. (2020). Protective Role of Casuarinin from Melaleuca Leucadendra Against Ethanol-Induced Gastric Ulcer in Rats. *Planta Med.* 86 (1), 32–44. doi:10.1055/a-1031-7328

Al-Shorbagy, M. Y., El Sayeh, B. M., and Abdallah, D. M. (2013). Additional Antiepileptic Mechanisms of Levetiracetam in Lithium-Pilocarpine Treated Rats. *PLoS One.* 8 (10), e76735. doi:10.1371/journal.pone.0076735

Alese, O. O., and Mabandla, M. V. (2019). Upregulation of Hippocampal Synaptophysin, GFAP and mGluR3 in a Pilocarpine Rat Model of Epilepsy with History of Prolonged Febrile Seizure. *J. Chem. Neuroanat.* 100, 101659. doi:10.1016/j.jchemneu.2019.101659

Argaud, L., Gomez, L., Gateau-Roesch, O., Couture-Lepetit, E., Loufouat, J., Robert, D., et al. (2005). Trimetazidine Inhibits Mitochondrial Permeability Transition Pore Opening and Prevents Lethal Ischemia-Reperfusion Injury. *J. Mol. Cel. Cardiol.* 39 (6), 893–899. doi:10.1016/j.yjmcc.2005.09.012

Beal, M. F. (2005). Mitochondria Take Center Stage in Aging and Neurodegeneration. *Ann. Neurol.* 58 (4), 495–505. doi:10.1002/ana.20624

Bendotti, C., Guglielmetti, F., Tortarolo, M., Samanin, R., and Hirst, W. D. (2000). Differential Expression of S100beta and Glial Fibrillary Acidic Protein in the Hippocampus after Kainic Acid-Induced Lesions and Mossy Fiber Sprouting in Adult Rat. *Exp. Neurol.* 161 (1), 317–329. doi:10.1006/exnr.1999.7262

Berkeley, J. L., Decker, M. J., and Levey, A. I. (2002). The Role of Muscarinic Acetylcholine Receptor-Mediated Activation of Extracellular Signal-Regulated Kinase 1/2 in Pilocarpine-Induced Seizures. *J. Neurochem.* 82 (1), 192–201. doi:10.1046/j.1471-4159.2002.00977.x

Cavaliere, C., Cirillo, G., Rosaria Bianco, M., Rossi, F., De Novellis, V., Maione, S., et al. (2007). Gliosis Alters Expression and Uptake of Spinal Glial Amino Acid Transporters in a Mouse Neuropathic Pain Model. *Neuron Glia Biol.* 3 (2), 141–153. doi:10.1017/S1740925X07000695

Choi, J. S., Kim, S. Y., Park, H. J., Cha, J. H., Choi, Y. S., Kang, J. E., et al. (2003). Upregulation of Gp130 and Differential Activation of STAT and P42/44 MAPK in the Rat hippocampus Following Kainic Acid-Induced Seizures. *Brain Res. Mol. Brain Res.* 119 (1), 10–18. doi:10.1016/j.molbrainres.2003.08.010

Cirillo, G., Bianco, M. R., Colangelo, A. M., Cavaliere, C., Daniele, de. L., Zaccaro, L., et al. (2011). Reactive Astrocytosis-Induced Perturbation of Synaptic Homeostasis Is Restored by Nerve Growth Factor. *Neurobiol. Dis.* 41 (3), 630–639. doi:10.1016/j.nbd.2010.11.012

Colangelo, A. M., Alberghina, L., and Papa, M. (2014). Astrogliosis as a Therapeutic Target for Neurodegenerative Diseases. *Neurosci. Lett.* 565, 59–64. doi:10.1016/j.neulet.2014.01.014

Danbolt, N. C. (2001). Glutamate Uptake. *Prog. Neurobiol.* 65 (1), 1–105. doi:10.1016/S0301-0082(00)00067-8

Dhote, V., and Balaraman, R. (2008). Anti-Oxidant Activity Mediated Neuroprotective Potential of Trimetazidine on Focal Cerebral Ischaemia-Reperfusion Injury in Rats. *Clin. Exp. Pharmacol. Physiol.* 35 (5-6), 630–637. doi:10.1111/j.1440-1681.2008.04845.x

Diano, S., Matthews, R. T., Patrylo, P., Yang, L., Beal, M. F., Barnstable, C. J., et al. (2003). Uncoupling Protein 2 Prevents Neuronal Death Including that

Occurring During Seizures: a Mechanism for Preconditioning. *Endocrinology.* 144 (11), 5014–5021. doi:10.1210/en.2003-0667

Diaz Verdugo, C., Myren-Svelstad, S., Aydin, E., Van Hoeymissen, E., Deneubourg, C., Vanderhaeghe, S., et al. (2019). Glia-Neuron Interactions Underlie State Transitions to Generalized Seizures. *Nat. Commun.* 10 (1), 3830. doi:10.1038/s41467-019-11739-z

Dutra, M. R. H., Feliciano, R. D. S., Jacinto, K. R., Gouveia, T. L. F., Brigidio, E., Serra, A. J., et al. (2018). Protective Role of UCP2 in Oxidative Stress and Apoptosis During the Silent Phase of an Experimental Model of Epilepsy Induced by Pilocarpine. *Oxid. Med. Cel. Longev.* 2018, 6736721. doi:10.1155/2018/6736721

Dutuit, M., Touret, M., Szymocha, R., Nehlig, A., Belin, M. F., and Didier-Bazès, M. (2002). Decreased Expression of Glutamate Transporters in Genetic Absence Epilepsy Rats Before Seizure Occurrence. *J. Neurochem.* 80 (6), 1029–1038. doi:10.1046/j.0022-3042.2002.00768.x

El-Sayed, S. S., El-Yamany, M. F., Salem, H. A., and El-Sahar, A. E. (2021). New Insights Into the Effects of Vinpocetine Against Neurobehavioral Comorbidities in a Rat Model of Temporal Lobe Epilepsy via the Downregulation of the Hippocampal PI3K/mTOR Signalling Pathway. *J. Pharm. Pharmacol.* 73 (5), 626–640. doi:10.1093/jpp/rgab011

Ellman, G. L. (1959). Tissue Sulfhydryl Groups. *Arch. Biochem. Biophys.* 82 (1), 70–77. doi:10.1016/0003-9861(59)90090-6

Frizzo, M. E., Frizzo, J. K., Amadio, S., Rodrigues, J. M., Perry, M. L., Bernardi, G., et al. (2007). Extracellular Adenosine Triphosphate Induces Glutamate Transporter-1 Expression in Hippocampus. *Hippocampus.* 17 (4), 305–315. doi:10.1002/hipo.20269

Glushakova, O. Y., Jeromin, A., Martinez, J., Johnson, D., Denslow, N., Streeter, J., et al. (2012). Cerebrospinal Fluid Protein Biomarker Panel for Assessment of Neurotoxicity Induced by Kainic Acid in Rats. *Toxicol. Sci.* 130 (1), 158–167. doi:10.1093/toxsci/kfs224

Hassanzadeh, G., Hosseini, A., Pasbakhsh, P., Akbari, M., Ghaffarpour, M., Takzare, N., et al. (2015). Trimetazidine Prevents Oxidative Changes Induced in a Rat Model of Sporadic Type of Alzheimer's Disease. *Acta Med. Iran.* 53 (1), 17–24. PMID: 25597600

Ingram, E. M., Wiseman, J. W., Tessler, S., and Emson, P. C. (2001). Reduction of Glial Glutamate Transporters in the Parietal Cortex and Hippocampus of the EL Mouse. *J. Neurochem.* 79 (3), 564–575. doi:10.1046/j.1471-4159.2001.00612.x

Jain, A., Mårtensson, J., Stole, E., Auld, P. A., and Meister, A. (1991). Glutathione Deficiency Leads to Mitochondrial Damage in Brain. *Proc. Natl. Acad. Sci. U. S. A.* 88 (5), 1913–1917. doi:10.1073/pnas.88.5.1913

Jain, S., Bharal, N., Khurana, S., Mediratta, P. K., and Sharma, K. K. (2011). Anticonvulsant and Antioxidant Actions of Trimetazidine in Pentylenetetrazole-Induced Kindling Model in Mice. *Naunyn. Schmiedebergs. Arch. Pharmacol.* 383 (4), 385–392. doi:10.1007/s00210-011-0606-1

Jain, S., Bharal, N., Mediratta, P. K., and Sharma, K. K. (2010). Trimetazidine Exerts Protection Against Increasing Current Electroshock Seizure Test in Mice. *Seizure.* 19 (5), 300–302. doi:10.1016/j.seizure.2010.04.001

Joo, M. S., Kim, W. D., Lee, K. Y., Kim, J. H., Koo, J. H., and Kim, S. G. (2016). AMPK Facilitates Nuclear Accumulation of Nrf2 by Phosphorylating at Serine 550. *Mol. Cel. Biol.* 36 (14), 1931–1942. doi:10.1128/mcb.00118-16

Kauppinen, T. M., and Swanson, R. A. (2007). The Role of Poly(ADP-Ribose) Polymerase-1 in CNS Disease. *Neuroscience* 145 (4), 1267–1272. doi:10.1016/j.neuroscience.2006.09.034

Lee, D. J., Hsu, M. S., Seldin, M. M., Arellano, J. L., and Binder, D. K. (2012). Decreased Expression of the Glial Water Channel Aquaporin-4 in the Intrahippocampal Kainic Acid Model of Epileptogenesis. *Exp. Neurol.* 235 (1), 246–255. doi:10.1016/j.expneurol.2012.02.002

Li, Y. Q., Xue, T., Xu, J., Xu, Z. C., Liu, H., and Chen, Y. M. (2009). ERK1/2 Activation in Reactive Astrocytes of Mice With Pilocarpine-Induced Status Epilepticus. *Neurol. Res.* 31 (10), 1108–1114. doi:10.1179/174313209X389839

Liang, L. P., and Patel, M. (2004). Mitochondrial Oxidative Stress and Increased Seizure Susceptibility in Sod2(-/+) Mice. *Free Radic. Biol. Med.* 36 (5), 542–554. doi:10.1016/j.freeradbiomed.2003.11.029

Lin, T. K., Chen, S. D., Lin, K. J., and Chuang, Y. C. (2020). Seizure-Induced Oxidative Stress in Status Epilepticus: Is Antioxidant Beneficial? *Antioxidants (Basel).* 9 (11), 1029. doi:10.3390/antiox9111029

Liu, Z., Chen, J. M., Huang, H., Kuznicki, M., Zheng, S., Sun, W., et al. (2016). The Protective Effect of Trimetazidine on Myocardial Ischemia/Reperfusion Injury Through Activating AMPK and ERK Signaling Pathway. *Metabolism.* 65 (3), 122–130. doi:10.1016/j.metabol.2015.10.022

Livak, K. J., and Schmittgen, T. D. (2001). Analysis of Relative Gene Expression Data Using Real-Time Quantitative PCR and the 2(-Delta Delta C(T)) Method. *Methods.* 25 (4), 402–408. doi:10.1006/meth.2001.1262

Miyazaki, T., Miyamoto, O., Janjua, N. A., Hata, T., Takahashi, F., and Itano, T. (2003). Reactive Gliosis in Areas Around Third Ventricle in Association with Epileptogenesis in Amygdaloid-Kindled Rat. *Epilepsy Res.* 56 (1), 5–15. doi:10.1016/j.eplepsyres.2003.08.002

Mohamed, M. A. E., Abdel-Rahman, R. F., Mahmoud, S. S., Khattab, M. M., and Safar, M. M. (2020). Metformin and Trimetazidine Ameliorate Diabetes-Induced Cognitive Impediment in Status Epileptic Rats. *Epilepsy Behav.* 104 (Pt A), 106893. doi:10.1016/j.yebeh.2019.106893

Morin, D., Sapena, R., Elimadi, A., Testa, B., Labidalle, S., Le Ridant, A., et al. (2000). [(3)H]-Trimetazidine Mitochondrial Binding Sites: Regulation by Cations, Effect of Trimetazidine Derivatives and Other Agents and Interaction With an Endogenous Substance. *Br. J. Pharmacol.* 130 (3), 655–663. doi:10.1038/sj.bjp.0703348

Neary, J. T., Kang, Y., Bu, Y., Yu, E., Akong, K., and Peters, C. M. (1999). Mitogenic Signaling by ATP/P2Y Purinergic Receptors in Astrocytes: Involvement of a Calcium-Independent Protein Kinase C, Extracellular Signal-Regulated Protein Kinase Pathway Distinct From the Phosphatidylinositol-Specific Phospholipase C/Calcium Pathway. *J. Neurosci.* 19 (11), 4211–4220. doi:10.1523/jneurosci.19-11-04211.1999

Neary, J. T., Kang, Y., Willoughby, K. A., and Ellis, E. F. (2003). Activation of Extracellular Signal-Regulated Kinase by Stretch-Induced Injury in Astrocytes Involves Extracellular ATP and P2 Purinergic Receptors. *J. Neurosci.* 23 (6), 2348–2356. doi:10.1523/jneurosci.23-06-02348.2003

Nicholls, D. G., and Ward, M. W. (2000). Mitochondrial Membrane Potential and Neuronal Glutamate Excitotoxicity: Mortality and Millivolts. *Trends Neurosci.* 23 (4), 166–174. doi:10.1016/S0166-2236(99)01534-9

Noh, H. S., Hah, Y. S., Nilufar, R., Han, J., Bong, J. H., Kang, S. S., et al. (2006). Acetoacetate Protects Neuronal Cells From Oxidative Glutamate Toxicity. *J. Neurosci. Res.* 83 (4), 702–709. doi:10.1002/jnr.20736

Nowak, P., Zagził, T., Konecki, J., Szczerbak, G., Szkilnik, R., Niwiński, J., et al. (2006). Trimetazidine Increases [3H]Glucose Uptake in Rat Brain. *Pharmacol. Rep.* 58 (4), 559–561. PMID: 16963803

Ortuño-Sahagún, D., González, R. M., Verdaguer, E., Huerta, V. C., Torres-Mendoza, B. M., Lemus, L., et al. (2014). Glutamate Excitotoxicity Activates the MAPK/ERK Signaling Pathway and Induces the Survival of Rat Hippocampal Neurons *In Vivo*. *J. Mol. Neurosci.* 52 (3), 366–377. doi:10.1007/s12031-013-0157-7

Payet, O., D'Aldin, C., Maurin, L., Bonne, C., and Muller, A. (2004). Anti-Excitotoxic Activity of Trimetazidine in the Retina. *J. Ocul. Pharmacol. Ther.* 20 (1), 85–92. doi:10.1089/108076804772745491

Peng, S., Zhao, M., Wan, J., Fang, Q., Fang, D., and Li, K. (2014). The Efficacy of Trimetazidine on Stable Angina Pectoris: A Meta-Analysis of Randomized Clinical Trials. *Int. J. Cardiol.* 177 (3), 780–785. doi:10.1016/j.ijcard.2014.10.149

Pfaffl, M. W. (2001). A New Mathematical Model for Relative Quantification in Real-Time RT-PCR. *Nucleic Acids Res.* 29 (9), e45. doi:10.1093/nar/29.9.e45

Phillis, J. W., Ren, J., and O'Regan, M. H. (2000). Transporter Reversal as a Mechanism of Glutamate Release From the Ischemic Rat Cerebral Cortex: Studies With DL-Threo-Beta-Benzyloxyaspartate. *Brain Res.* 880 (1), 224–312. doi:10.1016/S0006-8993(00)02303-9

Pierelli, G., Stanzione, R., Forte, M., Migliarino, S., Perelli, M., Volpe, M., et al. (2017). Uncoupling Protein 2: A Key Player and a Potential Therapeutic Target in Vascular Diseases. *Oxid. Med. Cel. Longev.* 2017, 7348372. doi:10.1155/2017/7348372

Pines, G., Danbolt, N. C., Bjørås, M., Zhang, Y., Bendahan, A., Eide, L., et al. (1992). Cloning and Expression of a Rat Brain L-Glutamate Transporter. *Nature.* 360 (6403), 464–467. doi:10.1038/360464a0

Racine, R. J. (1972). Modification of Seizure Activity by Electrical Stimulation. II. Motor Seizure. *Electroencephalogr. Clin. Neurophysiol.* 32 (3), 281–294. doi:10.1016/0013-4694(72)90177-0

Robel, S., Buckingham, S. C., Boni, J. L., Campbell, S. L., Danbolt, N. C., Riedemann, T., et al. (2015). Reactive Astrogliosis Causes the Development

of Spontaneous Seizures. *J. Neurosci.* 35 (8), 3330–3345. doi:10.1523/JNEUROSCI.1574-14.2015

Ronnett, G. V., Ramamurthy, S., Kleman, A. M., Landree, L. E., and Aja, S. (2009). AMPK in the Brain: Its Roles in Energy Balance and Neuroprotection. *J. Neurochem.* 109 (Suppl. 1), 17–23. doi:10.1111/j.1471-4159.2009.05916.x

Rothstein, J. D., Martin, L. J., and Kuncl, R. W. (1992). Decreased Glutamate Transport by the Brain and Spinal Cord in Amyotrophic Lateral Sclerosis. *N. Engl. J. Med.* 326 (22), 1464–1468. doi:10.1056/NEJM199205283262204

Rothstein, J. D., Patel, S., Regan, M. R., Haenggeli, C., Huang, Y. H., Bergles, D. E., et al. (2005). Beta-Lactam Antibiotics Offer Neuroprotection by Increasing Glutamate Transporter Expression. *Nature.* 433 (7021), 73–77. doi:10.1038/nature03180

Rowley, S., and Patel, M. (2013). Mitochondrial Involvement and Oxidative Stress in Temporal Lobe Epilepsy. *Free Radic. Biol. Med.* 62, 121–131. doi:10.1016/j.freeradbiomed.2013.02.002

Sandhiya, S., Dkhar, S. A., Pillai, A. A., George, M., Jayaraman, B., and Chandrasekaran, A. (2015). Comparison of Ranolazine and Trimetazidine on Glycemic Status in Diabetic Patients With Coronary Artery Disease - a Randomized Controlled Trial. *J. Clin. Diagn. Res.* 9 (1), OC01–5. doi:10.7860/jcdr/2015/10594.5448

Sanz, P., and Garcia-Gimeno, M. A. (2020). Reactive Glia Inflammatory Signaling Pathways and Epilepsy. *Int. J. Mol. Sci.* 21 (11), 4096. doi:10.3390/ijms21114096

Sedky, A. A., El Serafy, O. M. H., Hassan, O. A., Abdel-Kawy, H. S., Hasanin, A. H., and Raafat, M. H. (2017). Trimetazidine Potentiates the Antiepileptic Activity and Ameliorates the Metabolic Changes Associated With Pentylenetetrazole Kindling in Rats Treated With Valproic Acid. *Can. J. Physiol. Pharmacol.* 95 (6), 686–696. doi:10.1139/cjpp-2016-0263

Seifert, G., and Steinhäuser, C. (2013). Neuron-Astrocyte Signaling and Epilepsy. *Exp. Neurol.* 244, 4–10. doi:10.1016/j.expneurol.2011.08.024

Seki, Y., Feustel, P. J., Keller, R. W., Tranmer, B. I., and Kimelberg, H. K. (1999). Inhibition of Ischemia-Induced Glutamate Release in Rat Striatum by Dihydrokinate and an Anion Channel Blocker. *Stroke.* 30 (2), 433–440. doi:10.1161/01.STR.30.2.433

Shimamoto, K., LeBrun, B., Yasuda-Kamatani, Y., Sakaitani, M., Shigeri, Y., Yumoto, N., et al. (1998). DL-Threo-Beta-Benzyloxyaspartate, a Potent Blocker of Excitatory Amino Acid Transporters. *Mol. Pharmacol.* 53 (2), 195–201. doi:10.1124/mol.53.2.195

Stringer, J. L. (1996). Repeated Seizures Increase GFAP and Vimentin in the Hippocampus. *Brain Res.* 717 (1-2), 147–153. doi:10.1016/0006-8993(96)00059-5

Sullivan, P. G., Rabchevsky, A. G., Waldmeier, P. C., and Springer, J. E. (2005). Mitochondrial Permeability Transition in CNS Trauma: Cause or Effect of Neuronal Cell Death? *J. Neurosci. Res.* 79 (1-2), 231–239. doi:10.1002/jnr.20292

Tanaka, K., Watase, K., Manabe, T., Yamada, K., Watanabe, M., Takahashi, K., et al. (1997). Epilepsy and Exacerbation of Brain Injury in Mice Lacking the Glutamate Transporter GLT-1. *Science.* 276 (5319), 1699–1702. doi:10.1126/science.276.5319.1699

Tikhaze, A. K., Lankin, V. Z., Zharova, E. A., and Kolycheva, S. V. (2000). Trimetazidine as Indirect Antioxidant. *Bull. Exp. Biol. Med.* 130 (10), 951–953. doi:10.1023/a:1002801504611

Todd, A. C., and Hardingham, G. E. (2020). The Regulation of Astrocytic Glutamate Transporters in Health and Neurodegenerative Diseases. *Int. J. Mol. Sci.* 21 (24), 9607. doi:10.3390/ijms21249607

Torre, E. R., Lothman, E., and Steward, O. (1993). Glial Response to Neuronal Activity: GFAP-mRNA and Protein Levels Are Transiently Increased in the Hippocampus after Seizures. *Brain Res.* 631 (2), 256–264. doi:10.1016/0006-8993(93)91543-2

Trotti, D., Danbolt, N. C., and Volterra, A. (1998). Glutamate Transporters Are Oxidant-Vulnerable: A Molecular Link Between Oxidative and Excitotoxic Neurodegeneration? *Trends Pharmacol. Sci.* 19 (8), 328–334. doi:10.1016/S0165-6147(98)01230-9

Ueda, Y., Doi, T., Tsuru, N., Tokumaru, J., and Mitsuyama, Y. (2002). Expression of Glutamate Transporters and Ionotropic Glutamate Receptors in GLAST Knockout Mice. *Brain Res. Mol. Brain Res.* 104 (2), 120–126. doi:10.1016/S0169-328X(02)00325-X

Waldbaum, S., Liang, L. P., and Patel, M. (2010). Persistent Impairment of Mitochondrial and Tissue Redox Status during Lithium-Pilocarpine-Induced Epileptogenesis. *J. Neurochem.* 115 (5), 1172–1182. doi:10.1111/j.1471-4159.2010.07013.x

Waldbaum, S., and Patel, M. (2010). Mitochondria, Oxidative Stress, and Temporal Lobe Epilepsy. *Epilepsy Res.* 88 (1), 23–45. doi:10.1016/j.eplepsyres.2009.09.020

Wallace, D. C., Lott, M. T., Shoffner, J. M., and Brown, M. D. (1992). Diseases Resulting From Mitochondrial DNA point Mutations. *J. Inherit. Metab. Dis.* 15 (4), 472–479. doi:10.1007/BF01799605

Wallraff, A., Köhling, R., Heinemann, U., Theis, M., Willecke, K., and Steinhäuser, C. (2006). The Impact of Astrocytic gap Junctional Coupling on Potassium Buffering in the hippocampus. *J. Neurosci.* 26 (20), 5438–5447. doi:10.1523/JNEUROSCI.0037-06.2006

Yun, H., Park, S., Kim, M. J., Yang, W. K., Im, D. U., Yang, K. R., et al. (2014). AMP-Activated Protein Kinase Mediates the Antioxidant Effects of Resveratrol Through Regulation of the Transcription Factor FoxO1. *FEBS J.* 281 (19), 4421–4438. doi:10.1111/febs.12949

Zhang, J., Wang, Y., Liu, X., Dagda, R. K., and Zhang, Y. (2017). How AMPK and PKA Interplay to Regulate Mitochondrial Function and Survival in Models of Ischemia and Diabetes. *Oxid. Med. Cel. Longev.* 2017, 4353510. doi:10.1155/2017/4353510

Zini, R., Simon, N., Morin, C., d'Athis, P., and Tillement, J. P. (1996). Inhibition of Rat Cerebral Mitochondrial Respiration by Cyclosporins A, D, and G and Restoration With Trimetazidine. *C. R. Acad. Sci.* 319 (12), 1087–1092. PMID: 9091178

Conflict of Interest: The authors declare that the research was conducted in the absence of any commercial or financial relationships that could be construed as a potential conflict of interest.

Publisher's Note: All claims expressed in this article are solely those of the authors and do not necessarily represent those of their affiliated organizations, or those of the publisher, the editors, and the reviewers. Any product that may be evaluated in this article, or claim that may be made by its manufacturer, is not guaranteed or endorsed by the publisher.

frontiers in Pharmacology

ORIGINAL RESEARCH
published: 24 November 2021
doi: 10.3389/fphar.2021.770610

Fluoxetine Potentiates Phagocytosis and Autophagy in Microglia

Sung Hee Park[1†], *Young-Sun Lee*[1,2†], *Hyun-Jeong Yang*[3] *and Gyun Jee Song*[1,2*]

[1]*Department of Medical Science, Catholic Kwandong University College of Medicine, Gangneung, Korea,* [2]*The Convergence Institute of Healthcare and Medical Science, Catholic Kwandong University, International St. Mary's Hospital, Incheon, Korea,* [3]*Department of Integrative Biosciences, University of Brain Education, Cheonan, Korea*

Fluoxetine is a classic antidepressant drug, and its immunomodulatory effects have recently been reported in many disease models. In addition, it has strong antineuroinflammatory effects in stroke and neurodegenerative animal models. However, the effect of fluoxetine on microglia phagocytosis and its molecular mechanisms have not yet been studied. In this study, we investigated whether fluoxetine has a regulatory effect on microglial function. Microglia cell lines and primary mouse microglia were treated with fluoxetine, and the production of inflammatory cytokines and neurotrophic factors and the phagocytosis of amyloid β were measured. Fluoxetine significantly attenuated the production of lipopolysaccharide-induced proinflammatory cytokines and oxidative stress in microglia. Fluoxetine also significantly potentiated microglia phagocytosis and autophagy. In addition, autophagy flux inhibitors attenuated fluoxetine-induced phagocytosis. In conclusion, fluoxetine induces autophagy and potentiates phagocytosis in microglia, which can be a novel molecular mechanism of the neuroinflammatory and neuroprotective effects of fluoxetine.

Keywords: fluoxetine, microglia, phagocytosis, autophagy, neuroinflammation

OPEN ACCESS

Edited by:
Nesrine Salah El Dine El Sayed, Cairo University, Egypt

Reviewed by:
Rabab Sayed, Cairo University, Egypt
Muhammed Abdullatif Saad, Cairo University, Egypt

***Correspondence:**
Gyun Jee Song
gyunjeesong@gmail.com

†These authors have contributed equally to this work

Specialty section:
This article was submitted to Neuropharmacology, a section of the journal Frontiers in Pharmacology

Received: *04 September 2021*
Accepted: *07 October 2021*
Published: *24 November 2021*

Citation:
Park SH, Lee Y-S, Yang H-J and Song GJ (2021) Fluoxetine Potentiates Phagocytosis and Autophagy in Microglia. Front. Pharmacol. 12:770610. doi: 10.3389/fphar.2021.770610

INTRODUCTION

Microglia are innate immune cells of the central nervous system (CNS), and resting microglia in the mature brain are known to play a role in brain homeostasis (Lenz and Nelson, 2018). Microglia is very sensitive to the changes in the microenvironment, and they can be activated in response to infection or injury-induced molecules. Activated microglia cause morphological changes and an increase in surface receptors and release several types of substances (Song and Suk, 2017; Zhao et al., 2017). Among them, there are neurotrophic factors that affect the survival of neurons and have neuroprotective effects (Song et al., 2016a; Song et al., 2016b; Ramirez et al., 2017). Activated microglia also produce many proinflammatory and neurotoxic factors (Jha et al., 2018; Song et al., 2019; Gupta et al., 2020). These proinflammatory cytokines and molecules produced by these inflammatory activated microglia cause neuroinflammation, which can lead to neurodegenerative diseases (Ramirez et al., 2017; Hansen et al., 2018). For example, the treatment of neurons with tumor necrosis factor (TNF-α), interleukin 1β (IL-1β), and nitric oxide (NO) was reported to cause the loss of synapses and neuronal death, suggesting that the inflammatory activation of microglia plays an important role in neurodegenerative disease pathogenesis. Conversely, there are neuroprotective types of microglia (Kwon and Koh, 2020) that show anti-inflammatory and regenerative functions. Often known as M2 microglia, these cells can relieve inflammation through the secretion of anti-inflammatory molecules, mainly inhibit the production of proinflammatory cytokines, and release neurotrophic factors such as brain-derived neurotrophic factor (BDNF) and insulin-like growth factor 1 (Chen and Trapp, 2016). In addition, M2 microglia have been reported to clear tissue debris and misfolded proteins to maintain CNS homeostasis as CNS phagocytes.

Autophagy is one of the key intracellular functions that maintain cellular homeostasis by removing misfolded proteins and damaged organelles. As the aggregation of misfolded proteins and mitochondrial dysfunction are the main etiology of most neurodegenerative diseases, autophagy dysfunction is recently considered to play an important role in many neurodegenerative diseases (Plaza-Zabala et al., 2017; Corti et al., 2020). Therefore, it has been proposed that autophagy regulation in neurons may have a therapeutic effect in neurodegenerative diseases. More recently, the dysregulation of autophagy in microglia has been reported to contribute to neurodegenerative disease pathogenesis (Menzies et al., 2017; Cho et al., 2020). For example, autophagy disorders in microglia can affect immune functions such as phagocytosis or neuroinflammation (Plaza-Zabala et al., 2017). However, whether autophagy activation regulates phagocytosis in microglia remains uninvestigated.

Fluoxetine is selective serotonin reuptake inhibitors (SSRIs), which increases the extracellular level of serotonin by limiting its reuptake into the presynaptic cell, and is mainly used as a treatment for depressive syndrome. Serotonin is also known to affect immune regulation via different 5-hydroxytryptamine (5-HT) receptors (5-HTRs) expressed in cells of the innate and adaptive immune system (Herr et al., 2017). Serotonin inhibited the production of TNF-α in Lipopolysaccharide (LPS)-stimulated mononuclear cells, with effects inhibited by 5-HT2 receptor blockade (de las Casas-Engel et al., 2013; Herr et al., 2017). Fluoxetine can act as an agonist to the 5-HT2B (Peng et al., 2014), and 5-HT2B was detected at the mRNA level in microglia collected from adult mice (Kettenmann et al., 2011; Turkin et al., 2021). Therefore, SSRIs such as fluoxetine have anti-inflammatory effects in microglia through 5-HT2B; however, the mechanisms related to other microglial functions, such as phagocytosis, remain unknown.

Recently, fluoxetine has been reported to reduce neuroinflammation *in vitro* and *in vivo* animal models (Liu et al., 2011; Zhang et al., 2012; Liu et al., 2018). Fluoxetine reduces neuroinflammation by decreasing proinflammatory cytokine production (TNF-α, IL-1β, IL-6, etc.), phosphorylation of inducible NO synthase (iNOS), p38 mitogen-activated protein kinase, and nuclear factor κB (NF-κB) activity. It also reduces hippocampal neuronal damage caused by cerebral hemorrhage and has neuroprotective effects such as neurogenesis and the induction of cell proliferation (Khodanovich et al., 2018). Furthermore, fluoxetine has an autophagy induction capacity in other cell types. A few studies have shown that, when administered in disease models, fluoxetine causes autophagic activation (Sun et al., 2018).

In this study, we investigated whether fluoxetine has anti-inflammatory effects and induces autophagy and phagocytosis in microglia.

MATERIALS AND METHODS

Cell Culture

BV-2 cells, an immortalized mouse microglial cell line, were maintained in Dulbecco modified eagle medium (DMEM; Gibco, Grand Island, NY, USA) with 5% fetal bovine serum (FBS; Gibco) and 100 U/mL penicillin/streptomycin (Gibco). HAPI cells, an immortalized rat microglial cell line, were cultured in DMEM with 10% FBS and 100 U/mL penicillin/streptomycin at 37°C in a 5% CO_2 incubator.

Primary mixed glial cells (MGCs) were prepared from neonatal C57BL/6 mice on postnatal days 1–3, as previously described (Gupta et al., 2020), with minor modifications. All experiments were conducted in accordance with the institutional animal care committee of the Catholic Kwandong University (no. CKU 2020-012). The cell suspensions obtained from brain tissue dissections were cultured with DMEM supplemented with 10% FBS and 100 U/mL penicillin/streptomycin for 3 weeks, with medium changes every 3 days.

Microglia Isolation From Adult Mouse Brain

Primary mouse microglial cultures were performed using a mouse adult brain dissociation and microglia isolation kit (MACS; Mitenyi Biotec, Bergisch Gladbach, Germany). Briefly, the brains of wild-type C57Bl6/J mice (3 months old) were removed immediately after euthanasia and digested with digestion buffer (Miltenyi Biotec, 130-107-677) at 37°C for 40 min. After the removal of myelin debris, the cell suspension was filtered through a 70-μm cell strainer. Cell pellets were washed with phosphate-buffered saline (PBS) with 0.5% bovine serum albumin (BSA), followed by CD11b-positive selection (Miltenyi Biotec, 130-093-636) using a mini-MACS (Miltenyi Biotec, 130-042-201) column. CD11b-positive microglia were seeded on poly-L-lysine–coated coverslips and cultured in DMEM with 10% FBS.

Measurement of Nitric Oxide and Cell Viability Assay

The cells were plated on 96-well plates (4×10^4/well) in full serum DMEM media. The cells were treated with or without concentrations of fluoxetine (Sigma–Aldrich, St. Louis, MO, USA), in the absence or presence of LPS (100 ng/mL; Sigma–Aldrich), in serum-free media for 24 h. NO production was quantified by adding a Griess solution, and the absorbance was measured at 540 nm with a microplate reader. Standard curves were prepared based on the reference values of a serially diluted sodium nitrite solution. Cell viability was determined using the 3-[4, 5-dimethylthiazol-2-yl]-2,5-diphenyl tetrazolium bromide (MTT; Sigma–Aldrich) assay. Absorbance was measured at 570 nm.

Reverse Transcription–Polymerase Chain Reaction

Total RNA was extracted from the treated cells using the TRIZOL reagent (Invitrogen, Carlsbad, CA, USA), and cDNA was synthesized using Moloney murine leukemia virus reverse transcriptase (Promega) and oligo(dT) primers. Reverse transcription–polymerase chain reaction (RT-PCR) was performed with specific primer sets, as shown in **Table 1**, using a T100 Thermal Cycler (Bio-Rad Laboratories, Richmond, CA, USA). PCR products were detected under

TABLE 1 | Primers used for RT-PCR.

Target genes	Accession number	Forward primer (5′–3′)	Reverse primer (5′–3′)	Temp (°C)	Cycles
TNF-α	NM_013693.2	CATCTTCTCAAAATTCGAGTGACAA	ACTTGGGCAGATTGACCTCAG	60	24
IL-1β	NM_008361.4	GCAACTGTTCCTGAACTC	CTCGGAGCCTGTAGTGCA	60	29
IL-6	NM_031168.2	AGTTGCTTCTTGGGACTGA	TCCACGATTTCCCAGAGAAC	57	27
Arg-1	NM_007482	CGCCTTTCTCAAAAGGACAG	CCAGCTCTTCATTGGCTTTC	60	29
BDNF	NM_007540.4	CGCAAACATGTCTATGAGGGTTC	TAGTAAGGGCCCGAACATACGAT	60	30
GAPDH	NM_008084	ACCACAGTCCATGCCATCAC	TCCACCACCCTGTTGCTGTA	60	24

ultraviolet light following ethidium bromide (Sigma–Aldrich) staining.

Western Blot Assay

MGCs were treated with the following chemicals: fluoxetine (7.5 μM), 3-MA (50 μM; Sigma–Aldrich), chloroquine (CQ; 50 μM; Sigma–Aldrich), and LPS (100 ng/mL; Sigma–Aldrich) for 3 h. The cells were washed with cold PBS after various treatments and lysed with a RIPA lysis buffer (50 mM Tris-HCl, 150 mM NaCl, 0.1% sodium dodecyl sulfate (SDS), and 1% NP-40). Equal amounts of protein were separated on a 12% SDS–polyacrylamide gel and transferred to polyvinylidene difluoride membranes (Bio-Rad Laboratories). The blots were blocked with 5% skim milk for 1 h at room temperature and incubated with the following primary antibodies: rabbit antimicrotubule-associated protein light chain 3 (LC3; 1:1,000 dilution; MBL, Woburn, MA, USA) or mouse anti–β-actin (1:5,000 dilution; Sigma–Aldrich, St. Louis, MO, USA) overnight at 4°C. After washing, the membranes were incubated for 1 h at room temperature with horseradish peroxidase–conjugated secondary antibodies (1:2,000) in 5% skim milk. The blots were developed using an enhanced chemiluminescence detection kit (SuperSignal™ West Femto; Thermo Fisher, Franklin, MA, USA).

Phagocytosis Assay

The phagocytosis assay was performed with fluorescent zymosan bioparticles from *Saccharomyces cerevisiae* (pH-sensitive pHrodoTM Red dye conjugates; Life Technologies, Carlsbad, CA, USA) or oligomerized FITC–amyloid-β (M-2585; BACHEM, Bubendorf, Switzerland). Primary MGCs were seeded at a density of 2×10^4 cells/well in 96-well plates and cultured for 48 h. The cells were treated with LPS (1 μg/mL) and/or fluoxetine (5 μM) and/or bafilomycin (Baf; 10 nM; Sigma–Aldrich) for 24 h in serum-free DMEM. The cells were treated with zymosan red or FITC–amyloid-β in serum-free media for 2–3 h. In some experiments, we conducted time-lapse imaging using a fluorescence microscope (DP80; Olympus, Japan). Blindly labeled images were analyzed to quantify phagocytosis.

Immunofluorescence Assay

The cells were cultured on coverslips and stained for LC3 or Iba-1 expression. Briefly, the cells were fixed in 4% paraformaldehyde (Sigma–Aldrich) for 20 min and blocked with 1% BSA (Sigma–Aldrich) and 4% normal donkey serum with 0.1% Triton X-100 (Sigma–Aldrich) in PBS (PBST) for 1 h at room temperature. The cells were incubated with primary rabbit anti-LC3 (1:500, MBL, Nagoya, Japan) or rabbit anti–Iba-1 (1:200, Wako, Neuss, Germany) in 1% BSA in PBST at 4°C overnight and then incubated with Cy3-conjugated secondary antibody (1:500 dilutions, Jackson ImmunoResearch, West Grove, PA, USA) for 1 h. The coverslips were mounted using a VECTASHIELD® antifade mounting solution with DAPI (Vector Laboratories, Burlingame, CA, USA). Blindly labeled images were analyzed to quantify LC3 punta.

Statistical Analysis

Data are presented as mean ± standard error of the mean (SEM) from at least three independent experiments. Statistical significance was analyzed using unpaired Student *t* test to compare two groups and one-way analysis of variance (ANOVA; Tukey *post hoc* multiple-comparisons tests) for multiple groups. $p < 0.05$ was considered statistically significant.

RESULTS

Fluoxetine Inhibits the Production of LPS-Induced Proinflammatory Molecules in Microglia

The anti-inflammatory effect of fluoxetine was examined in the microglial cell line BV-2. When BV-2 cells were treated with LPS, NO increased, and when fluoxetine was treated with LPS, NO production was significantly inhibited in a concentration-dependent manner. A slight toxicity was observed at high concentrations (10 μM). Therefore, other experiments were conducted at nontoxic concentrations (7.5 and 5 μM) of fluoxetine with NO inhibition effect (**Figures 1A, B**). Next, we have investigated whether fluoxetine modulates the expression of the neurotoxic or neuroprotective genes in microglia. Fluoxetine treatment significantly reduced TNF-α mRNA production, an inflammatory cytokine in BV-2 (**Figures 1C, D**), but no significant differences in the expression of Arg1, an M2 microglia marker, and BDNF, a neurotrophic factor, were observed. This anti-inflammatory effect was also confirmed in HAPI cells, another microglia cell line (**Figures 1E, F**).

Fluoxetine Promotes Phagocytosis in Microglia

One of the important functions of microglia is the clearance of pathogens and aggregated proteins (Galloway et al., 2019). Therefore, in this study, we analyzed whether fluoxetine increases microglial phagocytosis. First, the phagocytosis of

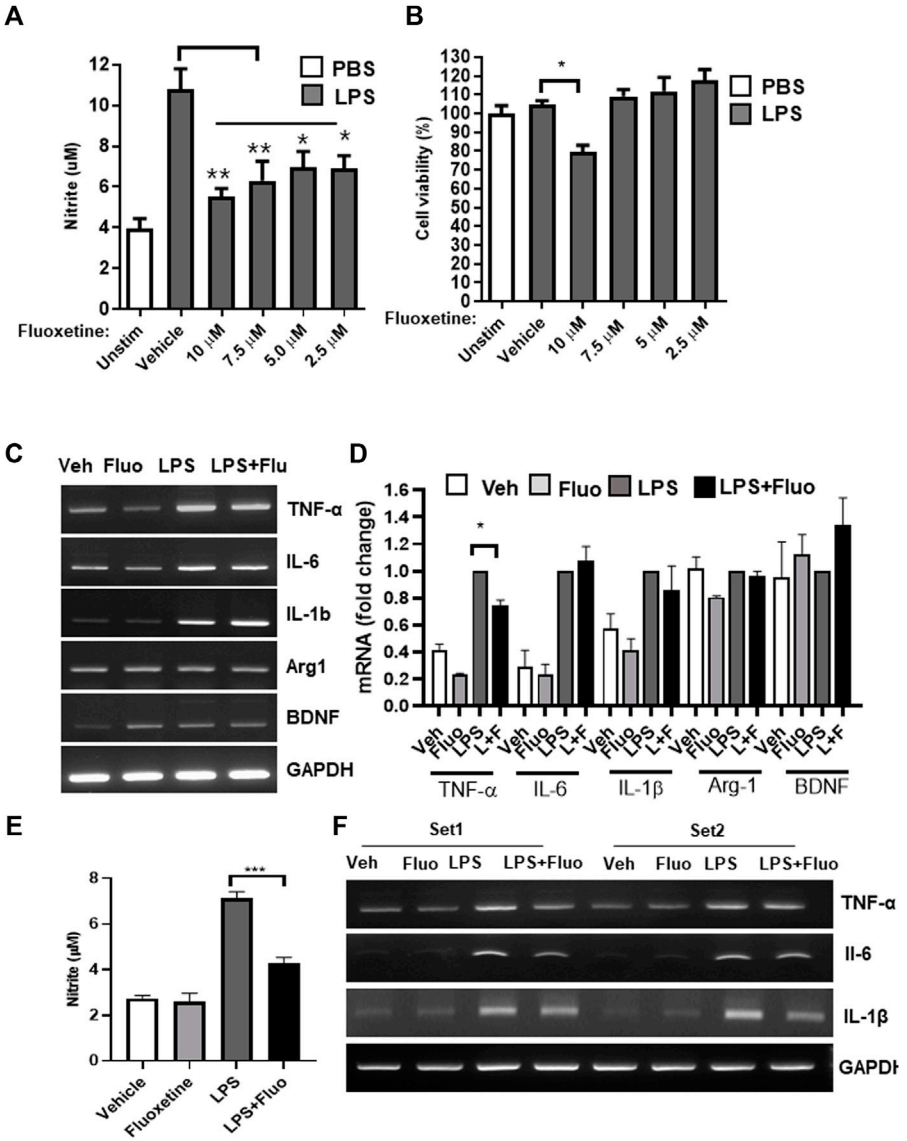

FIGURE 1 | Fluoxetine reduces inflammation in microglia. BV-2 cells were treated with the indicated concentrations of fluoxetine with or without LPS (100 ng/mL). After 24 h, NO production was measured using the Griess assay **(A)**, and cell viability was measured using the MTT assay **(B)**. **(C**, **D)** BV-2 cells were treated with 7.5 μM fluoxetine (fluo) with or without LPS. After 24 h, the mRNA expression levels of TNF-α, IL-6, IL-1β, Arg1, and BDNF were determined using RT-PCR. Fold changes were calculated as the ratio of the expression level in the LPS-only treated group. **(E)** A rat microglia cell line, HAPI cells, was also used to confirm the anti-inflammatory effect of fluoxetine. The cells were treated with 7.5 μM fluoxetine with or without LPS. NO production was measured after 24 h of incubation. **(F)** HAPI cells were treated with 7.5 μM fluoxetine for 6 h with or without LPS, and mRNA levels of inflammatory cytokines were measured using RT-PCR. Data are presented as the mean ± SEM. $^{*}p < 0.05$, $^{**}p < 0.01$, $^{***}p < 0.001$ compared with the LPS-only treated group in an one-way ANOVA with Tukey *post hoc* multiple-comparisons test. Veh, Vehicle. One-way ANOVA: **(A)** $F(5,18) = 9.387$, $p = 0.0002$; **(B)** $F(5,18) = 7.624$, $p = 0.0005$; **(D)** $F(3,8) = 134.8$, $p < 0.0001$; **(E)** $F(3,12) = 57.97$, $p < 0.0001$.

fluorescently labeled amyloid-β was observed in BV-2. Cells pretreated with fluoxetine were incubated with oligomerized amyloid $\beta_{1\text{-}42}$-GFP, and GFP engulfed by microglia was observed under a fluorescence microscope. As shown in **Figure 2A**, the phagocytosis of amyloid $\beta_{1\text{-}42}$-GFP increased with fluoxetine pretreatment. To digest phagocytosed particles, phagosomes fuse to lysosomes to form phagolysosomes. To determine whether fluoxetine increases phagolysosome formation, cells were treated with pHrodo-Red–labeled zymosan. When zymosan enters the phagolysosome, an organelle with a low pH, it turns into a strongly red fluorescent particle. As a result of counting and quantifying zymosan particles per cell, it was confirmed that phagocytosis significantly increased with fluoxetine in BV-2 in the presence or absence of LPS (**Figures 2B, C**). Next, primary microglia were used to confirm fluoxetine-induced phagocytosis. After isolating microglia from the adult mouse brain using a CD11b antibody, adult microglia were pretreated with fluoxetine for 24 h and then

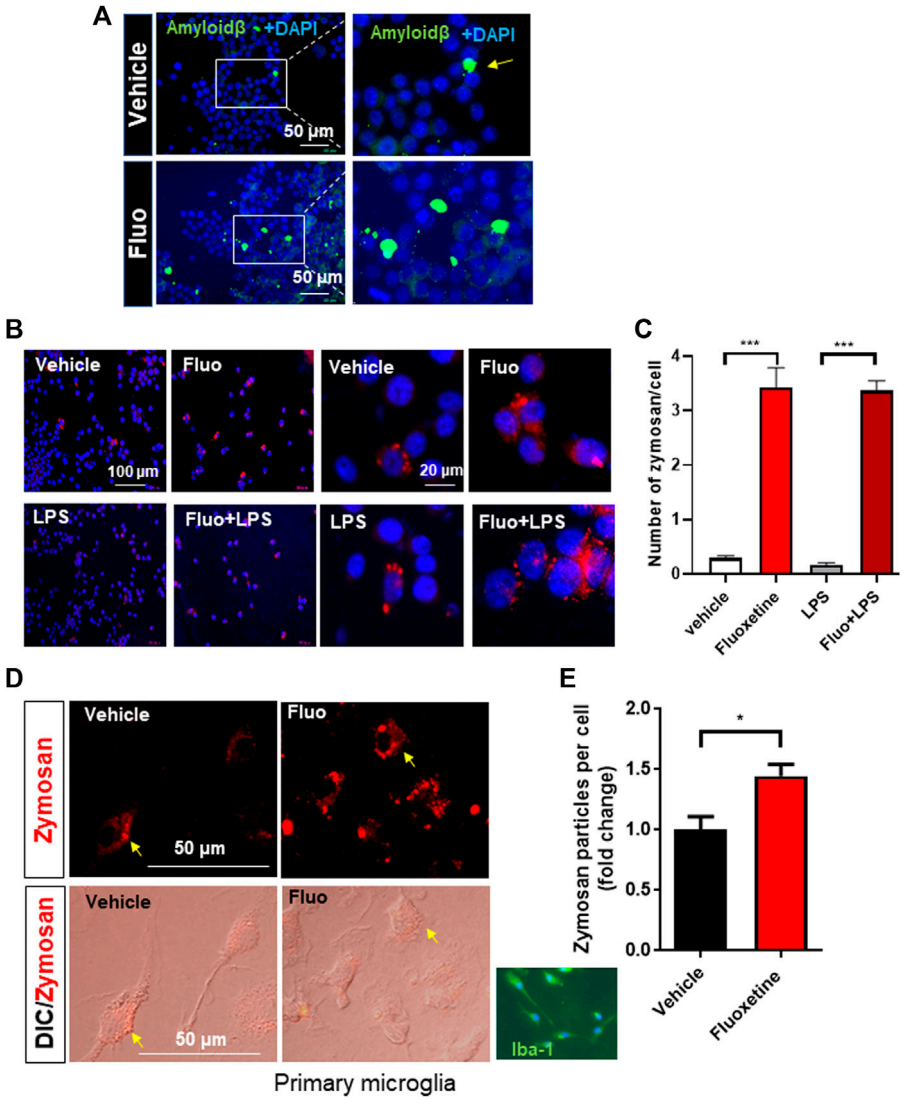

FIGURE 2 | Fluoxetine enhances phagocytosis in microglia. **(A)** BV-2 cells were seeded on coverslips in a 24-well plate and incubated overnight. The cells were then treated with fluoxetine (Fluo; 7.5 μM) for 16 h, followed by incubation with oligomerized amyloid β-GFP (100 μM in DMEM) for 3 h. The phagocytosed amyloid β-GFP was imaged under the fluorescence microscope. **(B)** BV-2 cells were treated with fluoxetine (7.5 μM) with or without LPS (100 ng/mL) for 16 h. The cells were then incubated with opsonized zymosan red particles for another 3 h. **(C)** The phagocytosed zymosan particles were counted and expressed as the number of zymosan particles per cell. More than 325 cells per group (total of >1,300 cells) were analyzed for quantification. **(D)** Primary microglia isolated from adult mice (Iba-1 microglial marker stained in green) was treated with fluoxetine (5 μM) for 24 h. The cells were then incubated with opsonized zymosan red particles for another 3 h. **(E)** The phagocytosed zymosan particles were counted and expressed as the fold change of the number of zymosan particles per cell. A total of 250 cells (117 and 133 cells per group) were analyzed for quantification. Data are presented as the mean ± SEM. $^{*}p < 0.05$, $^{***}p < 0.001$ compared with fluoxetine-treated cells in ANOVA with Tukey multiple-comparisons test or Student *t* test. One-way ANOVA: **(C)** $F(3,40) = 83.38$, $p < 0.0001$.

treated with zymosan particles for 3 h to obtain a fluorescence image. As shown in **Figures 2D, E**, red phagocytosed zymosan particles rapidly increased after entering the cell by fluoxetine.

Fluoxetine Increases Autophagy in Microglia

Autophagy is known to be involved in the regulation of microglial function (Lee et al., 2021). Therefore, we examined whether fluoxetine induces autophagy in microglia. First, microglia were treated with fluoxetine, and the levels of autophagosome protein LC3-I and LC3-II were measured using Western blot. We found that LC3-II accumulation (LC3-II/loading control β-actin) was increased by fluoxetine treatment in both cells with or without LPS treatment (**Figures 3A, B**). DMF, an autophagy inducer, was used as a positive control (Lee et al., 2021). To determine whether fluoxetine increases the autophagy flux, we perturbed it by treatment with its inhibitor CQ. The fluoxetine

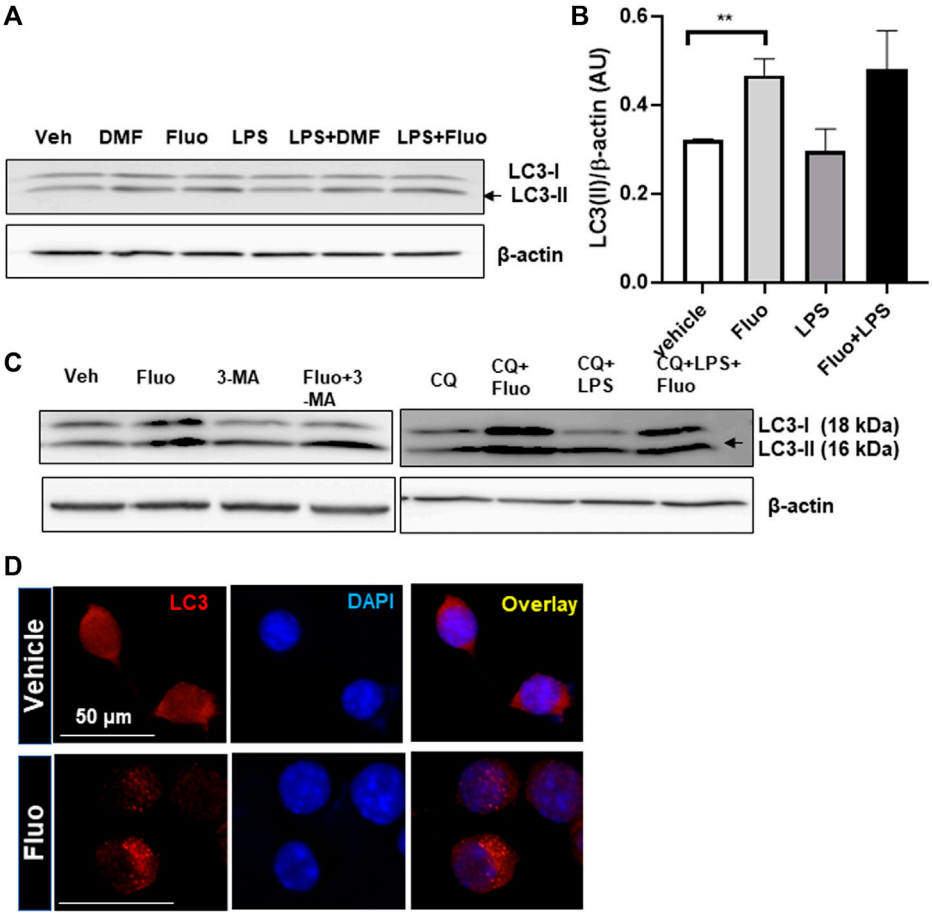

FIGURE 3 | Fluoxetine enhances autophagy in microglia. **(A)** HAPI cells were treated with DM*F*(4 μM), fluoxetine (7.5 μM), and/or LPS (100 ng/mL), as indicated, for 3 h. Cell lysates were immunoblotted for LC3-I and LC3-II. β-Actin was used as a loading control. **(B)** LC3-II quantification. Band intensity was quantified using ImageJ, and LC3-II band intensities were normalized based on β-actin band intensities. One-way ANOVA [$F(3,12) = 4.720$, $p = 0.0213$, n = 3–5/group]. The differences were not significant between groups after Tukey multiple-comparisons tests. Data are presented as means ± SEM. $^{**}p < 0.01$ compared with fluoxetine-treated cells in an unpaired *t* test. **(C)** Autophagy induction in primary MGCs isolated from the mouse brain with fluoxetine treatment. MGCs were treated with the following chemicals: fluoxetine (7.5 μM), 3-MA (50 μM), CQ (50 μM), and LPS (100 ng/mL) for 3 h. Cell lysates were immunoblotted for LC3-I and LC3-II. **(D)** Autophagosome formation labeled by LC3 in microglia. BV-2 cells were treated with fluoxetine (7.5 μ) for 3 h and immunostained for LC3 in red. Images were obtained with a 40× fluorescent microscope.

(7.5 μM)–induced LC3-II increase was potentiated under CQ treatment (**Figure 3C**). Autophagosome formation in microglia was visualized by immunofluorescence, which revealed that the LC3 puncta per cell were dramatically increased in fluoxetine-treated BV-2 cells (**Figure 3D**). Our data suggest that fluoxetine contributes to autophagy induction and flux.

Autophagy Inhibitor Decreases Fluoxetine-Induced Phagocytosis

To determine whether autophagy is required for the pro-phagocytic effects of fluoxetine, we perturbed the phagosome flux by treatment with Baf. Baf treatment increased LC3 puncta formation by inhibiting the autophagy flux (**Figure 4A**). The phagocytosis assay showed that Baf significantly inhibits fluoxetine-induced phagocytosis (**Figures 4B, C**). To test whether fluoxetine-induced phagocytosis potentiates the clearance of pathogens or phagocytosed materials, the cells were treated with zymosan fluorescence particles first and then with or without fluoxetine for another 3 h to induce clearance (**Figure 4D**). As shown in **Figure 4E**, fluoxetine rapidly removed the phagocytic zymosan particles. These results support the finding that an enhanced autophagic activity contributes to phagocytosis and the clearance of phagocytosed materials. Taken together, these results demonstrate that fluoxetine could contribute to autophagy activation to engulf and digest pathogens or misfolded proteins, which could exert neuroprotective effects.

DISCUSSION

Fluoxetine, an SSRI, is commonly prescribed to treat depression. Recent studies have suggested that fluoxetine

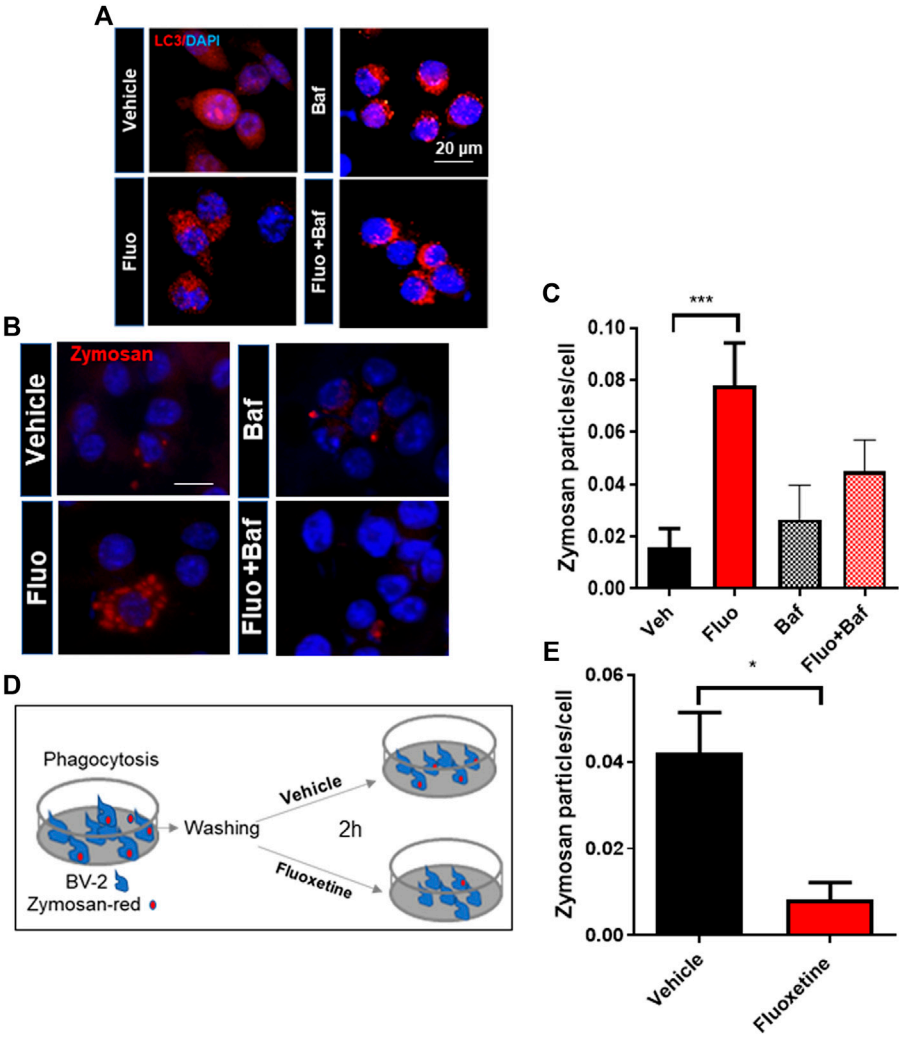

FIGURE 4 | The autophagy inhibitor decreases fluoxetine-induced phagocytosis. **(A)** Autophagosome formation visualized by LC3 immunostaining in BV-2 cells with fluoxetine (7.5 μM) and/or Baf (10 nM) for 3 h. **(B)** Fluoxetine-induced phagocytosis blocked by an autophagy flux inhibitor, Baf (10 nM). BV-2 cells were pretreated with fluoxetine (7.5 μM) for 3 h and then treated with zymosan red for another 3 h with and without Baf. The cells were imaged under a fluorescence microscope. **(C)** The phagocytosed zymosan particles were counted and expressed as the number of zymosan particles per cell. A total of 1,850 cells (520, 560, 370, and 400 per group) were analyzed for quantification. **(D, E)** Fluoxetine potentiates the clearance of phagocytosed materials. BV-2 cells were incubated with zymosan red for 3 h and then washed three times. The cells were further incubated with either vehicle or fluoxetine for 2 h to measure the clearance of phagocytosed zymosan particles. The fixed cells were imaged using fluorescence microscopy. Data are presented as means ± SEM. $^{*}p < 0.05$, $^{***}p < 0.001$ compared with fluoxetine-treated cells in ANOVA [$F(3,32) = 4.408$, $p = 0.0105$] with Tukey multiple-comparisons test **(C)** or Student *t* test **(E)**.

affords strong neuroprotective ability in many neurological disease models. However, the molecular mechanisms underlying fluoxetine-mediated neuroprotection have not yet been elucidated. In the present study, fluoxetine was shown to have antineuroinflammatory and prophagocytic effects. In particular, the results of fluoxetine's effects and mechanisms of action are reported in microglia, which are responsible for maintaining brain immunity and homeostasis. Fluoxetine not only inhibits the proinflammatory activity of microglia but also increases phagocytosis and autophagy. The effects of inhibiting brain inflammation and reducing the accumulation of misfolded protein aggregates are expected to be helpful in the treatment of neurodegenerative diseases such as AD and PD.

Fluoxetine was developed as an antidepressant, but its anti-inflammatory and brain-protective effects have also been reported. Previous studies on the effects of fluoxetine on microglia are consistent with our findings. According to an article reported by Lui et al. (2011) in *Neuropharmacology*, fluoxetine significantly inhibited LPS-stimulated proinflammatory cytokines and neurotoxic mediators in BV-2 cells, as in our study (**Figure 1**). In addition, fluoxetine exerts a neuroprotective effect against microglia-mediated neurotoxicity in neuron and glia cocultures (Zhang et al., 2012). Fluoxetine has neuroprotective

effects by reducing the production of proinflammatory factors, including NO, TNF-α, iNOS, and IL-1β, in early brain injury after subarachnoid hemorrhage (Liu et al., 2018). As a potential mechanism of the antineuroinflammatory effect of fluoxetine, fluoxetine-mediated NF-κB regulation has been proposed. Moreover, fluoxetine has been reported to display beneficial effects in models of neurological disorders, which may not be related to antineuroinflammatory effects (Gassen et al., 2015).

Recent studies have shown that fluoxetine is involved in the induction of autophagy, as summarized in a review article (Cho et al., 2020). Autophagy declines with age, and its deficit has been observed in the brain of many neurodegenerative diseases. Treatment with autophagy-inducing drugs led to a robust recovery rate and decline in clinical symptoms in rodent models of neurodegenerative diseases (Rusmini et al., 2019). Our recently published article also showed autophagy induction by DMF, reduced neuroinflammation by the inhibition of the M1 phenotype, and an increase in the M2 phenotype of microglia (Lee et al., 2021). Fluoxetine treatment exhibits autophagy induction in lymphoma (Cloonan and Williams, 2011) and adipose-derived stem cells (Sun et al., 2015). It significantly up-regulated autophagy-related genes and LC3 protein expression (Sun et al., 2015). Gassen et al. (2015) reported that fluoxetine activates autophagic pathways in an FKBP51-dependent manner. More recently, fluoxetine was found to activate autophagy in a rat subarachnoid hemorrhage brain injury model (Liu et al., 2018). In addition, fluoxetine reversed depressive behavior and up-regulated BDNF and autophagy-associated proteins (LC3-II) in normal mice. However, microglia-specific autophagy-deficient mice showed higher inflammatory levels and reduced BDNF expression (Tan et al., 2018). In their study, fluoxetine increased the expression of autophagy-related proteins ATG5, LC3-II, and BDNF, suggesting that fluoxetine-induced autophagy in the brain. Furthermore, Cx3Cr1Cre/ATG5loxp/loxp mice demonstrated a significantly lowered fluoxetine-induced BDNF overexpression. Interestingly, mouse brains with a microglia-specific autophagy deficiency showed the hyperactivation of microglia, as examined by Iba-1 staining in the hippocampal area of the brain. However, this study did not provide a mechanistic explanation of how fluoxetine mediates antidepressant effects through the autophagic pathway.

In this study, we showed the autophagy induction effect of fluoxetine in microglia. Serotonin and citalopram, another type of SSRI, are also known to have autophagy induction capacity in other cell types (Zschocke et al., 2011; Niture et al., 2018). In addition, SSRIs, such as escitalopram, fluoxetine, sertraline, paroxetine, and venlafaxine, are known to have an anti-inflammatory role (Dionisie et al., 2021). However, whether other members of SSRIs have anti-inflammatory effects and the ability to induce autophagy and phagocytosis in microglia, or whether these are fluoxetine-specific effects, is unclear. Further research on these topics is warranted.

Phagocytosis of dead cell debris and pathogens has been reported to be essential for the maintenance of brain homeostasis. Its dysfunction in microglia has been reported in patients with neurodegenerative diseases (Galloway et al., 2019). Recently, Berglund et al. (2020) reported that the deletion of Atg7 in microglia caused persistent neuroinflammation by driving microglial dysfunction in debris uptake and degradation. The reduced clearance capacity of microglia is most likely a consequence of the internalization of scavenger receptors due to impaired ATG7-dependent lysosomal degradation. The accumulation of intracellular proteins, including myelin and amyloid β, is associated with neurogenerative pathologies. ATG7-deficient microglia showed similar phenotypes to those of aged microglia. Therefore, molecules promoting the induction of autophagy might have a therapeutic potential. In this study, fluoxetine increased the canonical autophagosome formation examined by LC3 puncta and increases in LC3-II accumulation after treatment with CQ, an autophagy flux inhibitor.

The phagocytic capacity of microglia is essential for brain homeostasis maintenance. Especially, the dysfunction of microglia has been proposed as the common histology in aged brains and those with neurodegenerative diseases. Therefore, boosting the phagocytic capacity of microglia increases the clearance of neurotoxic proteins such as β-amyloid, α-synuclein, and TDP-43 (Boland et al., 2018). In our study, we found that fluoxetine has a prophagocytic function, a key function of microglia for maintaining brain homeostasis. We also showed that fluoxetine-induced phagocytosis is dependent on fluoxetine-mediated autolysophagosome formation in microglia.

Together, our findings demonstrate that fluoxetine has regulatory effects on autophagy and phagocytosis, which are necessary functions for microglia and CNS cellular homeostasis. We provide a novel mechanism for the neuroprotective and antineuroinflammatory effects of fluoxetine, which serves as a functional link between autophagy and phagocytosis capacity of microglia. We suggest that fluoxetine is an autophagic inducer in microglia and potentiates their phagocytic capacity. The initial step of autophagy is autophagosome formation, which fuses with lysosomal vesicles and mediates the delivery of cytoplasmic proteins to lysosomal vesicles to be degraded or recycled. Fluoxetine-induced autophagy increased LC3 puncta formation, as well as lysophagosome formation. An enhanced autophagic activity has been reported to promote Aβ clearance *in vitro* and in AD mice. Here, we find that fluoxetine treatment caused autophagic activation, as seen by increased LC3-II and LC3 punctate distribution and autophagosome accumulation. Furthermore, the fluoxetine-mediated increase in phagocytosis was blocked by the autophagy inhibitor Baf in microglia. Collectively, these data indicate that fluoxetine exerts an anti-inflammatory and neuroprotective effect in the brain through microglia, suggesting that modulating the autophagy–lysosomal pathway can be a promising therapy for the clearance of amyloid plaques in AD.

In conclusion, our study demonstrated that fluoxetine attenuated neuroinflammation and potentiated phagocytosis in microglia. A potential mechanism of fluoxetine-induced phagocytosis is, at least, partially involved in the activation of autophagy in microglia.

DATA AVAILABILITY STATEMENT

The original contributions presented in the study are included in the article, further inquiries can be directed to the corresponding author.

ETHICS STATEMENT

All animal experiments were reviewed and approved by the institutional animal care committee of the Catholic Kwandong University (No. CKU 2020-012).

AUTHOR CONTRIBUTIONS

SP and Y-SL performed experiments, data analysis, and wrote the manuscript; H-JY performed data analysis and reviewed the manuscript; GS designed the study, analyzed the data, and wrote the manuscript. All authors contributed to and approved the submitted version of the article.

FUNDING

This study was supported by grants from the National Research Foundation of Korea, Grant/Award Numbers 2016R1D1A1B01009186 and NRF-2019M3E5D2A01060293.

REFERENCES

Berglund, R., Guerreiro-Cacais, A. O., Adzemovic, M. Z., Zeitelhofer, M., Lund, H., Ewing, E., et al. (2020). Microglial Autophagy-Associated Phagocytosis Is Essential for Recovery from Neuroinflammation. *Sci. Immunol.* 5 (52), eabb5077. doi:10.1126/sciimmunol.abb5077

Boland, B., Yu, W. H., Corti, O., Mollereau, B., Henriques, A., Bezard, E., et al. (2018). Promoting the Clearance of Neurotoxic Proteins in Neurodegenerative Disorders of Ageing. *Nat. Rev. Drug Discov.* 17 (9), 660–688. doi:10.1038/nrd.2018.109

Chen, Z., and Trapp, B. D. (2016). Microglia and Neuroprotection. *J. Neurochem.* 136, 10–17. doi:10.1111/jnc.13062

Cho, K. S., Lee, J. H., Cho, J., Cha, G. H., and Song, G. J. (2020). Autophagy Modulators and Neuroinflammation. *Curr. Med. Chem.* 27 (6), 955–982. doi:10.2174/0929867325666181031144605

Cloonan, S. M., and Williams, D. C. (2011). The Antidepressants Maprotiline and Fluoxetine Induce Type II Autophagic Cell Death in Drug-Resistant Burkitt's Lymphoma. *Int. J. Cancer* 128 (7), 1712–1723. doi:10.1002/ijc.25477

Corti, O., Blomgren, K., Poletti, A., and Beart, P. M. (2020). Autophagy in Neurodegeneration: New Insights Underpinning Therapy for Neurological Diseases. *J. Neurochem.* 154 (4), 354–371. doi:10.1111/jnc.15002

de las Casas-Engel, M., Domínguez-Soto, A., Sierra-Filardi, E., Bragado, R., Nieto, C., Puig-Kroger, A., et al. (2013). Serotonin Skews Human Macrophage Polarization through HTR2B and HTR7. *J. Immunol.* 190 (5), 2301–2310. doi:10.4049/jimmunol.1201133

Dionisie, V., Filip, G. A., Manea, M. C., Manea, M., and Riga, S. (2021). The Anti-inflammatory Role of SSRI and SNRI in the Treatment of Depression: a Review of Human and Rodent Research Studies. *Inflammopharmacology* 29 (1), 75–90. doi:10.1007/s10787-020-00777-5

Galloway, D. A., Phillips, A. E. M., Owen, D. R. J., and Moore, C. S. (2019). Phagocytosis in the Brain: Homeostasis and Disease. *Front. Immunol.* 10, 790. doi:10.3389/fimmu.2019.00790

Gassen, N. C., Hartmann, J., Schmidt, M. V., and Rein, T. (2015). FKBP5/FKBP51 Enhances Autophagy to Synergize with Antidepressant Action. *Autophagy* 11 (3), 578–580. doi:10.1080/15548627.2015.1017224

Gupta, D. P., Park, S. H., Yang, H. J., Suk, K., and Song, G. J. (2020). Neuroprotective and Anti-neuroinflammatory Effects of a Poisonous Plant Croton Tiglium Linn. Extract. *Toxins (Basel)* 12 (4), 261–274. doi:10.3390/toxins12040261

Hansen, D. V., Hanson, J. E., and Sheng, M. (2018). Microglia in Alzheimer's Disease. *J. Cel Biol* 217 (2), 459–472. doi:10.1083/jcb.201709069

Herr, N., Bode, C., and Duerschmied, D. (2017). The Effects of Serotonin in Immune Cells. *Front. Cardiovasc. Med.* 4, 48. doi:10.3389/fcvm.2017.00048

Jha, M. K., Kim, J. H., Song, G. J., Lee, W. H., Lee, I. K., Lee, H. W., et al. (2018). Functional Dissection of Astrocyte-Secreted Proteins: Implications in Brain Health and Diseases. *Prog. Neurobiol.* 162, 37–69. doi:10.1016/j.pneurobio.2017.12.003

Kettenmann, H., Hanisch, U. K., Noda, M., and Verkhratsky, A. (2011). Physiology of Microglia. *Physiol. Rev.* 91 (2), 461–553. doi:10.1152/physrev.00011.2010

Khodanovich, M., Kisel, A., Kudabaeva, M., Chernysheva, G., Smolyakova, V., Krutenkova, E., et al. (2018). Effects of Fluoxetine on Hippocampal Neurogenesis and Neuroprotection in the Model of Global Cerebral Ischemia in Rats. *Int. J. Mol. Sci.* 19 (1), 162. doi:10.3390/ijms19010162

Kwon, H. S., and Koh, S. H. (2020). Neuroinflammation in Neurodegenerative Disorders: the Roles of Microglia and Astrocytes. *Transl Neurodegener* 9 (1), 42. doi:10.1186/s40035-020-00221-2

Lee, Y. S., Gupta, D. P., Park, S. H., Yang, H. J., and Song, G. J. (2021). Anti-Inflammatory Effects of Dimethyl Fumarate in Microglia via an Autophagy Dependent Pathway. *Front. Pharmacol.* 12, 612981. doi:10.3389/fphar.2021.612981

Lenz, K. M., and Nelson, L. H. (2018). Microglia and beyond: Innate Immune Cells as Regulators of Brain Development and Behavioral Function. *Front. Immunol.* 9, 698. doi:10.3389/fimmu.2018.00698

Liu, D., Wang, Z., Liu, S., Wang, F., Zhao, S., and Hao, A. (2011). Anti-inflammatory Effects of Fluoxetine in Lipopolysaccharide(LPS)-stimulated Microglial Cells. *Neuropharmacology* 61 (4), 592–599. doi:10.1016/j.neuropharm.2011.04.033

Liu, F. Y., Cai, J., Wang, C., Ruan, W., Guan, G. P., Pan, H. Z., et al. (2018). Fluoxetine Attenuates Neuroinflammation in Early Brain Injury after Subarachnoid Hemorrhage: a Possible Role for the Regulation of TLR4/MyD88/NF-Kb Signaling Pathway. *J. Neuroinflammation* 15 (1), 347. doi:10.1186/s12974-018-1388-x

Menzies, F. M., Fleming, A., Caricasole, A., Bento, C. F., Andrews, S. P., Ashkenazi, A., et al. (2017). Autophagy and Neurodegeneration: Pathogenic Mechanisms and Therapeutic Opportunities. *Neuron* 93 (5), 1015–1034. doi:10.1016/j.neuron.2017.01.022

Niture, S., Gyamfi, M. A., Kedir, H., Arthur, E., Ressom, H., Deep, G., et al. (2018). Serotonin Induced Hepatic Steatosis Is Associated with Modulation of Autophagy and Notch Signaling Pathway. *Cell Commun Signal* 16 (1), 78. doi:10.1186/s12964-018-0282-6

Peng, L., Gu, L., Li, B., and Hertz, L. (2014). Fluoxetine and All Other SSRIs Are 5-HT2B Agonists - Importance for Their Therapeutic Effects. *Curr. Neuropharmacol* 12 (4), 365–379. doi:10.2174/1570159X12666140828221720

Plaza-Zabala, A., Sierra-Torre, V., and Sierra, A. (2017). Autophagy and Microglia: Novel Partners in Neurodegeneration and Aging. *Int. J. Mol. Sci.* 18 (3), 598–625. doi:10.3390/ijms18030598

Ramirez, A. I., de Hoz, R., Salobrar-Garcia, E., Salazar, J. J., Rojas, B., Ajoy, D., et al. (2017). The Role of Microglia in Retinal Neurodegeneration: Alzheimer's Disease, Parkinson, and Glaucoma. *Front. Aging Neurosci.* 9, 214. doi:10.3389/fnagi.2017.00214

Rusmini, P., Cortese, K., Crippa, V., Cristofani, R., Cicardi, M. E., Ferrari, V., et al. (2019). Trehalose Induces Autophagy via Lysosomal-Mediated TFEB Activation in Models of Motoneuron Degeneration. *Autophagy* 15 (4), 631–651. doi:10.1080/15548627.2018.1535292

Song, G. J., Jung, M., Kim, J. H., Park, H., Rahman, M. H., Zhang, S., et al. (2016a). A Novel Role for Protein Tyrosine Phosphatase 1B as a Positive Regulator of Neuroinflammation. *J. Neuroinflammation* 13 (1), 86. doi:10.1186/s12974-016-0545-3

Song, G. J., Nam, Y., Jo, M., Jung, M., Koo, J. Y., Cho, W., et al. (2016b). A Novel Small-Molecule Agonist of PPAR-γ Potentiates an Anti-inflammatory M2 Glial Phenotype. *Neuropharmacology* 109, 159–169. doi:10.1016/j.neuropharm.2016.06.009

Song, G. J., Rahman, M. H., Jha, M. K., Gupta, D. P., Park, S. H., Kim, J. H., et al. (2019). A Bcr-Abl Inhibitor GNF-2 Attenuates Inflammatory Activation of Glia and Chronic Pain. *Front. Pharmacol.* 10, 543. doi:10.3389/fphar.2019.00543

Song, G. J., and Suk, K. (2017). Pharmacological Modulation of Functional Phenotypes of Microglia in Neurodegenerative Diseases. *Front. Aging Neurosci.* 9, 139. doi:10.3389/fnagi.2017.00139

Sun, B. K., Kim, J. H., Choi, J. S., Hwang, S. J., and Sung, J. H. (2015). Fluoxetine Decreases the Proliferation and Adipogenic Differentiation of Human Adipose-Derived Stem Cells. *Int. J. Mol. Sci.* 16 (7), 16655–16668. doi:10.3390/ijms160716655

Sun, D., Zhu, L., Zhao, Y., Jiang, Y., Chen, L., Yu, Y., et al. (2018). Fluoxetine Induces Autophagic Cell Death via eEF2K-AMPK-mTOR-ULK Complex axis in Triple Negative Breast Cancer. *Cell Prolif* 51 (2), e12402. doi:10.1111/cpr.12402

Tan, X., Du, X., Jiang, Y., Botchway, B. O. A., Hu, Z., and Fang, M. (2018). Inhibition of Autophagy in Microglia Alters Depressive-like Behavior via BDNF Pathway in Postpartum Depression. *Front. Psychiatry* 9, 434. doi:10.3389/fpsyt.2018.00434

Turkin, A., Tuchina, O., and Klempin, F. (2021). Microglia Function on Precursor Cells in the Adult Hippocampus and Their Responsiveness to Serotonin Signaling. *Front Cel Dev Biol* 9, 665739. doi:10.3389/fcell.2021.665739

Zhang, F., Zhou, H., Wilson, B. C., Shi, J. S., Hong, J. S., and Gao, H. M. (2012). Fluoxetine Protects Neurons against Microglial Activation-Mediated Neurotoxicity. *Parkinsonism Relat. Disord.* 18 S213–S217. doi:10.1016/S1353-8020(11)70066-9

Zhao, S. C., Ma, L. S., Chu, Z. H., Xu, H., Wu, W. Q., and Liu, F. (2017). Regulation of Microglial Activation in Stroke. *Acta Pharmacol. Sin* 38 (4), 445–458. doi:10.1038/aps.2016.162

Zschocke, J., Zimmermann, N., Berning, B., Ganal, V., Holsboer, F., and Rein, T. (2011). Antidepressant Drugs Diversely Affect Autophagy Pathways in Astrocytes and Neurons-Ddissociation from Cholesterol Homeostasis. *Neuropsychopharmacology* 36 (8), 1754–1768. doi:10.1038/npp.2011.57

Conflict of Interest: The authors declare that the research was conducted in the absence of any commercial or financial relationships that could be construed as a potential conflict of interest.

Publisher's Note: All claims expressed in this article are solely those of the authors and do not necessarily represent those of their affiliated organizations, or those of the publisher, the editors and the reviewers. Any product that may be evaluated in this article, or claim that may be made by its manufacturer, is not guaranteed or endorsed by the publisher.

frontiers in Pharmacology

ORIGINAL RESEARCH
published: 02 December 2021
doi: 10.3389/fphar.2021.747975

HEXA-018, a Novel Inducer of Autophagy, Rescues TDP-43 Toxicity in Neuronal Cells

Shinrye Lee[1†], Myungjin Jo[1†], Hye Eun Lee[2], Yu-Mi Jeon[1], Seyeon Kim[1,3], Younghwi Kwon[1,3], Junghwa Woo[1], Shin Han[4], Ji Young Mun[2] and Hyung-Jun Kim[1]**

[1]Dementia Research Group, Korea Brain Research Institute (KBRI), Daegu, South Korea, [2]Neural Circuit Research Group, Korea Brain Research Institute (KBRI), Daegu, South Korea, [3]Department of Brain and Cognitive Sciences, DGIST, Daegu, South Korea, [4]Hexa Pharmatec, Ansan-si, South Korea

The autophagy-lysosomal pathway is an essential cellular mechanism that degrades aggregated proteins and damaged cellular components to maintain cellular homeostasis. Here, we identified HEXA-018, a novel compound containing a catechol derivative structure, as a novel inducer of autophagy. HEXA-018 increased the LC3-I/II ratio, which indicates activation of autophagy. Consistent with this result, HEXA-018 effectively increased the numbers of autophagosomes and autolysosomes in neuronal cells. We also found that the activation of autophagy by HEXA-018 is mediated by the AMPK-ULK1 pathway in an mTOR-independent manner. We further showed that ubiquitin proteasome system impairment- or oxidative stress-induced neurotoxicity was significantly reduced by HEXA-018 treatment. Moreover, oxidative stress-induced mitochondrial dysfunction was strongly ameliorated by HEXA-018 treatment. In addition, we investigated the efficacy of HEXA-018 in models of TDP-43 proteinopathy. HEXA-018 treatment mitigated TDP-43 toxicity in cultured neuronal cell lines and *Drosophila*. Our data indicate that HEXA-018 could be a new drug candidate for TDP-43-associated neurodegenerative diseases.

Keywords: catechol, autophagy, mitochondrial dysfunction, TDP-43, ALS

OPEN ACCESS

Edited by:
Barbara Budzynska,
Medical University of Lublin, Poland

Reviewed by:
Basant K. Patel,
Indian Institute of Technology Hyderabad, India
Paola Bellosta,
University of Trento, Italy
Hamdi Yosra,
Tunis El Manar University, Tunisia

****Correspondence:***
Ji Young Mun
jymun@kbri.re.kr
Hyung-Jun Kim
kijang1@kbri.re.kr

[†]These authors have contributed equally to this work

Specialty section:
This article was submitted to Neuropharmacology, a section of the journal Frontiers in Pharmacology

Received: *27 July 2021*
Accepted: *05 November 2021*
Published: *02 December 2021*

Citation:
Lee S, Jo M, Lee HE, Jeon Y-M, Kim S, Kwon Y, Woo J, Han S, Mun JY and Kim H-J (2021) HEXA-018, a Novel Inducer of Autophagy, Rescues TDP-43 Toxicity in Neuronal Cells. Front. Pharmacol. 12:747975. doi: 10.3389/fphar.2021.747975

1 INTRODUCTION

The autophagy-lysosomal pathway (ALP) is an evolutionarily conserved catabolic mechanism that involves the degradation of unnecessary or abnormal proteins/organelles (Lee, 2012). The postmitotic and long-lived nature of neurons makes them vulnerable to proteotoxic stress induced by the accumulation of misfolded proteins or damaged organelles (Son et al., 2012). Thus, maintaining efficient ALP function is essential for neuronal survival, and dysfunction of the ALP is one of the common features of neurodegenerative diseases (Son et al., 2012).

TDP-43 is part of an evolutionarily conserved family of heterogeneous nuclear ribonucleoproteins that modulate multiple steps of RNA metabolic processes (Jo et al., 2020). Therefore, TDP-43 is mainly localized in the nucleus but also shuttles between the nucleus and the cytoplasm to perform various cellular functions. However, under pathological conditions, cytoplasmic transfer of TDP-43 increases, and mislocalized TDP-43 accumulates in the cytoplasm, which could contribute to neuronal dysfunction and toxicity (Van Deerlin et al., 2008). Cytoplasmic aggregation of TDP-43 in affected neurons is a pathological hallmark of many neurodegenerative diseases, including amyotrophic lateral sclerosis (ALS),

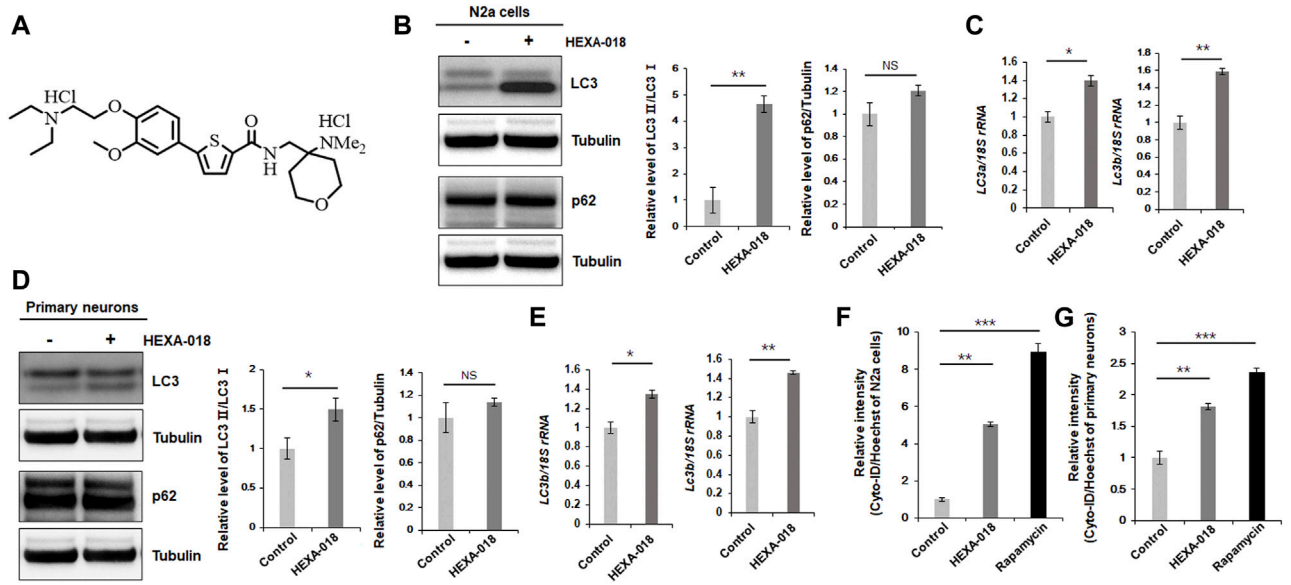

FIGURE 1 | HEXA-018 induces autophagy in neuronal cells. **(A)** Chemical structure of HEXA-018. **(B,C)** N2a cells were treated with HEXA-018 (5 μM) for 24 h. **(B)** Western blot analysis was performed to determine the amount of LC3-I/II or p62 protein. HEXA-018 significantly increased the LC3-II levels in N2a cells but did not affect total p62 protein levels. Quantification of the immunoblots was performed from 3 independent experiments. $^{**}p < 0.005$; *n. s.*, not significant (unpaired Student's *t*-test). **(C)** RT-PCR for *lc3a* and *lc3b* mRNA expression in HEXA-018-treated N2a cells. The quantification of *lc3a* and *lc3b* mRNA transcript levels is presented as the mean ± SEM from 3 independent real-time RT-PCR experiments. *18S rRNA* was used for normalization. $^{*}p < 0.05$; $^{**}p < 0.005$ (unpaired Student's *t*-test). **(D,E)** Primary neurons were treated with HEXA-018 (0.5 μM) for 24 h. **(D)** Western blot analysis was performed to determine LC3-I/II or p62 protein expression. Quantification of the immunoblots was performed from 3 independent experiments. $^{*}p < 0.05$; *n. s.,* not significant (unpaired Student's *t*-test). **(E)** RT-PCR for *lc3a* and *lc3b* mRNA expression in HEXA-018-treated primary neurons. The quantification of *lc3a* and *lc3b* mRNA transcription levels are presented as the mean ± SEM from 3 independent real-time RT-PCR experiments. *18S rRNA* was used for normalization. $^{*}p < 0.05$; $^{**}p < 0.005$ (unpaired Student's *t*-test). **(F,G)** N2a cells **(F)** and primary neurons **(G)** were treated with HEXA-018 (5 μM/0.5 μM) for 24 h. Rapamycin (200 nM) was used as a positive control. Cyto-ID fluorescence analysis was performed thereafter. The level of Cyto-ID fluorescence was significantly increased in the HEXA-018-treated cells, which indicates autophagic activation. The fluorescence signal intensity of Cyto-ID was normalized to that of Hoechst 33342. Data are presented as the mean ± SD from 3 independent experiments. $^{**}p < 0.005$; $^{***}p < 0.001$ (one-way ANOVA with Tukey's multiple comparison test).

frontotemporal dementia (FTD), Alzheimer's disease (AD), and limbic predominant age-related TDP-43 encephalopathy (LATE) (Huang et al., 2020).

Previous studies have shown that gain of function or overexpression of TDP-43 in neuronal cells is sufficient to cause neurodegeneration. Mislocalized and accumulated TDP-43 induces mitochondrial dysfunction and reactive oxidative species (ROS) production (Wang et al., 2019). Furthermore, oxidative stress exacerbates the cytotoxicity of TDP-43 (Prasad et al., 2019). Another mechanism of TDP-43-induced neurotoxicity is impairment of the ubiquitin proteasome system (UPS). The UPS is one of the major intracellular protein quality control systems, and it is a critical regulator of misfolded and aggregation-prone proteins, which have been found to accumulate in neurodegenerative diseases. Recent studies have shown that UPS impairment is implicated in the neurotoxicity of TDP-43 in mammalian cell models and *Drosophila* (Lee et al., 2020a; Lee et al., 2020b). In addition, TDP-43 toxicity is significantly suppressed by ALP activation (Barmada et al., 2014; Lee et al., 2020a). Moreover, some genes associated with TDP-43 proteinopathy, such as *SQSTM1*, valosin-containing protein (*VCP*), optineurin (*OPTN*), and TANK binding kinase 1 (*TBK1*), are closely linked to the ALP (de Boer et al., 2020). Therefore, modulation of the ALP could be a potential therapeutic approach for TDP-43 proteinopathy.

N-((4-(Dimethylamino)tetrahydro-2H-pyran-4-yl) methyl)-5-(4-(2-diethylamino)ethoxy-3-methoxyphenyl) thiophene-2-carboxamide hydrochloride (also called HEXA-018, **Figure 1A**) is a newly developed inducer of autophagy, but its effect in neuronal cells has not been studied (Han and Lee, 2020). In this study, we found that HEXA-018, a novel compound containing a catechol derivative structure, activated the autophagic pathway via an mTOR-independent pathway and mitigated neuronal toxicity induced by oxidative stress and ubiquitin proteasome system (UPS) impairment. Both oxidative stress and UPS impairment are major pathological features of TDP-43 proteinopathy. Moreover, HEXA-018 treatment reduced TDP-43-induced neurotoxicity in cells and *Drosophila*.

Therefore, we expect that the novel catechol derivative compound HEXA-018 might be a drug candidate for neurodegenerative diseases associated with TDP-43 accumulation.

2 MATERIALS AND METHODS

2.1 Reagents and Antibodies

The following reagents were purchased from the indicated providers: dimethyl sulfoxide (DMSO; Sigma, D8418), MG132 (Calbiochem/Merck-Millipore, 474791), rotenone (Sigma, R8875), rapamycin (InvivoGen, tlrl-rap), ULK1 inhibitor (MRT68921; Selleckchem, S7949), and mifepristone (RU-486; Sigma, M8046). We also received HEXA-018 from Hexa Pharmatec., which is not commercially available (Patent number, WO 2020/017878 A1).

The following antibodies were used for immunoblotting: GFP (Clontech, 632380), p62 (Sigma, P0067), LC3 (MBL, PM036), phospho-mTOR Ser2448 (Cell Signaling, 5536), phospho-mTOR Ser2481 (Cell Signaling, 2974), mTOR (Cell Signaling, 2983), phospho-ULK1 Ser757 (Cell Signaling, 6888), ULK1 (Abcam, ab128859), phospho-AMPKα1 Thr183 + AMPKα2 Thr172 (GeneTex, GTX130429), AMPKα1/α2 (GeneTex, GTX50863), Ref2(P) (Abcam, ab178440), HRP-conjugated anti-alpha-tubulin (Cell Signaling, 9099), HRP-conjugated rabbit IgG (Santa Cruz Biotechnology, sc-2004), and HRP-conjugated mouse IgG (Santa Cruz Biotechnology, sc-2005).

2.2 Cell Lines

The Neuro-2a (ATCC, N2a) mouse neuroblastoma cell line was maintained in Dulbecco's modified Eagle's medium (DMEM; Gibco, 11995-065) supplemented with 10% heat-inactivated fetal bovine serum (FBS; Gibco, 16000-044) and 50 μg/ml penicillin-streptomycin (Gibco, 15140-122). Cells were grown at 37°C in a humidified atmosphere containing 5% CO_2. All experiments were performed using cells from passages 5 to 15.

2.3 Mouse Cortical Neuron Cultures

Primary cultures of cerebral cortical neurons were prepared from 16-days embryonic mice as described previously (Enokido et al., 1992; Araki et al., 2000). Briefly, mouse embryos were decapitated, and the brains were rapidly removed and placed in a culture dish containing HBSS (Gibco, 14170-112). Cortices were isolated, transferred to a conical tube and washed twice in HBSS. Cortical tissues were enzymatically digested by 20 units/ml papain (Worthington Biochemical Corporation, LK003150) and 0.005% DNase I for 30 min at 37°C. The tissues were mechanically dissociated by gently pipetting up and down. The cortical cells were centrifuged at 800 × *g* for 10 min at room temperature. Then, the dissociated cells were seeded on plates coated with poly-D-lysine (Sigma-Aldrich, P7405) in neurobasal media containing 2 mM glutamine (Gibco, 25030-081), N2 supplement (Gibco, 17502-048), B27 supplement (Gibco, 17504-044), and penicillin-streptomycin. The culture media were changed initially after 5 days and then every 3 days. Animals used in the current research were acquired and cared for in accordance with the guidelines published in the National Institutes of Health *Guide for the Care and Use of Laboratory Animals*.

2.4 Cytotoxicity Tests

N2a cells (3×10^4 cells/ml) or primary neurons (8×10^4 cells/ml) were grown in 96-well plates and treated with MG132/rotenone or drugs as indicated for 24 h. DMSO was used as a negative control. For measurement of cytotoxicity, Cell Counting Kit-8 (CCK-8; Enzo Life Science, ALX-850-039-KI02) was used according to the manufacturer's instructions. Briefly, 10 μL of CCK-8 reagent was added to each well, and the plate was incubated at 37°C for 2 h. The absorbance at 450 nm was measured by using a microplate reader (Tecan). Cell viability is expressed as a percentage of the control. All experiments were performed in triplicate.

2.5 Flow Cytometric Analysis

N2a (30×10^4 cells/ml) or primary neurons (80×10^4 cells/ml) were detached with trypsin-EDTA and washed twice with cold PBS. The cells were then resuspended in 250 μL of binding buffer (10 mM HEPES, 140 mM NaCl, 2.5 mM $CaCl_2$ (pH 7.4)) and incubated with 3 μL of FITC-conjugated Annexin V (apoptotic cells; BD Biosciences) according to the manufacturer's guide. Then, cells were gently vortexed and incubated for 15 min at room temperature in the dark. After adding Propidium iodide (necrotic cells; 20 μg/ml), flow cytometry was performed within 1 h using MoFlo Astrios (Beckman Coulter).

2.6 Quantitative RT-PCR

N2a cells (20×10^4 cells/ml) or primary neurons (40×10^4 cells/ml) were treated with drug for 8 h, and RNA was extracted from cells by using TRIzol plus RNA Purification Kit (Invitrogen, 12183-555) according to the manufacturer's instructions. cDNA synthesis was performed at 37°C for 120 min with 100 ng of RNA using a High Capacity cDNA Reverse Transcription kit (Applied Biosystems, 4368814). Quantitative RT-PCR was performed using the one-step SYBR® PrimeScript™ RT-PCR kit (Takara Bio Inc, RR420A) according to the manufacturer's instructions, followed by detection using an Applied Biosystems 7500 Real-Time PCR system (Applied Biosystems). *18S rRNA* was used as an internal control. The $2^{-\Delta\Delta Ct}$ method was used to calculate relative changes in gene expression, as determined by real time PCR experiments (Livak and Schmittgen, 2001).

2.7 Immunoblot Analysis

Cells or 20 adult fly heads were homogenized in Cell Lysis Buffer (Cell Signaling Technology, 9803) with protease and phosphatase inhibitor cocktails. The protein concentration of the cell or fly head lysates was determined by a BCA protein assay (Thermo Fisher, 23225). Next, the protein extracts were mixed with 4x Bolt LDS Sample Buffer (Invitrogen) and 10x

Bolt Sample Reducing Agent (Invitrogen) and then boiled at 95°C for 5 min. An equal amount of protein from each sample was separated on Bolt 4–12% Bis-Tris gels (Invitrogen, NW04120BOX) or NuPAGE 3–8% Tris-Acetate gels (Invitrogen, EA0378BOX) and transferred to a polyvinylidene difluoride membrane (PVDF; Invitrogen, LC2005). After the membrane was blocked with 5% skim milk in TBS with 0.025% Tween 20, it was probed with antibodies as indicated and detected with an ECL Prime Kit (GE Healthcare, RPN2232). Samples from three independent experiments were used, and the relative expression levels were determined using a Fusion-FX system (Viber Lourmat).

2.8 Cyto-ID Autophagy Analysis

N2a cells (3×10^4 cells/ml) or primary neurons (8×10^4 cells/ml) were treated with rapamycin or drugs for 24 h, and the cells were assessed using the Cyto-I Green Autophagy Kit (Enzo Life Science, ENZ-51031-K200) according to the manufacturer's instructions. Briefly, Cyto-ID dye or Hoechst 33342 was added to each well of a 96-well plate. Then, the plate was incubated at 37°C for 30 min. Cells were washed in 1x Assay Buffer with 2% FBS. The fluorescence signals (excitation/emission 480/530 nm and 340/480 nm) were measured by using a FlexStation 3 Microplate Reader (Molecular Devices). The ratios of the 480/530 signals over the 340/480 signals were calculated for each sample, and the Cyto-ID fluorescence is represented as a percentage of the control. All experiments were performed in triplicate.

2.9 Autophagy Assessment

Instead of pellet embedding, flat embedding was used for autophagy assessment in cells (Ylä-Anttila et al., 2009). Without cell harvest, cells on coverslips were fixed at 4°C for 1 h in 2.5% glutaraldehyde and 2% paraformaldehyde in 0.1 M sodium cacodylate buffer (pH 7.4) and postfixed with 2% reduced osmium tetroxide (3% potassium ferrocyanide combined with an equal volume of 4% osmium tetroxide) for 30 min at 4°C. Then, the cells were stained with thiocarbohydrazide (TCH) and 2% osmium tetroxide in distilled water and *en bloc* in 1% uranyl acetate. The cells were then dehydrated via a graded ethanol series and embedded with an EMBed-812 Embedding Kit (EMS). The embedded samples were incubated for 48 h in 60°C. Resin blocks were incubated for 48 h at 60°C. The embedded samples were sectioned (60 nm) with an ultramicrotome (Leica), and the sections were then viewed on a Tecnai 20 transmission electron microscope (TEM; Thermo Fisher) at 120 kV. Images were captured with a US1000X-P camera 200. Stitching images were acquired using Photomontage software (Thermo Fisher). The numbers of autophagosomes and autolysosomes were counted in cells of almost the same size using ImageJ software (National Institutes of Health).

2.10 Mitochondrial Activity Assay

For assessment of neuronal mitochondrial dysfunction, N2a cells (4×10^4 cells/ml) and primary neurons (8×10^4 cells/ml) were seeded in XF24-well culture plates (Seahorse Bioscience). The cells were washed twice with XF Base Medium supplemented with 2 mM L-glutamine, 10 mM D-glucose and 1 mM sodium pyruvate (pH 7.4) and incubated at 37°C in a non-CO_2 incubator for 1 h. Mitochondrial dysfunction was evaluated using the XF Cell Mito Stress Test *Kit* (Seahorse Bioscience) according to the manufacturer's instructions, followed by measurement using an XF24 Extracellular Flux Analyzer (Seahorse Bioscience). The 24-well utility plate was hydrated, treated with 2 μM oligomycin, 2 μM carbonyl cyanide 4-(trifluoromethoxy) phenylhydrazone (FCCP), and 0.5 μM antimycin A + rotenone, and was then used to calibrate the analyzer. The basal oxygen consumption rate (OCR), ATP production, maximum reserve, and respiratory capacity were calculated as previously described (Dranka et al., 2011), with averages calculated from 4 wells per condition in each individual experiment. The OCR was normalized to the total protein concentration (OD). After the Seahorse analysis, the plate was centrifuged at 280 × *g* for 5 min. The media were aspirated, and the plate was washed twice with PBS. The cells were lysed in RIPA buffer. Protein concentrations in cell lysates were determined using a BCA assay kit.

2.11 IncuCyte Live Cell Imaging

N2a cells (2.5×10^3 cells/ml) were plated in 96-well plates and transfected with *Gfp (pCMV-AC-Gfp)* and human *TDP-43 (pCMV-AC-TDP-43-Gfp)* cDNA by using Lipofectamine 3000 reagent (Invitrogen, L3000-015) according to the manufacturer's instructions. Six hours after transfection, the cells were treated with HEXA-018 (5 μM) and subsequently treated with IncuCyte Red Cytotoxicity Reagent (50 nM; EssenBioscience, 4632). Images were collected with an IncuCyte Zoom System and a ×20 objective lens at 6 h intervals. Cell toxicity was analyzed with IncuCyte ZOOM software by counting the green and red double-positive cells.

2.12 Fly Strains

Drosophila stocks were maintained on standard cornmeal agar media at 24°C unless otherwise noted. UAS-TARDBP was described previously (Kim et al., 2014). All other stocks were from The Bloomington Stock Center.

2.13 Climbing and Lifespan Assays

Adult males (0–1 day old) were separated and transferred into experimental vials containing fly medium mixed with or without RU-486 at a density of 25 (for lifespan) or 25 (for climbing assay) flies per vial ($n > 100$). The number of dead flies was recorded daily, and the flies were transferred to fresh media every other day. Adult locomotor function was assessed by a previously described method (Feany and Bender, 2000), with 100 flies per genotype per time point in all experiments. Experiments were repeated twice to ensure consistent results.

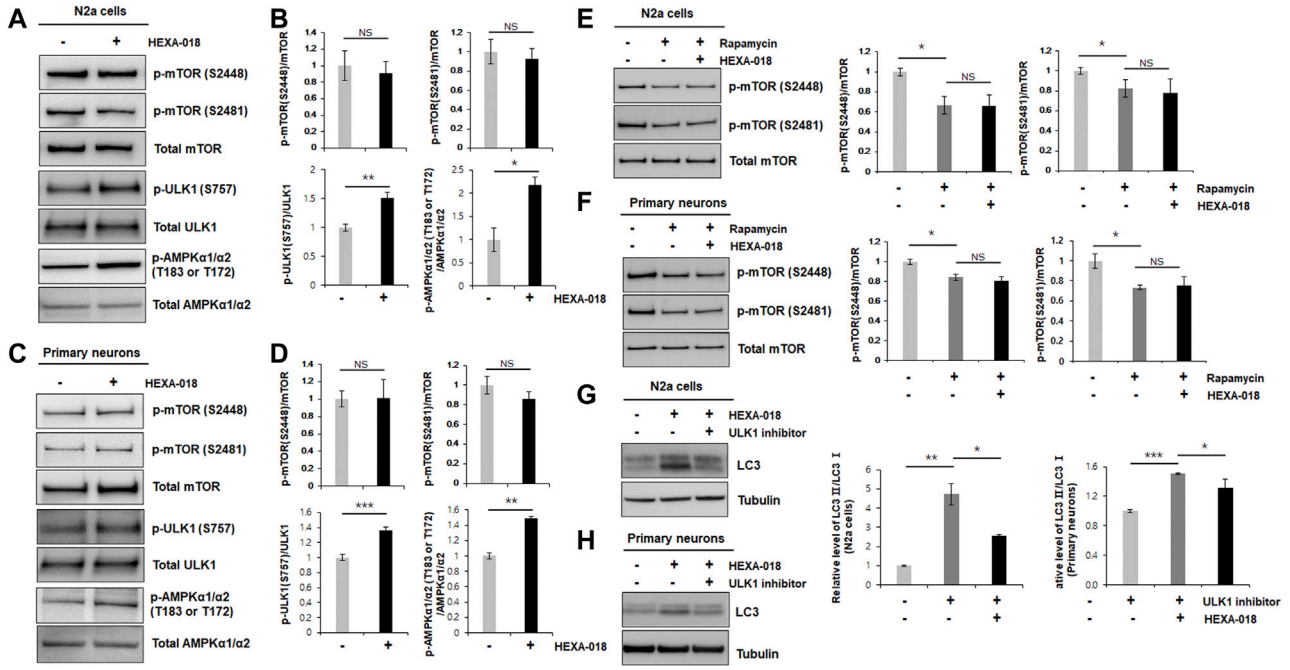

FIGURE 2 | HEXA-018 is an mTOR-independent activator of the ALP. **(A,B)** N2a cells were treated with HEXA-018 (5 μM) for 24 h, and then, the cells were harvested for total protein extraction. Western blot analysis was performed to determine phospho-mTOR (S2481 or S2488), total mTOR, phospho-ULK1 (S757), ULK1, p-AMPKα1/α2 (T183 or T172), or AMPKα1/α2 protein expression. Quantification of the immunoblots was performed from 3 independent experiments. Treatment with HEXA-018 did not affect phospho-mTOR levels but phospho-ULK1 and phospho-AMPK protein levels was significantly increased in N2a cells. $^{*}p < 0.05$; $^{**}p < 0.005$; *n. s.*, not significant (unpaired Student's *t*-test). **(C,D)** Primary neurons were treated with HEXA-018 (0.5 μM) for 24 h, and then, the cells were harvested for total protein extraction. Western blot analysis was performed to determine phospho-mTOR (S2481 or S2488), total mTOR, phospho-ULK1 (S757), ULK1, p-AMPKα1/α2 (T183 or T172), or AMPKα1/α2 protein expression. $^{**}p < 0.005$; $^{***}p < 0.001$; *n. s.*, not significant (unpaired Student's *t*-test). **(E,F)** N2a cells and primary neurons were pretreated with HEXA-018 (5 μM/0.5 μM) for 30 min and subsequently treated with rapamycin (200 nM) for 24 h, and then, the cells were harvested for total protein extraction. Western blot analysis was performed to determine phospho-mTOR (S2481 or S2488) or total mTOR protein expression. HEXA-018 treatment was not significantly changed following rapamycin-decreased phospho-mTOR levels in N2a cells and primary neurons. Data are presented as the mean ± SD of 3 independent experiments. $^{*}p < 0.05$; *n. s.*, not significants (one-way ANOVA with Tukey's multiple comparison test). **(G,H)** N2a cells were pretreated with HEXA-018 (5 μM) for 30 min and subsequently treated with ULK1 inhibitor (200 nM) for 24 h, and then, the cells were harvested for total protein extraction. Western blot analysis was performed to determine LC3-I/II protein expression. HEXA-018 increased LC3-II level was significantly decreased by ULK1 inhibition in N2a cells. Data are presented as the mean ± SD of 3 independent experiments. $^{*}p < 0.05$; $^{**}p < 0.005$ (one-way ANOVA with Tukey's multiple comparison test). **(H)** Primary neurons were pretreated with HEXA-018 (0.5 μM) for 30 min and subsequently treated with ULK1 inhibitor (20 nM) for 24 h, and then, the cells were harvested for total protein extraction. Western blot analysis was performed to determine LC3-I/II protein expression. $^{*}p < 0.05$; $^{***}p < 0.001$ (one-way ANOVA with Tukey's multiple comparison test).

3 RESULTS

3.1 HEXA-018 Induces Autophagy in an mTOR-independent Manner in Neuronal Cells

To investigate whether HEXA-018 activates the ALP, we examined the microtubule-associated protein light chain 3 (LC3-I/II) ratios in N2a cells following treatment with HEXA-018. The increase in the LC3-I/II ratio is a typical indicator of autophagic activation. We found that HEXA-018 treatment significantly increased the LC3-I/II ratio in N2a cells (**Figure 1B**). Another features of ALP activation are the reduction of p62 protein. However, HEXA-018 did not affect the protein level of p62 in neuronal cells (**Figure 1B**). We also observed that HEXA-018 treatment upregulated the transcription of *lc3a* and *lc3b* mRNA in N2a cells and primary neurons (**Figure 1C**). We confirmed these results in primary neurons treated with HEXA-018 (**Figures 2D,E**). For further confirmation of ALP activation, we used Cyto-ID fluorescence dye. Cyto-ID fluorescence dye specifically labels all types of autophagic vacuoles, including amphisomes or autolysosomes (Guo et al., 2015). Thus, the fluorescence intensities of Cyto-ID-stained cells indicate the level of ALP activation. Rapamycin is a well-known activator of the ALP (Thellung et al., 2019), so the fluorescence intensity of Cyto-ID-stained N2a cells and mouse primary neurons was strongly elevated by rapamycin treatment (**Figures 1F,G**). Consistent with these results, we observed that the HEXA-018-treated cells showed increased Cyto-ID fluorescence intensities in both N2a cells and primary neurons (**Figures 1F,G**). These results suggest that HEXA-018 activates the ALP in N2a cells and primary neurons.

The most well-studied regulatory mechanism of the ALP is the mTOR (mechanistic target of rapamycin) pathway. To determine

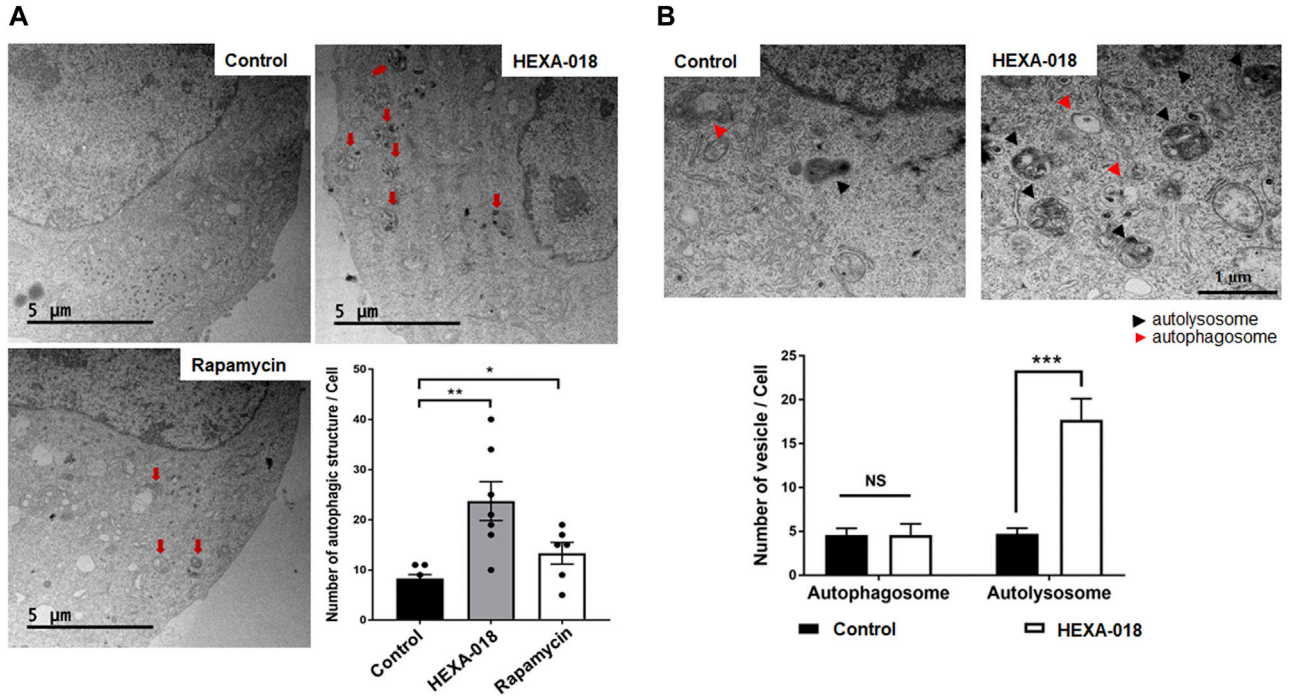

FIGURE 3 | HEXA-018 increases the formation of autolysosomes in neuronal cells. **(A)** Representative TEM images showing autophagy in N2a cells and Hexa-018- or rapamycin-treated cells. N2a cells were treated with HEXA-018 (5 μM) for 24 h and then analyzed. Rapamycin (200 nM) was used as a positive control. Electron microscopy images show that the number of autophagic structures and vesicles was significantly increased by HEXA-018 in N2a cells. The red arrows indicate autophagic structures. Quantification of the number of autophagic structures and vesicles per cell. *$p < 0.05$; **$p < 0.005$ (one-way ANOVA with Tukey's multiple comparison test). **(B)** The arrowheads indicate autophagosomes (red) and autolysosomes (black). Quantification of the number of autophagosomes and autolysosomes from the images ($n = 7$) is shown in the graph. The bar graph shows the mean ± SEM of the representative groups. ***$p < 0.001$; *n. s.*, not significant (one-way ANOVA with Tukey's multiple comparison test).

whether HEXA-018 induces autophagy via modulation of the mTOR pathway, we measured the phosphorylation level of mTOR in the HEXA-018-treated N2a cells and primary neurons. The phosphorylation of mTOR (Ser2481 and Ser2448) is critical for mTOR activation. However, the phosphorylation levels of mTOR were not affected by HEXA-018 treatment in N2a cells (**Figures 2A,B**). We confirmed these results in primary neurons treated with HEXA-018 (**Figures 2C,D**). These results suggest that HEXA-018 activates the ALP in an mTOR-independent manner. Previous studies demonstrated that the phosphorylation of ULK1 (Ser757) and AMPK1 (Thr183 and Thr172) is the major contributor of ALP activation in mTOR dependent and independent ALP (Jung et al., 2010; Roach, 2011; Din et al., 2012). We analyzed phosphorylation levels of ULK1 and AMPK1 in N2a cells and primary neurons treated with HEXA-018. We showed that HEXA-018 clearly increased the phosphorylation levels of ULK1 and AMPK1 (**Figures 2A–D**). We used rapamycin as a mTOR-dependent activator of autophagy. We found that the rapamycin treatment significantly decreased the mTOR phosphorylation, but HEXA-018 treatment did not change mTOR phosphorylation in rapamycin-treated neuronal cells (**Figures 2E,F**). Consistent with previous findings, we observed that rapamycin decreased the level of p62 protein in N2a cells and primary neurons (**Supplementary Figures 1A,B**). These results suggest that HEXA-018 significantly increased the ULK1 and AMPK1 phosphorylation levels, but mTOR phosphorylation levels were not affected by HEXA-018 treatment. In addition, HEXA-018 induced autophagy activation was significantly decreased by ULK1 inhibition in N2a cells and primary neurons (**Figures 2G,H**). Taken together, HEXA-018 activates the ALP via the ULK1-AMPK pathway in an mTOR-independent manner.

3.2 HEXA-018 Facilitates Autolysosome Formation in Neuronal Cells

Electron microscopy is one of the most precise ways to detect and quantify autophagic structures. To investigate whether HEXA-018 increases the number of autophagic vacuoles, we analyzed autophagic structures using transmission electron microscopy (TEM). With autophagy initiation, the phagophore fully surrounds its cargo and fuses to form the double-membrane autophagosome. After fusion with the lysosome, strong electron density represented as the criterion for identification of autolysosomes due to degradation of materials. Various autophagic structures, including autophagosomes and autolysosomes, were observed in N2a cells. The red arrows in **Figure 3A** indicate autophagic structures. The number of autophagic vacuoles was substantially increased after HEXA-

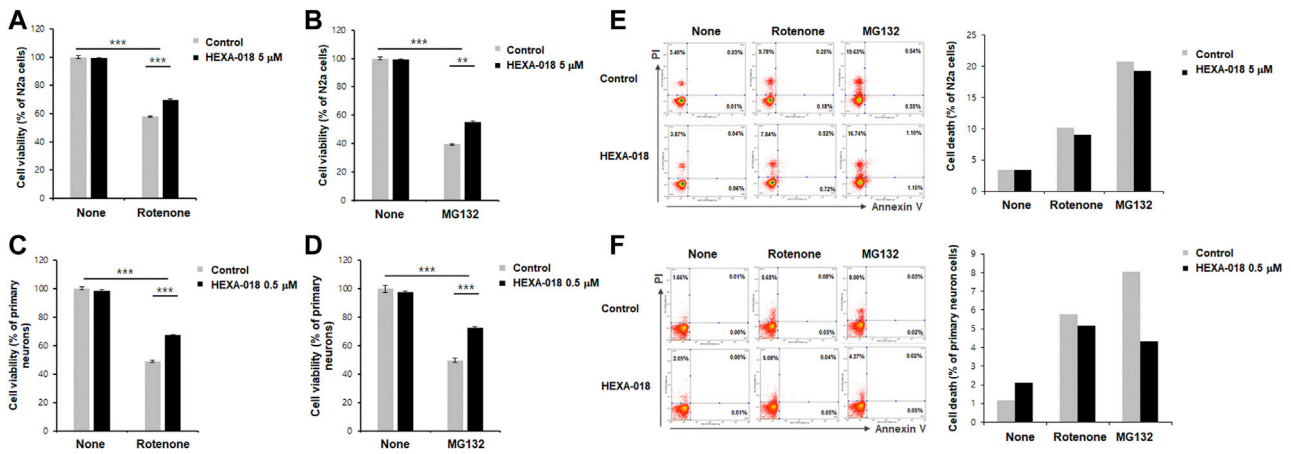

FIGURE 4 | HEXA-018 attenuates MG132-and rotenone-induced toxicity in neuronal cells. **(A,B)** N2a cells were pretreated with HEXA-018 (5 μM) for 30 min and subsequently treated with MG132 (5 μM, **(A)**) or rotenone (10 μM, **(B)**) for 24 h. CCK-8 analysis was performed thereafter. HEXA-018 significantly reduced MG132-or rotenone-induced neuronal toxicity in N2a cells. Data are presented as the mean ± SD of 3 independent experiments. $^{**}p < 0.005$; $^{***}p < 0.001$ (one-way ANOVA with Tukey's multiple comparison test). **(C,D)** Primary neurons were pretreated with HEXA-018 (0.5 μM) for 30 min and subsequently treated with MG132 (5 μM, **(C)**) or rotenone (10 μM, **(D)**) for 24 h. MG132-or rotenone-induced neuronal toxicity was also reduced by HEXA-018 treatment in primary neurons. CCK-8 analysis was performed thereafter. 5 μM or 0.5 μM were the maximum non-cytotoxic concentrations of HEXA-018 in N2a cells and primary neurons, respectively. HEXA-018 concentration was then assessed after 24 h treatment using the each highest concentrations showing no toxicity in N2a cells and primary neurons. Data are presented as the mean ± SD of 3 independent experiments. $^{***}p < 0.001$ (one-way ANOVA with Tukey's multiple comparison test). **(E,F)** N2a cells and primary neurons were pretreated with HEXA-018 (5/0.5 μM) for 30 min and subsequently treated with MG132 (5 μM) or rotenone (10 μM) for 24 h. FACS analysis was additional performed to assess cell viability after HEXA-018 treatment against neurotoxic drugs (10,000 cells per each condition). Representative scatter plots show that annexin V^-/PI^+ (upper left quadrant, necrosis) and annexin V^+/PI^+ (upper right quadrant, late apoptosis/necrosis) were significantly increased by MG132 or rotenone, but annexin V^+/PI^- (lower right quadrant, early apoptosis) was not significantly changed in N2a cells and primary neurons. The proportion of cells residing in each quadrant is represented as a percentage. The percentage of cell death (apoptosis and necrosis) in the flow cytometric analysis is shown ***(right)***.

018 or rapamycin treatment in N2a cells (**Figure 3A**). To investigate the regulatory role of HEXA-018 in autolysosome formation, we fluorescent puncta assay with DsRed-LC3-GFP, which is a well-established method to monitor autophagy flux (Sheen et al., 2011). This assay uses the characteristics that the GFP fluorescence is lost but DsRed fluorescence is stable in the lysosomal acidic environment. The autophagic vesicles, both autophagosome (yellow puncta) and autolysosome (red puncta), were significantly increased by HEXA-018 and rapamycin treatment in N2a cells (**Supplementary Figure S2**). We then further assessed the numbers of autophagosomes and autolysosomes in the control and HEXA-018-treated cells using TEM (**Figure 3B**). The number of autophagosomes was not significantly changed, but the number of autolysosomes was significantly increased in the HEXA-018-treated cells compared with the control cells (**Figure 3B**). These results strongly suggest that HEXA-018 activates the ALP. Considering that autolysosome formation was significantly increased by HEXA-018 treatment, HEXA-018 appears to promote the fusion of autophagosomes and lysosomes.

3.3 HEXA-018 Ameliorates UPS Impairment and ROS-Induced Neurotoxicity

MG132 (proteasome inhibitor) and rotenone (inducer of reactive oxygen species (ROS)) are currently accepted as neurotoxicity-inducing factors. Previous studies have shown that ALP activation mitigates MG132-or rotenone-induced neurotoxicity. Thus, we investigated the protective effect of HEXA-018 in MG132-or rotenone-treated N2a cells and primary neurons. HEXA-018 significantly attenuated the cytotoxicity of MG132 and rotenone in N2a cells (**Figures 4A,B**; **Supplementary Figures 3A,B**) and primary neurons (**Figures 4C,D**; **Supplementary Figures 3C,D**). We also confirmed these results using a different experimental approach based on flow cytometry using Annexin V and PI staining. We found that HEXA-018 attenuated the rotenone/MG132-induced necrotic cell death in N2a (**Figure 4E**; **Supplementary Figure 4A**) and primary neurons (**Figure 4F**; **Supplementary Figure 4B**). These results indicate that HEXA-018 mitigates UPS impairment and ROS-induced neurotoxicity.

Recent studies have suggested that overproduction of ROS leads to mitochondrial damage and that mitochondrial dysfunction is a key pathological feature of many neurodegenerative diseases, such as ALS, AD, and PD. Accumulating evidence suggests that autophagy activation suppresses rotenone-induced neurotoxicity such as mitochondrial dysfunction and oxidative stress in cell and mice (Chen et al., 2007; Lin et al., 2012; Xiong et al., 2013). Moreover, rotenone-induced α-synuclein aggregates are significantly decreased by rapamycin treatment (Yu et al., 2009). Thus, we next investigated whether HEXA-018 suppresses rotenone-induced mitochondrial dysfunction in neuronal cells. N2a cells and primary neurons were treated with HEXA-018 and rotenone, and then, we measured the cellular oxygen consumption rate (OCR) using the Seahorse

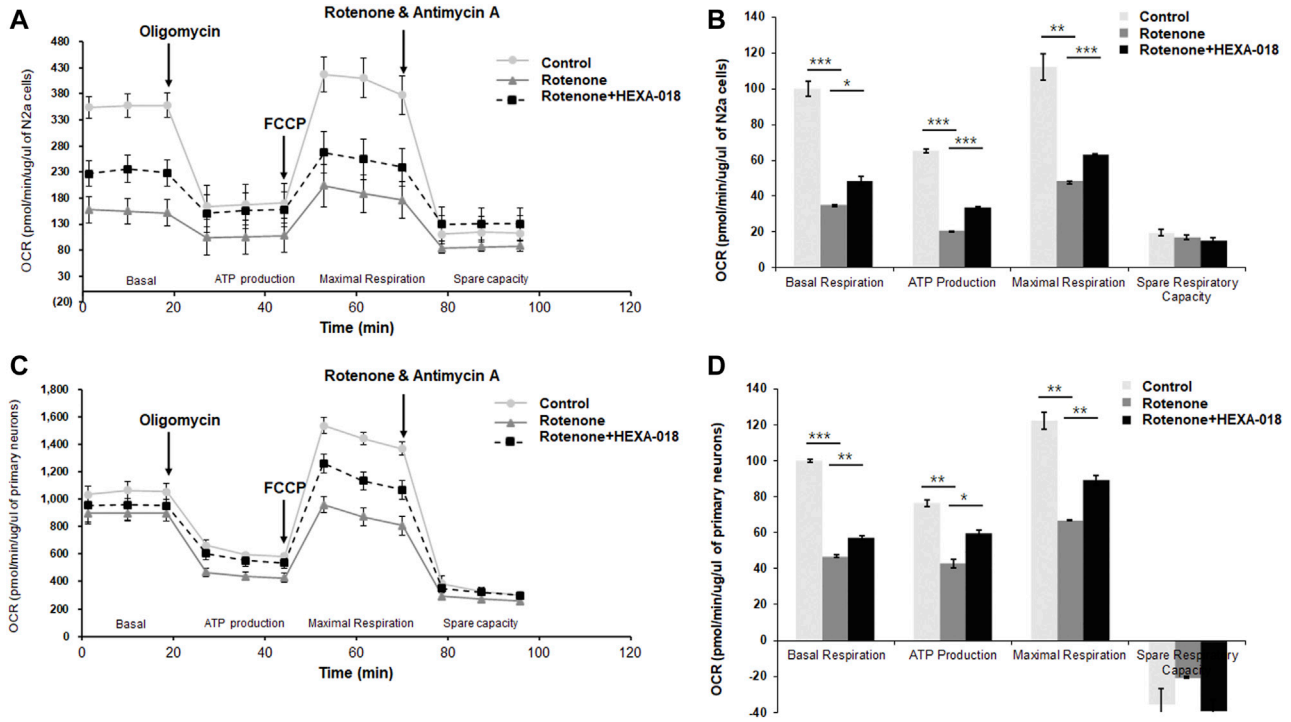

FIGURE 5 | HEXA-018 mitigates rotenone-induced mitochondrial dysfunction in neuronal cells. **(A,B)** N2a cells were pretreated with HEXA-018 (5 μM) for 30 min and subsequently treated with rotenone (10 μM) for 24 h and then analyzed. **(A)** Mitochondrial function was analyzed in N2a cells by detecting the basal OCR, ATP production, maximum reserve, and respiratory capacity with a Seahorse XF analyzer. The OCR was normalized to the total protein concentration. **(B)** Quantification of the OCR, ATP production, maximum reserve, and respiratory capacity as percentages of the basal values. Data are presented as the mean ± SD. $^{*}p < 0.05$; $^{**}p < 0.005$; $^{***}p < 0.001$ (two-way ANOVA with Tukey's multiple comparison test). **(C,D)** Primary neurons were pretreated with HEXA-018 (0.5 μM) for 30 min and subsequently treated with rotenone (10 μM) for 24 h and then analyzed. **(C)** Mitochondrial function was analyzed in primary neurons by detecting the basal OCR, ATP production, maximum reserve, and respiratory capacity with a Seahorse XF analyzer. The OCR was normalized to the total protein concentration. **(D)** Quantification of the OCR, ATP production, maximum reserve, and respiratory capacity as percentages of the basal values. Data are presented as the mean ± SD. $^{*}p < 0.05$; $^{**}p < 0.005$; $^{***}p < 0.001$ (two-way ANOVA with Tukey's multiple comparison test).

XF24 Extracellular Flux Analyzer and a mitochondrial stress test kit. OCR is an indicator of mitochondrial respiration, including basal respiration, ATP production, maximal respiration, and spare respiratory capacity. Analysis of mitochondrial respiratory parameters was performed by using oligomycin, FCCP, and antimycin A + rotenone. Notably, we found that the basal respiration, ATP production, and maximal respiratory parameters were markedly decreased in the rotenone-treated cells compared to the control cells. The rotenone-induced reductions in basal respiration, ATP production, and maximal respiration parameters were strongly ameliorated by HEXA-018 treatment, but the spare respiratory capacity was not altered (**Figures 5A–D**). Taken together, these findings suggest that HEXA-018 attenuates rotenone-induced mitochondrial dysfunction in neuronal cells.

3.4 HEXA-018 Suppresses TDP-43-Induced Toxicity in Mammalian Cells and Flies

Previous studies have indicated that overexpression of TDP-43 cause neuronal toxicity in mammalian and *Drosophila* neurons. In addition, oxidative stress and UPS impairment are key pathological features in TDP-43 proteinopathy. All these data suggest that HEXA-018 might attenuate TDP-43-induced neurotoxicity. Thus, we analyzed TDP-43 toxicity using a live cell imaging system (IncuCyte). GFP- or GFP-tagged TDP-43-expressing N2a cells were treated with HEXA-018, and the cell death of the GFP-expressing cells was monitored. As expected, TDP-43-induced neuronal toxicity was significantly suppressed by HEXA-018 treatment (**Figure 6A**).

We also assessed ALP activity in a *Drosophila in vivo* model. To evaluate ALP function, we expressed the Atg8a-GFP reporter in the fly nervous system. The ratio of free GFP to Atg8a-GFP correlates with ALP activity because globular GFP protein is much more resistant to acidic lysosomal conditions than Atg8a. By adopting this method, we examined the free GFP/Atg8a-GFP ratio in the fly model. We found that the ratio was significantly higher in the HEXA-018-treated flies than in the control flies (**Figure 6B**). Moreover, we found that Ref2(P) (*Drosophila* homologue of p62) protein level was not changed in Atg8a-GFP flies (**Figure 6C**). These data suggest that HEXA-018 activates the ALP in fly neurons. Given the strong *in vitro* evidence that HEXA-018 attenuates TDP-43-induced toxicity in neuronal cells, we next examined whether HEXA-018

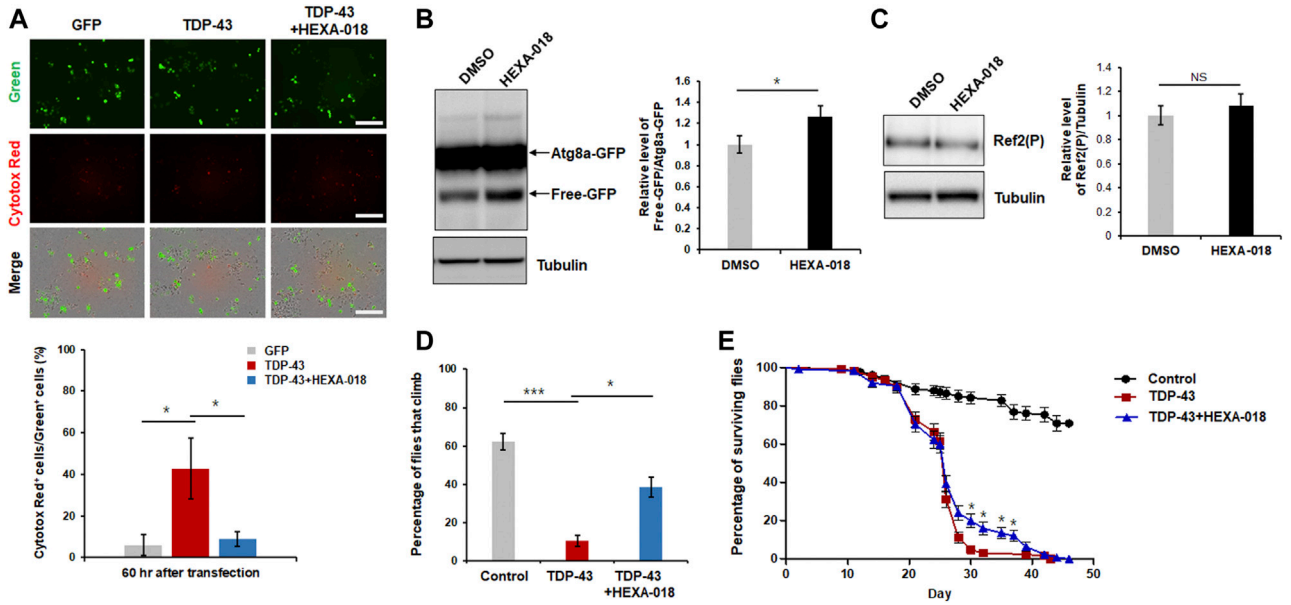

FIGURE 6 | HEXA-018 suppresses TDP-43-induced toxicity in neuronal cells and *Drosophila*. **(A)** N2a cells were transfected with the GFP or TDP-43-GFP expression construct for 6 h and subsequently treated with HEXA-018 (5 μM) for 54 h. Dying neuronal cells, as indicated by red fluorescence, were imaged every 3 h and quantified by counting double-fluorescent (green and red) cells using the IncuCyte system. HEXA-018 significantly reduced TDP-43-induced neuronal toxicity. Data are presented as the mean ± SD of 3 independent experiments. $^{*}p < 0.05$ (one-way ANOVA with Tukey's multiple comparison test). Scale bar, 200 μm. **(B)** HEXA-018 treatment increased ALP activation. Western blot analysis of Atg8a-GFP and free GFP protein levels in the head lysates of flies. Quantification of immunoblots was performed from 3 independent experiments, and protein levels were normalized to that of tubulin. Data are presented as the mean ± SD. Genotypes: *elavGS, UAS-Atg8a-GFP/+*. $^{*}p < 0.05$ (unpaired Student's *t*-test). **(C)** Western blot analysis of Ref2(P) protein levels in the head lysates of Atg8a-GFP flies. Quantification of immunoblots was performed from 3 independent experiments, and protein levels were normalized to that of tubulin. HEXA-018 treatment did not affect Ref2(P) protein level. Data are presented as the mean ± SD. Genotypes: *elavGS, UAS-Atg8a-GFP/+*. *n. s.*, not significant (unpaired Student's *t*-test). **(D,E)** Climbing ability and lifespan of TDP-43 flies fed HEXA-018 (10 μM) at the indicated time points. The TDP43-induced motility deficit was significantly reduced by treatment with HEXA-018. The percentages of flies that climbed or survived were quantified. Genotypes: control is *elavGS/+*, TDP-43 is *elavGS, UAS-TARDBP/+*. Data are presented as the mean ± SEM ($n = 4$ replicates per condition, each with $n = 25$ flies per sample). $^{*}p < 0.05$; $^{***}p < 0.001$ (one-way ANOVA with Tukey's multiple comparison test).

treatment suppresses TDP-43-induced toxicity in a *Drosophila* model of TDP-43 proteinopathy that expresses human TDP-43 in the nervous system (Kim et al., 2014; Lee et al., 2020a). We also found that HEXA-018 treatment significantly improved the TDP-43-induced climbing deficit and shortened lifespan compared with the control treatment (**Figures 6D,E**). Taken together, these results show that HEXA-018 ameliorates TDP-43 toxicity in fly and mammalian cell line models of TDP-43 proteinopathy via ALP activation.

4 DISCUSSION

In this study, we demonstrated the effect of HEXA-018, a novel compound containing a catechol derivative structure, as an inducer of autophagy. Recent studies have shown that the ALP has many roles, including cellular homeostasis, metabolism, development, antitumor properties, and innate defense (Levine and Kroemer, 2008; Mizushima and Levine, 2010; Mizushima and Komatsu, 2011; Wang and Levine, 2011; Kim and Lee, 2014). Moreover, dysregulation of the ALP is closely associated with neurodegenerative diseases, such as Alzheimer's disease, amyotrophic lateral sclerosis (ALS), and Parkinson's disease (Ravikumar et al., 2004; Crews et al., 2010; Spilman et al., 2010; Barmada et al., 2014; Hsueh et al., 2016). Thus, ALP activation is a promising therapeutic strategy for neurodegenerative diseases.

The mTOR signaling pathway is the most well-characterized negative regulator of the ALP (Dunlop and Tee, 2014). In addition, several studies have shown that rapamycin has beneficial effects in some animal models of age-associated neurodegenerative diseases via ALP activation (Jahrling and Laberge, 2015). However, mTOR activation in the brain plays essential roles in synapse development, neurotrophic factor synthesis, neuronal apoptosis and neuroinflammation (Kim, 2014; Jahrling and Laberge, 2015; Kim et al., 2018; Kim, 2020). Furthermore, human clinical studies have suggested that rapamycin induces various side effects, including immunosuppression, impaired wound healing, hyperlipidemia, and proteinuria (Stallone et al., 2009; Salmon, 2015). Thus,

developing mTOR-independent inducers of autophagy could be a promising therapeutic strategy for neurodegenerative diseases.

HEXA-018 is a novel compound with a catechol derivative structure. Previous studies have demonstrated that urushiol, a catechol derivative, induces autophagic flux (Go et al., 2017). Moreover, catechol derivatives mediate autophagy-mediated cell death in cancer cells (Hong et al., 1999; Kim et al., 2013; Go et al., 2017). In this study, we found that HEXA-018 activates the ALP in an mTOR-independent manner. HEXA-018 specifically increased the number of autolysosomes (**Figure 3B**). This result suggests that HEXA-018 facilitates the fusion of autophagosomes with lysosomes. The studied regulators of autophagosome-lysosome fusion are Ras-associated binding (Rab) GTPases, including Rab2 and Rab7 (Lorincz and Juhasz, 2020). However, the soluble N-ethylmaleimide–sensitive factor attachment protein receptor (SNARE) complex and vesicular transport system are also essential for the fusion process. Therefore, further studies are warranted to determine how HEXA-018 modulates the ALP. The possible mTOR-independent ALP activation pathways of HEXA-018 are Ca2+, inositol and IP3, ULK1/AMPK, and MAPK/JNK pathway (Williams et al., 2008; Decuypere et al., 2011; Kim et al., 2011; Zhao et al., 2013; Li et al., 2015). To elucidate the mechanism of HEXA-018 mediated ALP activation, we performed additional experiment to test whether HEXA-018 is related to the ULK1/AMPK pathway. We found that the HEXA-018 activates the ULK1/AMPK pathway. Moreover, ULK1 inhibition is sufficient to suppress HEXA-018-induced ALP activation. However, there is still a possibility that HEXA-018 could increase ALP activation via multiple pathways.

As for the concentration of HEXA-018, we have treated with several concentrations of HEXA-018 in primary neurons and N2a cells and then selected one concentration (for each cell types) that does not exhibit cytotoxicity itself and have significant protective effect against neurotoxic agents. Many studies have found significant differences between immortalized cell lines and primary neurons. Indeed, immortalized cells or those derived from tumors differ biologically from normal, differentiated neurons obtained from the fetal brain. Notably, HEXA-018 alone showed a dose dependent response with high doses (N2a cells; 100 μM and primary neurons; 1 μM) demonstrating significant toxicity while lower doses (N2a cells; 1, 5, 10 μM and primary neurons; 0.1, 0.5 μM) had no effect on cell toxicity using FACS analysis (**Supplementary Figure S3**). Moreover, treatment with rotenone and MG132 significantly increased the necrotic rates, but apoptotic rate were not affected in N2a cells and primary neurons by flow cytometry. The treatment with HEXA-018 also decreased the rotenone-induced necrotic rate (**Figures 4E,F**).

TDP-43 is the major component of inclusions or aggregates present in the neuronal cells of patients affected by ALS and frontotemporal lobal degeneration (FTLD) (Liscic et al., 2008; Scotter et al., 2015; James et al., 2016; Josephs et al., 2017). Importantly, TDP-43-induced UPS impairment plays a critical role in the pathogenesis of TDP-43 by regulating neurotoxicity. Moreover, ALP activation reduces TDP-43 aggregation, cytoplasmic mislocalization and toxicity in mouse and cultured neurons (Ayala et al., 2011; Avendano-Vazquez et al., 2012; Wang et al., 2012; Barmada et al., 2014). Taken together, all evidence suggests that regulation of ALP plays an important role in the TDP-43 proteinopathy model. We demonstrated that HEXA-018 significantly attenuated the ALP activation and behavioral defect induced by TDP-43-expressing cells and flies.

Our data suggest that HEXA-018 suppressed neuronal toxicity in cell and *Drosophila* models of TDP-43 proteinopathy. These results present the possibility that HEXA-018-mediated ALP activation may be a novel therapeutic intervention for neurodegenerative diseases with TDP-43 proteinopathy.

DATA AVAILABILITY STATEMENT

The original contributions presented in the study are included in the article/**Supplementary Material**, further inquiries can be directed to the corresponding authors.

ETHICS STATEMENT

This study was approved by the Institutional Animal Care and Use Committee (IACUC) at Korea Brain Research Institute (#IACUC-18-00019). All experiments were performed in accordance with the guidelines of the IACUC at the Korea Brain Research Institute.

AUTHOR CONTRIBUTIONS

SL, MJ, H-EL, SH, and J-YM and planned and performed the experiments. SK, YK, JW, and Y-MJ. provided ideas for the project and participated in writing the paper. SL, MJ, J-YM, and H-JK wrote the paper. All authors read and approved the final manuscript.

FUNDING

This work was supported by the KBRI Research Program of the Ministry of Science, ICT and Future Planning (21-BR-02-15, 21-BR-01-11) and Hexa Pharmatec.

SUPPLEMENTARY MATERIAL

The Supplementary Material for this article can be found online at: https://www.frontiersin.org/articles/10.3389/fphar.2021.747975/full#supplementary-material

REFERENCES

Araki, W., Yuasa, K., Takeda, S., Shirotani, K., Takahashi, K., and Tabira, T. (2000). Overexpression of Presenilin-2 Enhances Apoptotic Death of Cultured Cortical Neurons. *Ann. N. Y Acad. Sci.* 920, 241–244. doi:10.1111/j.1749-6632.2000.tb06929.x

Avendaño-Vázquez, S. E., Dhir, A., Bembich, S., Buratti, E., Proudfoot, N., and Baralle, F. E. (2012). Autoregulation of TDP-43 mRNA Levels Involves Interplay between Transcription, Splicing, and Alternative PolyA Site Selection. *Genes Dev.* 26, 1679–1684. doi:10.1101/gad.194829.112

Ayala, Y. M., De Conti, L., Avendaño-Vázquez, S. E., Dhir, A., Romano, M., D'ambrogio, A., et al. (2011). TDP-43 Regulates its mRNA Levels through a Negative Feedback Loop. *EMBO J.* 30, 277–288. doi:10.1038/emboj.2010.310

Barmada, S. J., Serio, A., Arjun, A., Bilican, B., Daub, A., Ando, D. M., et al. (2014). Autophagy Induction Enhances TDP43 Turnover and Survival in Neuronal ALS Models. *Nat. Chem. Biol.* 10, 677–685. doi:10.1038/nchembio.1563

Chen, Y., Mcmillan-Ward, E., Kong, J., Israels, S. J., and Gibson, S. B. (2007). Mitochondrial Electron-Transport-Chain Inhibitors of Complexes I and II Induce Autophagic Cell Death Mediated by Reactive Oxygen Species. *J. Cel Sci* 120, 4155–4166. doi:10.1242/jcs.011163

Crews, L., Spencer, B., Desplats, P., Patrick, C., Paulino, A., Rockenstein, E., et al. (2010). Selective Molecular Alterations in the Autophagy Pathway in Patients with Lewy Body Disease and in Models of Alpha-Synucleinopathy. *PLoS One* 5, e9313. doi:10.1371/journal.pone.0009313

de Boer, E. M. J., Orie, V. K., Williams, T., Baker, M. R., De Oliveira, H. M., Polvikoski, T., et al. (2020). TDP-43 Proteinopathies: a New Wave of Neurodegenerative Diseases. *J. Neurol. Neurosurg. Psychiatry* 92, 86–95. doi:10.1136/jnnp-2020-322983

Decuypere, J. P., Bultynck, G., and Parys, J. B. (2011). A Dual Role for Ca(2+) in Autophagy Regulation. *Cell Calcium* 50, 242–250. doi:10.1016/j.ceca.2011.04.001

Din, F. V., Valanciute, A., Houde, V. P., Zibrova, D., Green, K. A., Sakamoto, K., et al. (2012). Aspirin Inhibits mTOR Signaling, Activates AMP-Activated Protein Kinase, and Induces Autophagy in Colorectal Cancer Cells. *Gastroenterology* 142, 1504–1515.e3. doi:10.1053/j.gastro.2012.02.050

Dranka, B. P., Benavides, G. A., Diers, A. R., Giordano, S., Zelickson, B. R., Reily, C., et al. (2011). Assessing Bioenergetic Function in Response to Oxidative Stress by Metabolic Profiling. *Free Radic. Biol. Med.* 51, 1621–1635. doi:10.1016/j.freeradbiomed.2011.08.005

Dunlop, E. A., and Tee, A. R. (2014). mTOR and Autophagy: a Dynamic Relationship Governed by Nutrients and Energy. *Semin. Cel Dev Biol* 36, 121–129. doi:10.1016/j.semcdb.2014.08.006

Enokido, Y., Akaneya, Y., Niinobe, M., Mikoshiba, K., and Hatanaka, H. (1992). Basic Fibroblast Growth Factor Rescues CNS Neurons from Cell Death Caused by High Oxygen Atmosphere in Culture. *Brain Res.* 599, 261–271. doi:10.1016/0006-8993(92)90400-4

Feany, M. B., and Bender, W. W. (2000). A Drosophila Model of Parkinson's Disease. *Nature* 404, 394–398. doi:10.1038/35006074

Go, D. H., Lee, Y. G., Lee, D. H., Kim, J. A., Jo, I. H., Han, Y. S., et al. (2017). 3-Decylcatechol Induces Autophagy-Mediated Cell Death through the IRE1α/JNK/p62 in Hepatocellular Carcinoma Cells. *Oncotarget* 8, 58790–58800. doi:10.18632/oncotarget.17732

Guo, S., Liang, Y., Murphy, S. F., Huang, A., Shen, H., Kelly, D. F., et al. (2015). A Rapid and High Content Assay that Measures cyto-ID-stained Autophagic Compartments and Estimates Autophagy Flux with Potential Clinical Applications. *Autophagy* 11, 560–572. doi:10.1080/15548627.2015.1017181

Han, S., and Lee, J. H. (2020). *Novel Catechol Derivatives or Salt Thereof, Processes for Preparing the Same, and Pharmaceutical Compositions Comprising the Same*. PCT Patient. WO 2020/017878 A1. https://patents.google.com/patent/WO2020017878A1/en.

Hong, D. H., Han, S. B., Lee, C. W., Park, S. H., Jeon, Y. J., Kim, M. J., et al. (1999). Cytotoxicity of Urushiols Isolated from Sap of Korean Lacquer Tree (Rhus Vernicifera Stokes). *Arch. Pharm. Res.* 22, 638–641. doi:10.1007/BF02975339

Hsueh, K. W., Chiou, T. W., Chiang, S. F., Yamashita, T., Abe, K., Borlongan, C. V., et al. (2016). Autophagic Down-Regulation in Motor Neurons Remarkably Prolongs the Survival of ALS Mice. *Neuropharmacology* 108, 152–160. doi:10.1016/j.neuropharm.2016.03.035

Huang, W., Zhou, Y., Tu, L., Ba, Z., Huang, J., Huang, N., et al. (2020). TDP-43: From Alzheimer's Disease to Limbic-Predominant Age-Related TDP-43 Encephalopathy. *Front. Mol. Neurosci.* 13, 26. doi:10.3389/fnmol.2020.00026

Jahrling, J. B., and Laberge, R. M. (2015). Age-Related Neurodegeneration Prevention through mTOR Inhibition: Potential Mechanisms and Remaining Questions. *Curr. Top. Med. Chem.* 15, 2139–2151. doi:10.2174/1568026615666150610125856

James, B. D., Wilson, R. S., Boyle, P. A., Trojanowski, J. Q., Bennett, D. A., and Schneider, J. A. (2016). TDP-43 Stage, Mixed Pathologies, and Clinical Alzheimer's-Type Dementia. *Brain* 139, 2983–2993. doi:10.1093/brain/aww224

Jo, M., Lee, S., Jeon, Y. M., Kim, S., Kwon, Y., and Kim, H. J. (2020). The Role of TDP-43 Propagation in Neurodegenerative Diseases: Integrating Insights from Clinical and Experimental Studies. *Exp. Mol. Med.* 52, 1652–1662. doi:10.1038/s12276-020-00513-7

Josephs, K. A., Dickson, D. W., Tosakulwong, N., Weigand, S. D., Murray, M. E., Petrucelli, L., et al. (2017). Rates of Hippocampal Atrophy and Presence of post-mortem TDP-43 in Patients with Alzheimer's Disease: a Longitudinal Retrospective Study. *Lancet Neurol.* 16, 917–924. doi:10.1016/S1474-4422(17)30284-3

Jung, C. H., Ro, S. H., Cao, J., Otto, N. M., and Kim, D. H. (2010). mTOR Regulation of Autophagy. *FEBS Lett.* 584, 1287–1295. doi:10.1016/j.febslet.2010.01.017

Kim, K. H., and Lee, M. S. (2014). Autophagy--a Key Player in Cellular and Body Metabolism. *Nat. Rev. Endocrinol.* 10, 322–337. doi:10.1038/nrendo.2014.35

Kim, J., Kundu, M., Viollet, B., and Guan, K. L. (2011). AMPK and mTOR Regulate Autophagy through Direct Phosphorylation of Ulk1. *Nat. Cel Biol* 13, 132–141. doi:10.1038/ncb2152

Kim, S., Kim, D. H., Lee, S. H., Kim, M. J., Yoon, J. H., Chung, H. Y., et al. (2013). Urushiol Induces Apoptosis via a P53-Dependent Pathway in Human Gastric Cancer Cells. *J. Cancer Prev.* 18, 169–176. doi:10.15430/jcp.2013.18.2.169

Kim, H. J., Raphael, A. R., Ladow, E. S., Mcgurk, L., Weber, R. A., Trojanowski, J. Q., et al. (2014). Therapeutic Modulation of eIF2α Phosphorylation Rescues TDP-43 Toxicity in Amyotrophic Lateral Sclerosis Disease Models. *Nat. Genet.* 46, 152–160. doi:10.1038/ng.2853

Kim, S., Moon, G. J., Oh, Y. S., Park, J., Shin, W. H., Jeong, J. Y., et al. (2018). Protection of Nigral Dopaminergic Neurons by AAV1 Transduction with Rheb(S16H) against Neurotoxic Inflammation *In Vivo*. *Exp. Mol. Med.* 50, e440. doi:10.1038/emm.2017.261

Kim, S. R. (2014). Mammalian Target of Rapamycin Complex 1 as an Inducer of Neurotrophic Factors in Dopaminergic Neurons. *Neural Regen. Res.* 9, 2036–2037. doi:10.4103/1673-5374.147923

Kim, S. R. (2020). Beneficial Effects of AAV1-Rheb(S16H) Administration in the Adult Hippocampus. *Neural Regen. Res.* 15, 1479–1480. doi:10.4103/1673-5374.274335

Lee, S., Jeon, Y. M., Cha, S. J., Kim, S., Kwon, Y., Jo, M., et al. (2020a). PTK2/FAK Regulates UPS Impairment via SQSTM1/p62 Phosphorylation in TARDBP/TDP-43 Proteinopathies. *Autophagy* 16, 1396–1412. doi:10.1080/15548627.2019.1686729

Lee, S., Kwon, Y., Kim, S., Jo, M., Jeon, Y. M., Cheon, M., et al. (2020b). The Role of HDAC6 in TDP-43-Induced Neurotoxicity and UPS Impairment. *Front Cel Dev Biol* 8, 581942. doi:10.3389/fcell.2020.581942

Lee, J. A. (2012). Neuronal Autophagy: a Housekeeper or a Fighter in Neuronal Cell Survival? *Exp. Neurobiol.* 21, 1–8. doi:10.5607/en.2012.21.1.1

Levine, B., and Kroemer, G. (2008). Autophagy in the Pathogenesis of Disease. *Cell* 132, 27–42. doi:10.1016/j.cell.2007.12.018

Li, L., Tan, J., Miao, Y., Lei, P., and Zhang, Q. (2015). ROS and Autophagy: Interactions and Molecular Regulatory Mechanisms. *Cell Mol. Neurobiol.* 35, 615–621. doi:10.1007/s10571-015-0166-x

Lin, T. K., Cheng, C. H., Chen, S. D., Liou, C. W., Huang, C. R., and Chuang, Y. C. (2012). Mitochondrial Dysfunction and Oxidative Stress Promote Apoptotic Cell Death in the Striatum via Cytochrome C/Caspase-3 Signaling Cascade Following Chronic Rotenone Intoxication in Rats. *Int. J. Mol. Sci.* 13, 8722–8739. doi:10.3390/ijms13078722

Liscic, R. M., Grinberg, L. T., Zidar, J., Gitcho, M. A., and Cairns, N. J. (2008). ALS and FTLD: Two Faces of TDP-43 Proteinopathy. *Eur. J. Neurol.* 15, 772–780. doi:10.1111/j.1468-1331.2008.02195.x

Livak, K. J., and Schmittgen, T. D. (2001). Analysis of Relative Gene Expression Data Using Real-Time Quantitative PCR and the 2(-Delta Delta C(T)) Method. *Methods* 25, 402–408. doi:10.1006/meth.2001.1262

Lorincz, P., and Juhasz, G. (2020). Autophagosome-Lysosome Fusion. *J. Mol. Biol.* 432, 2462–2482. doi:10.1016/j.jmb.2019.10.028

Mizushima, N., and Komatsu, M. (2011). Autophagy: Renovation of Cells and Tissues. *Cell* 147, 728–741. doi:10.1016/j.cell.2011.10.026

Mizushima, N., and Levine, B. (2010). Autophagy in Mammalian Development and Differentiation. *Nat. Cel Biol* 12, 823–830. doi:10.1038/ncb0910-823

Prasad, A., Bharathi, V., Sivalingam, V., Girdhar, A., and Patel, B. K. (2019). Molecular Mechanisms of TDP-43 Misfolding and Pathology in Amyotrophic Lateral Sclerosis. *Front. Mol. Neurosci.* 12, 25. doi:10.3389/fnmol.2019.00025

Ravikumar, B., Vacher, C., Berger, Z., Davies, J. E., Luo, S., Oroz, L. G., et al. (2004). Inhibition of mTOR Induces Autophagy and Reduces Toxicity of Polyglutamine Expansions in Fly and Mouse Models of Huntington Disease. *Nat. Genet.* 36, 585–595. doi:10.1038/ng1362

Roach, P. J. (2011). AMPK -> ULK1 -> Autophagy. *Mol. Cel Biol* 31, 3082–3084. doi:10.1128/MCB.05565-11

Salmon, A. B. (2015). About-face on the Metabolic Side Effects of Rapamycin. *Oncotarget* 6, 2585–2586. doi:10.18632/oncotarget.3354

Scotter, E. L., Chen, H. J., and Shaw, C. E. (2015). TDP-43 Proteinopathy and ALS: Insights into Disease Mechanisms and Therapeutic Targets. *Neurotherapeutics* 12, 352–363. doi:10.1007/s13311-015-0338-x

Sheen, J. H., Zoncu, R., Kim, D., and Sabatini, D. M. (2011). Defective Regulation of Autophagy upon Leucine Deprivation Reveals a Targetable Liability of Human Melanoma Cells *In Vitro* and *In Vivo*. *Cancer Cell* 19, 613–628. doi:10.1016/j.ccr.2011.03.012

Son, J. H., Shim, J. H., Kim, K. H., Ha, J. Y., and Han, J. Y. (2012). Neuronal Autophagy and Neurodegenerative Diseases. *Exp. Mol. Med.* 44, 89–98. doi:10.3858/emm.2012.44.2.031

Spilman, P., Podlutskaya, N., Hart, M. J., Debnath, J., Gorostiza, O., Bredesen, D., et al. (2010). Inhibition of mTOR by Rapamycin Abolishes Cognitive Deficits and Reduces Amyloid-Beta Levels in a Mouse Model of Alzheimer's Disease. *PLoS One* 5, e9979. doi:10.1371/journal.pone.0009979

Stallone, G., Infante, B., Grandaliano, G., and Gesualdo, L. (2009). Management of Side Effects of Sirolimus Therapy. *Transplantation* 87, S23–S26. doi:10.1097/TP.0b013e3181a05b7a

Thellung, S., Corsaro, A., Nizzari, M., Barbieri, F., and Florio, T. (2019). Autophagy Activator Drugs: A New Opportunity in Neuroprotection from Misfolded Protein Toxicity. *Int. J. Mol. Sci.* 20, 901. doi:10.3390/ijms20040901

Van Deerlin, V. M., Leverenz, J. B., Bekris, L. M., Bird, T. D., Yuan, W., Elman, L. B., et al. (2008). TARDBP Mutations in Amyotrophic Lateral Sclerosis with TDP-43 Neuropathology: a Genetic and Histopathological Analysis. *Lancet Neurol.* 7, 409–416. doi:10.1016/S1474-4422(08)70071-1

Wang, R. C., and Levine, B. (2011). Calcipotriol Induces Autophagy in HeLa Cells and Keratinocytes. *J. Invest. Dermatol.* 131, 990–993. doi:10.1038/jid.2010.423

Wang, I. F., Chang, H. Y., Hou, S. C., Liou, G. G., Way, T. D., and James Shen, C. K. (2012). The Self-Interaction of Native TDP-43 C Terminus Inhibits its Degradation and Contributes to Early Proteinopathies. *Nat. Commun.* 3, 766. doi:10.1038/ncomms1766

Wang, P., Deng, J., Dong, J., Liu, J., Bigio, E. H., Mesulam, M., et al. (2019). TDP-43 Induces Mitochondrial Damage and Activates the Mitochondrial Unfolded Protein Response. *Plos Genet.* 15, e1007947. doi:10.1371/journal.pgen.1007947

Williams, A., Sarkar, S., Cuddon, P., Ttofi, E. K., Saiki, S., Siddiqi, F. H., et al. (2008). Novel Targets for Huntington's Disease in an mTOR-Independent Autophagy Pathway. *Nat. Chem. Biol.* 4, 295–305. doi:10.1038/nchembio.79

Xiong, N., Xiong, J., Jia, M., Liu, L., Zhang, X., Chen, Z., et al. (2013). The Role of Autophagy in Parkinson's Disease: Rotenone-Based Modeling. *Behav. Brain Funct.* 9, 13. doi:10.1186/1744-9081-9-13

Ylä-Anttila, P., Vihinen, H., Jokitalo, E., and Eskelinen, E. L. (2009). Monitoring Autophagy by Electron Microscopy in Mammalian Cells. *Methods Enzymol.* 452, 143–164. doi:10.1016/S0076-6879(08)03610-0

Yu, W. H., Dorado, B., Figueroa, H. Y., Wang, L., Planel, E., Cookson, M. R., et al. (2009). Metabolic Activity Determines Efficacy of Macroautophagic Clearance of Pathological Oligomeric Alpha-Synuclein. *Am. J. Pathol.* 175, 736–747. doi:10.2353/ajpath.2009.080928

Zhao, Y., Li, X., Ma, K., Yang, J., Zhou, J., Fu, W., et al. (2013). The axis of MAPK1/3-XBP1u-FOXO1 Controls Autophagic Dynamics in Cancer Cells. *Autophagy* 9, 794–796. doi:10.4161/auto.23918

Conflict of Interest: Author SH is the Chief Executive Officer of Hexa Pharmatec.

The remaining authors declare that the research was conducted in the absence of any commercial or financial relationships that could be construed as a potential conflict of interest.

Publisher's Note: All claims expressed in this article are solely those of the authors and do not necessarily represent those of their affiliated organizations, or those of the publisher, the editors and the reviewers. Any product that may be evaluated in this article, or claim that may be made by its manufacturer, is not guaranteed or endorsed by the publisher.

frontiers in Pharmacology

ORIGINAL RESEARCH
published: 22 December 2021
doi: 10.3389/fphar.2021.740966

Inhibition of Brain GTP Cyclohydrolase I Attenuates 3-Nitropropionic Acid-Induced Striatal Toxicity: Involvement of Mas Receptor/PI3k/Akt/CREB/ BDNF Axis

Aya M. Mustafa[1], *Mostafa A. Rabie*[2]*, *Hala F. Zaki*[2] *and Aya M. Shaheen*[1]

[1]*Department of Pharmacology and Toxicology, Faculty of Pharmacy, Egyptian Russian University, Cairo, Egypt,* [2]*Department of Pharmacology and Toxicology, Faculty of Pharmacy, Cairo University, Cairo, Egypt*

OPEN ACCESS

Edited by:
Anna Boguszewska-Czubara, Medical University of Lublin, Poland

Reviewed by:
Elizabeth Hernández-Echeagaray, National Autonomous University of Mexico, Mexico
Sumit Jamwal, Yale University, United States

***Correspondence:**
Mostafa A. Rabie
Mostafa.mohammed@pharma.cu.edu.eg

Specialty section:
This article was submitted to Neuropharmacology, a section of the journal Frontiers in Pharmacology

Received: *14 July 2021*
Accepted: *15 November 2021*
Published: *22 December 2021*

Citation:
Mustafa AM, Rabie MA, Zaki HF and Shaheen AM (2021) Inhibition of Brain GTP Cyclohydrolase I Attenuates 3-Nitropropionic Acid-Induced Striatal Toxicity: Involvement of Mas Receptor/ PI3k/Akt/CREB/ BDNF Axis. Front. Pharmacol. 12:740966. doi: 10.3389/fphar.2021.740966

GTP cyclohydrolase I (GTPCH I) is the rate-limiting enzyme for tetrahydrobiopterin (BH4) biosynthesis; the latter is an essential factor for iNOS activation that contributes neuronal loss in Huntington's disease (HD). The aim of the study was to investigate the neuroprotective effect of 2,4-diamino-6-hydroxypyrimidine (DAHP), GTPCH I enzyme inhibitor, against neuronal loss in 3-nitropropinic acid (3-NP)-induced HD in rats and to reveal the possible involved mechanisms mediated through PI3K/Akt axis and its correlation to Mas receptor (MasR). Rats received 3-NP (10 mg/kg/day; i.p.) with or without administration of DAHP (0.5 g/kg/day; i.p.) or wortmannin (WM), a PI3K inhibitor, (15 µg/kg/day; i.v.) for 14 days. DAHP improved cognitive, memory, and motor abnormalities induced by 3-NP, as confirmed by striatal histopathological specimens and immunohistochemical examination of GFAP. Moreover, DAHP treatment inhibited GTPCH I activity, resulting in decreased BH4 levels and iNOS activation. Also, DAHP upregulated the protein expression of survival protein; p85/p55 (pY458/199)-PI3K and pS473-Akt that, in turn, boosted the activation of striatal neurotrophic factors and receptor, pS133-CREB, BDNF and pY515-TrKB, which positively affect MasR protein expression and improve mitochondrial dysfunction, as indicated by enhancing both SDH and PGC-1α levels. Indeed, DAHP attenuates oxidative stress by increasing SOD activity and Nrf2 expression in addition to reducing neuro-inflammatory status by inhibiting NF-κB p65 and TNF-α expression. Interestingly, all the previous effects were blocked by co-administration of WM with DAHP. In conclusion, DAHP exerts neuroprotective effect against neuronal loss induced by 3-NP administration *via* inhibition of GTPCH I and iNOS activity and activation of MasR/PI3K/Akt/CREB/BDNF/TrKB axis besides its antioxidant and anti-inflammatory effect.

Keywords: 3-nitropropionic acid, mitochondrial dysfunction, mas receptor, PI3K/AKT signaling, DAHP 3

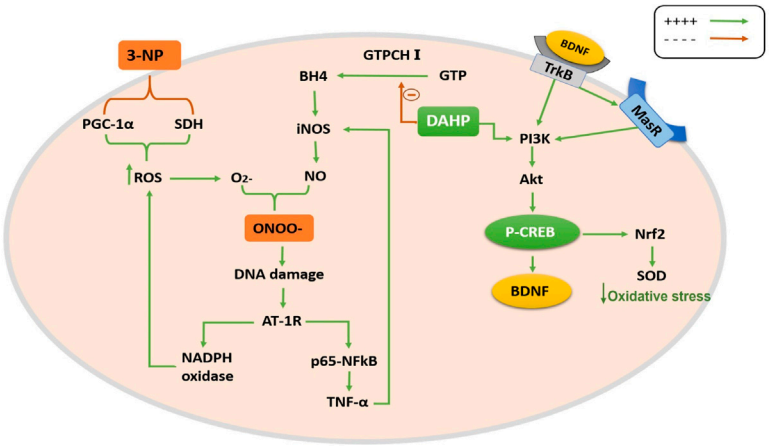

GRAPHICAL ABSTRACT |

1 INTRODUCTION

Huntington's disease (HD) is a progressive neurodegenerative disease characterized by motor and cognitive dysfunctions together with psychiatric manifestations (Shah et al., 1993; Roos, 2010), for which no cure or disease-modifying therapies are available until now (Tabrizi et al., 2019). Of note, inflammation mediated by microglia plays a crucial role in neurodegenerative diseases as Parkinson's disease (PD) (Gao et al., 2003), Alzheimer's disease (AD) (Salvati and Beenhakker, 2019), and HD (Sapp et al., 2001). Sustained and excessive activation of microglia along with massive production of proinflammatory cytokines is responsible, in part, for inflammation-induced neurodegeneration (Block et al., 2007; Glass et al., 2010). Nitric oxide (NO) produced by inducible nitric oxide synthase (iNOS) in the microglia is one of the chief proinflammatory factors that induce neuronal death (Liu et al., 2012). Thus, iNOS inhibition attenuated microglia-mediated neuronal death, revealing the pivotal role of NO in microglia-mediated neurotoxicity (Mander and Brown, 2005). Tetrahydrobiopterin (BH4), an essential cofactor for NOS activity and phenylalanine hydroxylase, tryptophan hydroxylase, and tyrosine hydroxylases (Thony et al., 2000). Tyrosine hydroxylase, the rate-limiting enzyme for dopamine biosynthesis, uses tetrahydrobiopterin and molecular oxygen to convert tyrosine to L-DOPA (Thony et al., 2000). GTP cyclohydrolase I (GTPCH I) is the rate- limiting enzyme and the first step in BH4 biosynthesis (Alp and Channon, 2004). Indeed, GTPCH I activation by various cytokines, such as tumor necrosis factor α (TNFα) and interferon γ (IFN-γ) is accompanied by increased BH4 level and NOS activity (Huang et al., 2005). In the present study, 3-nitropropionic acid (3-NP), irreversible inhibitor of mitochondrial succinate dehydrogenase, is used to mimic the pathological and motor abnormalities of HD (Brouillet et al., 2005; Kumar et al., 2011; Gao et al., 2015). 3-NP induces an oxidative stress status and impairs antioxidant defense mechanisms in the brain (Pérez-De La Cruz et al., 2009; Zafir et al., 2009) together with the production of proinflammatory cytokines, such as TNF-α, interleukin-6, and interleukin-1β (Jamwal and Kumar, 2016). The overproduction of reactive oxygen species and neuroinflammatory status results in marked elevation of iNOS activity and peroxynitrite (ONOO-) level, ultimately causing neuronal death (Pedraza-Chaverrí et al., 2009).

Noteworthy, the PI3K/Akt axis exerts a neuroprotective effect in neurodegenerative diseases, such as ischemic stroke, PD, and AD *via* enhancement of cAMP-responsive element-binding protein (CREB) expression with subsequent downstream protein, brain-derived neurotrophic factor (BDNF) leading to cellular proliferation and inhibition of apoptotic and inflammatory biomarkers that eventually ends up with improved cell survival (Jiang et al., 2013; Heras-Sandoval et al., 2014; Ribeiro et al., 2014; Zuo et al., 2016). Moreover, Sayed et al. (2020) reported the crucial function for PI3K and Akt proteins as cellular components in hampering HD (Sayed et al., 2020). It is previously reported that DAHP, GTPCH I inhibitor, demonstrated a neuroprotective effect in focal cerebral ischemia through activation of phosphoinositide-3-kinase/protein kinase B (PI3K/Akt) pathway (Li et al., 2015).

Based on the above data, the current study investigated the neuroprotective effect of 2, 4-diamino-6-hydroxypyrimidine (DAHP), brain GTPCH-1 inhibitor, against neuronal loss in 3-NP induced HD *via* iNOS inhibition. Moreover, the aim was extended to study the protective role of PI3K/Akt axis and its consequence on Mas receptor (MasR) activation against 3-NP induced neurotoxicity using wortmannin (WM) as a direct PI3K pathway inhibitor.

2 MATERIALS AND METHODS

2.1 Ethics Statement

The investigation complies with the Guide for the Care and Use of Laboratory Animals published by the US National

Institutes of Health (NIH publication No. 8023, revised 1978) adopted by the Ethics Research Committee of Faculty of Pharmacy, Cairo University (Cairo, Egypt; PT (2573). All efforts were done to minimize animal suffering during the experiment.

2.2 Animals

Male Wistar rats, weighing 180–200 g, were obtained from the animal facility of Faculty of Pharmacy, Cairo University (Cairo, Egypt). Before starting the experiment, the animals were allowed to acclimatize to laboratory conditions for 1 week. The animals were housed under controlled environmental conditions at constant temperature (23 ± 2°C), humidity (60 ± 10%), and a 12-/12-h light/dark cycle. The rats were allowed free access to standard chow diet and water *ad libitum*, and all behavioral tests were carried out in a sound isolated laboratory.

2.3 Experimental Design

The rats were randomly divided into five groups, (n = 14/group): Group I received dimethyl sulfoxide (DMSO) (0.2 ml/kg/day; i.p; Thermo Fisher, United States) and served as normal control group. Group II received DAHP (0.5 g/kg/day; i.p; Sigma-Aldrich, MO, United States) (Li et al., 2015) and served as normal drug group. Group III received 3-NP (10 mg/kg/day; i.p; Sigma-Aldrich, MO, United States) (Kumar et al., 2010). Group IV was treated with DAHP (0.5 g/kg/day; i.p; (Li et al., 2015) 1 h after 3-NP injection. Group V was treated with WM (15 μg/kg/day; i.v.; Sigma-Aldrich, MO, United States) after 3-NP injection and 15 min prior to DAHP administration (Yue et al., 2005). All treatments were conducted for 14 days, where 3-NP was dissolved in saline, and the pH was adjusted to 7.4 with NaOH. Meanwhile, DAHP and WM were dissolved in DMSO (Merck, Germany), and then WM was freshly diluted with saline. The animals were subjected to behavioral tests then further classified randomly into three subsets: first subset (n = 5) was used to assess parameters by Western blot technique, the second subset (n = 6) was used to measure parameters by ELISA technique, and the third subset (n = 3) was used for striatal histopathological examination and immunohistochemical assessment of glial fibrillary acidic protein (GFAP). The following **Scheme 1** summarizes the timeline for behavioral tests and treatments.

2.4 Behavioral Tests

Twenty-four hours after the last injection of 3-NP, DAHP, and/or WM, the rats were screened for motor performance using the open field and rotarod test. Additionally, memory was assessed using Morris water maze test and novel object recognition test. The tests were conducted on two consecutive days during the light cycle, Day 1) Open field and Rotarod test were performed and on the second day, Morris Water Maze and Novel object recognition tests were performed with 2-h respite period between the tests (Ramachandran and Thangarajan, 2016; Sayed et al., 2020).

2.4.1 Open Field Test

Open field test was carried out to assess spontaneous locomotor activity. The apparatus was a square box (80 × 80 × 40 cm) made of wood with red walls and black polished floor divided by white lines into 16 equal squares. The rats were individually placed at the center of the apparatus and allowed to explore the field for 5 min. An overhead camera was used to monitor the animals, and record ambulation frequency (the number of squares crossed by each rat) and rearing frequency (the number of rearings on the hind limbs). After each animal was tested, the floor was cleaned (Ramachandran and Thangarajan, 2018).

2.4.2 Rotarod Test

Motor coordination and grip strength were evaluated using rotarod apparatus (120-cm long, 3 cm in diameter, subdivided into four compartments by disks 24 cm in diameter and rotating at a constant speed of 20 rpm). For 3 days before experimental procedures, the animals were subjected to training sessions where the animal that continued on the rod for 5 min was chosen to carry out the experiment. After completion of OFT, the test was performed and fall off latency was recorded (Avila et al., 2010).

2.4.3 Morris Water Maze

The rats were screened for memory retention and spatial learning using the Morris water maze. The animals were trained to swim to a platform in a circular pool (150 cm in diameter and 60 cm in height with non-reflective interior surfaces) divided into four quadrants and filled with water up to 35-cm level and at a constant temperature of 25 ± 2°C. A movable circular platform (9 cm in diameter) was placed in the center of specific quadrant of the pool 1 cm below the water surface for acquisition test. A non-toxic soluble black paint was used to make the water opaque. Initially, the rats were subjected to three training sessions per day, each 120 s, for 4 days, in which the animals were left freely to find the platform from different starting positions. If the rat did not find the platform it was guided to it, and left on it for 30 s. Average time taken by the rat to reach the platform was recorded as acquisition latency. On the fifth day, a probe test was performed where the platform was removed and the animal was released facing the wall of the pool at quadrant opposite to the target quadrant, and was allowed to explore the pool for 1 min. The time spent by the animal swimming in the target quadrant was recorded using overhead camera (Suganya and Sumathi, 2017).

2.4.4 Novel Object Recognition Test

Novel object recognition test was performed to evaluate cognition and particularly recognition memory. The test was carried out in a black open field box measuring 50 × 25 × 50 cm. During habituation, the rats were allowed to explore the test box with no objects present for 10 min per day for two consecutive days. In the training sessions, each rat was placed in the test box with two identical objects placed in two corners (approximately 30-cm apart from each other). On the test day, the animals were introduced back in the test box, in which one of the familiar

objects was replaced with a novel object. The time spent exploring each object was recorded for 3 min using overhead camera during training and test sessions (Karasawa et al., 2008; Chen et al., 2019). Discrimination index, the difference in time spent exploring familiar and novel objects over the total time spent exploring both objects was calculated, and the time spent exploring familiar and novel objects as well (Arnt et al., 2010; Antunes and Biala, 2012).

2.5 Striatal Processing

At the end of behavioral tests, the rats were weighed and euthanized where the whole brains were quickly excised, washed with ice-cold saline, and dissected. Striata from each brain were immediately isolated and flash frozen in liquid nitrogen, then stored at −80°C.

2.5.1 Measurement of Tetrahydrobiopterin Levels and GTP Cyclohydrolase I Activity

BH4 levels and GTPCH I activity were assessed by high-performance liquid chromatography (HPLC) analysis using fluorescence detection as previously described (d'Uscio et al., 2003). Total biopterins including BH4 plus dihydropterin (BH2) plus oxidized biopterins were determined by acid oxidation, whereas BH2 and oxidized biopterins were determined by alkali oxidation. BH4 content was calculated from the difference between total biopterins to BH2 plus oxidized biopterins. GTPCH I activity was assessed using HPLC method with measurement of neopterin, after oxidation and phosphatase treatment of dihydroneopterin triphosphate.

2.5.2 Western Blot Analysis of Mas receptor, p85/p55 (pY458/199)-PI3K, pS473-Akt, pS133-cAMP Responsive Element-Binding Protein, Brain-Derived Neurotrophic Factor, pY515-TrkB, and Nuclear Factor Erythroid-2-Related Factor-2

The striata in the first subset were homogenized in radio immunoprecipitation assay (RIPA) buffer (150 mM NaCl, 1% Triton X-100, 0.5% sodium deoxycholate, 50 mM Tris HCl pH 8, and 0.1% SDS) supplied with freshly made protease–phosphatase inhibitors cocktail to maintain protein integrity. Bradford Protein Assay Kit (Bio BASIC Inc., ON, Canada) was used for quantitative striatal protein analysis. A 10-μg protein concentration of each sample was boiled with Laemmli buffer for 5 min and separated by SDS-PAGE and transferred to PVDF membrane that was blocked with 5% bovine serum albumin (BSA). Protein expression was evaluated by incubating membrane with primary antibodies (Thermo Fisher Scientific, MA, United States) against Mas receptor (0.25 μg/ml; cat#: PA5-43669), p85/p55 (pY458/199)-PI3K (1:1,000; cat#: PA5–17387), pS473-Akt (1:250; cat#: 700392), pS133-CREB (1:250; cat#: PA1-851B), BDNF (1:1,000; cat#: OSB00017W), pY515-TrkB (1:2,500; cat#: PA5–38076), nuclear factor erythroid-2-related factor-2 (Nrf2) (1:1,000; cat#: PA5–67520), and β-actin (1:1,000; cat#: PA5-16914) polyclonal antibody overnight at 4°C. Afterward, membranes were probed with horseradish peroxidase-conjugated goat anti-rabbit immunoglobulin (Dianova, Hamburg, Germany) for 2 h at room temperature. The amount of target proteins was quantified by densitometric analysis using Image analysis software on the ChemiDoc™ MP Imaging System (version 3) (Bio-Rad, CA, United States). The percentage of acrylamide used for all studied protein was 10% except for Nrf2 and TrKB, with a percentage of 8%. Results were normalized for β-actin protein expression and expressed as arbitrary units (AU).

2.5.3 ELISA Assay of Striatal Proliferator-Activated Receptor Gamma Coactivator 1-Alpha, Tumor Necrosis Factor-Alpha , Inducible Nitric Oxide Synthase , Nuclear Factor-κB, Succinate Dehydrogenase , and Superoxide Dismutase

Striata were rinsed and homogenized in PBS for quantitative determination of proliferator-activated receptor gamma coactivator 1-alpha (PGC-1α) (cat#: CSB-EL018425RA) and tumor necrosis factor-alpha (TNF-α) (cat#: CSB-E11987r) using CUSABIO ELISA kits (Wuhan, PRC). The MyBioSource ELISA kits (CA, United States) were used to determine iNOS (cat#: MBS263618), nuclear factor- κB p65 (NF-κB p65) (cat#: MBS015549), SDH (cat#: MBS3807968) and superoxide dismutase (SOD) (cat#: MBS036924). The procedures were performed according to the instructions of the manufacturer and the results were presented as pg/mg tissue protein for PGC-1α, TNF-α and NF-κB p65, ng/mg tissue protein for iNOS and SDH and U/mg tissue protein for SOD.

2.6 Histopathological Examination

Tissue samples were fixed in 10% neutral buffered formalin for 72 h with a change of formalin solution every day. The samples were washed, dehydrated, and processed in serial grades of ethanol, cleared in Xylene, synthetic wax infiltration, and embedded into Paraplast tissue embedding media. The 5-μm-thick sagittal brain sections were cut by rotatory microtome, stained with hematoxylin and eosin (H&E) and examined under light microscope for demonstration of striatal regions in different samples (Sidhu et al., 2018). All micrographs and data were obtained by using full HD microscopic camera operated by Leica application module for histological analysis (Leica Microsystems GmbH, Wetzlar, Germany) (Sayed et al., 2020).

2.7 Immunohistochemical Detection of Glial Fibrillary Acidic Protein

Deparaffinized 5-μm-thick tissue sections were cut and prepared for evaluation of astroglial alteration. Striatal sections were treated with 3% hydrogen peroxide for 20 min, washed with PBS, then incubated with mouse monoclonal glial fibrillary acidic protein (GFAP) antibody (Thermo Fisher Scientific Inc., United States) for 30 min. The sections were washed with PBS followed by incubation for 20 min with secondary antibody (Dako, Carpenteria, CA, United States), and then with horseradish peroxidase using the HRP Envision kit (Dako, Carpenteria, CA, United States). The reaction was visualized

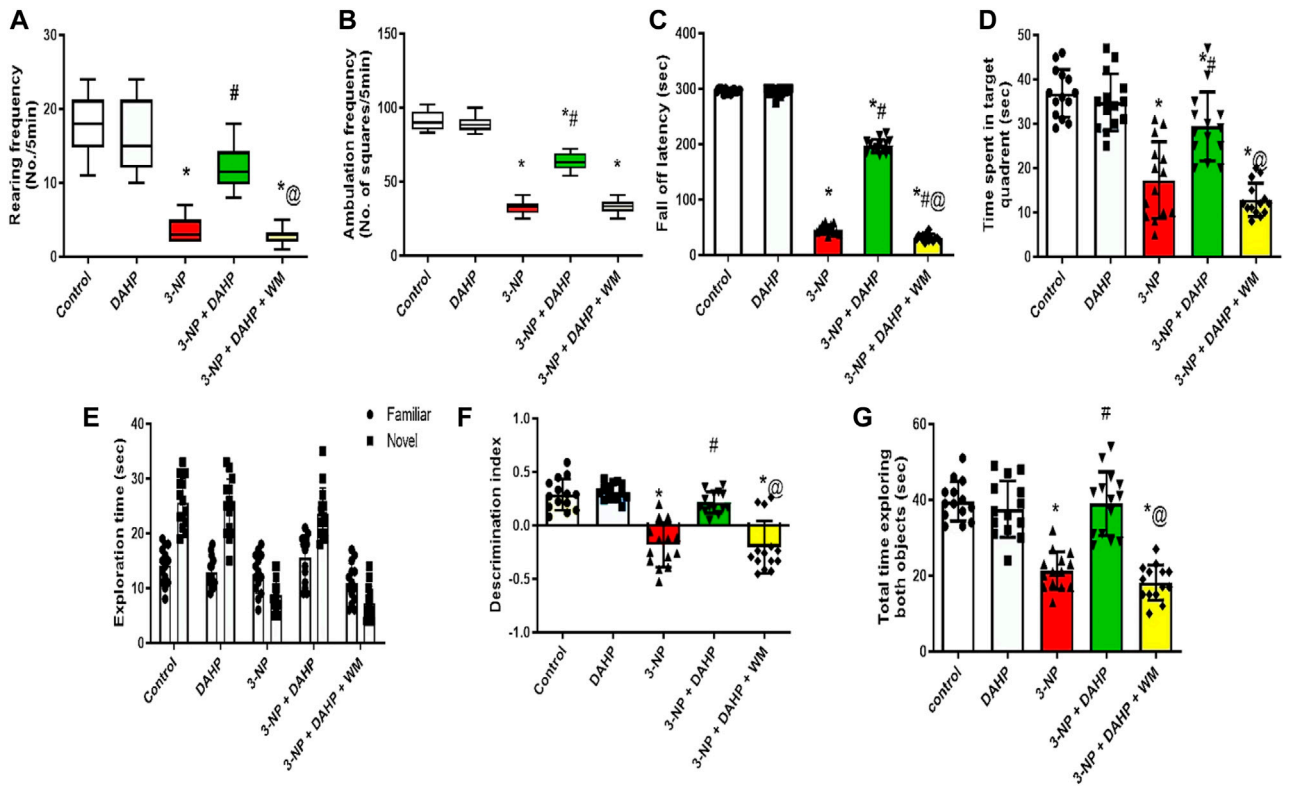

FIGURE 1 | Effect of DAHP on 3-NP-induced changes in **(A)** rearing frequency and **(B)** ambulation frequency in open field test and **(C)** fall off latency in rotarod test, as well as **(D)** time spent in target quadrant in Morris water maze test, **(E)** the exploration time of familiar and novel objects, **(F)** discrimination index and **(G)** Total time exploring both object in novel object recognition test. Rearing and ambulation frequency are presented as boxplots with median, 25th, and 75th percentile values using Kruskel–Wallis test followed by Dunn's as a *post-hoc* test. Parametric data are presented as mean ± SD of 14 rats per group, using one-way ANOVA followed by Tukey's *post-hoc* test. Differences in familiar and novel object exploration time for each group were tested using two-way ANOVA; F (4.65) = 3,667, F (4.65) = 36.3, F (4.65) = 32.7, F (4.65) = 44.7; $p < 0.05$. * vs. control, # vs. 3-NP, @ vs. 3-NP + DAHP. 3-NP, 3-nitropropionic acid; DAHP, 2,4-diamino-6-hydroxypyrimidine; WM, wortmannin.

with 3,3′-diaminobenzidine tetrahydrochloride (DAB Substrate Kit, Vector Laboratories Inc., Burlingame, CA, United States) for 10 min following another wash with PBS. Finally, the sections were counterstained with hematoxylin, dehydrated, and cleared in xylene then cover-slipped for microscopic analysis. Six randomly selected fields from striatum region were analyzed for determination of GFAP immunoreactive percentage areas in individual sections using full HD microscopic camera operated by Leica application module for histological analysis (Sayed et al., 2020).

2.8 Statistical Analysis

All data obtained were expressed as mean ± SD. Results were analyzed using one-way analysis of variance test (one-way ANOVA) followed by Tukey's multiple comparison test for all parameters, except ambulation frequency and rearing frequency which were analyzed using Kruskal–Wallis test followed by Dunn's multiple comparison test. Differences in familiar and novel object exploration time for each group were tested for significance by two-way ANOVA using objects and drug treatments as set variables. Statistical analysis was performed using GraphPad Prism software (version 5). For all statistical tests, statistical significance was set at $p < 0.05$.

3 RESULTS

For all measured parameters, no significant differences were recorded between control group and DAHP group; hence, comparisons were made relative to the control group only.

3.1 Effect of 2,4-Diamino-6-Hydroxypyrimidine on Behavioral and Motor Alteration as Well as Body Weight in 3-Nitropropinic Acid Rat Model

Huntington's disease (HD) displayed striatal dysfunction was associated with motor and cognitive impairment. In 3-NP rats, marked reduction in rearing frequency and ambulation frequency to 83.33 and 69.44%, respectively, showed in open field test, in addition to decrease in fall of latency to 84.39% in rotarod test. DAHP treatment reversed 3-NP effect that was demonstrated as an increase in rearing frequency and ambulation frequency by 3.8-

TABLE 1 | Effect of DAHP on 3-NP induced change in body weight.

Group	Final body weight (g)
Control	206.8 ± 7.100
DAHP	205.1 ± 6.184
3-NP	174.8 ± 4.522[a]
3-NP + DAHP	202.7 ± 5.427[a,b]
3-NP + DAHP + WM	172.9 ± 4.032[a,c]

Note. Data are presented as means ± SD, of 14 rats per group. Statistical analysis was performed using one-way ANOVA, followed by Tukey's post hoc *test; F (4.65) = 132;* p < *0.05. 3-NP, 3-nitropropionic acid; DAHP, 2, 4-diamino-6-hydroxypyrimidine; WM, wortmannin.*

[a]p < *0.05 vs. control.*

[b]p < *0.05 vs. 3-NP.*

[c]p < *0.05 vs. 3-NP + DAHP.*

and 2.5-fold, respectively, in open field test as well as increase in fall of latency by 4.3-fold in rotarod test. In the Morris water maze test, time spent in the target quadrant was reduced to 53.09% in 3-NP group. Furthermore, in novel object recognition test, 3-NP treated rats spent significantly less time exploring the novel object than familiar object (31.1%) and less time exploring the novel object in comparison with control group (65.97%) and showed significant decrease in discrimination index and the total time spent exploring both objects (46.12%) that was a clear indication on cognitive deficit. On the contrary, DAHP treated rats showed significant increase in time spent at the target quadrant by 1.7-fold in the Morris water maze test. This was accompanied by increase in time spent in exploring the novel object than the familiar one by 1.5-fold and increase in time spent in exploring the novel object compared with the 3-NP treated group by 2.7-fold and significant increase in discrimination index and the total time spent exploring both objects by 1.8-fold. Meanwhile, WM pretreatment abolished locomotor and behavioral modulation induced by DAHP in all previous tests (**Figure 1**).

Regarding body weight, 3-NP reduced the body weight to 15.47% compared with the control group. On the other hand, treatment with DAHP alleviated 3-NP induced body weight loss by 1.16-fold compared with 3-NP group. However, pre-treatment with WM reversed the effect of DAHP in 3-NP rats (**Table 1**).

3.2 Effect of 2,4-Diamino-6-Hydroxypyrimidine on Striatal GTP Cyclohydrolase I Activity, Tetrahydrobiopterin, and Inducible Nitric Oxide Synthase

The current study investigated for the first time the possible role of GTPCH I enzyme, the rate-limiting step in BH4 biosynthesis, on iNOS regulation in HD rat model. The 3-NP induced robust increase in GTPCH I activity, BH4 content, and iNOS content to 1.78-, 1.99-, and 4.97-fold, respectively, as compared with control group. On the other hand, treatment with DAHP, GTPCH I inhibitor, showed marked inhibition in GTPCH I, BH4, and iNOS by 33.60%, 34.82%, and 66.99%, respectively, compared with 3-NP group. These effects were reversed by the coadministration of WM with DAHP (**Figure 2**).

3.3 Effect of 2,4-Diamino-6-Hydroxypyrimidine on Striatal Succinate Dehydrogenase, Proliferator-Activated Receptor Gamma Coactivator 1-Alpha, Superoxide Dismutase, and Nuclear Factor Erythroid-2-Related Factor-2 in 3-Nitropropinic Acid Rat Model

The 3-NP intoxication showed severe mitochondrial dysfunction together with oxidative stress status demonstrated as significant reduction in striatal SDH level and PGC-1α protein expression as well as SOD and Nrf2 to reach 63.33, 54, 70.22, and 77.82%, respectively, compared with the control group. DHAP improved mitochondrial dysfunction and attenuated oxidative stress; displayed as significant increase in SDH level, PGC-1α protein expression, as well as SOD and Nrf2 by 2.1-, 1.9-, 2.3-, and 3.6-

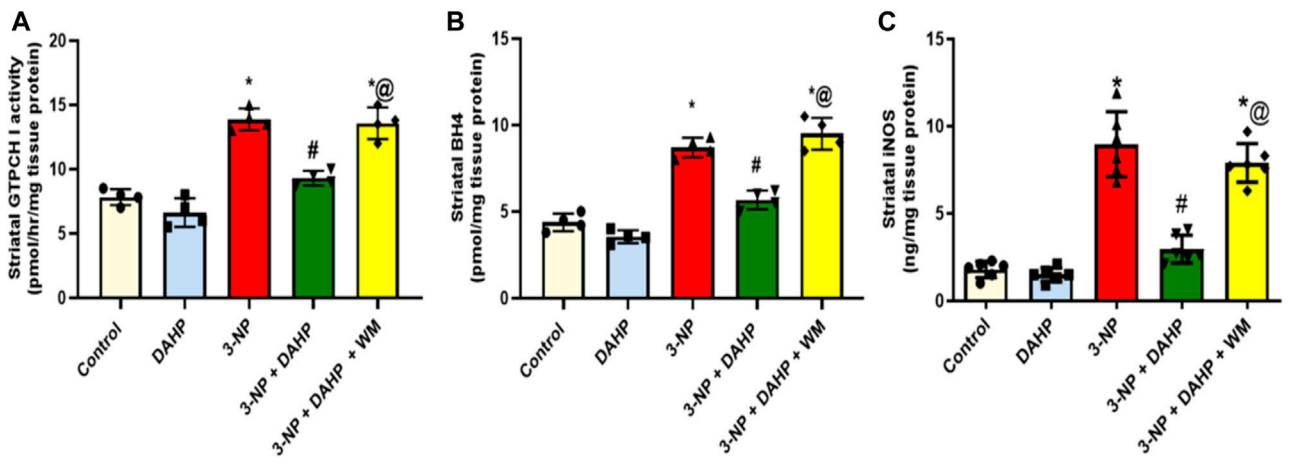

FIGURE 2 | Effect of DAHP on 3-NP induced alteration in striatal **(A)** GTPCH I activity, **(B)** BH4 and **(C)** iNOS level. Data are presented as mean ± SD of four to six rats per group, using one-way ANOVA followed by Tukey's *post-hoc* test; F (4.15) = 52.5, F (4.15) = 75, F (4.25) = 65.6; $p < 0.05$. * vs. control, # vs. 3-NP, @ vs. 3-NP + DAHP. 3-NP, 3-nitropropionic acid; DAHP, 2, 4-diamino-6-hydroxypyrimidine; WM, wortmannin; GTPCH I, GTP cyclohydrolase I; BH4, tetrahydrobiopterin; iNOS, inducible nitric oxide synthase.

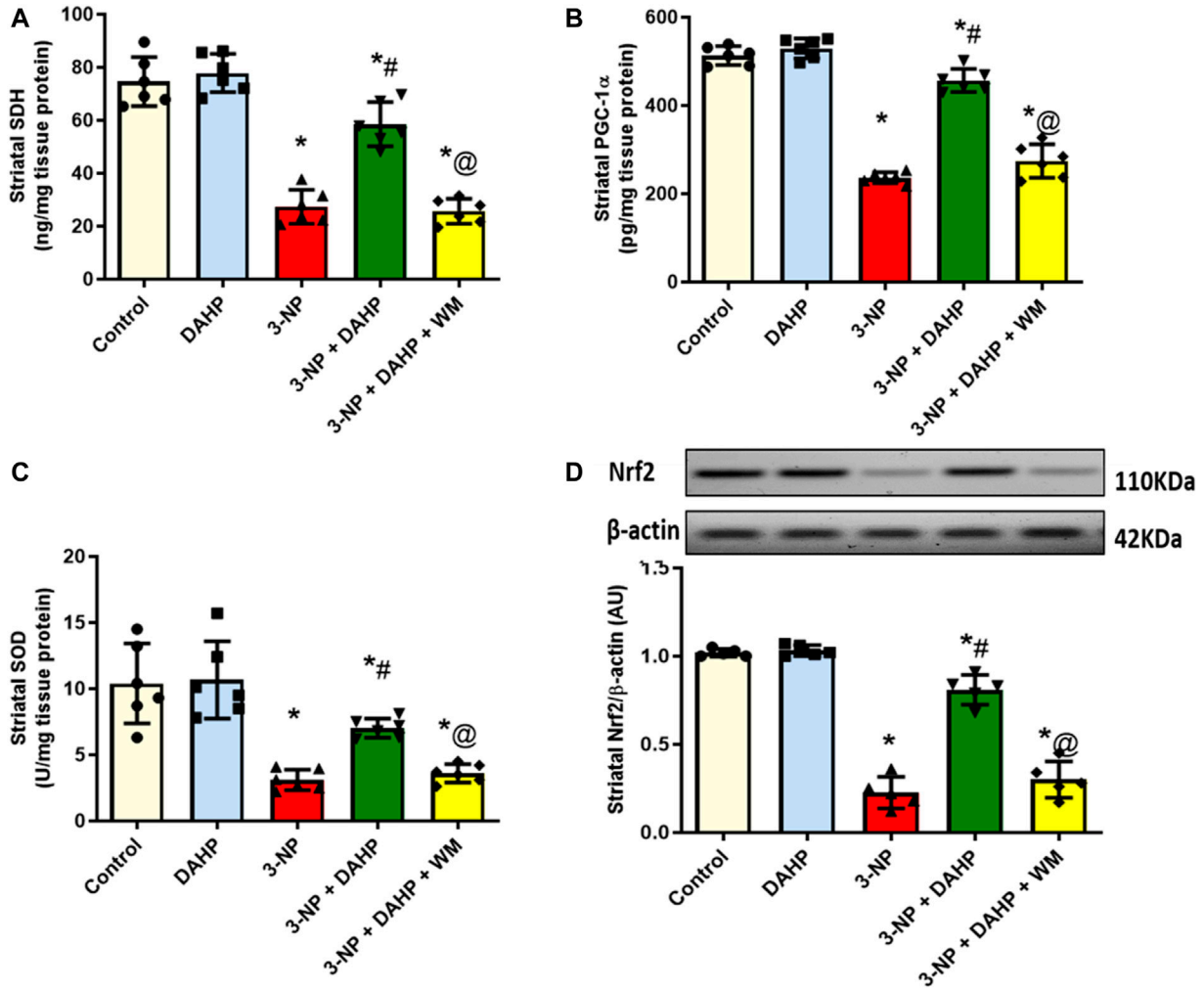

FIGURE 3 | Effect of DAHP on 3-NP induced alteration in striatal **(A)** SDH level, **(B)** PGC-1α content, **(C)** SOD activity and **(D)** Nrf2 protein expression. Data are presented as mean ± SD of five to six rats per group, using one-way ANOVA followed by Tukey's post hoc test; F (4.25) = 69.6, F (4.25) = 175.9, F (4.25) = 20.1, F (4.20) = 138.8; $p < 0.05$. * vs. control, # vs. 3-NP, @ vs. 3-NP + DAHP. 3-NP, 3-nitropropionic acid; DAHP, 2,4-diamino-6-hydroxypyrimidine; WM, wortmannin; SDH, succinate dehydrogenase; PGC-1α, proliferator-activated receptor gamma coactivator 1-alpha; SOD, superoxide dismutase; Nrf2, nuclear factor erythroid-2-related factor-2.

fold compared with 3-NP group. However, WM pre-treatment revoked DAHP-induced modification (**Figure 3**).

3.4 Effect of 2,4-Diamino-6-Hydroxypyrimidine on Striatal Neuroinflammatory Markers in 3-Nitropropinic Acid Rat Model

The 3-NP-induced neuroinflammatory status is demonstrated as a significant elevation of p65 nuclear factor-κB (p65 NF-κB) protein expression and tumor necrosis factor-alpha (TNF-α) level by 1.73- and 3.75-fold, respectively, compared with the normal rats. Furthermore, this elevation was abolished by DAHP administration to 49.13 and 38.05% relative to p65 NF-κB and TNF-α, respectively. On the other hand, WM pre-treatment largely obliterated DAHP anti-inflammatory effect and caused 1.96- and 2.52-fold rise in p65 NF-κB and TNF-α, respectively (**Figure 4**).

3.5 Effect of 2,4-Diamino-6-Hydroxypyrimidine on Striatal Contents of Mas Receptor, Phosphoinositide-3-Kinase, Phosphorylated-Serine-Threonine Kinase, Phosphorylated cAMP-Responsive Element-Binding Protein, Brain-Derived Neurotrophic Factor, and Phosphorylated Tyrosine Kinase B in 3-Nitropropinic Acid Rat Model

To assess the possible DAHP-induced neuroprotective effect on striatal MasR signaling, it was necessary to assess MasR, and its

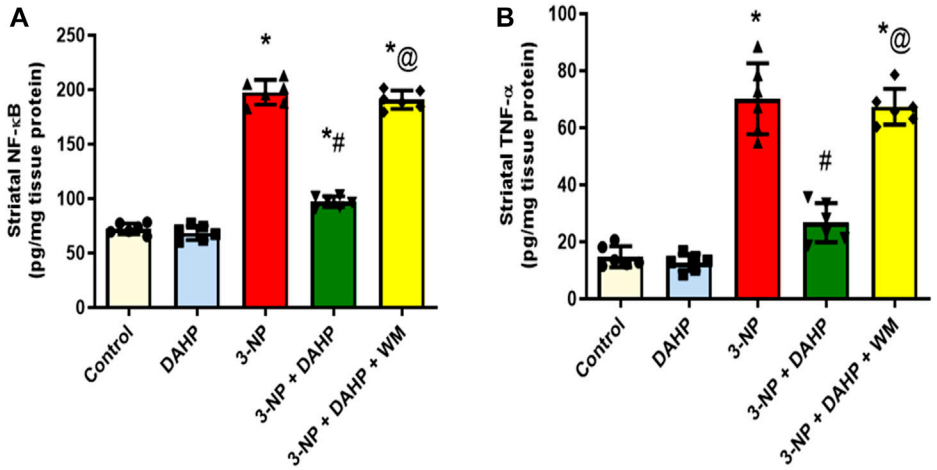

FIGURE 4 | Effect of DAHP on 3-NP induced alteration in striatal **(A)** p65 NF-κB and **(B)** TNF-α content. Data are presented as mean ± SD of six rats per group, using one-way ANOVA followed by Tukey's *post-hoc* test; F (4.25) = 418, F (4.25) = 91.2; $p < 0.05$. * vs. control, # vs. 3-NP, @ vs. 3-NP + DAHP. 3-NP, 3-nitropropionic acid; DAHP, 2,4-diamino-6-hydroxypyrimidine; WM, wortmannin; p65 NF-kB, p65 nuclear factor-kB; TNF-α, tumor necrosis factor-alpha.

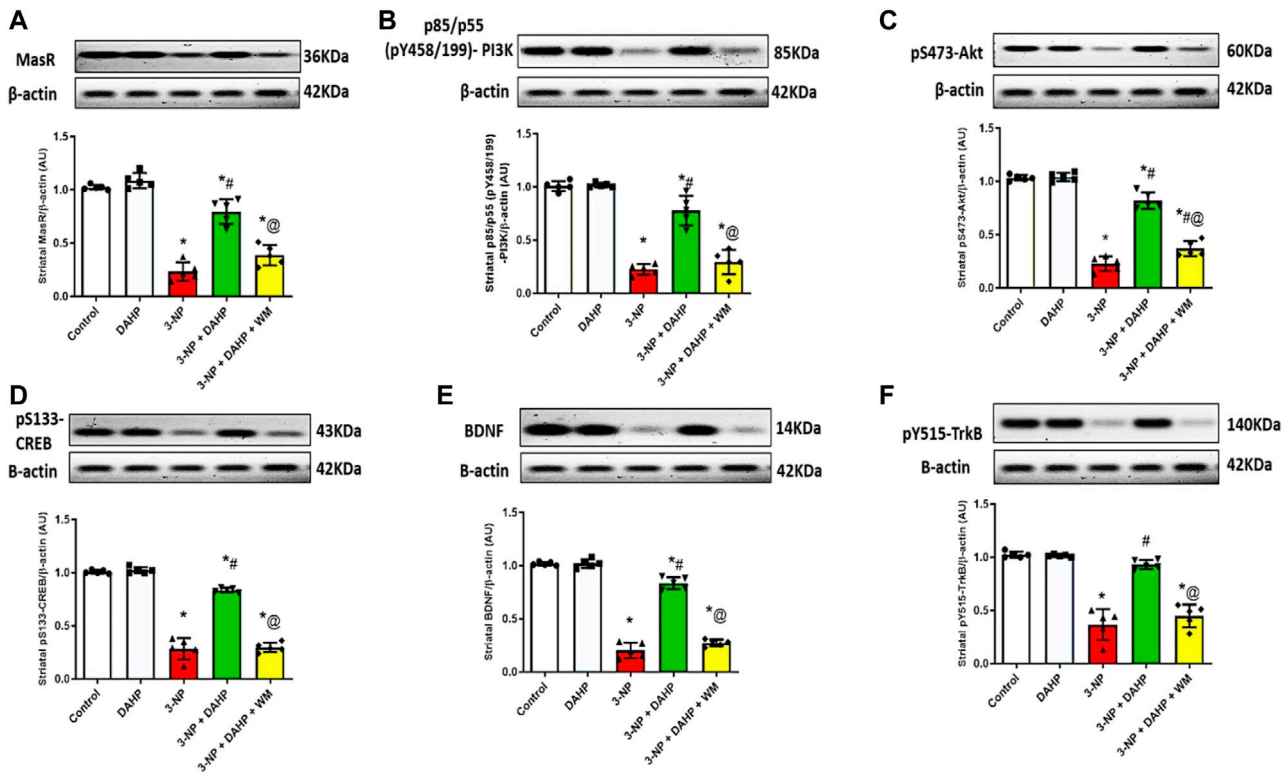

FIGURE 5 | Effect of DAHP on 3-NP induced alteration in striatal **(A)** MasR, **(B)** p-PI3K, **(C)** p-Akt, **(D)** p-CREB, **(E)** BDNF and **(F)** p-TrkB protein expression. Data are presented as mean± SD of five rats per group, using one-way ANOVA followed by Tukey's *post hoc* test; F (4.20) = 100.4, F (4.20) = 96.7, F (4.20) = 200.5, F (4.20) = 254.4, F (4.20) = 359.7, F (4.20) = 73.6; $p < 0.05$. * vs control, # vs 3-NP, @ vs 3-NP + DAHP. 3-NP, 3-nitropropionic acid; DAHP, 2, 4-diamino-6-hydroxypyrimidine; WM, wortmannin; MasR, Mas receptor; p-P13K, phosphorylated phosphoinositide-3-kinase; p-Akt, phosphorylated protein kinase B; p-CREBm phosphorylated cAMP responsive element-binding protein; BDNF, brain-derived neurotrophic factor; p-TrkB, phosphorylated tyrosine kinase B.

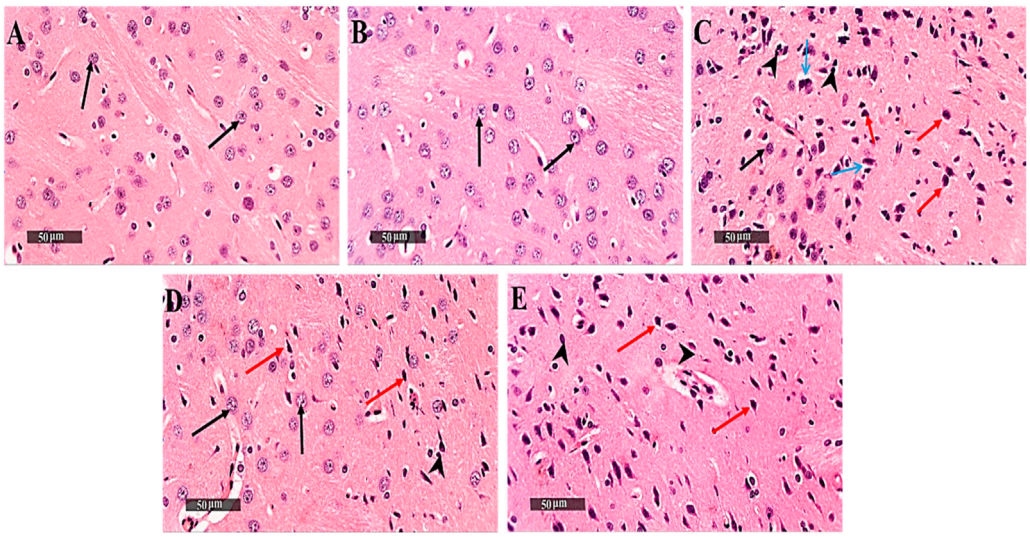

FIGURE 6 | Effect of DAHP on 3-NP induced striatal histopathological alterations. **(A–J)** photomicrographs represent staining of striatum with H&E (Scale bar 200 µm). **(A)** Control group, **(B)** DAHP alone treatment, **(C)** 3-NP group, **(D)** DAHP treated group and **(E)** WM treated group. Well organized apparent intact neurons (black arrow), degenerated neurons (red arrow), perineuronal edema (blue arrow) and severe astrogliosis (arrow head). 3-NP, 3-nitropropionic acid; DAHP, 2,4-diamino-6-hydroxypyrimidine; WM, wortmannin; H&E, hematoxylin and eosin.

down streaming signal transduction. In **Figure 5**, 3-NP caused a marked reduction in MasR protein expression together with the phosphorylated forms of PI3K, Akt, CREB, BDNF, and TrKB to 77.18, 77.82, 78.04, 71.88, 80.04, and 64.26%, respectively, compared with normal values. Oppositely, DAHP treatment elevated MasR, p-PI3K, p-Akt, p-CREB, BDNF, and p-TrKB receptor protein expression by 3.41-, 3.47-, 3.62-, 2.95-, 4.11-, and 2.5- fold, respectively, compared with the insult. This elevation was blocked by coadministration of WM with DAHP.

3.6 Effect of 2,4-Diamino-6-Hydroxypyrimidine on 3-Nitropropinic Acid Induced Striatal Histopathological Alterations

Control samples demonstrated normal histological features of striatum region with many well-organized apparent intact neurons with intact subcellular details. On the contrary, 3-NP rats showed severe neuronal loss accompanied with moderate perineuronal edema as well as severe astrogliosis was observed at external lesion border. Interestingly, DAHP treated group showed disappearance of circumscribed lesion records with significant reduction of glial cells infiltrates and appearance of mild records of perineuronal edema. Meanwhile, WM pre-treatment revoked DAHP effects and showed more extensive core lesions than in 3-NP rats (**Figure 6**).

3.7 Effect of 2,4-Diamino-6-Hydroxypyrimidine on 3-Nitropropinic Acid Induced Changes in Striatal Glial Fibrillary Acidic Protein Immunoreactivity

The immunoreactivity of striatal GFAP was assessed by immunostaining as an indicator of the magnitude of astrocyte activation. The 3-NP-treated rats with or without WM showed a significant increase in the immunoexpression of GFAP in striatum along with diffuse astrogliosis. On the other hand, striatal sections from the DAHP-treated group revealed marked reduction in GFAP immunoreactivity to 58.66%, compared with 3-NP-treated rats (**Figure 7**).

4 DISCUSSION

The current study demonstrated the first evidence for the neuroprotective effect of DAHP against 3-NP-induced neurotoxicity in rat model, which was supported by plethora of events; 1) inhibition of GTPCH I activity reduces BH4 biosynthesis resulting in reduction of nitrosative stress and alleviation of mitochondrial dysfunction, 2) activation of MasR/PI3K/Akt/CREB/BDNF/TrKB axis stimulates neurogenesis and suppresses neuroinflammatory status. These positive events were reflected on the behavioral tests showing improvement in motor performance and cognitive impairment, together with reduction in HD symptoms. On the other hand, the use of wortmannin, PI3K inhibitor, reverted the beneficial effects of DAHP.

Striatum is the central core area in the basal ganglia that controls motor coordination, administration of 3-NP produced striatal lesion, which led to motor dysfunction (Jang and Cho, 2016), cognitive impairment (Palfi et al., 1996), and poor retention of memory (Kumar et al., 2007). It was previously reported that 3-NP produces hippocampal lesions in CA1 and CA3 pyramidal neurons; the areas of the brain that is correlated with cognitive performance (Sugino et al., 1999; Kumar and Kumar, 2009). Also, 3-NP increased acetylcholinesterase activity in hippocampus compared with other brain areas suggesting the contribution of hippocampus in cognitive impairment. Furthermore, Borlongan et al. (1997) stated that

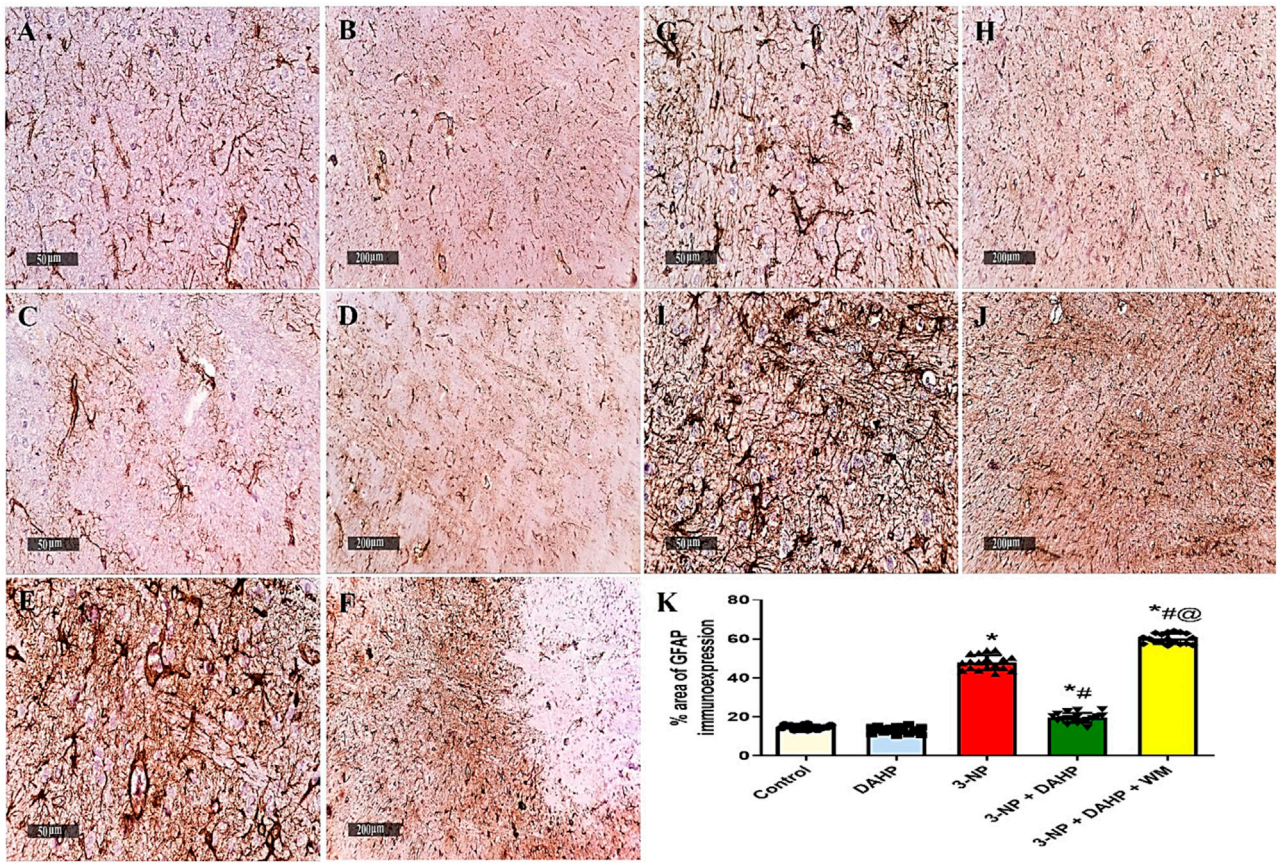

FIGURE 7 | Effect of DAHP on 3-NP induced striatal GFAP immunoreactivity. **(A–J)** photomicrographs represent immunohistochemical staining of GFAP in striatum (Scale bar 50 and 200 μm). **(A–B)** Control group, **(C–D)** DAHP alone treatment, **(E–F)** 3-NP group, **(G–H)** DAHP-treated group and **(I–J)** WM-treated group. **(K)** % area of GFAP immunoexpression. Data are presented as mean ± SD. of three rats per group, using one-way ANOVA followed by Tukey's post hoc test; F (4.25) = 643; $p < 0.05$. * vs control, # vs 3-NP, @ vs 3-NP + DAHP. 3-NP, 3-nitropropionic acid; DAHP, 2,4-diamino-6-hydroxypyrimidine; WM, wortmannin, GFAP, glial fibrillary acidic protein.

3-NP produces cerebral lesions in addition to lesions in other brain areas, including the hippocampus, thalamus, and brain cortex. In the current study, open field, rotarod, Morris water maze, and novel object recognition tests were used to evaluate motor, behavioral, and cognitive abnormalities induced by 3-NP.

Interestingly, DAHP treatment showed significant improvement in locomotor activity, spatial learning, memory retention, and cognitive performance over 3-NP rats indicating the positive effect of DAHP on 3-NP-induced neurotoxicity and degeneration. Moreover, 3-NP induced a significant decrease in the final body weight, which is considered as an indication of 3-NP neurotoxicity (Brouillet et al., 2005). This loss in body weight could be attributed to impairment of energy metabolism, mobilization of energy stores and lipid peroxidation (Pubill et al., 2001). DAHP treatment showed marked improvement in body weight compared with the 3-NP-treated group.

Mitochondrial dysfunction is one of the early pathological hallmarks of HD and one of the basic features of 3-NP model (Carmo et al., 2018). Indeed, 3-NP administration irreversibly inhibits SDH, key enzyme of electron transport chain, leading to inhibition of free fatty acid oxidation and release of massive amounts of reactive oxygen species (ROS) that eventually leads to striatal neurodegeneration (Hariharan et al., 2014; Danduga et al., 2018). Furthermore, 3-NP repressed PGC-1α expression as documented here and earlier (Ahmed et al., 2016). PGC-1α is a transcriptional coactivator that plays an important role in mitochondrial biogenesis and brain energy homeostasis. Accordingly, the suppressed PGC-1α protein expression could be another reason for mitochondrial dysfunction and striatal degeneration observed in 3-NP rats (Chen et al., 2012). Noteworthy, a previous study (St-Pierre et al., 2006) has reported the positive effect of PGC-1α in the expression of several ROS-detoxifying enzymes. Herein, DAHP treatment improved mitochondrial function through increasing SDH level and PGC-1α protein expression. Interestingly, PGC-1α gene possesses cAMP-responsive element (CRE) site for CREB, thus, increased p-CREB observed latter can be the reason for increased PGC-1α expression (Fernandez-Marcos and Auwerx, 2011; Kang et al., 2017).

Regarding oxidative stress, enhancement of Nrf2 protein expression is one of the direct transcriptional targets of CREB

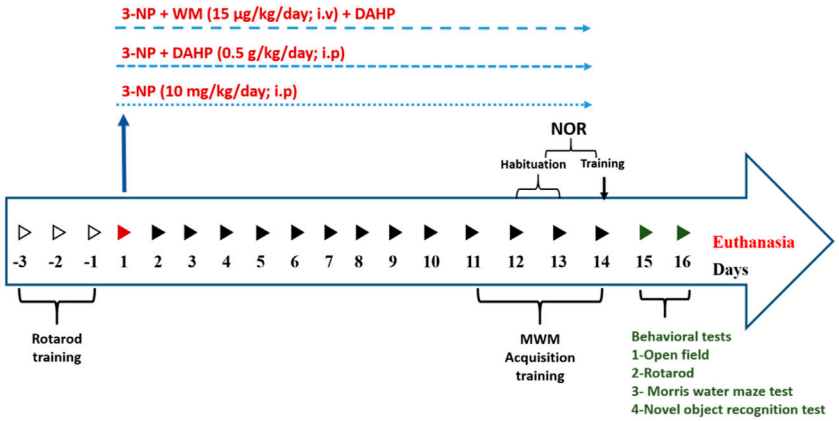

SCHEME 1 | Time schedule for DAHP and wortmannin administration and behavioral assessment in 3-Nitropropionic acid rat model.

(Katoh et al., 2001) that plays a vital role in the defense mechanism against oxidative stress *via* upregulation of antioxidant enzymes, scavenging ROS and enhancement of mitochondrial biogenesis (Satta et al., 2017). In current study, the antioxidant activity of DAHP was witnessed by significant increase in Nrf2 protein expression and SOD content. Of note, a greater protection against H_2O_2-induced DNA damage is observed in transgenic animals due to the upregulation of SOD (Reddy et al., 2004). Accordingly, the increase in SOD activity after DAHP treatment elaborates its protective effect against striatal damage caused by oxidative stress.

The 3-NP mimics HD pathogenesis through GABAergic neurons degeneration in the striatum by inducing microglial activation that causes excessive cytotoxic agents production such as nitric oxide, free radicals, and pro-inflammatory cytokines such as tumor necrosis factor-α (TNF-α) and interleukin-1β (IL-1β) (Bonsi et al., 2006; Ahuja et al., 2008). These proinflammatory cytokines have been reported to enhance GTPCH I activity, the rate limiting step for BH4 biosynthesis, that is required as essential cofactor for iNOS activation and NO production (Werner et al., 1993). Subsequently, NO interacts with superoxide to form peroxynitrite ($ONOO^-$), a toxic derivative that causes neuronal loss (Saha and Pahan, 2006). Previous studies demonstrated that iNOS has been involved in various neurodegenerative diseases including Alzheimer's disease, Parkinson's disease and HD (Dehmer et al., 2004; Lee et al., 2008). Noteworthy, iNOS expression was repressed after DAHP treatment in rat model of MACO due to inhibition of BH4 synthesis (Kidd et al., 2005). Similarly, in our study, DAHP inhibited iNOS expression through inhibition of GTPCH I activity and consequently reduction in BH4 levels, besides reducing TNF-α level following suppression of inflammatory response. Interestingly, in the current study DAHP treatment showed significant inhibition in NF-κB expression through PI3K/Akt pathway activation and suppression of microglial activity. These data is in line with those of Li et al. (2015), who proved that the anti-inflammatory effect of DAHP against cerebral ischemic model is mediated *via* inhibition of NF-κB expression.

Recently, central renin–angiotensin system (RAS) has been involved in the pathogenesis of several neurodegenerative diseases such as PD, AD, and HD (Tian et al., 2012; Rabie et al., 2018; Machado et al., 2020). Of note, Mas receptor (MasR), a RAS component that is expressed in different brain area, has been evoked as counter regulatory arm that opposed the devastating effect of ACE/Ang II/AT1R axis and offered neuroprotective effect through upregulation of PI3K/Akt (Jiang et al., 2013; Rabie et al., 2018). Activated PI3K triggers Akt phosphorylation, this axis entails activation/phosphorylation of CREB (Sakamoto et al., 2011). Phosphorylated CREB plays a substantial role in neurotrophin-mediated neuronal survival *via* transcription of BDNF (Bonni et al., 1999; Sayed et al., 2020) and its receptor TrKB (Song et al., 2015). Worth mentioning, increased BDNF stimulates neurogenesis and triggers TrKB phosphorylation to act as a positive feed-forward loop to re-stimulate MasR and PI3K/Akt axis to promote neuronal survival (Yao et al., 2012; Rabie et al., 2018). Moreover, activated p-TrKB re-activates CREB by phosphorylating it at the S133 site to sustain this cascade (Yoshii and Constantine-Paton, 2010).

Our study revealed that DAHP treatment showed neuroprotective effect against 3-NP *via* increment of MasR protein expression and activation of downstream PI3K/Akt/CREB/BDNF/TrKB cascade. These findings were in line with Li et al. (2015), who stated the neuroprotective effects of DAHP against focal cerebral ischemia was attributed to PI3K/Akt activation. Another evidence to confirm that DAHP neuroprotective effect was mediated through PI3K/Akt pathway was provided by WM, a PI3K inhibitor that abolished histological and biochemical modifications presented by DAHP through blocking the phosphorylation of PI3K and Akt in DAHP-treated rats.

In conclusion, the behavioral, histological, cellular, and neurochemical findings of the current study support for the first time the role of MasR/PI3K/Akt/CREB/BDNF/TrKB pathway activation and iNOS inhibition in the neuroprotective

effect of DAHP against neurotoxicity and mitochondrial dysfunction induced by 3-NP, thus, offering a new prospect for the possible role of BH4 inhibitors in HD.

DATA AVAILABILITY STATEMENT

The original contributions presented in the study are included in the article/**Supplementary Material**, further inquiries can be directed to the corresponding author.

ETHICS STATEMENT

The animal study was reviewed and approved by the Ethics Committee, Faculty of Pharmacy, Cairo University.

AUTHOR CONTRIBUTIONS

AM handled the conceptualization, methodology, investigation, formal analysis, and the writing of the original draft. AS was in charge of the software and validation. MR also handled the conceptualization, methodology, visualization, supervision, writing, review, and editing of the manuscript. HZ performed the data curation and supervision.

SUPPLEMENTARY MATERIAL

The Supplementary Material for this article can be found online at: https://www.frontiersin.org/articles/10.3389/fphar.2021.740966/full#supplementary-material

REFERENCES

Ahmed, L. A., Darwish, H. A., Abdelsalam, R. M., and Amin, H. A. (2016). Role of Rho Kinase Inhibition in the Protective Effect of Fasudil and Simvastatin against 3-nitropropionic Acid-Induced Striatal Neurodegeneration and Mitochondrial Dysfunction in Rats. *Mol. Neurobiol.* 53, 3927–3938. doi:10.1007/s12035-015-9303-2

Ahuja, M., Bishnoi, M., and Chopra, K. (2008). Protective Effect of Minocycline, a Semi-synthetic Second-Generation Tetracycline against 3-nitropropionic Acid (3-Np)-Induced Neurotoxicity. *Toxicology* 244, 111–122. doi:10.1016/j.tox.2007.11.003

Alp, N. J., and Channon, K. M. (2004). Regulation of Endothelial Nitric Oxide Synthase by Tetrahydrobiopterin in Vascular Disease. *Arterioscler Thromb. Vasc. Biol.* 24, 413–420. doi:10.1161/01.ATV.0000110785.96039.f6

Antunes, M., and Biala, G. (2012). The Novel Object Recognition Memory: Neurobiology, Test Procedure, and its Modifications. *Cogn. Process.* 13, 93–110. doi:10.1007/s10339-011-0430-z

Arnt, J., Bang-Andersen, B., Grayson, B., Bymaster, F. P., Cohen, M. P., DeLapp, N. W., et al. (2010). Lu AE58054, a 5-HT6 Antagonist, Reverses Cognitive Impairment Induced by Subchronic Phencyclidine in a Novel Object Recognition Test in Rats. *Int. J. Neuropsychopharmacol.* 13, 1021–1033. doi:10.1017/S1461145710000659

Avila, D. S., Colle, D., Gubert, P., Palma, A. S., Puntel, G., Manarin, F., et al. (2010). A Possible Neuroprotective Action of a Vinylic telluride against Mn-Induced Neurotoxicity. *Toxicol. Sci.* 115, 194–201. doi:10.1093/toxsci/kfq036

Block, M. L., Zecca, L., and Hong, J. S. (2007). Microglia-mediated Neurotoxicity: Uncovering the Molecular Mechanisms. *Nat. Rev. Neurosci.* 8, 57–69. doi:10.1038/nrn2038

Bonni, A., Brunet, A., West, A. E., Datta, S. R., Takasu, M. A., and Greenberg, M. E. (1999). Cell Survival Promoted by the Ras-MAPK Signaling Pathway by Transcription-dependent and -independent Mechanisms. *Science* 286, 1358–1362. doi:10.1126/science.286.5443.1358

Bonsi, P., Cuomo, D., Martella, G., Sciamanna, G., Tolu, M., Calabresi, P., et al. (2006). Mitochondrial Toxins in Basal Ganglia Disorders: from Animal Models to Therapeutic Strategies. *Curr. Neuropharmacol* 4, 69–75. doi:10.2174/157015906775203039

Borlongan, C. V., Koutouzis, T. K., Freeman, T. B., Hauser, R. A., Cahill, D. W., and Sanberg, P. R. (1997). Hyperactivity and Hypoactivity in a Rat Model of Huntington's Disease: the Systemic 3-nitropropionic Acid Model. *Brain Res. Brain Res. Protoc.* 1, 253–257. doi:10.1016/s1385-299x(96)00037-2

Brouillet, E., Jacquard, C., Bizat, N., and Blum, D. (2005). 3-Nitropropionic Acid: a Mitochondrial Toxin to Uncover Physiopathological Mechanisms Underlying Striatal Degeneration in Huntington's Disease. *J. Neurochem.* 95, 1521–1540. doi:10.1111/j.1471-4159.2005.03515.x

Carmo, C., Naia, L., Lopes, C., and Rego, A. C. (2018). Mitochondrial Dysfunction in Huntington's Disease. *Adv. Exp. Med. Biol.* 1049, 59–83. doi:10.1007/978-3-319-71779-1_3

Chen, J., Xu, Z. C., Xu, X. M., and Zhang, J. H. (2019). Animal Models of Acute Neurological Injury. AJNR Am J Neuroradiol, 30. e45. doi:10.1007/978-3-030-16082-1

Chen, L. W., Horng, L. Y., Wu, C. L., Sung, H. C., and Wu, R. T. (2012). Activating Mitochondrial Regulator PGC-1α Expression by Astrocytic NGF Is a Therapeutic Strategy for Huntington's Disease. *Neuropharmacology* 63, 719–732. doi:10.1016/j.neuropharm.2012.05.019

d'Uscio, L. V., Milstien, S., Richardson, D., Smith, L., and Katusic, Z. S. (2003). Long-term Vitamin C Treatment Increases Vascular Tetrahydrobiopterin Levels and Nitric Oxide Synthase Activity. *Circ. Res.* 92 (1), 88–95. doi:10.1161/01.res.0000049166.33035.62

Danduga, R. C. S. R., Dondapati, S. R., Kola, P. K., Grace, L., Tadigiri, R. V. B., and Kanakaraju, V. K. (2018). Neuroprotective Activity of Tetramethylpyrazine against 3-nitropropionic Acid Induced Huntington's Disease-like Symptoms in Rats. *Biomed. Pharmacother.* 105, 1254–1268. doi:10.1016/j.biopha.2018.06.079

Dehmer, T., Heneka, M. T., Sastre, M., Dichgans, J., and Schulz, J. B. (2004). Protection by Pioglitazone in the MPTP Model of Parkinson's Disease Correlates with IκBα Induction and Block of NFκB and iNOS Activation. *J. Neurochem.* 88, 494–501. doi:10.1046/j.1471-4159.2003.02210.x

Fernandez-Marcos, P. J., and Auwerx, J. (2011). Regulation of PGC-1α, a Nodal Regulator of Mitochondrial Biogenesis. *Am. J. Clin. Nutr.* 93, 884S–890S. doi:10.3945/ajcn.110.001917

Gao, H. M., Liu, B., Zhang, W., and Hong, J. S. (2003). Synergistic Dopaminergic Neurotoxicity of MPTP and Inflammogen Lipopolysaccharide: Relevance to the Etiology of Parkinson's Disease. *FASEB J.* 17, 1957–1959. doi:10.1096/fj.03-0203fje

Gao, Y., Chu, S. F., Li, J. P., Zhang, Z., Yan, J. Q., Wen, Z. L., et al. (2015). Protopanaxtriol Protects against 3-nitropropionic Acid-Induced Oxidative Stress in a Rat Model of Huntington's Disease. *Acta Pharmacol. Sin* 36, 311–322. doi:10.1038/aps.2014.107

Glass, C. K., Saijo, K., Winner, B., Marchetto, M. C., and Gage, F. H. (2010). Mechanisms Underlying Inflammation in Neurodegeneration. *Cell* 140, 918–934. doi:10.1016/j.cell.2010.02.016

Hariharan, A., Shetty, S., Shirole, T., and Jagtap, A. G. (2014). Potential of Protease Inhibitor in 3-nitropropionic Acid Induced Huntington's Disease like Symptoms: Mitochondrial Dysfunction and Neurodegeneration. *Neurotoxicology* 45, 139–148. doi:10.1016/j.neuro.2014.10.004

Heras-Sandoval, D., Pérez-Rojas, J. M., Hernández-Damián, J., and Pedraza-Chaverri, J. (2014). The Role of PI3K/AKT/mTOR Pathway in the Modulation of Autophagy and the Clearance of Protein Aggregates in Neurodegeneration. *Cell. Signal.* 26, 2694–2701. doi:10.1016/j.cellsig.2014.08.019

Huang, A., Zhang, Y. Y., Chen, K., Hatakeyama, K., and Keaney, J. F., Jr (2005). Cytokine-stimulated GTP Cyclohydrolase I Expression in Endothelial Cells Requires Coordinated Activation of Nuclear Factor-kappaB and Stat1/Stat3. *Circ. Res.* 96, 164–171. doi:10.1161/01.RES.0000153669.24827.DF

Jamwal, S., and Kumar, P. (2016). Spermidine Ameliorates 3-nitropropionic Acid (3-Np)-Induced Striatal Toxicity: Possible Role of Oxidative Stress, Neuroinflammation, and Neurotransmitters. *Physiol. Behav.* 155, 180–187. doi:10.1016/j.physbeh.2015.12.015

Jang, M., and Cho, I. H. (2016). Sulforaphane Ameliorates 3-Nitropropionic Acid-Induced Striatal Toxicity by Activating the Keap1-Nrf2-ARE Pathway and Inhibiting the MAPKs and NF-Kb Pathways. *Mol. Neurobiol.* 53, 2619–2635. doi:10.1007/s12035-015-9230-2

Jiang, T., Gao, L., Lu, J., and Zhang, Y. D. (2013). ACE2-Ang-(1-7)-Mas axis in Brain: a Potential Target for Prevention and Treatment of Ischemic Stroke. *Curr. Neuropharmacol.* 11, 209–217. doi:10.2174/1570159x11311020007

Kang, H., Khang, R., Ham, S., Jeong, G. R., Kim, H., Jo, M., et al. (2017). Activation of the ATF2/CREB-PGC-1α Pathway by Metformin Leads to Dopaminergic Neuroprotection. *Oncotarget* 8, 48603–48618. doi:10.18632/oncotarget.18122

Karasawa, J., Hashimoto, K., and Chaki, S. (2008). D-serine and a glycine Transporter Inhibitor Improve MK-801-Induced Cognitive Deficits in a Novel Object Recognition Test in Rats. *Behav. Brain Res.* 186, 78–83. doi:10.1016/j.bbr.2007.07.033

Katoh, Y., Itoh, K., Yoshida, E., Miyagishi, M., Fukamizu, A., and Yamamoto, M. (2001). Two Domains of Nrf2 Cooperatively Bind CBP, a CREB Binding Protein, and Synergistically Activate Transcription. *Genes Cells* 6, 857–868. doi:10.1046/j.1365-2443.2001.00469.x

Kidd, G. A., Hong, H., Majid, A., Kaufman, D. I., and Chen, A. F. (2005). Inhibition of Brain GTP Cyclohydrolase I and Tetrahydrobiopterin Attenuates Cerebral Infarction via Reducing Inducible NO Synthase and Peroxynitrite in Ischemic Stroke. *Stroke* 36, 2705–2711. doi:10.1161/01.STR.0000190000.98707.6d

Kumar, P., Kalonia, H., and Kumar, A. (2010). Possible Nitric Oxide Modulation in Protective Effect of FK-506 against 3-nitropropionic Acid-Induced Behavioral, Oxidative, Neurochemical, and Mitochondrial Alterations in Rat Brain. *Drug Chem. Toxicol.* 33, 377–392. doi:10.3109/01480541003642050

Kumar, P., and Kumar, A. (2009). Neuroprotective Effect of Cyclosporine and FK506 against 3-nitropropionic Acid Induced Cognitive Dysfunction and Glutathione Redox in Rat: Possible Role of Nitric Oxide. *Neurosci. Res.* 63, 302–314. doi:10.1016/j.neures.2009.01.005

Kumar, P., Padi, S. S., Naidu, P. S., and Kumar, A. (2007). Possible Neuroprotective Mechanisms of Curcumin in Attenuating 3-nitropropionic Acid-Induced Neurotoxicity. *Methods Find Exp. Clin. Pharmacol.* 29, 19–25. doi:10.1358/mf.2007.29.1.1063492

Kumar, P., Kalonia, H., and Kumar, A. (2011). Expression of Concern: Role of LOX/COX Pathways in 3-nitropropionic Acid-induced Huntington's Disease-like Symptoms in Rats: Protective Effect of Licofelone. *Br. J. Pharmacol.* 164, 644–654. doi:10.1111/j.1476-5381.2011.01418.x

Lee, S. T., Chu, K., Park, J. E., Hong, N. H., Im, W. S., Kang, L., et al. (2008). Atorvastatin Attenuates Mitochondrial Toxin-Induced Striatal Degeneration, with Decreasing iNOS/c-Jun Levels and Activating ERK/Akt Pathways. *J. Neurochem.* 104, 1190–1200. doi:10.1111/j.1471-4159.2007.05044.x

Li, W., Yang, Y., Hu, Z., Ling, S., and Fang, M. (2015). Neuroprotective Effects of DAHP and Triptolide in Focal Cerebral Ischemia via Apoptosis Inhibition and PI3K/Akt/mTOR Pathway Activation. *Front. Neuroanat.* 9, 48. doi:10.3389/fnana.2015.00048

Liu, P. W., Chen, M. F., Tsai, A. P., and Lee, T. J. (2012). STAT1 Mediates Oroxylin a Inhibition of iNOS and Pro-inflammatory Cytokines Expression in Microglial BV-2 Cells. *PLoS One* 7, e50363. doi:10.1371/journal.pone.0050363

Machado, T. C. G., Guatimosim, C., and Kangussu, L. M. (2020). The Renin-Angiotensin System in Huntington's Disease: Villain or Hero. *Protein Pept. Lett.* 27, 456–462. doi:10.2174/0929866527666200110154523

Mander, P., and Brown, G. C. (2005). Activation of Microglial NADPH Oxidase Is Synergistic with Glial iNOS Expression in Inducing Neuronal Death: a Dual-Key Mechanism of Inflammatory Neurodegeneration. *J. Neuroinflammation* 2, 20–15. doi:10.1186/1742-2094-2-20

Palfi, S., Ferrante, R. J., Brouillet, E., Beal, M. F., Dolan, R., Guyot, M. C., et al. (1996). Chronic 3-nitropropionic Acid Treatment in Baboons Replicates the Cognitive and Motor Deficits of Huntington's Disease. *J. Neurosci.* 16, 3019–3025. doi:10.1523/JNEUROSCI.16-09-03019.1996

Pedraza-Chaverrí, J., Reyes-Fermín, L. M., Nolasco-Amaya, E. G., Orozco-Ibarra, M., Medina-Campos, O. N., González-Cuahutencos, O., et al. (2009). ROS Scavenging Capacity and Neuroprotective Effect of α-mangostin against 3-nitropropionic Acid in Cerebellar Granule Neurons. *Exp. Toxicologic Pathol.* 61, 491–501. doi:10.1016/j.etp.2008.11.002

Pérez-De La Cruz, V., Elinos-Calderón, D., Robledo-Arratia, Y., Medina-Campos, O. N., Pedraza-Chaverrí, J., Ali, S. F., et al. (2009). Targeting Oxidative/nitrergic Stress Ameliorates Motor Impairment, and Attenuates Synaptic Mitochondrial Dysfunction and Lipid Peroxidation in Two Models of Huntington's Disease. *Behav. Brain Res.* 199, 210–217. doi:10.1016/j.bbr.2008.11.037

Pubill, D., Verdaguer, E., Canudas, A. M., Sureda, F. X., Escubedo, E., Camarasa, J., et al. (2001). Orphenadrine Prevents 3-nitropropionic Acid-Induced Neurotoxicity *In Vitro* and *In Vivo*. *Br. J. Pharmacol.* 132, 693–702. doi:10.1038/sj.bjp.0703869

Rabie, M. A., Abd El Fattah, M. A., Nassar, N. N., El-Abhar, H. S., and Abdallah, D. M. (2018). Angiotensin 1-7 Ameliorates 6-hydroxydopamine Lesions in Hemiparkinsonian Rats through Activation of MAS receptor/PI3K/Akt/BDNF Pathway and Inhibition of Angiotensin II Type-1 receptor/NF-Kb axis. *Biochem. Pharmacol.* 151, 126–134. doi:10.1016/j.bcp.2018.01.047

Ramachandran, S., and Thangarajan, S. (2016). A Novel Therapeutic Application of Solid Lipid Nanoparticles Encapsulated Thymoquinone (TQ-SLNs) on 3-nitroproponic Acid Induced Huntington's Disease-like Symptoms in Wistar Rats. *Chem. Biol. Interact* 256, 25–36. doi:10.1016/j.cbi.2016.05.020

Ramachandran, S., and Thangarajan, S. (2018). Thymoquinone Loaded Solid Lipid Nanoparticles Counteracts 3-Nitropropionic Acid Induced Motor Impairments and Neuroinflammation in Rat Model of Huntington's Disease. *Metab. Brain Dis.* 33, 1459–1470. doi:10.1007/s11011-018-0252-0

Reddy, V. N., Kasahara, E., Hiraoka, M., Lin, L. R., and Ho, Y. S. (2004). Effects of Variation in Superoxide Dismutases (SOD) on Oxidative Stress and Apoptosis in Lens Epithelium. *Exp. Eye Res.* 79, 859–868. doi:10.1016/j.exer.2004.04.005

Ribeiro, M., Rosenstock, T. R., Oliveira, A. M., Oliveira, C. R., and Rego, A. C. (2014). Insulin and IGF-1 Improve Mitochondrial Function in a PI-3K/Akt-dependent Manner and Reduce Mitochondrial Generation of Reactive Oxygen Species in Huntington's Disease Knock-In Striatal Cells. *Free Radic. Biol. Med.* 74, 129–144. doi:10.1016/j.freeradbiomed.2014.06.023

Roos, R. A. (2010). Huntington's Disease: A Clinical Review. *Orphanet J. Rare Dis.* 5, 40. doi:10.1186/1750-1172-5-40

Saha, R. N., and Pahan, K. (2006). Regulation of Inducible Nitric Oxide Synthase Gene in Glial Cells. *Antioxid. Redox Signal.* 8, 929–947. doi:10.1089/ars.2006.8.929

Sakamoto, K., Karelina, K., and Obrietan, K. (2011). CREB: a Multifaceted Regulator of Neuronal Plasticity and protection. *J. Neurochem.* 116, 1–9. doi:10.1111/j.1471-4159.2010.07080.x

Salvati, K., and Beenhakker, M. (2019). Astrocyte Receptor Rebirth. *Epilepsy Curr.* 19, 196–198. doi:10.1177/1535759719844267

Sapp, E., Kegel, K. B., Aronin, N., Hashikawa, T., Uchiyama, Y., Tohyama, K., et al. (2001). Early and Progressive Accumulation of Reactive Microglia in the Huntington Disease Brain. *J. Neuropathol. Exp. Neurol.* 60, 161–172. doi:10.1093/jnen/60.2.161

Satta, S., Mahmoud, A. M., Wilkinson, F. L., Yvonne Alexander, M., and White, S. J. (20172017). The Role of Nrf2 in Cardiovascular Function and Disease. *Oxid Med. Cel Longev* 2017, 9237263–9237318. doi:10.1155/2017/9237263

Sayed, N. H., Fathy, N., Kortam, M. A., Rabie, M. A., Mohamed, A. F., and Kamel, A. S. (2020). Vildagliptin Attenuates Huntington's Disease through Activation of GLP-1 Receptor/PI3K/Akt/BDNF Pathway in 3-Nitropropionic Acid Rat Model. *Neurotherapeutics* 17 (1), 252–268. doi:10.1007/s13311-019-00805-5

Shah, M., Datson, N., Srinidhi, L., Stanton, V., MacDonald, M., Allard, M., et al. (1993). A Novel Gene Containing a Trinucleotide Repeat that Is Expanded and Unstable on Huntington's Disease Chromosomes. The Huntington's Disease Collaborative Research Group. *Cell* 72, 971–983. doi:10.1016/0092-8674(93)90585-e

Sidhu, A., Diwan, V., Kaur, H., Bhateja, D., Singh, C. K., Sharma, S., et al. (2018). Nicotinamide Reverses Behavioral Impairments and Provides Neuroprotection in 3-nitropropionic Acid Induced Animal Model ofHuntington's Disease: Implication of Oxidative Stress- Poly(ADP- Ribose) Polymerase Pathway. *Metab. Brain Dis.* 33, 1911–1921. doi:10.1007/s11011-018-0297-0

Song, J. H., Yu, J. T., and Tan, L. (2015). Brain-Derived Neurotrophic Factor in Alzheimer's Disease: Risk, Mechanisms, and Therapy. *Mol. Neurobiol.* 52, 1477–1493. doi:10.1007/s12035-014-8958-4

St-Pierre, J., Drori, S., Uldry, M., Silvaggi, J. M., Rhee, J., Jäger, S., et al. (2006). Suppression of Reactive Oxygen Species and Neurodegeneration by the PGC-1 Transcriptional Coactivators. *Cell* 127, 397–408. doi:10.1016/j.cell.2006.09.024

Suganya, S. N., and Sumathi, T. (2017). Effect of Rutin against a Mitochondrial Toxin, 3-nitropropionicacid Induced Biochemical, Behavioral and Histological Alterations-A Pilot Study on Huntington's Disease Model in Rats. *Metab. Brain Dis.* 32, 471–481. doi:10.1007/s11011-016-9929-4

Sugino, T., Nozaki, K., Takagi, Y., Hattori, I., Hashimoto, N., and Yodoi, J. (1999). Expression and Distribution of Redox Regulatory Protein, Thioredoxin after Metabolic Impairment by 3-nitropropionic Acid in Rat Brain. *Neurosci. Lett.* 275, 145–148. doi:10.1016/s0304-3940(99)00763-6

Tabrizi, S. J., Ghosh, R., and Leavitt, B. R. (2019). Huntingtin Lowering Strategies for Disease Modification in Huntington's Disease. *Neuron* 101, 801–819. doi:10.1016/j.neuron.2019.01.039

Thöny, B., Auerbach, G., and Blau, N. (2000). Tetrahydrobiopterin Biosynthesis, Regeneration and Functions. *Biochem. J.* 347, 1–16. doi:10.1042/bj3470001

Tian, M., Zhu, D., Xie, W., and Shi, J. (2012). Central Angiotensin II-Induced Alzheimer-like Tau Phosphorylation in normal Rat Brains. *FEBS Lett.* 586, 3737–3745. doi:10.1016/j.febslet.2012.09.004

Werner, E. R., Werner-Felmayer, G., and Wachter, H. (1993). Tetrahydrobiopterin and Cytokines. *Proc. Soc. Exp. Biol. Med.* 203, 1–12. doi:10.3181/00379727-203-43566a

Yao, R. Q., Qi, D. S., Yu, H. L., Liu, J., Yang, L. H., and Wu, X. X. (2012). Quercetin Attenuates Cell Apoptosis in Focal Cerebral Ischemia Rat Brain via Activation of BDNF-TrkB-PI3K/Akt Signaling Pathway. *Neurochem. Res.* 37, 2777–2786. doi:10.1007/s11064-012-0871-5

Yoshii, A., and Constantine-Paton, M. (2010). Postsynaptic BDNF-TrkB Signaling in Synapse Maturation, Plasticity, and Disease. *Dev. Neurobiol.* 70, 304–322. doi:10.1002/dneu.20765

Yue, T. L., Bao, W., Gu, J. L., Cui, J., Tao, L., Ma, X. L., et al. (2005). Rosiglitazone Treatment in Zucker Diabetic Fatty Rats Is Associated with Ameliorated Cardiac Insulin Resistance and protection from Ischemia/reperfusion-Induced Myocardial Injury. *Diabetes* 54, 554–562. doi:10.2337/diabetes.54.2.554

Zafir, A., Ara, A., and Banu, N. (2009). *In vivo* Antioxidant Status: A Putative Target of Antidepressant Action. *Prog. Neuropsychopharmacol. Biol. Psychiatry* 33, 220–228. doi:10.1016/j.pnpbp.2008.11.010

Zuo, D., Lin, L., Liu, Y., Wang, C., Xu, J., Sun, F., et al. (2016). Baicalin Attenuates Ketamine-Induced Neurotoxicity in the Developing Rats: Involvement of PI3K/Akt and CREB/BDNF/Bcl-2 Pathways. *Neurotox. Res.* 30, 159–172. doi:10.1007/s12640-016-9611-y

Conflict of Interest: The authors declare that the research was conducted in the absence of any commercial or financial relationships that could be construed as a potential conflict of interest.

Publisher's Note: All claims expressed in this article are solely those of the authors and do not necessarily represent those of their affiliated organizations, or those of the publisher, the editors, and the reviewers. Any product that may be evaluated in this article, or claim that may be made by its manufacturer, is not guaranteed or endorsed by the publisher.

GLOSSARY

3-NP 3-nitropropionic acid
ACE angiotensin-converting enzyme
Akt serine–threonine kinase Akt
Ang II angiotensin II
ARE antioxidant response element
AT1R angiotensin type-1 receptor
ATP adenosine triphosphate
AU arbitrary unit
BDNF brain-derived neurotrophic factor
BH4 tetrahydrobiopterin
BSA bovine serum albumin
CBP CREB-binding protein
CRE cAMP-responsive element
CREB cAMP-responsive element-binding protein
DAB 3,3′-diaminobenzidine tetrahydrochloride
DAHP 2,4-diamino-6-hydroxypyrimidine
DMSO dimethyl sulfoxide
GFAP glial fibrillary acidic protein
GTPCH 1 GTP cyclohydrolase 1
H&E hematoxylin and eosin
HD Huntington's disease
HTT huntingtin
iNOS inducible nitric oxide syntheses
IL-1 interleukin-1
MASR MAS receptor
MCAO middle cerebral artery occlusion
NF-κB nuclear factor-κB
NO nitric oxide
Nrf2 nuclear factor erythroid-2-related factor-2
OFT open field test
ONOO- peroxynitrite
PGC-1α proliferator-activated receptor gamma coactivator 1-alpha
PI3K phosphoinositide-3-kinase
RAS renin–angiotensin system
RIPA radio immunoprecipitation assay
ROS reactive oxygen species
SDH succinate dehydrogenase
SOD superoxide dismutase
TNF-α tumor necrosis factor-alpha
TrkB tyrosine kinase B
WM wortmannin

frontiers in Pharmacology

ORIGINAL RESEARCH
published: 14 January 2022
doi: 10.3389/fphar.2021.772485

Neuroprotective Effect of Daidzein Extracted From *Pueraria* lobate Radix in a Stroke Model *Via* the Akt/mTOR/BDNF Channel

Meizhu Zheng[1], *Mi Zhou*[2], *Minghui Chen*[2], *Yao Lu*[2], *Dongfang Shi*[1], *Jing Wang*[2] *and Chunming Liu*[1]*

[1]The Central Laboratory, Changchun Normal University, Changchun, China, [2]College of Life Science, Changchun Normal University, Changchun, China

Daidzein is a plant isoflavonoid primarily isolated from *Pueraria lobate* Radix as the dry root of *P. lobata* (Wild.) Ohwi, have long been used as nutraceutical and medicinal herb in China. Despite the report that daidzein can prevent neuronal damage and improve outcome in experimental stroke, the mechanisms of this neuroprotective action have been not fully elucidated. The aim of this study was to determine whether the daidzein elicits beneficial actions in a stroke model, namely, cerebral ischemia/reperfusion (I/R) injury, and to reveal the underlying neuroprotective mechanisms associated with the regulation of Akt/mTOR/BDNF signal pathway. The results showed that I/R, daidzein treatment significantly improved neurological deficits, infarct volume, and brain edema at 20 and 30 mg/kg, respectively. Meanwhile, it was found out that the pretreatment with daidzein at 20 and 30 mg/kg evidently improved striatal dopamine and its metabolite levels. In addition, daidzein treatment reduced the cleaved Caspase-3 level but enhanced the phosphorylation of Akt, BAD and mTOR. Moreover, daidzein at 30 mg/kg treatment enhanced the expression of BDNF and CREB significantly. This protective effect of daidzein was ameliorated by inhibiting the PI3K/Akt/mTOR signaling pathway using LY294002. To sum up, our results demonstrated that daidzein could protect animals against ischemic damage through the regulation of the Akt/mTOR/BDNF channel, and the present study may facilitate the therapeutic research of stroke.

Keywords: daidzein, BDNF, neuroprotection, AKT/mTOR, ischemic stroke

OPEN ACCESS

Edited by:
Nesrine Salah El Dine El Sayed, Cairo University, Egypt

Reviewed by:
Yibo Ying, The Second Affiliated Hospital and Yuying Children's Hospital of Wenzhou Medical University, China
Ayman Elsahar, Cairo University, Egypt

***Correspondence:**
Chunming Liu
zhengmz605@mail.cncnc.edu.cn

Specialty section:
This article was submitted to Neuropharmacology, a section of the journal Frontiers in Pharmacology

Received: *08 September 2021*
Accepted: *01 December 2021*
Published: *14 January 2022*

Citation:
Zheng M, Zhou M, Chen M, Lu Y, Shi D, Wang J and Liu C (2022) Neuroprotective Effect of Daidzein Extracted From Pueraria *lobate Radix in a Stroke Model* Via *the Akt/mTOR/BDNF Channel. Front. Pharmacol. 12:772485. doi: 10.3389/fphar.2021.772485*

1 INTRODUCTION

As a common disease, ischemic stroke remains a major cause of mortality and neurological disability worldwide. The World Health Organization (WHO) has reported that around 15 million people suffer from stroke per year globally, making it a serious health issue that is also documented with high relapse rates (Campbell et al., 2019). Currently, the only effective solution to treatment is

Abbreviations: AD, Alzheimer's disease; BDNF, brain-derived neurotrophic factor; BAD, Bcl-2-associated death protein; CREB, cAMP-response element binding protein; DA, Dopamine; DOPAC, 3, 4-dihydroxyphenylacetic acid; DTT, dithiothreitol; ESI, electrospray ionization; GAPDH, glyceraldehyde 3-phosphate dehydrogenase; HE, hematoxylin-eosin staining; HPLC-MS/MS, high-performance liquid chromatography (HPLC)-tandem mass spectrometric (MS/MS); HRP, horseradish peroxidase; HVA, homovanillic acid; I/R, ischemia/reperfusion; NS, normal saline; NMDA, N-methyl-D-aspartate; mTOR, mammalian target of rapamycin; PVDF, polyvinylidene difluoride; PAGE, polyacrylamide gel electrophoresis;PI3K, phosphoinositide 3-kinases; SDS, sodium dodecyl sulfate; TTFA, trifluoracetic acid; TTC, 2,3,5-triphenyltetrazolium chloride.

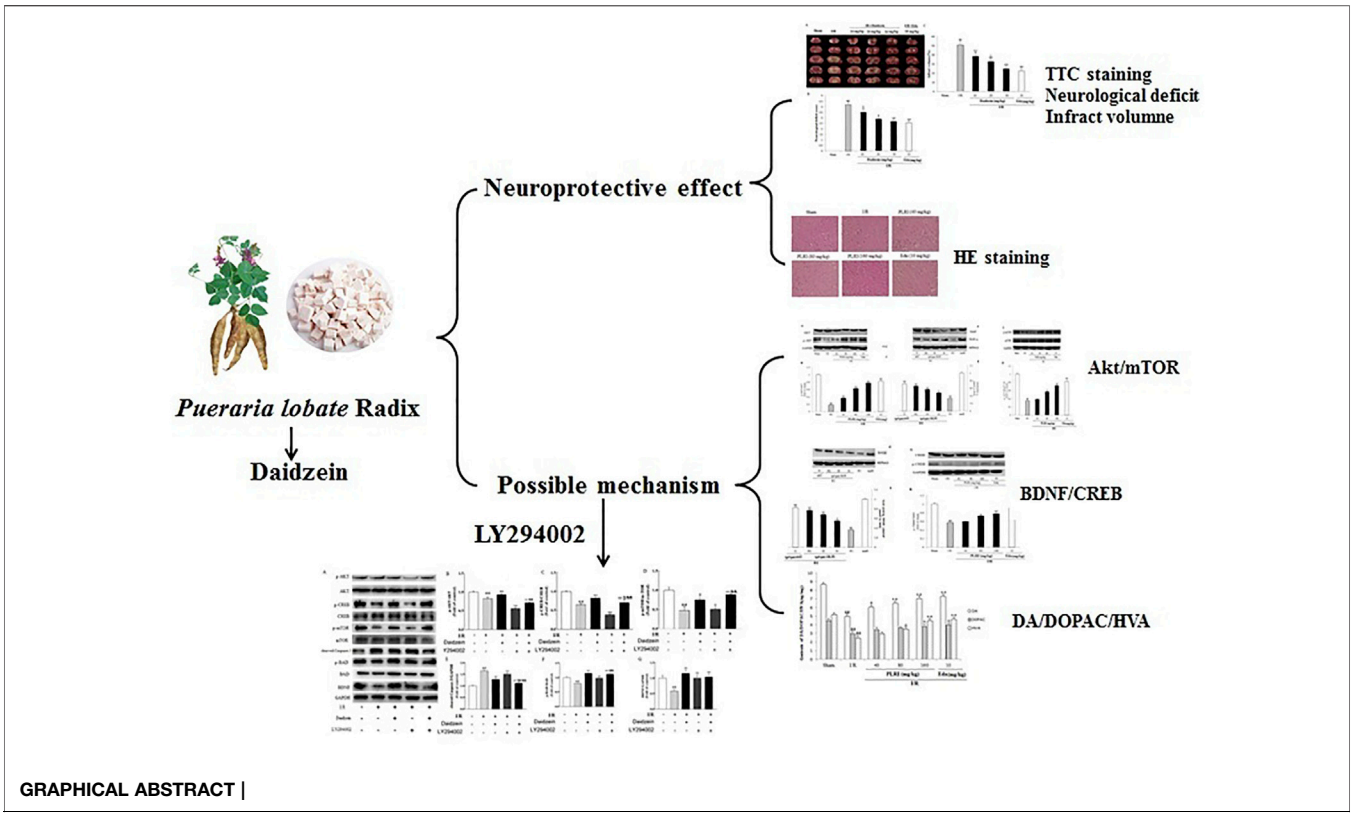

GRAPHICAL ABSTRACT |

thrombolysis. However, there are various restrictions which make it fit for only about 5% of all stroke patients. Due to the narrow window for administering rtPA (recombinant tissue plasminogen activator) treatment, only a small percentage of patients receive rtPA treatment during this therapeutic window (4.5 h) after the onset of stroke (Jiang et al., 2021). This has prompted the search for a chemical that could protect neurons from stroke-induced damage by interfering with the biochemical cascade that leads to cell death in the penumbra. Despite more and more studies focusing on the stroke system, there remain few effective therapeutic drugs suited to clinical applications (Zhang et al., 2020a). At present, there are four types of acetylcholinesterase inhibitors used to treat stroke (donepezil, galantamine, rivastigmine, and tacrine) and the agonist (memantine) of one N-methyl- D -aspartate (NMDA) receptor (Cheng et al., 2019). However, drugs can have adverse reactions due to indiscriminate effects on various central and peripheral organs and tissues (Chu, et al., 2019). For this reason, there is a necessity to explore the complementary and alternative therapies with greater effectiveness and less side effect.

Several mechanisms are found to be involved in cerebral ischemic injury including inflammatory responses, oxidative stress, neuronal apoptosis, excitotoxicity and mitochondrial dysfunction (Wang et al., 2020). So far, it has been suggested that excessive inflammation and immune response are the pathophysiological basis of ischemic brain injury after cerebral infarction (Lee et al., 2021). The phosphoinositide 3-kinase/ protein kinase B (PI3K/Akt) signaling regulates various processes including and inflammatory responses, cell growth, survival, metabolism in response to growth factors (Zheng et al., 2017). Previous studies have demonstrated the neuroprotective role of the PI3K/Akt pathway in ischemic stroke models (Xu et al., 2008). P-Akt can activate various downstream proteins, such as Bcl-2 associated death protein (Bad), caspase and so on. Apart from that, brain derived neurotrophic factor (BDNF) can help alleviate cerebral ischemia injury by interfering with apoptotic channels (Zhang et al., 2018). One of the main downstream effector of Akt is mammalian target of rapamycin (mTOR) that exists as 2 multi-protein complexes -mTORc1 and mTORc2 (Ma et al., 2020). The mTOR is a conserved serine/threonine kinase that regulates cell growth and proliferation. The serine/threonine kinase Akt is an upstream regulator of mTOR in mammalian cells, and it is well-known that autophagy is promoted by AKT and inhibited by mTOR (Wang et al., 2019). Accumulating evidence demonstrates that the AKT/mTOR signalling pathway can modulate neuroprotective activation following cerebral ischemia-reperfusion (I/R) (Zheng et al., 2017). For this reason, the AKT/mTOR/BDNF signaling channel is considered to be a potential therapeutic target for treating cerebral I/R impairment.

Daidzein, a monoterpene isoflavone isolated from *P.* lobate Radix, the dry roots of *Pueraria* lobate (Willd.) Ohwi (Radix Pueraria Lobate, Gegen), are officially quoted in the Chinese Pharmacopoeia as antipyretic and spasmolytic agent, as well as the medicine suitable for treating coronary heart diseases, cerebrovascular diseases and hyperlipidemia (Chinese

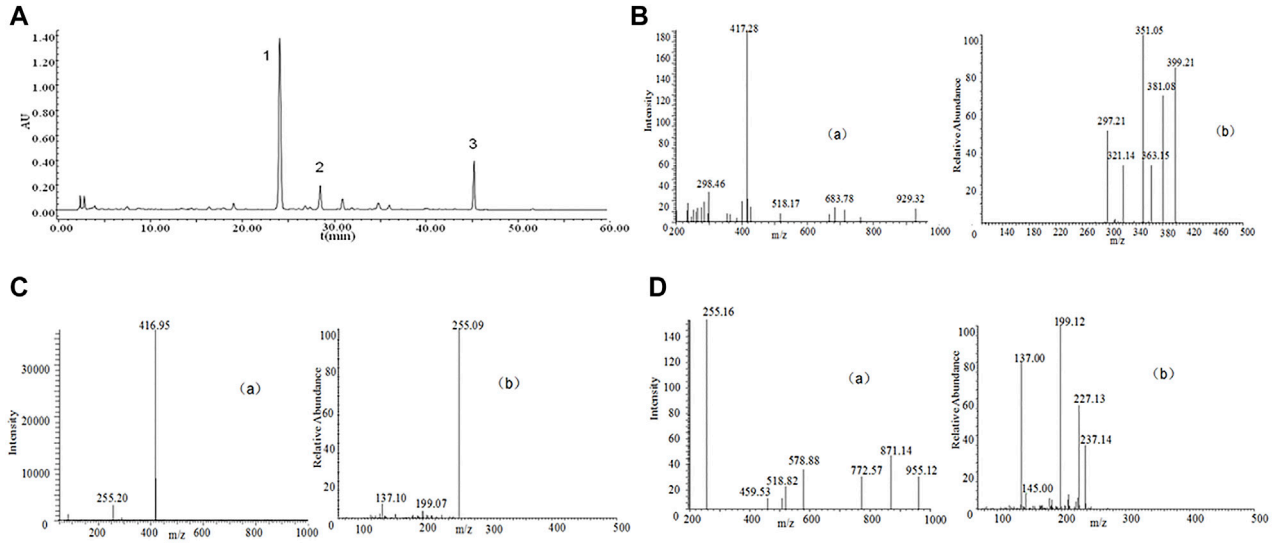

FIGURE 1 | High-performance liquid chromatography (HPLC) chromatograms and total ion chromatogram (TIC) of HPLC-electrospray ionization (ESI)-mass spectrometry (MS) of *P. lobate* Radix extract. **(A)** HPLC chromatograms of *Pueraria lobate* Radix extract **(B)** ESI-MS(a) and secondary mass spectrum of Puerarin (b) **(C)** ESI-MS(a) and secondary mass spectrum of Daidzin (b); **(D)** ESI-MS(a) and secondary mass spectrum of Daidzein (b). HPLC peaks were as follows: 1, Puerarin; 2, Daidzin; 3, Daidzein. Column: C18 column (250 × 4.6 mm id, 5 μm). Column temperature 25°C; mobile phase: consisted of acetonitrile (solvent A) and water containing 0.5% phosphoric acid (solvent B), The *P. lobate* Radix extract was analyzed using the following a gradient program: 0–5 min, 85–85% B; 5–10 min, 85–75% B; 10–20 min, 75–70% B; 20–35 min, 70–55% B; 35–40 min, 55–45% B; and 40–60 min, 45–45% B; flow rate: 0.8 ml/min; and detection wavelength at 250 nm. MS analysis was performed using a DAD instrument by an ESI interface. The mass spectrometer was operated in positive ion modes. The capillary voltage was set at −20 V. The spray voltage was set at 4.5 kV, and the capillary temperature at 250°C.

Pharmacopoeia Commission, 2010; Zhang et al., 2020b). According to recently conducted researches revealing the neuroprotective characteristics pertaining to isoflavones, the mentioned nature compounds can potentially mitigate nerve impairment and ameliorate stroke results (Burguete et al., 2016). Daidzein is effective in protecting neural cell from the cell death triggered by oxygen-glucose deprivation by activating receptor-γ under the action of peroxisome proliferator (Hurtado et al., 2012) and in improving poststroke sensorimotor outcomes in mice (Kim et al., 2015). *In vitro*, daidzein protect primary neurons from β-amyloid toxicity (Liu et al., 2012) and from thapsigargin-induced apoptosis (Linford and Dorsa, 2002). In addition, both molecules have been reported to be neuroprotective against glutamate excitotoxicity and oxygen–glucose deprivation (OGD) in cultured neurons (Song et al., 2020). However, the mechanisms of this neuroprotective action have not been fully elucidated.

Edaravone is referred to as one effective antioxidant that moppers free radicals responsible for various neurological disorders. According to the relevant animal research and clinics-related trials, edaravone is effective in protecting neuro from brain diseases (e.g., acute cerebral infarction) (Zheng and Chen, 2016), intracerebral hemorrhage (Dang et al., 2021), Parkinson's (Li et al., 2021a) and Alzheimer's disease (Feng et al., 2021), amyotrophic lateral sclerosis (Ortiz et al., 2020) as well as brain trauma (Shakkour et al., 2021). Therefore, Edaravone is treated as positive control herein.

Based on the study of how daidzein could reduce ischemic brain impairment, an investigation was conducted into the role of Akt/mTOR/BDNF signaling channels in mediating the effect of daidzein on cerebral ischemi.We then used LY294002, a PI3K inhibitor, to inhibit the PI3K/Akt/mTOR signaling pathway.

2 MATERIAL AND METHODS

2.1 Statement of Ethics

IACUC (Institutional Animal Care and Use Committee of Changchun Normal University, Changchun, China) provided the approval for the experiment protocol. Based on international standards on the ethical treatment of animals, all the experimental processes were carried out, and the minimal animal number was adopted for suffering minimization.

2.2 Chemicals

We obtained glycine, Tris, TritonX-100, DA, homovanillic acid (HVA), 3, 4-dihydroxyphenylacetic acid (DOPAC), MPTP, dithiothreitol (DTT), sodium dodecyl sulfate (SDS), and LY294002 from Sigma-Aldrich (St. Louis, MO, United States). From our institutional pharmacy, this study acquired Madopar (Shanghai Roche Led., Shanghai, China). Abcam (Dako, Cambridgeshire, United Kingdom) offered Rat anti- glyceraldehyde 3-phosphate dehydrogenase (GAPDH), anti-Akt (total) antibody, rabbit anti-BAD, rabbit anti-cleaved-Caspase-3 antibody, rabbit anti-phospho-Akt (Ser473) antibody, p-BAD, mTOR, p-mTOR, BDNF, CREB, and p-CREB antibodies, horseradish peroxidase (HRP)-conjugated anti-rabbit, and HRP-conjugated rat antibodies. All other chemicals exhibited great-purity analysis level and

TABLE 1 | The MS-MS fragmentation patterns of the isoflavonoids extracted from the *Pueraria* lobate Radix.

Peak	Retention time/min	MS, m/z	MS^2, m/z	Identified compounds
1	24.2	418.27, $[M + H]^+$	351.05, 399.21, 381.08	Puerarin
2	28.7	416.95, $[M + H]^+$	255.09	Daidzin
3	45.5	255.16, $[M + H]^+$	237.14, 227.13, 199.12	Daidzein

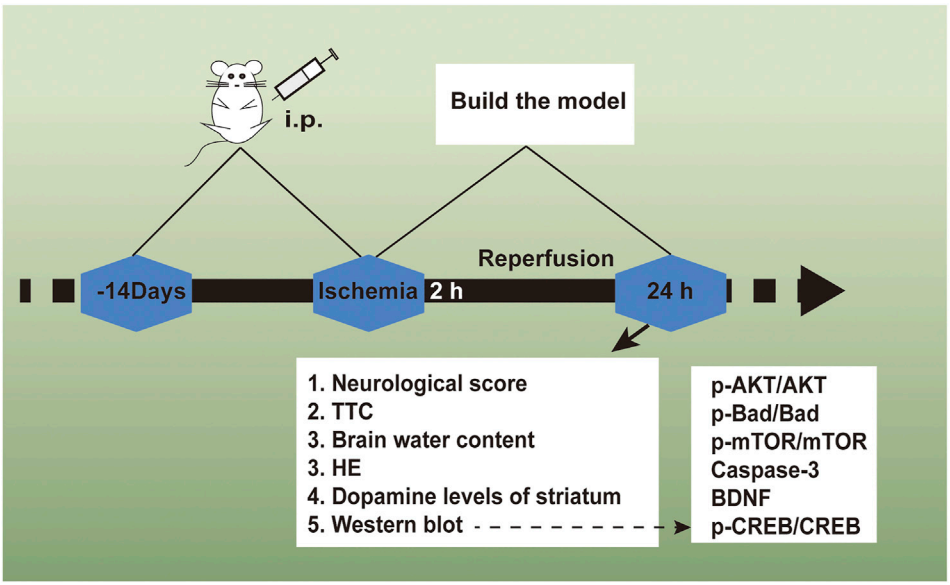

FIGURE 2 | The experimental flow chart of the protective effect exerted by Daidzein in ischemic stroke

originated in Shanghai Chemical Reagent Co., Ltd. (Shanghai, China).

2.3 Plant Material and Preparation of Daidzein Extracted from *P.* lobate Radix

Tong Ren Tang Medicinal Store (Changchun, China) in 2019 provided *P.* lobate Radix, under the identification by Prof. Shu-MinWang (Changchun University of Chinese Medicine). Voucher specimens (PLP-20–0628) have received the deposition at the Central Laboratory, Changchun Normal University.

P. lobate Radix (100 g each) received the crushing and 2 h extraction 3 times with reflux inside 70% ethanol under 1,000 ml. The extracts received the separate combination and filtering process via one Whatman #2 filter paper and then the concentration towards dryness with one rotary evaporator under 50°C. Analysis of the compounds in the *P. lobata* Radix extracts was performed on a Waters 2,695 extended by a C18 column (250 × 4.6 mm id, 5 μm), showing its containing 3.83% (w/w) of Puerarin, 1.09% (w/w) of Daidzin and containing 0.36% (w/w) of Daidzein (**Figure 1**; **Table 1**). The extraction rate of the *P. lobata* Radix (100 g) was 12.5%.

The binary mobile phase comprised water supplemented by 0.5% phosphoric acid (solvent B) and acetonitrile (solvent A). The flow ratio received the maintenance to be constant under 1.0 ml/min. The extracted from *P.* lobate Radix received the analysis with the use of the gradient program below: 0–5 min, 90–80% B; 5–20 min, 80–77% B; 20–35 min, 77–50% B; and 35–40 min, 50–50% B. The authors conducted the monitoring process for the peaks under 250 nm wavelength. Puerarin appeared at 24.2 min, Daidzin at 28.7 min, and Daidzein at 45.5 min (**Figure 1**).

2.4 Animals and Treatment

The Shanghai Experimental Animal Center, Chinese Academy of Sciences offered ICR rats (male, body weight 25–30 g). 72 adult rats received the random dividing process in 6 cohorts ($n = 12$): the daidzein 10 mg/kg cohort, the daidzein 20 mg/kg cohort, the daidzein 30 mg/kg cohort, the model cohort, the sham cohort, and the Edaravone cohort (10 mg/kg). The drug followed the intragastrical injection one time per day. With presurgery treating process conducted for 2 weeks, stroke received the inducing process inside the rat by I/R, following the previous description, under several modifications (Belayev et al., 1999). In brief, a 5 cm-long nylon filament (0.24–0.28 mm diameter) received the 2 h

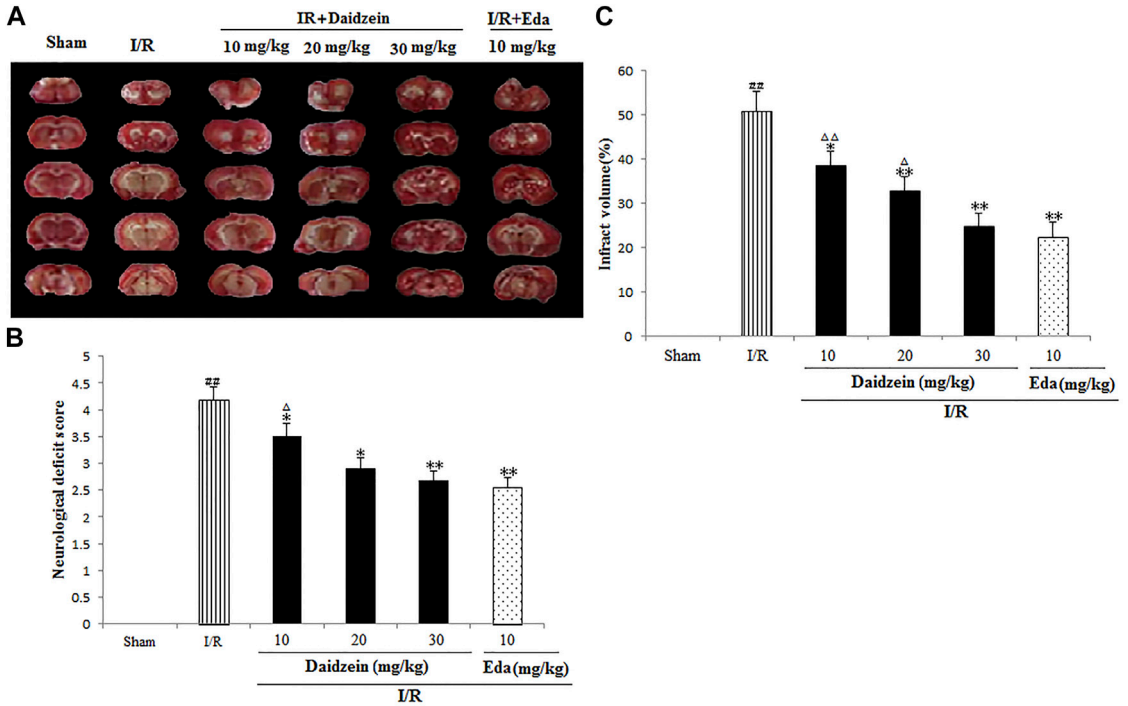

FIGURE 3 | Daidzein attenuated the neurological deficit values and infarct volume of after I/R. **(A)** The influence exerted by daidzein on neurological deficit values **(B)** Representative brain sections stained with TTC; **(C)** The influence exerted by daidzein on the infarct volume. $^{\#\#}p < 0.01$, in contrast to the Sham group; $^{*}p < 0.05$, $^{**}p < 0.05$ *vs.* I/R; $^{\triangle}p < 0.05$, $^{\triangle\triangle}p < 0.01$, compared with the Eda group.

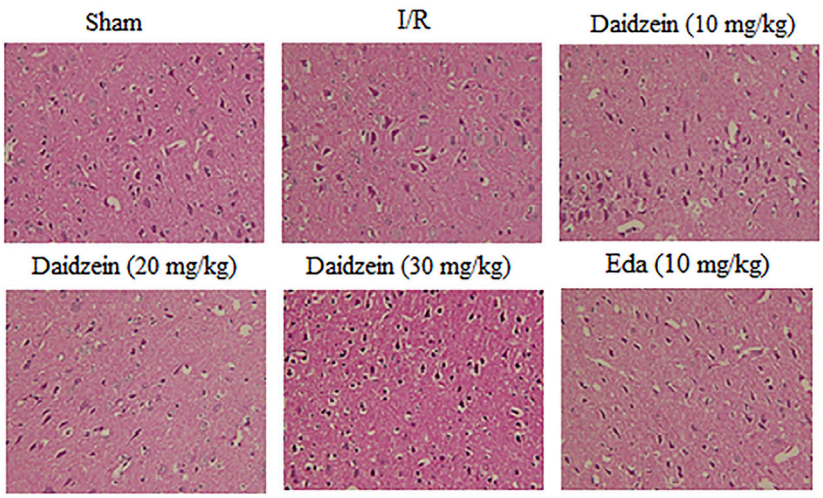

FIGURE 4 | HE staining of daidzein effect upon the ischemic damage after I/R. **(A)** Sham **(B)** I/R **(C)** I/R + daidzein (40 mg/kg) **(D)** I/R + daidzein (80 mg/kg) **(E)** I/R + daidzein (160 mg/kg) **(F)** I/R + Eda (10 mg/kg).

inserting process in the middle cerebral artery. Sham-operated rats received the identical surgical process as those in the MCAO cohort, with the exception of the middle cerebral artery occlusion. 10 min when ischemia was caused, the rats received the administration with daidzein (10, 20, 30 mg/kg) intraperitoneal injection or the identical normal saline volume (NS). When 2 h was passed, the nylon filament received the careful removal for allowing blood for returning into the ischemic artery. Subsequently, the suturing process was conducted for establishing reperfusion. When the ischemia/reperfusion experiment was completed, the rats were sacrificed, and the brains were immediately removed after the behavioral tests. 5 of them are for TTC, 4 for histopathology, western blot analysis and determination of

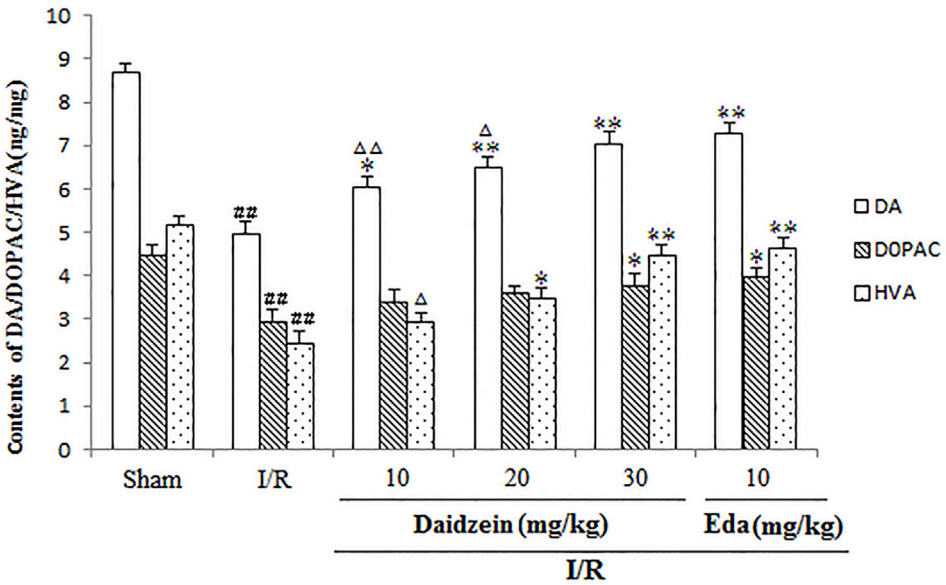

FIGURE 5 | Effects exerted by daidzein on homovanillic acid (HVA), 3, 4-dihydroxyphenylacetic acid (DOPAC), and dopamine (DA) within the striatum prior to I/R. Values have the expression to be means ± standard errors of the means (SEMs; $n = 6$). $^{\#\#}p < 0.01$, in contrast to the Sham group; $^{*}p < 0.05$, $^{**}p < 0.01$, in comparison with the I/R group; $^{\triangle}p < 0.05$, $^{\triangle\triangle}p < 0.01$, compared with the Eda group.

striatum dopamine levels, 3 for measurement of brain edema. **Figure 2** shows the timeline of the experimental flow chart.

2.4.1 Assessment for Neurological Impairments

Prior to the sacrificing process, with Longa's neurological severity scale, the animal neurological impairments received the evaluation 24 h when the sham or I/R surgery was conducted, following the previous description (Longa et al., 1989). At a 5-point scale, the neurological findings received the scoring: 0, no neurological impairments: 1: failing for overall stretching the fore-limbs and contralateral body; 2: circling for the surgery contralateral side; 3: falling for the surgery contralateral side; 4: depressed consciousness level and lacked spontaneously walking.

2.4.2 TTC Staining and Measuring Process of the Infarct Volume

At the time of neurological impairment evaluation, the rats received the sacrifice under deep anesthesia. For the purpose of TTC staining, 5 rats were randomly selected to comprise the respective cohort. The brains were carefully removed and the sectioning process was carried out in 6 2.0 mm-thick coronal sections. Then, the sections went through the 30 min staining process via 2% TTC in normal saline. Afterwards, the fixing process was conducted in 4% paraformaldehyde solution overnight. The infarct volume was calculated using the infarct size of the six sections multiplied by their thickness. An individual blinded to the treatment carried out all the infarct measuring processes.

2.4.3 Measurement of Brain Edema

The rats were killed 24 h after cerebral ischemia. Then, the brain samples were collected (Zhang et al., 2013). The ischemic area underwent the blotting process with care by using filter paper and then was weighed to obtain wet weights (WW). The ischemic hemispheres were dried for 24 h at 100°C, thus obtaining a constant weight as the dry weight (DW). Water content was calculated using the formula: H_2O (%) = (WW- DW)/ WW × 100%.

2.4.4 HE Staining

A crown zone (2–6 mm after optico chiasm, including hippocampus) of brain tissues was taken as in the embedding box. Then, conventional dehydration, paraffin embedding, slicing (4 μm thickness) and routine HE staining were performed in sequence. Brain tissue lesions were observed under optical microscope (OlympusBX51, Olympus, Japan).

2.5 Determination of Striatum Dopamine Levels

The striatum tissue was weighted and homogenized in 200 μl of ice-cold methanol. After 20 min of centrifugation at 14,000 rpm and 4°C, the supernatant was collected and then filtered using a 0.22 μm filter. Then, in accordance with Liquid Chromatography-Mass Spectrometry/Mass Spectrometry (LC-MS/MS), the solution was used to investigate dopamine (DA) and the relevant metabolites (e.g., 3, 4-dihydroxyphenylacetic acid (DOPAC)). LC-MS/MS analyses were conducted as previously described (Zheng et al., 2017).

2.6 Western Blot Analysis

When the evaluation was conducted for neurological impairments and TTC staining, the remaining rats' brains were employed to achieve the Western blotting investigation. The samples received

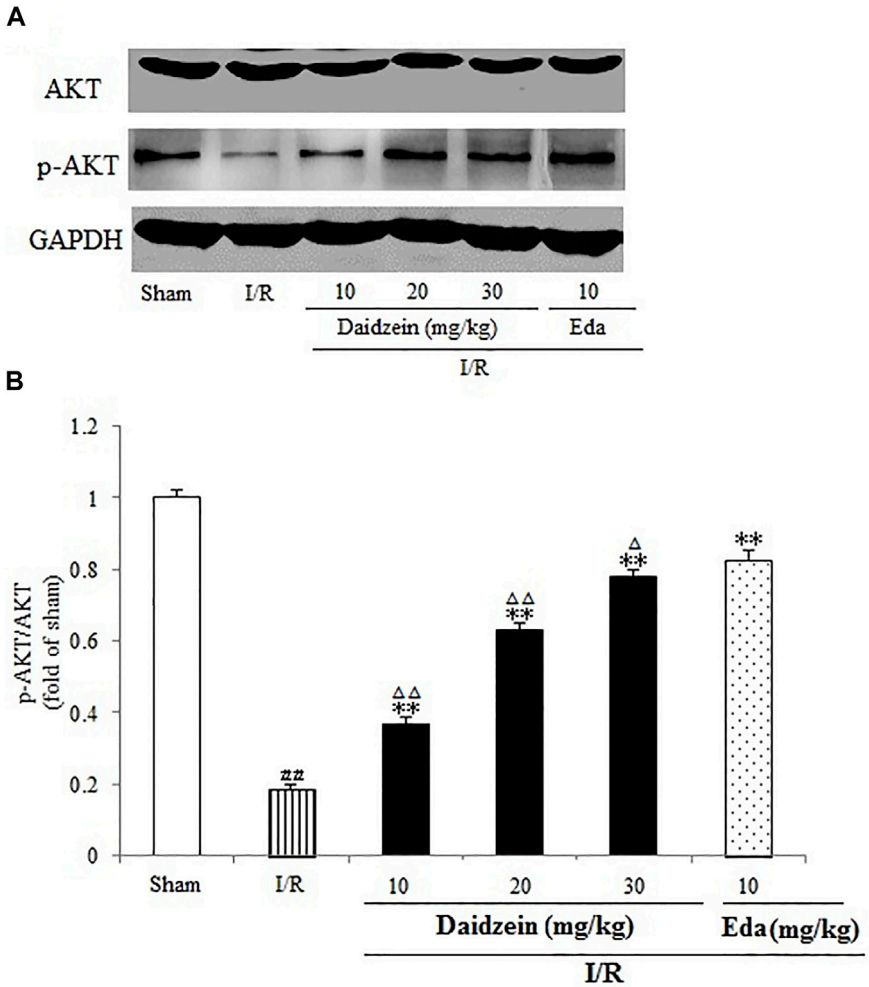

FIGURE 6 | Effects daidzein treatment on the expression of p-Akt and Akt levels in rats' brain infarct region. **(A)** Representative western blots. **(B)** Ratio of p-Akt/Akt. Values are indicated as means ± standard errors of the means (SEMs; $n = 3$). $^{\#\#}p < 0.01$ noticeably distinct from Sham; $^{**}p < 0.05$, noticeably distinct from I/R; $^{\triangle}p < 0.05$, $^{\triangle\triangle}p < 0.01$, compared with the Eda group.

the treating process by using a lysis buffer (0.1% sodium dodecyl sulfate (SDS), 0.5% sodium deoxycholate, 1% Triton X-100, 150 mM NaCl, and 50 mM Tris–HCl (pH8.0)) supplemented by a protease inhibitors cocktail (10 μg/ml leupeptin, 1 mM phenylmethylsulfonylfluo-ride, and2 μg/ml aprotinin). The membranes received the incubation by using major antibodies from the BAD, p-BAD, cleaved-Caspase-3, p-Akt, Akt, mTOR, p-mTOR, BDNF, CREB, p-CREB, and GAPDH proteins (1:1,000) throughout the night at 4°C. When the cleaning process was achieved, blots received the 45 min reaction process by using peroxidase-conjugated secondary antibodies. In addition, based on the enhanced chemiluminescence (ECL) detection system, the protein concentrations received the determination. The staining intensities of the protein bands received the measuring process, quantifying process, and normalizing process against GADPH staining based on the Quantity One software (Bio-Rad Laboratories; Hercules, CA, United States).

2.7 To Verify the Effects of Daidzein on the PI3K/Akt Pathway in I/R-Treated Rats

The 60 rats were then randomly divided into 5 groups: sham surgery group, I/R + saline group (rats were administrated with the same volume of physiological saline), I/R + daidzein (rats were treated with daidzein 30 mg/kg), I/R + daidzein + LY294002 group (rats were administrated with both daidzein and PI3K/Akt/mTOR inhibitor LY294002 0.3 mg/kg, Li et al., 2018), and I/R + LY294002 group (rats were treated with LY294002). All animal experiments were approved just as the protocols above.

At the end of the experiment, the rats were sacrificed, and their brains were harvested for Western blotting analysis.

2.7 Statistics

All data were expressed as the means ± SD from at least three independent experiments. The data were analyzed by Student's t test for two group comparisons or one-way analysis of variance

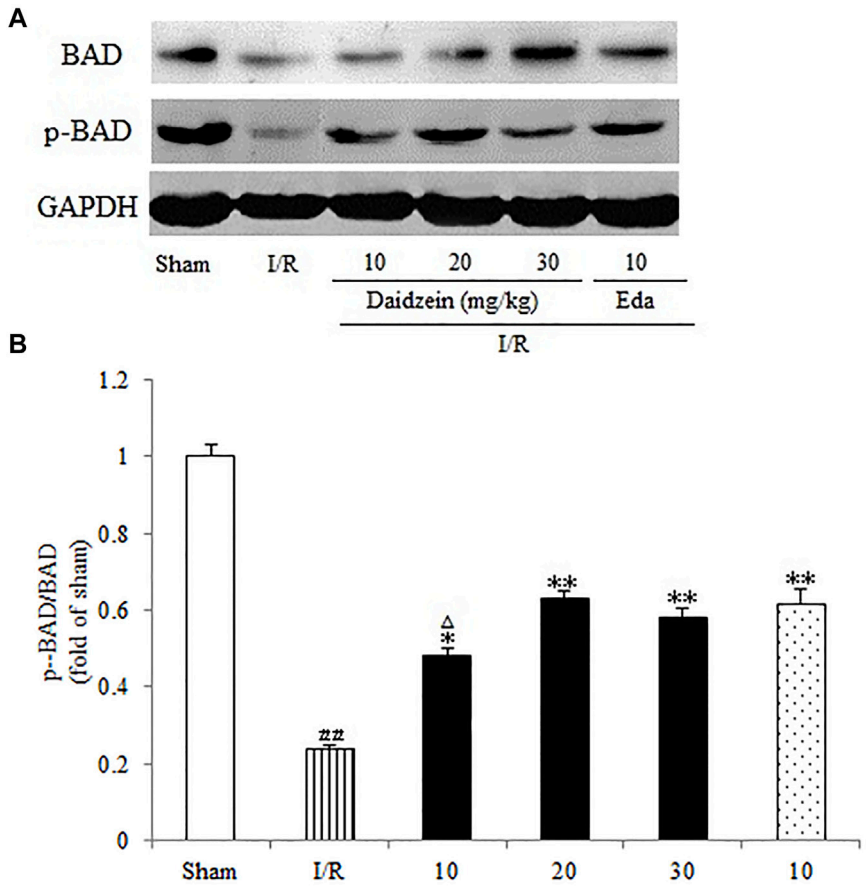

FIGURE 7 | Immunoblotting analysis of protein levels of p-mTOR/mTOR in rats' brain infarct region. **(A)** Representative western blots. **(B)** Ratio of p-mTOR/mTOR. Values are indicated as means ± standard errors of the means (SEMs; $n = 3$). $^{\#\#}p < 0.01$ noticeably distinct from Sham; $^{**}p < 0.05$, noticeably distinct from I/R; $^{\triangle}p < 0.05$, $^{\triangle\triangle}p < 0.01$, compared with the Eda group.

(ANOVA), followed by Dunnett's post hoc test for multiple comparisons, using Graph Pad Prism 6.0 (Graph Pad Software, La Jolla, CA, United States). Differences were considered significant with a p-value of less than 0.05.

3 RESULTS

3.1 Daidzein Down-Regulated Neurological Impairment Scores and Volume of Infarct in Rat After I/R

Neurological impairment was tested against a 5-point scale when ischemic stroke occurred, with higher score indicating greater severity of motor impairment. The results are shown in **Figure 3A**. The rats in the sham cohort suffered no neurological impairment. Accordingly, a neurological score of zero was maintained throughout the study. Neurological impairment was observed among the I/R cohort (e.g., irregular posture and less spontaneous activity). The aforementioned indicators were improved significantly among the daidzein cohort at 10, 20 and 30 mg/kg ($p < 0.05$, $p < 0.05$, $p < 0.01$) and Edaravone at 10 mg/kg ($p < 0.01$).

Ischemic brain edema was confirmation by the assessment of ischemic brain tissue for its cerebral water content. Brain water content was up-regulated evidently within the ischemia cohort in comparison with the sham cohort ($p < 0.05$). While a reduction to water content was observed in the daidzein cohort (10, 20 and 30 mg/kg) and Edaravone (10 mg/kg) cohort as compared to the ischemia cohort, suggesting that daidzein could reverse the formation of brain edema after ischemic stroke ($p < 0.05$, $p < 0.01$, $p < 0.01$, $p < 0.01$) (**Figures 3B,C**).

3.2 Effect of Daidzein on Pathological Brain Tissue Changes

According to HE staining results, there was no abnormality identified in the brain tissue of the sham cohort. To be specific, the neurons were arranged in an orderly way, the morphology was as normal, the nucleolus was clear, and the

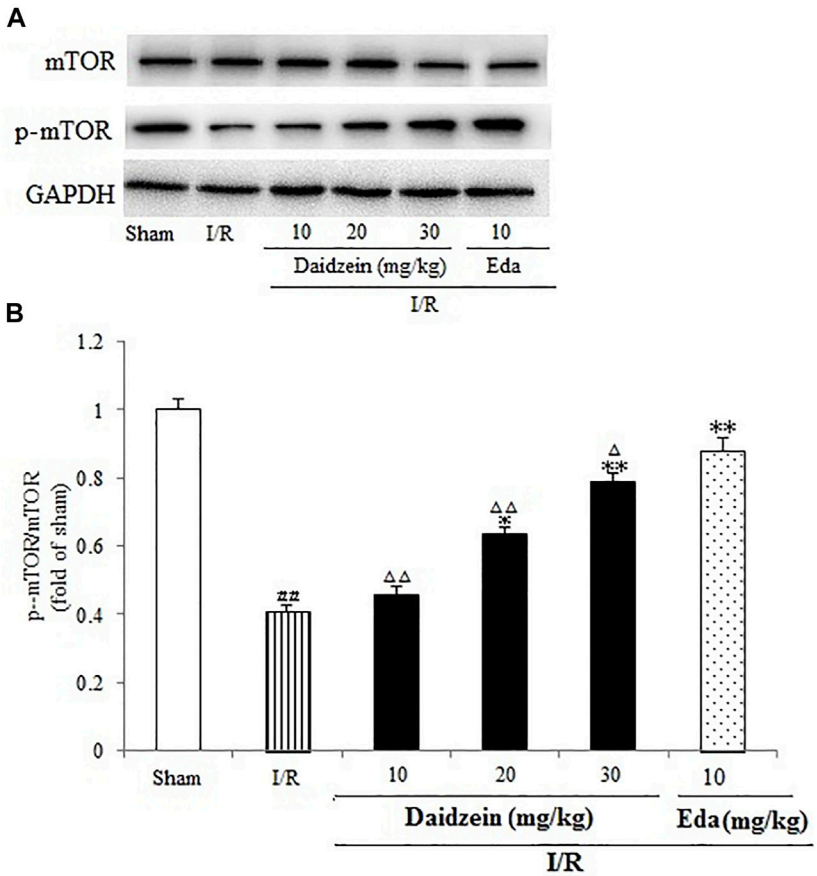

FIGURE 8 | Immunoblotting analysis indicating the Bcl-2/BAD ratio in rats' brain infarct region. **(A)** Representative protein bands of Bcl-2 and BAD. **(B)** Ratio of Bcl-2/BAD. Values are indicated as means ± standard errors of the means (SEMs; $n = 3$). $^{\#\#}p < 0.01$ noticeably distinct from Sham; $^{**}p < 0.05$, noticeably distinct from I/R; $^{\triangle}p < 0.05$, $^{\triangle\triangle}p < 0.01$, compared with the Eda group.

staining was uniform. The number of cells in the hippocampus was large and the cell level was high. Meanwhile, the cells in the cerebral cortex were abundant and there was no cell contraction observed. There was neither cell edema nor damage detected in the corpus callosum. Among the ischemia cohort, the cells in the hippocampus and cerebral cortex appeared loosened, edema, and contracted. Some brain white matter cells showed significant edema changes, the ischemic area was expanded, the neurons were squeezed. However, the pathological changes of neurons in the ischemic area were significantly reduced after the pretreatment with daidzein at 20 and 30 mg/kg and Edaravone at 10 mg/kg. These results suggest that daidzein contributed to nerve regeneration after traumatic nerve injury (**Figure 4**).

3.3 The Effects Exerted by Daidzein on DA and DA Metabolites within the Rat Striatum

Figure 4 shows the results of catecholamine measurement. According to this figure, stroke triggered a sharp decline in dopamine levels and the relevant metabolites as compared to the control ($p < 0.01$, $p < 0.01$, $p < 0.01$). The treatment using daidzein at 30 mg/kg caused the levels of DA, DOPAC and HVA to drop sharply ($p < 0.01$, $p < 0.05$, $p < 0.01$) (**Figure 5**). This is consistent with the effect of Edaravone at 10 mg/kg ($p < 0.01$).

3.4 Effect Exerted by Daidzein on Expression Levels of p-BAD, p-mTOR and p-Akt

Western blotting was performed to estimate the activity of downstream apoptosis-related proteins and PI3K/Akt signaling, as shown in **Figures 5**–**7**. As suggested by the results, I/R significantly reduced the expression ration of p-BAD/BAD, p- mTOR/mTOR and p-Akt/Akt as compared to the sham cohort ($p < 0.01$, $p < 0.01$, $p < 0.01$). Relative to the I/R cohorts, the treatment using daidzein (10, 20 and 30 mg/kg) elevated p-BAD/BAD, p-mTOR/mTOR and p-Akt/Akt ratios to a significant extent ($p < 0.01$, $p < 0.01$, $p < 0.01$; $p < 0.05$, $p < 0.01$; $p < 0.01$; $p < 0.01$, $p < 0.01$, $p < 0.01$) (**Figures 6**, **7**, **8**).

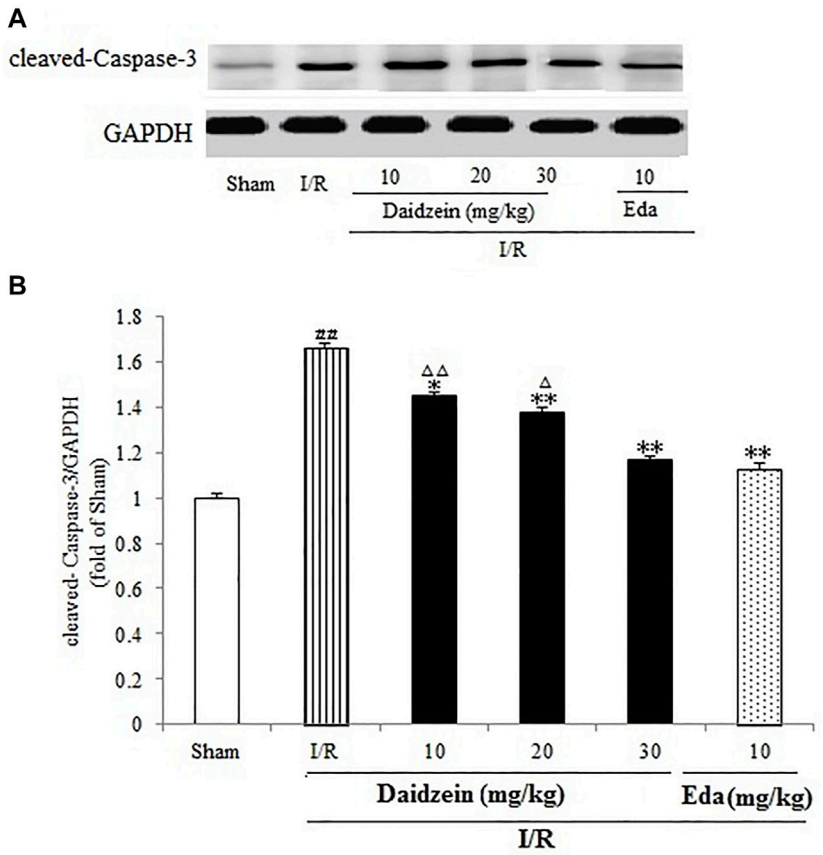

FIGURE 9 | Daidzein treatment decreases the cleaved Caspase-3 level promoted by I/R-treated Rats. **(A)** Immunoblotting analysis of cleavage Caspase-3. **(B)** Ratio of cleaved-Caspase-3/GAPDH. Values are indicated as means ± standard errors of the means (SEMs; $n = 3$). $^{\#\#}p < 0.01$ noticeably distinct from Sham; $^{**}p < 0.05$, noticeably distinct from I/R; $^{\triangle}p < 0.05$, $^{\triangle\triangle}p < 0.01$, compared with the Eda group.

3.5 Daidzein Attenuated Cleaved Caspase-3 Activation in I/R-Treated Mice

As shown in **Figure 9**, I/R treatment enhanced cleaved-Caspase-3 expression significantly in comparison with the sham cohort ($p < 0.01$). Daidzein (10, 20 and 30 mg/kg) preconditioning contributed significantly to reversing the increase of cleaved-Caspase-3 caused by I/R ($p < 0.05$, $p < 0.01$, $p < 0.01$), which was much lower compared with the Edaravone group ($p < 0.01$).

3.6 Influence Exerted by Daidzein on the Activation of BDNF/CREB Signaling

A further investigation was conducted into the levels pertaining to CREB and BDNF, which could alleviate the damage caused by ischemia (According to the results, the expression of BDNF was suppressed significantly after I/R surgery ($p < 0.01$). In contrast, it rose sharply after daidzein (10, 20 and 30 mg/kg) and Edaravone at 10 mg/kg treatment was achieved ($p < 0.05$, $p < 0.01$, $p < 0.01$, $p < 0.01$) (**Figure 10**).

As shown in **Figure 11**, I/R surgery reduced p-CREB/CREB rate noticeably, as compared to the sham cohort ($p < 0.01$). However, the decline in p-CREB/CREB rate was significant during the treatment with daidzein at 20 and 30 mg/kg ($p < 0.05$, $p < 0.01$) and Edaravone at 10 mg/kg, in comparison with the I/R cohort.

3.7 Confirm the Effects of Daidzein Inhibiting the PI3K/Akt/mTOR Signaling Pathway

To further investigate whether the neuro-protective effect of daidzein was regulated by the PI3K/Akt pathway, the PI3K inhibitor LY294002 was used to block the activity of PI3K. Daidzein improved p-Akt, p-mTOR, p-BAD, p-CREB and BDNF levels notably after I/R injury ($p < 0.01$, $p < 0.01$, $p < 0.01$, $p < 0.01$,$p < 0.01$, **Figures 12A–G**). Notably, Akt, mTOR, BAD and CREB phosphorylation levels and BDNF levels were reduced in the daidzein + LY294002 + I/R group compared with those in the daidzein + I/R group ($p < 0.01$, $p < 0.01$, $p < 0.01$, $p < 0.01$,$p < 0.01$). Moreover, daidzein reduced the cleaved-Caspase-3 level noticeably after I/R injury ($p < 0.01$), while level was improved in the daidzein + LY294002 + I/R group compared with those in the daidzein + I/R group ($p < 0.01$). The above data

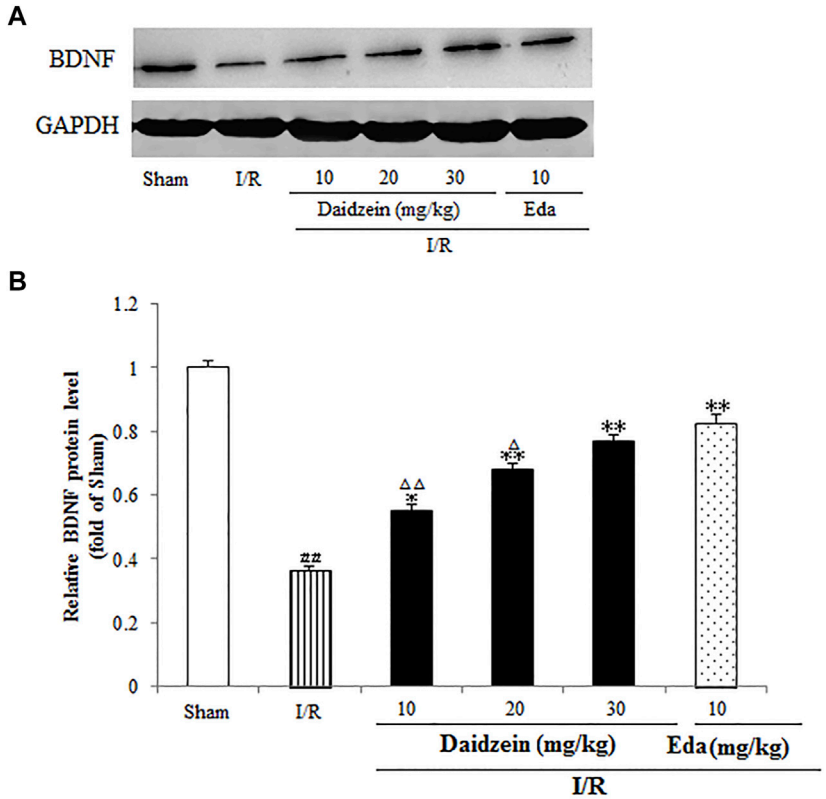

FIGURE 10 | Daidzein conducts the activation for BDNF/Akt/CREB signalling channel for providing neuro-repair in rats. **(A)** Quantifying process of the relative protein extent of BDNF. **(B)** Ratio of BDNF/GAPDH. I/R or daidzein-treatment rats' brain infarct region. Values are indicated as means ± standard errors of the means (SEMs; n = 3). $^{\#}p < 0.05$, noticeably distinct from sham; $^{*}p < 0.05$, noticeably distinct from I/R; $^{\triangle}p < 0.05$, $^{\triangle\triangle}p < 0.01$, compared with the Eda group.

suggest that daidzein modulated the phosphorylation of downstream targets of the PI3K/Akt pathway, while total Akt and mTOR levels were unaffected (**Figure 11**).

4 DISCUSSION

The aim of this study was at examining the potential mechanism of daidzein against ischemia/reperfusion (I/R). The experiment animal models for stroke were built to simulate the development of cerebral ischemia in humans (Zhou et al., 2021). As revealed from existing research, in the treatment with daidzein at 30 mg/kg per day, corresponding to the habitual intake of isoflavones in Asian adults after conversion (Lee et al., 2021) for 2 weeks, the protection for mice against stroke insult with I/R was conducted consecutively, based on the decrease in the infarct volume and the improvement of neurological impairment. Furthermore, daidzein was demonstrated to activate the PI3K/Akt/mTOR pathway, and LY294002, a specific PI3K inhibitor, significantly reversed the effects of daidzein. The mentioned results suggested daidzein can help alleviate ischemic neuron impairment and prevent I/R-triggered apoptosis, which is attributed at least partially to inhibiting PI3K/mTOR apoptosis channels and activating the BDNF/CREB channel during I/R.

It has been suggested in a number of studies that the dopamine content of extracellular fluid can be significantly increased after cerebral ischemia. Not only could DA produce excitotoxicity, it is also capable to induce the generation of oxygen free radicals, mitochondrial oxidative stress and the accumulation of intracellular calcium ions (Kaushik et al., 2020). As revealed by Li et al., ischemia and reperfusion can cause oxidative metabolites for DA to accumulate in the striatum, which improves the specificity in inducing the generation of oxygen free radicals and inflammatory cytokines (e.g., TNF-a, interleukin (IL)-1b and IL-6), and thus severely damages neurons. Moreover, electro-acupuncture treatment can effectively inhibit the release of DA to protect the brain (Li J et al., 2021). Accordingly, DA is considered to produce neuroprotective effects and promote the restoration of nerve function. As suggested by the results obtained in this study, however, daidzein is capable of reversing the reduction to DA extents and its metabolites, HVA and DOPAC, in the striatum of I/R-treated animals. The mentioned conflicting results may be attributed to the difference between the intra- and interstitial fluids being ignored. The above data suggests the potential of daidzein as a therapeutic option of stroke treatment.

The PI3K/Akt pathway, a major regulator of cell growth and survival, is critical to the mediation of myocardial cell survival in

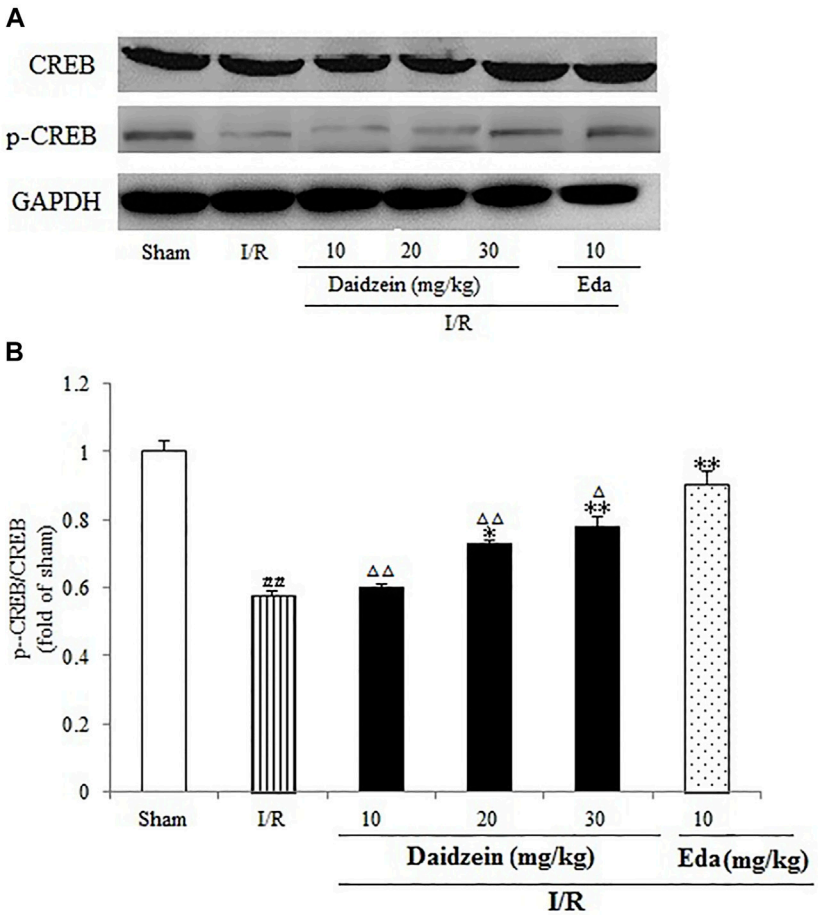

FIGURE 11 | Daidzein conducts the activation for BDNF/Akt/CREB signalling channel for providing neuro-repair in rats. **(A)** Representative protein bands of p-CREB and CREB. **(B)** p-CREB/CREB within the sham, I/R or daidzein-treatment rats' brain infarct region. Values are indicated as means ± standard errors of the means (SEMs; $n = 3$). $^{\#}p < 0.05$, noticeably distinct from sham; $^{*}p < 0.05$, noticeably distinct from I/R; $^{\triangle}p < 0.05$, $^{\triangle\triangle}p < 0.01$, compared with the Eda group.

numerous scenarios. Besides, it is responsible for axonal sprouting, which is of high significance to the post-stroke recovery of related functions (Qin et al., 2021). As demonstrated by existing studies, activation of PI3K/Akt can ameliorate I/R injury (Zhang et al., 2020). Furthermore, activation of the PI3K/Akt pathway can phosphorylate mTOR, which has been reported to protect against I/R injury by reducing autophagy and enhancing recovery in the heart (Saiprasad et al., 2014; Meng et al., 2020). Furthermore, the mTOR signal pathway was reported to be highly dependent on the neuroprotective effect in cerebral ischemia (Meng et al., 2020). According to another study, mTOR signal pathway achieved a vital function for protection against ischemic stroke (Li et al., 2021b). Moreover, Ren et al., confirmed that PI3K/Akt/mTOR signaling pathway could protect nerve energy cells by participating in oxidative stress and negatively regulating apoptosis (Ren et al., 2021). Consistent results were achieved here, which demonstrated that daidzein significantly up-regulated the expression levels of p-PI3K, p-Akt and p-mTOR, while LY294002, a specific inhibitor of PI3K, noticeably reversed the aforementioned effects of daidzein. The mentioned findings suggested that daidzein exerted neuroprotection via activating the PI3K/Akt/mTOR pathway.

Existing studies reported that cerebral ischemia down-regulates mTOR as well as Akt, which could prevent BAD translocation in the mitochondrial membrane. As it widely known as the principal mediators of apoptosis, while anti-apoptotic protein BAD could improve the survival of damaged cells by regulating permeabilization of the mitochondrial outer membrane. Though PAKT is capable of inhibiting the transport of BAD to mitochondrial membrane, Akt activation can facilitate the phosphorylation of Bad, thereby inhibiting the apoptotic activity and promoting the survival of cells (Wang A. R et al., 2021). It is already known that the increase of p-Bad contributes to the process of apoptosis inhibition. Apoptosis stimulation can lead to dephosphorylation of BAD, which activates Bax and Caspase-3 (Zhong et al., 2021). Caspase is only activated when caspase is cleaved and initiator caspases, such as caspase-3, are activated. Cleaved Caspase-3 is well known as an executioner protease of

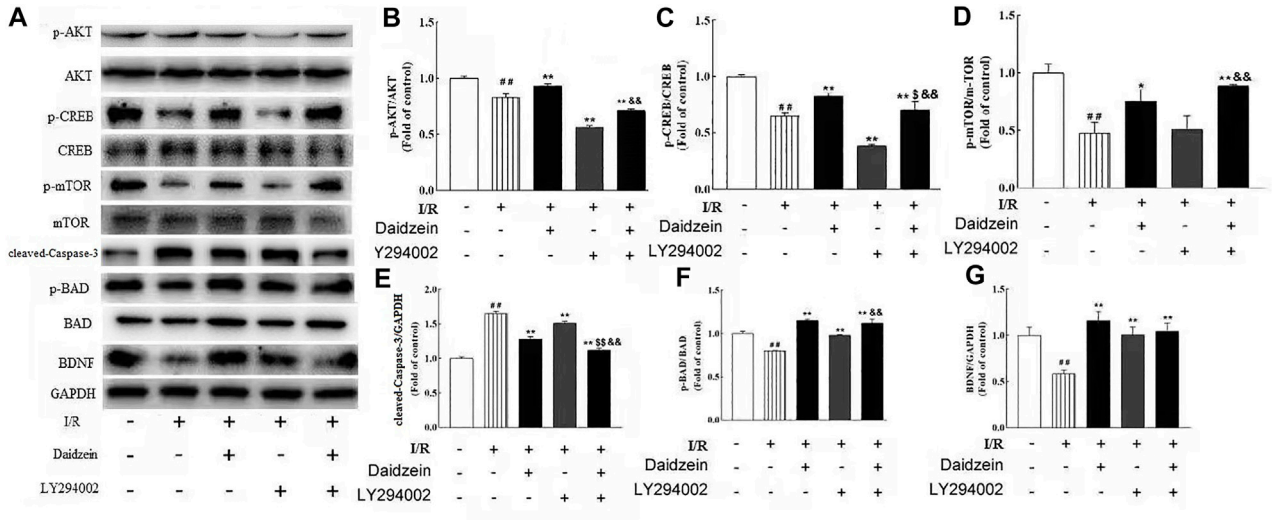

FIGURE 12 | Effect of kinase inhibitors LY294002 on neuroprotection of daidzein against I/R-induced ischemic damage in PIK3/AKT/mTOR pathway. **(A)** Representative western blots. **(B)** Ratio of p-Akt/Akt. **(C)** Ratio of p-CREB/CREB. **(D)** Ratio of p-mTOR/mTOR. **(E)** Ratio of cleaved-Caspase-3/GAPDH. **(F)** Ratio of p-BAD/ BAD. **(G)** Ratio of BDNF/GAPDH. Values are indicated as means ± standard errors of the means (SEMs; $n = 3$). $^{\#\#}p < 0.01$ noticeably distinct from Sham; $^{**}p < 0.05$, noticeably distinct from I/R; $^{\$}p < 0.05$, $^{\$\$}p < 0.01$, compared to the group treated with I/R+ daidzein; $^{\&\&}p < 0.01$compared to the group treated with I/R and LY294002

apoptosis following brain ischem, and the neuroprotection by resveratrol related to significantly upregulated the expression of p-AKT, p-mTOR, and BCL-2 and downregulated expression of cleaved Caspase-3 and BAX via the PI3K/Akt signaling pathway (Hou, et al., 2018). Consistent with these findings, we demonstrated that I/R increased the levels of cleaved-Caspase-3, while daidzein significantly decreased the expression of cleaved-Caspase-3. LY294002 remarkably ($p < 0.05$) eliminated cleaved-Caspase-3 reduction induced by daidzein.

Furthermore, neurotrophic factors (i.e., CREB and BDNF) can significantly impact the prevention and treatment of ischemic injury (Yang et al., 2018). By interfering with PI3K/Akt apoptotic channels, BDNF could protect against cerebral ischemic injury (Sheikholeslami et al., 2021). Phosphorylated CREB, an activated state of CREB, could up-regulate the expression of BDNF, while BDNF also promotes the activation of CREB through tropomyosin receptor kinase (Trk) B receptors (Zhang et al., 2012; Lan et al., 2014). According to an existing study, the repeated administration of Genistein (a monoterpene isoflavone) was found to improve CREB activity, up-regulate the BDNF expression, and protect the injured nerve of ischemic injury (Xu et al., 2021). Rapid release of BDNF contributed to reverse I/R-induced ischemic injury behaviors in rats (Wang M et al., 2021). Moreover, p-CREB is involved in neuronal apoptosis processes, which is mediated partially by BDNF. p-CREB overexpression inhibited neuronal apoptosis, whereas the inhibition of CREB activity accelerated neuronal apoptosis (Ren et al., 2021).

In this study, an increase in the expression of p-CREB, p-Akt and BDNF was identified after the daidzein treatment, which demonstrated that the BDNF/Akt/CREB signaling channel had a considerable impact on functional recovery after stroke. Despite plenty of researches where Akt and CREB were identified as the downstream targets of BDNF (Massa et al., 2010; Clarkson et al., 2015), CREB is phosphorylated by Akt according to a recent study, causing CREB-mediated expressing state of genes critical for neuronal survival, covering BDNF (Lu et al., 2013). Given the findings made in this study and others, BDNF, Akt, and CREB are suspected to be involved in a regulatory cycle. Plenty of studies indicated that BDNF is released by neurons and is mainly secreted via dendritic release (Zhu et al., 2021; Lee et al., 2020). Given the *in vitro* data used in this study, daidzein enhanced BDNF expression in primary cortical neuron culture (Zhang et al., 2018). In spite of this, how daidzein up-regulates BDNF expression should be investigated in depth, and the direct targets suitable for daidzein therapy should be identified.

To verify the effects of inhibiting the PI3K/Akt/mTOR signaling pathway on stroke model induced by ischemia/reperfusion in rats, LY294002 was intrathecally injected into rats, and the effects were subsequently studied. The results showed that LY294002 significantly alleviated the effect induced by I/R. Moreover, LY294002 significantly down-regulated the expressions of PI3K/Akt/mTOR signaling pathway related factors (**Figure 12**), which demonstrated that I/R injury was relieved, and that PI3K/Akt/mTOR signaling pathway inhibition might be effective to treat stroke induced by I/R.

5 CONCLUSION

In brief, the results of this study showed that daidzein has therapeutic potential for ischemia/reperfusion-induced brain injury. Although the potential system and feasibility of long-term use remain to be validated, the data still suggests that daidzein promotes neuronal regeneration after ischemic stroke by upregulating Akt/CREB and enhancing BDNF expression. In addition, daidzein may potentially be a new agent to be used in the prevention of focal cerebral ischemia, while also being inexpensive and easily available.

DATA AVAILABILITY STATEMENT

The original contributions presented in the study are included in the article/Supplementary Materials, further inquiries can be directed to the corresponding authors.

ETHICS STATEMENT

The animal study was reviewed and approved by Institutional Animal Care and Use Committee of Changchun Normal University, Changchun, China.

AUTHOR CONTRIBUTIONS

The present work was conducted in collaboration with all authors. Authors CL and ZMZ designed the study and wrote the methodology. The authors ZMZ and MC performed the experiments. MZ, JW, and DS performed the literature search and statistical analysis, author ZMZ wrote the paper, and author CL supervised the research. All authors have read and approved the final manuscript.

FUNDING

This study received the support from the Natural Science Foundation of Jilin Province, China (20210101031JC, 20180414028GH, JJKH20181168KJ, and JJKH20181185KJ), and the National Natural Science Foundation of China (grant numbers 31670358 and 31870336), and Supported by Natural Science Foundation of Changchun Normal University (2020-003).

ACKNOWLEDGMENTS

We would like to express our gratitude to Editage for English language editing.

REFERENCES

Belayev, L., Busto, R., Zhao, W., Fernandez, G., and Ginsberg, M. D. (1999). Middle Cerebral Artery Occlusion in the Mouse by Intraluminal Suture Coated with Poly-L-Lysine: Neurological and Histological Validation. *Brain Res.* 833, 181–190. doi:10.1016/S0006-8993(99)01528-0

Burguete, M. C., Torregrosa, G., Pérez-Asensio, F. J., Castelló-Ruiz, M., Salom, J. B., and Gil, J. V. (2006). Dietary Phytoestrogens Improve Stroke Outcome After Transient Focal Cerebral Ischemia in Rats. *Eur. J. Neurosci.* 23, 703–710. doi:10.1111/j.1460-9568.2006.04599.x

Campbell, B. C. V., De Silva, D. A., Macleod, M. R., Coutts, S. B., Schwamm, L. H., Davis, S. M., et al. (2019). Ischaemic Stroke. *Nat. Rev. Dis. Primers* 5, 70. doi:10.1038/s41572-019-0118-8

Cheng, Z., Zhang, M., Ling, C., Zhu, Y., Ren, H., Hong, C., et al. (2019). Neuroprotective Effects of Ginsenosides against Cerebral Ischemia. *Molecules* 24, 1102–1117. doi:10.3390/molecules24061102

Chinese Pharmacopoeia Commission (2010). *Pharmacopoeia of the People's Republic of China, Vol. 1*. Beijing: China Medical Science Press.

Chu, S. F., Zhang, Z., Zhou, X., He, W. B., Chen, C., Luo, P., et al. (2019). Ginsenoside Rg1 Protects against Ischemic/reperfusion-Induced Neuronal Injury through miR-144/Nrf2/ARE Pathway. *Acta Pharmacol. Sin.* 40, 13–25. doi:10.1038/s41401-018-0154-z

Clarkson, A. N., Parker, K., Nilsson, M., Walker, F. R., and Gowing, E. K. (2015). Combined Ampakine and BDNF Treatments Enhance Poststroke Functional Recovery in Aged Mice via AKT-CREB Signaling. *J. Cereb. Blood Flow Metab.* 35, 1272–1279. doi:10.1038/jcbfm.2015.33

Dang, L., Dong, X., Yang, J., Miranda, K., and Khan, I. (2021). Influence of Nanoparticle-Loaded Edaravone on Postoperative Effects in Patients with Cerebral Hemorrhage. *J. Nanosci. Nanotechnol.* 21 (2), 1202–1211. doi:10.1166/jnn.2021.18668

Feng, T., Yamashita, T., Sasaki, R., Tadokoro, K., Matsumoto, N., Hishikawa, N., et al. (2021). Protective Effects of Edaravone on white Matter Pathology in a Novel Mouse Model of Alzheimer's Disease with Chronic Cerebral Hypoperfusion. *J. Cereb. Blood Flow Metab.* 41 (6), 1437–1448. doi:10.1177/0271678X20968927

Hou, Y., Wang, K., Wan, W., Cheng, Y., Pu, X., and Ye, X. (2018). Resveratrol Provides Neuroprotection by Regulating the JAK2/STAT3/PI3K/AKT/mTOR Pathway after Stroke in Rats. *Genes Dis.* 155 (3), 245–255. doi:10.1016/j.gendis.2018.06.001

Hurtado, O., Ballesteros, I., Cuartero, M. I., Moraga, A., Pradillo, J. M., Ramírez-Franco, J., et al. (2012). Daidzein Has Neuroprotective Effects Through Ligand-Binding-Independent PPARγ Activation. *Neurochem. Int.* 61 (1), 119–127. doi:10.1016/j.neuint.2012.04.007

Jiang, L., Yin, X., Chen, Y. H., Chen, Y., Jiang, W., Zheng, H., et al. (2021). Proteomic Analysis Reveals Ginsenoside Rb1 Attenuates Myocardial Ischemia/reperfusion Injury through Inhibiting ROS Production from Mitochondrial Complex I. *Theranostics* 11 (4), 1703–1720. doi:10.7150/thno.43895

Kaushik, P., Ali, M., Tabassum, H., and Parvez, S. (2020). Post-ischemic Administration of Dopamine D2 Receptor Agonist Reduces Cell Death by Activating Mitochondrial Pathway Following Ischemic Stroke. *Life Sci.* 261, 118349. doi:10.1016/j.lfs.2020.118349

Kim, Y., Park, G. Y., Seo, Y. J., and Im, S. (2015). Effect of Anterior Cervical Osteophyte in Poststroke Dysphagia: A Case-Control Study. *Arch. Phys. Med. Rehabil.* 96 (7), 1269–1276. doi:10.1016/j.apmr.2015.02.026

Lan, X., Zhang, M., Yang, W., Zheng, Z., Wu, Y., Zeng, Q., et al. (2014). Effect of Treadmill Exercise on 5-HT, 5-HT1A Receptor and Brain Derived Neurophic Factor in Rats after Permanent Middle Cerebral Artery Occlusion. *Neurol. Sci.* 35, 761–766. doi:10.1007/s10072-013-1599-y

Lee, S., Hudobenko, J., McCullough, L. D., and Chauhan, A. (2021). Microglia Depletion Increase Brain Injury after Acute Ischemic Stroke in Aged Mice. *Exp. Neurol.* 336, 113530. doi:10.1016/j.expneurol.2020.113530

Lee, S. S., Kim, C. J., Shin, M. S., and Lim, B. V. (2020). Treadmill Exercise Ameliorates Memory Impairment through ERK-Akt-CREB-BDNF Signaling Pathway in Cerebral Ischemia Gerbils. *J. Exerc. Rehabil.* 16 (1), 49–57. doi:10.12965/jer.2040014.007

Li, C., Sui, C., Wang, W., Yan, J., Deng, N., Du, X., et al. (2021). Baicalin Attenuates Oxygen-Glucose Deprivation/Reoxygenation-Induced Injury by Modulating the BDNF-TrkB/PI3K/Akt and MAPK/Erk1/2 Signaling Axes in Neuron-

Astrocyte Cocultures. *Front. Pharmacol.* 12, 599543. doi:10.3389/fphar.2021.599543

Li, J., Dai, X., Zhou, L., Li, X., and Pan, D. (2021). Edaravone Plays Protective Effects on LPS-Induced Microglia by Switching M1/M2 Phenotypes and Regulating NLRP3 Inflammasome Activation. *Front. Pharmacol.* 12, 691773. doi:10.3389/fphar.2021.691773

Li, X., Hu, X., Wang, J., Xu, W., Yi, C., Ma, R., et al. (2018). Inhibition of Autophagy via Activation of PI3K/Akt/mTOR Pathway Contributes to the protection of Hesperidin against Myocardial Ischemia/reperfusion Injury. *Int. J. Mol. Med.* 42 (4), 1917–1924. doi:10.3892/ijmm.2018.3794

Li, Y., Xiang, L., Wang, C., Song, Y., Miao, J., and Miao, M. (2021a). Protection against Acute Cerebral Ischemia/reperfusion Injury by Leonuri Herba Total Alkali via Modulation of BDNF-TrKB-PI3K/Akt Signaling Pathway in Rats. *Biomed. Pharmacother.* 133, 111021. doi:10.1016/j.biopha.2020.111021

Li, Y., Xu, G., Hu, S., Wu, H., Dai, Y., Zhang, W., et al. (2021b). Electroacupuncture Alleviates Intestinal Inflammation and Barrier Dysfunction by Activating Dopamine in a Rat Model of Intestinal Ischaemia. *Acupunct Med.* 39 (3), 208–216. doi:10.1177/0964528420922232

Linford, N. J., and Dorsa, D. M. (2002). 17beta-Estradiol and the Phytoestrogen Genistein Attenuate Neuronal Apoptosis Induced by the Endoplasmic Reticulum Calcium-ATPase Inhibitor Thapsigargin. *Steroids* 67, 1029–1040. doi:10.1016/s0039-128x(02)00062-4

Liu, H., Liu, X., Wei, X., Chen, L., Xiang, Y., Yi, F., et al. (2012). Losartan, an Angiotensin II Type 1 Receptor Blocker, Ameliorates Cerebral Ischemia-Reperfusion Injury via PI3K/Akt-Mediated eNOS Phosphorylation. *Brain Res. Bull.* 89, 65–70. doi:10.1016/j.brainresbull.2012.06.010

Longa, E. Z., Weinstein, P. R., Carlson, S., and Cummins, R. (1989). Reversible Middle Cerebral Artery Occlusion without Craniectomy in Rats. *Stroke* 20, 84–91. doi:10.1161/01.STR.20.1.84

Lu, Y. Y., Li, Z. Z., Jiang, D. S., Wang, L., Zhang, Y., Chen, K., et al. (2013). TRAF1 Is a Critical Regulator of Cerebral Ischaemia-Reperfusion Injury and Neuronal Death. *Nat. Commun.* 4, 2852. doi:10.1038/ncomms3852

Ma, C., Wang, X., Xu, T., Zhang, S., Liu, S., Zhai, C., et al. (2020). An Integrative Pharmacology-Based Analysis of Refined Qingkailing Injection against Cerebral Ischemic Stroke: A Novel Combination of Baicalin, Geniposide, Cholic Acid, and Hyodeoxycholic Acid. *Front. Pharmacol.* 11, 519. doi:10.3389/fphar.2020.00519

Massa, S. M., Yang, T., Xie, Y. M., Shi, J., Bilgen, M., Joyce, J. N., et al. (2010). Small Molecule BDNF Mimetics Activate TrkB Signaling and Prevent Neuronal Degeneration in Rodents. *J. Clin. Invest.* 120 (5), 1774–1785. doi:10.1172/JCI41356

Meng, X., Mei, L., Zhao, C., Chen, W., and Zhang, N. (2020). miR-885 Mediated Cardioprotection against Hypoxia/reoxygenation-Induced Apoptosis in Human Cardiomyocytes via Inhibition of PTEN and BCL2L11 and Modulation of AKT/mTOR Signaling. *J. Cell Physiol.* 235 (11), 8048–8057. doi:10.1002/jcp.29460

Ortiz, J. F., Khan, S. A., Salem, A., Lin, Z., Iqbal, Z., and Jahan, N. (2020). Post-marketing Experience of Edaravone in Amyotrophic Lateral Sclerosis: A Clinical Perspective and Comparison with the Clinical Trials of the Drug. *Cureus* 12 (10), e10818. doi:10.7759/cureus.10818

Qin, Z. S., Zheng, Y., Zhou, X. D., Shi, D. D., Cheng, D., Shek, C. S., et al. (2021). Shexiang Baoxin Pill, a Proprietary Multi-Constituent Chinese Medicine, Prevents Locomotor and Cognitive Impairment Caused by Brain Ischemia and Reperfusion Injury in Rats: A Potential Therapy for Neuropsychiatric Sequelae of Stroke. *Front. Pharmacol.* 12, 665456. doi:10.3389/fphar.2021.665456

Ren, X., Wang, Z., and Guo, C. (2021). MiR-195-5p Ameliorates Cerebral Ischemia-Reperfusion Injury by Regulating the PTEN-AKT Signaling Pathway. *Neuropsychiatr. Dis. Treat.* 17, 1231–1242. doi:10.2147/NDT.S297975

Saiprasad, G., chitra, P., Manikandan, R., and Sudhandiran, G. (2014). Hesperidin Induces Apoptosis and Triggers Autophagic Markers through Inhibition of aurora-A Mediated Phosphoinositide-3-kinase/Akt/mammalian Target of Rapamycin and Glycogen Synthase Kinase-3 Beta Signalling Cascades in Experimental colon Carcinogenesis. *Eur. J. Cancer* 50, 2489–2507. doi:10.1016/j.ejca.2014.06.013

Shakkour, Z., Issa, H., Ismail, H., Ashekyan, O., Habashy, K. J., Nasrallah, L., et al. (2021). Drug Repurposing: Promises of Edaravone Target Drug in Traumatic Brain Injury. *Curr. Med. Chem.* 28 (12), 2369–2391. doi:10.2174/0929867327666200812221022

Sheikholeslami, M. A., Ghafghazi, S., Pouriran, R., Mortazavi, S. E., and Parvardeh, S. (2021). Attenuating Effect of Paroxetine on Memory Impairment Following Cerebral Ischemia-Reperfusion Injury in Rat: The Involvement of BDNF and Antioxidant Capacity. *Eur. J. Pharmacol.* 893, 173821. doi:10.1016/j.ejphar.2020.173821

Song, X., Gong, Z., Liu, K., Kou, J., Liu, B., and Liu, K. (2020). Baicalin Combats Glutamate Excitotoxicity via Protecting Glutamine Synthetase From ROS-Induced 20S Proteasomal Degradation. *Redox Biol.* 34, 101559. doi:10.1016/j.redox.2020.101559

Wang, A. R., Mi, L. F., Zhang, Z. L., Hu, M. Z., Zhao, Z. Y., Liu, B., et al. (2021). Saikosaponin A Improved Depression-like Behavior and Inhibited Hippocampal Neuronal Apoptosis after Cerebral Ischemia through P-Creb/bdnf Pathway. *Behav. Brain Res.* 403, 113138. doi:10.1016/j.bbr.2021.113138

Wang, G., Wang, T., Zhang, Y., Li, F., Yu, B., and Kou, J. (2019). Schizandrin Protects against OGD/R-Induced Neuronal Injury by Suppressing Autophagy: Involvement of the AMPK/mTOR Pathway. *Molecules* 24 (19), 3624. doi:10.3390/molecules24193624

Wang, M., Hayashi, H., Horinokita, I., Asada, M., Iwatani, Y., Liu, J. X., et al. (2021). Neuroprotective Effects of Senkyunolide I against Glutamate-Induced Cells Death by Attenuating JNK/caspase-3 Activation and Apoptosis. *Biomed. Pharmacother.* 140, 111696. doi:10.1016/j.biopha.2021.111696

Wang, Z., Kawabori, M., and Houkin, K. (2020). FTY720 (Fingolimod) Ameliorates Brain Injury through Multiple Mechanisms and Is a Strong Candidate for Stroke Treatment. *Curr. Med. Chem.* 27 (18), 2979–2993. doi:10.2174/0929867326666190308133732

Xu, X., Chua, C. C., Gao, J., Chua, K. W., Wang, H., Hamdy, R. C., et al. (2008). Neuroprotective Effect of Humanin on Cerebral Ischemia/Reperfusion Injury is Mediated by a PI3K/Akt Pathway. *Brain Res.* 1227, 12–18. doi:10.1016/j.brainres.2008.06.018

Xu, H., Wang, E., Chen, F., Xiao, J., and Wang, M. (2021). Neuroprotective Phytochemicals in Experimental Ischemic Stroke: Mechanisms and Potential Clinical Applications. *Oxid. Med. Cell Longev.* 2021, 6687386. doi:10.1155/2021/6687386

Yang, J., Yan, H., Li, S., and Zhang, M. (2018). Berberine Ameliorates MCAO Induced Cerebral Ischemia/Reperfusion Injury via Activation of the BDNF-TrkB-PI3K/Akt Signaling Pathway. *Neurochem. Res.* 43 (3), 702–710. doi:10.1007/s11064-018-2472-4

Zhang, G., Zhang, T., Li, N., Wu, L., Gu, J., Li, C., et al. (2018). Tetramethylpyrazine Nitrone Activates the BDNF/Akt/CREB Pathway to Promote post-ischaemic Neuroregeneration and Recovery of Neurological Functions in Rats. *Br. J. Pharmacol.* 175, 517–531. doi:10.1111/bph.14102

Zhang, J., Fu, B., Zhang, X., Chen, L., Zhang, L., Zhao, X., et al. (2013). Neuroprotective Effect of Bicyclol in Rat Ischemic Stroke: Down-Regulates TLR4, TLR9, TRAF6, NF-Kb, MMP-9 and Up-Regulates Claudin-5 Expression. *Brain Res.* 1528, 80–88. doi:10.1016/j.brainres.2013.06.032

Zhang, Y., He, Q., Yang, M., Hua, S., Ma, Q., Guo, L., et al. (2020b). Dichloromethane Extraction from Piper Nigrum L. And P. Longum L. to Mitigate Ischemic Stroke by Activating the AKT/mTOR Signaling Pathway to Suppress Autophagy. *Brain Res.* 1749, 147047. doi:10.1016/j.brainres.2020.147047

Zhang, Y., Yang, M., Ho, N. J., Mok, R. Y., Zhang, Z., Ge, B., et al. (2020a). Is it Safe to Take Radix Salvia Miltiorrhiza - Radix Pueraria Lobate Product with Warfarin and Aspirin? A Pilot Study in Healthy Human Subjects. *J. Ethnopharmacol.* 262, 113151. doi:10.1016/j.jep.2020.113151

Zhang, Z., Peng, D., Zhu, H., and Wang, X. (2012). Experimental Evidence of Ginkgo Biloba Extract EGB as a Neuroprotective Agent in Ischemia Stroke Rats. *Brain Res. Bull.* 87, 193–198. doi:10.1016/j.brainresbull.2011.11.002

Zheng, J., and Chen, X. (2016). Edaravone Offers Neuroprotection for Acute Diabetic Stroke Patients. *Ir. J. Med. Sci.* 185, 819–824. doi:10.1007/s11845-015-1371-9

Zheng, Y., Bu, J., Yu, L., Chen, J., and Liu, H. (2017). Nobiletin Improves Propofol-Induced Neuroprotection via Regulating Akt/mTOR and TLR 4/NF-Kb Signaling in Ischemic Brain Injury in Rats. *Biomed. Pharmacother.* 91, 494–503. doi:10.1016/j.biopha.2017.04.048

Zhong, H., Yu, H., Chen, B., Guo, L., Xu, X., Jiang, M., et al. (2021). Protective Effect of Total Panax Notoginseng Saponins on Retinal Ganglion Cells of an Optic Nerve Crush Injury Rat Model. *Biomed. Res. Int.* 2021, 4356949. doi:10.1155/2021/4356949

Zhou, Z., Xu, N., Matei, N., McBride, D. W., Ding, Y., Liang, H., et al. (2021). Sodium Butyrate Attenuated Neuronal Apoptosis via GPR41/Gβγ/PI3K/Akt Pathway after MCAO in Rats. *J. Cereb. Blood Flow Metab.* 41 (2), 267–281. doi:10.1177/0271678X20910533

Zhu, T., Wang, L., Xie, W., Meng, X., Feng, Y., Sun, G., et al. (2021). Notoginsenoside R1 Improves Cerebral Ischemia/Reperfusion Injury by Promoting Neurogenesis via the BDNF/Akt/CREB Pathway. *Front. Pharmacol.* 12, 615998. doi:10.3389/fphar.2021.615998

Conflict of Interest: The authors declare that the research was conducted in the absence of any commercial or financial relationships that could be construed as a potential conflict of interest.

Publisher's Note: All claims expressed in this article are solely those of the authors and do not necessarily represent those of their affiliated organizations, or those of the publisher, the editors, and the reviewers. Any product that may be evaluated in this article, or claim that may be made by its manufacturer, is not guaranteed or endorsed by the publisher.

frontiers in Pharmacology

REVIEW
published: 26 January 2022
doi: 10.3389/fphar.2022.781889

Lipoxins in the Nervous System: Brighter Prospects for Neuroprotection

Jiayu Zhang[1,2], *Zhe Li*[2], *Mingyue Fan*[2] *and Wei Jin*[2]*

[1]Graduate School of Hebei Medical University, Shijiazhuang, China, [2]Department of Neurology, Hebei General Hospital, Shijiazhuang, China

Lipoxins (LXs) are generated from arachidonic acid and are involved in the resolution of inflammation and confer protection in a variety of pathological processes. In the nervous system, LXs exert an array of protective effects against neurological diseases, including ischemic or hemorrhagic stroke, neonatal hypoxia-ischemia encephalopathy, brain and spinal cord injury, Alzheimer's disease, multiple sclerosis, and neuropathic pain. Lipoxin administration is a potential therapeutic strategy in neurological diseases due to its notable efficiency and unique superiority regarding safety. Here, we provide an overview of LXs in terms of their synthesis, signaling pathways and neuroprotective evidence. Overall, we believe that, along with advances in lipoxin-related drug design, LXs will bring brighter prospects for neuroprotection.

Keywords: lipoxins, neuroprotection, neurological diseases, resolution of inflammation, anti-oxidation

OPEN ACCESS

Edited by:
Barbara Budzynska,
Medical University of Lublin, Poland

Reviewed by:
Vasileia Ismini Alexaki,
University Hospital Carl Gustav Carus, Germany
Monika Gawrońska-Grzywacz,
Medical University of Lublin, Poland

***Correspondence:**
Wei Jin
jinwei8626@126.com

Specialty section:
This article was submitted to Neuropharmacology, a section of the journal Frontiers in Pharmacology

Received: *23 September 2021*
Accepted: *07 January 2022*
Published: *26 January 2022*

Citation:
Zhang J, Li Z, Fan M and Jin W (2022) Lipoxins in the Nervous System: Brighter Prospects for Neuroprotection. Front. Pharmacol. 13:781889. doi: 10.3389/fphar.2022.781889

1 INTRODUCTION

Resolution is a crucial stage of the inflammatory response, which is necessary to limit excessive tissue injury, minimize the development of chronic inflammation and re-establish homeostasis. During the process, specialized pro-resolving mediators (SPMs) with anti-inflammatory actions, including lipoxins (LXs), resolvins, protectins, and maresins, may be generated (Serhan, 2014). Among these endogenous local mediators, LXs, a class of arachidonate (arachidonic acid, AA)-derived eicosanoids, are the first to be recognized for functioning as "braking signals" in inflammation (Serhan et al., 1984). They are typically generated by lipoxygenase (LOX) interactions in a biosynthetic pathway known as transcellular biosynthesis (Serhan et al., 1994). In the past few decades, the actions of LXs in inflammation have been gradually determined. They can decrease the production of proinflammatory mediators, including interleukin (IL)-1, IL-6 and tumor necrosis factor (TNF)-α; facilitate the release of anti-inflammatory cytokines such as transforming growth factor-β1, IL-10 and prostaglandin E_2 (PGE_2); and consequently promote the resolution of inflammation. Additionally, they are found to inhibit neutrophil chemotaxis and infiltration, promote the phagocytic clearance of apoptotic cells by macrophages, and stimulate the accumulation of a nonphlogistic type of monocytes/macrophages (Lawrence et al., 2002; Maderna and Godson, 2009). Owing to their wide spectrum of anti-inflammatory and pro-resolving properties, a multitude of studies have investigated the potential protective effects of LXs on a variety of diseases and the underlying mechanism.

It has become widely appreciated that, in addition to classic infectious diseases such as encephalitis, excessive inflammation also occurs in the pathogenesis of many other neurologicaldiseases including stroke, neurotrauma, and neurodegenerative diseases (Ransohoff, 2016; Devanney et al., 2020; Mészáros et al., 2020). Moderate neuroinflammation orchestrated by

microglia, macrophages and lymphocytes is a beneficial response to foreign challenge or tissue injury, which can ultimately lead to the restoration of tissue structure and function. Generally, this type of inflammatory response is self-limiting under the strict control of endogenous mechanisms (Lawrence et al., 2002). However, prolonged inflammation can override the beneficial actions and contribute to the disease course. Taking ischemic stroke as an example, microglia-associated neuroinflammation can play an important role in isolating damaged brain tissue and clearing dead cell debris in the central nervous system (CNS), whereas the vast release of proinflammatory cytokines can lead to secondary brain tissue injury and cause poor functional recovery (Hanisch and Kettenmann, 2007). Thus, targeting the resolution of inflammation has become a promising therapeutic strategy for the treatment of neurological diseases, and LXs have drawn scientists' attention.

Interestingly, in addition to their involvement in the regulation of inflammation, LXs have also been found to have antioxidative, antiapoptotic, autophagy-moderating actions (Wu et al., 2012c; Jin et al., 2014; Jia et al., 2015; Prieto et al., 2015). In this review, we aimed to summarize the current knowledge about the many effects that LXs have on the nervous system and to discuss their roles in different CNS cell types, as well as their therapeutic potential for neurological diseases.

2 THE SYNTHESIS OF LIPOXINS

Endogenous LXs can be categorized into two types: native LXs composed of lipoxin A_4 (5*S*,6*R*,15*S*-trihydroxy-7,9,13-*trans*-11-*cis*-eicosatetraenoic acid, LXA_4) and lipoxin B_4 (5*S*,14*R*,15*S*-trihydroxy-6,10,12-*trans*-8-*cis* eicosatetraenoic acid, LXB_4) and aspirin-triggered lipoxins (ATLs), including aspirin-triggered lipoxin A_4 (15-epi-LXA_4, $ATLA_4$) and aspirin-triggered lipoxin B_4 (15-epi-LXB_4, $ATLB_4$). Compared to native LXs, ATLs are more resistant to metabolic inactivation and have an enhanced ability to evoke bioactions.

Native LXA_4 and LXB_4 are positional isomers typically generated from AA mediated by LOXs. There are two main pathways of native LX biosynthesis in human cells and tissues. One way comprises sequential lipoxygenation of AA by 15-LOX in epithelial cells and monocytes and by 5-LOX in neutrophils. In this pathway, not only are LXs synthesized, but leukotriene (LT) formation is also reduced (Serhan et al., 1984). The other involves the conversion of LTA_4, the 5-LOX epoxide product, to LXA_4 or LXB_4 by the LOX-synthetase activity of 12-LOX in platelets, which occurs when platelets adhere to neutrophils (Serhan and Sheppard, 1990). For ATL, aspirin can acetylate cyclooxygenase-2 (COX-2) and switch its catalytic activity from generating the intermediate for prostaglandins (PGs) and thromboxanes (TXs) to an *R*-LOX action, thus producing 15*R*-hydroxyeicosatetraenoic acid (15*R*-HETE). Then, the product is rapidly converted to ATL by 5-LOX (Clària and Serhan, 1995).

Actually, aside from aspirin, several drugs can induce the synthesis of LXA_4. Pioglitazone and atorvastatin have been reported to increase myocardial levels of 15-epi-LXA_4 produced by both COX-2 and 5-LOX (Birnbaum et al., 2006). Rosiglitazone can switch the generation of proinflammatory LTB4 to LXA_4 *via de novo* synthesis of 5-LOX, thus contributing to neuroprotection in experimental stroke (Sobrado et al., 2009).

LXs have been identified in brain tissues and cerebrospinal fluid (CSF), but the specific cell types responsible for generating and secreting LXs have not been illustrated explicitly. In addition to neutrophils, immune cells and endothelial cells (Ke et al., 2017), both microglia and astrocytes have shown the capacity to produce LXs. Immunohistochemical analysis of human hippocampal tissue revealed the localization of 15-LOX-2 in both astrocytes and microglia but not in neurons (Wang et al., 2015). Likewise, another key enzyme involved in LX synthesis, 5-LOX, and its activating protein (FLAP) are also expressed in human microglia (Klegeris and McGeer, 2003). It has been confirmed that human microglia can release LXA_4 after lipopolysaccharide (LPS)- treatment (Zhu et al., 2015). In the inner retina, astrocytes are able to synthesize LXA_4 and LXB_4 to participate in neuroprotection (Livne-Bar et al., 2017). At present, it is not clear which cell types in the CNS are the predominant source of LXs, but single-cell sequencing techniques coupled with lipidomics may be of help to address this problem in the future.

To increase the half-life of LXs, a range of stable, biologically active analogs have been designed and played an important role in studying actions of LXs. They were proven to be as potent as endogenous LXs in a series of *in vitro* and *in vivo* animal models, but only LXA_4 methyl ester (LXA_4 ME) and BML-111 (5*S*,6*R*,7-trihydroxyheptanoic acid methyl ester) were tested in the nervous system. Besides, since reliable commercial sources of LXB_4 have only recently become available, most experiments on LXs in the CNS or their roles in neuroprotection are performed using LXA_4, ATL and their analogs. Consequently, there is limited knowledge about LXB_4.

3 THE LIPOXIN RECEPTOR AND SIGNALING PATHWAY

The actions of LXA_4 and ATL are primarily mediated by a distinct G protein-coupled receptor (GPR) of the formyl peptide receptor superfamily (FPR). In the course of receptor identification, several different names have been used, including formyl peptide receptor 2 (FPR2), formyl peptide receptor-like 1 (FPRL1), LXA_4 receptors (LXA_4R), and ALX (Ye et al., 2009). According to the International Union of Basic and Clinical Pharmacology-recommended nomenclature (Ye et al., 2009), we use the term FPR2/ALX to refer to the receptor in this article regardless of species. FPR2/ALX is expressed in several types of leukocytes, including neutrophils, monocytes/macrophages and activated T cells (Cattaneo et al., 2013). Recently, the expression of FPR2/ALX has also been investigated in brain cells, but the conclusions remain controversial. In animal experiments, a study using double immunofluorescence and western blotting found that, in the rat brain, FPR2/ALX was highly expressed in neurons, moderately expressed in microglia, and not expressed in

astrocytes (Liu G.J. et al., 2020). However, FPR2/ALX was detected to be expressed in both primary astrocytes and microglia in a rat meningitis model by using reverse transcription-polymerase chain reaction (RT-PCR) and immunofluorescence (Braun et al., 2011; Abdelmoaty et al., 2013). In humans, the first evidence of FPR expression was reported in 1998 *via* immunocytochemistry (ICC) (Becker et al., 1998). Research detected FPR in brain and spinal cord sections and found positive results in neurons, astrocytes and Schwann cells but negative results in oligodendrocytes and microglia. Inconsequently, another study in 2015 revealed FPR2/ALX expression in both astrocytes and microglia through immunohistochemistry in human hippocampal tissue (Wang et al., 2015). Moreover, neural stem cells (NSCs) can also express FPR2/ALX, which has been confirmed by ICC, RT-PCR and western blotting in rodent pups (Wang et al., 2016). In our view, FPR2/ALX has a wide distribution in the nervous system, and the different results for FPR2/ALX localization may be attributed to the way it was detected. When using ICC or immunohistochemistry, the high expression in neurons may cover up the expression in other cells, causing the absence of observations. A study using RT-PCR indicated that FPR2/ALX mRNA expression was greatest in the brainstem, followed by the spinal cord, thalamus/hypothalamus, cerebral neocortex, hippocampus, cerebellum and striatum (Ho et al., 2018). Therefore, another factor that cannot be ignored is that the expression level of FPR2/ALX varies in different regions of the brain and spinal cord.

The expression of FPR2/ALX usually increases in pathological conditions. In a rat subarachnoid hemorrhage (SAH) model, FPR2/ALX expression was significantly increased and maintained from 24 h to approximately 3 days (Guo et al., 2016; Liu G.J. et al., 2020). Compared to the control brain, a higher FPR2/ALX level was also detected in Alzheimer's disease (AD) (Wang et al., 2015). Moreover, FPR2/ALX has also been observed to be altered in the spinal cord after peripheral inflammation (Abdelmoaty et al., 2013). FPR2/ALX is a versatile receptor that can bind to a variety of ligands and exert different functions, including both proinflammatory and pro-resolving functions (Cattaneo et al., 2013). It has not yet been ascertained whether the increase in FPR2/ALX triggers inflammatory damage or acts as an endogenous compensatory outcome for the reduced SPMs in the pathological brain to perform neuroprotection. Tylek et al. (2021) introduced the dual actions of FPR2/ALX on inflammatory response regulation in the brain and explained them by the concept of biased agonism. Interestingly, LXs did not show "dual-faced" effects on FPR2/ALX and have been always acting as anti-inflammatory mediators.

Through FPR2/ALX, LXA_4 blocks the mitogen-activated protein kinase (MAPK) pathway and attenuates nuclear factor kappa B (NF-κB) activation (Wang et al., 2011), which are two pathways that promote inflammation and neurodegeneration. ATL also depresses the Janus kinase 2 (JAK2)/signal transducer and activator of transcription 3 (STAT3) signaling pathway and triggers the expression of suppressor of cytokine signaling-2/3. Consequently, neuroinflammation and the induction of neuropathic pain are suppressed (Machado et al., 2006; Wang et al., 2014). Moreover, ATL has been shown to activate the protein kinase B (Akt) pathway (Lu et al., 2018), interact with nuclear factor erythroid 2-related factor 2 (Nrf2) and its downstream antioxidant enzymes (Jin et al., 2014), and abrogate nicotinamide adenine dinucleotide phosphate (NADPH) oxidase-dependent reactive oxygen species (ROS) generation (Wu et al., 2012c). In these ways, activation of FPR2/ALX exerts neuroprotection (**Figure 1**). LXA_4 can also induce microtubule-associated protein 1 light chain 3 (MAP1LC3)-II from MAP1LC3-I and the degradation of sequestosome 1 as well as the formation of $MAP1LC3C^+$ autophagosomes, which modulate apoptosis and autophagy in inflammation. The effect may be related to the activation of MAPK1 and the Nrf2 pathways (Prieto et al., 2015). Furthermore, FPR2/ALX is also the receptor for axonal or dendritic outgrowth (Ho et al., 2018) and the contributor to the migration and differentiation of NSCs (Wang et al., 2016), suggesting its important roles in cell proliferation and differentiation.

LXA_4 and ATL can also bind to other receptors (**Figure 1**). LXA_4 can inhibit the cysteinyl leukotriene receptor in vascular endothelial cells (Norel and Brink, 2004) and activate the aryl hydrocarbon receptor in dendritic cells (Schaldach et al., 1999; Machado et al., 2006), thus mediating anti-inflammatory actions. In the CNS, LXA_4 can bind to GPR32, which was discovered in differentiated neuroblastoma cells (Zhu et al., 2016). LXA_4 is also an endogenous allosteric enhancer of the cannabinoid 1 receptor, exerting cannabimimetic effects in the brain (Pamplona et al., 2012). Peroxisome proliferator-activated receptor gamma (PPARγ) has been illustrated to serve as a master gatekeeper of cytoprotective stress responses (Cai et al., 2018). LXA_4 can act as an agonist of PPARγ, thereby mitigating inflammation and neutralizing oxidative stress (Sobrado et al., 2009).

As a positional isomer of LXA_4, LXB_4 carries alcohol groups at the carbon 5S, 14R, and 15S positions instead of the C-5S, 6R, and 15S positions presented in LXA_4. Although LXB_4 shares several similar bioactivities with LXA_4 (Lefer et al., 1988; Takano et al., 1998; Ariel et al., 2003), it has shown differences from LXA_4 in many ways. In terms of actions, LXB_4 enhances human memory B cell antibody production, while LXA_4 confers exactly the reverse effect (Kim et al., 2018). In addition, the generation of LXB_4 is regulated by NLR family pyrin domain containing 3 (NLRP3) inflammasome activity (Lee et al., 2017), and the ω-oxidation products of LXB_4 are equipotent with the parent molecule in polymorphonuclear leukocytes (Maddox and Serhan, 1996), which are not seen in LXA_4. More interestingly, distinct from LXA_4 signaling, LXB_4 does not bind to ALXR (Fiore et al., 1994) and does not induce an increase in cytosolic calcium as a component of the signal transduction events following monocyte interaction (Romano et al., 1996). In the one and only study on LXB_4 neuroprotection, it demonstrated more potent protection than LXA_4, and the actions were independent of FPR2/ALX and resolvin D2 receptor (GPR18) (Livne-Bar et al., 2017). With respect to its possible remarkable neuroprotective role, LXB_4 and its downstream signaling are worth further investigation.

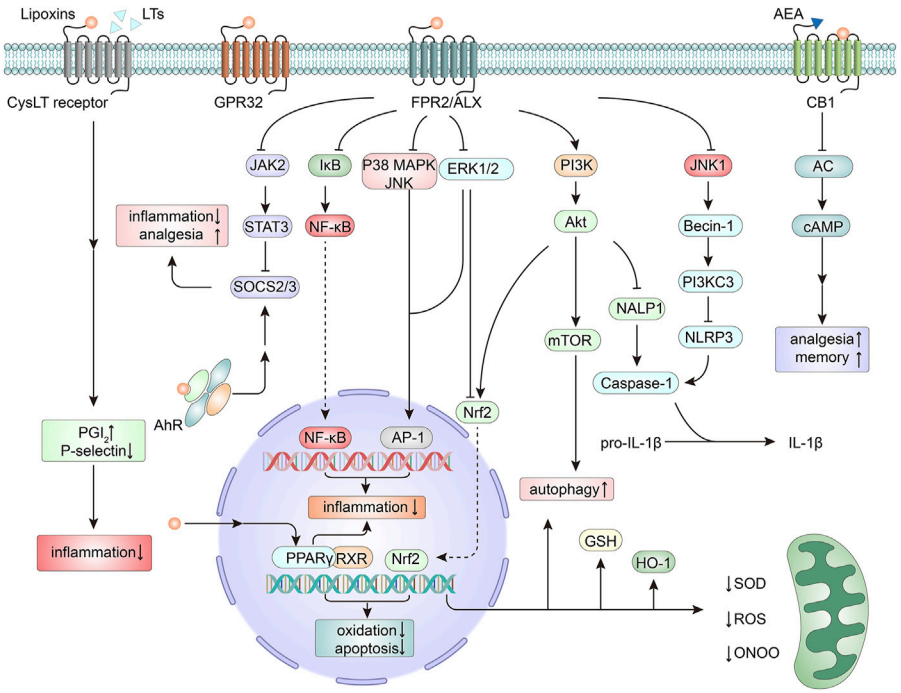

FIGURE 1 | Mechanisms of neuroprotection by lipoxins (LXs). The actions of LXs are mainly mediated by the activation of the formyl peptide receptor 2/LXA_4 receptor (FPR2/ALX). Downstream from the activation of FPR2/ALX, several signaling pathways are triggered, thus modulating the expression of genes and proteins related to inflammation (Machado et al., 2006; Wang et al., 2011; Wang et al., 2014), apoptosis (Zhu et al., 2020), oxidation (Wu et al., 2012c; Jin et al., 2014), autophagy (Prieto et al., 2015), and pain signaling (Wang et al., 2014). As antagonists of cysteinyl leukotriene (CysLT) receptors, LXs compete for binding sites with leukotrienes (LTs) and mediate an anti-inflammatory action (Norel and Brink, 2004). LXs can bind to G protein-coupled receptor 32 (GPR32) (Zhu et al., 2016) and act as an endogenous allosteric enhancer of the cannabinoid 1 (CB1) receptor (Pamplona et al., 2012). LXs can also exert agonistic action on peroxisome proliferator-activated receptor gamma (PPARγ) (Sobrado et al., 2009), thereby mitigating inflammation and neutralizing oxidative stress. In addition, by activating the nuclear receptor aryl hydrocarbon receptor (AhR), LXs promote the expression of suppressor of cytokine signaling 2 (SOCS2), thus exerting effects on anti-inflammation and analgesia (Schaldach et al., 1999; Machado et al., 2006). AC, adenylate cyclase; AEA, anandamide; Akt, protein kinase B, PKB; AP-1, activating protein-1; cAMP, cyclic adenosine monophosphate; ERK, extracellular signal regulated kinase; GSH, glutathione; HO-1, heme oxygenase-1; IκB, inhibitor κB; JAK2, Janus kinase 2; JNK, c-Jun N-terminal kinase; MAPK, mitogen-activated protein kinase; mTOR, mammalian target of rapamycin; NALP1, NAcht leucine-rich-repeat protein 1; NF-κB, nuclear factor kappa B; Nrf2, nuclear factor erythroid 2-related factor 2; ONOO, peroxynitrite; PG, prostaglandin; PI3K, phosphoinositide-3-kinase; ROS, reactive oxygen species; RXR, retinoid X receptor; SOD, superoxide dismutase; STAT3, signal transducer and activator of transcription 3.

4 PROTECTIVE EFFECTS OF LIPOXINS IN CENTRAL NERVOUS SYSTEM CELLS

The roles of LXs have been assessed in different CNS cell populations exposed to various stimuli. Herein, we specifically focus upon evidence for the effects of LXs in different CNS cell types, involving not only protection but also modulation (**Figure 2**).

4.1 Neural Stem Cells

NSCs can proliferate, migrate and differentiate into neurons, astrocytes and/or oligodendrocytes. During the pathological process, NSCs can proliferate, migrate to lesions and rebuild the damaged neuronal network in response to extracellular signal changes. It was reported that stable analogs of LXA_4 and $ATLA_4$ could directly regulate the growth of NSCs isolated from embryonic mouse brains by improving growth-related gene expression, including epidermal growth factor receptor, cyclin E, p27, and caspase 8 (Wada et al., 2006). Another study demonstrated that FPR2/ALX detected in NSCs can promote NSC migration through F-actin polymerization and skew NSC differentiation to neurons, implying that LXs may serve as candidates for the treatment of brain or spinal cord injury (Wang et al., 2016).

4.2 Neurons

The protective effects of LXs on neurons have also been extensively studied. LXs can reduce neuronal death in response to a variety of stimuli, including staurosporine, glutamate, paraquat, serum deprivation and oxygen-glucose deprivation (Zhu et al., 2016; Livne-Bar et al., 2017; Zhu et al., 2020), which has been explained to be related to their anti-inflammatory, anti-apoptotic and antioxidative effects (Zhu et al., 2016; Zhu et al., 2020). Furthermore, FPR2/ALX mediated axonal and dendritic outgrowth, suggesting that LXs may promote neuronal repair by activating FPR2/ALX (Ho et al., 2018).

4.3 Microglia

Microglia are the resident immune cells of the CNS. They are activated in response to pathological insults and harmful

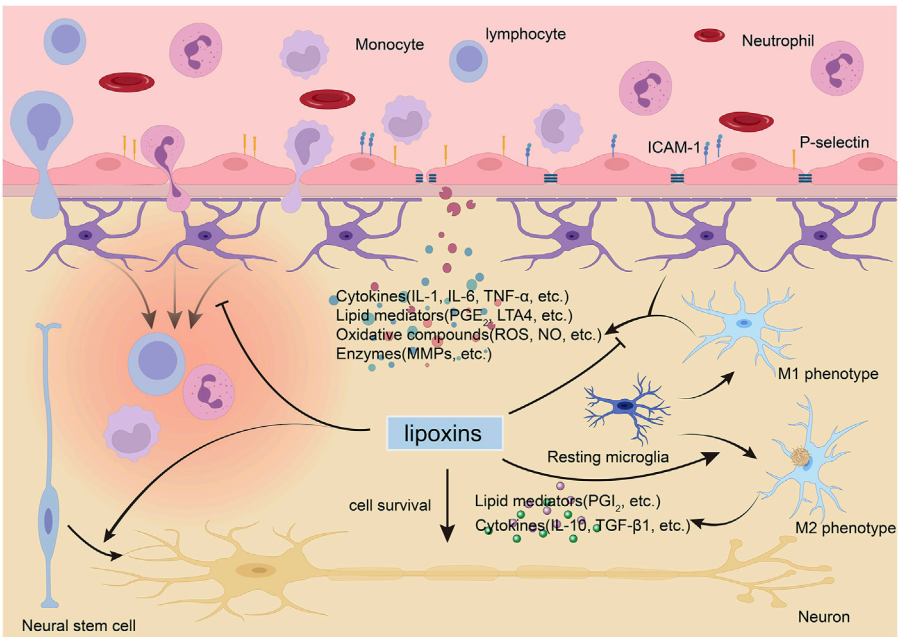

FIGURE 2 | Lipoxins (LXs) exert protective and modulatory actions in the brain. During neurological diseases, the blood-brain barrier (BBB) is disturbed and allows circulating immune cells and proteins to enter the brain. LXs can inhibit the activation and migration of immune cells (Liu et al., 2019), modulate activated endothelial leukocyte interactions (Smith et al., 2015), and maintain the integrity of the BBB by suppressing the expression of proinflammatory mediators and matrix metallopeptidases (MMPs) (Wu et al., 2012b; Hawkins et al., 2014). LXs can modulate glial cell activity to block harmful cytokine release (Wang et al., 2011; Wu et al., 2012a; Yao et al., 2014) and switch activated microglia to the anti-inflammatory, tissue-repairing M2 phenotype instead of the proinflammatory, tissue-damaging M1 phenotype (Taetzsch et al., 2015). LXs can also promote the survival of neurons (Zhu et al., 2020) and inducted the differentiation of neural stem cell to neurons (Wada et al., 2006). ICAM, intercellular cell adhesion molecule-1; IL, interleukin; LT, leukotriene; NO, nitric oxide; PG, prostaglandin; ROS, reactive oxygen species; TGF-β1, transforming growth factor β1; TNF, tumor necrosis factor.

stimuli, a process termed polarization. Activated microglia have been largely classified into two phenotypes, namely, classically activated (M1, proinflammatory) or alternatively activated (M2, anti-inflammatory) microglia. Proinflammatory microglia produce inflammatory mediators and exert detrimental effects. Conversely, anti-inflammatory microglia phagocytose cell fragments, dampen the inflammatory response and promote tissue repair. A study demonstrated that proinflammatory microglia could downregulate their capacity to produce LXA_4, further worsening the imbalance between proinflammation and anti-inflammation (Feng et al., 2017). ATL attenuates LPS-induced proinflammatory responses and the production of nitric oxide by inhibiting the activation of NF-κB and MAPKs *via* FPR2/ALX in BV-2 microglial cells (Wang et al., 2011). ATL could also abrogate NADPH oxidase-mediated ROS generation, subsequently inhibiting oxidase activation (Wu et al., 2012c) and M1 activation in microglia (Taetzsch et al., 2015). Recently, studies have demonstrated that LXs regulated microglial activation through the Notch signaling pathway (Wu et al., 2019b; Li et al., 2021), working as a repressor of inflammatory reactions in the brain. In fact, the supposed dichotomy between M1 and M2 phenotypes is oversimplified. Recent transcriptomics and proteomics studies have identified a multitude of activated microglial phenotypes in diverse disease stages (Beaino et al., 2021). To boost the correct microglial phenotype, it is necessary to further study the role and the underlying mechanism of LXs in regulating microglial activation, especially *in vivo*.

The effects of LXs on macrophages in the resolution of inflammation have been elucidated. LXs could mediate macrophage recruitment, improve the nonphlogistic phagocytosis of apoptotic neutrophils by macrophages (Godson et al., 2000), and increase macrophage survival *via* inhibition of apoptosis (Prieto et al., 2010) and regulation of autophagy (Prieto et al., 2015). In addition, LXs could also shift the macrophage phenotypic profile to an M2 state (Vasconcelos et al., 2015). Recently, disease-associated microglia (DAM) have attracted the attention of scientists. DAM are phagocytic cells conserved in mice and human and are associated with neurodegenerative diseases, such as AD and amyotrophic lateral sclerosis (Keren-Shaul et al., 2017). They are localized near amyloid plaques (Aβ) and participate in the dismantling and digestion of Aβ. Similar phagocytosis of DAM and macrophages suggests that there may also be a link between LXs and DAM. However, to date, we have not found studies on the roles of SPMs in DAM. The issue may become a hot spot of research 1 day in the future.

4.4 Astrocytes

In the CNS, as crucial players in maintaining brain homeostasis, astrocytes contribute to the formation of the BBB, secrete neurotrophic factors and modulate synaptic transmission.

Although not all astrocytic responses attenuate inflammation, their predominant function is to protect the brain from injury by regulating the neuroinflammatory response (Cekanaviciute and Buckwalter, 2016). Anti-inflammatory and antioxidant effects of LXs have been characterized in astrocytes. LXA_4 could inhibit IL-1β-induced IL-8 and intercellular cell adhesion molecule-1 (ICAM-1) expression in 1321N1 human astrocytoma cells, thus reducing the infiltration of immune cells (Decker et al., 2009). In neonatal rat astrocyte primary cultures suffering oxygen-glucose deprivation/recovery, LXA_4 inhibited LTC4 and LTA4 biosynthesis as well as 5-LOX translocation through an extracellular signal-regulated kinase (ERK) signal transduction pathway (Wu et al., 2012a). In response to LPS-induced neurotoxicity, ATL suppressed the production of nitric oxide and PGE_2 through an NF-κB-dependent mechanism (Yao et al., 2014). In addition, LXA_4 was found to downregulate the expression of aquaporin 4, which may be another anti-inflammatory target of LXA_4 (Wu et al., 2019a). Furthermore, LXA_4 could induce heme oxygenase-1 (HO-1) expression and glutathione (GSH) release as well as Nrf2 expression, of which nuclear translocation was partly ascribed to excess p62 accumulation, hence diminishing oxidative stress (Wu et al., 2015).

In the context of CNS inflammation, there is sophisticated crosstalk between astrocytes and other cells in the CNS (Linnerbauer et al., 2020). Moreover, the roles of astrocytes can be multifaceted. The regulation of astrocytes by LXs remains to be further studied. Whether LXs can regulate the communication between astrocytes and other cells cannot be ignored, either.

In addition to the cells mentioned above, LXs also regulate the activation and migration of leukocytes (Liu et al., 2019), exert anti-inflammatory and antiangiogenic effects on endothelial cells (Baker et al., 2009), and modulate activated endothelial leukocyte interactions (Smith et al., 2015), which are not discussed here.

5 PROTECTIVE EFFECTS OF LIPOXINS AGAINST NEUROLOGICAL DISEASES

5.1 Ischemic Stroke

The exact mechanisms responsible for ischemic stroke are not fully understood. Inflammation following ischemia-reperfusion plays a pivotal role in the pathophysiology of ischemic stroke and related brain injury (Mizuma and Yenari, 2017; Rajkovic et al., 2018). The generation of LXA_4 after ischemic stroke has been detected in both animal models and clinical patients. Marcheselli et al. (2003) determined the LXA_4 production in the hippocampus of mice after 1 h of middle cerebral artery occlusion (MCAO) followed by reperfusion and found a tendency for an increase in plasma LXA_4 levels after injury, which peaked within 8 h and lasted for 24 h. Similarly, plasma LXA_4 levels were measured, and it was determined that they increase in rats after global cerebral ischemia (GCI). Due to the long interval between observations, LXA_4 did not change up to 6 h but tended to increase at 24 and 72 h and remained elevated until 168 h post-GCI (Jung et al., 2020). In the blood of patients after ischemic stroke, there was also a significant increase in LXA_4 on the seventh day after the incident, indicating that LXA_4 is one of the most important derivatives after an early incident of ischemic stroke (Szczuko et al., 2020).

The neuroprotection of LXs has been well established in ischemic stroke. It was first evaluated by Sobrado et al. (2009), who demonstrated that intracerebroventricular administration of LXA_4 (1 nmol) caused a decrease in both infarct volume and neurological deficit scores after MCAO and confirmed that it was partially mediated by PPARγ. Then, You Shang et al. conducted further investigation on the efficacy of LXs using LXA_4 ME in the same model and reconfirmed the neuroprotection of LXs in ischemic stroke (Wu Y. et al. 2010). They found that LXA_4 ME could suppress neutrophil infiltration and lipid peroxidation levels, inhibit the activation of microglia and astrocytes and modulate the ratio of proinflammatory cytokines and anti-inflammatory cytokines, which were associated with the inhibition of the NF-κB pathway (Wu et al., 2010; Ye et al., 2010). In a later experiment, they demonstrated that LXA_4 ME could also improve blood-brain barrier (BBB) integrity through the upregulation of metallopeptidase inhibitor-1 and the subsequent downregulation of matrix metallopeptidase (MMP)-9 expression and activity (Wu et al., 2012b). Recently, it was also shown that LXA_4 exerted a neuroprotective effect on ischemic stroke by regulating microglial M1/M2 polarization *via* the Notch signaling pathway (Li et al., 2021). In accordance with these findings, it has been shown that BML-111, another LXA_4 analog, could also alleviate neuroinflammation and maintain BBB integrity after ischemic stroke by decreasing the levels of MMP-9 and MMP-3 and protecting tight junction proteins in an ALX-dependent manner (Hawkins et al., 2014). In the following experiment, researchers attempted to further confirm the long-term effects of BML-111 on neurological recovery at 4 weeks after ischemic stroke in rats, but frustratingly, they failed (Hawkins et al., 2017). Vital et al. have focused on the ATL effects within the cerebral microvasculature. They found that ATL activated FPR2/3 and inhibited leukocyte-endothelial interactions to initiate endogenous pro-resolution (Smith et al., 2015) and inhibited neutrophil-platelet aggregation to prevent secondary embolism (Vital et al., 2016).

Le Wu et al. explored the anti-inflammatory and antioxidant mechanisms underlying the neuroprotective effects of LXA_4 in ischemic stroke. They demonstrated that LXA_4 could inhibit 5-LOX translocation and leukotriene biosynthesis both *in vivo* and *in vitro*, which are partly mediated by FPR2/ALX and through an ERK signal transduction pathway (Wu et al., 2012a). They also confirmed *in vivo* and *in vitro* that LXA_4 could induce Nrf2 expression and its nuclear translocation, as well as HO-1 expression and GSH synthesis (Wu et al., 2013; Wu et al., 2015). Of interest, these pathways may be independent of FPR2/ALX and more closely related to p62 accumulation.

Cognitive impairment and depression are the most common complications of stroke, and it seems that LXs are associated with

the outcomes. In terms of poststroke cognitive impairment (PSCI), it was reported that, compared with patients without PSCI, the levels of LXA_4 were significantly reduced in PSCI patients, and the LXA_4 levels were positively correlated with the Mini-Mental State Examination scores (Wang et al., 2021). Inspiringly, LXA_4 pretreatment has been verified to improve cognitive function in aged rats after global cerebral ischemia-reperfusion (Wu et al., 2018). Regarding poststroke depression, it was shown that the changes in the Beck Depression Inventory-II scores of patients after stroke were inversely correlated with LXA_4 level, hinting that LXA_4 may also be a protective factor for the prevention of depression after stroke (Kotlega et al., 2020). In addition, it was investigated that the activation of FPR 2/3 could inhibit the action of glucocorticoids on the hypothalamic-pituitary-adrenal axis and maintain hippocampal homeostasis by preventing neuronal damage associated with depression (Peritore et al., 2020). Therefore, it is conceivable that LXs may confer neuroprotection in depression through the activation of FPR 2/3.

For ischemic stroke, diabetes mellitus is one of the major risk factors, and atherogenesis is the most common etiology. Excitingly, LXA_4 has been reported to protect against inflammatory reactions in diabetic cerebral ischemia/reperfusion (I/R) injury, and its mechanism may be related to the inhibition of TNF-α and NF-κB expression (Han et al., 2016). Besides, LXA_4 and ATL could compromise foam cell formation, oxidized low-density lipoprotein-induced inflammation and apoptotic signaling in macrophages during atherogenesis, which could be instructive for ischemic stroke prevention (Petri et al., 2017; Mai et al., 2018).

In conclusion, LXs are a promising therapeutic agent to better resolve the aggressive inflammatory state after ischemic stroke and limit irrecoverable neuronal damage. At present, the observed neuroprotective effects of LXA_4 can last at least 72 h in the model of MCAO/reperfusion when administered immediately after ischemia (Wu et al., 2012a). Although BML-111 failed to show long-term neuroprotective effects, it remains to be explored whether other LX analogs can be protective up to weeks following ischemia and contribute to long-term functional recovery. On the other hand, in terms of LX administration, which dose to use, when to administer it, and how frequently may influence the results, offering new ideas for us to obtain a long-term protection from LXs (Han et al., 2016).

5.2 Hemorrhagic Stroke

Subarachnoid hemorrhage and intracerebral hemorrhage (ICH) are the two types of hemorrhagic stroke, in which inflammation is a vital pathologic manifestation of early brain injury and a crucial factor related to the outcome (Lucke-Wold et al., 2016; Xue and Yong, 2020). It has been confirmed that LXs can exert protective effects in SAH. The expression of endogenous LXA_4 was decreased and its receptor FPR2/ALX was increased in the hippocampal and cerebral arteries after SAH, indicating a depletion of anti-inflammation (Guo et al., 2016). Exogenously injected LXA_4 (1.0 nmol) at 1.5 h after SAH could significantly alleviate the pathology of SAH, including reducing brain edema, preserving BBB integrity, improving neurological scores, and enhancing spatial learning and memory abilities. In this experiment, the FPR2/p38 MAPK signaling pathway was shown to be involved in the anti-inflammatory pathway elicited by LXA_4 (Guo et al., 2016). In addition, LXA_4 could significantly ameliorate endothelial dysfunction, recover microflow and protect against inflammation by inhibiting neutrophil infiltration. The beneficial effects of LXA_4 on endothelial function might be partly dependent on the inhibition of NF-κB via the FPR2/ERK1/2 pathway (Liu et al., 2019).

The preemptive treatment of unruptured intracranial aneurysms (IAs) is the first goal in the prevention of SAH. Frustratingly, except for open surgery and endovascular intervention, there is no noninvasive medical treatment for IAs. By targeting inflammation, nonsteroid anti-inflammatory drugs (NSAIDs) and statins exert a suppressive effect on IAs (Aoki et al., 2008; Hasan et al., 2011). Recently, eicosapentaenoic acid, the precursor of resolvin E1 targeting GPR120, was also reported to suppress the size of IAs and degenerative changes in the media in rats by suppressing NF-κB activation (Abekura et al., 2020). Considering the strong modulation of inflammation of SPMs, LXs may also have an effect on IAs. LXA_4 may serve as an alternative treatment for SAH and is worthy of further exploration.

For ICH, it has been reported that LXA_4 ME could inhibit neuronal apoptosis, decrease the levels of proinflammatory cytokines and improve neurologic function by inhibiting the NF-kB-dependent MMP-9 pathway in a rat model of ICH (Song et al., 2019). LX treatment may be a potential therapy after brain hemorrhage. In the future, more studies are needed to determine the potential role of LXs in ICH and to clarify the protective mechanism.

5.3 Neonatal Hypoxia-Ischemia Encephalopathy

Neonatal hypoxia-ischemia (HI) encephalopathy is the most common clinical brain injury in the perinatal period (Hagberg et al., 2015). Recently, the neuroprotective effects of LXA_4 were reported in a rat model of neonatal HI brain injury (Zhu et al., 2020). LXA_4 treatment suppressed acute inflammation and oxidative stress following brain injury in addition to preventing BBB disruption by regulating the IκB/NF-κB signaling pathway, which consequently attenuated HI brain damage. Furthermore, LXA_4 succeeded in exerting long-term neuroprotection, which involved promoting the recovery of neuronal function and tissue structure 7 days post-HI and ameliorating motor and learning functioning 21 days after HI. Moreover, LXA_4 significantly inhibited neuronal apoptosis both *in vivo* and *in vitro* experiments. Although there is a lack of sufficient research support, LXA_4 raises new hope for HI, and further studies are required to elucidate the mechanisms underlying protection. Additionally, it is valuable to explore whether combined LXA_4 treatment with hypothermia, the only effective treatment recognized in HI clinical practice, can produce more pronounced improvements in HIE.

5.4 Traumatic Brain Injury

In traumatic brain injury (TBI), following mechanical damage from an impact, called "primary injury," a complex cascade of physiologic reactions will result in a secondary injury, among which primary BBB disruption and inflammatory response are the critical pathological steps (Jassam et al., 2017). AA products involving 5-HETE, 12-HETE and TXB2 were all increased in patients' CSF 1–4 days following TBI (Shearer and Walker, 2018). In contrast, plasma LXA_4 levels showed a tendency to decrease after TBI from 6 h up to 168 h in a controlled cortical impact rat model of TBI (Jung et al., 2020). These results indicate that proinflammatory activity rather than resolving activity is the dominant theme in TBI, which may lead to detrimental consequences, including increased intracranial pressure, brain edema, and brain herniation.

Neuroinflammation is proposed as an important manipulable aspect of secondary injury in animal and human studies. LXA_4 treatment was shown to effectively reduce BBB permeability, brain edema and lesion volume 24 h post-TBI in mice (Luo et al., 2013). These protective effects of LXA_4 were associated with the inhibition of proinflammatory cytokines (TNF-α, IL-1β and IL-6) and the activation of MAPK pathways (p-ERK and p-JNK but not p-p38). Of interest, LXA_4 enhanced the activation of ALXR in astrocytes instead of microglia at 24 h after injury, but the exact mechanism is still unclear. The limitation of the study was that it only focused on the effects of LXA_4 on the early changes within 24 h after TBI. In fact, the efficacy of TBI therapies is influenced by the type (focal vs. diffuse), stage (acute vs. chronic), severity, and location of the injury. Moreover, TBI can cause lifelong and dynamic influences such as sustained cognitive and psychiatric disorders, sleep-wake disturbances and neurodegeneration (Moretti et al., 2012; Sandsmark et al., 2017; Wilson et al., 2017). Therefore, more studies about the protective effect of LXs on TBI remain to be conducted.

5.5 Spinal Cord Injury

After spinal cord injury (SCI), incomplete or delayed resolution usually occurs and can lead to detrimental effects, including propagated tissue damage and impaired wound healing. First, the clearance of inflammatory cells containing neutrophils, macrophages, microglia and lymphocytes was impaired after SCI. Second, the synthesis of SPMs was delayed after contusion injury. The levels of 12-HETE and 15-HETE, which are pathway markers of the synthesis of LXA_4, did not increase until 14 days after injury (Francos-Quijorna et al., 2017).

Exogenous administration of LXs has shown protective effects against SCI in animal models. LXA_4 suppressed the damage induced by I/R in rabbits through its antiapoptotic and antioxidant activities (Liu et al., 2015). In a model of spinal cord hemisection, LXA_4 inhibited microglial activation, moderated neuroinflammation and attenuated mechanical allodynia (Martini et al., 2016). Moreover, LXA_4 upregulated Akt/Nrf2/HO-1 signaling, contributing to the improvement in functional recovery, attenuation of allodynia and hyperalgesia, reduction of lesion volume and inhibition of apoptotic signaling after SCI (Lu et al., 2018). Recently, BML-111 has also been reported to protect against SCI by suppressing inflammation and oxidative stress (Liu J. et al., 2020). Collectively, LXs may be considered a potential therapeutic agent for SCI and its associated complications.

5.6 Alzheimer's Disease

The AD brain is marked by the accumulation of extracellular senile plaques and intracellular neurofibrillary tangles composed of Aβ and hyperphosphorylated-tau protein (p-tau), respectively. The etiological mechanisms underlying these neuropathological changes remain unclear, but dysregulation of glial cells, especially microglia, and elevated neuroinflammation make great contributions to disease progression (Heneka et al., 2015). The decreased levels of LXA_4 are in line with the fact that the inflammation fails to be resolved in the AD brain. In the brain of 3xTg-AD mice, the levels of LXA_4 were significantly lower than those in the brains of nontransgenic mice. As the best-known risk factor for AD, age reduced LXA_4 levels with a pattern that showed a greater impact in AD mice (Dunn et al., 2015). Similar results were also found in the hippocampus of 5xFAD mice (Kantarci et al., 2018) and neurons from APP/PS1 mice (Lee et al., 2018). The latter study also uncovered that the decrease in 15-R-LXA_4 might be related to the reduction in neural sphingosine kinase 1. Generally, sphingosine kinase 1 can acetylate COX2 to increase SPM secretion, increase microglial phagocytosis and improve AD-like brain pathology, including abnormal inflammation and neuronal dysfunction.

Marianne Schultzberg's team analyzed postmortem brain tissues and CSF samples from AD patients concerning the production of SPM. In accordance with the findings in mice, the levels of LXA_4 were reduced in both the postmortem CSF and hippocampus of AD patients (Wang et al., 2015). The decline in LXA_4 synthesis was independent of the enzyme 15-LOX-2 since its expression in AD brains was elevated. They also found a positive correlation between the Mini-Mental State Examination scores and the levels of LXA_4, showing the importance of LXA_4 in maintaining normal cognition. Of interest, they verified the AD-related alterations in the entorhinal cortex, but no difference was found with regard to LXA_4, revealing its tissue-specific expression (Dunn et al., 2015). In the study, they also detected the level of FPR2/ALX and found an increase in AD brains, which would make the tissue more responsive to pro-resolving signaling. However, the influence of LXA_4 on the chemotaxis and production of reactive oxygen species in phagocytic cells also occurs *via* FPR2/ALX (Tiffany et al., 2001), which makes the role of the FPR2/ALX in AD progression more complicated.

In AD, several lines of evidence have shown the neuroprotective effect of LXA_4. It was first demonstrated in the cortex and hippocampus of mice and BV2 microglial cells exposed to Aβ1–42. LXA_4 inhibited the production of IL-1β and TNF-α *via* the NF-κB signaling pathway both *in vivo* and *in vitro* (Wu et al., 2011). LXA_4 also displayed neuroprotection against spatial memory impairment induced by Aβ1–40 in a cannabinoid 1 receptor-dependent manner in mice (Pamplona et al., 2012). Whether PPAR-γ mediates the neuroprotective effects of LXA_4 remains unknown, but the levels of PPAR-γ were markedly higher in AD than in the control compensatory reaction to the decreased levels of LXA_4 (Wang et al., 2015). In addition,

LXA_4 alleviated oxidative stress-driven neuroinflammation in rats by targeting redox-sensitive proteins, including heat shock protein 72 and HO-1 (Trovato et al., 2016).

ATL also exerted neuroprotective effects on AD-like pathology in mice. ATL switched microglia from the classic phenotype to the alternative phenotype, thus improving the phagocytic function of microglia. Altered microglia promoted clearance of Aβ deposits and ultimately reduced synaptotoxicity and restored cognitive function in Tg2576 mice. According to the study, ATL can activate FPR2/ALX and reduce NF-κB activation in astrocytes, sequentially potentiating the action of alternative microglia (Medeiros et al., 2013). However, there was no significant effect on $A\beta_{42}$ phagocytosis in CHME-3 microglia using LXA_4 (Zhu et al., 2016). Apart from reducing Aβ levels, ATL could also decrease the levels of p-tau and enhance the cognitive performance of 3xTg-AD mice (Dunn et al., 2015). The decrease in p-tau was in part due to the inhibition of tau kinases GSK-3β and p38 MAPK. Additionally, microglial and astrocyte reactivity was inhibited by ATL treatment.

Combining LXA_4 with other SPMs is a promising strategy to reverse the neuroinflammatory process associated with AD pathology since different SPMs have distinct selective functions and can regulate the process at multiple levels. Strong support is provided by the fact that combined treatment with LXA_4 and resolvin E1 resolved AD-associated neuroinflammation and restored cognitive deficits more effectively than LXA_4 treatment alone in 5xFAD mice (Kantarci et al., 2018). There have been several investigations on AD patients treated with dietary supplementation with SPM precursors (Kotani et al., 2006; Janssen and Kiliaan, 2014). For instance, it was shown that dietary supplementation with 240 mg/d AA and docosahexaenoic acid for 90 days improved the immediate memory and attention scores of patients with mild cognitive dysfunction. However, clinical trials in which human AD patients are directly treated with SPMs to correct the deficiency have not yet been performed.

Previous studies on AD tended to focus on "anti-inflammation" rather than "pro-resolution." Although epidemiological studies have suggested that patients with protracted NSAID use have a lower prevalence of dementia (McGeer et al., 1996), clinical trials with NSAIDs have thus far yielded disappointing results (Cunningham and Skelly, 2012; Cudaback et al., 2014; Heneka et al., 2015). In contrast to "anti-inflammatory" treatments, SPMs do not block the enzymatic activity to regulate the inflammatory process. Instead, they interact with specific receptors to promote the beneficial and restorative aspects of inflammation. The LX dysregulation in neurodegeneration is attracting more and more attentions (Kim et al., 2020). We think that the intervention of LXs based on inflammatory resolution may give AD a chance to return to normal.

5.7 Multiple Sclerosis

Excessive neuroinflammation is a crucial pathological hallmark of multiple sclerosis (MS). Gijs Kooij and his colleagues revealed that the majority of SPMs, including LXA_4 and LXB_4, were significantly reduced in MS and correlated with disease progression through targeted lipid metabololipidomics in the plasma of MS patients (Kooij et al., 2020). They also found that the expression of SPM-related biosynthetic enzymes and receptors in blood-derived leukocytes of MS patients was impaired. *In vitro*, LXA_4 and LXB_4 were found to reduce MS-derived monocyte activation and cytokine production, improve BBB function and inhibit monocyte transmigration in MS patients (Kooij et al., 2020). *In vivo*, LXA_4 administration ameliorated clinical signs of experimental autoimmune encephalomyelitis (EAE) in mice by normalizing the EAE-induced spinal cord lipidome and modulating Th1 and Th17 responses (Derada Troletti et al., 2021), which further highlighted the potential clinical application of LXs for MS.

5.8 Chronic Cerebral Hypoperfusion

Chronic cerebral hypoperfusion (CCH) is a chronic and silent disease characterized by sustained defects in brain perfusion. In recent years, as increasing evidence suggests the critical roles of CCH in the initiation and progression of vascular dementia and AD (Duncombe et al., 2017), CCH has garnered increasing attention from scientists and clinicians. Interestingly, LXs have been shown to exert beneficial effects against cognitive and neuropathological changes in CCH. LXA_4 ME could exert neuroprotection in CCH by regulating endoplasmic reticulum stress and macroautophagy (Jia et al., 2015). LXA_4 ME could also attenuate oxidative injury and reduce neuronal apoptosis related to CCH through activation of the ERK/Nrf2 signaling pathway in the rat hippocampus (Jin et al., 2014). Therefore, it is conceivable that the application of LXs in the future might provide beneficial effects for patients with CCH and ameliorate the related decline in cognition.

5.9 Neuropathic Pain

Neuropathic pain is attributed to lesions affecting the somatosensory nervous system that alter its structure and function so that pain occurs spontaneously and responses to noxious and innocuous stimuli are pathologically amplified (Costigan et al., 2009). There is abundant evidence for the involvement of inflammatory mediators in neuropathic pain. The development of allodynia and hyperalgesia is correlated with the release of TNF-α, IL-1β and IL-6, whereas antagonism or their knockout leads to the opposite effect. The mechanism of their action is not well established; nevertheless, they can directly excite nociceptors or indirectly maintain sensory abnormalities by modulating synaptic transmission and pain hypersensitivity (Marchand et al., 2005). It has been determined that the spinal cord, especially the astrocytes within it, can express FPR2/ALX *in vivo* and in culture (Svensson et al., 2007; Abdelmoaty et al., 2013; Wang et al., 2014). LX treatment has been reported to alleviate neuropathic pain under various pathological conditions, including opioid-induced hyperalgesia, peripheral nerve injury and spinal cord injury. The effect of LX on analgesics is primarily associated with its anti-inflammatory and pro-resolution properties.

LXA_4 ME attenuated morphine antinociceptive tolerance and withdrawal-induced hyperalgesia. This prevention was correlated with the inactivation of NF-κB, inhibition of proinflammatory

TABLE 1 | Summary of *in vitro* studies on the neuroprotective effects of lipoxins.

Cell type	Model	Agent	Effects	References
Neural stem cells				
Murine neural stem cells	—	ATL, LXA_4	Attenuated growth of NSCs by inducing the expression of epidermal growth factor receptor, cyclin E, p27, and caspase 8	Wada et al. (2006)
Neurons				
SH-SY5Y cells	STS-induced neurotoxicity	LXA_4	Anti-apoptosis by targeting GPR32	Zhu et al. (2016)
HT-22 cells	Glutamate-induced neurotoxicity	LXA_4, LXB_4	LXA_4: cell death reduced by targeting FPR2/ALX; LXB_4: cell death reduced by influencing mitochondrial activity	Livne-Bar et al. (2017)
Rat primary cortical neurons	OGD	LXA_4	Anti-apoptosis, anti-inflammation and anti-oxidation by inhibiting IκB/NF-κB pathway	Zhu et al. (2020)
Mouse primary cortical neurons	Serum deprivation	LXA_4, LXB_4	Cell death reduced only by LXB_4	Livne-Bar et al. (2017)
RGCs	PQ-induced oxidative stress	LXA_4, LXB_4	LXA_4: RGC survival rescued; LXB_4: both RGC survival and neurite degeneration rescued	Livne-Bar et al. (2017)
Microglia				
BV2 cells	Stimulated by LPS	ATL	NO, iNOS, IL-1β and TNF-α reduced by inhibiting NF-κB, ERK, p38 MAPK and AP-1 signaling pathways; ROS reduced by inhibiting the function of NADPH oxidase; regulated the activation and polarization of microglia via the Notch Signaling Pathway	Wang et al. (2011), Wu et al. (2012c), Wu et al. (2019b)
BV2 cells	OGDR	LXA_4	Regulated the polarization of microglia through the Notch signaling pathway	Li et al. (2021)
BV2 cells	Stimulated by $A\beta_{1-42}$	LXA_4	IL-1β and TNF-α reduced by inhibiting NF-κB signal pathway	Wu et al. (2011)
Human CHME3 cells	Stimulated by $A\beta_{42}$	LXA_4	No significant effect on microglial activation and phagocytosis	Zhu et al. (2016)
Astrocytes				
Rat primary astrocytes	OGDR	LXA_4	LTB_4, LTC_4 and 5-LOX nuclear translocation reduced involving ALXR/ERK pathway; anti-oxidation by activating Nrf2 pathway and increasing the level of HO-1, GSH, and p62	Wu et al. (2012a), Wu et al. (2015)
Rat primary astrocytes	Stimulated by LPS	ATL, LXA_4	NO, PGE2, iNOS and COX-2 reduced by inhibiting NF-κB signal pathway; down-regulate the expression of AQP4	Yao et al. (2014), Wu et al. (2019a)
1321N1 human astrocytoma cells	IL-1β-induced stimulation	LXA_4	IL-8 and ICAM-1 reduced by inhibiting NF-κB signal pathway	Decker et al. (2009)

AP-1, activating protein-1; ATL, aspirin-triggered lipoxin A_4; Aβ, β-amyloid; COX-2, cyclooxygenase 2; ERK, extracellular signal-regulated kinase; FPR2/ALX, formyl peptide receptor 2/ LXA_4 receptor; GPR, G protein-coupled receptor; GSH, glutathione; HO-1, heme oxygenase; IFN, interferon; IL, interleukin; iNOS, inducible nitric oxide synthase; IκB, inhibitor κB; LOX, lipoxygenase; LPS, lipopolysaccharide; LT, leukotriene; LX, lipoxin; MAPK, mitogen-activated protein kinase; NADPH, nicotinamide adenine dinucleotide phosphate; NF-κB, nuclear factor kappa B; NO, nitric oxide; Nrf2, nuclear factor erythroid 2-related factor 2; OGD/R, oxygen-glucose deprivation/recovery; PQ, paraquat; RGCs, retinal ganglion cells; ROS, reactive oxygen species; STS, staurosporine; TNF, tumor necrosis factor.

cytokines (IL-1β, IL-6, and TNF-α), and upregulation of anti-inflammatory cytokines (IL-10 and transforming growth factor-β1). According to the authors' perspective, the actions of LXA_4 ME were achieved by interacting with the Toll-like receptor 4 cascade, which has been verified as a contributor to painful neuropathy (Tanga et al., 2005), rather than opioid receptors (Jin et al., 2012). However, another study revealed the involvement of the μ-receptor/phosphoinositide-3-kinase (PI3K)-Akt signaling/NAcht leucine-rich-repeat protein 1 (NALP1) inflammasome cascade in this process and found that ATL could block this signaling cascade (Tian et al., 2015).

In chronic constriction injury (CCI)-induced neuropathic pain, ALT potently suppresses thermal and mechanical hyperalgesia and significantly inhibits NALP1 inflammasome activation, caspase-1 cleavage, and IL-1β maturation (Li et al., 2013). Further investigation indicated that the analgesic effect of ATL was mediated by inhibiting spinal JAK2/STAT3 signaling through FPR2/ALX and hence suppressing spinal neuroinflammation in CCI rats (Wang et al., 2014). In line with this discovery, LXA_4 exerted similar antinociceptive effects in a model of chronic dorsal root ganglia compression in rats (Sun et al., 2012). Moreover, LXA_4 potently alleviated radicular pain in a rat model of noncompressive lumbar disc herniation by attenuating the activation of NF-κB/p65, p-ERK and p-JNK, but not p-p38, in the dorsal root ganglion (Miao et al., 2015). Another study showed that LXA_4 inhibited NLRP3 activation and autophagy in the dorsal root ganglion by regulating the JNK1/beclin-1/PI3KC3 axis, thus participating in its analgesic effects (Jin et al., 2020).

LXA_4 also exhibited analgesic activity against SCI-induced neuropathic pain, as evidenced by an increase in the mechanical paw withdrawal threshold in a model of SCI in both mice and rats (Martini et al., 2016; Lu et al., 2018). The antinociceptive effects of LXA_4 were mediated by FPR2/ALX and might be partly attributable to the decline in TNF-α from microglia (Martini et al., 2016). In addition, LXs could prevent the phosphorylation of ERK and JNK in astrocytes by activating FPR2/ALX (Svensson et al., 2007; Hu et al., 2012).

Recently, roles of SPMs in neuropathic pain were elucidated, suggesting that SPM can be promising targets to counteract neuropathic pain (Leuti et al., 2021). SPM represent the endogenous inhibitors of transient receptor potential cation channel subfamily V member 1 (TRPV1), which has been

TABLE 2 | Summary of *in vivo* studies on the neuroprotective effects of lipoxins.

Disease type	Object	Substance	Outcome	Mechanism	References
Ischemia/ reperfusion injury	Rat; mice	LXA_4, LXA_4 ME, ATL, BML-111	Infarct volume, brain water content, tissue damage, hemorrhagic transformation, neurologic deficit and cognitive impairment attenuated; BBB dysfunction ameliorated; the reactivity of the cerebral microvasculature inhibited; the cognitive function improved	Anti-apoptosis; inhibition of neutrophil infiltration, lipid peroxidation, and astrocyte activation; anti-inflammation; inhibition of 5-LOX translocation and leukotriene biosynthesis; downregulation of MMP-9 and MMP-3 expression and upregulation of TIMP-1 expression; involvement of the ERK signal transduction pathway; PPARγ agonistic actions; activation of neutrophil FPR2/3 regulating leukocyte-endothelial interactions and NPA formation; activation of Nrf2/HO-1/GSH signaling	Sobrado et al. (2009), Wu et al. (2010), Ye et al. (2010), Wu et al. (2012a), Wu et al. (2013), Hawkins et al. (2014), Smith et al. (2015), Han et al. (2016), Vital et al. (2016), Hawkins et al. (2017), Wu et al. (2018)
Intracerebral Hemorrhage	Rat	LXA_4 ME	Neuronal apoptosis and cerebral edema reduced; neurologic function improved; the levels of proinflammatory cytokines decreased	Inhibition in NF-kB-dependent MMP-9 pathway	Song et al. (2019)
Subarachnoid hemorrhage	Rat	LXA_4	Brain water content and BBB permeability decreased; neurological functions and spatial learning and memory abilities improved; cerebrovascular endothelial dysfunction ameliorated; microflow recovered	Anti-inflammation (FPR2/p38 MAPK pathway); suppression infiltration of neutrophils; inhibition of NF-κB via the FPR2/ERK1/2 pathway	Guo et al. (2016), Liu et al. (2019)
Hypoxia/ischemia neonatal brain injury	Rat	LXA_4	Cerebral edema, infarct volume, and inflammatory responses reduced; neuronal function and tissue structure recovered; motor, learning and memory functions ameliorated; the integrity of the BBB maintained	Anti-inflammation; anti-apoptosis; anti-oxidation; inhibition of IκB/NF-κB pathway	Zhu et al. (2020)
Traumatic brain injury	Mice	LXA_4	Cerebral edema, infarct volume and BBB breakdown reduced	Anti-inflammation; downregulation MAPK pathway with FPR2/ALX in astrocytes	Luo et al. (2013)
Spinal cord injury	Rabbit	LXA_4	Neurological function improved; allodynia and hyperalgesia attenuated; lesion reduced	Anti-apoptosis; anti-oxidation; upregulation of Akt/Nrf2/HO-1 signaling	Liu et al. (2015), Martini et al. (2016), Lu et al. (2018), Liu J. et al. (2020)
Alzheimer's disease	Mouse	ATL, BML-111	Cognitive impairment reduced; the expression of synaptic proteins increased; the levels of p-tau and Aβ reduced	Anti-inflammation; anti-oxidation; activation of microglia in a non-phlogistic phenotype; suppression of NF-κB activation; anti-apoptosis; modulation of CB1 receptors; inhibition of the tau kinases GSK-3β and p38 MAPK.	Wu et al. (2011), Pamplona et al. (2012), Medeiros et al. (2013), Dunn et al. (2015), Kantarci et al. (2018)
Multiple sclerosis	Mouse	LXA4	Clinical signs of experimental autoimmune encephalomyelitis ameliorated	Modulation of Th1 and Th17 response and the EAE-induced spinal cord lipidom	Derada Troletti et al. (2021)
Chronic cerebral hypoperfusion	Rat	LXA_4 ME	Cognitive impairment reduced	Activation of ERK/Nrf2 signaling pathway; regulation of endoplasmic reticulum stress and macroautophagy	Jin et al. (2014), Jia et al. (2015)
Neuropathic pain	Mice; rat	LXA_4, ATL, LXA_4 ME	Mechanical allodynia in opioid-induced hyperalgesia, peripheral nerve injury and spinal cord injury attenuated	Anti-inflammation; inhibition of microglial activation through FPR2/ALX; inhibition of JAK2/STAT3 signaling; inactivation of NF-κB, ERK and p-JNK; inhibition of μ-receptor/Pl3k-Akt signaling/NALP1 inflammasome cascade; anti-autophagy by regulating the JNK1/beclin-1/Pl3KC3 axis	Tanga et al. (2005), Sun et al. (2012), Li et al. (2013), Wang et al. (2014), Miao et al. (2015), Tian et al. (2015), Martini et al. (2016), Lu et al. (2018), Jin et al. (2020)
Plasmodium berghei- infection	Mice	LXA_4	Survival prolonged, endothelial dysfunction ameliorated		Shryock et al. (2013), Souza et al. (2015)

(Continued on following page)

TABLE 2 | (*Continued*) Summary of *in vivo* studies on the neuroprotective effects of lipoxins.

Disease type	Object	Substance	Outcome	Mechanism	References
				Inhibition of IL-12 production and CD8(+) IFN-γ (+) T cells; modulation of ICAM-1 and HO-1 expression	
Toxoplasma gondii infection	Mice	LXA_4	Survival prolonged	Regulation of proinflammatory responses	Aliberti et al. (2002)
Retinal diseases	Mice	LXA_4, LXB_4	The progression of retinal degeneration delayed; photoreceptors rescued	Modulation of microglial activities and anti-inflammation	Livne-Bar et al. (2017), Lu et al. (2019)

Akt, protein kinase B, PKB; ALXR, lipoxin A4 receptor; Aβ, Amyloid-beta; BBB, blood-brain barrier; CB1, cannabinoid receptor 1; ER, endoplasmic reticulum; ERK, extracellular signal-regulated kinase; FPR2/ALX, formyl peptide receptor 2/LXA_4 receptor; GSH, glutathione; HO-1, heme oxygenase-1; IκB, inhibitor κB; JAK2, Janus kinase 2; JNK, c-Jun N-terminal kinase; LOX, lipoxygenase; LX, lipoxin; LXA_4 ME, lipoxin A_4 methyl ester; MAPK, mitogen-activated protein kinase; MMP, matrix metalloproteinase; NALP1, NAcht leucine-rich-repeat protein 1; NF-κB, nuclear factor kappa B; NPA, neutrophil-platelet aggregation; Nrf2, nuclear factor erythroid 2-related factor 2; PI3k, phosphoinositide-3-kinase; PPAR, peroxisome proliferator-activated receptor; SOCS, suppressors of cytokine signaling; STAT3, signal transducer and activator of transcription 3; TIMP, metallopeptidase inhibitor.

confirmed with Resolvin E1 and protectin 1. To date, it remains unknown whether LXs has an effect on TRPV1. Due to the intricated relationship between inflammation and pain, it is necessary to better understand the cellular and molecular pathways associated to the analgesia of LXs.

5.10 Others

In recent years, the protection of LXs has been underscored in a variety of central nervous system infections. First, LXs generated in a 5-LO-dependent manner have been demonstrated to control proinflammatory and type 1 T helper cells' immune responses against *M. tuberculosis* infection (Bafica et al., 2005). Aspirin can improve outcomes from tuberculosis meningitis, which is speculated to be related to the production of ATL (Tobin et al., 2012). However, in a randomized placebo-controlled trial of adjunctive aspirin treatment in adults with tuberculosis meningitis, ATL concentrations were not changed by aspirin treatment, but it confirmed that SPM concentrations, including ATL in CSF, were associated with disease severity and outcome (Colas et al., 2019). In *Plasmodium berghei*-infected mice, LXA_4 not only prolonged survival by inhibiting IL-12 production and CD8(+) IFN-γ(+) T cells (Shryock et al., 2013) but also ameliorated endothelial dysfunction by modulating ICAM-1 and HO-1 expression in brain tissue (Souza et al., 2015). Moreover, by generating LXA_4 (Aliberti et al., 2002), wild-type mice avoid succumbing to encephalitis after *Toxoplasma gondii* infection. Notably, it has been proven that FPR2/ALX plays a pivotal role in glial cell activation in bacterial infection of the CNS (Braun et al., 2011), hinting that LXs may also have an effect on bacterial meningitis.

There is also evidence of the neuroprotective effect of LXs on epilepsy and retinal diseases. The LXA_4 level and FPR2/ALX expression in the cortex and hippocampi of rats were greater in pentylenetetrazole-kindled rats than in the saline group. Aspirin can downregulate the levels of FPR2/ALX and LXA_4, elevating the seizure threshold and helping achieve seizure control (Abd-Elghafour et al., 2017). Astrocyte-derived LXA_4 and LXB_4 have been reported to have a protective effect on the retina against acute kainic acid-induced injury and chronic glaucoma *in vivo* and to simultaneously dampen paraquat-induced oxidative stress *in vitro* (Livne-Bar et al., 2017). Recently, it was further characterized that intravitreal injection of LXA_4 delayed the progression of retinal degeneration in mice through the modulation of microglial activities to suppress retinal inflammation and rescue photoreceptors (Lu et al., 2019).

6 CONCLUSION AND PERSPECTIVES

LXs present opportunities to intervene in and promote human brain health. The neuroprotection of LXs has been well established in CNS cell types (**Table 1**). LXs can exert an array of protective effects on neurological diseases, including ischemic or hemorrhagic stroke, neonatal hypoxia-ischemia encephalopathy, brain and spinal cord injury, AD, MS, CCH, and neuropathic pain, showing great therapeutic potential for neuroinflammatory and neurodegenerative disorders (**Table 2**).

In terms of the treatment efficiency and potential risks, LXs might show superior advantages among the clinical therapeutic options for neurological diseases in the future. On the one hand, LXs present notable potency at a microgram dose of the compound and manifest protection in a broad spectrum of diseases not limited to the CNS, such as type 2 diabetes mellitus, hypertension, and coronary heart disease (Das, 2018). This means that applying LXs in patients with both neurological disorders and others diseases can benefit more than we expected. On the other hand, as an innate SPM, LXs are involved in physiological functions of the body and can be rapidly metabolized and inactivated, which may signify little interference with the healthy physiological process and few side effects for patients. Nevertheless, inflammation is a complex course. In acute events of the CNS, such as stroke, applying LXs at an incorrect time or in an overdose might impede the natural processes of focus clearance and functional recovery. In chronic neuroinflammation and neurodegeneration, whether persistence of anti-inflammation by LXs could impair innate immune responses and result in adverse effects, such as neoplasia, is an issue worth considering. In addition, improper use of LXs may possibly augment the effects of resolution. For instance, overdose of LXs might result in excessive phagocytosis of macrophages leading to synapse destruction. However, all above are based on our speculations. In the future, more

studies on the adverse effects of LXs are essential before their clinical application.

Before the extensive use of LXs in humans, there are also other important issues for researchers to consider. Regarding pharmacodynamic, to date, most studies have interpreted the neuroprotective effects of LXs with their pro-resolving activity in neuroinflammation. Whether LXs exert direct protective effects in the CNS remains to be seen, and more research is needed to understand the specific role that LXs play in each given disease. Concerning pharmacokinetics, there are two major factors to consider. To our knowledge, no studies have provided explicit evidence for the BBB permeability of LXs. If LXs are beneficial in CNS diseases only when administered by intrathecal injection instead of oral or intravenous administration, they will cause great pain to patients due to repeated punctures and will be limited in use. The other major factor is that natural LXs are characterized by rapid metabolic inactivation, temperature sensitivity and a lack of tissue specificity. Chemical modification of LX structures and the development of more LX analogs could render them more effective for therapeutic use in nervous diseases. Recently, a drug delivery system composed of neutrophil membrane-derived nanovesicles was loaded with SPMs specifically targeting inflamed brain endothelium during I/R, thus protecting against brain damage during ischemic stroke (Dong et al., 2019). Advanced nanocarrier provides a strategy for lipoxin-related drug design. We believe that along with the advances in drug design, LXs will spring more new surprises down our road against neurological diseases.

AUTHOR CONTRIBUTIONS

WJ conceived and designed review; JZ, ZL, and MF wrote and revised manuscript; JZ, ZL, MF, and WJ approved final version of manuscript.

FUNDING

This work was supported by the National Natural Science Foundation of China (No. 81701082) and Specialist leader training project subsidized by Hebei government in 2018.

REFERENCES

Abd-Elghafour, B. A., El-Sayed, N. M., Ahmed, A. A., Zaitone, S. A., and Moustafa, Y. M. (2017). Aspirin and (Or) omega-3 Polyunsaturated Fatty Acids Protect against Corticohippocampal Neurodegeneration and Downregulate Lipoxin A4 Production and Formyl Peptide Receptor-like 1 Expression in Pentylenetetrazole-Kindled Rats. *Can. J. Physiol. Pharmacol.* 95, 340–348. doi:10.1139/cjpp-2016-0060

Abdelmoaty, S., Wigerblad, G., Bas, D. B., Codeluppi, S., Fernandez-Zafra, T., El-Awady, S., et al. (2013). Spinal Actions of Lipoxin A4 and 17(R)-resolvin D1 Attenuate Inflammation-Induced Mechanical Hypersensitivity and Spinal TNF Release. *PLoS One* 8 (9), e75543. doi:10.1371/journal.pone.0075543

Abekura, Y., Ono, I., Kawashima, A., Takizawa, K., Koseki, H., Miyata, H., et al. (2020). Eicosapentaenoic Acid Prevents the Progression of Intracranial Aneurysms in Rats. *J. Neuroinflammation* 17 (1), 129. doi:10.1186/s12974-020-01802-8

Aliberti, J., Serhan, C., and Sher, A. (2002). Parasite-induced Lipoxin A4 Is an Endogenous Regulator of IL-12 Production and Immunopathology in Toxoplasma Gondii Infection. *J. Exp. Med.* 196 (9), 1253–1262. doi:10.1084/jem.20021183

Aoki, T., Kataoka, H., Ishibashi, R., Nozaki, K., and Hashimoto, N. (2008). Simvastatin Suppresses the Progression of Experimentally Induced Cerebral Aneurysms in Rats. *Stroke* 39 (4), 1276–1285. doi:10.1161/STROKEAHA.107.503086

Ariel, A., Chiang, N., Arita, M., Petasis, N. A., and Serhan, C. N. (2003). Aspirin-triggered Lipoxin A4 and B4 Analogs Block Extracellular Signal-Regulated Kinase-dependent TNF-Alpha Secretion from Human T Cells. *J. Immunol.* 170 (12), 6266–6272. doi:10.4049/jimmunol.170.12.6266

Bafica, A., Scanga, C. A., Serhan, C., Machado, F., White, S., Sher, A., et al. (2005). Host Control of *Mycobacterium tuberculosis* Is Regulated by 5-lipoxygenase-dependent Lipoxin Production. *J. Clin. Invest.* 115 (6), 1601–1606. doi:10.1172/JCI23949

Baker, N., O'Meara, S. J., Scannell, M., Maderna, P., Godson, C., and Godson, C. (2009). Lipoxin A4: Anti-inflammatory and Anti-angiogenic Impact on Endothelial Cells. *J. Immunol.* 182 (6), 3819–3826. doi:10.4049/jimmunol.0803175

Beaino, W., Janssen, B., Vugts, D. J., de Vries, H. E., and Windhorst, A. D. (2021). Towards PET Imaging of the Dynamic Phenotypes of Microglia. *Clin. Exp. Immunol.* 206, 282–300. doi:10.1111/cei.13649

Becker, E. L., Forouhar, F. A., Grunnet, M. L., Boulay, F., Tardif, M., Bormann, B. J., et al. (1998). Broad Immunocytochemical Localization of the Formylpeptide Receptor in Human Organs, Tissues, and Cells. *Cell Tissue Res.* 292 (1), 129–135. doi:10.1007/s004410051042

Birnbaum, Y., Ye, Y., Lin, Y., Freeberg, S. Y., Nishi, S. P., Martinez, J. D., et al. (2006). Augmentation of Myocardial Production of 15-Epi-Lipoxin-A4 by Pioglitazone and Atorvastatin in the Rat. *Circulation* 114 (9), 929–935. doi:10.1161/CIRCULATIONAHA.106.629907

Braun, B. J., Slowik, A., Leib, S. L., Lucius, R., Varoga, D., Wruck, C. J., et al. (2011). The Formyl Peptide Receptor Like-1 and Scavenger Receptor MARCO Are Involved in Glial Cell Activation in Bacterial Meningitis. *J. Neuroinflammation* 8 (1), 11. doi:10.1186/1742-2094-8-11

Cai, W., Yang, T., Liu, H., Han, L., Zhang, K., Hu, X., et al. (2018). Peroxisome Proliferator-Activated Receptor γ (PPARγ): A Master Gatekeeper in CNS Injury and Repair. *Prog. Neurobiol.* 163-164, 27–58. doi:10.1016/j.pneurobio.2017.10.002

Cattaneo, F., Parisi, M., and Ammendola, R. (2013). Distinct Signaling Cascades Elicited by Different Formyl Peptide Receptor 2 (FPR2) Agonists. *Int. J. Mol. Sci.* 14 (4), 7193–7230. doi:10.3390/ijms14047193

Cekanaviciute, E., and Buckwalter, M. S. (2016). Astrocytes: Integrative Regulators of Neuroinflammation in Stroke and Other Neurological Diseases. *Neurotherapeutics* 13, 685–701. doi:10.1007/s13311-016-0477-8

Clària, J., and Serhan, C. N. (1995). Aspirin Triggers Previously Undescribed Bioactive Eicosanoids by Human Endothelial Cell-Leukocyte Interactions. *Proc. Natl. Acad. Sci. U S A.* 92 (21), 9475–9479. doi:10.1073/pnas.92.21.9475

Colas, R. A., Nhat, L. T. H., Thuong, N. T. T., Gómez, E. A., Ly, L., Thanh, H. H., et al. (2019). Proresolving Mediator Profiles in Cerebrospinal Fluid Are Linked with Disease Severity and Outcome in Adults with Tuberculous Meningitis. *FASEB J.* 33 (11), 13028–13039. doi:10.1096/fj.201901590R

Costigan, M., Scholz, J., and Woolf, C. J. (2009). Neuropathic Pain: a Maladaptive Response of the Nervous System to Damage. *Annu. Rev. Neurosci.* 32, 1–32. doi:10.1146/annurev.neuro.051508.135531

Cudaback, E., Jorstad, N. L., Yang, Y., Montine, T. J., and Keene, C. D. (2014). Therapeutic Implications of the Prostaglandin Pathway in Alzheimer's Disease. *Biochem. Pharmacol.* 88 (4), 565–572. doi:10.1016/j.bcp.2013.12.014

Cunningham, C., and Skelly, D. T. (2012). Non-steroidal Anti-inflammatory Drugs and Cognitive Function: Are Prostaglandins at the Heart of Cognitive Impairment in Dementia and Delirium. *J. Neuroimmune Pharmacol.* 7 (1), 60–73. doi:10.1007/s11481-011-9312-5

Das, U. N. (2018). Ageing: Is There a Role for Arachidonic Acid and Other Bioactive Lipids? A Review. *J. Adv. Res.* 11, 67–79. doi:10.1016/j.jare.2018.02.004

Decker, Y., McBean, G., and Godson, C. (2009). Lipoxin A4 Inhibits IL-1beta-induced IL-8 and ICAM-1 Expression in 1321N1 Human Astrocytoma Cells. *Am. J. Physiol. Cel Physiol* 296 (6), C1420–C1427. doi:10.1152/ajpcell.00380.2008

Derada Troletti, C., Enzmann, G., Chiurchiù, V., Kamermans, A., Tietz, S. M., Norris, P. C., et al. (2021). Pro-resolving Lipid Mediator Lipoxin A4 Attenuates Neuro-Inflammation by Modulating T Cell Responses and Modifies the Spinal Cord Lipidome. *Cell Rep* 35, 109201. doi:10.1016/j.celrep.2021.109201

Devanney, N. A., Stewart, A. N., and Gensel, J. C. (2020). Microglia and Macrophage Metabolism in CNS Injury and Disease: The Role of Immunometabolism in Neurodegeneration and Neurotrauma. *Exp. Neurol.* 329, 113310. doi:10.1016/j.expneurol.2020.113310

Dong, X., Gao, J., Zhang, C. Y., Hayworth, C., Frank, M., and Wang, Z. (2019). Neutrophil Membrane-Derived Nanovesicles Alleviate Inflammation to Protect Mouse Brain Injury from Ischemic Stroke. *ACS Nano* 13 (2), 1272–1283. doi:10.1021/acsnano.8b06572

Duncombe, J., Kitamura, A., Hase, Y., Ihara, M., Kalaria, R. N., and Horsburgh, K. (2017). Chronic Cerebral Hypoperfusion: a Key Mechanism Leading to Vascular Cognitive Impairment and Dementia. Closing the Translational gap between Rodent Models and Human Vascular Cognitive Impairment and Dementia. *Clin. Sci. (Lond)* 131 (19), 2451–2468. doi:10.1042/CS20160727

Dunn, H. C., Ager, R. R., Baglietto-Vargas, D., Cheng, D., Kitazawa, M., Cribbs, D. H., et al. (2015). Restoration of Lipoxin A4 Signaling Reduces Alzheimer's Disease-like Pathology in the 3xTg-AD Mouse Model. *J. Alzheimers Dis.* 43 (3), 893–903. doi:10.3233/JAD-141335

Feng, X., Valdearcos, M., Uchida, Y., Lutrin, D., Maze, M., and Koliwad, S. K. (2017). Microglia Mediate Postoperative Hippocampal Inflammation and Cognitive Decline in Mice. *JCI Insight* 2 (7), e91229. doi:10.1172/jci.insight.91229

Fiore, S., Maddox, J. F., Perez, H. D., and Serhan, C. N. (1994). Identification of a Human cDNA Encoding a Functional High Affinity Lipoxin A4 Receptor. *J. Exp. Med.* 180 (1), 253–260. doi:10.1084/jem.180.1.253

Francos-Quijorna, I., Santos-Nogueira, E., Gronert, K., Sullivan, A. B., Kopp, M. A., Brommer, B., et al. (2017). Maresin 1 Promotes Inflammatory Resolution, Neuroprotection, and Functional Neurological Recovery after Spinal Cord Injury. *J. Neurosci.* 37 (48), 11731–11743. doi:10.1523/JNEUROSCI.1395-17.2017

Godson, C., Mitchell, S., Harvey, K., Petasis, N. A., Hogg, N., and Brady, H. R. (2000). Cutting Edge: Lipoxins Rapidly Stimulate Nonphlogistic Phagocytosis of Apoptotic Neutrophils by Monocyte-Derived Macrophages. *J. Immunol.* 164 (164), 1663–1667. doi:10.4049/jimmunol.164.4.1663

Guo, Z., Hu, Q., Xu, L., Guo, Z. N., Ou, Y., He, Y., et al. (2016). Lipoxin A4 Reduces Inflammation through Formyl Peptide Receptor 2/p38 MAPK Signaling Pathway in Subarachnoid Hemorrhage Rats. *Stroke* 47 (2), 490–497. doi:10.1161/STROKEAHA.115.011223

Hagberg, H., Mallard, C., Ferriero, D. M., Vannucci, S. J., Levison, S. W., Vexler, Z. S., et al. (2015). The Role of Inflammation in Perinatal Brain Injury. *Nat. Rev. Neurol.* 11 (4), 192–208. doi:10.1038/nrneurol.2015.13

Han, J. Q., Liu, C. L., Wang, Z. Y., Liu, L., Cheng, L., and Fan, Y. D. (2016). Anti-inflammatory Properties of Lipoxin A4 Protect against Diabetes Mellitus Complicated by Focal Cerebral Ischemia/reperfusion Injury. *Neural Regen. Res.* 11 (4), 636–640. doi:10.4103/1673-5374.180750

Hanisch, U. K., and Kettenmann, H. (2007). Microglia: Active Sensor and Versatile Effector Cells in the normal and Pathologic Brain. *Nat. Neurosci.* 10 (11), 1387–1394. doi:10.1038/nn1997

Hasan, D. M., Mahaney, K. B., Brown, R. D., Jr, Meissner, I., Piepgras, D. G., Huston, J., et al. (2011). Aspirin as a Promising Agent for Decreasing Incidence of Cerebral Aneurysm Rupture. *Stroke* 42 (11), 3156–3162. doi:10.1161/STROKEAHA.111.619411

Hawkins, K. E., DeMars, K. M., Alexander, J. C., de Leon, L. G., Pacheco, S. C., Graves, C., et al. (2017). Targeting Resolution of Neuroinflammation after Ischemic Stroke with a Lipoxin A4 Analog: Protective Mechanisms and Long-Term Effects on Neurological Recovery. *Brain Behav.* 7, e00688. doi:10.1002/brb3.688

Hawkins, K. E., DeMars, K. M., Singh, J., Yang, C., Cho, H. S., Frankowski, J. C., et al. (2014). Neurovascular protection by post-ischemic Intravenous Injections of the Lipoxin A4 Receptor Agonist, BML-111, in a Rat Model of Ischemic Stroke. *J. Neurochem.* 129 (1), 130–142. doi:10.1111/jnc.12607

Heneka, M. T., Carson, M. J., El Khoury, J., Landreth, G. E., Brosseron, F., Feinstein, D. L., et al. (2015). Neuroinflammation in Alzheimer's Disease. *Lancet Neurol.* 14 (4), 388–405. doi:10.1016/S1474-4422(15)70016-5

Ho, C. F., Ismail, N. B., Koh, J. K., Gunaseelan, S., Low, Y. H., Ng, Y. K., et al. (2018). Localisation of Formyl-Peptide Receptor 2 in the Rat Central Nervous System and its Role in Axonal and Dendritic Outgrowth. *Neurochem. Res.* 43 (8), 1587–1598. doi:10.1007/s11064-018-2573-0

Hu, S., Mao-Ying, Q. L., Wang, J., Wang, Z. F., Mi, W. L., Wang, X. W., et al. (2012). Lipoxins and Aspirin-Triggered Lipoxin Alleviate Bone Cancer Pain in Association with Suppressing Expression of Spinal Proinflammatory Cytokines. *J. Neuroinflammation* 9, 278. doi:10.1186/1742-2094-9-278

Janssen, C. I., and Kiliaan, A. J. (2014). Long-chain Polyunsaturated Fatty Acids (LCPUFA) from Genesis to Senescence: the Influence of LCPUFA on Neural Development, Aging, and Neurodegeneration. *Prog. Lipid Res.* 53, 1–17. doi:10.1016/j.plipres.2013.10.002

Jassam, Y. N., Izzy, S., Whalen, M., McGavern, D. B., and El Khoury, J. (2017). Neuroimmunology of Traumatic Brain Injury: Time for a Paradigm Shift. *Neuron* 95 (6), 1246–1265. doi:10.1016/j.neuron.2017.07.010

Jia, Y., Jin, W., Xiao, Y., Dong, Y., Wang, T., Fan, M., et al. (2015). Lipoxin A4 Methyl Ester Alleviates Vascular Cognition Impairment by Regulating the Expression of Proteins Related to Autophagy and ER Stress in the Rat hippocampus. *Cell Mol Biol Lett.* 20 (3), 475–487. doi:10.1515/cmble-2015-0027

Jin, H., Li, Y. H., Xu, J. S., Guo, G. Q., Chen, D. L., and Bo, Y. (2012). Lipoxin A4 Analog Attenuates Morphine Antinociceptive Tolerance, Withdrawal-Induced Hyperalgesia, and Glial Reaction and Cytokine Expression in the Spinal Cord of Rat. *Neuroscience* 208, 1–10. doi:10.1016/j.neuroscience.2012.02.009

Jin, J., Xie, Y., Shi, C., Ma, J., Wang, Y., Qiao, L., et al. (2020). Lipoxin A4 Inhibits NLRP3 Inflammasome Activation in Rats with Non-compressive Disc Herniation through the JNK1/Beclin-1/PI3KC3 Pathway. *Front. Neurosci.* 14, 799. doi:10.3389/fnins.2020.00799

Jin, W., Jia, Y., Huang, L., Wang, T., Wang, H., Dong, Y., et al. (2014). Lipoxin A4 Methyl Ester Ameliorates Cognitive Deficits Induced by Chronic Cerebral Hypoperfusion through Activating ERK/Nrf2 Signaling Pathway in Rats. *Pharmacol. Biochem. Behav.* 124, 145–152. doi:10.1016/j.pbb.2014.05.023

Jung, J. S., Kho, A. R., Lee, S. H., Choi, B. Y., Kang, S. H., Koh, J. Y., et al. (2020). Changes in Plasma Lipoxin A4, Resolvins and CD59 Levels after Ischemic and Traumatic Brain Injuries in Rats. *Korean J. Physiol. Pharmacol.* 24 (2), 165–171. doi:10.4196/kjpp.2020.24.2.165

Kantarci, A., Aytan, N., Palaska, I., Stephens, D., Crabtree, L., Benincasa, C., et al. (2018). Combined Administration of Resolvin E1 and Lipoxin A4 Resolves Inflammation in a Murine Model of Alzheimer's Disease. *Exp. Neurol.* 300, 111–120. doi:10.1016/j.expneurol.2017.11.005

Ke, Y., Zebda, N., Oskolkova, O., Afonyushkin, T., Berdyshev, E., Tian, Y., et al. (2017). Anti-Inflammatory Effects of OxPAPC Involve Endothelial Cell-Mediated Generation of LXA4. *Circ. Res.* 121 (3), 244–257. doi:10.1161/CIRCRESAHA.116.310308

Keren-Shaul, H., Spinrad, A., Weiner, A., Matcovitch-Natan, O., Dvir-Szternfeld, R., Ulland, T. K., et al. (2017). A Unique Microglia Type Associated with Restricting Development of Alzheimer's Disease. *Cell* 169, 1276–e17. doi:10.1016/j.cell.2017.05.018

Kim, C., Livne-Bar, I., Gronert, K., and Sivak, J. M. (2020). Fair-Weather Friends: Evidence of Lipoxin Dysregulation in Neurodegeneration. *Mol. Nutr. Food Res.* 64, e1801076. doi:10.1002/mnfr.201801076

Kim, N., Lannan, K. L., Thatcher, T. H., Pollock, S. J., Woeller, C. F., and Phipps, R. P. (2018). Lipoxin B4 Enhances Human Memory B Cell Antibody Production via Upregulating Cyclooxygenase-2 Expression. *J. Immunol.* 201 (11), 3343–3351. doi:10.4049/jimmunol.1700503

Klegeris, A., and McGeer, P. L. (2003). Toxicity of Human Monocytic THP-1 Cells and Microglia toward SH-Sy5y Neuroblastoma Cells Is Reduced by Inhibitors of 5-lipoxygenase and its Activating Protein FLAP. *J. Leukoc. Biol.* 73 (3), 369–378. doi:10.1189/jlb.1002482

Kooij, G., Troletti, C. D., Leuti, A., Norris, P. C., Riley, I., Albanese, M., et al. (2020). Specialized Pro-resolving Lipid Mediators Are Differentially Altered in

Peripheral Blood of Patients with Multiple Sclerosis and Attenuate Monocyte and Blood-Brain Barrier Dysfunction. *Haematologica* 105, 2056–2070. doi:10.3324/haematol.2019.219519

Kotani, S., Sakaguchi, E., Warashina, S., Matsukawa, N., Ishikura, Y., Kiso, Y., et al. (2006). Dietary Supplementation of Arachidonic and Docosahexaenoic Acids Improves Cognitive Dysfunction. *Neurosci. Res.* 56 (2), 159–164. doi:10.1016/j.neures.2006.06.010

Kotlega, D., Zembron-Lacny, A., Golab-Janowska, M., Nowacki, P., and Szczuko, M. (2020). The Association of Free Fatty Acids and Eicosanoids with the Severity of Depressive Symptoms in Stroke Patients. *Int. J. Mol. Sci.* 21, 5220. doi:10.3390/ijms21155220

Lawrence, T., Willoughby, D. A., and Gilroy, D. W. (2002). Anti-inflammatory Lipid Mediators and Insights into the Resolution of Inflammation. *Nat. Rev. Immunol.* 2 (10), 787–795. doi:10.1038/nri915

Lee, J. Y., Han, S. H., Park, M. H., Baek, B., Song, I. S., Choi, M. K., et al. (2018). Neuronal SphK1 Acetylates COX2 and Contributes to Pathogenesis in a Model of Alzheimer's Disease. *Nat. Commun.* 9 (1), 1479. doi:10.1038/s41467-018-03674-2

Lee, S., Nakahira, K., Dalli, J., Siempos, I. I., Norris, P. C., Colas, R. A., et al. (2017). NLRP3 Inflammasome Deficiency Protects against Microbial Sepsis via Increased Lipoxin B4 Synthesis. *Am. J. Respir. Crit. Care Med.* 196 (6), 713–726. doi:10.1164/rccm.201604-0892OC

Lefer, A. M., Stahl, G. L., Lefer, D. J., Brezinski, M. E., Nicolaou, K. C., Veale, C. A., et al. (1988). Lipoxins A4 and B4: Comparison of Icosanoids Having Bronchoconstrictor and Vasodilator Actions but Lacking Platelet Aggregatory Activity. *Proc. Natl. Acad. Sci. U S A.* 85 (21), 8340–8344. doi:10.1073/pnas.85.21.8340

Leuti, A., Fava, M., Pellegrini, N., and Maccarrone, M. (2021). Role of Specialized Pro-resolving Mediators in Neuropathic Pain. *Front. Pharmacol.* 12, 717993. doi:10.3389/fphar.2021.717993

Li, Q., Tian, Y., Wang, Z. F., Liu, S. B., Mi, W. L., Ma, H. J., et al. (2013). Involvement of the Spinal NALP1 Inflammasome in Neuropathic Pain and Aspirin-Triggered-15-Epi-Lipoxin A4 Induced Analgesia. *Neuroscience* 254, 230–240. doi:10.1016/j.neuroscience.2013.09.028

Li, Q. Q., Ding, D. H., Wang, X. Y., Sun, Y. Y., and Wu, J. (2021). Lipoxin A4 Regulates Microglial M1/M2 Polarization after Cerebral Ischemia-Reperfusion Injury via the Notch Signaling Pathway. *Exp. Neurol.* 339, 113645. doi:10.1016/j.expneurol.2021.113645

Linnerbauer, M., Wheeler, M. A., and Quintana, F. J. (2020). Astrocyte Crosstalk in CNS Inflammation. *Neuron* 108, 608–622. doi:10.1016/j.neuron.2020.08.012

Liu, G. J., Tao, T., Wang, H., Zhou, Y., Gao, X., Gao, Y. Y., et al. (2020). Functions of Resolvin D1-Alx/fpr2 Receptor Interaction in the Hemoglobin-Induced Microglial Inflammatory Response and Neuronal Injury. *J. Neuroinflammation* 17 (1), 239. doi:10.1186/s12974-020-01918-x

Liu, J., Peng, L., and Li, J. (2020). The Lipoxin A4 Receptor Agonist BML-111 Alleviates Inflammatory Injury and Oxidative Stress in Spinal Cord Injury. *Med. Sci. Monit.* 26, e919883. doi:10.12659/MSM.919883

Liu, L., Zhang, P., Zhang, Z., Hu, Q., He, J., Liu, H., et al. (2019). LXA4 Ameliorates Cerebrovascular Endothelial Dysfunction by Reducing Acute Inflammation after Subarachnoid Hemorrhage in Rats. *Neuroscience* 408, 105–114. doi:10.1016/j.neuroscience.2019.03.038

Liu, Z. Q., Zhang, H. B., Wang, J., Xia, L. J., and Zhang, W. (2015). Lipoxin A4 Ameliorates Ischemia/reperfusion Induced Spinal Cord Injury in Rabbit Model. *Int. J. Clin. Exp. Med.* 8 (8), 12826–12833.

Livne-Bar, I., Wei, J., Liu, H. H., Alqawlaq, S., Won, G. J., Tuccitto, A., et al. (2017). Astrocyte-derived Lipoxins A4 and B4 Promote Neuroprotection from Acute and Chronic Injury. *J. Clin. Invest.* 127 (12), 4403–4414. doi:10.1172/JCI77398

Lu, T., Wu, X., Wei, N., Liu, X., Zhou, Y., Shang, C., et al. (2018). Lipoxin A4 Protects against Spinal Cord Injury via Regulating Akt/nuclear Factor (Erythroid-derived 2)-like 2/heme Oxygenase-1 Signaling. *Biomed. Pharmacother.* 97, 905–910. doi:10.1016/j.biopha.2017.10.092

Lu, Z., Zhang, H., Zhang, X., Gao, Y., and Yin, Z. Q. (2019). Lipoxin A4 Delays the Progression of Retinal Degeneration via the Inhibition of Microglial Overactivation. *Biochem. Biophys. Res. Commun.* 516 (3), 900–906. doi:10.1016/j.bbrc.2019.06.137

Lucke-Wold, B. P., Logsdon, A. F., Manoranjan, B., Turner, R. C., McConnell, E., Vates, G. E., et al. (2016). Aneurysmal Subarachnoid Hemorrhage and Neuroinflammation: A Comprehensive Review. *Int. J. Mol. Sci.* 17 (4), 497. doi:10.3390/ijms17040497

Luo, C. L., Li, Q. Q., Chen, X. P., Zhang, X. M., Li, L. L., Li, B. X., et al. (2013). Lipoxin A4 Attenuates Brain Damage and Downregulates the Production of Pro-inflammatory Cytokines and Phosphorylated Mitogen-Activated Protein Kinases in a Mouse Model of Traumatic Brain Injury. *Brain Res.* 1502, 1–10. doi:10.1016/j.brainres.2013.01.037

Machado, F. S., Johndrow, J. E., Esper, L., Dias, A., Bafica, A., Serhan, C. N., et al. (2006). Anti-inflammatory Actions of Lipoxin A4 and Aspirin-Triggered Lipoxin Are SOCS-2 Dependent. *Nat. Med.* 12 (3), 330–334. doi:10.1038/nm1355

Maddox, J. F., and Serhan, C. N. (1996). Lipoxin A4 and B4 Are Potent Stimuli for Human Monocyte Migration and Adhesion: Selective Inactivation by Dehydrogenation and Reduction. *J. Exp. Med.* 183 (1), 137–146. doi:10.1084/jem.183.1.137

Maderna, P., and Godson, C. (2009). Lipoxins: Resolutionary Road. *Br. J. Pharmacol.* 158 (4), 947–959. doi:10.1111/j.1476-5381.2009.00386.x

Mai, J., Liu, W., Fang, Y., Zhang, S., Qiu, Q., Yang, Y., et al. (2018). The Atheroprotective Role of Lipoxin A4 Prevents oxLDL-Induced Apoptotic Signaling in Macrophages via JNK Pathway. *Atherosclerosis* 278, 259–268. doi:10.1016/j.atherosclerosis.2018.09.025

Marchand, F., Perretti, M., and McMahon, S. B. (2005). Role of the Immune System in Chronic Pain. *Nat. Rev. Neurosci.* 6 (7), 521–532. doi:10.1038/nrn1700

Marcheselli, V. L., Hong, S., Lukiw, W. J., Tian, X. H., Gronert, K., Musto, A., et al. (2003). Novel Docosanoids Inhibit Brain Ischemia-Reperfusion-Mediated Leukocyte Infiltration and Pro-inflammatory Gene Expression. *J. Biol. Chem.* 278 (44), 43807–43817. doi:10.1074/jbc.M305841200

Martini, A. C., Berta, T., Forner, S., Chen, G., Bento, A. F., Ji, R. R., et al. (2016). Lipoxin A4 Inhibits Microglial Activation and Reduces Neuroinflammation and Neuropathic Pain after Spinal Cord Hemisection. *J. Neuroinflammation* 13 (1), 75. doi:10.1186/s12974-016-0540-8

McGeer, P. L., Schulzer, M., and McGeer, E. G. (1996). Arthritis and Anti-inflammatory Agents as Possible Protective Factors for Alzheimer's Disease: a Review of 17 Epidemiologic Studies. *Neurology* 47 (2), 425–432. doi:10.1212/wnl.47.2.425

Medeiros, R., Kitazawa, M., Passos, G. F., Baglietto-Vargas, D., Cheng, D., Cribbs, D. H., et al. (2013). Aspirin-triggered Lipoxin A4 Stimulates Alternative Activation of Microglia and Reduces Alzheimer Disease-like Pathology in Mice. *Am. J. Pathol.* 182 (5), 1780–1789. doi:10.1016/j.ajpath.2013.01.051

Mészáros, Á., Molnár, K., Nógrádi, B., Hernádi, Z., Nyúl-Tóth, Á., Wilhelm, I., et al. (2020). Neurovascular Inflammaging in Health and Disease. *Cells* 9, 1614. doi:10.3390/cells9071614

Miao, G. S., Liu, Z. H., Wei, S. X., Luo, J. G., Fu, Z. J., and Sun, T. (2015). Lipoxin A4 Attenuates Radicular Pain Possibly by Inhibiting Spinal ERK, JNK and NF-κB/p65 and Cytokine Signals, but Not P38, in a Rat Model of Non-compressive Lumbar Disc Herniation. *Neuroscience* 300, 10–18. doi:10.1016/j.neuroscience.2015.04.060

Mizuma, A., and Yenari, M. A. (2017). Anti-Inflammatory Targets for the Treatment of Reperfusion Injury in Stroke. *Front. Neurol.* 8, 467. doi:10.3389/fneur.2017.00467

Moretti, L., Cristofori, I., Weaver, S. M., Chau, A., Portelli, J. N., and Grafman, J. (2012). Cognitive Decline in Older Adults with a History of Traumatic Brain Injury. *Lancet Neurol.* 11 (12), 1103–1112. doi:10.1016/S1474-4422(12)70226-0

Norel, X., and Brink, C. (2004). The Quest for New Cysteinyl-Leukotriene and Lipoxin Receptors: Recent Clues. *Pharmacol. Ther.* 103 (1), 81–94. doi:10.1016/j.pharmthera.2004.05.003

Pamplona, F. A., Ferreira, J., Menezes de Lima, O., Jr, Duarte, F. S., Bento, A. F., Forner, S., et al. (2012). Anti-inflammatory Lipoxin A4 Is an Endogenous Allosteric Enhancer of CB1 Cannabinoid Receptor. *Proc. Natl. Acad. Sci. U S A.* 109 (51), 21134–21139. doi:10.1073/pnas.1202906109

Peritore, A. F., Crupi, R., Scuto, M., Gugliandolo, E., Siracusa, R., Impellizzeri, D., et al. (2020). The Role of Annexin A1 and Formyl Peptide Receptor 2/3 Signaling in Chronic Corticosterone-Induced Depression-like Behaviors and Impairment in Hippocampal-dependent Memory. *CNS Neurol. Disord. Drug Targets* 19 (1), 27–43. doi:10.2174/1871527319666200107094732

Petri, M. H., Laguna-Fernandez, A., Arnardottir, H., Wheelock, C. E., Perretti, M., Hansson, G. K., et al. (2017). Aspirin-triggered Lipoxin A4 Inhibits

Atherosclerosis Progression in Apolipoprotein E-/- Mice. *Br. J. Pharmacol.* 174 (22), 4043–4054. doi:10.1111/bph.13707

Prieto, P., Cuenca, J., Través, P. G., Fernández-Velasco, M., Martín-Sanz, P., and Boscá, L. (2010). Lipoxin A4 Impairment of Apoptotic Signaling in Macrophages: Implication of the PI3K/Akt and the ERK/Nrf-2 Defense Pathways. *Cell Death Differ* 17, 1179–1188. doi:10.1038/cdd.2009.220

Prieto, P., Rosales-Mendoza, C. E., Terrón, V., Toledano, V., Cuadrado, A., López-Collazo, E., et al. (2015). Activation of Autophagy in Macrophages by Pro-resolving Lipid Mediators. *Autophagy* 11 (10), 1729–1744. doi:10.1080/15548627.2015.1078958

Rajkovic, O., Potjewyd, G., and Pinteaux, E. (2018). Regenerative Medicine Therapies for Targeting Neuroinflammation after Stroke. *Front. Neurol.* 9, 734. doi:10.3389/fneur.2018.00734

Ransohoff, R. M. (2016). How Neuroinflammation Contributes to Neurodegeneration. *Science* 353, 777–783. doi:10.1126/science.aag2590

Romano, M., Maddox, J. F., and Serhan, C. N. (1996). Activation of Human Monocytes and the Acute Monocytic Leukemia Cell Line (THP-1) by Lipoxins Involves Unique Signaling Pathways for Lipoxin A4 versus Lipoxin B4: Evidence for Differential Ca2+ Mobilization. *J. Immunol.* 157 (5), 2149–2154.

Sandsmark, D. K., Elliott, J. E., and Lim, M. M. (2017). Sleep-Wake Disturbances after Traumatic Brain Injury: Synthesis of Human and Animal Studies. *Sleep* 40, 40. doi:10.1093/sleep/zsx044

Schaldach, C. M., Riby, J., and Bjeldanes, L. F. (1999). Lipoxin A4: a New Class of Ligand for the Ah Receptor. *Biochemistry* 38 (23), 7594–7600. doi:10.1021/bi982861e

Serhan, C. N., Fiore, S., and Levy, B. D. (1994). Cell-cell Interactions in Lipoxin Generation and Characterization of Lipoxin A4 Receptors. *Ann. N. Y Acad. Sci.* 744, 166–180. doi:10.1111/j.1749-6632.1994.tb52734.x

Serhan, C. N., Hamberg, M., and Samuelsson, B. (1984). Lipoxins: Novel Series of Biologically Active Compounds Formed from Arachidonic Acid in Human Leukocytes. *Proc. Natl. Acad. Sci. U S A.* 81 (17), 5335–5339. doi:10.1073/pnas.81.17.5335

Serhan, C. N. (2014). Pro-resolving Lipid Mediators Are Leads for Resolution Physiology. *Nature* 510, 92–101. doi:10.1038/nature13479

Serhan, C. N., and Sheppard, K. A. (1990). Lipoxin Formation during Human Neutrophil-Platelet Interactions. Evidence for the Transformation of Leukotriene A4 by Platelet 12-lipoxygenase *In Vitro*. *J. Clin. Invest.* 85 (3), 772–780. doi:10.1172/JCI114503

Shearer, G. C., and Walker, R. E. (2018). An Overview of the Biologic Effects of omega-6 Oxylipins in Humans. *Prostaglandins Leukot. Essent. Fatty Acids* 137, 26–38. doi:10.1016/j.plefa.2018.06.005

Shryock, N., McBerry, C., Salazar Gonzalez, R. M., Janes, S., Costa, F. T., and Aliberti, J. (2013). Lipoxin A_4 and 15-Epi-Lipoxin A_4 Protect against Experimental Cerebral Malaria by Inhibiting IL-12/IFN-γ in the Brain. *PLoS One* 8 (4), e61882. doi:10.1371/journal.pone.0061882

Smith, H. K., Gil, C. D., Oliani, S. M., and Gavins, F. N. (2015). Targeting Formyl Peptide Receptor 2 Reduces Leukocyte-Endothelial Interactions in a Murine Model of Stroke. *FASEB J.* 29 (5), 2161–2171. doi:10.1096/fj.14-263160

Sobrado, M., Pereira, M. P., Ballesteros, I., Hurtado, O., Fernández-López, D., Pradillo, J. M., et al. (2009). Synthesis of Lipoxin A4 by 5-lipoxygenase Mediates PPARgamma-dependent, Neuroprotective Effects of Rosiglitazone in Experimental Stroke. *J. Neurosci.* 29 (12), 3875–3884. doi:10.1523/JNEUROSCI.5529-08.2009

Song, Y., Yang, Y., Cui, Y., Gao, J., Wang, K., and Cui, J. (2019). Lipoxin A4 Methyl Ester Reduces Early Brain Injury by Inhibition of the Nuclear Factor Kappa B (NF-κb)-dependent Matrix Metallopeptidase 9 (MMP-9) Pathway in a Rat Model of Intracerebral Hemorrhage. *Med. Sci. Monit.* 25, 1838–1847. doi:10.12659/MSM.915119

Souza, M. C., Pádua, T. A., Torres, N. D., Souza Costa, M. F., Candéa, A. P., Maramaldo, T., et al. (2015). Lipoxin A4 Attenuates Endothelial Dysfunction during Experimental Cerebral Malaria. *Int. Immunopharmacol* 24 (2), 400–407. doi:10.1016/j.intimp.2014.12.033

Sun, T., Yu, E., Yu, L., Luo, J., Li, H., and Fu, Z. (2012). LipoxinA(4) Induced Antinociception and Decreased Expression of NF-Kb and Pro-inflammatory Cytokines after Chronic Dorsal Root Ganglia Compression in Rats. *Eur. J. Pain* 16 (1), 18–27. doi:10.1016/j.ejpain.2011.05.005

Svensson, C. I., Zattoni, M., and Serhan, C. N. (2007). Lipoxins and Aspirin-Triggered Lipoxin Inhibit Inflammatory Pain Processing. *J. Exp. Med.* 204 (2), 245–252. doi:10.1084/jem.20061826

Szczuko, M., Kotlęga, D., Palma, J., Zembroń-Łacny, A., Tylutka, A., Gołąb-Janowska, M., et al. (2020). Lipoxins, RevD1 and 9, 13 HODE as the Most Important Derivatives after an Early Incident of Ischemic Stroke. *Sci. Rep.* 10 (1), 12849. doi:10.1038/s41598-020-69831-0

Taetzsch, T., Levesque, S., McGraw, C., Brookins, S., Luqa, R., Bonini, M. G., et al. (2015). Redox Regulation of NF-Kb P50 and M1 Polarization in Microglia. *Glia* 63, 423–440. doi:10.1002/glia.22762

Takano, T., Clish, C. B., Gronert, K., Petasis, N., and Serhan, C. N. (1998). Neutrophil-mediated Changes in Vascular Permeability Are Inhibited by Topical Application of Aspirin-Triggered 15-Epi-Lipoxin A4 and Novel Lipoxin B4 Stable Analogues. *J. Clin. Invest.* 101 (4), 819–826. doi:10.1172/JCI1578

Tanga, F. Y., Nutile-McMenemy, N., and DeLeo, J. A. (2005). The CNS Role of Toll-like Receptor 4 in Innate Neuroimmunity and Painful Neuropathy. *Proc. Natl. Acad. Sci. U S A.* 102 (16), 5856–5861. doi:10.1073/pnas.0501634102

Tian, Y., Liu, M., Mao-Ying, Q. L., Liu, H., Wang, Z. F., Zhang, M. T., et al. (2015). Early Single Aspirin-Triggered Lipoxin Blocked Morphine Anti-nociception Tolerance through Inhibiting NALP1 Inflammasome: Involvement of PI3k/Akt Signaling Pathway. *Brain Behav. Immun.* 50, 63–77. doi:10.1016/j.bbi.2015.06.016

Tiffany, H. L., Lavigne, M. C., Cui, Y. H., Wang, J. M., Leto, T. L., Gao, J. L., et al. (2001). Amyloid-beta Induces Chemotaxis and Oxidant Stress by Acting at Formylpeptide Receptor 2, a G Protein-Coupled Receptor Expressed in Phagocytes and Brain. *J. Biol. Chem.* 276 (26), 23645–23652. doi:10.1074/jbc.M101031200

Tobin, D. M., Roca, F. J., Oh, S. F., McFarland, R., Vickery, T. W., Ray, J. P., et al. (2012). Host Genotype-specific Therapies Can Optimize the Inflammatory Response to Mycobacterial Infections. *Cell.* 148 (3), 434–446. doi:10.1016/j.cell.2011.12.023

Trovato, A., Siracusa, R., Di Paola, R., Scuto, M., Fronte, V., Koverech, G., et al. (2016). Redox Modulation of Cellular Stress Response and Lipoxin A4 Expression by Coriolus Versicolor in Rat Brain: Relevance to Alzheimer's Disease Pathogenesis. *Neurotoxicology* 53, 350–358. doi:10.1016/j.neuro.2015.09.012

Tylek, K., Trojan, E., Regulska, M., Lacivita, E., Leopoldo, M., and Basta-Kaim, A. (2021). Formyl Peptide Receptor 2, as an Important Target for Ligands Triggering the Inflammatory Response Regulation: a Link to Brain Pathology. *Pharmacol. Rep.* 73, 1004–1019. doi:10.1007/s43440-021-00271-x

Vasconcelos, D. P., Costa, M., Amaral, I. F., Barbosa, M. A., Águas, A. P., and Barbosa, J. N. (2015). Modulation of the Inflammatory Response to Chitosan through M2 Macrophage Polarization Using Pro-resolution Mediators. *Biomaterials* 37, 116–123. doi:10.1016/j.biomaterials.2014.10.035

Vital, S. A., Becker, F., Holloway, P. M., Russell, J., Perretti, M., Granger, D. N., et al. (2016). Formyl-Peptide Receptor 2/3/Lipoxin A4 Receptor Regulates Neutrophil-Platelet Aggregation and Attenuates Cerebral Inflammation: Impact for Therapy in Cardiovascular Disease. *Circulation* 133 (22), 2169–2179. doi:10.1161/CIRCULATIONAHA.115.020633

Wada, K., Arita, M., Nakajima, A., Katayama, K., Kudo, C., Kamisaki, Y., et al. (2006). Leukotriene B4 and Lipoxin A4 Are Regulatory Signals for Neural Stem Cell Proliferation and Differentiation. *FASEB J.* 20 (11), 1785–1792. doi:10.1096/fj.06-5809com

Wang, G., Zhang, L., Chen, X., Xue, X., Guo, Q., Liu, M., et al. (2016). Formylpeptide Receptors Promote the Migration and Differentiation of Rat Neural Stem Cells. *Sci. Rep.* 6, 25946. doi:10.1038/srep25946

Wang, X., Miao, Z., Xu, X., Schultzberg, M., and Zhao, Y. (2021). Reduced Levels of Plasma Lipoxin A4 Are Associated with Post-Stroke Cognitive Impairment. *J. Alzheimers Dis.* 79 (2), 607–613. doi:10.3233/JAD-201050

Wang, X., Zhu, M., Hjorth, E., Cortés-Toro, V., Eyjolfsdottir, H., Graff, C., et al. (2015). Resolution of Inflammation Is Altered in Alzheimer's Disease. *Alzheimers Dement* 11 (1), 40–42. doi:10.1016/j.jalz.2013.12.024

Wang, Y. P., Wu, Y., Li, L. Y., Zheng, J., Liu, R. G., Zhou, J. P., et al. (2011). Aspirin-triggered Lipoxin A4 Attenuates LPS-Induced Pro-inflammatory Responses by

Inhibiting Activation of NF-Kb and MAPKs in BV-2 Microglial Cells. *J. Neuroinflammation* 8, 95. doi:10.1186/1742-2094-8-95

Wang, Z. F., Li, Q., Liu, S. B., Mi, W. L., Hu, S., Zhao, J., et al. (2014). Aspirin-triggered Lipoxin A4 Attenuates Mechanical Allodynia in Association with Inhibiting Spinal JAK2/STAT3 Signaling in Neuropathic Pain in Rats. *Neuroscience* 273, 65–78. doi:10.1016/j.neuroscience.2014.04.052

Wilson, L., Stewart, W., Dams-O'Connor, K., Diaz-Arrastia, R., Horton, L., Menon, D. K., et al. (2017). The Chronic and Evolving Neurological Consequences of Traumatic Brain Injury. *Lancet Neurol.* 16 (10), 813–825. doi:10.1016/S1474-4422(17)30279-X

Wu, H. S., Guo, P. P., Jin, Z., Li, X. Y., Yang, X., Ke, J. J., et al. (2018). Effects of Lipoxin A4 Pretreatment on Cognitive Function of Aged Rats after Global Cerebral Ischemia Reperfusion. *Curr. Med. Sci.* 38 (4), 666–671. doi:10.1007/s11596-018-1928-8

Wu, J., Ding, D., Wang, X., Li, Q., Sun, Y., Li, L., et al. (2019a). Regulation of Aquaporin 4 Expression by Lipoxin A4 in Astrocytes Stimulated by Lipopolysaccharide. *Cell Immunol* 344, 103959. doi:10.1016/j.cellimm.2019.103959

Wu, J., Ding, D. H., Li, Q. Q., Wang, X. Y., Sun, Y. Y., and Li, L. J. (2019b). Lipoxin A4 Regulates Lipopolysaccharide-Induced BV2 Microglial Activation and Differentiation via the Notch Signaling Pathway. *Front Cel Neurosci* 13, 19. doi:10.3389/fncel.2019.00019

Wu, J., Wang, A., Min, Z., Xiong, Y., Yan, Q., Zhang, J., et al. (2011). Lipoxin A4 Inhibits the Production of Proinflammatory Cytokines Induced by β-amyloid *In Vitro* and *In Vivo*. *Biochem. Biophys. Res. Commun.* 408, 382–387. doi:10.1016/j.bbrc.2011.04.013

Wu, L., Li, H. H., Wu, Q., Miao, S., Liu, Z. J., Wu, P., et al. (2015). Lipoxin A4 Activates Nrf2 Pathway and Ameliorates Cell Damage in Cultured Cortical Astrocytes Exposed to Oxygen-Glucose Deprivation/Reperfusion Insults. *J. Mol. Neurosci.* 56 (4), 848–857. doi:10.1007/s12031-015-0525-6

Wu, L., Liu, Z. J., Miao, S., Zou, L. B., Cai, L., Wu, P., et al. (2013). Lipoxin A4 Ameliorates Cerebral Ischaemia/reperfusion Injury through Upregulation of Nuclear Factor Erythroid 2-related Factor 2. *Neurol. Res.* 35 (9), 968–975. doi:10.1179/1743132813Y.0000000242

Wu, L., Miao, S., Zou, L. B., Wu, P., Hao, H., Tang, K., et al. (2012a). Lipoxin A4 Inhibits 5-lipoxygenase Translocation and Leukotrienes Biosynthesis to Exert a Neuroprotective Effect in Cerebral Ischemia/reperfusion Injury. *J. Mol. Neurosci.* 48 (1), 185–200. doi:10.1007/s12031-012-9807-4

Wu, Y., Wang, Y. P., Guo, P., Ye, X. H., Wang, J., Yuan, S. Y., et al. (2012b). A Lipoxin A4 Analog Ameliorates Blood-Brain Barrier Dysfunction and Reduces MMP-9 Expression in a Rat Model of Focal Cerebral Ischemia-Reperfusion Injury. *J. Mol. Neurosci.* 46 (3), 483–491. doi:10.1007/s12031-011-9620-5

Wu, Y., Zhai, H., Wang, Y., Li, L., Wu, J., Wang, F., et al. (2012c). Aspirin-triggered Lipoxin A_4 Attenuates Lipopolysaccharide-Induced Intracellular ROS in BV2 Microglia Cells by Inhibiting the Function of NADPH Oxidase. *Neurochem. Res.* 37 (8), 1690–1696. doi:10.1007/s11064-012-0776-3

Wu, Y., Ye, X. H., Guo, P. P., Xu, S. P., Wang, J., Yuan, S. Y., et al. (2010). Neuroprotective Effect of Lipoxin A4 Methyl Ester in a Rat Model of Permanent Focal Cerebral Ischemia. *J. Mol. Neurosci.* 42 (2), 226–234. doi:10.1007/s12031-010-9355-8

Xue, M., and Yong, V. W. (2020). Neuroinflammation in Intracerebral Haemorrhage: Immunotherapies with Potential for Translation. *Lancet Neurol.* 19 (12), 1023–1032. doi:10.1016/S1474-4422(20)30364-1

Yao, C., Yang, D., Wan, Z., Wang, Z., Liu, R., Wu, Y., et al. (2014). Aspirin-triggered Lipoxin A4 Attenuates Lipopolysaccharide Induced Inflammatory Response in Primary Astrocytes. *Int. Immunopharmacol* 18 (1), 85–89. doi:10.1016/j.intimp.2013.10.028

Ye, R. D., Boulay, F., Wang, J. M., Dahlgren, C., Gerard, C., Parmentier, M., et al. (2009). International Union of Basic and Clinical Pharmacology. LXXIII. Nomenclature for the Formyl Peptide Receptor (FPR) Family. *Pharmacol. Rev.* 61, 119–161. doi:10.1124/pr.109.001578

Ye, X. H., Wu, Y., Guo, P. P., Wang, J., Yuan, S. Y., Shang, Y., et al. (2010). Lipoxin A4 Analogue Protects Brain and Reduces Inflammation in a Rat Model of Focal Cerebral Ischemia Reperfusion. *Brain Res.* 1323, 174–183. doi:10.1016/j.brainres.2010.01.079

Zhu, J. J., Yu, B. Y., Fu, C. C., He, M. Z., Zhu, J. H., Chen, B. W., et al. (2020). LXA4 Protects against Hypoxic-Ischemic Damage in Neonatal Rats by Reducing the Inflammatory Response via the IκB/NF-Kb Pathway. *Int. Immunopharmacol* 89 (Pt B), 107095. doi:10.1016/j.intimp.2020.107095

Zhu, M., Wang, X., Hjorth, E., Colas, R. A., Schroeder, L., Granholm, A. C., et al. (2016). Pro-Resolving Lipid Mediators Improve Neuronal Survival and Increase Aβ42 Phagocytosis. *Mol. Neurobiol.* 53 (4), 2733–2749. doi:10.1007/s12035-015-9544-0

Zhu, M., Wang, X., Schultzberg, M., and Hjorth, E. (2015). Differential Regulation of Resolution in Inflammation Induced by Amyloid-B42 and Lipopolysaccharides in Human Microglia. *J. Alzheimers Dis.* 43 (4), 1237–1250. doi:10.3233/JAD-141233

Conflict of Interest: The authors declare that the research was conducted in the absence of any commercial or financial relationships that could be construed as a potential conflict of interest.

Publisher's Note: All claims expressed in this article are solely those of the authors and do not necessarily represent those of their affiliated organizations, or those of the publisher, the editors and the reviewers. Any product that may be evaluated in this article, or claim that may be made by its manufacturer, is not guaranteed or endorsed by the publisher.

GLOSSARY

AA arachidonic acid
AD Alzheimer's disease
Akt protein kinase B
ATL aspirin-triggered lipoxins
$ATLA_4$ aspirin-triggered lipoxin A_4
$ATLB_4$ aspirin-triggered lipoxin B_4
Aβ amyloid β
BBB blood-brain barrier
CCH chronic cerebral hypoperfusion
CNS central nervous system
COX-2 cyclooxygenase-2
CSF cerebrospinal fluid
DAM disease-associated microglia
ERK extracellular signal-regulated kinase
FPR2 formyl peptide receptor 2
GPR G protein-coupled receptor
HI hypoxia-ischemia
HO-1 heme oxygenase-1
IAs intracranial aneurysms
ICAM-1 intercellular cell adhesion molecule-1
ICC immunocytochemistry
ICH intracerebral hemorrhage
IL interleukin
JAK2 Janus kinase 2
LOX lipoxygenase
LPS lipopolysaccharide
LT leukotriene
LXA_4 ME LXA_4 methyl ester
LXs lipoxins
MAP1LC3 microtubule-associated protein 1 light chain 3
MAPK mitogen-activated protein kinase
MMP-9 matrix metallopeptidase 9
MS multiple sclerosis
NADPH abrogate nicotinamide adenine dinucleotide phosphate
NF-κB nuclear factor kappa B
Nrf2 erythroid 2-related factor 2
NSAIDs non-steroid anti-inflammatory drugs
NSCs neural stem cells
PGE2 prostaglandin E2
PGs prostaglandins
PI3k phosphoinositide-3-kinase
PPARγ peroxisome proliferator-activated receptors gamma
PSCI post-stroke cognitive impairment
p-tau phosphorylated-tau protein
ROS reactive oxygen species
RT-PCR reverse transcription-polymerase chain reaction
SAH subarachnoid hemorrhage
SCI spinal cord injury
SPMs specialized pro-resolving mediators
STAT3 signal transducer and activator of transcription 3
TBI traumatic brain injury
TNF tumor necrosis factor
TXs thromboxanes

frontiers in Pharmacology

ORIGINAL RESEARCH
published: 03 February 2022
doi: 10.3389/fphar.2022.822499

Alzheimer's Disease Enhanced Tonic Inhibition is Correlated With Upregulated Astrocyte GABA Transporter-3/4 in a Knock-In *APP* Mouse Model

Yousif Aldabbagh[1†], *Anam Islam*[1†], *Weicong Zhang*[1], *Paul Whiting*[2] *and Afia B. Ali*[1*]

[1]*UCL School of Pharmacy, London, United Kingdom,* [2]*Alzheimer's Research UK Drug Discovery Institute, Queen Square Institute of Neurology, London, United Kingdom*

OPEN ACCESS

Edited by:
Nesrine Salah El Dine El Sayed, Cairo University, Egypt

Reviewed by:
Walaa Wadie, Cairo University, Egypt
Marta Valenza, Sapienza University of Rome, Italy

***Correspondence:**
Afia B. Ali
afia.b.ali@ucl.ac.uk

[†]*These authors have contributed equally to this work*

Specialty section:
This article was submitted to Neuropharmacology, a section of the journal Frontiers in Pharmacology

Received: *25 November 2021*
Accepted: *12 January 2022*
Published: *03 February 2022*

Citation:
Aldabbagh Y, Islam A, Zhang W, Whiting P and Ali AB (2022) Alzheimer's Disease Enhanced Tonic Inhibition is Correlated With Upregulated Astrocyte GABA Transporter-3/4 in a Knock-In APP *Mouse Model. Front. Pharmacol. 13:822499. doi: 10.3389/fphar.2022.822499*

Cognitive decline is a major symptom in Alzheimer's disease (AD), which is strongly associated with synaptic excitatory-inhibitory imbalance. Here, we investigated whether astrocyte-specific GABA transporter 3/4 (GAT3/4) is altered in *APP* knock-in mouse model of AD and whether this is correlated with changes in principal cell excitability. Using the $APP^{NL\text{-}F/NL\text{-}F}$ knock-in mouse model of AD, aged-matched to wild-type mice, we performed *in vitro* electrophysiological whole-cell recordings combined with immunohistochemistry in the CA1 and dentate gyrus (DG) regions of the hippocampus. We observed a higher expression of GAD67, an enzyme that catalyses GABA production, and GAT3/4 in reactive astrocytes labelled with GFAP, which correlated with an enhanced tonic inhibition in the CA1 and DG of 12–16 month-old $APP^{NL\text{-}F/NL\text{-}F}$ mice compared to the age-matched wild-type animals. Comparative neuroanatomy experiments performed using post-mortem brain tissue from human AD patients, age-matched to healthy controls, mirrored the results obtained using mice tissue. Blocking GAT3/4 associated tonic inhibition recorded in CA1 and DG principal cells resulted in an increased membrane input resistance, enhanced firing frequency and synaptic excitation in both wild-type and $APP^{NL\text{-}F/NL\text{-}F}$ mice. These effects exacerbated synaptic hyperactivity reported previously in the $APP^{NL\text{-}F/NL\text{-}F}$ mice model. Our data suggest that an alteration in astrocyte GABA homeostasis is correlated with increased tonic inhibition in the hippocampus, which probably plays an important compensatory role in restoring AD-associated synaptic hyperactivity. Therefore, reducing tonic inhibition through GAT3/4 may not be a good therapeutic strategy for AD

Keywords: alzheheimer's disease, hippocampus, GABA, excitation, astrocytes, amyloid-β, dentate gyrus

Abbreviations: Aβ, amyloid-β; AD, Alzheimer's disease; App, β-amyloid precursor protein; CA1, Cornu Ammonis; GABA, γ-aminobutyric acid; GAD67, glutamate decarboxylase 67; GAT3/4, GABA Transporter-3/4; GFAP, glial fibrillary acidic protein; sEPSPs, spontaneous excitatory postsynaptic potentials; sIPSPs, spontaneous inhibitory postsynaptic potentials.

1 INTRODUCTION

Alzheimer's disease (AD) is the most prevalent cause of dementia in the elderly, affecting 6–8% of the world's population over 65 years old (WHO, 2017). AD is a progressive disorder that leads to cognitive deficits which severely reduce quality of life (Burns and Iliffe, 2009), and is described macroscopically by loss of brain volume and shrinkage of cortical gyri, with the entorhinal cortex and hippocampus being heavily affected (Stelzma et al., 1995).

The major pathological hallmarks of AD are neuroinflammation, presence of severe neuropathological lesions, including amyloid-β (Aβ) plaques, synaptic loss, and neuronal death. One of the key cell types that modulate the neuroinflammatory response in AD are astrocytes, the most abundant glial cells in the brain, supported by glial fibrillary acidic protein (GFAP). Aβ plaques have been shown to localise and trigger the activation of astrocytes (Akiyama, 2000) and it is well established that prolonged neuroinflammation maintained by reactive astrocytes can have catastrophic effects on the neuronal environment and potentiate neurodegeneration in AD (Medeiros and LaFerla, 2013). Recent studies have shown that Aβ-induced dysfunction of astrocytes networks can lead to dysregulated neuronal networks and a positive feedback loop with Aβ formation and deposition; with similar effects not seen in the non-pathological ageing brain (Gómez-Gonzalo et al., 2017; Lines et al., 2022)

Astrocytes also play a key role in the 'tripartite' synapse where the perisynaptic astrocytic processes envelop the pre- and postsynaptic elements of neurons; consequently, maintaining neuronal homeostasis by the uptake of excess neurotransmitters or release of gliotransmitters such as ?-aminobutyric acid (GABA), thus modulating synaptic signalling (Parpura et al., 1994; Delekate et al., 2014; Jo et al., 2014; Ishibashi et al., 2019; Patel et al., 2019). For example, under "normal" physiological conditions, astrocytes uptake excessive neuronally released glutamate from the synapse through Na^+-coupled excitatory amino acid transporters (EAAT1/EAAT2) (Lehre and Danbolt, 1998; Kojima et al., 1999), and GABA through astrocyte-specific GABA transporters, GAT3/4 (Liu et al., 1993), abundantly found on astrocytic processes (Ribak et al., 1996; Conti et al., 2004), which are thought to be crucial for setting the level of background tonic inhibition. However, these mechanisms seem to alter during pathological conditions, which can lead to reversal of such transporters and extrusion of GABA into the synaptic space, ultimately impacting the fine-tuning of inhibitory synapses (Conti et al., 2004; Héja et al., 2012). Interestingly, following subcortical stroke an enhanced tonic inhibition, via astrocytes was shown to induce neuronal glucose hypometabolism, impairing functional recovery and neuronal activity (Nam et al., 2020). Similarly, evidence suggests that elevated levels of tonic inhibition in the dentate gyrus (DG), impaired synaptic plasticity as well as memory function via GAT3/4 in a 5xFAD mouse model (Wu et al., 2014). These findings have huge relevance in understanding the role of astrocytes in maintaining synaptic homeostasis in altered physiological states such as AD-associated synaptic hyperexcitability, a phenotype that spans from human studies to animals, and iPSC cell models (Hazra et al., 2013; Busche and Konnerth, 2016; Ghatak et al., 2019; Petrache et al., 2019). AD-associated hyperexcitability is thought to spread the disease pathology between brain subregions (Khan et al., 2014; Petrache et al., 2019). The process by which this develops remains to be fully answered, with one hypothesis referring to the selective aberrant behaviour of inhibitory neurotransmitter GABA-containing interneurons (Rice et al., 2020; Shi et al., 2020; Xu et al., 2020; Reid et al., 2021), despite an elevated background inhibition observed in AD by others (Jo et al., 2014; Wu et al., 2014). Surprisingly, the levels of astrocyte glutamate decarboxylase 67 (GAD67), an enzyme that converts glutamate to GABA, is shown to be elevated in astrocytes in AD patients and mouse models of AD (Wu et al., 2014). This suggests an altered role of astrocytes in GABA homeostasis via GAT3/4, which is thought to be related to the modified inhibitory tone of local neuronal circuits (Lee et al., 2011). Therefore, in this study, we investigated whether elevated GAD67 and GAT3/4 levels are associated with a higher background inhibitory tone and whether this correlated with intrinsic and synaptic excitability of hippocampal principal cells in a knock-in mouse model of AD.

2 MATERIALS AND METHODS

2.1 Mouse Animal Procedures

All the procedures in this study were carried out in accordance with the British Home Office regulations under the Animal Scientific Procedure Act 1986, under the project licence PPL: P1ADA633A held by the principal investigator, Dr Afia Ali. All procedures were approved by both internal and external UCL ethics committees, and in accordance with the ARRIVE guidelines for reporting experiments involving animals (McGrath et al., 2010). A total of 78 animals (disease model and wild-type) were used in this study. The animals had *ad-libitum* access to food and water and were reared in cages of maximum of 5 inhabitants, with a day: night cycle of 12 h: 12 h.

The knock-in $APP^{NL\text{-}F/NL\text{-}F}$ AD mouse model was used for this study (Saito et al., 2014). This mouse model was chosen because it faithfully reproduces the effect of AD Aβ pathology without overexpression artefacts in a time-dependent manner. The $APP^{NL\text{-}F/NL\text{-}F}$ model has two familial AD (FAD) mutations: KM670/671NL (Swedish) and I716F (Iberian). The former increases β-site cleavage of APP to produce elevated amounts of both Aβ40 and Aβ42, whereas the latter promotes γ-site cleavage at C-terminal position 42, thereby increasing the Aβ42/Aβ40 ratio in favour of the more hydrophobic Aβ42 as seen in clinical AD. Thus, the $APP^{NL\text{-}F/NL\text{-}F}$ mouse model shows Aβ accumulation and related pathology in an age-dependent manner, with initial accumulation shown at 6 months (Saito et al., 2014). The knock-in line was crossed with C57BL/6 mice and the resulting heterozygous pairs were used for breeding but excluded from experiments. Only male $APP^{NL\text{-}F/NL\text{-}F}$ and age-matched wild-type (C57BL/6) mice, aged between 12 and 16 months were included.

Animals were genotyped via standard polymerase chain reaction using the following four primers: 5′-ATCTCGGAA

TABLE 1 | *Patient demographic details of human cases used for neuroanatomy experiments.*

Cases ID	Group	Regions Used	Age (years)	Sex	Post-mortem Delay (hours)	Brain Weight (g)	Braak Staging	CERAD Score	Thal Staging
1	AD	CA1	67	Male	35.27	1,223	Braak 6	CERAD 3	Thal 5
2	AD	CA1	55	Female	47.50	1,100	Braak 6	Frequent	—
3	AD	CA1	90	Male	89	1,200	Braak 4	CERAD 0	Thal 1
4	AD	CA1	86	Male	96.1	1,203	Braak 6	CERAD 3	Thal 5
5	AD	CA1	68	Male	70.05	1,522	Braak 6	—	Thal 5
6	AD	CA1, DG	69	Male	35.04	891	Braak 6	Frequent	Thal 5
7	AD	CA1, DG	88	Male	58.1	1,084	Braak 6	—	Thal 5
8	AD	CA1, DG	70	Male	60.25	1,224	—-	—	—
9	AD	CA1, DG	62	Female	76.20	996	Braak 6	Frequent	Thal 5
10	AD	DG	63	Male	31.42	1,042	Braak 6	CERAD 3	Thal 5
11	AD	DG	64	Male	95.5	1,280	Braak 6	—	Thal 5
12	AD	DG	65	Male	34.25	1,089	Braak 5 or 6	C3	A3
13	AD	DG	79	Male	61.19	1,423	Braak 5 or 6	C3	A3
14	Control	CA1	101	Male	60.35	1,450	Braak 1	CERAD 0	—
15	Control	CA1	79	Male	105.5	1,355	Braak 2	—	—
16	Control	CA1	88	Male	96	1,240	Braak 2	CERAD 1	Thal 3
17	Control	CA1	71	Female	76	1,214	Braak 3	CERAD 2	Thal 2
18	Control	CA1	86	Female	120	1,234	Braak 2	—	—
19	Control	CA1	80	Female	49.10	1,242	Braak 2	—	—
20	Control	CA1	83	Male	105.00	1,244	Braak 4	CERAD 2	Thal 3
21	Control	CA1, DG	94	Female	89.25	1,541	Braak 3	Sparse	—
22	Control	CA1, DG	88	Male	27.30	1,300	Braak 4	—	Thal 3
23	Control	DG	76	Male	79	1,366	Braak 2	Cerad 0	Thal 1
24	Control	DG	80	Female	53	1,130	Braak 2	Cerad 0	Thal 3
25	Control	DG	84	Female	53	1,283	Braak 2	—	Thal 3
26	Control	DG	90	Male	46	1,213	Braak 4	Cerad 2	Thal 3
27	Control	DG	96	Female	60	1,032	Braak 2	—	Thal 2

GTGAAGATG-3′, 5′-TGTAGATGAGAACTTAAC-3′, 5′-ATC TCGGAAGTGAATCTA-3′, and 5′-CGTATAATGTATGCT ATACGAAG-3′ as previously described (Saito et al., 2014).

2.2 Tissue Collection and Preparation

2.2.1 Mouse Brain Tissue

Tissue preparation was carried out as previously described (Petrache et al., 2019; Shi et al., 2020). All experiments were performed single-blinded. Mice were deeply anaesthetized using inhalation of isoflurane 4% followed by intraperitoneal injection of 60 mg/kg phenobarbitone. The level of anaesthesia was monitored using pedal and tail pinch reflexes, rate, depth, and pattern of respiration through observation and the colour of mucous membranes and skin. The mice were then perfused transcardially with artificial cerebrospinal fluid (ACSF) containing (in mM) 248 sucrose, 3.3 KCl, 1.4 NaH2PO4, 2.5 CaCl2, 1.2 MgCl2, 25.5 NaHCO3, and 15 glucose, bubbled with 95% O_2 and 5% CO_2. The animals were then decapitated, the brain removed and 300 μm thick coronal sections of the cortex and hippocampus were cut in ice-cold standard ACSF using an automated vibratome (Leica, Germany). This standard ACSF contained (in mM): 121 NaCl, 2.5 KCl, 1.3 $NaH2PO_4$, two $CaCl_2$, one $MgCl_2$, 20 glucose and 26 $NaHCO_3$, equilibrated with 95% O_2 and 5% CO_2 (pH, 7.3, osmolarity, 300–310 m Osm).

The brain slices were then incubated in ACSF for 30 min at 37°C and transferred to room temperature prior to recording. Brain slices were placed in a submerged chamber and superfused with ACSF at a rate of 1–2 ml/min for electrophysiological recordings.

For neuroanatomical studies, one-half of the brains were immediately fixed after perfusion in 4% paraformaldehyde and 0.1% glutaraldehyde in 0.1M phosphate buffer for 24 h prior to sectioning.

2.3 Human Brain Tissue

A total of 27 hippocampal post-mortem brain tissue sections from 13 AD patients and 14 age-matched control individuals were obtained from Queen Square Brain Bank for Neurological Disorders, UCL Institute of Neurology, according to the Human Tissue Act (HTA) 2004 and under the HTA license. Ethical approval was obtained from the local research ethics committee for the national hospital for Neurology and Neurosurgery. The information for cases used throughout is detailed in **Table 1**.

2.4 Electrophysiology

Whole-cell somatic recordings were performed using patch electrodes with resistances of 8–11 MΩ made from filamented borosilicate glass capillaries (Harvard Apparatus, UK) and filled with a solution containing (in mM): 134 K gluconate, 10 HEPES, 10 phosphocreatine, two Na2ATP, 0.2 Na2GTP, and 0.2% w/v biocytin (pH, 7.3, osmolarity, 300–310 mOsm). Excitatory CA1 pyramidal cells or DG granule cells were

selected for recording based on Soma shape using video microscopy under near infrared differential interference contrast illumination. Cells were visualised on a monitor (Panasonic, UK) using an upright microscope (Leica, Germany) under near infrared differential interference contrast (DIC). Images were enhanced using a camera control unit (Hamamatsu, Japan). Cells were further characterized by their electrophysiological properties obtained from injecting a series of 500 m depolarizing and hyperpolarizing current pulses. Recorded cells were filled with biocytin-dye and neurons were further identified based on their gross morphology (see below).

Spontaneous postsynaptic potentials were recorded from passive membrane responses as mixed spontaneous excitatory postsynaptic potentials (sEPSPs) and spontaneous inhibitory postsynaptic potentials (sIPSPs) at resting membrane potential, and were collected in 60 s frame samples, repeated at 0.33 Hz. The reversal potential of inhibitory events mediated by $GABA_A$ receptors was approx.—7 mV. Recordings were carried out under the current clamp mode of operation (NPI SEC 05LX amplifier; NPI electronics, Germany), low pass filtered at 2 KHz and digitized at 5 KHz using a CED 1401 interface (Cambridge Electronic Design, UK). Current-clamp mode allowed for the recording of the intrinsic biophysical properties of the neurons and the natural synaptic voltages to be measured, cells with stable membrane potentials were selected for pharmacological experiments. Input resistance was monitored throughout experiments by means of a hyperpolarizing current step (-10 pA, 10 m). The input resistance was determined from voltage changes in response to hyperpolarizing current steps (-25 pA, 500 m) and calculated from the steady state voltage change. Signal (Cambridge Electronic Design, UK) was used to acquire recordings and generate current steps. The average amplitudes of spontaneous events and their frequency was measured manually from single sweep data sets of 60 s recordings, including a total sweep range of 30–50 frames (*i.e.,* 30–50 min of recording), synaptic noise was taken as ± 0.15mV from baseline, for example values above +0.15mV was considered as synaptic events.

For *in vitro* pharmacological studies, the $GABA_A$ receptor antagonist, bicuculline (100 μM, Tocris Bioscience, UK), SNAP5114 (50 μM, Tocris Bioscience, UK), GAT3/4 inhibitor, were bath-applied. Different sub-sets of principal cells were used for each pharmacological protocols, where subsequent addition of the drug was not performed. Drug concentrations were within the range of their reported biological activity with efficacy and in line with previous *in vitro* studies (Wu et al., 2014). Average data points after drug application were obtained after steady-state responses were attained with the drugs, which was ~15–20 min after onset of the bath-application. Changes in membrane potential caused by drug application were allowed to reach a steady state after ~15–20 min, and then manually taken to resting membrane potential values to record the spontaneous events to compare the changes to control condition.

2.5 Neuroanatomical Procedures and Analysis

2.5.1 Recovery of Biocytin-Labelled Cells Post-Electrophysiological Recordings

After electrophysiological recordings with pharmacological protocols, the slices were fixed in 4% paraformaldehyde and 0.1% glutaraldehyde in 0.1M phosphate buffer for 24 h, embedded in 6% gelatine then re-sectioned at 70 μm. For fluorescence labelling, the sections were permeated using 0.1% Triton X-100 and incubated with Streptavidin-Alexa 488 conjugate (Thermofisher, United States) for 48 h followed by image acquisition, via confocal laser scanning microscope (LSM 880 Zeiss, Germany). After image acquisition the sections were washed and incubated in avidin-biotin complex (ABC) overnight at 4°C, followed by the 3-3-diaminobenzidine (DAB) staining. Recovered cells were reconstructed manually from consecutive slices at ×100 objective under a Leica DMR microscope with an attached drawing tube.

2.6 Immunohistochemical Procedures and Analysis

Ventral hippocampal coronal slices were sectioned at 70 μm thickness using a vibratome (Leica, Germany) from the same region of the DG and CA1 in reference to mouse brain atlases. The brain sections were incubated in 0.1M phosphate buffer solution (PBS) for 24 h on a microplate shaker (VWR, UK). Sections were permeated using 0.3% tris-buffered saline and Triton (TBS-T) solution. This was followed by 1% H_2O_2 incubation at room temperature, prepared using 30% stock solution (Sigma-Aldrich, United States) and diluted with deionised water (Sigma-Aldrich, United States). Sections were subsequently washed using TBS-T solution before the blocking procedure using 20% animal serum in PBS. Incubation in primary antibodies was performed for 48 h at 4°C, and subsequent incaution in secondary antibodies was for 3 h at room temperature (**Table 2**). Following incubation in secondary antibodies, the sections were counterstained using DAPI (1:1000 dilution in H_2O, Sigma-Aldrich, United States) and mounted with Vectashield (Vector Laboratories, UK). For immunoperoxidase analysis, the slices were incubated in avidin-biotin-horseradish peroxidase complex (Vector Laboratories, UK) solution, processed with DAB, and subsequently dehydrated and mounted (Khan et al., 2018).

Human slices (**Table 1**) followed a similar procedure to mouse brain sections with permeation using TBS-T solution and H_2O_2, followed by blocking procedures using 20% animal serum diluted in PBS. The slices were incubated with primary and then subsequently secondary antibody solutions in accordance with dilutions in **Table 2** below, before being counterstained with DAPI (1:1000 dilution in H_2O, Sigma-Aldrich, United States).

2.7 Confocal Microscopy

From each brain section, an average of two Z-stacks at ×20 and ×63 objective were taken using the Zeiss LSM880 confocal microscope in unison with the Zeiss Zen Black imaging

TABLE 2 | List of antibodies and dilutions used in this study.

Primary Antibodies					
Company	**Antibody Target**	**Species**	**Dilution with TBS-T**	**Catalog Number**	**Country**
Agilent Technologies	GFAP	Rat	1:1000	13–0300	United States
Merck Millipore	GAD67	Mouse	1:1000	MAB5406	United States
Abcam	GAT3/4	Rabbit	1:100	ab431	United Kingdom
Secondary Antibodies					
Company	**Antibody Name**	**Targeted Species**	**Dilution with TBS-T**	**Catalog Number**	**Country**
Molecular Probes (now Invitrogen)	Alexa 568	Rat	1:500	A-11077	United States
Abcam	Alexa 488	Rabbit	1:500	ab150077	United Kingdom
Abcam	Alexa 488	Rat	1:500	ab150165	United Kingdom
Sigma-Aldrich	FITC	Mouse	1:200	F2653	United States
Invitrogen	Texas Red	Rabbit	1:750	T2767	United States
Vector laboratories	Biotinylated anti-rabbit	Rabbit	1:500	BA-1000	United States

software from the DG and CA1. Regions of interest (ROI), CA1 (including stratum oriens, stratum pyramidale and stratum lacunosum) and DG (including the molecular layer, granule cell layer and polymorphic layer), were located using the manual joystick through the ×20 objective lens by systematically searching the slice and consistent evaluation of location in reference to appropriate mouse and human atlases. Z stack images were taken at a resolution of 1024x1024 pixels with 12–14 Z steps through the depth of the slice and with application of appropriate filters to complement secondary antibody fluorescence: DAPI (405λm), FITC/Alexa 488 (488λm), Texas Red/Alexa 568 (561/594λm) and Alexa 647 (640λm).

Single-blinded image analysis was undertaken using the ImageJ software using an automated macro. The Z-stack images were split into their constituent colour channels. Following this, all astrocytes in a given image were selected through the Huang auto thresholding method in the ImageJ software, to demarcate signal from background and produce the ROI (Huang and Wang, 1994). Integrated Density (mean intensity of fluorescence multiplied by area) was calculated for each ROI in the in the x20 Z-stack images and an average taken, with markers such as GAD67 and GAT3/4 measured in astrocyte areas demarcated by GFAP staining using the ROI produced.

2.8 Statistics

The statistical analysis was performed using GraphPad Prism version 9.0 for Windows and Microsoft Excel. Based on the differences observed between control and diseased data sets obtained in our preliminary studies, an $n \geq 5$ was ideal for this study in order to reveal a statistical difference of >80% power assuming a 5% significance level and a two-sided test for both electrophysiology and neuroanatomy experiments.

All figures displaying error bars represent ± the standard error of the mean. The *"n"* is given as the number of observations and is equal to the number of animals used or human patients, unless otherwise stated. For all statistical tests performed, a 95% confidence interval was used ($p \leq .05$).

Various statistical tests were performed depending on the parameters used and each figure legends detail the specific statistical test used. A two-way analysis of aariance (ANOVA) corrected for multiple comparisons was used to indicate the presence of significance in neuroanatomical and pharmacological experiments between genotypes or comparisons within a genotype.

3 RESULTS

Neuroanatomical studies combined with somatic whole-cell patch recordings were performed on CA1 and DG excitatory cells from 12 to 16 month-old wild-type and $APP^{NL\text{-}F/NL\text{-}F}$ knock-in mouse model. Comparative studies using human hippocampal post-mortem brain tissue were also performed for the neuroanatomical studies.

3.1 Elevated Reactive Astrocytes Correlated With Increased Enzyme for GABA and GAT3/4 Levels in AD

GFAP is a widely used marker of reactive astrocytes, effectively labelling both astrocytic branches and processes in the brain regions investigated here, such as the CA1 and DG of the hippocampus (Zhang et al., 2019). To measure the alteration of the GABA content within astrocytes, we used GAD67 labelling, an enzyme responsible for catalysing the conversion of glutamate to GABA (see methods). In addition, we also stained for astrocyte specific GABA transporter, GAT3/4, to investigate the anatomical changes of astrocytes in AD. **Table 3** shows data from all neuroanatomy experiments. **Figure 1** illustrates the results from the analysis of immunofluorescence staining (GFAP, GAD67 and GAT3/4) from mouse and human brain slices which included the CA1 and DG regions of the hippocampus (see also **Table 3**).

Quantitively, the results showed a significant increase in the levels of GFAP in the $APP^{NL\text{-}F/NL\text{-}F}$ AD mouse model when

TABLE 3 | *Table gives actual values of all neuroanatomy data. All values are stated as mean ± SEM. * denotes significant difference (Two-way ANOVA with Šidák's post-hoc multiple comparisons test within a genotype, p ≤ .05) between wild-type and APP$^{NL-F/NL-F}$ mice and human control and human AD cases.*

Tissue	Marker	Region	Wild-type Mean and SEM	APP$^{NL-F/NL-F}$ Mean and SEM
Mouse	GFAP	CA1	8688.82 ± 503.37*	23304.28 ± 2133.60
		DG	8048.76 ± 751.05*	20712.32 ± 2630.37
	GAD67	CA1	4044.04 ± 957.70*	29846.41 ± 3031.23
		DG	6150.76 ± 1797.84*	30769.63 ± 3400.83
	GAT3	CA1	7630.53 ± 1949.88*	20273.58 ± 3730.67
		DG	9533.01 ± 1991.68*	28260.11 ± 2576.60
Human Post-Morten	GFAP	CA1	35322.72 ± 5372.42*	172,552.25 ± 53059.32
		DG	35858.81 ± 3604.18*	168,141.18 ± 32198.47
	GAD67	CA1	30107.36 ± 2491.94*	63793.49 ± 10124.91
		DG	30080.54 ± 2637.88*	62207.25 ± 4578.53
	GAT3	CA1	32237.57 ± 9879.24*	105,136.08 ± 27010.54
		DG	25161.01 ± 5716.40*	183,891.46 ± 23122.87

compared to age-matched wild-type mice (**Figure 1A**). The average integrated density for GFAP increased significantly by, 168.21 ± 15.40% in the CA1 region and similarly in the DG region by, 157.34 ± 19.98%. These results were mimicked in the CA1 and DG of human AD patients, when compared to the human control patient group (**Figure 1C**). Human GFAP levels increased significantly by, 338.50 ± 119.46% in CA1, and by 368.90 ± 70.64% in the DG. The results of the two-way ANOVA revealed a main effect of genotype, but not of the brain area and no interaction among the two factors analysed. The Šidák's post-hoc multiple comparisons test showed a strong statistical difference among the expression of GFAP in AD tissue ($n = 12$, $^{****}p \leq .0001$, for mouse study and $n = 10$, $^{**}p \leq .01$ for human study).

GAD67 is expressed by neurons and astrocytes and the overall levels of GAD67 increased in AD tissue. Here we focused on analysing the GAD67 levels in reactive astrocytes, Šidák's post-hoc multiple comparisons test showed a statistically significant difference between the genotypes, with no significant regional difference within or between the genotypes. There was an increase in GAD67 in astrocytes AD tissue, indicative of increased GABA levels in reactive astrocytes of CA1 and DG of the *APP$^{NL-F/NL-F}$* mouse model when compared to wild-type control mice (**Figure 1F**) by, 638.04 ± 64.80% in CA1, and by, 400.26 ± 44.24% in DG ($n = 5$, $^{****}p \leq .0001$). Similarly, average levels of GAD67, specifically in astrocytes, significantly increased (**Figure 1I**) in post-mortem brains of Alzheimer's patients by, 111.89 ± 17.76%, and 106.80 ± 7.86% in the CA1 and DG, respectively, when compared to age-matched CA1 and DG of control human patients ($n = 5$, $^{**}p \leq .01$).

To understand astrocyte mediated shutting of GABA and its effects on GABA homeostasis, we analysed the levels of the GAT3/4 GABA transporter within astrocytes. Here, Šidák's post-hoc multiple comparisons test showed a statistical difference between the expression of GAT3/4 between genotypes, which was markedly increased in *APP$^{NL-F/NL-F}$* mice when compared to age-matched wild-type control mice by, 165 ± 30.49% and 196.44 ± 17.91 in CA1 and DG, respectively ($n = 5$, $^{**}p \leq .01$), (**Figure 1G**). In comparison, GAT3/4 levels also increased in AD patients compared to the expression levels in control human tissue by, 226.13 ± 58.09% and 630.86 ± 79.33% in CA1 and DG, respectively ($n = 5$, $^{**}p \leq .01$), (**Figure 1J**). The results of the two-way ANOVA revealed no interaction among genotype and brin region.

3.2 Higher Levels of Tonic Inhibition Observed in CA1 and DG of the *APP$^{NL-F/NL-F}$* AD Model

Whole-cell electrophysiological recordings from principal neurons in either CA1 (**Figure 2A**) or DG (**Figure 2B**), revealed a background, tonic inhibition mediated via GAT3/4 in both CA1 and DG of wild-type and *APP$^{NL-F/NL-F}$* mice. **Table 4** shows data from electrophysiology experiments. **Figures 2C,D** and E-F illustrates the experiments performed to show the tonic inhibition revealed by blockade of GAT3/4 with a selective inhibitor, using SNAP-5114 (50 μM), that altered the resting membrane potential (depolarisation) of all cells recorded. These effects were seen within 20–30 min of bath-application of the drug and suggests that the astrocytic GAT3/4 contributed to the tonic inhibition after acute treatment with the inhibitor.

To investigate the involvement of GABA and whether the tonic inhibition was higher in *APP$^{NL-F/NL-F}$* mice, we bath applied $GABA_A$ receptor antagonist, bicuculline (100 μM), to a subset of neurons (**Figures 2G,H**), which resulted in a change in the resting membrane potential that induced an increase in depolarization in all principal cells and an increase in the input resistance recorded in both wild-type and AD tissue.

The results of the Two-way ANOVA revealed a main effect of genotype and drug effect with interaction between both factors. The Tukey's post-hoc multiple comparisons test, revealed a significantly greater change in the AD tissue with bicuculline by, 102.63 ± 0.34% and 134.23 ± 0.28% in CA1 and DG respectively ($n = 5$, $^{***}p \leq .001$) compared to neurons recorded in wild-type CA1 and DG principal cells, similar findings were reported previously by others (Wu et al., 2014). Subsequent bath addition of SNAP-5114 after bicuculline did not affect depolarization any further in CA1 and DG,

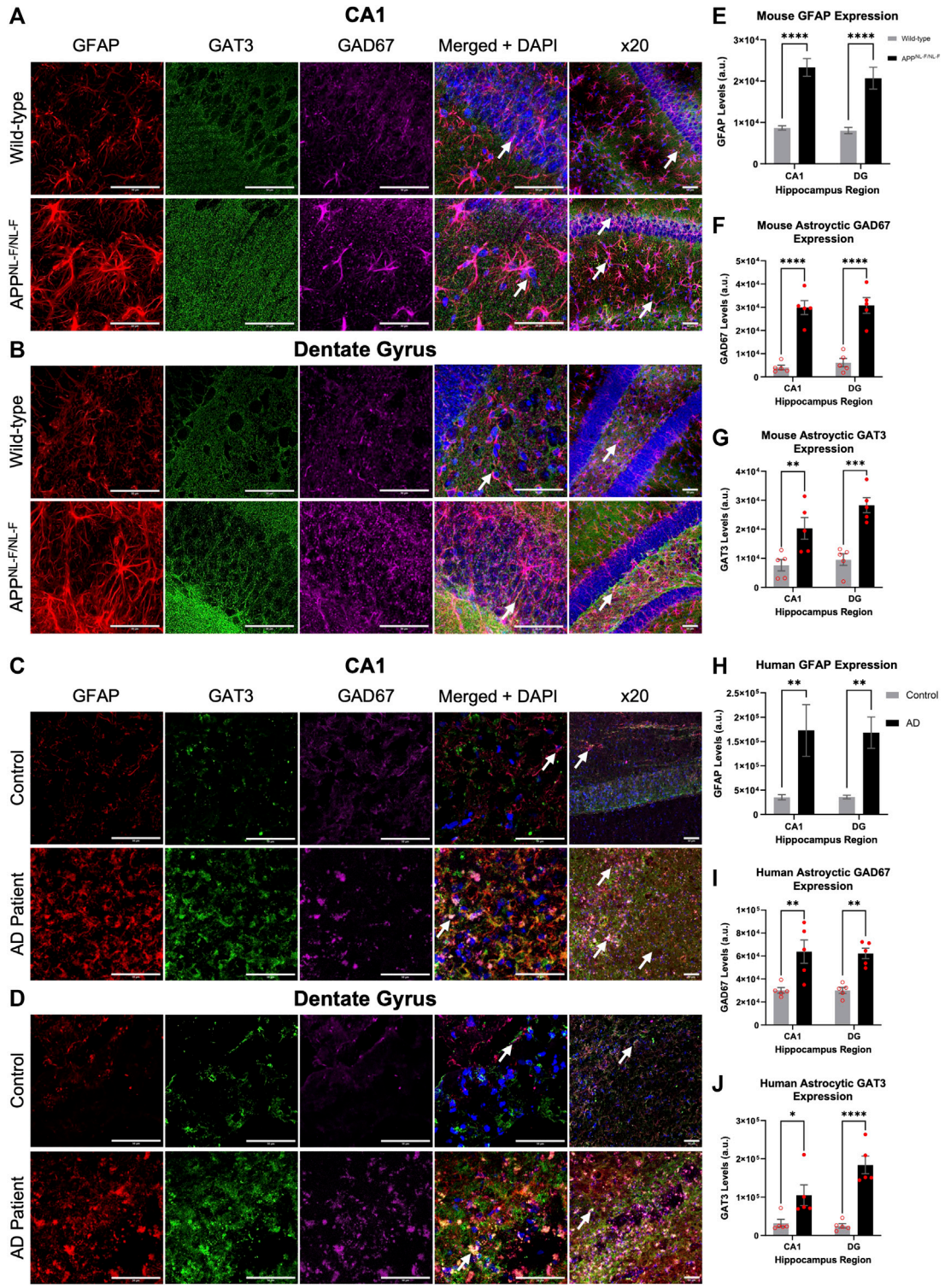

FIGURE 1 | Reactive astrocytes express increased levels of GAT3/4 and GAD67 in AD. **(A–D)** Z-stack images of the CA1 and DG regions of mice show increased Gram-positive astrocytes express increased levels of the astrocyte-specific GABA transporter 3/4 (GAT3/4) colocalised with GAD67 (GABA-producing enzyme) in the *APP*$^{NL\text{-}F/NL\text{-}F}$ mouse model of AD compared to age-matched wild-type animals. This finding was also consistent in post-mortem brain tissue of AD patients when compared to age-matched controls. White arrows show examples of colocalization at ×63 and ×20 magnification (scale bar = 50 μm). **(E–J)** Graphs show data of astrocytic GFAP, GAD67 and GAT3/4 expression in CA1 and DG, respectively, in mice and human post-mortem brain tissue. The data suggest an increased expression of GFAP, GAD67 and GAT3/4 levels in both, CA1 and DG regions of the AD model as well as in the AD human patient group compared to their control counterparts (*$p \leq .05$, **$p \leq .01$, ***$p \leq .001$, ****$p \leq .0001$; Two-way ANOVA with Šidák's post-hoc multiple comparisons test).

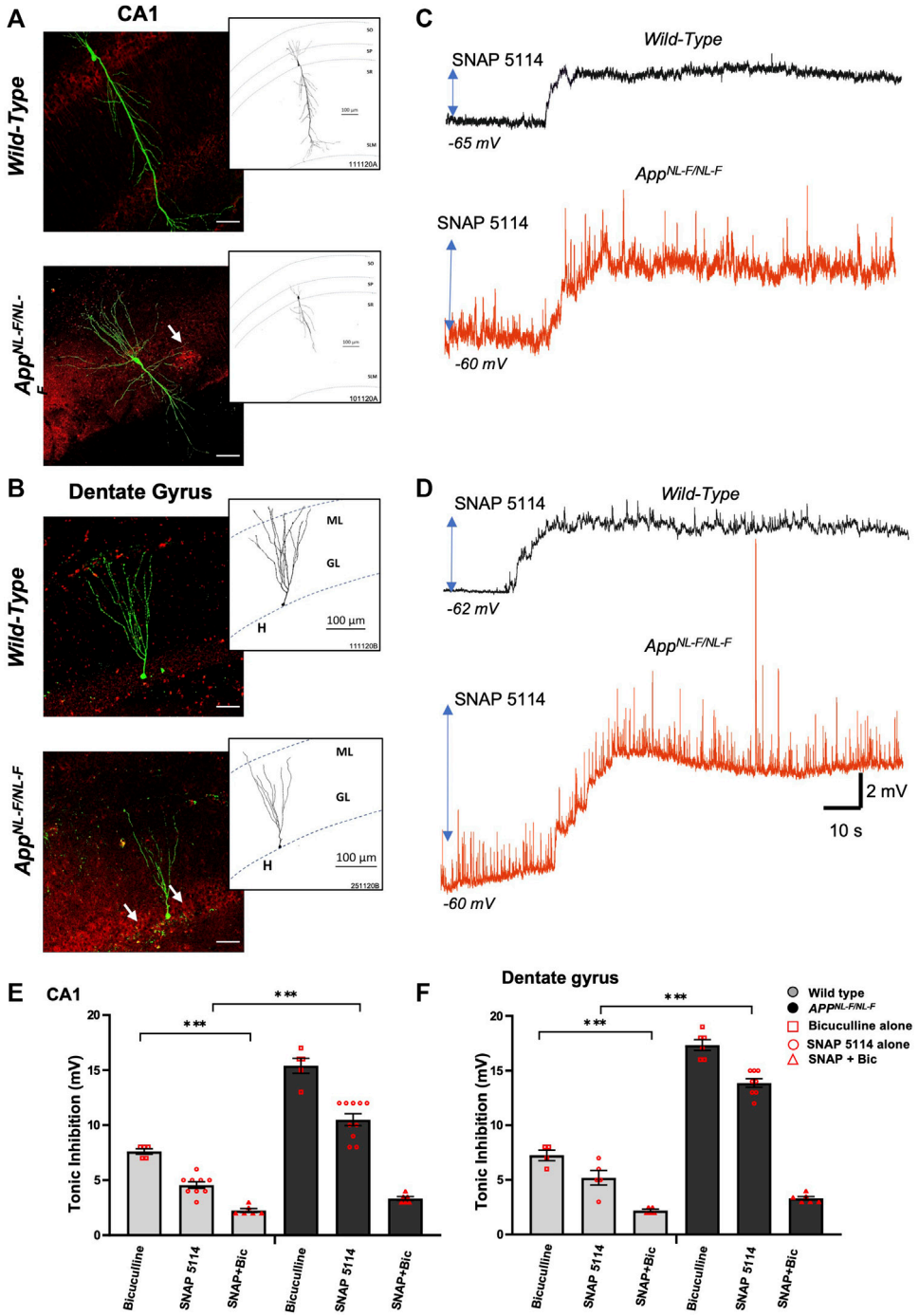

FIGURE 2 | Higher tonic inhibition observed in CA1 and DG of $APP^{NL\text{-}F/NL\text{-}F}$ mice. **(A,B)** Double immunofluorescence performed on whole-cell recorded, biocytin-labelled cells in CA1 and DG with streptavidin (Alexa 488, green) co-labelled with Aβ (Texas red, red) in wild-type and $APP^{NL\text{-}F/NL\text{-}F}$ mice (scale bar 50 µm). The white arrows show Aβ accumulation/plaques which were expressed in higher levels in the AD model. The inserts show reconstructed examples of biocytin-labelled pyramidal and granule cells in control and AD mice, which indicated a reduced dendritic complexity in both types of neurons in the AD model. **(C,D)** Whole-cell electrophysiological recordings from CA1 pyramidal cells and DG granule cells in control conditions (black trace) and after bath-application of the GAT3/4 antagonist, SNAP 5114 (50 µM) (red traces), which depolarised cell membranes, suggesting tonic inhibition under the control of GAT3/4 in all cells recorded. All whole-cell recordings in AD tissue were in close proximity to plaques. **(E,F)** Illustrates the % change in tonic inhibition after bath-application of bicuculline alone in one group of cells, and bath application of SNAP 5114 alone with subsequent bath application of SNAP + bicuculline in a separate group of cells (100 µM) in CA1 and DG principal cells from wild-type and $APP^{NL\text{-}F/NL\text{-}F}$ mice (Two-way ANOVA with Tukey's post-hoc multiple comparisons test, $^{*}p \leq .05$, $^{**}p \leq .01$, $^{***}p \leq .001$, $^{****}p \leq .0001$).

TABLE 4 | *Table gives actual values of all electrophysiology data. All values are stated as mean ± SEM. *denotes significant difference ($p \leq .05$) between wild-type control and experimental values. **denotes significant difference ($p \leq .05$) between wild-type and $APP^{NL\text{-}F/NL\text{-}F}$ values. A two-way ANOVA was performed corrected for multiple comparisons ($\alpha = 0.05$), with a post-hoc Tukey's test.*

	DG		CA1	
	sEPSP frequency (Hz)			
	Control	**SNAP 5114**	**Control**	**SNAP 5114**
Wild-type	1.79 ± 0.17 (*n = 5*)	2.90 ± 0.29 (*n = 5*) *	2.44 ± 0.15 (*n = 9*)	4.09 ± 0.20 (*n = 9*) *
$APP^{NL\text{-}F/NL\text{-}F}$	3.60 ± 0.16 (*n = 8*) **	4.50 ± 0.16 (*n = 6*) **	3.40 ± 0.13 (*n = 7*) **	4.66 ± 0.17 (*n = 6*)
	sEPSP amplitude (mV)			
Wild-type	0.89 ± 0.11 (*n = 5*)	1.60 ± 0.18 (*n = 5*) *	0.81 ± 0.07 (*n = 9*)	1.39 ± 0.10 (*n = 10*) *
$APP^{NL\text{-}F/NL\text{-}F}$	1.45 ± 0.11 (*n = 8*)	2.20 ± 0.19 (*n = 6*)	1.46 ± 0.06 (*n = 7*) **	2.43 ± 0.09 (*n = 6*) **
	sIPSP frequency (Hz)			
Wild-type	1.46 ± 0.18 (*n = 5*)	2.42 ± 0.28 (*n = 5*) *	1.75 ± 0.15 (*n = 9*)	3.06 ± 0.23 (*n = 9*) *
$APP^{NL\text{-}F/NL\text{-}F}$	1.00 ± 0.10 (*n = 8*)	2.67 ± 0.25 (*n = 7*)	0.94 ± 0.09 (*n = 8*) **	2.56 ± 0.27 (*n = 7*)
	sIPSP amplitude (mV)			
Wild-type	0.70 ± 0.07 (*n = 5*)	1.40 ± 0.11 (*n = 5*) *	0.92 ± 0.12 (*n = 9*)	1.58 ± 0.14 (*n = 9*) *
$APP^{NL\text{-}F/NL\text{-}F}$	0.51 ± 0.04 (*n = 8*)	1.32 ± 0.24 (*n = 6*)	0.54 ± 0.07 (*n = 8*)	1.12 ± 0.13 (*n = 7*)
	Resting membrane potential (mV)			
Wild-type	-72.00 ± 1.00 (*n = 6*)	-66.84 ± 1.45 (*n = 6*) *	-66.00 ± 0.82 (*n = 8*)	-61.62 ± 0.80 (*n = 8*) *
$APP^{NL\text{-}F/NL\text{-}F}$	-64.00 ± 0.78 (*n = 8*) **	-50.12 ± 0.81 (*n = 8*) **	-62.00 ± 0.53 (*n = 10*) **	-52.70 ± 0.98 (*n = 10*) **
	Tonic inhibition amplitude (mV)			
		DG		
	SNAP 5114	Bicuculline	SNAP 5114 + Bicuculline	
Wild-type	5.20 ± 0.66 (*n = 5*)	7.20 ± 0.48 (*n = 4*)	2.20 ± 0.12 (*n = 5*) *	
$APP^{NL\text{-}F/NL\text{-}F}$	13.90 ± 0.40 (*n = 8*) **	17.30 ± 0.50 (*n = 6*) **	3.30 ± 0.16 (*n = 6*)	
		CA1		
	SNAP 5114	Bicuculline	SNAP 5114 + Bicuculline	
Wild-type	4.50 ± 0.29 (*n = 9*)	7.60 ± 0.24 (*n = 5*) *	2.25 ± 0.17 (*n = 6*) *	
$APP^{NL\text{-}F/NL\text{-}F}$	10.50 ± 0.53 (*n = 10*) **	15.40 ± 0.68 (*n = 5*) **	3.34 ± 0.16 (*n = 6*)	

suggesting that the effects of SNAP-5114 are mediated by $GABA_A$ receptors.

In CA1, bath-application of SNAP-5114 (alone) resulted in a change in the average resting membrane potential of -66 ± 0.82 mV to -61.6 ± 0.80 mV and -62.8 ± 0.53 mV to -52.7 ± 0.97 mV in age-matched wild-type and $APP^{NL\text{-}F/NL\text{-}F}$ mice, respectively (**Table 4**) (*n = 8 wild type, n = 10 for* $APP^{NL\text{-}F/NL\text{-}F}$, $^{**}p \leq .01$ *for wild-type and* $^{***}p \leq .001$ *for* $APP^{NL\text{-}F/NL\text{-}F}$). Similarly, in the dentate gyrus, application of SNAP-5114 resulted in membrane depolarization, with a significant change in the average resting membrane potential of -72 ± 1 mV to -66.8 ± 1.4 mV in wild-type animals, and a change of -64 ± 0.77 mV to -50.1 ± 0.81 mV in the $APP^{NL\text{-}F/NL\text{-}F}$ mice (*n* = 6 wild-type, *n = 8* $APP^{NL\text{-}F/NL\text{-}F}$, $^{*}p \leq .05$ *for wild-type,* $^{***}p \leq .001$ *for* $APP^{NL\text{-}F/NL\text{-}F}$).

The overall tonic inhibition revealed by blockade of GAT3/4, in CA1 was in the range of 4–6 mV, and 8–12 mV in wild-type and $APP^{NL\text{-}F/NL\text{-}F}$ mice, respectively (**Table 4**), illustrating an enhanced tonic inhibition in the AD model by 130.5 ± 0.31% (*n = 9* wild-type, *n = 10* $APP^{NL\text{-}F/NL\text{-}F}$, $^{****}p \leq .0001$). Interestingly, the overall tonic inhibition was higher in the dentate gyrus, showing an increase of, 166.8 ± 0.25% in the $APP^{NL\text{-}F/NL\text{-}F}$ mice compared to age-matched wild-type mice (range: 13–15 mV, *n = 5* wild-type, *n = 8* $APP^{NL\text{-}F/NL\text{-}F}$, $^{****}p \leq .0001$).

The involvement of GABA in the total tonic inhibition was revealed by the change of membrane potential after subsequent bath-application of 100 μM bicuculline (in the presence of SNAP 5114) to block all $GABA_A$-mediated synaptic events. The subsequent tonic inhibition with bicuculline + SNAP-5114, was in the range of 2–3 mV and 3–4 mV in the CA1 and DG, respectively (see **Table 4**).

3.3 GAT3/4 Exacerbates Excitability in the AD Model

To explore the cells excitability after blocked tonic inhibition, the resting membrane potential (RMP), input resistance (R input) and neuronal firing properties that are contributing factors to the differences in excitability (**Figure 3**) together with the changes in spontaneous synaptic events (**Figure 4**) were measured.

Figure 3 (A-B) shows RPM of principal cells, which were more depolarised in the $APP^{NL\text{-}F/NL\text{-}F}$ mice in both CA1 and DG, and further depolarized after the bath application of SNAP 5114. The

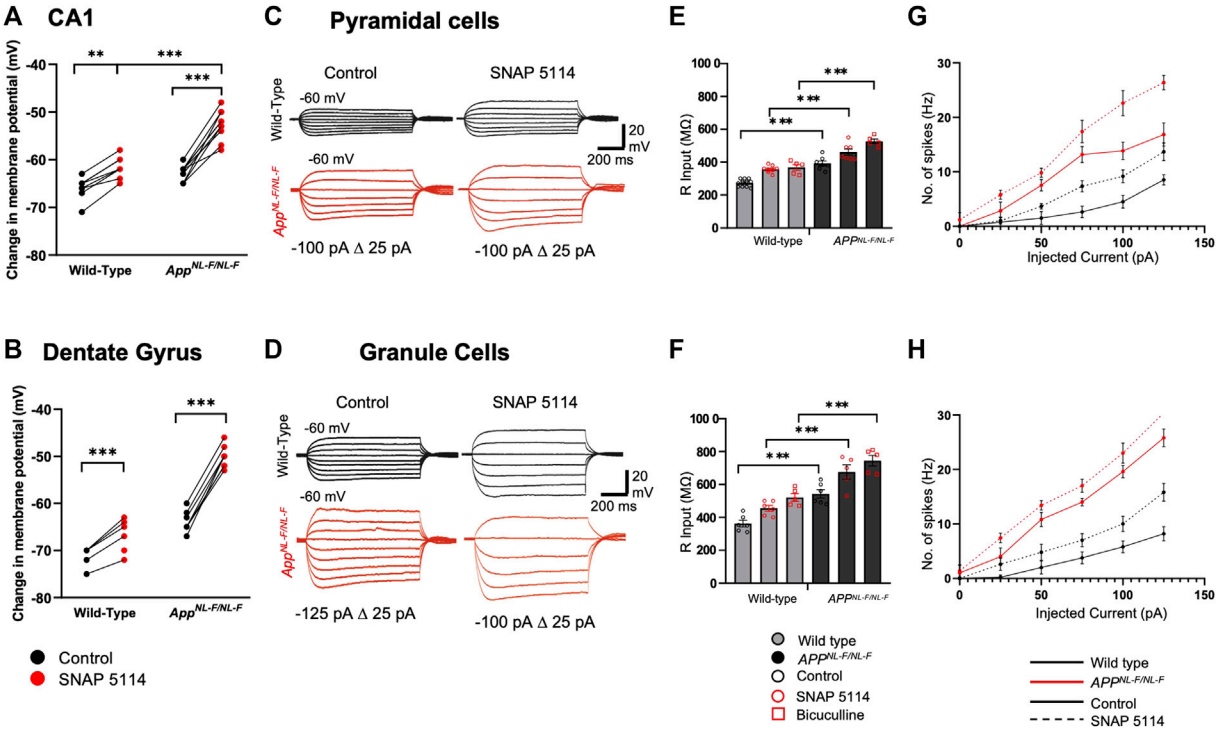

FIGURE 3 | Subthreshold and excitability responses of CA1 and DG principal cells after blockade of tonic inhibition. Whole cell current clamp recordings from CA1 and DG pyramidal cells from wild-type and $APP^{NL\text{-}F/NL\text{-}F}$ mice in control, after bath application with SNAP 5114 or bicuculline. **(A,B)** Graphs detail the change in the resting membrane potential for individual CA1 (upper) and DG (lower) pyramidal cells during bath-application of SNAP 5114 (Two-way ANOVA with Tukey's multiple comparison test, $^{*}p \leq .05$, $^{**}p \leq .01$, $^{***}p \leq .001$, $^{****}p \leq .0001$). **(C,D)** Voltage responses from CA1 and DG pyramidal cells to 500 m step current injections ranging from −125 to 50 pA in 25 pA increments. For clarity control and SNAP 5114 results are shown. **(E,F)** Input resistance was significantly higher in both CA1 and DG after bath application of SNAP 5114 and bicuculline ($n \geq 5$ for each cohort, Two-way ANOVA with post hoc Tukey's test for multiple comparisons, $^{*}p \leq .05$, $^{**}p \leq .01$, $^{***}p \leq .001$, $^{****}p \leq .0001$). **(G,H)** Relations between injected current and firing frequency for CA1 and DG pyramidal cells that were more excitable after drug application in wild-type and $APP^{NL\text{-}F/NL\text{-}F}$ mice. The input-output curves displayed a pseudo-linear relationship between no. of spikes generated with increasing current injections in wild-type and the AD model ($n \geq 5$ cells per cohort).

input resistance of the principal cells recorded ranged from, 240 to 300 and 340–600 MΩ under control conditions in CA1 and DG, respectively. As expected, blocking of $GABA_A$ receptors with bicuculine resulted in an increase in the input resistance by, 34.57 ± 4.55% in wild-type mice, and 34.49 ± 3.43% in $APP^{NL\text{-}F/NL\text{-}F}$ mice ($n = 5$, $^{***}p \leq .001$) in CA1. Similarly, in DG there was an increase by, 43.95 ± 7.11% in wild-type mice, and 37.08 ± 8.70% in $APP^{NL\text{-}F/NL\text{-}F}$ mice ($n = 5$, $^{***}p \leq .001$) (**Figures 3C–F**). Blocking GAT3/4 with SNAP 5114 also significantly increased input resistance by, 30.67 ± 1.82% ($n = 8$, $^{***}p \leq .001$), and 17.64 ± 2.84% ($n = 7$, $^{**}p \leq .01$) of control conditions in wild-type and $APP^{NL\text{-}F/NL\text{-}F}$ in CA1, respectively. Similarly, in DG, with bath application of SNAP 5114, there was an increase in input resistance by, 25.57 ± 3.59% and 24.53 ± 8.53% of control conditions in wild-type and $APP^{NL\text{-}F/NL\text{-}F}$, respectively ($n = 6$, $^{*}p \leq .05$), shown in **Figure 3** (C-F). These changes were associated with increased firing frequency of pyramidal cells after bath application of SNAP 5114 and bicuculline in both genotypes and regions studied (**Figures 3G,H**).

Spontaneous synaptic events recorded from principal cells displayed hyperactivity in the $APP^{NL\text{-}F/NL\text{-}F}$ mice in contrast to age-matched wild type mice; this activity was further exacerbated by bath-application of the GAT3/4 inhibitor SNAP-5114, which significantly increased the amplitude and frequency of the sEPSPs. The EPSP amplitude was significantly increased in both CA1 and DG of $APP^{NL\text{-}F/NL\text{-}F}$ mice by, 66.9 ± 0.14% and 51 ± 0.19% ($n = 6$, $^{**}p \leq .01$) of control values, respectively. Furthermore, the frequency of sEPSPs was significantly increased in both hippocampal regions of $APP^{NL\text{-}F/NL\text{-}F}$ mice by, 35 ± 0.27% ($n = 7$, $^{***}p \leq .001$) and 24.9 ± 0.26% ($n = 6$, $^{*}p \leq .05$) in CA1 and DG, respectively. This illustrates a further enhancement of the aberrant hyperactivity in the AD model (**Figure 4** red traces). The increase in hyperexcitability as a result of bath-application of SNAP-5114 is also indicated by the change in the cells subthreshold values, and membrane potential to firing threshold in the AD model (**Figure 3**).

The sIPSP amplitude and frequency also increased with bath application of SNAP-5114 in CA1 and DG, but only significant differences were seen in the $APP^{NL\text{-}F/NL\text{-}F}$ mice in both CA1 and DG ($n = 9$, $^{***}p \leq 0.001$) (**Figure 3** E-F and K-L, see **Table 4** for values).

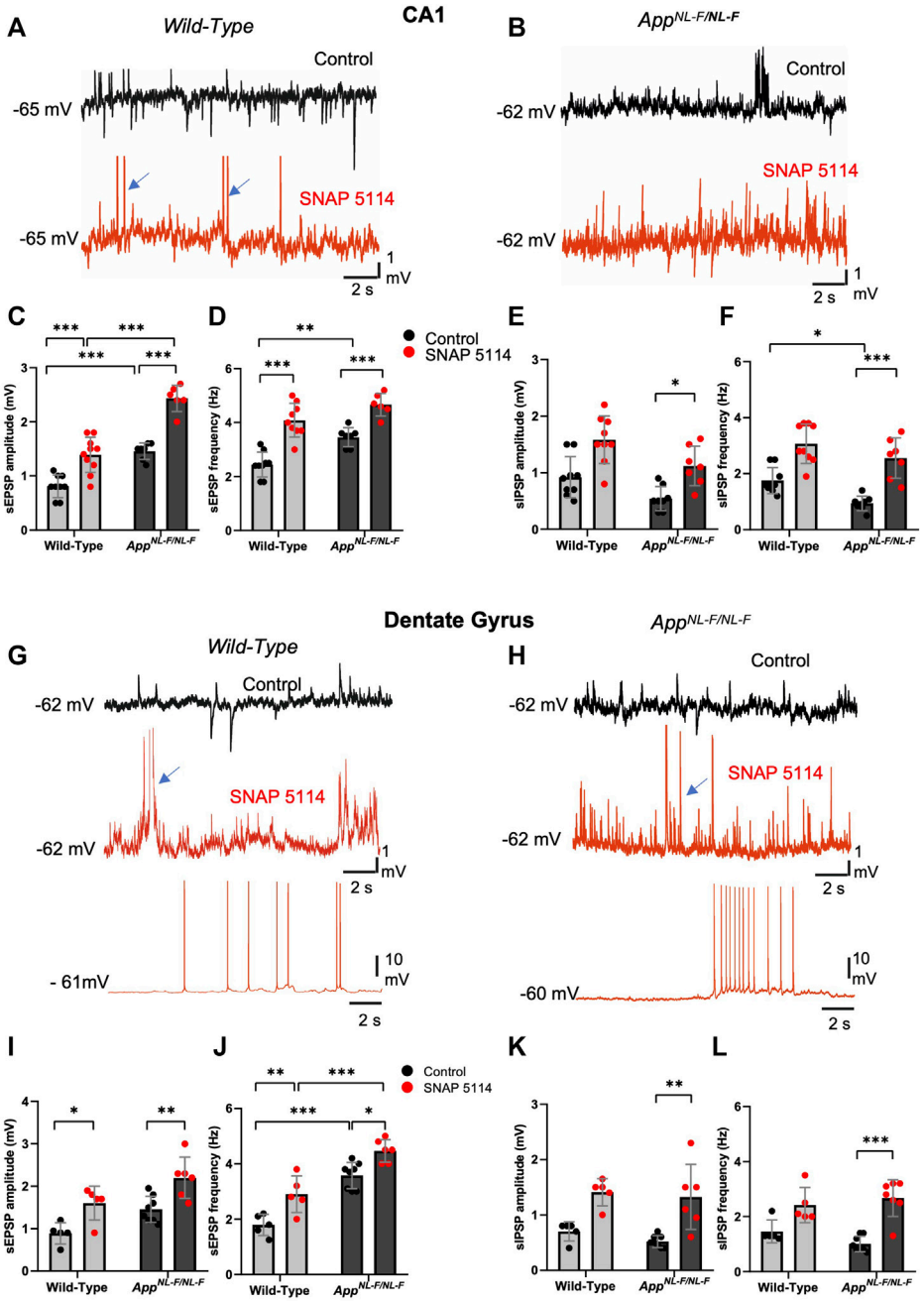

FIGURE 4 | The effect of GAT3/4 on spontaneous synaptic activity. **(A,B** and **G,H)** Whole-cell recordings of CA1 pyramidal cells and DG granule cells showing single sweep traces of spontaneous synaptic events recorded at the cells resting membrane potential, in control (black traces) and after subsequent addition bath-application of SNAP 5114 (red trace) in 12-months old wild-type and $APP^{NL\text{-}F/NL\text{-}F}$ mice. Traces show an increased level of spontaneous excitation, increased sEPSP and action potential firing with SNAP 5114 bath application in both wild-type and $APP^{NL\text{-}F/NL\text{-}F}$ mice. The blue arrows indicate truncated action potentials. **(C–F,I–L)** Graphs show frequency and amplitude of sEPSPs and sIPSPs in each of these regions in wild-type age matched to $APP^{NL\text{-}F/NL\text{-}F}$ mice recorded in control conditions and after subsequent addition of SNAP 5114 (Two-way ANOVA with multiple comparisons test, $*p \leq .05$, $**p \leq .01$, $***p \leq .001$, $****p \leq .0001$)

4 DISCUSSION

This study reveals novel data concerning the possible role of the GABA transporter GAT3/4 in AD, and provides a mechanistic insight into the pathophysiology of AD in terms of synaptic imbalance governed by astrocyte-specific mechanisms that contribute to altered background tonic inhibition in the first knock-in $APP^{NL\text{-}F/NL\text{-}F}$ mouse model of AD. Our key findings

corroborate other studies in the field, which show an enhanced inflammatory response as a result of reactive astrocytes, correlating with an elevated expression of GAD67 and GAT3/4 in hippocampal regions in AD models (Kersanté et al., 2013; Wu et al., 2014; Heneka et al., 2015; Carter et al., 2019). Nevertheless, it should be noted that while GFAP is a key component of most reactive astrocytes, its increase is not necessarily proportional to the level of inflammation especially due to the differences in basal levels of GFAP and physiological responses (Sosunov et al., 2014; Zhang et al., 2019; Escartin et al., 2021).

Our key findings firstly indicate anatomical alterations, including an elevated level of the GAD67 enzyme expressed by astrocytes. This suggests an increase in GABA production in astrocytes, correlated with elevated levels of the astrocyte-specific GAT3/4 in both CA1 and DG regions of the hippocampus in our mouse model of AD. This is consistent with our comparative studies using post-mortem human brain tissue from AD patients. It should be noted that, although some studies suggest GAT3/4 is exclusively expressed in astrocytes (Minelli et al., 1996; Lee et al., 2006), it is conceivable that these receptors are predominantly, but not exclusively expressed on astrocytes. Therefore, in the present study we have measured the expression of GAT3/4 only from astrocyte region as stained by GFAP and performed electrophysiological experiments using GAT3/4 specific pharmacological agent (Dhar et al., 2002).

Secondly, we observed a significant physiological change in synaptic balance in the hippocampus of $APP^{NL\text{-}F/NL\text{-}F}$ mouse model, which showed a higher level of baseline spontaneous synaptic excitation, reduced phasic spontaneous inhibitory events, and an increased background tonic inhibition which was revealed after blocking the GAT3/4 with SNAP-5114. These observations are known collectively as AD-associated hyperexcitation, reported in this study as well as by others (Hazra et al., 2013; Busche and Konnerth, 2016; Ghatak et al., 2019). Previously, using the $APP^{NL\text{-}F/NL\text{-}F}$ mouse model we showed that the AD-associated synaptic imbalance initiates in the entorhinal cortex, an interface for hippocampal-cortical communication, and one of the first regions to be severely affected preceding typical AD pathology. This further spreads the pathology to the CA1 and later to other cortical regions (Khan et al., 2014; Petrache et al., 2019), and corroborates preclinical imaging studies in human patients (Khan et al., 2014). We suggest that the resulting increased synaptic hyperactivity, due to disrupted glutamate levels in various cortical regions, triggers the reactive astrocytes to uptake the excess glutamate, as part of their physiological role in maintaining synaptic homeostasis. This probably leads to the subsequent conversion of the excess glutamate to GABA via the upregulated GAD67 enzyme responsible for catalysing glutamate decarboxylation. However, this is in contrast with some studies that report no significant change in the levels of overall GAD67 or its content within astrocytes using the APP/PS1 mouse model of AD, which differentially expresses Aβ42/Aβ40 expression (Jo et al., 2014) compared to the $APP^{NL\text{-}F/NL\text{-}F}$ mouse model. Furthermore, previous data shows the enhancement of the putrescine metabolic pathway for GABA production as the main mechanism for elevated GABA levels (Héja et al., 2012). Thus, the GAD pathway to produce GABA may be upregulated as an overspill mechanism which functions alongside putrescine metabolism in GABA production, however further research is necessary in knock-in models of AD.

The mechanisms by which GAT3/4 contributes to modulating tonic inhibition are complex and could emulate the multiple roles transporters play in maintaining synaptic homeostasis through interactions of neurons and astrocytes. These mechanisms are likely disrupted in pathological conditions, such as AD. Other studies have also shown the involvement of other GABA transporter (GAT1/2) in pathology such as typical absence seizures in thalamocortical neuronal circuits using genetically modified rat models (Cope et al., 2009). The alternative involvement of other GABA transporters may be due to differential expression and levels of the GABA transporters, especially GAT1 and GAT3 in the CNS. Not only this but often these different transporters may be expressed on different structures such as neuronal membranes and astrocytes respectively (Madsen et al., 2010; Zhou and Danbolt, 2013). Under healthy physiological conditions, astrocyte-specific GAT3/4 plays a role in maintaining the 'correct' extracellular environment for neuronal function and tonic inhibition, modulating network behaviour through the uptake of excess GABA from the synaptic environment. In addition, the activity of GAT3 has also been shown to inhibit neuronal glutamate release via the activation of presynaptic adenosine A1 receptors due to a rise in intracellular astrocytic Na^+ and Ca^{2+} through the Na/Ca exchange, leading to the subsequent release of ATP/Adenosine from the astrocyte (Boddum et al., 2016). Therefore, through such mechanisms, the blockade of GAT3 with SNAP in WT mice may lead to the less significant depolarization seen in our results. Furthermore, the neuropathological role of GABA transporters in astrocytes remains to be fully explored and is further complicated by the conflicting data reported previously. For example, some studies suggest that dampening of GAT3/4 transporter mechanisms results in an increase in tonic inhibition. This is evidenced either via elevating GAT3/4 activity, in a Rett syndrome rodent model, leading to a lowered tonic inhibition (Dong et al., 2020), or reducing the transporter expression, in a Parkinsonian rodent model, leading to an increase in tonic inhibition (Chazalon et al., 2018). These observations are contrary to our results in an AD model which show that the blockade of GAT3/4 results in reduced tonic inhibition in $APP^{NL\text{-}F/NL\text{-}F}$ mice in both the CA1 and DG regions, suggesting that GAT3/4 switches from 'clearing' excess extracellular GABA, to extruding GABA. This corroborates with previously published data using the 5xFAD model (Wu et al., 2014).

The differences in these observations could be related to the differential neurological disease models, and a proposed mechanism by which reversal of GAT3/4 function leading to the expulsion of GABA from the astrocytes could be related to AD-associated hyperexcitation in neurons which impact on the intra-astrocyte homeostasis. Thus, the enhanced tonic inhibition in AD may be due to the increased uptake of excess extracellular glutamate (as a direct impact of hyperexcitation) by astrocytes through EAAT1/2 co-transporters resulting in an increase in the intracellular $[Na^+]$. This has been shown to lead to a reversal of GAT3/4 channel mechanisms; resulting in the efflux and

expulsion of GABA instead of its uptake from the synaptic cleft (Héja et al., 2009, 2012; Wójtowicz et al., 2013). Our hypothesis is also supported by evidence that the blockade of EAAT in astrocytes results in elevated extracellular glutamate levels followed by neuronal death in the hippocampal CA1 and DG regions, suggesting that the elevated tonic inhibition via GAT3/4 serves as a *protective* mechanism in AD (Montiel et al., 2005; Héja et al., 2009). This is also supported by our data showing that blocking the tonic inhibition resulted with an increase in input resistance of principal cells which will raise the neuron's voltage level quicker, impacting on the resting membrane potential and in turn result in the cell being more readily available to fire action potentials, thus a more excitable state. This synaptic hyperexcitability was evident in both wild-type and AD tissue with bath application of the GAT3/4 blocker, which is not the desired outcome in a system that is altered and in a 'hyperactive' state as indicated by the differences in the resting membrane potentials observed between mice cohorts in control conditions. The increase in the amplitude and frequency of the spontaneous and inhibitory events in the present study is probably a direct outcome of the change in membrane potential favouring an increased driving force for GABA through $GABA_A$ receptors (Bonin et al., 2007; Herd et al., 2008).

Furthermore, it has been suggested that blocking the upregulated tonic inhibition mediated by α5 subunit-containing $GABA_A$ receptors was beneficial in targeting AD, as it favoured an enhancement of long-term potentiation (LTP), a recognised memory parameter (Wu et al., 2014). Our experimental protocol allowed for changes in neuronal membrane and synaptic excitability to be measured, and we consistently observed that blocking GAT3/4 in our AD model resulted in increased firing of principal cells, which could indeed lead to acute enhancement of LTP. Nevertheless, the long-term effects of this change and whether learning or memory are maintained, the pathology of AD halted, or neuronal damage exacerbated by prolonged hyperexcitation, is yet to be determined.

The mechanisms by which tonic inhibition was enhanced through $GABA_A$ receptors is an interesting point, as various neuronal sub-types of $GABA_A$ receptors have been implicated, including, the α5, α4/6 and δ-subunit-containing $GABA_A$ receptors (Caraiscos et al., 2004; Glykys et al., 2008; Lee and Maguire, 2014). It is well documented that the synaptic and extra-synaptic α5 $GABA_A$ subunit is "preserved" in AD, as shown in human tissue as well as mouse models of AD (Howell et al., 2000; Petrache et al., 2020). We have also previously shown that this receptor is upregulated in principal cells and interneurons and is responsible for the exacerbation of hyperactivity of principal neurons adding to the spread of aberrant excitation observed in AD brain tissue (Shi et al., 2020). Additionally, it has been shown that the δ subunit which is primarily correlated with the α6 and α4 subunits (Quirk et al., 1995; Jechlinger et al., 1998), is involved in tonic inhibition via slowing of the acute desensitization and recovery rate of GABA-induced currents in mouse fibroblast cells (Saxena and Macdonald, 1994). This was further established in mice where $GABA_A$ δ-subunit gene knockout caused convulsive seizures and faster decay rates of sIPSPs (Spigelman et al., 2002). However, the role that these synaptic and extra-synaptic $GABA_A$ receptor subunits play in AD pathogenesis is yet to be explored further.

In conclusion, our data are consistent with the hypothesis that AD pathogenesis in the hippocampus is associated with an elevated GABA content in reactive astrocytes, which together with an increased expression of GAT3/4 transporters may lead to an augmented tonic inhibition. Since bath-application of SNAP-5114 in our experiments, exacerbated AD-related synaptic hyperactivity (which is predicted to progress AD pathogenesis), the therapeutic inhibition of the GAT3/4 transporter in AD may be a questionable strategy.

DATA AVAILABILITY STATEMENT

The raw data supporting the conclusion of this article will be made available by the authors, without undue reservation.

ETHICS STATEMENT

The animal study was reviewed and approved by the British Home Office.

AUTHOR CONTRIBUTIONS

YA: contributed to and performed human and mouse neuroanatomical staining and confocal microscope imaging of GFAP, GAD67, and GAT3/4, and data analysis of immunofluorescence staining, and also contributed to writing the manuscript and preparation of figures. AI: performed human and mouse immunofluorescence staining and confocal image acquisition for GAT3/4, GFAP, and GAD67, post hoc recovery and reconstruction of neurons and contributed in preparing the manuscript. WZ: performed human and mouse immunofluorescence staining and confocal image acquisition for GAT3/4, GFAP, and GAD67. PW: advised on pharmacological experiments, provided the pharmacological tools and contributed to editing the manuscript. AA: designed and coordinated the project, performed all electrophysiological whole-cell recordings, supervised neuroanatomical studies, performed data analysis, and prepared the manuscript.

FUNDING

Experiments were performed using equipment funded by the UCL Alzheimer's Research UK (ARUK) Network pump priming awards (ARUK-NC2020-UCL), ARUK Drug Discovery Institution grant (ARUK DDI: 520909) and Wellcome Trust (UK) and the Medical Research Council (UK) awarded to AA (GO501263).

ACKNOWLEDGMENTS

We would like to thank Professors Takashi Saito, Takaomi C. Saido, RIKEN Center for Brain Science, Japan for the $APP^{NL-F/NL-F}$ mouse model of AD.

REFERENCES

Akiyama, H., Barger, S., Barnum, S., Bradt, B., Bauer, J., Cole, G. M., et al. (2000). Inflammation and Alzheimer's Disease. *Neurobiol. Aging* 21, 383–421. doi:10.1016/s0197-4580(00)00124-x

Boddum, K., Jensen, T. P., Magloire, V., Kristiansen, U., Rusakov, D. A., Pavlov, I., et al. (2016). Astrocytic GABA Transporter Activity Modulates Excitatory Neurotransmission. *Nat. Commun.* 7 (1 7), 13572. doi:10.1038/ncomms13572

Bonin, R. P., Martin, L. J., MacDonald, J. F., and Orser, B. A. (2007). Alpha5GABAA Receptors Regulate the Intrinsic Excitability of Mouse Hippocampal Pyramidal Neurons. *J. Neurophysiol.* 98, 2244–2254. doi:10.1152/jn.00482.2007

Burns, A., and Iliffe, S. (2009). Alzheimer's Disease. *BMJ* 338, b158–471. doi:10.1136/bmj.b158

Busche, M. A., and Konnerth, A. (2016). Impairments of Neural Circuit Function in Alzheimer's Disease. *Phil. Trans. R. Soc. B: Biol. Sci.* 371, 20150429. doi:10.1098/rstb.2015.0429

Caraiscos, V. B., Elliott, E. M., You-Ten, K. E., Cheng, V. Y., Belelli, D., Newell, J. G., et al. (2004). Tonic Inhibition in Mouse Hippocampal CA1 Pyramidal Neurons Is Mediated by Alpha5 Subunit-Containing Gamma-Aminobutyric Acid Type A Receptors. *Proc. Natl. Acad. Sci. U S A.* 101, 3662–3667. doi:10.1073/pnas.0307231101

Carter, S. F., Herholz, K., Rosa-Neto, P., Pellerin, L., Nordberg, A., and Zimmer, E. R. (2019). Astrocyte Biomarkers in Alzheimer's Disease. *Trends Mol. Med.* 25, 77–95. doi:10.1016/j.molmed.2018.11.006

Chazalon, M., Paredes-Rodriguez, E., Morin, S., Martinez, A., Cristóvão-Ferreira, S., Vaz, S., et al. (2018). GAT-3 Dysfunction Generates Tonic Inhibition in External Globus Pallidus Neurons in Parkinsonian Rodents. *Cell Rep* 23, 1678–1690. doi:10.1016/j.celrep.2018.04.014

Conti, F., Minelli, A., and Melone, M. (2004). GABA Transporters in the Mammalian Cerebral Cortex: Localization, Development and Pathological Implications. *Brain Res. Brain Res. Rev.* 45, 196–212. doi:10.1016/j.brainresrev.2004.03.003

Cope, D. W., Di Giovanni, G., Fyson, S. J., Orbán, G., Errington, A. C., Lorincz, M. L., et al. (2009). Enhanced Tonic GABAA Inhibition in Typical Absence Epilepsy. *Nat. Med.* 15 (12 15), 1392–1398. doi:10.1038/nm.2058

Delekate, A., Füchtemeier, M., Schumacher, T., Ulbrich, C., Foddis, M., and Petzold, G. C. (2014). Metabotropic P2Y1 Receptor Signalling Mediates Astrocytic Hyperactivity *In Vivo* in an Alzheimer's Disease Mouse Model. *Nat. Commun.* 5 (1 5), 5422. doi:10.1038/ncomms6422

Dhar, T. G., Borden, L. A., Tyagarajan, S., Smith, K. E., Branchek, T. A., Weinshank, R. L., et al. (2002). Design, Synthesis and Evaluation of Substituted Triarylnipecotic Acid Derivatives as GABA Uptake Inhibitors: Identification of a Ligand with Moderate Affinity and Selectivity for the Cloned Human GABA Transporter GAT-3. *J. Med. Chem.* 37, 2334–2342. Available at: https://pubs.acs.org/doi/abs/10.1021/jm00041a012 (Accessed December 29, 2021). doi:10.1021/jm00041a012

Dong, Q., Kim, J., Nguyen, L., Bu, Q., and Chang, Q. (2020). An Astrocytic Influence on Impaired Tonic Inhibition in Hippocampal CA1 Pyramidal Neurons in a Mouse Model of Rett Syndrome. *J. Neurosci.* 40, 6250–6261. doi:10.1523/JNEUROSCI.3042-19.2020

Escartin, C., Galea, E., Lakatos, A., O'Callaghan, J. P., Petzold, G. C., Serrano-Pozo, A., et al. (2021). Reactive Astrocyte Nomenclature, Definitions, and Future Directions. *Nat. Neurosci.* 24, 312–325. Available at: http://www.nature.com/articles/s41593-020-00783-4 (Accessed December 23, 2021). doi:10.1038/s41593-020-00783-4

Ghatak, S., Dolatabadi, N., Trudler, D., Zhang, X., Wu, Y., Mohata, M., et al. (2019). Mechanisms of Hyperexcitability in Alzheimer's Disease hiPSC-Derived Neurons and Cerebral Organoids vs. Isogenic Control. *eLife* 8, 50333. doi:10.7554/elife.50333

Glykys, J., Mann, E. O., and Mody, I. (2008). Which GABA(A) Receptor Subunits Are Necessary for Tonic Inhibition in the hippocampus? *J. Neurosci.* 28, 1421–1426. doi:10.1523/JNEUROSCI.4751-07.2008

Gómez-Gonzalo, M., Martin-Fernandez, M., Martínez-Murillo, R., Mederos, S., Hernández-Vivanco, A., Jamison, S., et al. (2017). Neuron-astrocyte Signaling Is Preserved in the Aging Brain. *Glia* 65, 569–580. doi:10.1002/glia.23112

Hazra, A., Gu, F., Aulakh, A., Berridge, C., Eriksen, J. L., and Žiburkus, J. (2013). Inhibitory Neuron and Hippocampal Circuit Dysfunction in an Aged Mouse Model of Alzheimer's Disease. *PLoS ONE* 8, e64318. doi:10.1371/journal.pone.0064318

Héja, L., Barabás, P., Nyitrai, G., Kékesi, K. A., Lasztóczi, B., Töke, O., et al. (2009). Glutamate Uptake Triggers Transporter-Mediated GABA Release from Astrocytes. *PLoS ONE* 4, e7153. Available at: www.plosone.org (Accessed June 17, 2021). doi:10.1371/journal.pone.0007153

Héja, L., Nyitrai, G., Kékesi, O., Dobolyi, A., Szabó, P., Fiáth, R., et al. (2012). Astrocytes Convert Network Excitation to Tonic Inhibition of Neurons. *BMC Biol.* 10, 26. doi:10.1186/1741-7007-10-26

Heneka, M. T., Carson, M. J., El Khoury, J., Landreth, G. E., Brosseron, F., Feinstein, D. L., et al. (2015). Neuroinflammation in Alzheimer's Disease. *Lancet Neurol.* 14, 388–405. doi:10.1016/S1474-4422(15)70016-5

Herd, M. B., Haythornthwaite, A. R., Rosahl, T. W., Wafford, K. A., Homanics, G. E., Lambert, J. J., et al. (2008). The Expression of GABAA Beta Subunit Isoforms in Synaptic and Extrasynaptic Receptor Populations of Mouse Dentate Gyrus Granule Cells. *J. Physiol.* 586, 989–1004. doi:10.1113/jphysiol.2007.146746

Howell, O., Atack, J. R., Dewar, D., McKernan, R. M., and Sur, C. (2000). Density and Pharmacology of Alpha5 Subunit-Containing GABA(A) Receptors Are Preserved in hippocampus of Alzheimer's Disease Patients. *Neuroscience* 98, 669–675. doi:10.1016/s0306-4522(00)00163-9

Huang, L-K., and Wang, M-J. J. (1994). Image Thresholding by Minimizing the Measures of Fuzziness. *Patttern Recognit.* 28, 41. doi:10.1016/0031-3203(94)E0043-K

Ishibashi, M., Egawa, K., and Fukuda, A. (2019). Diverse Actions of Astrocytes in GABAergic Signaling. *Int. J. Mol. Sci.* 20 (12), 2964. doi:10.3390/ijms20122964

Jechlinger, M., Pelz, R., Tretter, V., Klausberger, T., and Sieghart, W. (1998). Subunit Composition and Quantitative Importance of Hetero-Oligomeric Receptors: GABAA Receptors Containing Alpha6 Subunits. *J. Neurosci.* 18, 2449–2457. doi:10.1523/jneurosci.18-07-02449.1998

Jo, S., Yarishkin, O., Hwang, Y. J., Chun, Y. E., Park, M., Woo, D. H., et al. (2014). GABA from Reactive Astrocytes Impairs Memory in Mouse Models of Alzheimer's Disease. *Nat. Med.* 20, 886–896. doi:10.1038/nm.3639

Kersanté, F., Rowley, S. C., Pavlov, I., Gutièrrez-Mecinas, M., Semyanov, A., Reul, J. M., et al. (2013). A Functional Role for Both -aminobutyric Acid (GABA) Transporter-1 and GABA Transporter-3 in the Modulation of Extracellular GABA and GABAergic Tonic Conductances in the Rat hippocampus. *J. Physiol.* 591, 2429–2441. doi:10.1113/jphysiol.2012.246298

Khan, A. A., Shekh-Ahmad, T., Khalil, A., Walker, M. C., and Ali, A. B. (2018). Cannabidiol Exerts Antiepileptic Effects by Restoring Hippocampal Interneuron Functions in a Temporal Lobe Epilepsy Model. *Br. J. Pharmacol.* 175, 2097–2115. doi:10.1111/bph.14202

Khan, U. A., Liu, L., Provenzano, F. A., Berman, D. E., Profaci, C. P., Sloan, R., et al. (2014). Molecular Drivers and Cortical Spread of Lateral Entorhinal Cortex Dysfunction in Preclinical Alzheimer's Disease. *Nat. Neurosci.* 17, 304–311. doi:10.1038/nn.3606

Kojima, S., Nakamura, T., Nidaira, T., Nakamura, K., Ooashi, N., Ito, E., et al. (1999). Optical Detection of Synaptically Induced Glutamate Transport in Hippocampal Slices. *J. Neurosci.* 19, 2580–2588. doi:10.1523/jneurosci.19-07-02580.1999

Lee, M., Schwab, C., and Mcgeer, P. L. (2011). Astrocytes Are GABAergic Cells that Modulate Microglial Activity. *Glia* 59, 152–165. doi:10.1002/glia.21087

Lee, T. S., Bjørnsen, L. P., Paz, C., Kim, J. H., Spencer, S. S., Spencer, D. D., et al. (2006). GAT1 and GAT3 Expression Are Differently Localized in the Human Epileptogenic hippocampus. *Acta Neuropathol.* 111, 351–363. Available at: https://pubmed.ncbi.nlm.nih.gov/16456667/(Accessed December 29, 2021). doi:10.1007/s00401-005-0017-9

Lee, V., and Maguire, J. (2014). The Impact of Tonic GABAA Receptor-Mediated Inhibition on Neuronal Excitability Varies across Brain Region and Cell Type. *Front. Neural Circuits* 8, 3. doi:10.3389/fncir.2014.00003

Lehre, K. P., and Danbolt, N. C. (1998). The Number of Glutamate Transporter Subtype Molecules at Glutamatergic Synapses: Chemical and Stereological Quantification in Young Adult Rat Brain. *J. Neurosci.* 18, 8751–8757. doi:10.1523/jneurosci.18-21-08751.1998

Lines, J., Baraibar, A. M., Fang, C., Martin, E. D., Aguilar, J., Lee, M. K., et al. (2022). Astrocyte-neuronal Network Interplay Is Disrupted in Alzheimer's Disease Mice. *Glia* 70 (2), 368–378. doi:10.1002/glia.24112

Liu, Q. R., López-Corcuera, B., Mandiyan, S., Nelson, H., and Nelson, N. (1993). Molecular Characterization of Four Pharmacologically Distinct Gamma-Aminobutyric Acid Transporters in Mouse Brain [corrected]. *J. Biol. Chem.* 268, 2106–2112. doi:10.1016/s0021-9258(18)53968-5

Madsen, K. K., White, H. S., and Schousboe, A. (2010). Neuronal and Non-neuronal GABA Transporters as Targets for Antiepileptic Drugs. *Pharmacol. Ther.* 125, 394–401. doi:10.1016/j.pharmthera.2009.11.007

McGrath, J. C., Drummond, G. B., McLachlan, E. M., Kilkenny, C., and Wainwright, C. L. (2010). Guidelines for Reporting Experiments Involving Animals: The ARRIVE Guidelines. *Br. J. Pharmacol.* 160, 1573–1576. doi:10.1111/j.1476-5381.2010.00873.x

Medeiros, R., and LaFerla, F. M. (2013). Astrocytes: Conductors of the Alzheimer Disease Neuroinflammatory Symphony. *Exp. Neurol.* 239, 133–138. doi:10.1016/j.expneurol.2012.10.007

Minelli, A., DeBiasi, S., Brecha, N. C., Zuccarello, L. V., and Conti, F. (1996). GAT-3, a High-Affinity GABA Plasma Membrane Transporter, Is Localized to Astrocytic Processes, and it Is Not Confined to the Vicinity of GABAergic Synapses in the Cerebral Cortex. *J. Neurosci.* 16, 6255–6264. Available at: https://www.jneurosci.org/content/16/19/6255 (Accessed December 29, 2021). doi:10.1523/jneurosci.16-19-06255.1996

Montiel, T., Camacho, A., Estrada-Sánchez, A. M., and Massieu, L. (2005). Differential Effects of the Substrate Inhibitor L-Trans-Pyrrolidine-2,4-Dicarboxylate (PDC) and the Non-substrate Inhibitor DL-Threo-Beta-Benzyloxyaspartate (DL-TBOA) of Glutamate Transporters on Neuronal Damage and Extracellular Amino Acid Levels in Rat Brain *In Vivo*. *Neuroscience* 133, 667–678. doi:10.1016/j.neuroscience.2004.11.020

Nam, M. H., Cho, J., Kwon, D. H., Park, J. Y., Woo, J., Lee, J. M., et al. (2020). Excessive Astrocytic GABA Causes Cortical Hypometabolism and Impedes Functional Recovery after Subcortical Stroke. *Cel Rep* 32, 107975. doi:10.1016/j.celrep.2020.107975

Parpura, V., Basarsky, T. A., Liu, F., Jeftinija, K., Jeftinija, S., and Haydon, P. G. (1994). Glutamate-mediated Astrocyte-Neuron Signalling. *Nature* 369, 744. doi:10.1038/369744a0

Patel, D. C., Tewari, B. P., Chaunsali, L., and Sontheimer, H. (2019). Neuron-glia Interactions in the Pathophysiology of Epilepsy. *Nat. Rev. Neurosci.* 20, 282–297. doi:10.1038/s41583-019-0126-4

Petrache, A. L., Khan, A. A., Nicholson, M. W., Monaco, A., Kuta-Siejkowska, M., Haider, S., et al. (2020). Selective Modulation of α5 GABAA Receptors Exacerbates Aberrant Inhibition at Key Hippocampal Neuronal Circuits in APP Mouse Model of Alzheimer's Disease. *Front Cel Neurosci* 14, 568194. doi:10.3389/fncel.2020.568194

Petrache, A. L., Rajulawalla, A., Shi, A., Wetzel, A., Saito, T., Saido, T. C., et al. (2019). Aberrant Excitatory-Inhibitory Synaptic Mechanisms in Entorhinal Cortex Microcircuits during the Pathogenesis of Alzheimer's Disease. *Cereb. Cortex* 29, 1834–1850. doi:10.1093/cercor/bhz016

Quirk, K., Whiting, P. J., Ragan, C. I., and McKernan, R. M. (1995). Characterisation of delta-subunit Containing GABAA Receptors from Rat Brain. *Eur. J. Pharmacol.* 290, 175–181. doi:10.1016/0922-4106(95)00061-5

Reid, H. M. O., Chen-Mack, N., Snowden, T., and Christie, B. R. (2021). Understanding Changes in Hippocampal Interneurons Subtypes in the Pathogenesis of Alzheimer's Disease: A Systematic Review. *Brain Connect.* 11, 159–179. doi:10.1089/brain.2020.0879

Ribak, C. E., Tong, W. M. Y., and Brecha, N. C. (1996). GABA Plasma Membrane Transporters, GAT-1 and GAT-3, Display Different Distributions in the Rat Hippocampus. *J Comp Neurol.* 367, 595. doi:10.1002/(SICI)1096-9861(19960415)367:4<595:AID-CNE9>3.0.CO;2-#

Rice, H. C., Marcassa, G., Chrysidou, I., Horré, K., Young-Pearse, T. L., Müller, U. C., et al. (2020). Contribution of GABAergic Interneurons to Amyloid-β Plaque Pathology in an APP Knock-In Mouse Model. *Mol. Neurodegener* 15, 3. doi:10.1186/s13024-019-0356-y

Saito, T., Matsuba, Y., Mihira, N., Takano, J., Nilsson, P., Itohara, S., et al. (2014). Single App Knock-In Mouse Models of Alzheimer's Disease. *Nat. Neurosci.* 17, 661–663. doi:10.1038/nn.3697

Saxena, N. C., and Macdonald, R. L. (1994). Assembly of GABAA Receptor Subunits: Role of the delta Subunit. *J. Neurosci.* 14, 7077–7086. doi:10.1523/jneurosci.14-11-07077.1994

Shi, A., Petrache, A. L., Shi, J., and Ali, A. B. (2020). Preserved Calretinin Interneurons in an App Model of Alzheimer's Disease Disrupt Hippocampal Inhibition via Upregulated P2Y1 Purinoreceptors. *Cereb. Cortex* 30, 1272–1290. doi:10.1093/cercor/bhz165

Sosunov, A. A., Wu, X., Tsankova, N. M., Guilfoyle, E., McKhann, G. M., and Goldman, J. E. (2014). Phenotypic Heterogeneity and Plasticity of Isocortical and Hippocampal Astrocytes in the Human Brain. *J. Neurosci.* 34, 2285–2298. Available at: https://www.jneurosci.org/lookup/doi/10.1523/JNEUROSCI.4037-13 (Accessed December 23, 2021). doi:10.1523/JNEUROSCI.4037-13.2014

Spigelman, I., Li, Z., Banerjee, P. K., Mihalek, R. M., Homanics, G. E., and Olsen, R. W. (2002). Behavior and Physiology of Mice Lacking the GABAA-Receptor delta Subunit. *Epilepsia* 43, 3–8. doi:10.1046/j.1528-1157.43.s.5.8.x

Stelzma, R. A., Norman Schnitzlein, H., and Murllagh, F. R. (1995). An English I'ranslation of Alzheimer's 1907 Paper, "ijber eine eigenartige Erlranliung der Hirnrinde. *Clin. Anat.* 8, 429. doi:10.1002/ca.980080612

WHO (2017). *Global Action Plan on the Public Health Response to Dementia 2017-2025*. Geneva, Switzerland: WHO Document Production Services.

Wójtowicz, A. M., Dvorzhak, A., Semtner, M., and Grantyn, R. (2013). Reduced Tonic Inhibition in Striatal Output Neurons from Huntington Mice Due to Loss of Astrocytic GABA Release through GAT-3. *Front. Neural Circuits* 7, 188. doi:10.3389/fncir.2013.00188

Wu, Z., Guo, Z., Gearing, M., and Chen, G. (2014). Tonic Inhibition in Dentate Gyrus Impairs Long-Term Potentiation and Memory in an Alzheimer's [corrected] Disease Model. *Nat. Commun.* 5, 4159. Available at: http://www.nature.com/articles/ncomms5159. doi:10.1038/ncomms5159

Xu, Y., Zhao, M., Han, Y., and Zhang, H. (2020). GABAergic Inhibitory Interneuron Deficits in Alzheimer's Disease: Implications for Treatment. *Front. Neurosci.* 14, 660. doi:10.3389/fnins.2020.00660

Zhang, Z., Ma, Z., Zou, W., Guo, H., Liu, M., Ma, Y., et al. (2019). The Appropriate Marker for Astrocytes: Comparing the Distribution and Expression of Three Astrocytic Markers in Different Mouse Cerebral Regions. *Biomed. Res. Int.* 2019, 9605265. Available at: https://www.hindawi.com/journals/bmri/2019/9605265/(Accessed August 18, 2021). doi:10.1155/2019/9605265

Zhou, Y., and Danbolt, N. C. (2013). GABA and Glutamate Transporters in Brain. *Front. Endocrinol. (Lausanne)* 4, 165. doi:10.3389/fendo.2013.00165

Conflict of Interest: The authors declare that the research was conducted in the absence of any commercial or financial relationships that could be construed as a potential conflict of interest.

Publisher's Note: All claims expressed in this article are solely those of the authors and do not necessarily represent those of their affiliated organizations, or those of the publisher, the editors and the reviewers. Any product that may be evaluated in this article, or claim that may be made by its manufacturer, is not guaranteed or endorsed by the publisher.

frontiers in Neuroscience

ORIGINAL RESEARCH
published: 11 February 2022
doi: 10.3389/fnins.2022.792970

Bee Venom Effect on Glioblastoma Cells Viability and Gelatinase Secretion

Agata Małek[1], Joanna Kocot[1], Kamila Mitrowska[2], Andrzej Posyniak[2] and Jacek Kurzepa[1]**

[1] Department of Medical Chemistry, Medical University of Lublin, Lublin, Poland, [2] Department of Pharmacology and Toxicology, National Veterinary Research Institute, Puławy, Poland

Background: The involvement of MMP-2 and MMP-9 in the pathogenesis of various kinds of cancers including glioblastoma is well documented. The evaluation of the anticancer potential of honey bee (*Apis mellifera*) venom (BV) consisting of the inhibition of MMP-2 and MMP-9 secretion in a glioblastoma cell culture model was the aim of the study.

Methods: 8-MG-BA and GAMG human primary glioblastoma cell lines vs. HT-22 mouse hippocampal neuronal cells were applied for the study. The BV dose (0.5, 1.0, 1.25, 1.5, 1.75, 2.0, 2.5, and 5.0 μg/ml) and time-dependent (24, 48, 72 h) cytotoxicity was evaluated with the tetrazolium-based colorimetric assay (MTT test). MMP-2 and MMP-9 activities in the cell culture medium under different BV concentrations were determined by gelatin zymography.

Results: A dose and time-dependent BV effect on cytotoxicity of both glioblastoma cell lines and hippocampus line was observed. The weakest, but statistically important effect was exerted by BV on HT-22 cells. The greatest cytotoxic effect of BV was observed on the 8-MG-BA line, where a statistically significant reduction in viability was observed at the lowest BV dose and the shortest incubation time. The reduction of both gelatinases secretion was observed at 8-MG-BA and GAMG lines without significant effect of HT-22 cell line.

Conclusion: *In vitro* studies indicate that BV has both cytotoxic and inhibitory effects on the secretion of MMP-2 and MMP-9 in selected lines of glioma, suggesting anticancer properties of BV.

Keywords: bee venom, glioblastoma, anticancer potential, MMP-2, MMP-9

OPEN ACCESS

Edited by:
Riham Salah El Dine, Cairo University, Egypt

Reviewed by:
Josipa Vlainic, Rudjer Boskovic Institute, Croatia
Xiangping Chu, University of Missouri–Kansas City, United States

****Correspondence:***
Agata Małek
a.malek9506@gmail.com
Jacek Kurzepa
kurzepa@yahoo.com

Specialty section:
This article was submitted to Neuropharmacology, a section of the journal Frontiers in Neuroscience

Received: *11 October 2021*
Accepted: *24 January 2022*
Published: *11 February 2022*

Citation:
Małek A, Kocot J, Mitrowska K, Posyniak A and Kurzepa J (2022) Bee Venom Effect on Glioblastoma Cells Viability and Gelatinase Secretion. Front. Neurosci. 16:792970. doi: 10.3389/fnins.2022.792970

INTRODUCTION

Clinically, the classification of gliomas includes four grades, with grade four glioblastoma representing the most malignant type and also known as glioblastoma multiforme (GBM) (Atiq and Parhar, 2020). GBM is a highly aggressive brain tumor. Different grade GBMs are the most frequent primary malignant brain tumors (15% of all intracranial neoplasms and up to 50% of all primary malignant brain tumors) (Linhares et al., 2020). Despite significant progress in GBM treatment

research, it remains a great therapeutic challenge. Current treatment methods include surgical tumor resection with chemotherapy and radiotherapy thereafter. However, even with advanced surgical techniques such as e.g., fluorescence-guided resection, the complete removal of cancer cells is almost impossible because tumor cells located at the edges of tumors in perivascular niches remain in most cases (Atiq and Parhar, 2020). Therefore, the new kind of therapy together with the applying of various natural compounds seems to be an interesting research topic that gives hope for finding an effective treatment for glioblastoma. Bee venom (BV) is a biotoxin (apitoxin) synthesized and secreted by a venom gland placed in the abdominal cavity of a bee. BV is a complex mixture containing several biologically active components with a variety of pharmaceutical properties (Rady et al., 2017; Carpena et al., 2020). The most prevalent component of BV is a representative polypeptide group—melittin, composed of 26 amino acids. Phospholipase A_2 (PLA_2) is believed to be the second most abundant one (Choo et al., 2010; Sciani et al., 2010; Lee et al., 2016), while the third component is apamine (Rady et al., 2017). In BV samples collected from honey bees (*Apis mellifera*) in Poland, the content of the mentioned substances has been amounted to 61.15–70.15% (average 64.40%) for melittin, 11.24–15.05% (average 13.00%) for PLA_2 and 2.09–4.18% (average 3.10%) for apamine (Rybak-Chmielewska and Szczęsna, 2006).

The anticancer properties or the ability to prevent the chemotherapy-induced side effects of BV as well as its selective components have already been reported. Jamasbi et al. (2018) have revealed the effectiveness of melittin against gastric cancer cells. The authors compared the monomeric form of this peptide with its dimer form and found the former being more cytotoxic at low concentrations (1–5 μM), while at higher concentrations (10 μM) the cytotoxic effect of both forms was comparable. Kim et al. (2015), in turn, proved that PLA_2 could prevent inflammatory responses in cisplatin-induced acute kidney injury. According to Zhou et al. (2013) both melittin and apamine have been shown to trigger apoptotic cell death in hepatocellular carcinoma cells (HepG2). Zheng et al. (2015) in turn, suggested that BV could inhibit colon cancer cell growth, and its antiproliferative effect may be related to the induction of apoptosis by activation of DR4 and DR5 and inhibition of NF-κB signaling pathway.

When considering the therapeutic properties of BV components against the tumor located within the Central Nervous System (CNS), their ability to penetrate the blood-brain barrier (BBB) should be especially considered. Earlier studies show that both apamine and melittin have the ability to cross the BBB, which allows the BV components to be considered as chemical compounds with potential therapeutic properties exhibiting activity within the CNS (Upadhyay, 2014; Wehbe et al., 2019).

Matrix metalloproteinases (MMPs), including gelatinases (MMP-2 and MMP-9), exert pleiotropic effects under pathological and physiological conditions (Boguszewska-Czubara et al., 2019; Drankowska et al., 2019). MMPs also play a key role in cancer invasion and metastasis. Many studies have reported elevated MMPs expression and/or activity in cancer cells that metastasize to distant organs including the lungs, liver, lymph nodes, or adrenal medullary (Yelken et al., 2017). MMP-9 has been considerably involved in glioblastoma progression. Its overexpression correlates with increased invasive glioma grades, whereas a decrease of MMP-9 expression is associated with favorable outcome and response to Temozolomide treatment (Quesnel et al., 2020). Zhang et al. (2019) reported the positive expression of MMP-2 in glioma was closely related to the tumor diameter, severity of peritumoral edema, degree of enhancement, and pathological grade of tumor observed in magnetic resonance imaging (MRI). In addition, MMP-2 was highly expressed in brain glioma, and it was considered as a negative factor for prognosis (Zhang et al., 2019).

In the available literature data, studies evaluating the ability of BV to inhibit glioblastoma cell growth and metastasis are scarce. Considering this fact, the aim of the current study was to examine the *in vitro* influence of BV on cell viability and the BV induced secretion of MMP-2 and MMP-9 by glioblastoma cell lines (GAMG, 8-MG-BA) vs. hippocampal cells (HT-22).

MATERIALS AND METHODS

Bee Venom

Samples of *Apis mellifera* bee venom were collected from a private apiary located in Siedliszcze (Lublin region, Eastern Poland), by stimulating the bees with electric current pulses using Bee Venom Collector BVC 5.0 2017 (IGK Electronics Ltd., Varna, Bulgaria). The general scheme of bee venom collection procedure was illustrated by in Ref. (Carpena et al., 2020). The samples collected between May and September 2017 were pooled together and stored in the dark at 5°C until analysis (Rybak-Chmielewska and Szczęsna, 2006; Kokot et al., 2009). The bee venom stock solution of 1 mg/ml in PBS was prepared, vortexed for 1 min, sonicated for 10 min, and filtered (Matysiak et al., 2011). The stock solutions were prepared directly before each experiment and then diluted in a complete medium to obtain the required concentration.

The Determination of Melittin Content in the Bee Venom Sample

The determination of melittin content was performed in Department of Pharmacology and Toxicology of the National Veterinary Research Institute (Poland) by liquid chromatography with tandem mass spectrometry (LC-MS/MS) according to the method of Zhou et al. (2010) with some modifications. Briefly, the bee venom sample (2 mg) was weighed and dissolved in 1 ml of water followed by vortexing for 5 min. Next, the tube was centrifuged at 10,000 rpm at 4°C for 10 min. The supernatant was filtered through a 0.22-μm nylon syringe filter and diluted 100 times with 0.1% formic acid before the LC-MS/MS analysis. For separation and identification of melittin in BV extract, an ExionLC AC system consisting of a binary gradient pump, autosampler, column oven, and system controller coupled to QTRAP 5,500 linear ion trap quadrupole mass spectrometer (AB Sciex) with electrospray ionization (ESI) interface was used. Data acquisition and analysis were accomplished with Analyst 1.6.3. Mass spectrometric analysis was performed in positive ESI mode. The following instrument conditions were used: ion

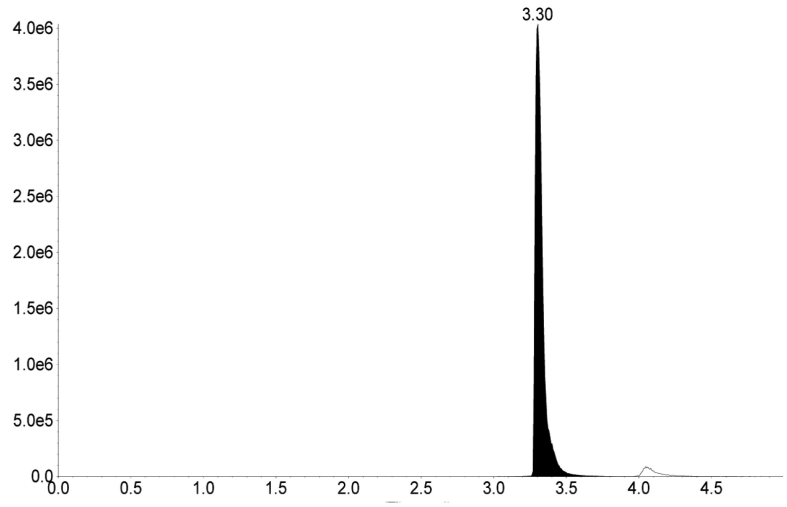

FIGURE 1 | MRM chromatogram of melittin (m/z 712.8–> 70.0) in the bee venom sample.

source temperature 300°C, curtain gas 20 psi, nebulizer gas 50 psi, heater gas 60 psi, ion spray voltage 3,500 V. Quantitation of analyte was performed by monitoring the following SRM transitions: m/z 712.8–> 70.0, collision energy 140 V with dwell time 100 ms. The chromatographic separation was performed on a Kinetex octadecyl analytical column (2.6 μm, 150 × 2.1 mm) with an octadecyl guard cartridge (Phenomenex, Torrance, CA, United States). The mobile phase A consisted of 0.1% formic acid in acetonitrile, while the mobile phase B contains 0.1% formic acid in water. Linear gradient steps were used with initial conditions set at 5% of the mobile phase A, held for 0.5 min, increasing to 95% from 0.51 to 2.00 min, and then returned to the initial composition of the mobile phase A (5%) from 2.01 to 5.00 min. The flow rate of the mobile phase was 0.25 ml/min. The column temperature was 30°C and the injection volume was 5 μ l.

Cell Culture

The human glioblastoma cell lines were obtained from Leibniz Institute, DSMZ—German Collection of Microorganisms and Cells Cultures GmbH (GAMG—ACC 242; 8-MG-BA—ACC 432). As control cells, immortalized mouse hippocampal cell line, HT-22 (Sigma Aldrich, Saint Louis, MO, United States) was used. The cells were cultured in Dulbecco's Modified Eagle Medium (DMEM), GAMG and HT-22 and in Eagle's Minimum Essential Medium (EMEM)—8-MG-BA, supplemented with 10% (v/v) fetal bovine serum, penicillin (10,000 U/ml), streptomycin (10 mg/ml) and amphotericin B (250 μg/ml). The cells were incubated at 37°C, 5% CO_2 atmosphere. The cells were maintained in the logarithmic growth phase by regular passage at 80% confluence.

Cell Viability Assay

The cytotoxicity of the bee venom was studied against human glioblastoma cell lines (GAMG and 8-MG-BA) vs. neuronal (hippocampal) cell line (HT-22) used as a control line. After 24-h incubation in growth medium with an addition of 10% fetal bovine serum (FBS) on 96-well plates, the cells were treated with the following concentrations of bee venom: 0 (vehicle), 0.5, 1.0, 1.25, 1.5, 1.75, 2.0, 2.5, and 5.0 μg/ml in medium without FBS. The cells were cultured at 37°C in the presence of 5% CO_2-air for the next 24, 48, and 72 h. The bee venom cytotoxicity was evaluated using the MTT colorimetric method based on the ability of viable cells to the transformation of yellow, soluble tetrazolium salts [3-(4,5-dimethylthiazol-2-yl)-2,5-diphenyltetrazolium bromide, MTT] to purple insoluble formazan, by cellular dehydrogenases. After incubation with bee venom solution, cell cultures were supplemented with 10 μl per well of 5 mg/ml MTT (Sigma-Aldrich, Saint Louis, MO, United States) stock in PBS, and the incubation was continued for 4 h at 37°C. Next, the medium with MTT was removed, and the formed crystals were dissolved in 100 μl of DMSO. The solution absorbance was measured at 570 nm, using a spectrophotometric plate reader Epoch, BioTek Instruments (Vermont, United States). The relative cytotoxic activity was determined as the amount of bee venom capable of reducing 50% of cell viability (IC50 value). The experiment was performed three times with triplicates for each concentration.

Analysis of Matrix Metalloproteinase-2 and Matrix Metalloproteinase-9 Activity in Cell Culture Supernatants

After 72-h incubation with the following concentration of BV 1.0, 1.5, 2.0, 2.5, 5.0 μl/ml, the media from the cells were collected to measure the secreted MMP-2 and MMP-9 activities. The concentrations of BV used for MMPs analysis as well as the 72 h incubation time were chosen on the base of the cell viability assay. The experiment was performed three times with duplicates for each concentration (n = 6). MMP-2 and MMP-9 activities were evaluated with the use of gelatin zymography according to previously applied methods (Golab et al., 2014). Briefly, 80 μl of cell culture media was mixed with 20 μL of

sample loading buffer containing 10% sodium dodecyl sulfate (SDS) and incubated for 30 min at room temp. Next, the proteins were separated by polyacrylamide gel electrophoresis (PAGE) on a 10% gel supplemented with 0.05% gelatin type A from porcine skin; G2500 (Sigma-Aldrich, St. Louis, MO, United States). After electrophoresis, the gels were washed with 2.5% Triton X-100 three times for 20 min each to remove SDS. Next, 48-h-incubation was performed at 37°C in the buffer pH 7.2 containing 1% Triton X-100. The gels were stained with the solution containing 0.1% Coomassie Blue R-250, 20% methanol, and 10% glacial acetic acid in distilled water and destained in 10% solution of acetic acid thereafter. The MMP-2 and MMP-9 were detected as colorless bands (digested gelatin) on a blue background (undigested gelatin). Zymography allows detecting both pro-active (latent) and active forms of MMPs as the SDS is used to activate non-proteolytic pro-MMPs into MMPs with catalytical activity without changing their molecular mass. The enzymes were identified by comparing their localization with molecular mass standards (SM0441) (Fermentas Life Sciences, St. Leon-Rot, Germany). Zymographic gels were scanned and quantified with ImageJ software (National Institute of Health, Bethesda, MD, United States). The activities of MMP-2 and MMP-9 were expressed as the optical density (OD) of the substrate lysis zone.

Statistical Analysis

Statistical analysis was performed using GraphPad Prism 8 software. Non-linear regression (curve fit) was used to establish IC50 values of BV after 24, 48, and 72 h of incubation for all three cell lines. The results of cells viability were expressed as mean values as well as standard deviation, and the statistical significance of the differences between the control vehicle and the other groups of each three cell lines in 3 time points was evaluated using a two-way analysis of variance (ANOVA) followed by Tukey's *post-hoc* test. Values were considered significant with $p < 0.05$.

RESULTS

Melittin Content in Bee Venom

Melittin content in the bee venom sample was found to be 69.0 ± 0.1% of dry weight (**Figure 1**).

The Effect of Bee Venom on Cells Viability *in vitro* (IC50 Estimation)

To analyze the effect of BV on cells viability, the inhibitory concentration of BV (IC50) was assessed depending on the incubation time; 24, 48, and 72 h. The most significant time-dependent effect of BV was observed on GAMG cells, where the increase of incubation time from 24 to 72 h decreased the IC50 from 1.519 to 0.274 ng/ml (more than 5-fold reduction in BV dose when incubated for 72 vs. 24 h). The lowest value of BV IC50 after 24 h incubation was noticed for 8-MG-BA cells (0.7027 ng/ml). IC50 for these cells did not change significantly after longer incubation times (0.6998 and 0.6527 ng/ml after 48 and 72 h, respectively). The highest IC50 value of BV was noticed for HT-22 cells at each of the time intervals, suggesting the low sensitivity of these cells to BV. The increase of incubation time from 24 to 72 h resulted in the decrease of IC50 value for HT-22 from 2.259 ng/ml to 1.383 ng/ml for HT-22 cells. All results were expressed in **Figure 2**.

The Bee Venom Effect on Matrix Metalloproteinase-2 and Matrix Metalloproteinase-9 Secretion

The dose-dependent effect of BV on MMP-2 and MMP-9 secretion from GAMG and 8-MG-BA cells was revealed. After 72 h of incubation with BV at concentration 1.5 μl/ml and higher, the significant reduction of MMP-2 and MMP-9 secretion from GAMG cells was noticed. Similar inhibitory effect was observed on 8-MG-BA cells, however, a statistical significant reduction of gelatinase secretion was already observed at BV concentration of 1.0 μl/ml. There was no significantly visible effect of BV on MMP-2 and MMP-9 secretion from HT-22 cells at any analyzed concentrations. The representative zymograms were shown in **Figure 3**.

DISCUSSION

Among the various agents that influence the development, progression, and metastasis of cancer, there are many natural compounds that have pleiotropic properties and possess chemopreventive potential, e.g., soybean isoflavones, curcumin, retinoids, resveratrol, epigallocatechin or cannabinoids. Some effects of them are well documented in the literature, for example, curcumin, resveratrol are known as strong antioxidants. The anticancer potential of the remaining compounds requires further research, as is the case with, for example, cannabinoids; animal studies showed that the activation of cannabinoid receptors 1 and 2 by tetrahydrocannabinol (THC) results in impaired proliferation and invasion of cancer cells, induces apoptosis (accumulation of ceramides in culture), and further reduces the tumor volume (McAllister et al., 2005; Galanti et al., 2008; Marcu et al., 2010; Abrams, 2016). Therapeutic administration of bee venom to treat various diseases, initially primarily arthritis or ailments related to joints and muscles, has been used in traditional Chinese medicine from 1,000 to 3,000 BC (Zhang et al., 2018). The application of BV is widespread in the treatment of not only immune-mediated diseases but also cancer. Both *in vitro* and *in vivo* studies have confirmed that the main BV constituent, melittin, is responsible not only for the cytotoxic effect, but also for the immunomodulatory and proapoptotic effect against various types of cancer cells (Oršolić, 2012). BV has been shown to have an antiproliferative effect on cancer cells via several mechanisms. It induces apoptosis through the activation of death DR4 and DR5 death receptors. In addition, melittin reduces tumor growth and metastasis (Liu et al., 2002). BV inhibits cancer cells growing also due to the activation of caspase 3 and 9 pathways and inhibition of NF-κB pathway signaling, leading to inhibition of the expression of proliferative and antiapoptotic genes encoding Bcl-2, cyclooxygenase-2 (COX-2),

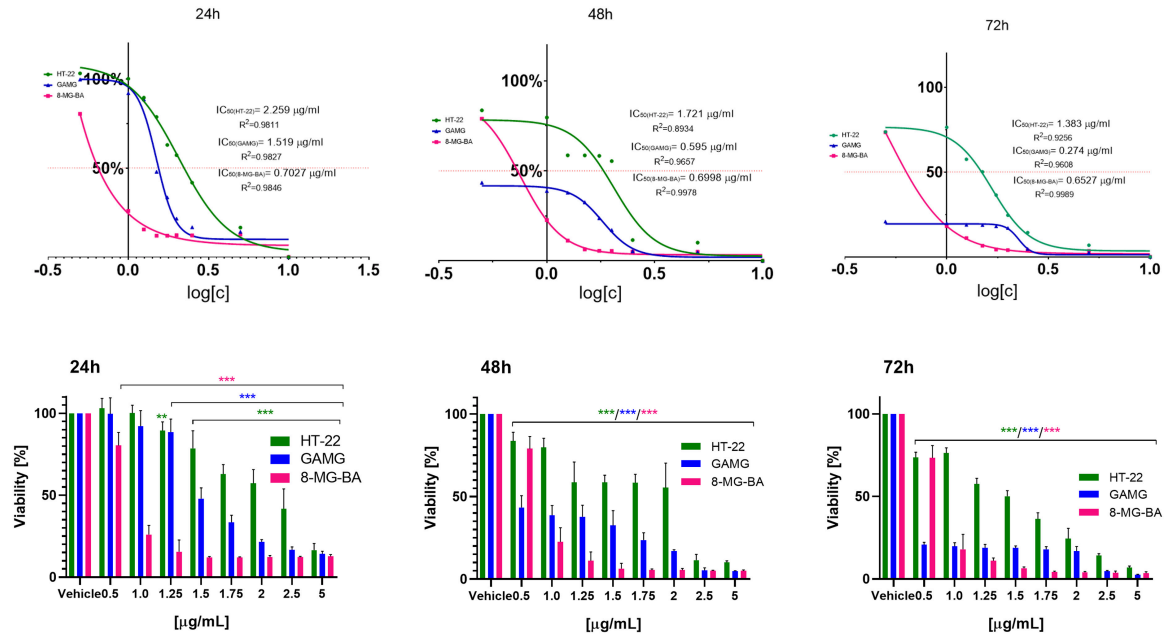

FIGURE 2 | The IC50 values (µg/ml) and cells viability (%) regarding GAMG, 8-MG-BA and HT-22 cells after 24, 48, and 72 h of incubation with BV; $^{**}p < 0.01$, $^{***}p < 0.001$ vs. GAMG, 8-MG-BA and HT-22 vehicle, respectively; Tukey test.

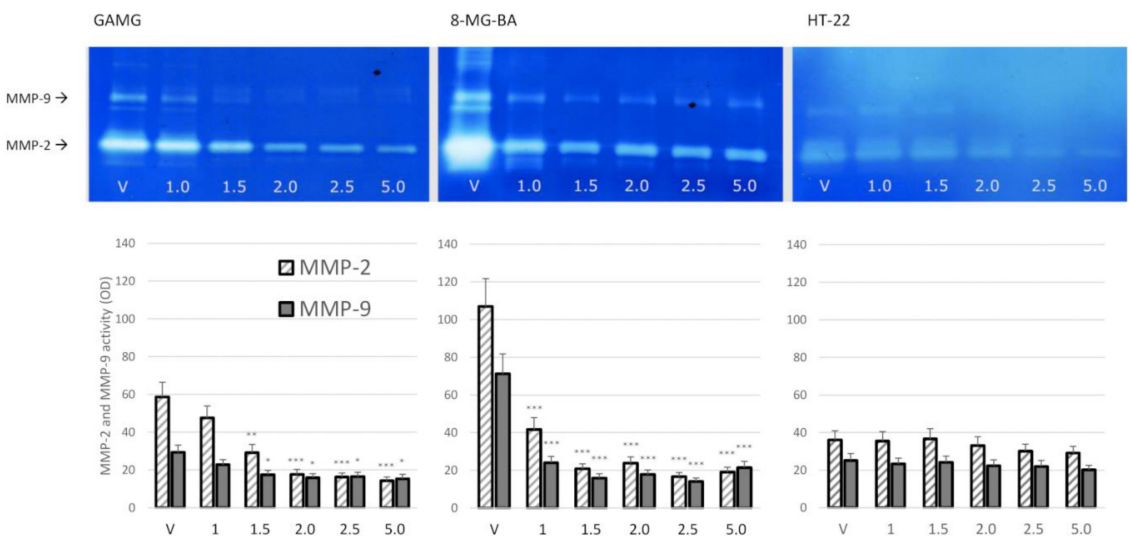

FIGURE 3 | BV effect on MMP-2 and MMP-9 secretion from GAMG, 8-MG-BA, and HT-22 cells. Significant decrease of gelatinase secretion was observed in GAMG and 8-MG-BA cells after 72 h of incubation with different concentrations of BV. The effect of BV on MMP-2 and MMP-9 secretion from HT-22 cells did not reach statistical significance. ANOVA with Tukey *post-hoc* test. $^{*}p < 0.05$, $^{**}p < 0.01$, $^{***}p < 0.01$ compared to controls (V, vehiculum).

cellular inhibitor of apoptosis 2 (cIAP-2), inducible nitric oxide synthase (iNOS) and cytosolic phospholipase A2 (cPLA2) (Park et al., 2014).

Finally, it is worth emphasizing that the potential of BV in the treatment of SARS-CoV-2 infections has also recently been recognized. It has been noted that in Wuhan, China, beekeepers, as a group exposed to frequent bee bites, are more resistant to COVID-19 infection, probably due to regulation of the immune response, which can cause an increase in the titer of IgE and IgG antibodies (Kasozi et al., 2020).

The obtained results showed a statistically significant effect of unfractionated bee venom on the viability of glioblastoma cells and physiological hippocampal cells. The observed effect was different for each cell type tested. Earlier reports indicated different chemosensitivity of glioblastoma cell lines (Wolff et al., 1999). Glioblastoma cell malignancy and drug sensitivity are

related to the cell of origin; nervous stem cell-like origin causes higher malignancy and drug sensitivity than others (Jiang et al., 2017). After an incubation time of 24 h, 8-MG-BA was proved to be more sensitive cells to BV effects than other tested cell lines; during each applied concentration of BV, the viability of 8-MG-BA cells was the lowest among the analyzed configurations. Moreover, the IC50 for BV was the lowest after 24 h incubation with respect to 8-MG-BA cells. However, after 48 h of incubation, the viability of GAMG cells significantly decreased. The IC50 for GAMG decreased threefold compared to the 24 h incubation and was less than the IC50 for 8-MG-BA after 48 h incubation. Extending the incubation time to 72 h did not significantly affect the IC50 value for 8-MG-BA cells, however, a decrease in IC50 for GAMG cells was observed at this time of incubation. When GAMG cells were incubated with bee venom for longer periods of time, we observe a significant decrease in cell viability even at lower concentrations compared to shorter incubation times. Thus, the longer the incubation the significantly greater the cytotoxic effect against GAMG cells without the need for higher doses of BV. For GAMG cell line, the incubation time of bee venom also proved to be a significant factor affecting cell viability, and by modifying the treatment time we can obtain a satisfactory effect even at lower doses of active substance. Summarizing this part, the studies showed the dose-dependent and time-dependent sensitivity of the tested cells to bee venom.

The glial cells were more sensitive to BV effects than the nerve cells of the hippocampus. For higher concentrations and/or longer incubation times with bee venom of HT-22 line cells, a reduction in the viability of hippocampal cells used as a control was also observed. Thus, bee venom may exhibit some inhibitory effects on neuronal cell viability in the brain. It is therefore worth emphasizing the necessity of caution in the selection of appropriate doses that will simultaneously be effective against tumor cells and will not significantly affect the viability of neuronal cells, so as not to impair their essential functions that they perform in numerous processes.

Substrate-zymography, applied in this study, still represents the most simple, sensitive, and quantifiable assay for MMPs analysis, which is able to identify, simultaneously in the same sample, the entire panel of enzymes that are capable of degrading a specific substrate. The identification of gelatinase activity is possible by using gelatin as a substrate (gelatin zymography). Moreover, zymography showing the activity of MMPs, but not directly the amount of protein, provides additional information on the activity of these enzymes in the tested sample (Lowrey et al., 2008; Ricci et al., 2016).

The study also showed a dose-dependent effect of bee venom on the secretion and activities of MMP-2 and MMP-9 in the culture medium. When analyzing the activity of both gelatinases in GAMG cells, depending on the dose of the BV used for incubation, a gradual reduction in activity can be observed. A statistically significant reduction in MMP-2 and MMP-9 activity was obtained at concentrations higher than 1 mg/ml. The reduction in the activity of gelatinases may be explained simply by the reduced expression and secretion of these enzymes to the extracellular space under the influence of BV. The observed decrease in the activity of MMP-2 and MMP-9 cannot be explained by the decreased cell viability, as cell death under the influence of BV would lead to the release of intracellular reservoirs of MMP-2 and MMP-9 into the medium. In such cases, it could even result in an increase in the activity of these enzymes.

The active ingredients of BV have the ability to pass through the BBB and can therefore be used in the treatment of diseases of the CNS (Gu et al., 2020). BV has proven to be an effective treatment in animal models of Alzheimer's Disease, Parkinson's Disease, Epilepsy, Multiple Sclerosis, and Amyotrophic Lateral Sclerosis (Silva et al., 2015). The sensitivity of several cancer cells, including renal, lung, liver, prostate, bladder, and mammary cancer cells to BV peptides such as melittin and phospholipase A2 together with the known permeability of these peptides through BBB allows to hope that BV may also be active against cancer located in the CNS (Oršolić, 2012).

CONCLUSION

In conclusion, the performed studies showed a dose and time-dependent effect of unfractionated bee venom on the survival of neoplastic cells of glial origin. Moreover, an inhibitory effect on the secretion of both gelatinases was demonstrated, which may have a potential impact on tumor spread.

Further research should focus on elucidating the molecular mechanism of the observed effect and on identifying the active components of the venom exhibiting these properties.

DATA AVAILABILITY STATEMENT

The raw data supporting the conclusions of this article will be made available by the authors, without undue reservation.

AUTHOR CONTRIBUTIONS

JKu, AM, and JKo participated in research design. AM, KM, and AP conducted to the experiments. AM, JKu, KM, and AP wrote and contributed to the writing of the manuscript. JKu supervised the work. JKu and JKo initiated the research. All authors contributed to the article and approved the submitted version.

REFERENCES

Abrams, D. I. (2016). Integrating cannabis into clinical cancer care. *Curr. Oncol.* 23, S8–S14. doi: 10.3747/co.23.3099

Atiq, A., and Parhar, I. (2020). Anti-neoplastic potential of flavonoids and polysaccharide phytochemicals in glioblastoma. *Molecules* 25:E4895. doi: 10.3390/molecules25214895

Boguszewska-Czubara, A., Budzynska, B., Skalicka-Wozniak, K., and Kurzepa, J. (2019). Perspectives and new aspects of metalloproteinases' inhibitors in the

therapy of CNS disorders: from chemistry to medicine. *Curr. Med. Chem.* 26, 3208–3224. doi: 10.2174/0929867325666180514111500

Carpena, M., Nuñez-Estevez, B., Soria-Lopez, A., and Simal-Gandara, J. (2020). Bee Venom: an updating review of its bioactive molecules and its health applications. *Nutrients* 12:3360. doi: 10.3390/nu12113360

Choo, Y. M., Lee, K. S., Yoon, H. J., Kim, B. Y., Sohn, M. R., Roh, J. Y., et al. (2010). Dual function of a bee venom serine protease: prophenoloxidase-activating factor in arthropods and fibrin(ogen)olytic enzyme in mammals. *PLoS One* 5:e10393. doi: 10.1371/journal.pone.0010393

Drankowska, J., Kos, M., Kościuk, A., Marzęda, P., Boguszewska-Czubara, A., Tylus, M., et al. (2019). MMP targeting in the battle for vision: recent developments and future prospects in the treatment of diabetic retinopathy. *Life Sci.* 229, 149–156. doi: 10.1016/j.lfs.2019.05.038

Galanti, G., Fisher, T., Kventsel, I., Shoham, J., Gallily, R., Mechoulam, R., et al. (2008). Δ9-Tetrahydrocannabi-nol inhibits cell cycle progression by downregulation of E2F1 inhuman glioblastoma multiforme cells. *Acta Oncol.* 47, 1062–1070.

Golab, P., Boguszewska-Czubara, A., Kielbus, M., and Kurzepa, J. (2014). The rtPA increases MMP-9 activity in serum during ischaemic stroke. *Neurol. Neurochir. Pol.* 48, 309–314. doi: 10.1016/j.pjnns.2014.07.012

Gu, H., Han, S. M., and Park, K. K. (2020). Therapeutic effects of apamin as a bee venom component for non-neoplastic disease. *Toxins* 12:195. doi: 10.3390/toxins12030195

Jamasbi, E., Lucky, S. S., Li, W., Hossain, M. A., Gopalakrishnakone, P., and Separovic, F. (2018). Effect of dimerized melittin on gastric cancer cells and antibacterial activity. *Amino Acids* 50, 1101–1110. doi: 10.1007/s00726-018-2587-6

Jiang, Y., Marinescu, V. D., Xie, Y., Jarvius, M., Maturi, N. P., Haglund, C., et al. (2017). Glioblastoma cell malignancy and drug sensitivity are affected by the cell of origin. *Cell Rep.* 18, 977–990. doi: 10.1016/j.celrep.2017.01.003

Kasozi, K. I., Niedbała, G., Alqarni, M., Zirintunda, G., Ssempijja, F., Musinguzi, S. P., et al. (2020). Bee Venom - a potential complementary medicine candidate for SARS-CoV-2 infections. *Front. Public Health* 8:594458. doi: 10.3389/fpubh.2020.594458

Kim, H., Lee, H., Lee, G., Jang, H., Kim, S. S., Yoon, H., et al. (2015). Phospholipase A2 inhibits cisplatin-induced acute kidney injury by modulating regulatory T cells by the CD206 mannose receptor. *Kidney Int.* 88, 550–559. doi: 10.1038/ki.2015.147

Kokot, Z. J., Matysiak, J., Kłos, J., Kędzia, B., and Hołderna-Kędzia, E. (2009). Application of principal component analysis for evaluation of chemical and antimicrobial properties of honey bee (*apis mellifera*) venom. *J. Apic. Res. Bee. World* 48, 168–175. doi: 10.3896/IBRA.1.48.3.04

Lee, K. S., Kim, B. Y., Yoon, H. J., Choi, Y. S., and Jin, B. R. (2016). Secapin, a bee venom peptide, exhibits anti-fibrinolytic, anti-elastolytic, and anti-microbial activities. *Dev. Comp. Immunol.* 63, 27–35. doi: 10.1016/j.dci.2016.05.011

Linhares, P., Carvalho, B., Vaz, R., and Costa, B. M. (2020). Glioblastoma: is there any blood biomarker with true clinical relevance? *Int. J. Mol. Sci.* 21:5809. doi: 10.3390/ijms21165809

Liu, X., Chen, D., Xie, L., and Zhang, R. (2002). Effect of honey bee venom on proliferation of K1735M2 mouse melanoma cells in-vitro and growth of murine B16 melanomas in-vivo. *J. Pharm. Pharmacol.* 54, 1083–1089. doi: 10.1211/002235702320266235

Lowrey, G. E., Henderson, N., Blakey, J. D., Corne, J. M., and Johnson, S. R. (2008). MMP-9 protein level does not reflect overall MMP activity in the airways of patients with COPD. *Respir. Med.* 102, 845–851.

Marcu, J. P., Christian, R. T., Lau, D., Zielinski, A. J., Horowitz, M. P., Lee, J., et al. (2010). Cannabidiol enhancesthe inhibitory effects of Δ9- tetrahydrocannabinol on human glioblastoma cell proliferation and survival. *Mol. Cancer Ther.* 9, 180–189.

Matysiak, J., Schmelzer, C. E., Neubert, R. H., and Kokot, Z. J. (2011). Characterization of honeybee venom by MALDI-TOF and nanoESI-QqTOF mass spectrometry. *J. Pharm. Biomed. Anal.* 54, 273–278. doi: 10.1016/j.jpba.2010.08.020

McAllister, S. D., Chan, C., Taft, R. J., Luu, T., Abood, M. E., Moore, D. H., et al. (2005). Cannabinoids selec-tively inhibit proliferation and induce death of cultured human glioblastoma multiforme cells. *J. Neuro Oncol.* 74, 31–40. doi: 10.1007/s11060-004-5950-2

Oršolić, N. (2012). Bee venom in cancer therapy. *Cancer Metastasis Rev.* 31, 173–194. doi: 10.1007/s10555-011-9339-3

Park, H. G., Kyung, S. S., Lee, K. S., Kim, B. Y., Choi, Y. S., Yoon, H. J., et al. (2014). Dual function of a bee (*Apis cerana*) inhibitor cysteine knot peptide that acts as an antifungal peptide and insecticidal venom toxin. *Dev. Comp. Immunol.* 47, 247–253. doi: 10.1016/j.dci.2014.08.001

Quesnel, A., Karagiannis, G. S., and Filippou, P. S. (2020). Extracellular proteolysis in glioblastoma progression and therapeutics. *Biochim. Biophys. Acta Rev. Cancer* 1874:188428. doi: 10.1016/j.bbcan.2020.188428

Rady, I., Siddiqui, I. A., Rady, M., and Mukhtara, H. (2017). Melittin, a major peptide component of bee venom, and its conjugates in cancer therapy. *Cancer Lett.* 402, 16–31. doi: 10.1016/j.canlet.2017.05.010

Ricci, S., D'Esposito, V., Oriente, F., Formisano, P., and Di Carlo, A. (2016). Substrate-zymography: a still worthwhile method for gelatinases analysis in biological samples. *Clin. Chem. Lab. Med.* 54, 1281–1290.

Rybak-Chmielewska, H., and Szczęsna, H. (2006). HPLC study of chemical composition of honeybee (*Apis mellifera L.*) venom. *J. Apic. Sci.* 48, 103–109.

Sciani, J. M., Marques-Porto, R., Lourenço Junior, A., Orsi Rde, O., Ferreira Junior, R. S., Barraviera, B., et al. (2010). Identification of a novel melittin isoform from *Africanized Apis mellifera* venom. *Peptides* 31, 1473–1479. doi: 10.1016/j.peptides.2010.05.001

Silva, J., Monge-Fuentes, V., Gomes, F., Lopes, K., dos Anjos, L., Campos, G., et al. (2015). Pharmacological alternatives for the treatment of neurodegenerative disorders: wasp and bee venoms and their components as new neuroactive tools. *Toxins* 7, 3179–3209. doi: 10.3390/toxins7083179

Upadhyay, R. K. (2014). Drug delivery systems, CNS protection, and the blood brain barrier. *Biomed. Res. Int.* 2014:869269. doi: 10.1155/2014/869269

Wehbe, R., Frangieh, J., Rima, M., El Obeid, D., Sabatier, J. M., and Fajloun, Z. (2019). Bee Venom: overview of main compounds and bioactivities for therapeutic interests. *Molecules* 24:2997. doi: 10.3390/molecules24162997

Wolff, J., Trilling, T., Mölenkamp, G., Egeler, R. M., and Jürgens, H. (1999). Chemosensitivity of glioma cells in vitro: a meta analysis. *J. Cancer Res. Clin. Oncol.* 125, 481–486. doi: 10.1007/s004320050305

Yelken, B. Ö, Balcı, T., Süslüer, S. Y., Kayabaşı, Ç, Avcı, Ç. B., Kırmızıbayrak, P. B., et al. (2017). The effect of tomatine on metastasis related matrix metalloproteinase (MMP) activities in breast cancer cell model. *Gene* 627, 408–411. doi: 10.1016/j.gene.2017.06.054

Zhang, H., Ma, Y., Wang, H., Xu, L., and Yu, Y. (2019). MMP-2 expression. *Oncol Lett.* 17, 1826–1832. doi: 10.3892/ol.2018.9806

Zhang, S., Liu, Y., Ye, Y., Wang, X.-R., Lin, L.-T., Xiao, L.-Y., et al. (2018). Bee venom therapy: potential mechanisms and therapeutic applications. *Toxicon* 148, 64–73. doi: 10.1016/j.toxicon.2018.04.012

Zheng, J., Lee, H. L., Ham, Y. W., Song, H. S., Song, M. J., and Hong, J. T. (2015). Anti-cancer effect of bee venom on colon cancer cell growth by activation of death receptors and inhibition of nuclear factor kappa B. *Oncotarget* 6, 44437–44451. doi: 10.18632/oncotarget.6295

Zhou, J., Qi, Y., Diao, Q., Wu, L., Du, X., Li, Y., et al. (2013). Cytotoxicity of melittin and apamin in human hepatic L02 and HepG2 cells in vitro. *J. Toxicol. Toxin. Rev.* 32, 60–67. doi: 10.3109/15569543.2013.852108

Zhou, J., Zhao, J., Zhang, S., Shen, J., Qi, Y., Xue, X., et al. (2010). Quantification of melittin and apamin in bee venom lyophilized powder from Apis mellifera by liquid chromatography-diode array detector-tandem mass spectrometry. *Anal. Biochem.* 404, 171–178. doi: 10.1016/j.ab.2010.05.014

Conflict of Interest: The authors declare that the research was conducted in the absence of any commercial or financial relationships that could be construed as a potential conflict of interest.

frontiers in Neuroscience

ORIGINAL RESEARCH
published: 14 February 2022
doi: 10.3389/fnins.2022.832478

Blood Glutamate Scavenging With Pyruvate as a Novel Preventative and Therapeutic Approach for Depressive-Like Behavior Following Traumatic Brain Injury in a Rat Model

Dmitry Frank[1†], Benjamin F. Gruenbaum[2†], Ilan Shelef[3], Vladislav Zvenigorodsky[3], Olena Severynovska[4], Ron Gal[1], Michael Dubilet[1], Alexander Zlotnik[1], Ora Kofman[5†] and Matthew Boyko[1†]*

[1] Department of Anesthesiology and Critical Care, Soroka University Medical Center, Ben-Gurion University of the Negev, Be'er Sheva, Israel, [2] Department of Anesthesiology and Perioperative Medicine, Mayo Clinic, Jacksonville, FL, United States, [3] Department of Radiology, Soroka University Medical Center, Ben-Gurion University of the Negev, Be'er Sheva, Israel, [4] Department of Physiology, Faculty of Biology, Ecology and Medicine, Dnepropetrovsk State University, Dnepropetrovsk, Ukraine, [5] Department of Psychology, Zlotowski Center for Neuroscience, Ben-Gurion University of the Negev, Be'er Sheva, Israel

OPEN ACCESS

Edited by:
Barbara Budzynska,
Medical University of Lublin, Poland

Reviewed by:
Monika Gawrońska-Grzywacz,
Medical University of Lublin, Poland
Pushpa Sharma,
Uniformed Services University of the Health Sciences, United States

***Correspondence:**
Matthew Boyko
matthewboykoresearch@gmail.com

[†] These authors have contributed equally to this work

Specialty section:
This article was submitted to Neuropharmacology, a section of the journal Frontiers in Neuroscience

Received: 09 December 2021
Accepted: 07 January 2022
Published: 14 February 2022

Citation:
Frank D, Gruenbaum BF, Shelef I, Zvenigorodsky V, Severynovska O, Gal R, Dubilet M, Zlotnik A, Kofman O and Boyko M (2022) Blood Glutamate Scavenging With Pyruvate as a Novel Preventative and Therapeutic Approach for Depressive-Like Behavior Following Traumatic Brain Injury in a Rat Model. Front. Neurosci. 16:832478. doi: 10.3389/fnins.2022.832478

Depression is a common and serious complication following traumatic brain injury (TBI). Both depression and TBI have independently been associated with pathologically elevated extracellular brain glutamate levels. In the setting of TBI, blood glutamate scavenging with pyruvate has been widely shown as an effective method to provide neuroprotection by reducing blood glutamate and subsequent brain glutamate levels. Here we evaluate pyruvate as a novel approach in the treatment and prevention of post-TBI depression-like behavior in a rat model. Rats were divided into five groups: (1) sham-operated control with pyruvate, (2) sham-operated control with placebo, (3) post-TBI with placebo, (4) post-TBI given preventative pyruvate, and (5) post-TBI treated with pyruvate. These groups had an equal number of females and males. Rats were assessed for depressive-like behavior, neurological status, and glutamate levels in the blood and brain. Post-TBI neurological deficits with concurrent elevations in glutamate levels were demonstrated, with peak glutamate levels 24 h after TBI. Following TBI, the administration of either prophylactic or therapeutic pyruvate led to reduced glutamate levels, improved neurologic recovery, and improved depressive-like behavior. Glutamate scavenging with pyruvate may be an effective prophylactic and therapeutic option for post-TBI depression by reducing associated elevations in brain glutamate levels.

Keywords: depression, glutamate scavenging, neuroprotection, pyruvate, traumatic brain injury

Abbreviations: ADC, apparent diffusion coefficient; CSF, cerebrospinal fluid; EAATs, excitatory amino acid transporters; MRI, magnetic resonance imaging; NSS, Neurological severity score; NMDA, *N*-methyl-D-aspartate; TR/TE, repetition time/echo time; TR/TM/TE, repetition time/mixing time/echo time; SENSE, SENSitivity Encoding; STEAM, STimulated Echo Acquisition Mode; TBI, traumatic brain injury; TSE, turbo spin echo.

INTRODUCTION

The majority of survivors of moderate and severe traumatic brain injury (TBI) suffer from chronic neuropsychiatric consequences, including cognitive defects, depression, anxiety, social withdrawal and aggression (Tateno et al., 2003; McAllister, 2008; Jorge and Arciniegas, 2014; Hicks et al., 2019; Rauen et al., 2020). While these behavioral sequelae may at first be attributable to the emotional burdens of physical disability, these symptoms are not correlated with the severity of the initial injury or with pain (Bodnar et al., 2019) and can persist for decades (Hoofien et al., 2001; Koponen et al., 2002). Despite their significant impacts on functional recovery, quality of life, and resumption of employment (Rivara et al., 2011), these chronic neuropsychiatric conditions following TBI are often overlooked, undiagnosed and untreated.

Depressive disorders are generally treated by targeting the serotoninergic, adrenergic, and/or dopaminergic systems with medication that increases synaptic access of these neurotransmitters (Robinson et al., 1984; Currier et al., 1992; Andersen et al., 1994; Wiart et al., 2000). However, treatment for depressive disorders is effective in approximately two thirds of patients. For those suffering from depression following TBI, the selective serotonin reuptake inhibitor Sertraline (Zoloft) was found to be no more effective than placebo (Fann et al., 2017). As post-TBI depression remains difficult to manage, novel therapeutic approaches that specifically target this and related neuropsychiatric conditions have been of great clinical interest.

A growing body of evidence points to the involvement of the glutamatergic system in the etiology and treatment of TBI and depression, both independently and in parallel (O'Neil et al., 2018). Glutamate levels in the brain have been shown to contribute to the pathophysiology and neurological dysfunction seen after TBI (Zauner et al., 1996b; Koura et al., 1998; Zhang et al., 2001; Shutter et al., 2004; Mao et al., 2019). Post-TBI excess extracellular glutamate release leads to cell swelling, apoptosis, and neuronal death (Zauner et al., 1996a; Koura et al., 1998), and the maintenance of glutamate homeostasis is critical in improving neurological outcome (Zauner et al., 1996b; Hong et al., 2001; Zhang et al., 2001; Shutter et al., 2004; Mao et al., 2019). Depression and many mood disorders are similarly affected by the glutamatergic system (Levine et al., 2000; Krystal et al., 2002; Sanacora et al., 2003, 2012; Mitani et al., 2006; Maeng and Zarate, 2007; Pittenger et al., 2007; Mitchell and Baker, 2010; Zarate et al., 2010; Machado-Vieira et al., 2012; McCarthy et al., 2012; Tokita et al., 2012) of evidence indicates that future therapeutic options for depression will be comprised of modalities based on this system (Sanacora et al., 2008; Gruenbaum et al., 2020). Recent literature suggests that a susceptibility to depression may be caused by glutamatergic disturbances after TBI (O'Neil et al., 2018). Therefore, limiting excess glutamate concentrations following TBI may be a vital strategy to target both the neurologic and psychiatric progression of the condition.

Neurological motor symptoms of TBI have been shown to be attenuated by decreasing glutamate levels or function in the brain with dextorphan (Faden et al., 1989), *N*-methyl-D-aspartate (NMDA) antagonists (Mei et al., 2018), stimulation of excitatory amino acid transporters (EAATs) (Goodrich et al., 2013), or antibiotics and other drugs that block calcium channels or glutamate release (McConeghy et al., 2012; Hicks et al., 2019). However, these treatments can also limit the essential effects of glutamate, leading to adverse side effects (Ikonomidou and Turski, 2002; Hardingham and Bading, 2003; Muir, 2006). For example, human clinical trials of NMDA receptor antagonists have not only failed to demonstrate clinical neuroprotective efficacy but led to worsened neurological outcome and an increased mortality rate following TBI (Morris et al., 1998; Muir, 2006). Moreover, other preclinical studies have found that direct or indirect stimulation of NMDA receptors mitigated the severity of neurological deficits in hippocampal-based memory in adult rats (Temple and Hamm, 1996; Biegon et al., 2004) and in rat pups (Sta Maria et al., 2017; Biegon et al., 2018) after TBI.

An alternative approach is to eliminate excess toxic glutamate, rather than interfering with ongoing excitatory transmission *via* receptor antagonists. This can be accomplished by enhancing the brain-to-blood glutamate efflux, which occurs naturally *via* the endothelial transport systems, to eliminate excess glutamate from the brain's interstitial fluid (Teichberg, 2007; Teichberg et al., 2009). Glutamate co-substrates pyruvate and oxaloacetate convert glutamate into its inactive form 2-ketoglutarate *via* blood resident enzymes glutamate-pyruvate transaminase and glutamate-oxaloacetate transaminase (Gonzalez et al., 2005; Leibowitz et al., 2012; Gray et al., 2014). Previous studies have established an association between brain glutamate and blood glutamate levels (Shaw et al., 1995; Ferrarese et al., 2001). A reduction in blood glutamate helps to form an ideal glutamate concentration gradient that causes excess glutamate to move from the brain's extracellular fluid into the blood (Zlotnik et al., 2011a, 2012a; Rogachev et al., 2012; Boyko et al., 2014). This process impedes secondary brain injury that can occur as a result of glutamate neurotoxicity (O'Kane et al., 1999; Teichberg et al., 2009; Boyko et al., 2014).

Glutamate reduction, unlike the use of NMDA receptor antagonists, does not impact glutamate receptors or glutamate-mediated synaptic activity. Instead, this process only removes pathologically-elevated glutamate levels in the brain without impeding the function of neural circuits that depend on glutamate transmission (Leibowitz et al., 2012; Boyko et al., 2014; Zhumadilov et al., 2015). Known as blood glutamate scavenging, this method for reduction of excess glutamate has been proposed as an effective method to ameliorate neurological conditions after TBI (Zlotnik et al., 2007, 2008, 2009, 2010, 2012b) and depressive symptoms after stroke (Frank et al., 2019a; Gruenbaum et al., 2020). The aim of this study was to employ a novel approach of blood glutamate scavenging with pyruvate for the prevention and treatment of post-TBI depressive-like behaviors in a rat model. We further analyzed the impact of gender differences on the development of post-TBI depressive-like behaviors and on subsequent treatment with blood glutamate scavenging.

MATERIALS AND METHODS

Animals

The experiments were conducted in accordance with the recommendation of the Declarations of Helsinki and Tokyo and the Guidelines for the Use of Experimental Animals of the European Community. The experiments were approved by the Animal Care Committee of Ben-Gurion University of the Negev (Beer-Sheva, Israel). A total of 134 male and 133 female Sprague-Dawley rats were used in this experiment. All rats weighed between 300 and 350 g. Purina Chow and water were made available *ad libitum*. The temperature in the room was maintained at 22°C, with a 12 h light–dark cycle. All the tests were conducted in the dark phase between 8 am and 4 pm.

Experimental Design

The timeline of the experiment is illustrated in **Figure 1**. All rats were divided into two main groups, sham-operated and TBI. The rats were randomly assigned, but each group had an equal number of females and males (**Table 1**). 24 h after induction of TBI or sham surgery, all rats were divided into five groups: (1) sham-operated control group given pyruvate, (2) sham-operated control group given placebo, (3) post-TBI control group given placebo, (4) post-TBI group given preventative pyruvate, (5) post-TBI group treated with pyruvate (**Table 1**). Each of the five groups was randomly divided into two subgroups: (A) a group for behavioral tests and (B) a group for testing blood and cerebrospinal fluid (CSF), and outcomes from magnetic resonance imaging (MRI) with anesthesia (**Table 1**). At 24 h after TBI or sham protocol, we collected a sample of CSF and blood from the rats in subgroup B. On day 3 of the study, two groups (the post-TBI group given preventative pyruvate and the sham-operated control group given pyruvate) began to receive pyruvate for 30 days (**Figure 1**, Axis A). Within subgroup A, behavioral tests were performed after the completion of treatment at 1-month post-TBI, and 2 months after the completion of treatment. After the TBI induction or sham operation, the rats from the therapeutic protocol received no treatment for a month. After 1-month, behavioral tests (subgroup A) or blood CSF measurements (subgroup B) were taken, followed by treatment with pyruvate (**Figure 1**, Axis B) at a dose described below. Behavioral tests at 6 months were performed only for the sham-operated control group given placebo and post-TBI rats given placebo (**Figure 1**).

Drugs and Doses

Pyruvate (Sigma Israel Chemicals, Rehovot, Israel, catalog number P2256) was kept at a temperature of 2–4°C prior to use. Immediately before administration, it was dissolved in drinking water. Doses of 180 mg/kg/day were administered to rats in the experimental groups divided into two daily doses of 90 mg/kg for 30 days. A fresh solution of pyruvate was made every 12 h. The placebo groups received an equal dose of water without pyruvate. The dose of pyruvate was based on previous data that demonstrated by magnetic resonance spectroscopy that a dose of 180 mg/kg/day was optimal for reducing blood and brain glutamate by about 25–35% (Frank et al., 2019a).

Traumatic Brain Injury

Traumatic brain injury was performed, as previously described (Jones et al., 2008; Kabadi et al., 2010; Frank et al., 2021a,b). Rats received inhaled isoflurane as anesthetic with 5% for induction and 1.5–2.5% for maintenance, with equal parts medical air and oxygen. Prior to incision, the scalp was infiltrated with 0.5% bupivacaine. It was then perforated and reflected laterally with the left temporal muscle, while the underlying periosteum was dissected to reveal the skull. Craniotomy was performed at 5-mm using a trephine (Roboz Surgical Instrument Co., Gaithersburg, MD, United States) fastened to the drill bit of an electrical drill (Stoelting, Wood Dale, IL, United States). The center of the craniotomy was positioned 4 mm lateral and 4 mm posterior to bregma. A Luer 3-way stopcock was fixed and additionally held in place by cyanoacrylate adhesive and dental acrylic. The injury was then effected by a pressure pulse of 2.2 atmospheres (Jones et al., 2008; Kabadi et al., 2010). TBI was induced by a fluid-percussion device over 21–23 ms through the 3-way stopcock. The fluid pulse from the piston plunger, through involvement by the pendulum, was enacted *via* continuous saline fluid into the dura to allow for efficient transmission of the pressure pulse. Rats in the sham-operated control groups underwent the same procedure but without the administration of the fluid pulse.

Rats were monitored by a pulse-oximeter during the surgery to ensure uninterrupted measurements of heart rate and blood oxygen levels. After TBI induction, the incision was sutured, and the rats were allowed to recover from anesthesia.

Neurological Severity Score

Two blinded observers calculated Neurological Severity Score (NSS), as previously described (Boyko et al., 2011a, 2013a; Ohayon et al., 2012; Zlotnik et al., 2012a; Frank et al., 2021b). Points were assigned for motor function and behavioral changes for an overall score between 0, indicating an intact neurological state, and 25, representing highest neurological impairment. The following criteria were evaluated: the ability to exit a circle (3-point scale), gait on a wide surface (3-point scale), gait on a narrow surface (4-point scale), effort to remain on a narrow surface (2-point scale), reflexes (5-point scale), seeking behavior (2-point scale), beam walking (3-point scale), and beam balance (3-point scale).

Sucrose Preference Test

The sucrose preference test was performed as described previously as a method to evaluate anhedonia, which reflects depressive-like symptoms, in a rodent model (Boyko et al., 2013a, 2015). Two bottles of sucrose solution were placed in each rat's cage, consisting of 1% (w/v) solution. The rat became acclimated to having two bottles in the cage, which allowed the rat to avoid neophobia during the sucrose preference test, for which two bottles were necessary. Similarly, one of the bottles was replaced by water for 24 h so that the rat could adjust to having one bottle of water and one bottle of sucrose.

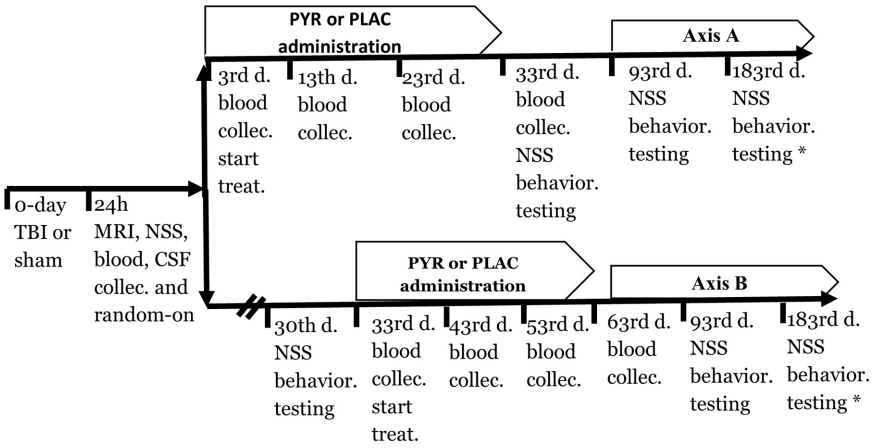

FIGURE 1 | A timeline of the protocol for preventative (axis A) and treatment (axis B) approach. CSF, Cerebrospinal fluid; NSS, Neurological severity score; PLAC, Placebo; PYR, Pyruvate; TBI, Traumatic brain injury.

TABLE 1 | The total number of rats in each of the experimental groups.

Study groups	Experimental procedures		Number of rats	
	MRI, CSF, and blood collection	Neuro-behavioral tests	Female	Male
Sham-operated controls given pyruvate	10f	15f	25	25
	10m	15m		
Sham-operated controls given placebo	10f	15f	25	25
	10m	15m		
Post-TBI rats given placebo	10f	15f	25	25
	10m	15m		
Post-TBI rats given preventative pyruvate	10f	15f	25	25
	10m	15m		
Post-TBI rats treated with pyruvate	10f	15f	25	25
	10m	15m		
The total number of rats			125	125

After this habituation, the rats were deprived of food and water for 12 h. At 9:00 am, the sucrose preference test was performed. The rats were housed in individual cages with free access to two bottles, one with 100 ml of sucrose solution (1% w/v) and the other with 100 ml of water, for 4 h. After this period, the volume (ml) of the consumed sucrose solution and water was recorded. Sucrose preference was calculated as sucrose preference (%) = sucrose consumption (ml)/[sucrose consumption (ml)+water consumption (ml)] × 100% (Boyko et al., 2013b, 2019b).

Open Field Test

The standard open field test evaluates locomotor, exploratory, and anxiety-related depressive-like behaviors in animal models based on novel conditions (Boyko et al., 2013a). The open field test measures exploratory activity in a novel environment. The open field boxes were round black plastic arenas 2 m in diameter, 60 cm high walls situated in a darkened room. For analysis, the arena was cleaned with 10% ethanol after each behavioral recording.

A video camera was mounted 200 cm above the open field arena and recorded all experiments. Locomotor activity was recorded for 5 min by a Logitech HD Pro Webcam C920. Analysis after the recording was performed with Ethovision XT software (Noldus, Wageningen, Netherlands) (Frank et al., 2019b). The recordings were analyzed based on total distance traveled.

Magnetic Resonance Imaging

Diffusion-weighted imaging and T2 MRI were performed at 48 h following TBI, as described previously (Frank et al., 2019a). The rats underwent general anesthesia and were maintained with 1.5% isoflurane in oxygen. A 3T MRI was used (Ingenia, Philips Medical Systems, Best, Netherlands) using an eight-channel receive-only coil. Localizing T2w turbo spin echo (TSE) sequences were obtained in sagittal and coronal planes with TR/TE = 3,000/80 ms, turbo factor = 15, water-fat shift = 1.6 pixels, resolution (freq × phase × slice) = 0.47 mm × 0.41 mm × 2.0 mm and one average for a scan time of 1:00 min. In the axial direction the scan parameters included

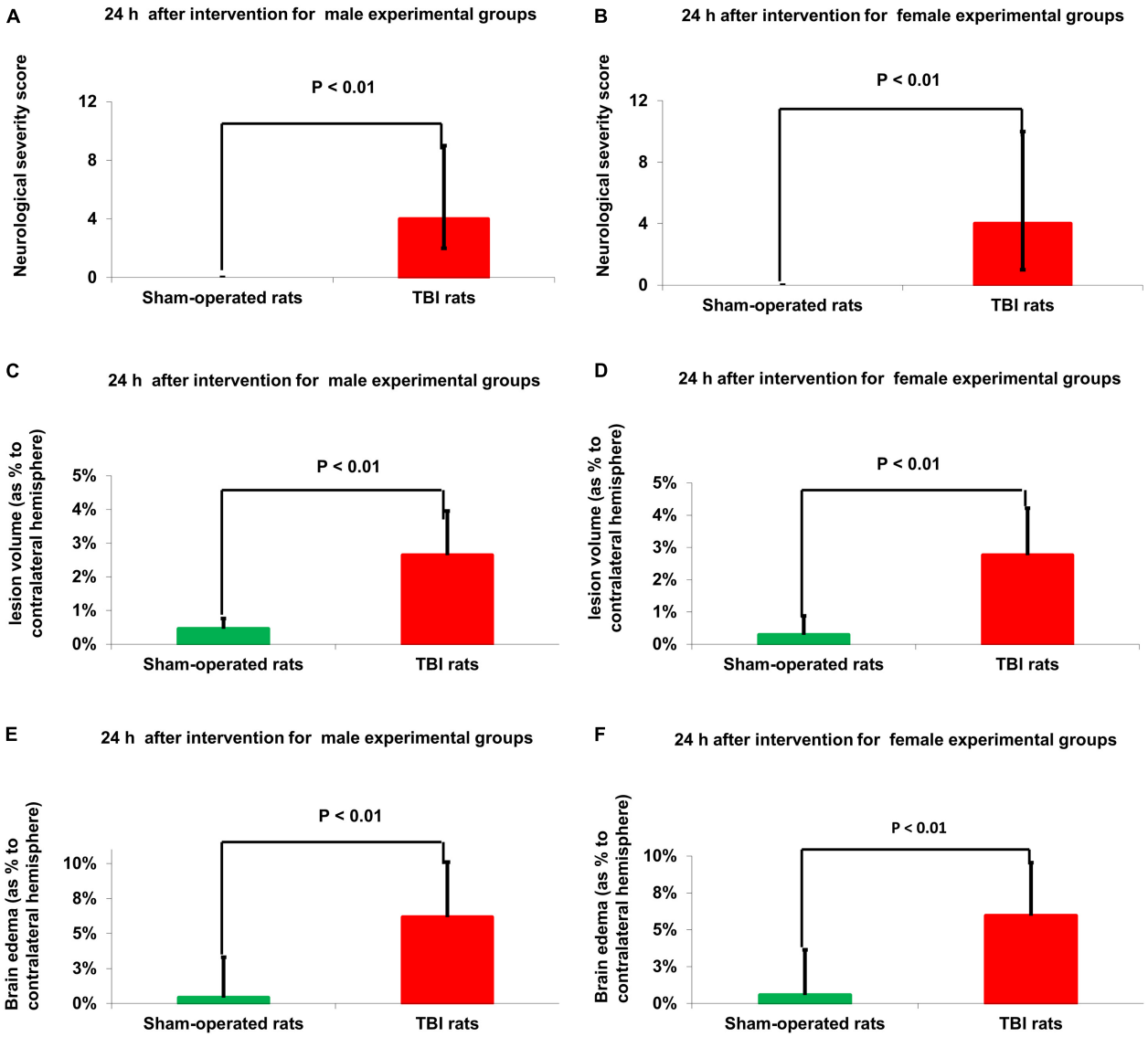

FIGURE 2 | Neurological outcome **(A,B)** and MRI-determined lesion volume **(C,D)** and brain edema **(E,F)**. Compared to sham-operated controls, the NSS at 24 h was significantly greater in male [$p < 0.01$ **(A)**] and female [$p < 0.01$ **(B)**] rats after TBI. The data are measured as a count and expressed as median and 25–75 percentile range. Compared to sham-operated rats, the lesion volume at 24 h was significantly greater in the male [$p < 0.01$ **(C)**] and female [$p < 0.01$ **(D)**] TBI groups. The data is expressed as a mean percentage of the contralateral hemisphere ± SD. Compared to sham-operated rats, the brain edema at 24 h was significantly greater in the male [$p < 0.01$, **(E)**] and female [$p < 0.01$ **(F)**] TBI groups. The data are expressed as a mean percentage of the contralateral hemisphere ± SD. TBI: Traumatic brain injury.

repetition time/echo time (TR/TE) = 3,000/80 ms, turbo factor = 14, water-fat shift = 1.6 pixels, resolution (freq × phase × slice) = 0.37 mm × 0.33 mm × 2.0 mm. Four averages were acquired for a scan time of 4:54 min. Diffusion tensor imaging in 6 directions was performed in the axial direction using a multi-shot STimulated Echo Acquisition Mode (STEAM) spin-echo, echo-planar sequence with repetition time/mixing time/echo time (TR/TM/TE) = 1,355/15.0/143 ms, SENSitivity Encoding (SENSE) reduction factor = 1.5, turbo factor = 19, b = 1,000 s/mm2, resolution (freq × phase × slice) = 0.55 mm × 0.55 mm × 2.0 mm with spectrally-selective fat suppression. Five signal averages were acquired for a scan time of 8:40 min. T2 perfusion studies were obtained using a dynamic, single-shot gradient-echo epi sequence with spectrally-selective fat suppression. The scan parameters were TR/TE = 1,300/40 ms, resolution (freq × phase × slice) = 0.64 mm × 0.69 mm × 2.0 mm, and one signal average giving a scan time of 1.3sec/dynamic. A total of 150 dynamics were acquired for a scan time of 3:19 min. We utilized the Intellispace Portal workstation (V5.0.0.20030, Philips Medical Systems, Best, Netherlands) for the post-processing of the perfusion studies.

Magnetic Resonance Imaging Analysis

An expert blinded to the groups performed image analysis. We generated quantitative apparent diffusion coefficient (ADC) maps, in units of square millimeters per second, in Philips software package (Ingenia, Philips Medical Systems, Best, Netherlands). Analysis was performed using ImageJ software (version 1.50i, National Institutes of Health, Bethesda, Maryland), as previously described (Boyko et al., 2019c). These thresholds indicated all pixels of ADC characteristics on each slice. The viability thresholds were 0.53X10-3mm^2/s for ADC images (Bardutzky et al., 2005; Boyko et al., 2019c). Calculation of lesion volume was performed by the RICH method and included the correction for tissue swelling, according to the following formula (Boyko et al., 2013b):

$$Corrected\ lesion\ volume = \frac{Lesion\ volume \times Contralateral\ hemisphere\ size}{Ipsilateral\ hemisphere\ size}$$

Calculation of brain edema was also performed by the RICH method. The calculation of brain edema by the RICH technique was done by comparing the contralateral and ipsilateral hemispheres, and performed using the following formula (Boyko et al., 2011a):

$$Brain\ edema = \frac{Volume\ of\ the\ right\ hemisphere - Volume\ of\ the\ left\ hemisphere}{Volume\ of\ the\ left\ hemisphere}$$

The lesion volume and brain edema were measured as a percentage of the total brain (Boyko et al., 2019a).

Determination of Blood Glutamate

Whole blood (200 μl aliquot) had its protein removed by adding an equal volume of ice-cold 1 M perchloric acid, followed by utilization of a centrifuge at 10,000 × *g* for 10 min at 4°C. The supernatant was obtained for future analysis if necessary, and adjusted to pH 7.2, with 2 M K2CO3, and stored at −80°C.

To measure the glutamate concentration, the fluorometric method of Graham and Aprison (1966) was used (Graham and Aprison, 1966). A 60 μl aliquot from the perchloric acid supernatant was combined with 90 μl of a 0.3 M glycine; 0.25 M hydrazine hydrate buffer adjusted to pH 8.6 with 1 M H2SO4 and containing 11.25 U of glutamate dehydrogenase in 10 mM Nicotinamide adenine dinucleotide. After incubation for 30 to 45 min at room temperature, the fluorescence was measured at 460 nm with excitation at 350 nm. A glutamate standard curve was established with concentrations ranging from 0 to 6 μM. All determinations were done at least in duplicates (Boyko et al., 2011b).

Blood Sample Collection

Blood was collected from the tail vein for the determination of blood glutamate levels *via* a 24- guage Neoflon (Becton Dickinson, Helsingborg, Sweden) catheter. After the blood sample was collected, the catheter was removed from the vein (Boyko et al., 2012).

Cerebrospinal Fluid Sample Collection

Rats were anesthetized and the cisterna magna was cannulated, as previously described (Boyko et al., 2012), and 0.1 to 0.2 ml of CSF were gently aspirated.

Determination of Cerebrospinal Fluid Glutamate

Fresh CSF (110 μl) was mixed with perchloric acid (25 μl) of 0.3 M, and then centrifuged at 10,000 × *g* for 10 min at 4°C. The pellet was discarded and the supernatant was collected, adjusted to pH 7.2 with 12.5 μl of 2 M K2CO3 and stored at −80°C for later analysis (Boyko et al., 2012). Analysis was performed by fluorometric method as described above for blood samples.

Statistical Analysis

Statistical analysis was performed with the SPSS 20 package (SPSS Inc., Chicago, IL, United States). The Kolmogorov–Smirnov test was used, to consider the number of rats in each group for deciding the appropriate test for the comparisons between the different parameters. For non-parametric data, we used the transformation test or other suitable tests. The significance of comparisons between groups were determined using the Kruskal–Wallis and Mann–Whitney (for nonparametric data) and one-way ANOVA with Bonferroni *post hoc* test or the Student's *t*-tests (for parametric data). Mortality rate was analyzed with chi-square and Fisher's exact tests. Results were considered statistically significant when $P < 0.05$, and highly significant when $P < 0.01$.

RESULTS

Mortality

The survival rate was calculated in the first 3 days following TBI or sham-operated procedure. During this period, the rats were not administered pyruvate. The mortality rate in sham-operated control rats was 0% in both gender groups, which was significantly lower than male (10.71%, p = 2.6E-02, chi-square and Fisher's exact test, 2-sided) and female (9.64%, p = 2.5E-02, chi-square and Fisher's exact test, 2-sided) rats following TBI.

Neurological Severity Score

There were no baseline neurological deficits observed in any of the rats before TBI or sham-operated procedure. The sham-operated control groups did not show any neurological deficit at any time point throughout the experiment. Compared to sham-operated controls, the NSS at 24 h was significantly greater in male [4(2–5) n = 75 vs. 0(0-0) n = 50, U = 45, p = 2.7E-21, r = 0.85] and female [4(3–6) n = 75 vs. 0(0-0) n = 50, U = 0, p = 4.5E-22, r = 0.86] rats after TBI, according to Mann–Whitney test (**Figures 2A,B**). No statistically significant differences were found between the 15 male and female groups, at time points of 30, 90, and 180 days, according to Kruskal–Wallis one-way analysis (see **Figure 1** and **Table 1**). The data are measured as a count and expressed as median and 25–75 percentile range.

Magnetic Resonance Imaging-Determined Lesion Volume

Compared to sham-operated rats, the lesion volume at 24 h was significantly greater in the female [2.71% ± 1.29% vs.0.46% ± 0.24%, $t(48) = -7.21$, $p = 3.4E\text{-}09$] and male [2.68% ± 1.32% vs. 0.45% ± 0.28%, $t(48) = -7.26$, $p = 3E\text{-}09$] TBI groups, according to Student's *t*-test (**Figures 2C,D**). The data are expressed as a mean percentage of the contralateral hemisphere ± SD.

Magnetic Resonance Imaging-Determined Brain Edema

Compared to sham-operated rats, the brain edema at 24 h was significantly greater in the female [5.98% ± 2.83% vs. 0.57% ± 0.29%, $t(48) = -5.5$, $p = 1.4E\text{-}06$] and male [6.15% ± 3.26% vs. 0.41% ± 0.24%, $t(48) = -5.6$, $p = 1E\text{-}06$] TBI groups, according to Student's *t*-test (**Figures 2E,F**). The data are expressed as a mean percentage of the contralateral hemisphere ± SD.

Concentration of Cerebrospinal Fluid Glutamate

Compared to sham-operated rats, the concentration of CSF glutamate at 24 h was significantly greater in the female [25.27 μM/L ± 13.13 μM/L vs. 3.6 μM/L ± 6.28 μM/L, $t(48) = -6.9$, $p = 1.2E\text{-}08$] and male [26.27 μM/L ± 16.39 μM/L vs. 2.1 μM/L ± 5.76 μM/L, $t(48) = -6.4$, $p = 6.1E\text{-}08$] TBI groups, according to Student's *t*-test (**Figures 3A,B**). The data are measured in μM/L and expressed as mean ± SD.

Concentration of Blood Glutamate

At baseline, there were no significant differences in blood glutamate concentration between treatment groups.

Compared to sham-operated rats, the concentration of blood glutamate at 24 h was significantly greater in the female [121% ± 20% vs. 100% ± 18%, $t(48) = 3.87$, $p < 0.01$] and male [114% ± 18% vs. 100% ± 17%, $t(48) = 2.75$, $p < 0.01$] TBI groups, according to Student's *t*-test. The data are measured in μM/L presented as a percentage from sham-operated rats and expressed as mean ± SD.

For male rats, at day 10 after pyruvate administration or placebo protocol, there were significant differences in blood glutamate levels between sham-operated rats given placebo (107% ± 8.6%), sham-operated rats given pyruvate (80.4% ± 4.4%), post-TBI given placebo (109.5% ± 9.4%), post-TBI rats given preventative pyruvate (77.6% ± 4.5%), and post-TBI rats treated with pyruvate (80.3% ± 6.1%) [Kruskal–Wallis, χ^2 (4) = 12.9, $p = 1.2E\text{-}02$]. A subsequent Mann–Whitney test indicated that male blood glutamate levels were significantly decreased in the sham-operated rats given pyruvate ($U = 21$, $p = 2.8E\text{-}02$, $r = -0.49$), post-TBI rats given preventative pyruvate ($U = 18$, $p = 1.6E\text{-}02$, $r = -0.02$), and post-TBI rats treated with pyruvate ($U = 22$, $p = 3.4E\text{-}02$, $r = -0.47$), compared to sham-operated rats given placebo. At day 20, there were significant differences in male blood glutamate levels between sham-operated rats given placebo (101.2% ± 7.3%), sham-operated rats given pyruvate (82.7% ± 5.1%), post-TBI given placebo (105.2% ± 4.8%), post-TBI rats given preventative pyruvate (80.6% ± 3.5%) and post-TBI rats treated with pyruvate (77.4% ± 3.5%) [Kruskal–Wallis, $\chi 2$ (4) = 11, $p = 2.6E\text{-}02$]. A subsequent Mann–Whitney test indicated that male blood glutamate levels were significantly decreased in the post-TBI rats given preventative pyruvate ($U = 24$, $p = 4.9E\text{-}02$, $r = -0.44$) and post-TBI rats treated with pyruvate ($U = 20$, $p = 2.3E\text{-}02$, $r = -0.51$), compared to the sham-operated control group given placebo. Also on day 20, male blood glutamate levels in the sham-operated rats given pyruvate were lower than in the sham-operated control rats given placebo, although this difference did not reach statistical significance. At day 30, there were significant differences in male blood glutamate levels between sham-operated rats given placebo (99.4% ± 5.9%), sham-operated rats given pyruvate (75.9% ± 5.2%), post-TBI given placebo (93.1% ± 7.1%), post-TBI rats given preventative pyruvate (77.9% ± 5.4%) and post-TBI rats treated with pyruvate (79.9% ± 3.6%) [Kruskal–Wallis, $\chi 2$ (4) = 10.1, $p = 3.9E\text{-}02$]. A subsequent Mann–Whitney test indicated that male blood glutamate levels were significantly decreased in the sham-operated controls given pyruvate ($U = 16$, $p = 1E\text{-}02$, $r = -0.58$), post-TBI rats given preventative pyruvate ($U = 75$, $p = 2.3E\text{-}02$, $r = -0.51$) and post-TBI rats treated with pyruvate ($U = 75$, $p = 2.3E\text{-}02$, $r = -0.51$), compared to sham-operated rats given placebo (**Figure 3C**).

For female rats, at day 10, there were significant differences in blood glutamate levels between sham-operated rats given placebo (98.7% ± 6.7%), sham-operated rats given pyruvate (80% ± 4.3%), post-TBI given placebo (104.5% ± 7%), post-TBI rats given preventative pyruvate (80.1% ± 3%) and post-TBI rats treated with pyruvate (78.7% ± 4.4%) [Kruskal–Wallis, $\chi 2$ (4) = 12.8, $p = 1.2E\text{-}02$]. A subsequent Mann–Whitney test indicated that at day 10, female blood glutamate levels were significantly decreased in the sham-operated controls given pyruvate ($U = 23$, $p = 4.1E\text{-}02$, $r = -0.46$), post-TBI rats given preventative pyruvate ($U = 23$, $p = 4.1E\text{-}02$, $r = -0.46$), and post-TBI rats treated with pyruvate ($U = 24$, $p = 4.9E\text{-}02$, $r = -0.45$), compared to sham-operated rats given placebo. At day 20, there were significant differences in female blood glutamate levels between sham-operated rats given placebo (103.4% ± 5.1%), sham-operated rats given pyruvate (81.1% ± 5.7%), post-TBI given placebo (100.3% ± 6.1%), post-TBI rats given preventative pyruvate (86.4% ± 4.9%) and post-TBI rats treated with pyruvate (83.2% ± 5%) [Kruskal–Wallis, $\chi 2$ (4) = 11.8, $p = 1.9E\text{-}02$]. A subsequent Mann–Whitney test indicated that at day 20, female blood glutamate levels were significantly decreased in the sham-operated controls given pyruvate ($U = 18$, $p = 1.6E\text{-}02$, $r = -0.54$), post-TBI rats given preventative pyruvate ($U = 24$, $p = 4.9E\text{-}02$, $r = -0.44$), and post-TBI rats treated with pyruvate ($U = 18$, $p = 1.6E\text{-}02$, $r = -0.54$), compared to sham-operated rats given placebo. At day 30, there were significant differences in female blood glutamate levels between sham-operated rats given placebo 101.2% ± 5.4%), sham-operated rats given pyruvate (82.9% ± 4%), post-TBI given placebo (97.6% ± 5.3%), post-TBI rats given preventative pyruvate (80.4% ± 5.6%) and post-TBI rats treated with pyruvate (74.2% ± 3.7%) [Kruskal–Wallis,

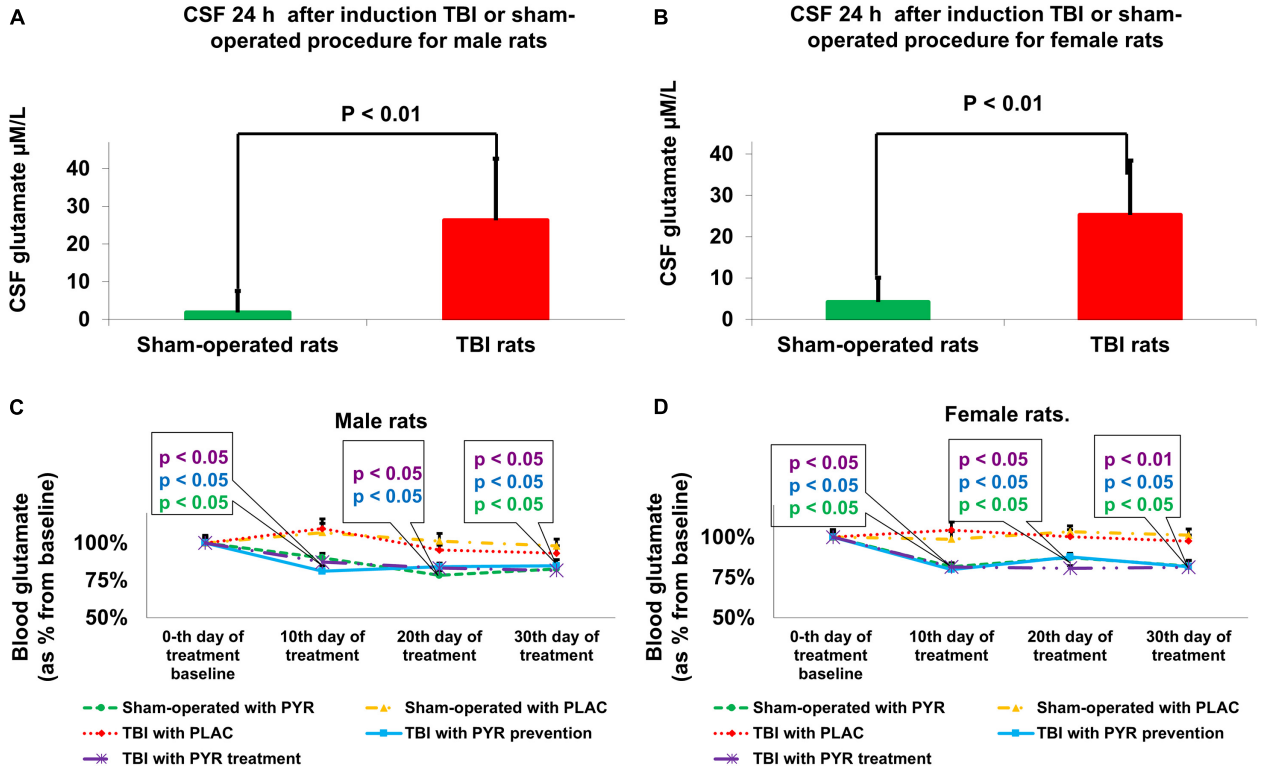

FIGURE 3 | Brain **(A,B)** and blood **(C,D)** glutamate concentrations. Compared to sham-operated rats, the concentrations of CSF glutamate at 24 h was significantly greater in the male [$p < 0.01$, **(A)**] and female [$p < 0.01$ **(B)**] TBI groups. The data are measured in μM/L and expressed as mean ± SD. Blood glutamate levels were decreased in male [$p < 0.05$ **(C)**] and female [$p < 0.05$ **(D)**] groups that received preventative or therapeutic pyruvate. The data are measured in μM/L presented as a percentage from baseline and expressed as mean ± SEM. CSF, Cerebrospinal fluid; PLAC, Placebo; PYR, Pyruvate; TBI, Traumatic brain injury.

$\chi 2$ (4) = 14.6, p = 5.7E-03]. A subsequent Mann–Whitney test indicated that at day 30, female blood glutamate levels were significantly decreased in the sham-operated controls given pyruvate (U = 19, p = 1.9E-02, r = −0.52), post-TBI rats given preventative pyruvate (U = 21, p = 2.8E-02, r = −0.49) and post-TBI rats treated with pyruvate (U = 11 p = 3.2E-02, r = −0.66), compared to sham-operated controls given placebo (**Figure 3D**).

As expected (Puig et al., 2000), blood glutamate levels in post-TBI rats treated with placebo were not statistically significantly different than in the sham-operated control rats treated with placebo. The data are measured in μfvM/L presented as a percentage from baseline and expressed as mean ± SEM.

Sucrose Preference

For male rats at day 30, a one-way ANOVA showed a significant difference in the percentage of sucrose preference between the study groups F(4,65) = 13.5, p = 4.8E-08. *Post hoc* analysis with a Bonferroni test showed a significant decrease between post-TBI rats given placebo (76.2% ± 1.9%, p = 4E-05) and post-TBI rats treated with pyruvate (75.4% ± 2%, p = 8.7E-06) compared to sham-operated controls given placebo (91.1% ± 1.2%). At day 90, a one-way ANOVA showed a significant difference in the percentage of sucrose preference between the study groups F(4,65) = 11.11, p = 6.3E-07. *Post hoc* analysis with a Bonferroni test showed a significant decrease in post-TBI rats given placebo (73% ± 3.1%, p = 6.5E-05) compared to sham-operated controls given placebo (89.9% ± 1.7%) (**Figures 4A,C,E**).

For female rats at day 30, a one-way ANOVA showed a significant difference in the percentage of sucrose preference between the study groups F(4, 68) = 16.27, p = 2.2E-09. *Post hoc* analysis with a Bonferroni test showed a significant decrease in post-TBI rats given placebo (77% ± 2.2%, p = 7.5E-06) and post-TBI rats treated with pyruvate (77.1% ± 1.6%, p = 8.2E-06), compared to sham-operated controls given placebo (91.4% ± 1.3%). At day 90, a one-way ANOVA showed a significant difference in the percentage of sucrose preference between the study groups F(4,65) = 21.29, p = 3.0E-11. *Post hoc* analysis with a Bonferroni test showed a significant decrease in post-TBI rats given placebo (64.5% ± 4.8%, p = 1.4E-08) compared to sham-operated controls given placebo (89.8% ± 1.2%) (**Figures 4B,D,F**). The data are measured in ml presented as percentage and expressed as mean ± SEM.

Open-Field Test

For male rats at day 30, a one-way ANOVA showed a significant difference in the total distance traveled between the study groups F(4,72) = 6.49, p = 1.6E-08. *Post hoc* analysis with a Bonferroni test showed a significant increase in post-TBI rats given placebo (31.21 m ± 2.5 m, p = 2.9E-03) and post-TBI rats treated with pyruvate (28.93 m ± 4.25 m,

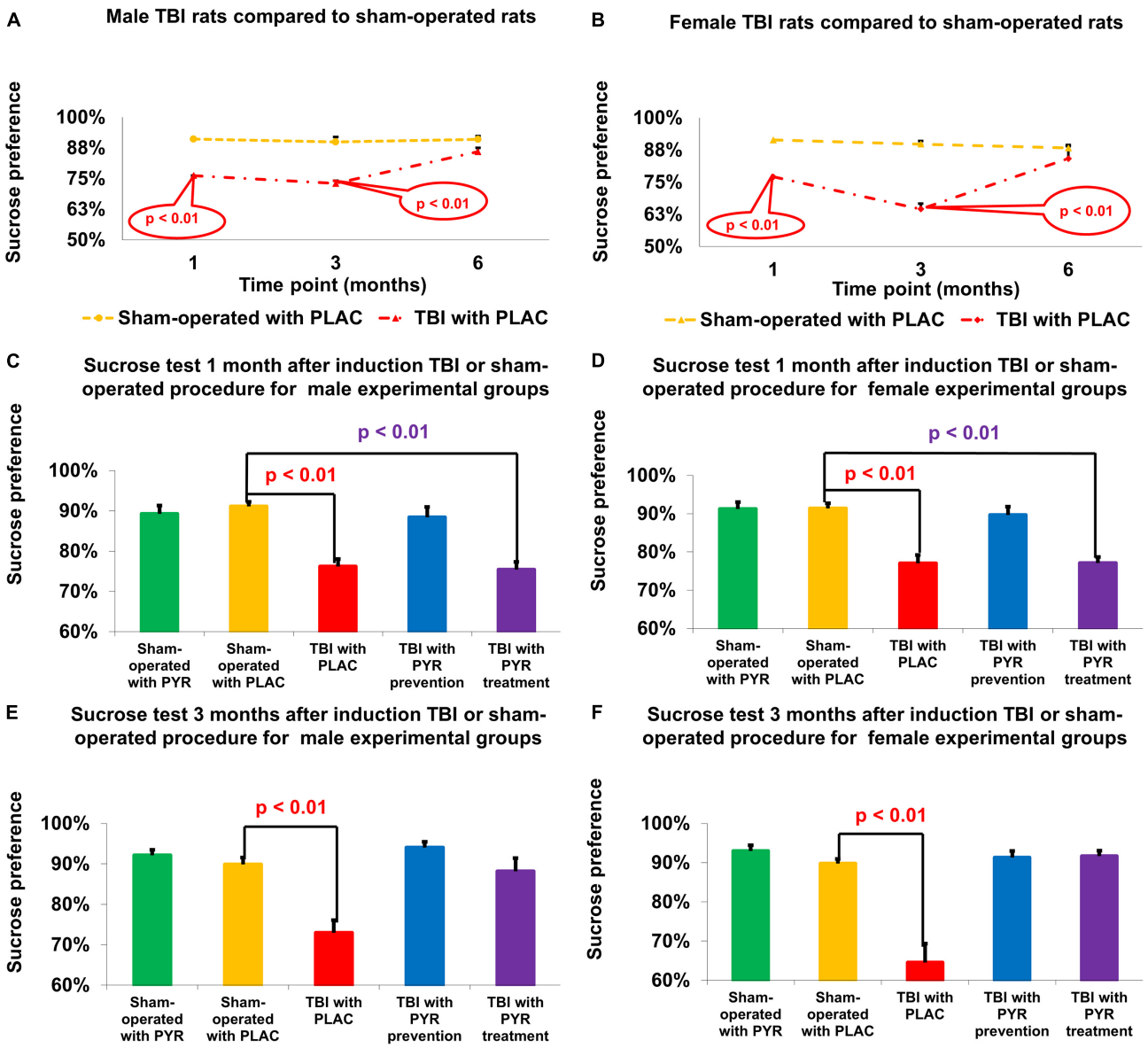

FIGURE 4 | Sucrose preference test. There was a decrease in sucrose preference at 1 and 3 months following TBI for male **(A)** and female **(B)** rats given placebo compared to sham-operated controls ($p < 0.01$). For male **(C)** and female **(D)** rats at day 30, there was a significant decrease in sucrose preference in post-TBI rats given placebo ($p < 0.01$) and post-TBI rats treated with pyruvate ($p < 0.01$) compared to sham-operated controls given placebo. For male **(E)** and female **(F)** rats at day 90, there was a significant decrease in sucrose preference in post-TBI rats given placebo ($p < 0.01$) compared to sham-operated controls given placebo. The data are measured as a percentage and presented as mean ± SEM. PLAC, Placebo; PYR, Pyruvate; TBI, Traumatic brain injury.

p = 2.9E-02), compared to sham-operated controls given placebo (19.3 m ± 0.77 m). At day 90, a one-way ANOVA showed a significant difference in the total distance traveled between the study groups $F(4,70) = 19.74$, p = 6.5E-11. *Post hoc* analysis with a Bonferroni test showed a significant increase in post-TBI rats given placebo (30.52 m ± 1.94 m, p = 8.1E-10) compared to sham-operated controls given placebo (18.84 m ± 0.72 m) (**Figures 5A,C,E**).

For female rats at day 30, a one-way ANOVA showed a significant difference in the total distance traveled between the study groups $F(4,72) = 4.4$, p = 3.1E-03. *Post hoc* analysis with a Bonferroni test showed a significant increase in post-TBI rats given placebo (29.89 m ± 2.33 m, p = 2.3E-02) and post-TBI rats treated with pyruvate (29.37 m ± 5.12 m, p = 3.5E-02), compared to sham-operated controls given placebo (18.65 m ± 0.69 m). At day 90, a one-way ANOVA showed significant difference in the total distance traveled between the study groups $F(4,69) = 9.25$, p = 4.8E-06. *Post hoc* analysis with a Bonferroni test showed a significant increase in distance traveled by post-TBI rats given placebo (27.55 m ± 2.06 m, p = 1.6E-05) compared

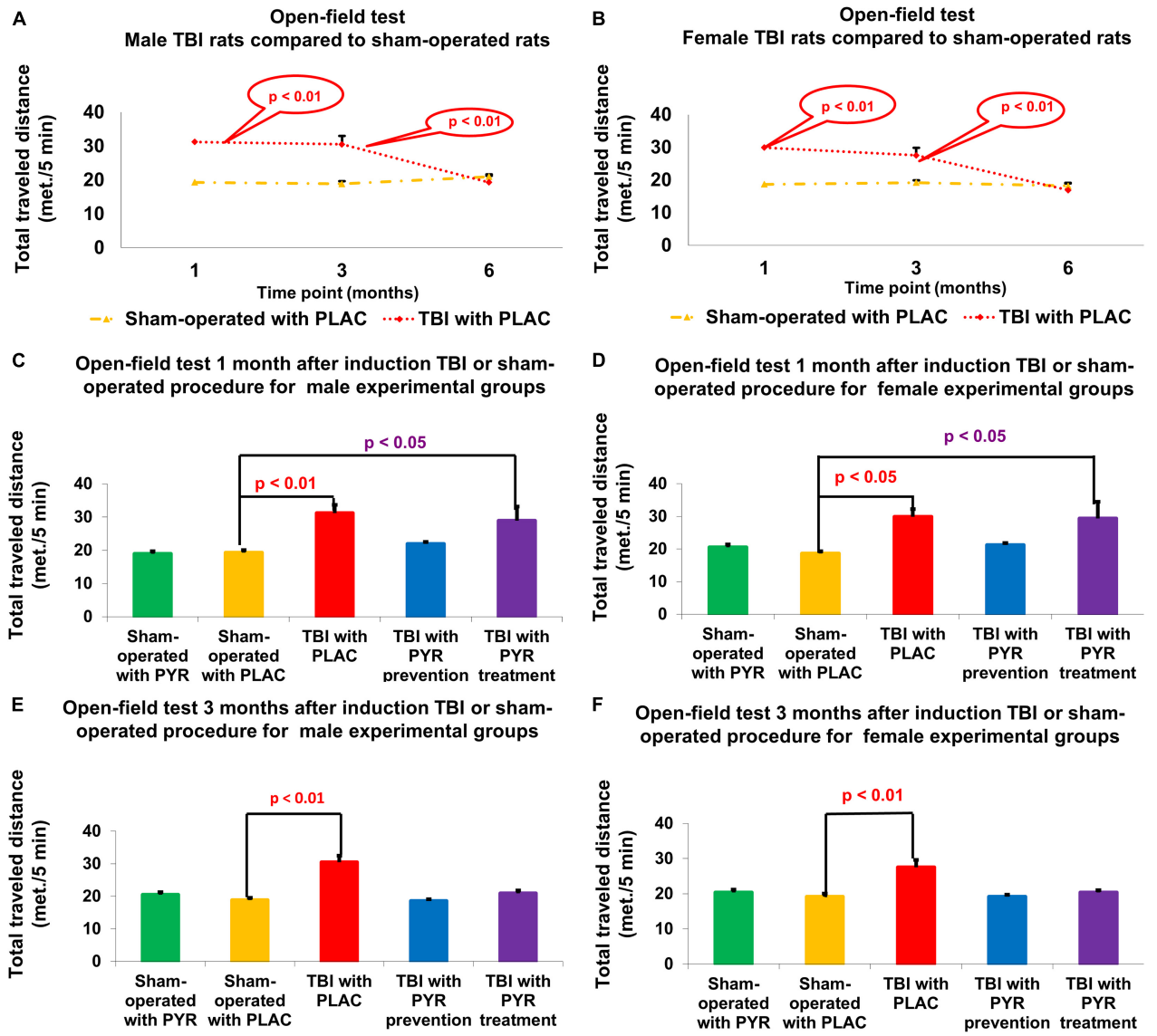

FIGURE 5 | Open-field test. There was an increase in the total traveled distance at 1 and 3 months following TBI for male **(A)** and female **(B)** rats given placebo compared to sham-operated controls ($p < 0.05$). For male **(C)** and female **(D)** rats at day 30, there was a significant increase in total distance traveled in post-TBI rats given placebo ($p < 0.01$) and post-TBI rats treated with pyruvate ($p < 0.01$) compared to sham-operated controls given placebo. For male **(E)** and female **(F)** rats at day 90, there was a significant increase in total distance traveled in post-TBI rats given placebo ($p < 0.01$) compared to sham-operated controls given placebo. The data are measured as cm/5 min and presented as mean ± SEM. PLAC, Placebo; PYR, Pyruvate; TBI, Traumatic brain injury.

to sham-operated controls given placebo (19.19 m ± 0.88 m) (**Figures 5B,D,F**). The data are measured as meter/5 min and presented as mean ± SEM.

DISCUSSION

In this study, we investigated blood glutamate scavenging activity from pyruvate administration and its mechanisms as a viable option for antidepressant treatment in a rat model of post-traumatic depression. Specifically, we studied the effects of pyruvate on anhedonia and elevated locomotor activity (Bhatt et al., 2017) as a consequence of post-traumatic behavioral mood disorders. Additionally, we considered brain glutamate levels and blood glutamate scavenging, MRI findings, and neurological outcomes between male and female rodent groups, and we used both a prophylactic and a therapeutic pyruvate treatment protocol. Our results determined that pyruvate likely has an antidepressant effect on the brain *via* its participation in blood glutamate scavenging.

Our hypotheses on the following neurological conditions were confirmed by our study. We determined that the mortality rate in the TBI group was higher than in the sham group. Cerebral edema and lesion volume were significantly higher

in the TBI group compared to the sham group (**Figures 2C–F**). We observed that neurological deficits were significantly greater in the TBI group compared to the sham group, which spontaneously recovered by 1 month (**Figures 2A,B** and section results > neurological performance). In addition, the concentration of glutamate was increased in the cerebrospinal fluid at 24 h as a consequence of TBI (**Figures 3A,B**). We have previously shown that the administration of pyruvate is effective in reducing cerebrospinal fluid glutamate levels in rodent models of subarachnoid hemorrhage (Boyko et al., 2012) and stroke (Frank et al., 2019a; Gruenbaum et al., 2020). A significant process of blood glutamate scavenging occurred in groups that received pyruvate treatment compared to placebo groups (**Figures 3C–D**). All the above results applied to both the male and female cohorts (**Figures 2**, **3**). At days 10–30 following TBI, the glutamate levels in rats given placebo did not differ from the levels in naïve rats treated with placebo. In previous studies in the setting of stroke, an increase in blood glutamate levels was seen in the first 24 h, but the levels dropped to baseline at 48 h and beyond (Puig et al., 2000).

To study the efficacy of pyruvate as an antidepressant therapy, we used two behavioral tests. The first was the sucrose preference test that measures the level of anhedonia, one of the most common symptoms of depressive disorders (American Psychiatric Pub, 2013). The sucrose preference test is a standard test for assessing anhedonia in rat models and has allowed for the development of new therapeutic antidepressant treatments (Gururajan et al., 2019). In our study, the TBI rats developed anhedonia at higher rates compared to sham rats and then spontaneously recovered 6 months after TBI (**Figures 4A,B**). In contrast, the post-TBI rats who were administered pyruvate prophylactically showed no symptoms of anhedonia and did not differ from the results of the sham rat group at 1 and 3 months following TBI (**Figures 4B–F**).

Traumatic brain injury rats that received pyruvate only after they developed anhedonia symptoms, showed a therapeutic effect of the treatment at 3 months. Thus, pyruvate has proven to be effective in two approaches: in the prophylactic treatment protocol as well as the therapy protocol (**Figure 4**). Pyruvate showed equal rates of efficacy in both the male and female cohorts (**Figure 4**).

The second behavioral test which we used was an open field test, a common method used to detect high emotionality and locomotor hyperactivity (Ramamoorthy et al., 2008) in post-TBI rats (Lewen et al., 1999; Pandey et al., 2009) and mice (Li et al., 2006; Pullela et al., 2006; Tucker et al., 2016). These manifestations are associated with depressive status (Pandey et al., 2009) and show high response rates to antidepressant drugs (Lewen et al., 1999; Pandey et al., 2009; Bhatt et al., 2017; Jindal et al., 2017). The hyperlocomotion that we recorded in the TBI group during the open field test is attributable to damage caused by the brain insult to the cerebral cortex, striatum, and olfactory bulbs (Viggiano, 2008). An increase in total distance traveled in the olfactory bulbectomized model of depression is well documented in the literature (Kalueff and Tuohimaa, 2004). Assessment of hyperlocomotive behavior as a consequence of TBI is also used to verify new models of TBI (Kane et al., 2012).

Our study supports the hypothesis that hyperlocomotion after TBI is associated with dysregulation of the glutamatergic system, in particular by high levels of extracellular glutamate. The association between dysregulation of the glutamatergic system and hyperlocomotion has been widely reported (Takahata and Moghaddam, 2003; Abekawa et al., 2007; Hackler et al., 2010; Egerton et al., 2020). It was previously observed that activation of metabotropic glutamate receptors increases both horizontal and vertical locomotor activity and this activity is impeded by administration of a receptor antagonist, fluphenazine (Kim and Vezina, 1997). Gainetdinov et al. (2001) showed that drugs that enhance glutamatergic transmission, such as positive modulators of L-α-amino-3-hydroxy-5-methylisoxazole-4-propionate glutamate receptors, suppress the hyperactivity of mice lacking the dopamine transporter (Gainetdinov et al., 2001). The involvement of the glutamate system in the development of attention-deficit disorder, hyperactivity, and other behavioral motor disorders has also been previously described (Procaccini et al., 2013; Maksimovic et al., 2014a,b; Miller, 2019; Aitta-Aho et al., 2019). Halberstadt et al. (2011) demonstrated that loss of mGlu5 receptor activity either pharmacologically or through gene deletion leads to locomotor hyperactivity in mice. These studies strongly indicate that dysregulation of the glutamatergic system, alone or in combination with other major neurotransmitter systems such as dopamine, GABA, and the serotonin system, may induce hyper-locomotive effects that are controlled by drugs that regulate glutamate homeostasis (Tucker et al., 2016). Although the precise brain circuitry and pharmacological targets involved in the suppression of locomotor behavior require further elucidation, our data support the possibility that glutamatergic transmission in the hippocampus could be therapeutically applied to dampen the hyper-excitable hippocampus and other brain circuitries.

In our study, we found that TBI rats were more likely to travel farther distances in the open field compared to the sham group until 6 months following TBI. In addition, more TBI rats developed hyperlocomotion activity compared to sham rats and then spontaneously recovered 6 months after TBI. In contrast, the rats after TBI from the protocol of preventive treatment with pyruvate showed no symptoms of hyperlocomotive activity and did not differ from sham rats at 1 and 3 months following TBI. TBI rats that were in the treatment group and did not receive pyruvate after TBI developed symptoms of hyperlocomotion and only then began to receive pyruvate as a therapeutic approach. Thus, pyruvate showed its efficacy both as a prophylactic protocol and as a therapeutic protocol. Pyruvate showed equal effective results in both male and female cohorts.

The similarities between the male and female cohorts in the outcomes of the sucrose preference test and the open field test elucidate our understanding of gender differences concerning depression and anxiety. Women tend to suffer more often from major depressive disorder (Kovacs et al., 1989; Weissman et al., 1993; Bebbington, 1998; Merikangas et al., 2010) and anxiety (Angst and Dobler-Mikola, 1985; Kessler et al., 1994; Bruce et al., 2005). In rodent models, different rat strains can display significant gender disparities in models of depression (Kokras and Dalla, 2014), though it is generally observed that female

rodents appear more active in the open field test, with less anxiety (Ter Horst et al., 2009; Kokras and Dalla, 2014). In our study, the use of the sucrose preference test in addition to the open field test assisted in developing more comprehensive neurological findings.

While it was outside of the scope of this study, we have previously observed that women display lower levels of blood glutamate concentration at baseline, and in conditions such as amyotrophic lateral sclerosis, rheumatoid arthritis, and growth hormone deficiency (Stover and Kempski, 2005). We have also determined that progesterone and estrogen have neuroprotective properties that act to reduce blood glutamate levels (Zlotnik et al., 2011b; Tsesis et al., 2013). We followed recommendations in the literature to include both sexes in this model (Rubin and Lipton, 2019), and, therefore our results accurately show the possible regulatory effects of pyruvate in similar ways across both groups. We hypothesize that more research on the topic of gender differences will support the use of pyruvate as a pharmacological approach that addresses depression for both men and women.

In our study, we began treatment on the third day after TBI. Usually, however, new therapeutic modalities are administered in the first hours after a brain injury (Tucker et al., 2016). We based our methodology on previous evidence that pyruvate has a neuroprotective effect in models of stroke and subarachnoid hemorrhage and, when administered in the first hours, reduces cerebral edema, infarction zone and blood brain barrier breakdown (Frank et al., 2019a). A reduction in damage to the brain tissue after pyruvate administration can potentially affect the development of behavioral outcomes after TBI. To neutralize the effect of histological outcomes on behavioral ones, we started pyruvate administration on the third day after TBI.

In summary, we have provided significant evidence that the process of blood glutamate scavenging by pyruvate induces antidepressant properties. These properties result in the prevention or treatment of anhedonia and hyperlocomotion that are caused by glutamate deregulation after TBI in rats. These conditions are symptoms of depressive-like conditions in rodent models. When analyzed in conjunction with previously observed neuroprotective properties of blood glutamate scavenging, it has become more apparent that blood glutamate scavengers should be considered as a viable treatment option for post-TBI depression.

DATA AVAILABILITY STATEMENT

The raw data supporting the conclusion of this article will be made available by the corresponding author (MB), upon reasonable request.

ETHICS STATEMENT

The animal study was reviewed and approved by the experiments were approved by the Animal Care Committee of Ben-Gurion University of the Negev (Be'er Sheva, Israel).

AUTHOR CONTRIBUTIONS

DF, BG, OK, and MB: study conception, data collection, data analysis, manuscript writing and editing, and final approval of manuscript. IS, VZ, OS, RG, MD, and AZ: data collection, data analysis, manuscript editing, and final approval of manuscript. All authors contributed to the article and approved the submitted version.

ACKNOWLEDGMENTS

We would like to thank Adam Abu Gama, Department of Orthopedic Surgery, Soroka Medical Center, Ben-Gurion University, Be'er Sheva, Israel, Mamdoch Abu Rabia of the Department of Anesthesiology and Critical Care, Soroka University Medical Center, and Rom Kahana of the Department of Anesthesiology Assuta Medical Centers, Israel, for their outstanding help in behavioral examination and analysis of the results by computer software. We would also like to thank Stella Cherninson and Alena Muraveva of the Department of Radiology, Soroka University Medical Center, Ben-Gurion University of the Negev, Be'er Sheva, Israel, for their outstanding help with the analysis of MR images by computer software and for carrying out measurements. We would also like to thank Valeria Frishman, laboratory assistant and Amos Douvdevani Head, Research Lab., from the Department of Clinical Biochemistry, Soroka Medical Center, Ben-Gurion University, for his help with the biochemical analysis.

REFERENCES

Abekawa, T., Ito, K., and Koyama, T. (2007). Different effects of a single and repeated administration of clozapine on phencyclidine-induced hyperlocomotion and glutamate releases in the rat medial prefrontal cortex at short-and long-term withdrawal from this antipsychotic. *Naunyn Schmiedebergs Arch. Pharmacol.* 375, 261–271. doi: 10.1007/s00210-007-0154-x

Aitta-Aho, T., Maksimovic, M., Dahl, K., Sprengel, R., and Korpi, E. R. (2019). Attenuation of novelty-induced hyperactivity of Gria1-/-mice by cannabidiol and hippocampal inhibitory chemogenetics. *Front. Pharmacol.* 10:309. doi: 10.3389/fphar.2019.00309

American Psychiatric Pub (2013). *Diagnostic and Statistical Manual of Mental Disorders (DSM-5§)*. Washington, DC: American Psychiatric Pub.

Andersen, G., Vestergaard, K., and Lauritzen, L. (1994). Effective treatment of poststroke depression with the selective serotonin reuptake inhibitor citalopram. *Stroke* 25, 1099–1104. doi: 10.1161/01.str.25.6.1099

Angst, J., and Dobler-Mikola, A. (1985). The zurich study. V. Anxiety and phobia in young adults. *Eur. Arch. Psychiatry Neurol. Sci.* 235, 171–178. doi: 10.1007/BF00380989

Bardutzky, J., Shen, Q., Henninger, N., Bouley, J., Duong, T. Q., and Fisher, M. (2005). Differences in ischemic lesion evolution in different rat strains using diffusion and perfusion imaging. *Stroke* 36, 2000–2005. doi: 10.1161/01.STR.0000177486.85508.4d

Bebbington, P. E. (1998). Sex and depression. *Psychol. Med.* 28, 1–8. doi: 10.1007/bf00288013

Bhatt, S., Mahesh, R., Jindal, A., and Devadoss, T. (2017). Neuropharmacological and neurochemical evaluation of Nn-propyl-3-ethoxyquinoxaline-2-carboxamide (6n): a novel serotonergic 5-HT3 receptor antagonist for co-morbid antidepressant-and anxiolytic-like potential using traumatic brain injury model in rats. *J. Basic Clin. Physiol. Pharmacol.* 28, 93–100. doi: 10.1515/jbcpp-2016-0057

Biegon, A., Fry, P. A., Paden, C. M., Alexandrovich, A., Tsenter, J., and Shohami, E. (2004). Dynamic changes in N-methyl-D-aspartate receptors after closed head injury in mice: implications for treatment of neurological and cognitive deficits. *Proc. Natl. Acad. Sci. U.S.A.* 101, 5117–5122. doi: 10.1073/pnas.0305741101

Biegon, A., Liraz-Zaltsman, S., and Shohami, E. (2018). Stimulation of N-methyl-D-aspartate receptors by exogenous and endogenous ligands improves outcome of brain injury. *Curr. Opin. Neurol.* 31, 687–692. doi: 10.1097/WCO.0000000000000612

Bodnar, C. N., Roberts, K. N., Higgins, E. K., and Bachstetter, A. D. (2019). A systematic review of closed head injury models of mild traumatic brain injury in mice and rats. *J. Neurotrauma* 36, 1683–1706. doi: 10.1089/neu.2018.6127

Boyko, M., Azab, A. N., Kuts, R., Gruenbaum, B. F., Gruenbaum, S. E., Melamed, I., et al. (2013a). The neuro-behavioral profile in rats after subarachnoid hemorrhage. *Brain Res.* 1491, 109–116. doi: 10.1016/j.brainres.2012.10.061

Boyko, M., Kutz, R., Gruenbaum, B. F., Cohen, H., Kozlovsky, N., Gruenbaum, S. E., et al. (2013b). The influence of aging on poststroke depression using a rat model via middle cerebral artery occlusion. *Cogn. Affect Behav. Neurosci.* 13, 847–859. doi: 10.3758/s13415-013-0177-3

Boyko, M., Gruenbaum, S. E., Gruenbaum, B. F., Shapira, Y., and Zlotnik, A. (2014). Brain to blood glutamate scavenging as a novel therapeutic modality: a review. *J. Neural. Transm. (Vienna)* 121, 971–979. doi: 10.1007/s00702-014-1181-7

Boyko, M., Kuts, R., Gruenbaum, B. F., Tsenter, P., Grinshpun, J., Frank, D., et al. (2019a). An alternative model of laser-induced stroke in the motor cortex of rats. *Biol. Proc. Online* 21:9. doi: 10.1186/s12575-019-0097-x

Boyko, M., Kutz, R., Grinshpun, J., Zvenigorodsky, V., Gruenbaum, B. F., Gruenbaum, S. E., et al. (2019b). The effect of depressive-like behavior and antidepressant therapy on social behavior and hierarchy in rats. *Behav. Brain Res.* 370:111953. doi: 10.1016/j.bbr.2019.111953

Boyko, M., Zvenigorodsky, V., Grinshpun, J., Shiyntum, H. N., Melamed, I., Kutz, R., et al. (2019c). Establishment of novel technical methods for evaluating brain edema and lesion volume in stroked rats: a standardization of measurement procedures. *Brain Res.* 1718, 12–21. doi: 10.1016/j.brainres.2019.04.022

Boyko, M., Kutz, R., Grinshpun, J., Zvenigorodsky, V., Gruenbaum, S. E., Gruenbaum, B. F., et al. (2015). Establishment of an animal model of depression contagion. *Behav. Brain Res.* 281, 358–363. doi: 10.1016/j.bbr.2014.12.017

Boyko, M., Melamed, I., Gruenbaum, B. F., Gruenbaum, S. E., Ohayon, S., Leibowitz, A., et al. (2012). The effect of blood glutamate scavengers oxaloacetate and pyruvate on neurological outcome in a rat model of subarachnoid hemorrhage. *Neurotherapeutics* 9, 649–657. doi: 10.1007/s13311-012-0129-6

Boyko, M., Ohayon, S., Goldsmith, T., Novack, L., Novack, V., Perry, Z. H., et al. (2011a). Morphological and neuro-behavioral parallels in the rat model of stroke. *Behav. Brain Res.* 223, 17–23. doi: 10.1016/j.bbr.2011.03.019

Boyko, M., Zlotnik, A., Gruenbaum, B. F., Gruenbaum, S. E., Ohayon, S., Kuts, R., et al. (2011b). Pyruvate's blood glutamate scavenging activity contributes to the spectrum of its neuroprotective mechanisms in a rat model of stroke. *Eur. J. Neurosci.* 34, 1432–1441. doi: 10.1111/j.1460-9568.2011.07864.x

Bruce, S. E., Yonkers, K. A., Otto, M. W., Eisen, J. L., Weisberg, R. B., Pagano, M., et al. (2005). Influence of psychiatric comorbidity on recovery and recurrence in generalized anxiety disorder, social phobia, and panic disorder: a 12-year prospective study. *Am. J. Psychiatry* 162, 1179–1187. doi: 10.1176/appi.ajp.162.6.1179

Currier, M., Murray, G., and Welch, C. (1992). Electroconvulsive therapy for poststroke depressed geriatric patients. *J. Neuropsychiatry Clin. Neurosci.* 4, 140–144. doi: 10.1176/jnp.4.2.140

Egerton, A., Grace, A. A., Stone, J., Bossong, M. G., Sand, M., and Mcguire, P. (2020). Glutamate in schizophrenia: neurodevelopmental perspectives and drug development. *Schizophr. Res.* 223, 59–70. doi: 10.1016/j.schres.2020.09.013

Faden, A. I., Demediuk, P., Panter, S. S., and Vink, R. (1989). The role of excitatory amino acids and NMDA receptors in traumatic brain injury. *Science* 244, 798–800. doi: 10.1126/science.2567056

Fann, J. R., Bombardier, C. H., Temkin, N., Esselman, P., Warms, C., Barber, J., et al. (2017). Sertraline for major depression during the year following traumatic brain injury: a randomized controlled trial. *J. Head Trauma Rehabil.* 32, 332–342. doi: 10.1097/HTR.0000000000000322

Ferrarese, C., Aliprandi, A., Tremolizzo, L., Stanzani, L., De Micheli, A., Dolara, A., et al. (2001). Increased glutamate in CSF and plasma of patients with HIV dementia. *Neurology* 57, 671–675. doi: 10.1212/wnl.57.4.671

Frank, D., Gruenbaum, B. F., Melamed, I., Grinshpun, J., Benjamin, I., Vzhetson, N., et al. (2021a). A metric test for assessing spatial working memory in adult rats following traumatic brain injury. *J. Vis. Exp.* 171, doi: 10.3791/62291

Frank, D., Gruenbaum, B. F., Shelef, I., Zvenigorodsky, V., Benjamin, Y., Shapoval, O., et al. (2021b). A novel histological technique to assess severity of traumatic brain injury in rodents: comparisons to neuroimaging and neurological outcomes. *Front. Neurosci.* 15:733115. doi: 10.3389/fnins.2021.733115

Frank, D., Kuts, R., Tsenter, P., Gruenbaum, B. F., Grinshpun, Y., Zvenigorodsky, V., et al. (2019a). The effect of pyruvate on the development and progression of post-stroke depression: a new therapeutic approach. *Neuropharmacology* 155, 173–184. doi: 10.1016/j.neuropharm.2019.05.035

Frank, D., Zlotnik, A., Kofman, O., Grinshpun, J., Severynovska, O., Brotfain, E., et al. (2019b). Early life stress induces submissive behavior in adult rats. *Behav. Brain Res.* 372:112025. doi: 10.1016/j.bbr.2019.112025

Gainetdinov, R. R., Mohn, A. R., Bohn, L. M., and Caron, M. G. (2001). Glutamatergic modulation of hyperactivity in mice lacking the dopamine transporter. *Proc. Natl. Acad. Sci. U.S.A.* 98, 11047–11054. doi: 10.1073/pnas.191353298

Gonzalez, S. V., Nguyen, N. H., Rise, F., and Hassel, B. (2005). Brain metabolism of exogenous pyruvate. *J. Neurochem.* 95, 284–293. doi: 10.1111/j.1471-4159.2005.03365.x

Goodrich, G. S., Kabakov, A. Y., Hameed, M. Q., Dhamne, S. C., Rosenberg, P. A., and Rotenberg, A. (2013). Ceftriaxone treatment after traumatic brain injury restores expression of the glutamate transporter, GLT-1, reduces regional gliosis, and reduces post-traumatic seizures in the rat. *J. Neurotrauma* 30, 1434–1441. doi: 10.1089/neu.2012.2712

Graham, L., and Aprison, M. (1966). Fluorometric determination of aspartate, glutamate, and γ-aminobutyrate in nerve tissue using enzymic method. *Anal. Biochem.* 15, 487–497. doi: 10.1016/0003-2697(66)90110-2

Gray, L. R., Tompkins, S. C., and Taylor, E. B. (2014). Regulation of pyruvate metabolism and human disease. *Cell Mol. Life Sci.* 71, 2577–2604. doi: 10.1007/s00018-013-1539-2

Gruenbaum, B. F., Kutz, R., Zlotnik, A., and Boyko, M. (2020). Blood glutamate scavenging as a novel glutamate-based therapeutic approach for post-stroke depression. *Ther. Adv. Psychopharmacol.* 10:2045125320903951. doi: 10.1177/2045125320903951

Gururajan, A., Reif, A., Cryan, J. F., and Slattery, D. A. (2019). The future of rodent models in depression research. *Nat. Rev. Neurosci.* 20, 686–701. doi: 10.1038/s41583-019-0221-6

Hackler, E., Byun, N., Jones, C., Williams, J., Baheza, R., Sengupta, S., et al. (2010). Selective potentiation of the metabotropic glutamate receptor subtype 2 blocks phencyclidine-induced hyperlocomotion and brain activation. *Neuroscience* 168, 209–218. doi: 10.1016/j.neuroscience.2010.02.057

Halberstadt, A. L., Lehmann-Masten, V. D., Geyer, M. A., and Powell, S. B. (2011). Interactive effects of mGlu5 and 5-HT 2A receptors on locomotor activity in mice. *Psychopharmacology* 215, 81–92. doi: 10.1007/s00213-010-2115-1

Hardingham, G. E., and Bading, H. (2003). The Yin and Yang of NMDA receptor signalling. *Trends Neurosci.* 26, 81–89. doi: 10.1016/S0166-2236(02)00040-1

Hicks, A. J., Clay, F. J., Hopwood, M., James, A. C., Jayaram, M., Perry, L. A., et al. (2019). The efficacy and harms of pharmacological interventions for aggression after traumatic brain injury—systematic review. *Front. Neurol.* 10:1169. doi: 10.3389/fneur.2019.01169

Hong, Z., Xinding, Z., Tianlin, Z., and Liren, C. (2001). Excitatory amino acids in cerebrospinal fluid of patients with acute head injuries. *Clin. Chem.* 47, 1458–1462.

Hoofien, D., Gilboa, A., Vakil, E., and Donovick, P. J. (2001). Traumatic brain injury (TBI) 10? 20 years later: a comprehensive outcome study of psychiatric

symptomatology, cognitive abilities and psychosocial functioning. *Brain Inj.* 15, 189–209. doi: 10.1080/026990501300005659

Ikonomidou, C., and Turski, L. (2002). Why did NMDA receptor antagonists fail clinical trials for stroke and traumatic brain injury? *Lancet Neurol.* 1, 383–386. doi: 10.1016/s1474-4422(02)00164-3

Jindal, A., Mahesh, R., Bhatt, S., and Pandey, D. (2017). Molecular modifications by regulating cAMP signaling and oxidant-antioxidant defence mechanisms, produce antidepressant-like effect: a possible mechanism of etazolate aftermaths of impact accelerated traumatic brain injury in rat model. *Neurochem. Int.* 111, 3–11. doi: 10.1016/j.neuint.2016.12.004

Jones, N. C., Cardamone, L., Williams, J. P., Salzberg, M. R., Myers, D., and O'brien, T. J. (2008). Experimental traumatic brain injury induces a pervasive hyperanxious phenotype in rats. *J. Neurotrauma* 25, 1367–1374. doi: 10.1089/neu.2008.0641

Jorge, R. E., and Arciniegas, D. B. (2014). Mood disorders after TBI. *Psychiatr. Clin.* 37, 13–29. doi: 10.1016/j.psc.2013.11.005

Kabadi, S. V., Hilton, G. D., Stoica, B. A., Zapple, D. N., and Faden, A. I. (2010). Fluid-percussion–induced traumatic brain injury model in rats. *Nat. Protoc.* 5:1552. doi: 10.1038/nprot.2010.112

Kalueff, A. V., and Tuohimaa, P. (2004). Experimental modeling of anxiety and depression. *Acta Neurobiol. Exp.* 64, 439–448.

Kane, M. J., Angoa-Pérez, M., Briggs, D. I., Viano, D. C., Kreipke, C. W., and Kuhn, D. M. (2012). A mouse model of human repetitive mild traumatic brain injury. *J. Neurosci. Methods* 203, 41–49. doi: 10.1016/j.jneumeth.2011.09.003

Kessler, R. C., Mcgonagle, K. A., Zhao, S., Nelson, C. B., Hughes, M., Eshleman, S., et al. (1994). Lifetime and 12-month prevalence of DSM-III-R psychiatric disorders in the United States: results from the National Comorbidity Survey. *Arch. Gen. Psychiatry* 51, 8–19. doi: 10.1001/archpsyc.1994.03950010008002

Kim, J.-H., and Vezina, P. (1997). Activation of metabotropic glutamate receptors in the rat nucleus accumbens increases locomotor activity in a dopamine-dependent manner. *J. Pharmacol. Exp. Ther.* 283, 962–968.

Kokras, N., and Dalla, C. (2014). Sex differences in animal models of psychiatric disorders. *Br. J. Pharmacol.* 171, 4595–4619. doi: 10.1111/bph.12710

Koponen, S., Taiminen, T., Portin, R., Himanen, L., Isoniemi, H., Heinonen, H., et al. (2002). Axis I and II psychiatric disorders after traumatic brain injury: a 30-year follow-up study. *Am. J. Psychiatry* 159, 1315–1321. doi: 10.1176/appi.ajp.159.8.1315

Koura, S., Doppenberg, E., Marmarou, A., Choi, S., Young, H., and Bullock, R. (1998). "Relationship between excitatory amino acid release and outcome after severe human head injury," in *Proceedings of the Intracranial Pressure and Neuromonitoring in Brain Injury* (Berlin: Springer), 244–246. doi: 10.1007/978-3-7091-6475-4_70

Kovacs, M., Gatsonis, C., Paulauskas, S. L., and Richards, C. (1989). Depressive disorders in childhood: IV. A longitudinal study of comorbidity with and risk for anxiety disorders. *Arch. Gen. Psychiatry.* 46, 776–782. doi: 10.1001/archpsyc.1989.01810090018003

Krystal, J. H., Sanacora, G., Blumberg, H., Anand, A., Charney, D. S., Marek, G., et al. (2002). Glutamate and GABA systems as targets for novel antidepressant and mood-stabilizing treatments. *Mol. Psychiatry* 7 (Suppl. 1), S71–S80. doi: 10.1038/sj.mp.4001021

Leibowitz, A., Boyko, M., Shapira, Y., and Zlotnik, A. (2012). Blood glutamate scavenging: insight into neuroprotection. *Int. J. Mol. Sci.* 13, 10041–10066. doi: 10.3390/ijms130810041

Levine, J., Panchalingam, K., Rapoport, A., Gershon, S., Mcclure, R. J., and Pettegrew, J. W. (2000). Increased cerebrospinal fluid glutamine levels in depressed patients. *Biol. Psychiatry* 47, 586–593. doi: 10.1016/s0006-3223(99)00284-x

Lewen, A., Fredriksson, A., Li, G. L., Olsson, Y., and Hillered, L. (1999). Behavioural and morphological outcome of mild cortical contusion trauma of the rat brain: influence of NMDA-receptor blockade. *Acta. Neurochirurgica* 141, 193–202. doi: 10.1007/s007010050286

Li, S., Kuroiwa, T., Katsumata, N., Ishibashi, S., Sun, L. Y., Endo, S., et al. (2006). Transient versus prolonged hyperlocomotion following lateral fluid percussion injury in mongolian gerbils. *J. Neurosci. Res.* 83, 292–300. doi: 10.1002/jnr.20720

Machado-Vieira, R., Ibrahim, L., Henter, I. D., and Zarate, C. A. Jr. (2012). Novel glutamatergic agents for major depressive disorder and bipolar disorder. *Pharmacol. Biochem. Behav.* 100, 678–687. doi: 10.1016/j.pbb.2011.09.010

Maeng, S., and Zarate, C. A. Jr. (2007). The role of glutamate in mood disorders: results from the ketamine in major depression study and the presumed cellular mechanism underlying its antidepressant effects. *Curr. Psychiatry Rep.* 9, 467–474. doi: 10.1007/s11920-007-0063-1

Maksimovic, M., Aitta-Aho, T., and Korpi, E. R. (2014a). Reversal of novelty-induced hippocampal c-Fos expression in GluA1 subunit-deficient mice by chronic treatment targeting glutamatergic transmission. *Eur. J. Pharmacol.* 745, 36–45. doi: 10.1016/j.ejphar.2014.10.005

Maksimovic, M., Vekovischeva, O. Y., Aitta-Aho, T., and Korpi, E. R. (2014b). Chronic treatment with mood-stabilizers attenuates abnormal hyperlocomotion of GluA1-subunit deficient mice. *PLoS One* 9:e100188. doi: 10.1371/journal.pone.0100188

Mao, Y., Zhuang, Z., Chen, Y., Zhang, X., Shen, Y., Lin, G., et al. (2019). Imaging of glutamate in acute traumatic brain injury using chemical exchange saturation transfer. *Quant. Imaging Med. Surg.* 9:1652. doi: 10.21037/qims.2019.09.08

McAllister, T. W. (2008). Neurobehavioral sequelae of traumatic brain injury: evaluation and management. *World Psychiatry* 7, 3–10. doi: 10.1002/j.2051-5545.2008.tb00139.x

McCarthy, D. J., Alexander, R., Smith, M. A., Pathak, S., Kanes, S., Lee, C. M., et al. (2012). Glutamate-based depression GBD. *Med. Hypotheses* 78, 675–681. doi: 10.1016/j.mehy.2012.02.009

McConeghy, K. W., Hatton, J., Hughes, L., and Cook, A. M. (2012). A review of neuroprotection pharmacology and therapies in patients with acute traumatic brain injury. *CNS Drugs* 26, 613–636. doi: 10.2165/11634020-000000000-00000

Mei, Z., Qiu, J., Alcon, S., Hashim, J., Rotenberg, A., Sun, Y., et al. (2018). Memantine improves outcomes after repetitive traumatic brain injury. *Behav. Brain Res.* 340, 195–204. doi: 10.1016/j.bbr.2017.04.017

Merikangas, K. R., He, J.-P., Burstein, M., Swanson, S. A., Avenevoli, S., Cui, L., et al. (2010). Lifetime prevalence of mental disorders in US adolescents: results from the National Comorbidity Survey Replication–Adolescent Supplement (NCS-A). *J. Am. Acad. Child Adolesc. Psychiatry* 49, 980–989.

Miller, E. M., Quintero, J. E., Pomerleau, F., Huettl, P., Gerhardt, G. A., and Glaser, P. E. (2019). Chronic methylphenidate alters tonic and phasic glutamate signaling in the frontal cortex of a freely-moving rat model of ADHD. *Neurochem. Res.* 44, 89–101.

Mitani, H., Shirayama, Y., Yamada, T., Maeda, K., Ashby, C. R. Jr., and Kawahara, R. (2006). Correlation between plasma levels of glutamate, alanine and serine with severity of depression. *Prog. Neuropsychopharmacol. Biol. Psychiatry* 30, 1155–1158. doi: 10.1016/j.pnpbp.2006.03.036

Mitchell, N. D., and Baker, G. B. (2010). An update on the role of glutamate in the pathophysiology of depression. *Acta. Psychiatr. Scand.* 122, 192–210. doi: 10.1111/j.1600-0447.2009.01529.x

Morris, G. F., Juul, N., Marshall, S. B., Benedict, B., and Marshall, L. F. (1998). Neurological deterioration as a potential alternative endpoint in human clinical trials of experimental pharmacological agents for treatment of severe traumatic brain injuries. Executive Committee of the International Selfotel Trial. *Neurosurgery* 43, 1369–1372; discussion 1372–1364.

Muir, K. W. (2006). Glutamate-based therapeutic approaches: clinical trials with NMDA antagonists. *Curr. Opin. Pharmacol.* 6, 53–60. doi: 10.1016/j.coph.2005.12.002

Ohayon, S., Boyko, M., Saad, A., Douvdevani, A., Gruenbaum, B. F., Melamed, I., et al. (2012). Cell-free DNA as a marker for prediction of brain damage in traumatic brain injury in rats. *J. Neurotrauma* 29, 261–267. doi: 10.1089/neu.2011.1938

O'Kane, R. L., Martinez-Lopez, I., Dejoseph, M. R., Vina, J. R., and Hawkins, R. A. (1999). Na(+)-dependent glutamate transporters (EAAT1, EAAT2, and EAAT3) of the blood-brain barrier. A mechanism for glutamate removal. *J. Biol. Chem.* 274, 31891–31895. doi: 10.1074/jbc.274.45.31891

O'Neil, D. A., Nicholas, M. A., Lajud, N., Kline, A. E., and Bondi, C. O. (2018). Preclinical models of traumatic brain injury: emerging role of glutamate in the pathophysiology of depression. *Front. Pharmacol.* 9:579. doi: 10.3389/fphar.2018.00579

Pandey, D. K., Yadav, S. K., Mahesh, R., and Rajkumar, R. (2009). Depression-like and anxiety-like behavioural aftermaths of impact accelerated traumatic brain injury in rats: a model of comorbid depression and anxiety? *Behav. Brain Res.* 205, 436–442. doi: 10.1016/j.bbr.2009.07.027

Pittenger, C., Sanacora, G., and Krystal, J. H. (2007). The NMDA receptor as a therapeutic target in major depressive disorder. *CNS Neurol. Disord. Drug Targets* 6, 101–115. doi: 10.2174/187152707780363267

Procaccini, C., Maksimovic, M., Aitta-Aho, T., Korpi, E. R., and Linden, A. M. (2013). Reversal of novelty-induced hyperlocomotion and hippocampal c-Fos expression in GluA1 knockout male mice by the mGluR2/3 agonist LY354740. *Neuroscience* 250, 189–200. doi: 10.1016/j.neuroscience.2013.07.010

Puig, N., Dávalos, A., Adan, J., Piulats, J., Martínez, J. M., and Castillo, J. (2000). Serum amino acid levels after permanent middle cerebral artery occlusion in the rat. *Cerebrovasc. Dis.* 10, 449–454. doi: 10.1159/000016106

Pullela, R., Raber, J., Pfankuch, T., Ferriero, D. M., Claus, C. P., Koh, S.-E., et al. (2006). Traumatic injury to the immature brain results in progressive neuronal loss, hyperactivity and delayed cognitive impairments. *Devel. Neurosci.* 28, 396–409. doi: 10.1159/000094166

Ramamoorthy, R., Radhakrishnan, M., and Borah, M. (2008). Antidepressant-like effects of serotonin type-3 antagonist, ondansetron: an investigation in behaviour-based rodent models. *Behav. Pharmacol.* 19, 29–40. doi: 10.1097/FBP.0b013e3282f3cfd4

Rauen, K., Reichelt, L., Probst, P., Schäpers, B., Müller, F., Jahn, K., et al. (2020). Quality of life up to 10 years after traumatic brain injury: a cross-sectional analysis. *Health Qual. Life Outcomes* 18, 1–12. doi: 10.1186/s12955-020-01391-3

Rivara, F. P., Koepsell, T. D., Wang, J., Temkin, N., Dorsch, A., Vavilala, M. S., et al. (2011). Disability 3, 12, and 24 months after traumatic brain injury among children and adolescents. *Pediatrics* 128, e1129–e1138. doi: 10.1542/peds.2011-0840

Robinson, R. G., Lipsey, J. R., and Pearlson, G. D. (1984). The occurrence and treatment of poststroke mood disorders. *Compr. Ther.* 10, 19–24.

Rogachev, B., Ohayon, S., Saad, A., Vorobiovsky, V., Gruenbaum, B. F., Leibowitz, A., et al. (2012). The effects of hemodialysis on blood glutamate levels in chronic renal failure: implementation for neuroprotection. *J. Crit. Care* 27, 743 e741–e747. doi: 10.1016/j.jcrc.2012.07.002

Rubin, T. G., and Lipton, M. L. (2019). Sex differences in animal models of traumatic brain injury. *J. Exp. Neurosci.* 13:1179069519844020. doi: 10.1177/1179069519844020

Sanacora, G., Rothman, D. L., Mason, G., and Krystal, J. H. (2003). Clinical studies implementing glutamate neurotransmission in mood disorders. *Ann. N. Y. Acad. Sci.* 1003, 292–308. doi: 10.1196/annals.1300.018

Sanacora, G., Treccani, G., and Popoli, M. (2012). Towards a glutamate hypothesis of depression: an emerging frontier of neuropsychopharmacology for mood disorders. *Neuropharmacology* 62, 63–77. doi: 10.1016/j.neuropharm.2011.07.036

Sanacora, G., Zarate, C. A., Krystal, J. H., and Manji, H. K. (2008). Targeting the glutamatergic system to develop novel, improved therapeutics for mood disorders. *Nat. Rev. Drug Discov.* 7, 426–437. doi: 10.1038/nrd2462

Shaw, P. J., Forrest, V., Ince, P. G., Richardson, J. P., and Wastell, H. J. (1995). CSF and plasma amino acid levels in motor neuron disease: elevation of CSF glutamate in a subset of patients. *Neurodegeneration* 4, 209–216. doi: 10.1006/neur.1995.0026

Shutter, L., Tong, K. A., and Holshouser, B. A. (2004). Proton MRS in acute traumatic brain injury: role for glutamate/glutamine and choline for outcome prediction. *J. Neurotrauma* 21, 1693–1705. doi: 10.1089/neu.2004.21.1693

Sta Maria, N. S., Reger, M. L., Cai, Y., Baquing, M. A. T., Buen, F., Ponnaluri, A., et al. (2017). D-cycloserine restores experience-dependent neuroplasticity after traumatic brain injury in the developing rat brain. *J. Neurotrauma* 34, 1692–1702. doi: 10.1089/neu.2016.4747

Stover, J. F., and Kempski, O. S. (2005). Anesthesia increases circulating glutamate in neurosurgical patients. *Acta Neurochir. (Wien)* 147, 847–853. doi: 10.1007/s00701-005-0562-y

Takahata, R., and Moghaddam, B. (2003). Activation of glutamate neurotransmission in the prefrontal cortex sustains the motoric and dopaminergic effects of phencyclidine. *Neuropsychopharmacology* 28, 1117–1124. doi: 10.1038/sj.npp.1300127

Tateno, A., Jorge, R. E., and Robinson, R. G. (2003). Clinical correlates of aggressive behavior after traumatic brain injury. *J. Neuropsychiatry Clin. Neurosci.* 15, 155–160. doi: 10.1176/jnp.15.2.155

Teichberg, V., Cohen-Kashi-Malina, K., Cooper, I., and Zlotnik, A. (2009). Homeostasis of glutamate in brain fluids: an accelerated brain-to-blood efflux of excess glutamate is produced by blood glutamate scavenging and offers protection from neuropathologies. *Neuroscience* 158, 301–308. doi: 10.1016/j.neuroscience.2008.02.075

Teichberg, V. I. (2007). From the liver to the brain across the blood–brain barrier. *Proc. Natl. Acad. Sci.U.S.A.* 104, 7315–7316. doi: 10.1073/pnas.0702450104

Temple, M. D., and Hamm, R. J. (1996). Chronic, post-injury administration of D-cycloserine, an NMDA partial agonist, enhances cognitive performance following experimental brain injury. *Brain Res.* 741, 246–251. doi: 10.1016/s0006-8993(96)00940-7

Ter Horst, G. J., Wichmann, R., Gerrits, M., Westenbroek, C., and Lin, Y. (2009). Sex differences in stress responses: focus on ovarian hormones. *Physiol. Behav.* 97, 239–249. doi: 10.1016/j.physbeh.2009.02.036

Tokita, K., Yamaji, T., and Hashimoto, K. (2012). Roles of glutamate signaling in preclinical and/or mechanistic models of depression. *Pharmacol. Biochem. Behav.* 100, 688–704. doi: 10.1016/j.pbb.2011.04.016

Tsesis, S., Gruenbaum, B. F., Ohayon, S., Boyko, M., Gruenbaum, S. E., Shapira, Y., et al. (2013). The effects of estrogen and progesterone on blood glutamate levels during normal pregnancy in women. *Gynecol. Endocrinol.* 29, 912–916. doi: 10.3109/09513590.2013.813467

Tucker, L. B., Fu, A. H., and Mccabe, J. T. (2016). Performance of male and female C57BL/6J mice on motor and cognitive tasks commonly used in pre-clinical traumatic brain injury research. *J. Neurotrauma* 33, 880–894. doi: 10.1089/neu.2015.3977

Viggiano, D. (2008). The hyperactive syndrome: metanalysis of genetic alterations, pharmacological treatments and brain lesions which increase locomotor activity. *Behav. Brain Res.* 194, 1–14. doi: 10.1016/j.bbr.2008.06.033

Weissman, M. M., Bland, R., Joyce, P. R., Newman, S., Wells, J. E., and Wittchen, H.-U. (1993). Sex differences in rates of depression: cross-national perspectives. *J. Affect. Disord.* 29, 77–84. doi: 10.1016/0165-0327(93)90025-f

Wiart, L., Petit, H., Joseph, P. A., Mazaux, J. M., and Barat, M. (2000). Fluoxetine in early poststroke depression: a double-blind placebo-controlled study. *Stroke* 31, 1829–1832. doi: 10.1161/01.str.31.8.1829

Zarate, C. Jr., Machado-Vieira, R., Henter, I., Ibrahim, L., Diazgranados, N., and Salvadore, G. (2010). Glutamatergic modulators: the future of treating mood disorders? *Harv. Rev. Psychiatry* 18, 293–303. doi: 10.3109/10673229.2010.511059

Zauner, A., Bullock, R., Kuta, A., Woodward, J., and Young, H. (1996a). "Glutamate release and cerebral blood flow after severe human head injury," in *Proceedings of the Clinical Aspects of Microdialysis* (Berlin: Springer), 40–44. doi: 10.1007/978-3-7091-6894-3_9

Zauner, A., Bullock, R., Kuta, A. J., Woodward, J., and Young, H. F. (1996b). Glutamate release and cerebral blood flow after severe human head injury. *Acta Neurochir. Suppl.* 67, 40–44. doi: 10.1007/978-3-7091-6894-3_9

Zhang, H., Zhang, X., Zhang, T., and Chen, L. (2001). Excitatory amino acids in cerebrospinal fluid of patients with acute head injuries. *Clin. Chem.* 47, 1458–1462. doi: 10.1093/clinchem/47.8.1458

Zhumadilov, A., Boyko, M., Gruenbaum, S. E., Brotfain, E., Bilotta, F., and Zlotnik, A. (2015). Extracorporeal methods of blood glutamate scavenging: a novel therapeutic modality. *Expert. Rev. Neurother.* 15, 501–508. doi: 10.1586/14737175.2015.1032259

Zlotnik, A., Gruenbaum, B. F., Klin, Y., Gruenbaum, S. E., Ohayon, S., Sheiner, E., et al. (2011a). The effects of insulin, glucagon, glutamate, and glucose infusion on blood glutamate and plasma glucose levels in naive rats. *J. Neurosurg. Anesthesiol.* 23, 323–328. doi: 10.1097/ANA.0b013e3182299b15

Zlotnik, A., Gruenbaum, B. F., Mohar, B., Kuts, R., Gruenbaum, S. E., Ohayon, S., et al. (2011b). The effects of estrogen and progesterone on blood glutamate levels: evidence from changes of blood glutamate levels during the menstrual cycle in women. *Biol. Reprod.* 84, 581–586. doi: 10.1095/biolreprod.110.088120

Zlotnik, A., Gruenbaum, S. E., Artru, A. A., Rozet, I., Dubilet, M., Tkachov, S., et al. (2009). The neuroprotective effects of oxaloacetate in closed head injury in rats is mediated by its blood glutamate scavenging activity: evidence from the use of maleate. *J. Neurosurg. Anesthesiol.* 21, 235–241. doi: 10.1097/ANA.0b013e3181a2bf0b

Zlotnik, A., Gurevich, B., Cherniavsky, E., Tkachov, S., Matuzani-Ruban, A., Leon, A., et al. (2008). The contribution of the blood glutamate scavenging activity of

pyruvate to its neuroprotective properties in a rat model of closed head injury. *Neurochem. Res.* 33, 1044–1050. doi: 10.1007/s11064-007-9548-x

Zlotnik, A., Gurevich, B., Tkachov, S., Maoz, I., Shapira, Y., and Teichberg, V. I. (2007). Brain neuroprotection by scavenging blood glutamate. *Exp. Neurol.* 203, 213–220. doi: 10.1016/j.expneurol.2006.08.021

Zlotnik, A., Klin, Y., Gruenbaum, B. F., Gruenbaum, S. E., Ohayon, S., Leibowitz, A., et al. (2012a). beta2 adrenergic-mediated reduction of blood glutamate levels and improved neurological outcome after traumatic brain injury in rats. *J. Neurosurg. Anesthesiol.* 24, 30–38. doi: 10.1097/ANA.0b013e318232deaa

Zlotnik, A., Sinelnikov, I., Gruenbaum, B. F., Gruenbaum, S. E., Dubilet, M., Dubilet, E., et al. (2012b). Effect of glutamate and blood glutamate scavengers oxaloacetate and pyruvate on neurological outcome and pathohistology of the hippocampus after traumatic brain injury in rats. *Anesthesiology* 116, 73–83. doi: 10.1097/ALN.0b013e31823d7731

Zlotnik, A., Klin, Y., Kotz, R., Dubilet, M., Boyko, M., Ohayon, S., et al. (2010). Regulation of blood L-glutamate levels by stress as a possible brain defense mechanism. *Exp. Neurol.* 224, 465–471. doi: 10.1016/j.expneurol.2010.05.009

Conflict of Interest: The authors declare that the research was conducted in the absence of any commercial or financial relationships that could be construed as a potential conflict of interest.

Publisher's Note: All claims expressed in this article are solely those of the authors and do not necessarily represent those of their affiliated organizations, or those of the publisher, the editors and the reviewers. Any product that may be evaluated in this article, or claim that may be made by its manufacturer, is not guaranteed or endorsed by the publisher.

frontiers in Pharmacology

ORIGINAL RESEARCH
published: 07 March 2022
doi: 10.3389/fphar.2022.840320

A Loading Dose of Dexmedetomidine With Constant Infusion Inhibits Intraoperative Neuromonitoring During Thoracic Spinal Decompression Surgery: A Randomized Prospective Study

Tun Liu[1], Yue Qin[1], Huaguang Qi[2], Zhenguo Luo[1], Liang Yan[3], Pengfei Yu[4], Buhuai Dong[1], Songchuan Zhao[3], Xucai Wu[1], Zhen Chang[3], Zhian Liu[5], Xuemei Liu[2], Tao Yuan[2], Houkun Li[3], Li Xiao[1] and Gang Wang[5]*

[1]Department of Anesthesiology, Xi'an Honghui Hospital, Xi'an Jiaotong University Health Science Center, Xi'an, China, [2]Department of Functional Inspection Section, Xi'an Honghui Hospital, Xi'an Jiaotong University Health Science Center, Xi'an, China, [3]Department of Spine Surgery, Xi'an Honghui Hospital, Xi'an Jiaotong University Health Science Center, Xi'an, China, [4]Department of Gastrointestinal Surgery, Xijing Hospital of Digestive Diseases, Xijing Hospital, Fourth Military Medical University, Xi'an, China, [5]The Key Laboratory of Biomedical Information Engineering, Ministry of Education, School of Life Science and Technology, Institute of Biomedical Engineering, Xi'an Jiaotong University, Xi'an, China

OPEN ACCESS

Edited by:
Nesrine Salah El Dine El Sayed, Cairo University, Egypt

Reviewed by:
Susanna Byram, Loyola University Medical Center, United States
Parthiban Velayutham, Advanced Centre for Treatment, India

***Correspondence:**
Tun Liu
spine001@163.com

Specialty section:
This article was submitted to Neuropharmacology, a section of the journal Frontiers in Pharmacology

Received: 21 December 2021
Accepted: 27 January 2022
Published: 07 March 2022

Citation:
Liu T, Qin Y, Qi H, Luo Z, Yan L, Yu P, Dong B, Zhao S, Wu X, Chang Z, Liu Z, Liu X, Yuan T, Li H, Xiao L and Wang G (2022) A Loading Dose of Dexmedetomidine With Constant Infusion Inhibits Intraoperative Neuromonitoring During Thoracic Spinal Decompression Surgery: A Randomized Prospective Study. Front. Pharmacol. 13:840320. doi: 10.3389/fphar.2022.840320

Background: The effect of a bolus dose of dexmedetomidine on intraoperative neuromonitoring (IONM) parameters during spinal surgeries has been variably reported and remains a debated topic.

Methods: A randomized, double-blinded, placebo-controlled study was performed to assess the effect of dexmedetomidine (1 μg/kg in 10 min) followed by a constant infusion rate on IONM during thoracic spinal decompression surgery (TSDS). A total of 165 patients were enrolled and randomized into three groups. One group received propofol- and remifentanil-based total intravenous anesthesia (TIVA) (T group), one group received TIVA combined with dexmedetomidine at a constant infusion rate (0.5 μg kg^{-1} h^{-1}) (D_1 group), and one group received TIVA combined with dexmedetomidine delivered in a loading dose (1 μg kg^{-1} in 10 min) followed by a constant infusion rate (0.5 μg kg^{-1} h^{-1}) (D_2 group). The IONM data recorded before test drug administration was defined as the baseline value. We aimed at comparing the parameters of IONM.

Results: In the D_2 group, within-group analysis showed suppressive effects on IONM parameters compared with baseline value after a bolus dose of dexmedetomidine. Furthermore, the D_2 group also showed inhibitory effects on IONM recordings compared with both the D_1 group and the T group, including a statistically significant decrease in SSEP amplitude and MEP amplitude, and an increase in SSEP latency. No significance was found in IONM parameters between the T group and the D_1 group.

Conclusion: Dexmedetomidine delivered in a loading dose can significantly inhibit IONM parameters in TSDS. Special attention should be paid to the timing of a bolus dose of

dexmedetomidine under IONM. However, dexmedetomidine delivered at a constant speed does not exert inhibitory effects on IONM data.

Keywords: dexmedetomidine, intraoperative neuromonitoring, thoracic spinal decompression surgery, motor evoked potential (MEP), somatosensory evoked potential (SSEP)

1 INTRODUCTION

Thoracic spinal decompression surgery (TSDS) is not as prevalent as cervical or lumbar spinal decompression surgery (Eggspuehler et al., 2007). Due to the rarity of thoracic spinal stenosis and the lack of adequate clinical experience (Stokes et al., 2019), TSDS confers a high risk for neurologic injury and even paralysis (Nuwer and Schrader, 2019). IONM is commonly used during spine surgery to provide real-time feedback of spinal neurological function. Early detection of neurologic dysfunction, using IONM, can alert the surgical team to initiate therapeutic interventions to limit or prevent further injury (Nuwer et al., 2012a; Melachuri et al., 2020). Previous studies reported that inhaled anesthetics are known to attenuate motor evoked potential (MEP) and somatosensory evoked potential (SSEP) as demonstrated by lower amplitude and increased latency on the waveforms (Zentner et al., 1976; Haghighi et al., 1990; Zentner et al., 1992; Chin Ted Chong et al., 2014). Furthermore, attenuated signals could erroneously be interpreted as neurologic injury or diminish the ability to appropriately monitor for neurologic injury (Nuwer et al., 2012b; Nuwer and Schrader, 2019; CoreyWalker and Park, 2020). Propofol has become one of the primary medications used for total intravenous anesthesia (TIVA) during spinal surgery with IONM (Macdonald et al., 2013; CoreyWalker and Park, 2020). Furthermore, remifentanil infusion offers the advantage of quicker recovery from anesthesia, which can facilitate the wake-up test (Imani et al., 2006), and has less variability in SSEP morphology (Samra et al., 2001). Moreover, it was demonstrated that propofol–remifentanil-based TIVA has an advantage over inhalation–intravenous combined anesthesia, because TIVA exerts less influence on synaptic transmission and has minimal effects on the amplitude and latency of IONM (Hermanns et al., 2007; CoreyWalker and Park, 2020). Those effects lead to a lower rate of false-positive waveform changes compared with inhaled anesthetics (Macdonald et al., 2013; CoreyWalker and Park, 2020). However, propofol had a dose-dependent inhibitory effect on MEP amplitude (Nathan et al., 2003; CoreyWalker and Park, 2020); the latest guideline recommended that propofol infusion rate <100 $mg\,kg^{-1}min^{-1}$ is the best recommendation under MEP monitoring (CoreyWalker and Park, 2020). So, maintaining lower propofol infusion rates by adding other types of intravenous anesthetics that do not adversely affect IONM signals can be beneficial.

The usage of dexmedetomidine in general anesthesia has both opioid-sparing (Nan Lin et al., 2019) and propofol-sparing (Ngwenyama et al., 2008) effects. So, dexmedetomidine has been increasingly used as an adjuvant to general anesthesia (Deiner et al., 2017; Silva-et al., 2019). However, effects of dexmedetomidine on SSEP and MEP remain a topic of hot debate (Endrit Bala et al., 2008; Tobias et al., 2008; Mahmoud et al., 2010; Rozet et al., 2015; Holt et al., 2020). Some authors demonstrated that dexmedetomidine does not influence IONM parameters when delivered by a loading dose and then followed by a constant infusion rate in adults (Lin et al., 2014; Rozet et al., 2015) and adolescents (Tobias et al., 2008). However, some authors demonstrated that dexmedetomidine administration can exert inhibitory effects on IONM (Mohamed Mahmoud et al., 2017; Holt et al., 2020). Moreover, dexmedetomidine enhances inhibitory synaptic transmission through activation of descending noradrenergic (NA) system (Yan Lu, 2007; Yusuke Funai a and Anthony, 2014). Furthermore, NA produces postsynaptic hyperpolarization (Grudt and Perl, 2002; Yan Lu, 2007). So, systemic administration of dexmedetomidine can therefore theoretically inhibit IONM to different degrees by enhancing inhibitory synaptic neurotransmission in both sensory and motor neurons.

We hypothesized that dexmedetomidine delivered in a loading dose (1 $g\,kg^{-1}$ in 10 min) and then at a constant infusion rate (0.5 $\mu g\,kg^{-1}\ h^{-1}$) has inhibitory effects on IONM recording. However, dexmedetomidine at a constant rate of infusion (0.5 $\mu g\,kg^{-1}\ h^{-1}$) would not significantly impact IONM data. To test our hypothesis, we performed a randomized, double-blinded, placebo-controlled trial in adult patients who underwent TSDS in our hospital.

2 METHODS

2.1 Ethics

Ethical approval for this study was provided by the Ethical Committee of Xi'an Honghui Hospital, Xi'an Jiaotong University Health Science Center, Xi'an, China, on October 1, 2018 (reference number No. 201801032) prior to patient enrolment and the start of the trial. The trial was registered at ChineseClinicalTrialRegistry.cn (Number: ChiCTR1800018685, October 3, 2018) prior to patient enrollment. Written informed consent was obtained from all subjects participating in the trial. This manuscript adheres to the applicable Consolidated Standards of Reporting Trials (CONSORT) guidelines.

2.2 Patients

A total of 210 patients were assessed for eligibility in our hospital. Inclusion criteria are as follows: (1) age between 18 and 60 years and ASA status from I to III; and (2) magnetic resonance image (MRI) studies showed thoracic spinal stenosis evidence (Tun Liu et al., 2021). Exclusion criteria are as follows: (1) poor quality of

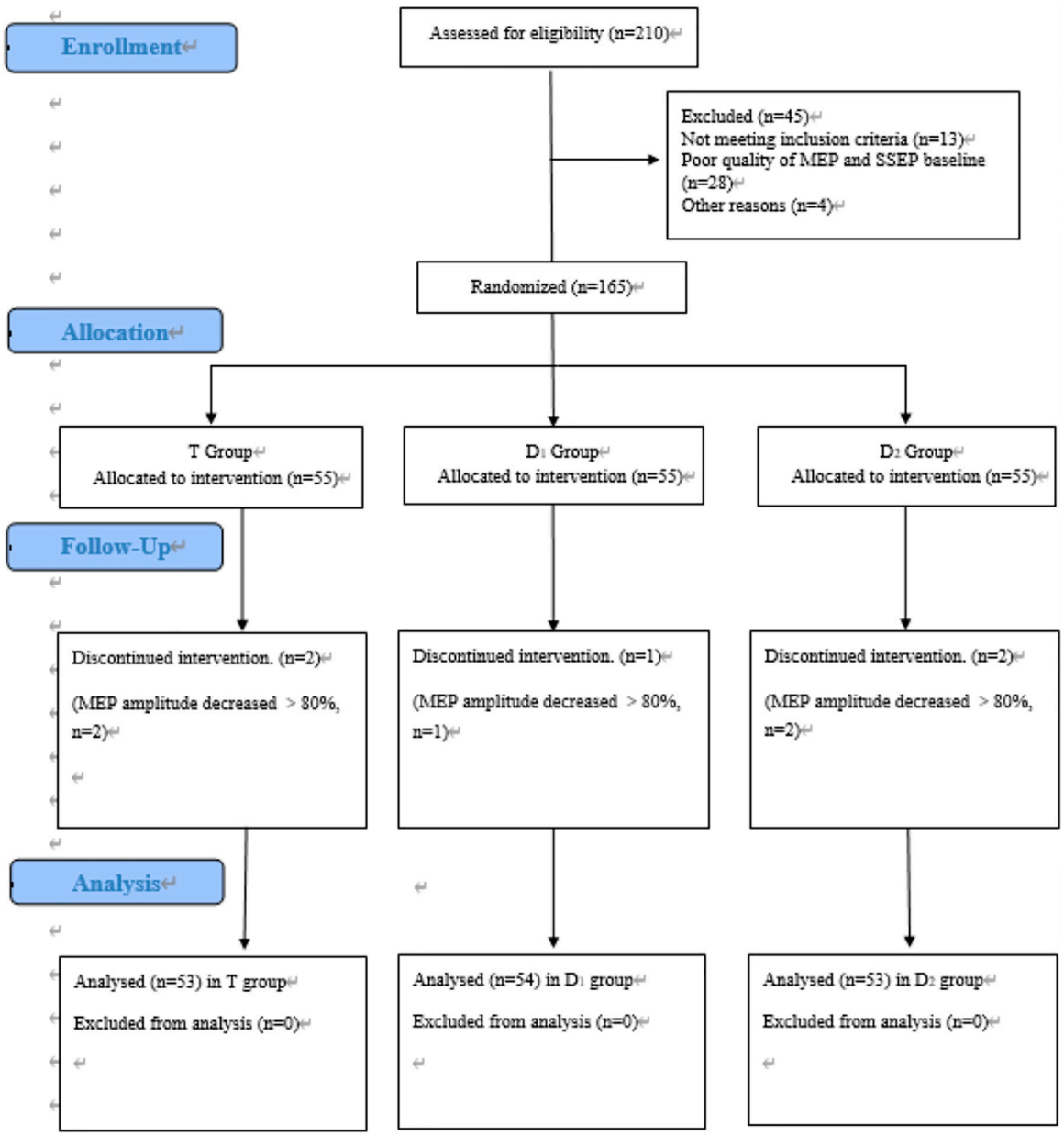

FIGURE 1 | CONSORT flow diagram of patients' inclusion. MEP, motor evoked potential. SSEP, somatosensory evoked potential. T group: propofol- and remifentanil-based total intravenous anesthesia (TIVA) group; D_1 group: TIVA combined with dexmedetomidine at a constant infusion rate; D_2 group: TIVA combined with dexmedetomidine delivered by a loading dose and then by a constant infusion rate.

waveforms baseline; (2) patients who were unable to provide informed consent; (3) patients who were alcohol or drug abusers; and (4) not meeting inclusion criteria. After our inclusion and exclusion criteria were discussed, 165 patients identified as enrolled in the trial, and 160 patients finally completed the trial. Our study flowchart is shown in **Figure 1**. Anesthesia-related assessments were completed by an independent anesthesiologist in the post-anesthesia care unit (PACU); orthopedic-related assessments were completed by an independent orthopedic surgeon in the 6-month follow-ups.

2.3 Randomization and Blinding

Randomization was generated by SPSS v24.0 statistics software (IBM; Armonk, NY). The randomization results were concealed in sealed, prenumbered, opaque envelopes prepared by an independent bio-statistician. Those envelopes were kept in a box until required. From the start of muscle incision to muscle closure in the operation room, consecutively recruited patients were randomly assigned to receive an intravenous bolus of dexmedetomidine 1 $\mu g\,kg^{-1}$ infusion over 10 min, then followed by continuous dexmedetomidine infusion at a rate of

0.5 μg kg^{-1} h^{-1} (the D_2 group), or a volume matched bolus of 0.9% saline over 10 min, then followed by continuous dexmedetomidine infusion at a rate of 0.5 μg kg^{-1} h^{-1} (the D_1 group), or a volume matched bolus and continuous infusion of 0.9% saline (the T group) in a 1:1:1 ratio, according to the random number allocation. An independent anesthesiologist was in charge of preparing and allocating the testing drugs to the corresponding anesthesiologists. An independent team of neurophysiologists was in charge of recording IONM data. So, the anesthesiologists, surgeons, neurophysiologists, and patients were blinded to treatment groups.

2.4 Anesthesia Protocol

Anesthesia induction was consistent with our previous protocol (Tun Liu et al., 2021). Anesthesia was induced by propofol 1.5–2.0 mg kg^{-1} and sufentanil 0.4–0.6 μg kg^{-1}, midazolam 0.01 mg kg^{-1}, and cisatracurium 0.10–0.15 mg kg^{-1}. From tracheal intubation until surgical exposure, cisatracurium 1.5–2.5 mg kg^{-1} min^{-1} was maintained. A real-time train-of-four (TOF) ratio was recorded before eliciting MEP signals to rule out undesirable suppressive effects brought by muscle relaxants on IONM.

Anesthesia was maintained by the Diprifusor propofol infusion system, with a target-controlled infusion (TCI) of propofol 2.0–4.0 μg ml^{-1} and 0.15–0.30 μg kg^{-1} min^{-1}. In the D_1 group, dexmedetomidine was infused at 0.5 μg kg^{-1}h^{-1} at a constant infusion rate from muscle incision to muscle closure. In the D_2 group, dexmedetomidine was delivered by a loading dose (1.0 μg kg^{-1} over 10 min) and then followed by a constant infusion rate (0.5 μg kg^{-1} h^{-1}). The depth of anesthesia was adjusted by varying the propofol or remifentanil doses based on bispectral monitor (BIS, Aspect Medical Systems Inc, United States), and MAP was maintained between 70 and 80 mmHg and augmented by ephedrine as needed.

2.5 Acquisition of SSEP and MEP Signals

We recorded MEP to abductor hallucis (AH) muscles in the lower extremities and the first dorsal interosseous muscles in the upper extremities (control). Because previous studies demonstrated that AH muscles had the highest rate, even if the patients with preoperative severe motor deficit (Kobayashi et al., 1976a; Kobayashi et al., 1976b). The stimulation electrodes were inserted subcutaneously over motor cortex regions C3–C4 according to the 10/20 EEG international system. Recording electrodes are placed into the AH muscles and the first dorsal interosseous muscles. MEPs were elicited by subcutaneous needle electrodes by stimulating at a constant voltage ((220–360 V) and five to eight train pulses, with a duration of 300 μs. The signal analysis time was 100 m. The bandpass filter was between 10 and 1,500 Hz (Zhuang et al., 1976). The stimulations were delivered by a commercially available IONM stimulator (Cascade, Cadwell Laboratories Inc., United States) with responses recorded on the same device used for obtaining SSEP. The amplitudes of MEP were measured by recording baseline-to-first negative peak voltages.

We recorded SSEP to the median nerve for the upper extremity (control) and the posterior tibial nerve for the lower extremity. SSEPs were recorded using adhesive gel Ag-AgCl electrodes placed at Cz and Fpz positions for active and reference according to the 10/20 EEG international system. We performed median nerve stimulation bilaterally at the wrist, and performed posterior tibial nerve stimulation bilaterally at the head of the fibula or the medial malleolus of the ankle. The parameters of recording SSEP were as follows: the median nerve was stimulated at 15 mA, and the posterior tibial nerves were stimulated at 25 mA. The bandpass filter was between 30 and 300 Hz, and the waveforms were displayed in a 100-m window. The single pulse was set between 5.1 and 5.7 Hz. We measured the amplitude of P38-N45 and the latency of P38. To minimize signal interference, 300 to 400 stimulation repetition is averaged to obtain each SSEP sweep (Wang et al., 2017).

MEP peak-to-peak amplitudes, as well as amplitudes and latencies of SSEP obtained before administration of our testing drugs (dexmedetomidine or saline), were defined as baseline values. After administration of the testing drug, time course of the relative amplitude and relative latency of the evoked potentials in each group were calculated as follows: relative value (%) = absolute value/baseline value×100% (Furutani et al., 2019). Because absolute amplitudes of MEP differ greatly in patients, comparison of absolute amplitudes among different groups was very difficult (Furutani et al., 2019).

We adopted IONM warning criteria as our study drug discontinuation criteria, including the following: (1) a change in SSEP was defined as a decrease of greater than 50% in amplitude and/or 10% increase in latency of the baseline cortical wave, or as reported per each case; and (2) a change in MEP was defined as a decrease of more than 80% in amplitude of the baseline value, or as reported per case (Nuwer et al., 2012c; Nuwer and Schrader, 2019).

2.6 Time Points Set for Measuring IONM Parameters

MEP parameters were measured at seven time points: T_1: Before dexmedetomidine or placebo infusion (at the same time as the start of muscle incision), we defined it as "baseline value"; T_2: 10 min after dexmedetomidine or placebo infusion; T_3: 20 min after dexmedetomidine or placebo infusion; T_4: At the start of spine decompression; T_5: 10 min after decompression; T_6: 20 min after decompression; and T_7: Muscle closure. SSEP parameters were measured at nine time points: T_1: Before the start of dexmedetomidine or placebo infusion (at the same time as the start of muscle incision), we defined it as "baseline value"; T_2: 5 min after dexmedetomidine infusion; T_3: 10 min after infusion; T_4: 15 min after infusion; T_5: 20 min after infusion and then every 10 min until decompression; T_6: At the start of spine decompression; T_7: 5 min after spine decompression; T_8: 10 min after spine decompression and then every 10 min until muscle closure; and T_9: Surgery over.

2.7 Endpoints

The primary endpoint of the study was designed to evaluate the effects of dexmedetomidine by different approaches of

administration on the amplitude and the latency of both SSEP and MEP in patients during TSDS.

Our secondary endpoints were aimed at evaluating the effects of dexmedetomidine on the intraoperative anesthetic requirement (consumption of propofol and remifentanil), hemodynamic stability (MAP and HR), anesthesia recovery time (time interval from cessation of anesthesia to following verbal commands and tracheal extubation) (Ku et al., 2002) in the operation room ,and postoperative pain scores assessed by VAS score in the PACU.

2.8 Sample Size Calculation and Statistical Analysis

Sample size calculation was performed by PASS 15 software (NCSS LLC, United States). Based on our pre-trial data (n = 24) on SSEP amplitude after 15 min of the test drug (dexmedetomidine or saline) infusion, SSEP amplitudes in the T, the D_1, and the D_2 groups were 1.83 ± 1.13 μV, 1.78 ± 1.61 μV, and 1.56 ± 1.90 μV, respectively. We chose the T and the D_1 groups to calculate their sample size. Forty patients per group was the smallest sample size required to demonstrate a difference between the T group and the D_1 group with an effect size of 0.8, a statistical power of 80%, an allocation ratio of the two groups of 1: 1, and a two-sided α level of 0.05. Considering possible intraoperative waveform changes during the surgery, we planned to recruit at least 50 patients into each group.

All data were analyzed using SPSS24.0 statistics software (SPSS24.0, Chicago, IL, United States). All measurement and enumeration data are presented as the mean± standard deviations (X± S D). The amplitude and latency of both MEP and SSEP were analyzed using the Mann–Whitney U test. Demographic data, hemodynamic parameters, anesthesia recovery time, and intraoperative anesthetic requirement were analyzed using the independent t-test among different groups. Within-group analysis was used. Qualitative or categorical variables were compared using the chi-square test or the Fisher test as appropriate. All reported p values less than 0.05 were considered to indicate statistical significance.

3 RESULTS

Between October 2018 and December 2020, a total of 210 patients were assessed for eligibility, and 160 patients finally completed the trial. **Figure 1** shows the flow diagram of the enrollment.

3.1 Comparison of the General Data of the Study Population

Compared with the T group, patients in the D_1 group (591.9 ± 102.5 vs. 787.8 ± 68.3, $p < 0.05$) and the D_2 group (539.4 ± 70.1 vs. 787.8 ± 68.3, $p < 0.05$) showed much less propofol consumption. Furthermore, patients in the D_1 group (2,512.5 ± 280.4 vs. 2,981.9 ± 465.8, $p < 0.05$) and the D_2 group (2,315.5 ± 338.5 vs. 2,981.9 ± 465.8, $p < 0.05$) also showed much less remifentanil consumption. Moreover, patients in the D_2 group showed more ephedrine consumption than those in the D_1 group (20.1 ± 8.6 vs. 11.1 ± 8.1, $p < 0.05$) and the T group (20.1 ± 8.6 vs. 9.6 ± 7.0, $p < 0.05$). Furthermore, the D_2 group showed a longer anesthesia recovery time, compared with the D_1 group (15.7 ± 4.1 vs. 12.6 ± 2.8, $p < 0.05$) and the T group (15.7 ± 4.1 vs. 14.9 ± 3.7, $p < 0.05$). Although the differences have statistical significance, they are in the order of 2 or 3 min, which is not clinically relevant. No significance was found among the different groups in terms of age, sex, weight, height, symptom duration, operation time, bleeding volume, surgical location, MAP, or heart rate (HR) before the start of anesthesia induction, and VAS score after general anesthesia recovery in the PACU. As depicted in **Table 1**. Furthermore, bleeding volume in our study was 569.15 ± 217.30 ml. In particular, massive blood loss in a short time (>500 ml in less than 30 min) during the decompression procedure was observed in 31 patients.

3.2 Comparison of SSEP and MEP Parameters

3.2 1 Comparison of the IONM Baseline Values Among Different Groups

No significance was found in both amplitude and latency before the start of dexmedetomidine or placebo infusion among different groups. SSEP amplitude baseline values in the T, the D_1, and the D_2 groups were 1.87 ± 1.05 μV, 1.91 ± 1.11 μV, and 1.86 ± 1.08 μV, respectively. SSEP latency baseline value in the T, the D_1, and the D_2 groups were 42.81 ± 3.94 m, 43.12 ± 3.36 m, and 42.98 ± 3.40 m, respectively.

3.2.2 Comparison of Time Course of the Relative Amplitude and Relative Latency of the Evoked Potentials

In the D_2 group, within-group analysis showed suppressive effects on IONM parameters compared with baseline value after dexmedetomidine (1 μg kg^{-1} in 10 min) infusion, including a significant decrease in SSEP amplitude (lasted for 25 min) and MEP amplitude (lasted for at least 10 min), and an increase in SSEP latency (lasted for 10 min). Compared with the D_1 group and the T group, the D_2 group also showed inhibitory effects on IONM recordings, including a significantly lower SSEP amplitude (lasted for 15 min) and MEP amplitude (lasted for at least 10 min) and a significantly prolonged SSEP latency (lasted for 10 min). No significance was found in IONM data between the T group and the D_1 group, as depicted in **Figure 2**. Furthermore, in the D_2 group, within-group analysis showed that a bolus of dexmedetomidine (1 μg kg^{-1} in 10 min) could increase SSEP latency by 5.50% ± 3.51%, and decreased MEP amplitude and SSEP amplitude by 27.13% ± 12.30% and 24.75% ± 15.04%, respectively, compared with the baseline value.

3.3 Comparison of MAP and HR Parameters

No significance was found in MAP and HR before the start of dexmedetomidine or placebo infusion among different groups (**Table 1**). In the D_2 group, within-group analysis showed a significant decrease in MAP and HR compared with baseline after dexmedetomidine (1 μg kg^{-1} in 10 min) infusion and lasted

TABLE 1 | The general data of the three groups.

	T group (n = 53)	D_1 group (n = 54)	D_2 group (n = 53)
Demographic data			
Age (years)	42.3 ± 16.2	43.4 ± 15.3	42.9 ± 15.7
Sex (M/F)	30/23	29/25	31/23
Height (cm)	168.7 ± 6.2	168.1 ± 5.6	169.2 ± 6.4
Weight (kg)	60.2 ± 12.8	61.2 ± 11.3	61.9 ± 10.7
Symptom duration (months)	4.7 ± 5.3	5.0 ± 4.6	4.9 ± 4.1
Perioperative data			
Operation time (min)	212.3 ± 105.1	209.0 ± 99.7	204.6 ± 101.2
Bleeding volume (ml)	563.2 ± 213.1	571.2 ± 200.2	559.2 ± 220.4
MAP before anesthesia induction (mmHg)	74.3 ± 5.5	74.8 ± 6.7	73.9 ± 6.3
HR before anesthesia induction (bpm)	75.2 ± 5.1	75.7 ± 6.3	75.4 ± 6.8
Surgical location			
$T_{1\text{-}8}$ (n =)	7	6	6
$T_{9\text{-}12}$ (n =)	46	48	47
VAS score in PACU	4.6 ± 1.4	4.9 ± 0.8	4.8 ± 1.1
Anaesthesia recovery time (min)	14.9 ± 3.7	12.6 ± 2.8[a]	15.7 ± 4.1[c]
Propofol consumption (mg)	787.8 ± 68.3	591.9 ± 102.5[a]	539.4 ± 70.1[b,c]
Remifentanil consumption (ug)	2,981.9 ± 465.8	2,512.5 ± 280.4[a]	2,315.5 ± 338.3[b,c]
Ephedrine consumption (mg)	9.6 ± 7.0	11.1 ± 8.1	20.1 ± 8.6[b,c]
IONM baseline value			
SSEP amplitude (μV)	1.87 ± 1.05	1.91 ± 1.11	1.86 ± 1.08
SSEP latency (ms)	42.81 ± 3.94	43.12 ± 3.36	42.98 ± 3.40

VAS: visual analogue scale; PACU: post anesthesia care unit. IONM: intraoperative neuromonitoring; SSEP: somatosensory evoked potential; MEP: motor evoked potential; T group: propofol- and remifentanil-based total intravenous anesthesia group; D_1 group: TIVA, combined with dexmedetomidine at a constant infusion rate; D_2 group: TIVA, combined with dexmedetomidine delivered by loading dose and then by a constant infusion rate. Data were expressed as mean ± standard deviations (X±SD) for VAS, score, time of anesthesia recovery, propofol consumption, remifentanil consumption, and ephedrine consumption. The amplitude and latency of both MEP and SSEP were analyzed using the Mann–Whitney U test. Demographic data, hemodynamic parameters, anesthesia recovery time, and intraoperative anesthetic requirement were analyzed using the independent t-test among different groups. Qualitative or categorical variables were compared using the chi-square test or the Fisher test as appropriate.

[a]$p < 0.05$, *D_1 group compared with the T group.*

[b]$p < 0.05$, *D_2 group compared with the T group.*

[c]$p < 0.05$, *D_2 group compared with the D_1 group.*

for 15 min. Furthermore, a significant decrease in the MAP and HR was found between the T group and the D_2 group after a bolus dose of dexmedetomidine. As is depicted in **Figure 3**. This indicates an unstable cardiovascular system after dexmedetomidine was delivered by a bolus dose. In contrast, after the testing drug was delivered only at a constant infusion rate in the D_1 group, no significant difference in MAP or HR at various time points was found, and both parameters were maintained within the clinically normal range.

4 DISCUSSION

Our study aimed at exploring effects of dexmedetomidine by different approaches of administration on the amplitude and the latency of both SSEP and MEP in patients during TSDS. The T group received TIVA, the D_1 group received TIVA combined with a constant infusion rate of dexmedetomidine, and the D_2 group received TIVA combined with dexmedetomidine delivered in a loading dose and then at a constant infusion rate. Within-group analysis showed that dexmedetomidine in the D_2 group exerted inhibitory effects on amplitude of both SSEP and MEP, as well as latency of SSEP. Compared with both the T group and the D_1 group, patients in the D_2 group also showed a significant decrease in amplitude of the waveforms and an increase in SSEP latency. Here, we demonstrated that dexmedetomidine delivered in a loading dose and then at a constant infusion rate had inhibitory effects on IONM recording in TSDS. However, dexmedetomidine delivered only at a constant infusion rate did not influence IONM parameters.

4.1 Time Points Set for Measuring IONM Parameters

Rozet et al. (2015) demonstrated that dexmedetomidine delivery by a bolus dose (0.6 μg kg^{-1} infused in 10 min) and followed by 0.6 μg kg^{-1} h^{-1} did not affect SSEP and MEP in adult patients during spine surgery. However, Rozet recorded both amplitude and latency twice within the first 30 min after dexmedetomidine administration and then recorded IONM parameters every 30 min until 240 min after dexmedetomidine administration. Statistically significant change in IONM parameters would likely be missed and ignored, because based on our results, compared with the T group and the D_1 group, the significant inhibitory effects of dexmedetomidine delivered in a bolus dose on SSEP amplitude, SSEP latency, and MEP amplitude lasted for 15 min, 10 min, and at least 10 min, respectively. If the interval of IONM recording is more than 15 min within the first 30 min after dexmedetomidine (1 μg kg^{-1}), it would likely miss the statistically significant change in amplitude and latency of evoked potentials.

Furutani et al. obtained MEP waveforms at 2, 4, 6, 8, and 10 min after a bolus dose of the testing drug (Furutani et al.,

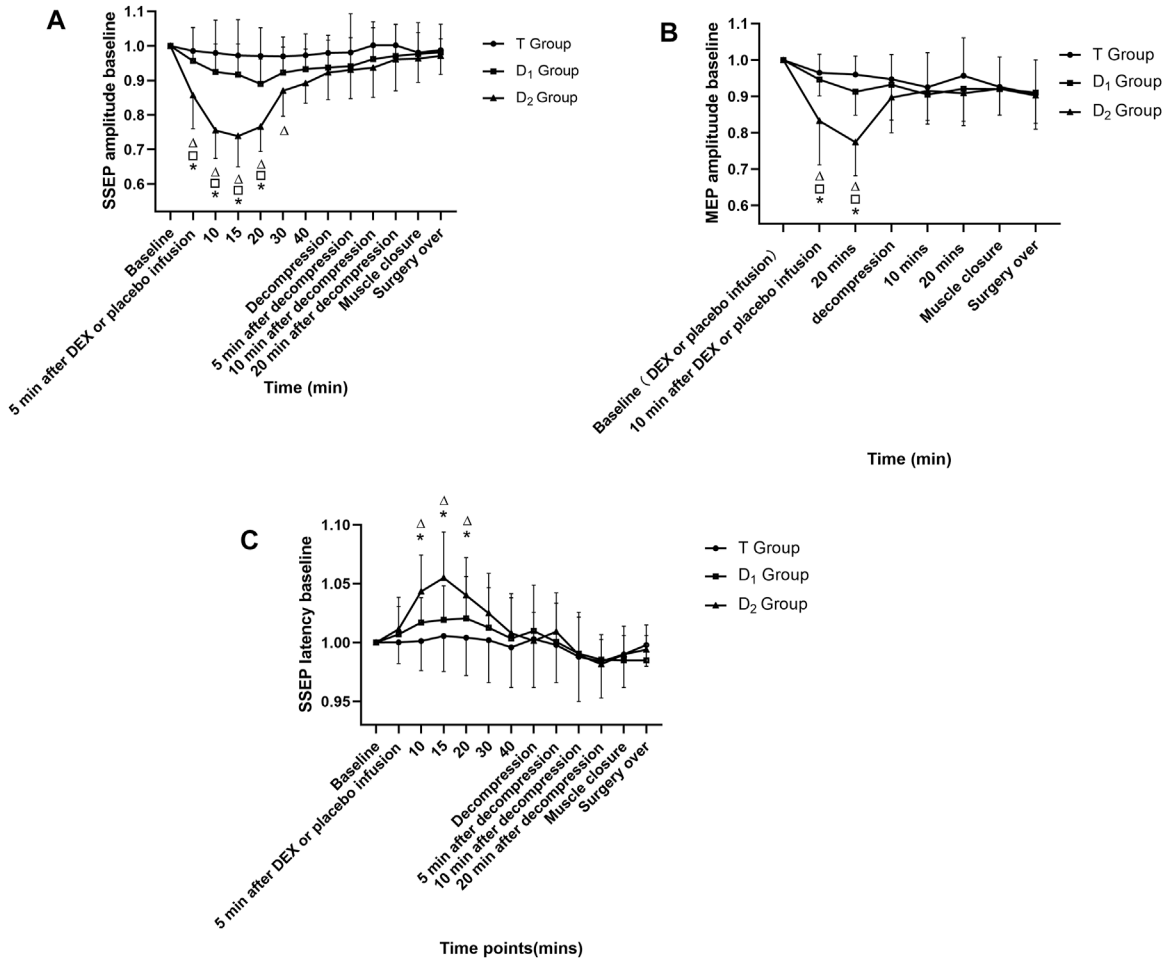

FIGURE 2 | Time course of SSEP and MEP amplitude variability, as well as SSEP latency variability in the three groups. △Compared with baseline value (after muscle incision, but before dexmedetomidine or placebo infusion) at corresponding time points, $p < 0.05$; compared with the D_1 group at corresponding time points, $p < 0.05$; * compared with the T group at corresponding time points, $p < 0.05$. DEX: dexmedetomidine; the T group: propofol- and remifentanil-based total intravenous anesthesia group; the D_1 group: TIVA combined with dexmedetomidine at a constant infusion rate; the D_2 group: TIVA combined with dexmedetomidine delivered by a loading dose and then by a constant infusion rate.

2019). However, we limited the frequency of MEP recording. First, MEP recording has more possibilities of adverse events (Yoshida et al., 1976a). Second, according to the latest guidance (Nuwer et al., 2012a) and our previous study (Tun Liu et al., 2021), it was recommended that every high-risk procedure (Yoshida et al., 1976b) (posterior decompression in OPLL patients and correction in deformity patients) after 10–20 min (Tun Liu et al., 2021), which is a critical time point, needs to put special emphasis on the change of IONM. Therefore, we recorded IONM parameters before and after high-risk procedures or according to specific needs during surgery to judge whether patients have spinal injuries.

4.2 Effects of Dexmedetomidine on Both Amplitude and Latency

Yusuke Funai and Anthony (2014) demonstrated that dexmedetomidine infusion enhances inhibitory synaptic transmission in the superficial dorsal horn (SDH) by activating the descending noradrenergic (NA) system. Then, NA can produce postsynaptic hyperpolarization (Grudt and Perl, 2002; Yan Lu, 2007). So, systemic administration of dexmedetomidine can therefore theoretically inhibit IONM parameters to different degrees by enhancing inhibitory synaptic neurotransmission in both motor and sensory neurons, especially when dexmedetomidine was delivered by a bolus dose (1 $\mu g\,kg^{-1}$ in 10 min), because larger doses of dexmedetomidine can lead to obvious inhibitory synaptic neurotransmission in neurons, thus resulting in attenuated amplitude and latency of the evoked potentials (Mohamed Mahmoud et al., 2010; Chen et al., 2015). Hence, IONM parameters would be more likely to be inhibited after dexmedetomidine 1 $\mu g\,kg^{-1}$ in 10 min. On the contrary, IONM waveforms would be less likely to be affected when smaller doses of dexmedetomidine were administered (at a constant infusion rate, 0.5 $\mu g\,kg^{-1}\,h^{-1}$)

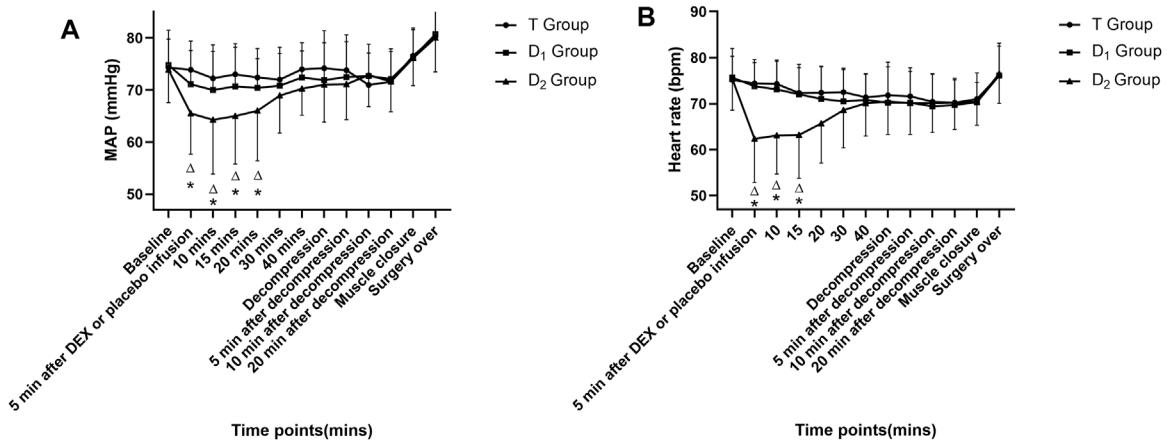

FIGURE 3 | Time course of intraoperative mean arterial pressure (MAP) (as depicted in 3A) and heart rate (HR) (as depicted in 3B) in the three groups. △ Compared with baseline value (after muscle incision, but before dexmedetomidine or placebo infusion) at corresponding time points, $p < 0.05$; * compared with the T group at corresponding time points, $p < 0.05$. DEX: dexmedetomidine; the T group: propofol- and remifentanil-based total intravenous anesthesia group; the D_1 group: TIVA combined with dexmedetomidine at a constant infusion rate; the D_2 group: TIVA combined with dexmedetomidine delivered by a loading dose and then by a constant infusion rate.

(Endrit Bala et al., 2008; Chen et al., 2015; Li et al., 2016; Liu et al., 2021).

Mahmoud et al. (2010) and Mohamed Mahmoud et al. (2017) reported that dexmedetomidine delivered by loading dose and then a constant infusion rate added to TIVA can decrease MEP amplitude in patients aged between 10 and 25 years. We excluded patients aged under 18 years old and abandon inhalation anesthetics in our study, for two reasons: (1) dexmedetomidine is not recommended for adolescents according to the FDA (SudIvya Sharma, 2013); and (2) accuracy of IONM could be adversely affected by the immature neural pathways of adolescents, and the differences between adolescents and adults in neuron structure and organization can increase the bias to the conclusion[26]. Although we exclude adolescent patients, we also reached a similar conclusion: dexmedetomidine (1 μg kg^{-1} in 10–20 min) does exert statistically inhibitory effects on IONM parameters. In our study, dexmedetomidine (1 μg kg^{-1} in 10 min) can inhibit IONM parameters within warning criteria (Nuwer and Schrader, 2019; Tun Liu et al., 2021). The suppressive effects on MEP and SSEP lasted for more than 10 min, and no more than 25 min, respectively. Therefore, we recommended that anesthesiologists should consider the time point of a bolus dose of dexmedetomidine administration during spine surgery.

4.3 Effects of Dexmedetomidine on Cardiovascular Stability

MAP could influence human autoregulation by maintaining stable cerebral blood flow (CBF) and spinal cord blood flow (SCBF) (Crystal et al., 2014; Meng et al., 2019). Furthermore, previous studies revealed that hypotension intraoperatively can increase the likelihood of neurologic deficits by reducing spinal cord perfusion pressure (Joshua Yang et al., 2018; CoreyWalker and Park, 2020). Schwan et al. (2020) reported that evoked potential waveforms can be lost after recurrent bradycardia during spinal surgery. So, bradycardia and hypotension should be avoided strictly during spinal surgeries, according to the latest guidance (Vitale et al., 2014; CoreyWalker and Park, 2020). A loading dose of dexmedetomidine (1 μg/kg in 10 min) has inhibitory effects on both MAP and HR, and lasted for 15 min. Anesthesiologists and neurophysiologists should be aware of this effect.

Lieberman et al. demonstrated that the serum concentration of propofol may increase dramatically during hemorrhage in a swine model (JeremyLieberman, 2013; Lieberman et al., 2018a; Lieberman et al., 2018b). Furthermore, hemorrhage is associated with a decrease in MEP amplitude (Lieberman et al., 2018b). Furthermore, elevated levels of propofol infusion can occasionally lead to hyperlactacidemia (Parke et al., 1992; Marinella, 1996). Therefore, to avoid excessive propofol consumption, using an adjuvant in general anesthesia that does not have an adverse influence on IONM and cardiovascular stability can be beneficial. We demonstrated that dexmedetomidine administrated at a constant infusion rate does not influence IONM or cardiovascular stability and has propofol-sparing effects.

4.4 Limitations

Our study has some limitations. Firstly, a decrease in MAP and HR after dexmedetomidine (1 μg kg^{-1}) could be identified by the attending anesthesiologists and might confound our blinding. However, it is less likely to affect our results, because the IONM parameters were recorded by an independent and blinded neurophysiologist. Secondly, we do not have MEP waveforms 20 min after dexmedetomidine (1 μg kg^{-1}) until decompression, because we limited the frequency of MEP recording. So, the inhibitory effects of dexmedetomidine (1 μg kg^{-1} in 10 min) on MEP amplitude might last for more than 10 min. However, there is no significant difference in MEP amplitude among different groups at the start of spine decompression, indicating adequate

time to eliminate the adverse effects of dexmedetomidine on MEP amplitude. So, the inhibitory effects of dexmedetomidine ($1\ \mu g\ kg^{-1}$) were less likely to affect our MEP waveforms before and after high-risk procedures.

5 CONCLUSION

A bolus dose of dexmedetomidine with a constant infusion rate can significantly increase the latency of SSEP and reduce the amplitude of both SSEP and MEP in TSDS. Special attention should be paid to the timing of dexmedetomidine ($1\ \mu g\ kg^{-1}$ in 10 min) administration under IONM. However, dexmedetomidine can be delivered at a constant rate ($0.5\ \mu g\ kg^{-1}\ h^{-1}$) because it does not exert an inhibitory effect on IONM parameters.

DATA AVAILABILITY STATEMENT

The original contributions presented in the study are included in the article/**Supplementary Material**, further inquiries can be directed to the corresponding author.

ETHICS STATEMENT

Ethical approval for this study was provided by the Ethical Committee of Xi'an Honghui Hospital, Xi'an Jiaotong University Health Science Center, Xi'an, China, on October 1, 2018 (reference number No. 201801032) prior to patient enrolment and the start of the trial. The patients/participants provided their written informed consent to participate in this study.

AUTHOR CONTRIBUTIONS

TL: Design and initiation of the study, patient recruitment, monitoring of processes, compilation of the CRF database, statistical analyses, composition of the first draft of the manuscript, and preparation of the figures. YQ, HQ, ZL, PY, BD, SZ, XW, ZC, ZL, XL, TY, HL, and LX: Design and initiation of the study, patient recruitment, monitoring of processes, compilation of the CRF database, statistical analyses, composition of the first draft of the manuscript, and preparation of the figures. GW, TY, and XL: Contributed to the interpretation of the data. Revision and approval of the final version of the paper: all authors.

FUNDING

This work was supported in part by the National Natural Science Foundation of China under Grants 32071372 and 31571000.

ACKNOWLEDGMENTS

We thank Nan Qin, Minyan Xu, LY, and Shuangqiang Yi from the Department of Anesthesiology, Xi'an Honghui Hospital, Xi'an Jiaotong University Health Science Center who helped in patients' testing drug or placebo allocation before anesthesia induction and anesthesia-related assessments in the PACU. We thank Yang Yuan, Xiao Song, Chuangli Li, Chunmiao Hou, and Yuchen Wang from the Department of Functional Inspection Section, Xi'an Honghui Hospital, Xi'an Jiaotong University Health Science Center who provided insight, knowledge, and neurophysiology-technical support that greatly assisted our research activities. We thank Wentao Wang, Junsong Yang, Ruiguo Wang, and Jiayuan Wu from the Department of Spine Surgery, Xi'an Honghui Hospital, Xi'an Jiaotong University Health Science Center who helped in patients' follow-up investigation.

SUPPLEMENTARY MATERIAL

The Supplementary Material for this article can be found online at: https://www.frontiersin.org/articles/10.3389/fphar.2022.840320/full#supplementary-material

REFERENCES

Chen, Z., Lin, S., and Shao, W. (2015). Effects on Somatosensory and Motor Evoked Potentials of Senile Patients Using Different Doses of Dexmedetomidine during Spine Surgery. *Irish J. Med. Sci.* 184, 813–818. doi:10.1007/s11845-014-1178-0

Chin Ted Chong, M., Anaes, M. M, FanzcaManninen, P., Frcpc, M. D., Vanitha Sivanaser, M., et al. (2014). Direct Comparison of the Effect of Desflurane and Sevoflurane on Intraoperative Motor-Evoked Potentials Monitoring. *J. Neurosurg. Anesthesiol* 26, 306–312. doi:10.1097/ANA.0000000000000041

CoreyWalker, H. J. K. T., and Park, P. (2020). *Neuroanesthesia Guidelines for Optimizing Transcranial Motor Evoked Potentials Neuromonitoring during Deformity and Complex Spinal Surgery: A Delphi Consensus Study*. SPINE.

Crystal, G. J., Czinn, E. A., and Salem, M. R. (2014). The Mechanism of Increased Blood Flow in the Brain and Spinal Cord during Hemodilution. *Anesth. Analg* 118, 637–643. doi:10.1213/ANE.0000000000000078

Deiner, S., Luo, X., Lin, H. M., Sessler, D. I., Saager, L., Sieber, F. E., et al. (2017). Intraoperative Infusion of Dexmedetomidine for Prevention of Postoperative Delirium and Cognitive Dysfunction in Elderly Patients Undergoing Major Elective Noncardiac Surgery: A Randomized Clinical Trial. *JAMA Surg.* 152, e171505. doi:10.1001/jamasurg.2017.1505

Eggspuehler, A., Sutter, M. A., Grob, D., Porchet, F., Jeszenszky, D., and Dvorak, J. (2007). Multimodal Intraoperative Monitoring (MIOM) during Surgical Decompression of Thoracic Spinal Stenosis in 36 Patients. *Eur. Spine J.* 16 (Suppl. 2), S216–S220. doi:10.1007/s00586-007-0425-8

Endrit Bala, D. I. S., Nair, D. R., McLain, R., and Dalton, J. E. (2008). Ehab Farag, Motor and Somatosensory Evoked Potentials Are Well Maintained in Patients Given Dexmedetomidine during Spine Surgery. *Anesthesiology* 109, 417–425. doi:10.1097/ALN.0b013e318182a467

Furutani, K., Deguchi, H., Matsuhashi, M., Mitsuma, Y., Kamiya, Y., and Baba, H. (2019). A Bolus Dose of Ketamine Reduces the Amplitude of the Transcranial Electrical Motor-Evoked Potential. *J. Neurosurg. Anesthesiology Publish Ahead Print*. doi:10.1097/ana.0000000000000653

Grudt, T. J., and Perl, E. R. (2002). Correlations between Neuronal Morphology and Electrophysiological Features in the Rodent Superficial Dorsal Horn. *J. Physiol.* 540, 189–207. doi:10.1113/jphysiol.2001.012890

Haghighi, S. S., Green, K. D., Oro, J. J., Drake, R. K., and Kracke, G. R. (1990). Depressive Effect of Isoflurane Anesthesia on Motor Evoked Potentials. *Neurosurgery* 26, 993–997. doi:10.1097/00006123-199006000-00012

Hermanns, H., Lipfert, P., Meier, S., Jetzek-Zader, M., Krauspe, R., and Stevens, M. F. (2007). Cortical Somatosensory-Evoked Potentials during Spine Surgery in Patients with Neuromuscular and Idiopathic Scoliosis under Propofol-Remifentanil Anaesthesia. *Br. J. Anaesth.* 98, 362–365. doi:10.1093/bja/ael365

Holt, F., Strantzas, S., Zaarour, C., Chamlati, R., Vreugdenhil, I., Luginbuehl, I., et al. (2020). The Effect of Dexmedetomidine on Motor-Evoked Potentials during Pediatric Posterior Spinal Fusion Surgery: a Retrospective Case-Control Study. *Can. J. Anaesth.* doi:10.1007/s12630-020-01758-6

Imani, F., Jafarian, A., Hassani, V., and Khan, Z. H. (2006). Propofol-alfentanil vs Propofol-Remifentanil for Posterior Spinal Fusion Including Wake-Up Test. *Br. J. Anaesth.* 96, 583–586. doi:10.1093/bja/ael075

JeremyLieberman, J. F. A. (2013). Russ Lyon, Mark D. Rollins, Effect of Hemorrhage and Hypotension on Transcranial Motor-Evoked Potentials in Swine. *Anesthesiology* 119, 1109–1119. doi:10.1097/ALN.0b013e31829d4a92

Joshua Yang, B., Skaggs, D. L., Mmm, M. D., Priscella Chan, M. S., Suken, A., Shah, M. D., et al. (2018). Raising Mean Arterial Pressure Alone Restores 20% of Intraoperative Neuromonitoring Losses. *SPINE* 43, 890–894. doi:10.1097/BRS.0000000000002461

Kobayashi, K., Imagama, S., Ando, K., Yoshida, G., Ando, M., Kawabata, S., et al. (1976a). Characteristics of Cases with Poor Transcranial Motor-Evoked Potentials Baseline Waveform Derivation in Spine Surgery: A Prospective Multicenter Study of the Monitoring Committee of the Japanese Society for Spine Surgery and Related Research. *Spine (Phila Pa.* 46, E1211–E1219.

Kobayashi, K., Imagama, S., Yoshida, G., Ando, M., Kawabata, S., Yamada, K., et al. (1976b). Effects of Preoperative Motor Status on Intraoperative Motor-Evoked Potential Monitoring for High-Risk Spinal Surgery: A Prospective Multicenter Study. *Spine (Phila Pa.* 46, E694–E700.

Ku, A. S., Hu, Y., Irwin, M. G., Chow, B., Gunawardene, S., Tan, E. E., et al. (2002). Effect of Sevoflurane/nitrous Oxide versus Propofol Anaesthesia on Somatosensory Evoked Potential Monitoring of the Spinal Cord during Surgery to Correct Scoliosis. *Br. J. Anaesth.* 88, 502–507. doi:10.1093/bja/88.4.502

Li, Y., Meng, L., Peng, Y., Qiao, H., Guo, L., Han, R., et al. (2016). Effects of Dexmedetomidine on Motor- and Somatosensory-Evoked Potentials in Patients with Thoracic Spinal Cord Tumor: a Randomized Controlled Trial. *BMC Anesthesiol* 16, 51. doi:10.1186/s12871-016-0217-y

Lieberman, J. A., Feiner, J., Rollins, M., Lyon, R., and Jasiukaitis, P. (2018). Changes in Transcranial Motor Evoked Potentials during Hemorrhage Are Associated with Increased Serum Propofol Concentrations. *J. Clin. Monit. Comput.* 32, 541–548. doi:10.1007/s10877-017-0057-4

Lieberman, J. A., Feiner, J., Rollins, M., Lyon, R., and Jasiukaitis, P. (2018). Correction to: Changes in Transcranial Motor Evoked Potentials during Hemorrhage Are Associated with Increased Serum Propofol Concentrations. *J. Clin. Monit. Comput.* 32, 581. doi:10.1007/s10877-017-0075-2

Lin, S., Dai, N., Cheng, Z., Shao, W., and Fu, Z. (2014). Effect of Dexmedetomidine-Etomidate-Fentanyl Combined Anesthesia on Somatosensory- and Motor-Evoked Potentials in Patients Undergoing Spinal Surgery. *Exp. Ther. Med.* 7, 1383–1387. doi:10.3892/etm.2014.1555

Liu, X., Li, Y., Kang, L., and Wang, Q. (2021). Recent Advances in the Clinical Value and Potential of Dexmedetomidine. *J. Inflamm. Res.* 14, 7507–7527. doi:10.2147/JIR.S346089

Macdonald, D. B., Skinner, S., Shils, J., and Yingling, C. (2013). Intraoperative Motor Evoked Potential Monitoring - a Position Statement by the American Society of Neurophysiological Monitoring. *Clin. Neurophysiol.* 124, 2291–2316. doi:10.1016/j.clinph.2013.07.025

Mahmoud, M., Sadhasivam, S., Salisbury, S., Nick, T. G., Schnell, B., Sestokas, A. K., et al. (2010). Susceptibility of Transcranial Electric Motor-Evoked Potentials to Varying Targeted Blood Levels of Dexmedetomidine during Spine Surgery. *Anesthesiology* 112, 1364–1373. doi:10.1097/ALN.0b013e3181d74f55

Marinella, M. A. (1996). Lactic Acidosis Associated with Propofol. *Chest* 109, 292. doi:10.1378/chest.109.1.292

Melachuri, S. R., Stopera, C., Melachuri, M. K., Anetakis, K., Crammond, D. J., Castellano, J. F., et al. (2020). The Efficacy of Somatosensory Evoked Potentials in Evaluating New Neurological Deficits after Spinal Thoracic Fusion and Decompression. *J. Neurosurg. Spine*, 1–6. doi:10.3171/2019.12.SPINE191157

Meng, L., Wang, Y., Zhang, L., and McDonagh, D. L. (2019). Heterogeneity and Variability in Pressure Autoregulation of Organ Blood Flow: Lessons Learned over 100+ Years. *Crit. Care Med.* 47, 436–448. doi:10.1097/CCM.0000000000003569

Mohamed Mahmoud, M. D., Sadhasivam, S., Sestokas, A. K., Paul Samuels, M. D., and John McAuliffe, M. D. (2017). Loss of Transcranial Electric Motor Evoked Potentials during Pediatric Spine Surgery with Dexmedetomidine. *Anesthesiology* 106, 393–396. doi:10.1097/00000542-200702000-00027

Mohamed Mahmoud, S. S., Salisbury, S., and Nick, T. G. (2010). Beverly Schnell, Anthony K. Sestokas, Cheryl Wiggins, Au. Paul Samuels, Thomas Kabalin, John McAuliffe., Susceptibility of Transcranial Electric Motor-Evoked Potentials to Varying Targeted Blood Levels of Dexmedetomidine during Spine Surgery. *Anesthesiology*, 1364–1373. doi:10.1097/ALN.0b013e3181d74f55

Nan Lin, M., Vutskits, L., Bebawy, J. F., and Gelb, A. W. (2019). Perspectives on Dexmedetomidine Use for Neurosurgical Patients. *J. Neurosurg. Anesthesiol* 31, 366–377. doi:10.1097/ANA.0000000000000554

Nathan, N., Tabaraud, F., Lacroix, F., Moulies, D., Viviand, X., Lansade, A., et al. (2003). Influence of Propofol Concentrations on Multipulse Transcranial Motor Evoked Potentials. *Br. J. Anaesth.* 91, 493–497. doi:10.1093/bja/aeg211

Ngwenyama, N. E., Anderson, J., Hoernschemeyer, D. G., and Tobias, J. D. (2008). *Effects of Dexmedetomidine on Propofol and Remifentanil Infusion Rates during Total Intravenous Anesthesia for Spine Surgery in Adolescents*. Pediatric Anesthesia.

Nuwer, M. R., Emerson, R. G., Galloway, G., Legatt, A. D. F. A. A. N., Lopez, J., Minahan, R., et al. (2012a). Evidence-based Guideline Update: Intraoperative Spinal Monitoring with Somatosensory and Transcranial Electrical Motor Evoked Potentials. *Neurology*, 585–589. doi:10.1097/WNP.0b013e31824a397e

Nuwer, M. R., and Schrader, L. M. (2019). Spinal Cord Monitoring. *Handb Clin. Neurol.* 160, 329–344. doi:10.1016/B978-0-444-64032-1.00021-7

Nuwer, M. R., Emerson, R. G., Galloway, G., Legatt, A. D., Lopez, J., Minahan, R., et al. (2012c). Evidence-based Guideline Update: Intraoperative Spinal Monitoring with Somatosensory and Transcranial Electrical Motor Evoked Potentials. *J. Clin. Neurophysiol.* 29, 101–108. doi:10.1097/WNP.0b013e31824a397e

Nuwer, M. R., Emerson, R. G., Galloway, G., Legatt, A. D., Lopez, J., Minahan, R., et al. (2012b). Therapeutics, N. Technology Assessment Subcommittee of the American Academy of, and S. American Clinical Neurophysiology, Evidence-Based Guideline Update: Intraoperative Spinal Monitoring with Somatosensory and Transcranial Electrical Motor Evoked Potentials: Report of the Therapeutics and Technology Assessment Subcommittee of the American Academy of Neurology and the American Clinical Neurophysiology Society. *Neurology* 78, 585–589. doi:10.1212/WNL.0b013e318247fa0e

Parke, J. E. S. T. J., Rice, A. S. C., Greenaway, C. L., Bray, R. J., Smith, P. J., Waldmann, C. S., et al. (1992). Metabolic Acidosis and Fatal Myocardial Failure after Propofol Infusion in Children: Five Case Reports. *BMJ* 305, 613–616. doi:10.1136/bmj.305.6854.613

Rozet, I., Metzner, J., Brown, M., Treggiari, M. M., Slimp, J. C., Kinney, G., et al. (2015). Dexmedetomidine Does Not Affect Evoked Potentials during Spine Surgery. *Anesth. Analg* 121, 492–501. doi:10.1213/ANE.0000000000000840

Samra, M. S. K., Dy, E. A., Welch, K. B., Ms, L. K., Reegept, L., and Graziano, G. P. (2001). Remifentanil- and Fentanyl-Based Anesthesia for Intraoperative Monitoring of Somatosensory Evoked Potentials. *Anesth. Analg* 92, 1510–1515. doi:10.1097/00000539-200106000-00031

Schwan, C. P., Pedersen, M. R., Tavanaiepour, K., Tavanaiepour, D., Hoefnagel, A. L., and Mongan, P. D. (2020). Acute Recurrent Bradycardia with Evoked Potential Loss during Transforaminal Lumbar Interbody Fusion. *Anaesth. Rep.* 8, 63–66. doi:10.1002/anr3.12049

Silva-, J. M., Jr, Katayama, H. T., Nogueira, F. A. M., Moura, T. B., Alves, T. L., and de Oliveira, B. W. (2019). Comparison of Dexmedetomidine and Benzodiazepine for Intraoperative Sedation in Elderly Patients: a Randomized Clinical Trial. *Reg. Anesth. Pain Med.* 44, 319–324. doi:10.1136/rapm-2018-100120

Stokes, S. M., Wakeam, E., Antonoff, M. B., Backhus, L. M., Meguid, R. A., Odell, D., et al. (2019). Optimizing Health before Elective Thoracic Surgery:

Systematic Review of Modifiable Risk Factors and Opportunities for Health Services Research. *J. Thorac. Dis.* 11, S537–S554. doi:10.21037/jtd.2019.01.06

SudIvya Sharma, P. J. (2013). Dexmedetomidine and Anesthesia. *Indian J. Clin. Pract.* 24, 223–225.

Tobias, J. D., Goble, T. J., Bates, G., Anderson, J. T., and Hoernschemeyer, D. G. (2008). Effects of Dexmedetomidine on Intraoperative Motor and Somatosensory Evoked Potential Monitoring during Spinal Surgery in Adolescents. *Paediatr. Anaesth.* 18, 1082–1088. doi:10.1111/j.1460-9592.2008.02733.x

Tun Liu, B. D., Qi, H., Yan, L., Zhao, S., Liu, Z., Liu, X., et al. (2021). The Prognostic Value of Intraoperative Neuromonitoring by Combining Somatosensoryand Motor-Evoked Potentials for Thoracic Spinal Decompression Surgery in Patients with Neurological Deficit. *Spine* 54, 25–33. doi:10.1097/brs.0000000000003989

Vitale, M. G., Skaggs, D. L., Pace, G. I., Wright, M. L., Matsumoto, H., Anderson, R. C., et al. (2014). Best Practices in Intraoperative Neuromonitoring in Spine Deformity Surgery: Development of an Intraoperative Checklist to Optimize Response. *Spine Deform* 2, 333–339. doi:10.1016/j.jspd.2014.05.003

Wang, S., Yang, Y., Zhang, J., Tian, Y., Shen, J., and Wang, S. (2017). Frequent Neuromonitoring Loss during the Completion of Vertebral Column Resections in Severe Spinal Deformity Surgery. *Spine J.* 17, 76–80. doi:10.1016/j.spinee.2016.08.002

Yan Lu, E. R. P. (2007). Selective Action of Noradrenaline and Serotonin on Neurones of the Spinal Superficial Dorsal Horn in the Rat. *J. Physiol.* 582, 127–136. doi:10.1113/jphysiol.2007.131565

Yoshida, G., Ando, M., Imagama, S., Kawabata, S., Yamada, K., Kanchiku, T., et al. (1976b). Alert Timing and Corresponding Intervention with Intraoperative Spinal Cord Monitoring for High-Risk Spinal Surgery. *Spine (Phila Pa.* 44, E470–E479. doi:10.1097/BRS.0000000000002900

Yoshida, G., Imagama, S., Kawabata, S., Yamada, K., Kanchiku, T., Fujiwara, Y., et al. (1976a). Adverse Events Related to Transcranial Electric Stimulation for Motor-Evoked Potential Monitoring in High-Risk Spinal Surgery. *Spine (Phila Pa.* 44, 1435–1440. doi:10.1097/BRS.0000000000003115

Yusuke Funai, A. B., and Anthony, E. (2014). Pickering C, Daisuke Uta a, Kiyonobu Nishikawa B, Takashi Mori B, Akira Asada B, Keiji Imoto A,d, Hidemasa Furue A,d,⇑, Systemic Dexmedetomidine Augments Inhibitory Synaptic Transmission in the Superficial Dorsal Horn through Activation of Descending Noradrenergic Control: An *In Vivo* Patch-Clamp Analysis of Analgesic Mechanisms. *PAIN* 115, 617–628. doi:10.1016/j.pain.2013.12.018

Zentner, J., Albrecht, T., and Heuser, D. (1992). Influence of Halothane, Enflurane, and Isoflurane on Motor Evoked Potentials. *Neurosurgery* 31, 298–305. doi:10.1227/00006123-199208000-00015

Zentner, J., Thees, C., Pechstein, U., Scheufler, K. M., Würker, J., and Nadstawek, J. (1976). Influence of Nitrous Oxide on Motor-Evoked Potentials. *Spine (Phila Pa.* 22, 1002–1006. doi:10.1097/00007632-199705010-00012

Zhuang, Q., Wang, S., Zhang, J., Zhao, H., Wang, Y., Tian, Y., et al. (1976). How to Make the Best Use of Intraoperative Motor Evoked Potential Monitoring? Experience in 1162 Consecutive Spinal Deformity Surgical Procedures. *Spine (Phila Pa.* 39, E1425–E1432. doi:10.1097/BRS.0000000000000589

Conflict of Interest: The authors declare that the research was conducted in the absence of any commercial or financial relationships that could be construed as a potential conflict of interest.

Publisher's Note: All claims expressed in this article are solely those of the authors and do not necessarily represent those of their affiliated organizations, or those of the publisher, the editors and the reviewers. Any product that may be evaluated in this article, or claim that may be made by its manufacturer, is not guaranteed or endorsed by the publisher.

frontiers in Pharmacology

ORIGINAL RESEARCH
published: 23 March 2022
doi: 10.3389/fphar.2022.766744

Alpha-Asaronol Alleviates Dysmyelination by Enhancing Glutamate Transport Through the Activation of PPARγ-GLT-1 Signaling in Hypoxia-Ischemia Neonatal Rats

Yuhang Ge[1,2†], Fei Zhen[3†], Ziqi Liu[1], Zhaowei Feng[1], Gui Wang[1], Chu Zhang[1], Xingqi Wang[4], Ying Sun[5], Xiaohui Zheng[5], Yajun Bai[5] and Ruiqin Yao[1]**

[1]Department of Cell Biology and Neurobiology, Xuzhou Key Laboratory of Neurobiology, Xuzhou Medical University, Xuzhou, China, [2]Department of Human Anatomy, Xuzhou Medical University, Xuzhou, China, [3]Hongze Huaian District People's Hospital, Hongze, China, [4]Key Laboratory for Biotechnology on Medicinal Plants of Jiangsu Province, School of Life Science, Jiangsu Normal University, Xuzhou, China, [5]Key Laboratory of Synthetic and Natural Functional Molecule Chemistry of the Ministry of Education, College of Chemistry and Materials Science, Northwest University, Xi'an, China

OPEN ACCESS

Edited by:
Barbara Budzynska,
Medical University of Lublin, Poland

Reviewed by:
Junhui Wang,
University of Toronto, Canada
Sachchida Nand Rai,
University of Allahabad, India
Haiyun Xu,
Wenzhou Medical University, China

***Correspondence:**
Ruiqin Yao
wenxi_yao@163.com
Yajun Bai
baiyj@nwu.edu.cn

†These authors have contributed equally to this work

Specialty section:
This article was submitted to Neuropharmacology, a section of the journal Frontiers in Pharmacology

Received: 30 August 2021
Accepted: 21 February 2022
Published: 23 March 2022

Citation:
Ge Y, Zhen F, Liu Z, Feng Z, Wang G, Zhang C, Wang X, Sun Y, Zheng X, Bai Y and Yao R (2022) Alpha-Asaronol Alleviates Dysmyelination by Enhancing Glutamate Transport Through the Activation of PPARγ-GLT-1 Signaling in Hypoxia-Ischemia Neonatal Rats. Front. Pharmacol. 13:766744. doi: 10.3389/fphar.2022.766744

Preterm white matter injury (PWMI) is the most common form of brain damage in premature infants caused by hypoxia-ischemia (HI), inflammation, or excitotoxicity. It is characterized by oligodendrocyte precursor cell (OPC) differentiation disorder and dysmyelination. Our previous study confirmed that alpha-asarone (α-asaronol), a major compound isolated from the Chinese medicinal herb *Acorus gramineus* by our lab, could alleviate neuronal overexcitation and improve the cognitive function of aged rats. In the present study, we investigated the effect and mechanism of α-asaronol on myelination in a rat model of PWMI induced by HI. Notably, α-asaronol promoted OPC differentiation and myelination in the corpus callosum of PWMI rats. Meanwhile, the concentration of glutamate was significantly decreased, and the levels of PPARγ and glutamate transporter 1 (GLT-1) were increased by α-asaronol treatment. *In vitro,* it was also confirmed that α-asaronol increased GLT-1 expression and recruitment of the PPARγ coactivator PCG-1a in astrocytes under oxygen and glucose deprivation (OGD) conditions. The PPARγ inhibitor GW9662 significantly reversed the effect of α-asaronol on GLT-1 expression and PCG-1a recruitment. Interestingly, the conditioned medium from α-asaronol-treated astrocytes decreased the number of OPCs and increased the number of mature oligodendrocytes. These results suggest that α-asaronol can promote OPC differentiation and relieve dysmyelination by regulating glutamate levels *via* astrocyte PPARγ-GLT-1 signaling. Although whether α-asaronol binds to PPARγ directly or indirectly is not investigated here, this study still indicates that α-asaronol may be a promising small molecular drug for the treatment of myelin-related diseases.

Keywords: α-asaronol, glutamic acid, PPARγ, white matter injury, oligodendrocyte precursor cells

HIGHLIGHTS

α-Asaronol promotes OPC differentiation and alleviates dysmyelination.
α-Asaronol decreases the concentration of glutamate in the brains of PWMI model rats.
α-Asaronol increases the expression of GLT-1 and PPARγ in astrocytes.
The promyelination effect of α-asaronol is due to glutamate uptake mediated by PPARγ-GLT-1 signaling.

INTRODUCTION

Premature white matter injury (PWMI) is the leading cause of child death worldwide and has become a global health priority. Although the survival rate of premature infants has improved due to the increasing importance of developing a neonatal intensive care unit, survivors will have a high risk of life-long disabilities, including cerebral palsy, epilepsy, and impairment of cognition and behavior (Younge et al., 2017). During the development of the oligodendroglial lineage, oligodendrocyte precursor cells (OPCs) are predominant at the early stage with capabilities of migration, differentiation, and remyelination in the central nervous system (CNS) (Back et al., 2001), and mature oligodendrocytes are responsible for forming myelin membranes around axons, enabling fast saltatory nerve conduction and axon integrity protection. Due to immaturity of the periventricular vasculature, OPCs are intrinsically vulnerable to adverse milieu such as infection, inflammation, and hypoxia-ischemia (HI), resulting in proliferation and differentiation disorders and eventually causing white matter injuries (Back, 2017).

Glutamate-mediated excitotoxicity has been shown to cause abnormal white matter development or WMI in neonatal rodents. Neonatal mouse hyperoxia disrupts glutamate homeostasis, and high extracellular glutamate levels lead to immature oligodendroglia apoptosis and white matter maturation delay and eventually reduce white matter diffusivity in adults (Schmitz et al., 2011). Enhancement of extracellular glutamate uptake by upregulating glutamate transporters significantly reduced HI-induced PWMI (Yeh et al., 2017). Maintenance of extracellular glutamate homeostasis is based on functional sodium-dependent glutamate transporters. Five subtypes of excitatory amino acid transporters (EAATs) are designated EAAT1-EAAT5, which belong to the solute carrier 1 (SLC1) family of transmembrane amino acid transporters (Rose et al., 2018; Magi et al., 2019). Astrocytic excitatory amino acid transporter 2 (EAAT2), also known as glutamate transporter 1 (GLT-1), plays an important role in cleaning up to 95% of glutamate (Haugeto et al., 1996). Perinatal infection/inflammation and HI contribute to the depletion of adenosine triphosphate (ATP) in the preterm brain, leading to disruption of GLT-1 in both expression and reversal function, while glutamate uptake is an energy-dependent process (Murugan et al., 2013).

Recently, we isolated α-asaronol from the rhizome of *Acorus calamus* var. *angustatus* Besser (Bai et al., 2020). It is a metabolite of α-asarone, which has long been a traditional medicine for the treatment of cardio-cerebrovascular disease (Limón et al., 2009; Lam et al., 2017). Although studies have revealed that α-asarone exhibits neuroprotective effects on epilepsy (Pages et al., 2010; Huang et al., 2013), Alzheimer's disease (Chen et al., 2020), and stroke (Lee et al., 2018), the nonnegligible side effects of its carcinogenic and genotoxic potential limit its application (Chamorro et al., 1993; Marczewska et al., 2013). With the synthesis of α-asaronol in our lab (Bai et al., 2019), its pharmacokinetics (Sun et al., 2019) and biological activities were gradually evaluated, such as antioxidative stress (He et al., 2018), alleviating neurotoxicity, and anticonvulsant (Jin et al., 2020) and anti-epilepsy by balancing neurotransmitters (data unpublished). However, the effect of α-asaronol on myelination in PWMI neonatal rats and the underlying mechanisms remain elusive.

In this study, we found that α-asaronol could effectively promote myelination and decrease the high level of glutamate triggered by HI in encephalic regions of postnatal pups. Meanwhile, GLT-1 expression was also increased in the model rats treated with α-asaronol. We predicted the potential target of α-asaronol using molecular docking analyses and further confirmed that α-asaronol regulates GLT-1 by activating peroxisome proliferator-activated receptor γ (PPARγ) by recruiting peroxisome proliferator-activated receptor-γ coactivator-1 alpha (PGC-1α) (Jin et al., 2020). Our study suggests that α-asaronol can relieve glutamate excitotoxicity and promote OPC differentiation and myelination by activating PPARγ-GLT-1 signaling in a rat model of PWMI.

MATERIALS AND METHODS

Animals and Drug Treatment

Adult male and female Sprague–Dawley (SD) rats were obtained from the Center of Experimental Animals of Xuzhou Medical University and bred in a sterile animal barrier system. The rats were maintained with a normal diet under a 12:12 h light:dark cycle. Postnatal 3-day rats (n ≈ 210) were randomly divided into the sham, hypoxia-ischemia (HI + normal saline group (HI + NS), and HI + α-asaronol groups (HI + ASA). The PWMI neonatal rat model was established as described previously (Vannucci and Vannucci, 1997). Briefly, pups were anesthetized with 2.5% isoflurane (Shandong Keyuan Pharmaceutical Co., Jinan, Shandong Province, China). The right common carotid artery was isolated and ligated from distal and proximal ends. After the skin was sutured and disinfected, the pups were returned to their mother's cage, allowed to recover for 2 h, and then exposed to 8% O_2 (92% N_2 saturation) at 37°C for 2 h. The sham group underwent the same procedures without ligation of the common carotid artery. The rats were exposed to room air after hypoxia. For α-asaronol treatment, pups were treated with different doses of α-asaronol (25 mg/kg, 50 mg/kg, 100 mg/kg) at 1 h after hypoxia, every 8 h, twice a day.

Tissue Preparation

At P3 + 12 h, P3 + 4 d, and P3 + 7 d (time after surgery), pups from each group were anesthetized with 2.5% isoflurane and sacrificed. For high-performance liquid chromatography (HPLC), western blot, and real-time quantitative PCR (RT–qPCR) tests, all the tissue samples were picked up on an ice pack and stored at −70°C. For immunofluorescence, pups were intracardially perfused with saline followed by fixation with 4% cold paraformaldehyde and then postfixed in 4% paraformaldehyde for 6 h at 4°C followed by 15% and 30% sucrose until the water was replaced completely. All procedures in the experiment were consistent with Chinese legislation on the use and care of laboratory animals and were approved by the Xuzhou Medical University committee for animal experiments.

Primary Cell Culture and Treatment

Primary mixed cells were isolated and cultured from the brains of P0~P2 SD rats. Briefly, the cerebral cortex was separated, cut into 1 mm^3 pieces, and centrifuged at 1,000 rpm for 2 min to remove the supernatant. Digestion of sediment was performed according to the instructions of the digestion kit, and then the digestion was terminated with DMEM/F-12 (1:1) medium (HyClone, United States) containing 10% fetal bovine serum (FBS, Gibco). The samples were centrifuged at 1,200 rpm for 5 min, and the supernatant was discarded. The cells were resuspended in DMEM/F-12 (1:1) medium and placed into a T25 culture flask at 1×10^6 cells/cm^2. The medium was changed every 2–3 days. Approximately 8–9 days after plating, the flasks were shaken at 200 rpm for 1 h on a cell shaker to remove microglial cells. After reincubation for 2–4 h at 37°C, the flasks were shaken at 200 rpm for 18 h, and then the supernatant was collected and centrifuged. Finally, OPCs were resuspended and plated onto coverslips in 24-well plates coated with poly-D-lysine (0.1 mg/ml, Sigma).

The astrocytes on the bottom of the flasks were digested with 0.25% trypsin and plated onto 100 mm Petri dishes. In order to observe the effect and mechanism of α-asaronol on GLT-1 expression, astrocytes (passages 3 to 7) were divided into normal culture group (control), glucose deprivation/reperfusion group (OGD/R) [astrocytes were washed with sterile phosphate-buffered saline (PBS), and incubated in glucose-free DMEM in an anaerobic incubator containing 95% N_2 and 5% CO_2 for 6 h at 37°C and then reoxygen for 12 h], OGD/R + α-asaronol group (astrocytes were pretreated with 1, 10, or 100 μM α-asaronol for 24 h before OGD), and OGD/R + α-asaronol + GW9662 group [astrocytes were pretreated with α-asaronol and 4 μM GW9662 (Meryer Chemical Technology Co., Ltd., Shanghai, China) for 24 h before OGD]. To clarify whether α-asaronol influences OPC differentiation by regulating GLT-1 expression and glutamate levels, a conditioned medium from the above four groups was used to treat OPCs for 3–5 days.

In this study, a conditioned medium from primary neurons was used to promote GLT-1 maturation of astrocytes *in vitro*. Briefly, the brains of P0~P1-day-old SD rats were collected, and the hippocampi were isolated. After the hippocampus was cut into small pieces, 0.25% trypsin with 0.125% ethylene diamine tetraacetonitrile was added to digest the small pieces at 37°C for 15 min. Digestion was terminated with DMEM/F-12 (1:1) medium containing 10% FBS. After the cells were gently blown into single cells using a pipette, the suspension was filtered with a 200-mesh sieve and centrifuged at 1,200 rpm for 5 min. The precipitate was resuspended in PBS and centrifuged again. The supernatant was discarded, and the cells were resuspended in neurobasal-A medium (Gibco, 10888022) supplemented with cytarabine (Aladdin, 147-94-4, 5 μmol/L) and seeded into Petri dishes for 24 h. After washing with PBS, the cytarabine-free neurobasal-A medium was changed. The conditioned medium from neurons was collected after 7 days.

Immunofluorescence Staining

For immunohistofluorescence, 20 μm serial cryosections were made and collected on polylysine-coated slides. For immunocytofluorescence, cells grown on coverslips were washed with 0.01 mol/L PBS and then fixed with 4% paraformaldehyde for 15 min at room temperature. After washing with PBS, brain sections or cells were blocked in PBS with 0.3% Triton X-100 and 10% goat serum for 1 h or 20 min at room temperature and then incubated with primary antibody at 4°C overnight and secondary antibody for 2 h at room temperature. Both antibody incubations were followed by washing with PBS. Finally, 2-(4-amidinophenyl)-6-indolecarbamidine (DAPI, Beyotime, C1005) was used to label nuclei. Staining specificity was assessed by omitting the primary antibody. Quantitative analysis of immunofluorescence staining was performed using ImageJ software (NIH, Bethesda, MD, United States). Primary and secondary antibodies were as follows: rabbit oligodendrocyte lineage transcription factor 2 (Olig2, Proteintech, 13999-1-AP, 1:200), rabbit glial fibrillary acidic protein (GFAP, Proteintech, 16825-1-AP, 1:400), mouse GLT-1 (Santa Cruz, sc-365634, 1:200), rabbit GLT-1 (Abcam, ab41621, 1:400), mouse GLT-1 (Santa Cruz, sc-365634, 1:100), mouse myelin basic protein (MBP, Santa Cruz, sc-271524, 1:500), mouse Protein APC (CC1, Invitrogen, MA1-25884, 1:50), rabbit platelet-derived growth factor receptor-alpha (PDGFRα, Abcam, ab203491, 1:400), rabbit ATPase, Na^+/K^+ transporting, alpha 1 polypeptide (ATP1α1, Proteintech, 14418-1-AP, 1:500), goat anti-mouse IgG (H + L) Alexa Fluor ®555-conjugated, or goat anti-rabbit IgG (H + L) Alexa Fluor ®555 (1:500, Cell signaling technology).

Western Blot

The ipsilateral hemispheres of the rats were dissected and homogenized at P3 + 12 h, P3 + 4 d, and P3 + 7 d after surgery. The homogenates were centrifuged at 12,000 rpm for 20 min at 4°C. The concentration of protein in the supernatant was determined using bicinchoninic acid (Beyotime, China). The protein samples (20 μL) were separated by sodium dodecyl sulfate–polyacrylamide gel electrophoresis (SDS–PAGE) and then transferred to nitrocellulose membranes (Millipore Corporation, MA, United States). The membranes were blocked with 5% nonfat milk at room temperature for 2 h, followed by overnight incubation at 4°C with anti-PDGFRα antibody (Abcam, ab203491, 1:500), anti-MBP antibody (Santa

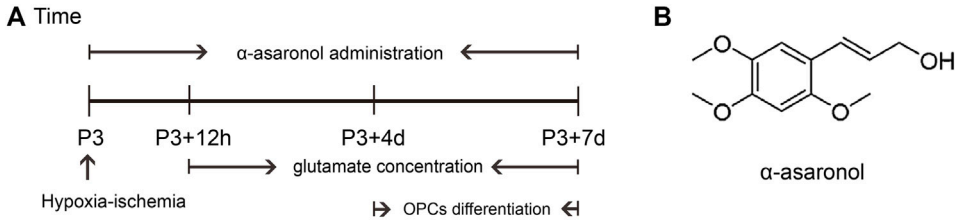

FIGURE 1 | Schematic diagram of the experimental design *in vivo*. **(A)** Schedule of animal experiments. **(B)** Molecular structure formula of α-asaronol.

Cruz, sc-271524, 1:500), anti-GLT-1 antibody (Santa Cruz, sc-365634, 1:1,000), anti-ATP1α1 antibody (Proteintech, 14418-1-AP, 1:5,000), anti-PPARγ antibody (Proteintech, 22061-1-AP, 1:500), anti phospho-AMPA receptor 2 (GluA2) (Tyr876) antibody (p-GluR2, CST 4027s, 1:1,000), anti-GluR2 antibody (CST 13607s, 1:1,000), and anti-β-actin antibody (Proteintech, 20536-1-AP, 1:2000). After washing, the membranes were incubated with goat anti-mouse or goat anti-rabbit secondary antibodies (Abcam, ab216776 and ab216773, 1:5,000) for 2 h at room temperature. The bands on the membrane were scanned with an Odyssey infrared scanner (LI-COR Biosciences, Lincoln, NE, United States), and the density of the bands was analyzed with ImageJ software.

Immunoprecipitation (Co-IP)

For PPAR-γ activation analysis, the astrocytes were collected and homogenized in 1/3 (w/v) ice-cold lysis buffer. Equal amounts of protein (500 μg) were precleared using protein A-Sepharose beads (40 μL) for 1 h at 4°C and then incubated with 5 μL of rabbit polyclonal anti-PPARγ antibody (Proteintech, 16643-1-AP) or mouse monoclonal anti-IgG (Cell Signaling Technology, Danvers, MA). The immune complex was affinity-precipitated with protein A-Sepharose beads and washed six times with 25 mM buffer (pH 7.4) containing 10 mM $MgCl_2$, 1 mM NaF, 1% NP-40, and 1 mM Na_3VO_4. The immunoprecipitates were separated by SDS–PAGE. The levels of PGC-1α and histone deacetylase 3 (HDAC3) were analyzed by western blot using rabbit polyclonal anti-PGC-1α antibody (Novus, NBP1-04676, 1:1,000) and mouse anti-HDAC3 antibody (Santa Cruz, sc-376957, 1:1,000).

High-Performance Liquid Chromatography

The ipsilateral hemispheres were isolated from the rats after HI for different times (P3 + 12, P3 + 4 d, P3 + 7 d). Tissue samples were treated with a mixture of methanol and distilled water (1:1) at a ratio of 100 mg/ml. The homogenate was centrifuged at 12,000 rpm for 20 min at 4°C, and the supernatant was collected. The sediment was added to ice-cold acetonitrile and homogenized and centrifuged. The supernatant was collected, and the pellet was resuspended, homogenized, and centrifuged again. The supernatant from the first and second centrifugation was mixed and dried with a rotary evaporator, and the content was dissolved in 80 μL distilled water for derivation. Standards and samples were mixed with 80 μL of 0.1 mM borate saline buffer (pH = 8.6), 160 μL distilled water, and 80 μL of 4 mM 9-fluorenylmethyl chloroformate (Fmoc-Cl) in a 40°C bath for 5 min for derivation. The derived product was filtered with a 0.22 μm Millipore filter membrane for chromatographic detection. The chromatographic analysis was performed using a Waters e2695 (Waters, United States) and UV detector at a wavelength of 265 nm. The analytical column (Hypersil ODS2, 260 × 4.0 mm, 5 μm particle size, Elite, China) was maintained at 30°C. The flow rate was set at 1 ml/min, and elution was performed using a linear gradient of mobile phases A (50 mM sodium acetate containing 1% tetrahydrofuran, pH = 4.8) and B (acetonitrile). HPLC was also used to detect the concentration of glutamate in the medium from the cultured astrocytes.

Cell Viability Analysis

The CCK-8 (Beyotime Biotechnology Inc., Shanghai, China) assay was carried out to estimate cell viability. Primary astrocytes were seeded into 96-well plates at a density of 4×10^3 cells per well and cultured for 2 days. After incubation with a fresh medium containing 1, 10, or 100 μM α-asaronol for 24 h, the cells were subjected to OGD for 6 h and reoxygenation for 12 h. Astrocytes were incubated with CCK-8 reagent for 1 h in the dark (5% CO_2 at 37°C). The optical density (OD) value was measured at a wavelength of 450 nm on a microplate reader (BioTek, United States).

Real-Time Quantitative PCR

RT-qPCR was used to investigate the transcript levels of GLT-1 and PPARγ. Total RNA from the pups (P3 + 12 h, P3 + 4 d, P3 + 7 d) from each group was extracted using TRIzol reagent (Invitrogen, United States). Extracted RNA was reverse-transcribed into cDNA using HiScript® II Q RT Super Mix for qPCR (Vazyme, China). RT-qPCR was performed using SYBR Green qPCR Master Mix (MCE, United States) and Roche Light Cycler 480 II (Roche, Switzerland). β-Actin was used as an internal standard. The relative gene expression was calculated according to the $2^{-\Delta\Delta Ct}$ method. The primers were as follows: GLT-1 (forward, GAAGACATCCCGTTC ACAAGA; reverse, TGATGCTTTATCCCCACAGAC) and PPARγ (forward, GTTCAAGGACGGGATGAATGTCTTA; reverse, CAT CAGCTTGGCCTGCTCAC).

Molecular Docking Simulation

Molecular modeling was performed using Sybyl-x 2.0 software from Tripos Inc. (St. Louis, MO). The PPARγ structure used

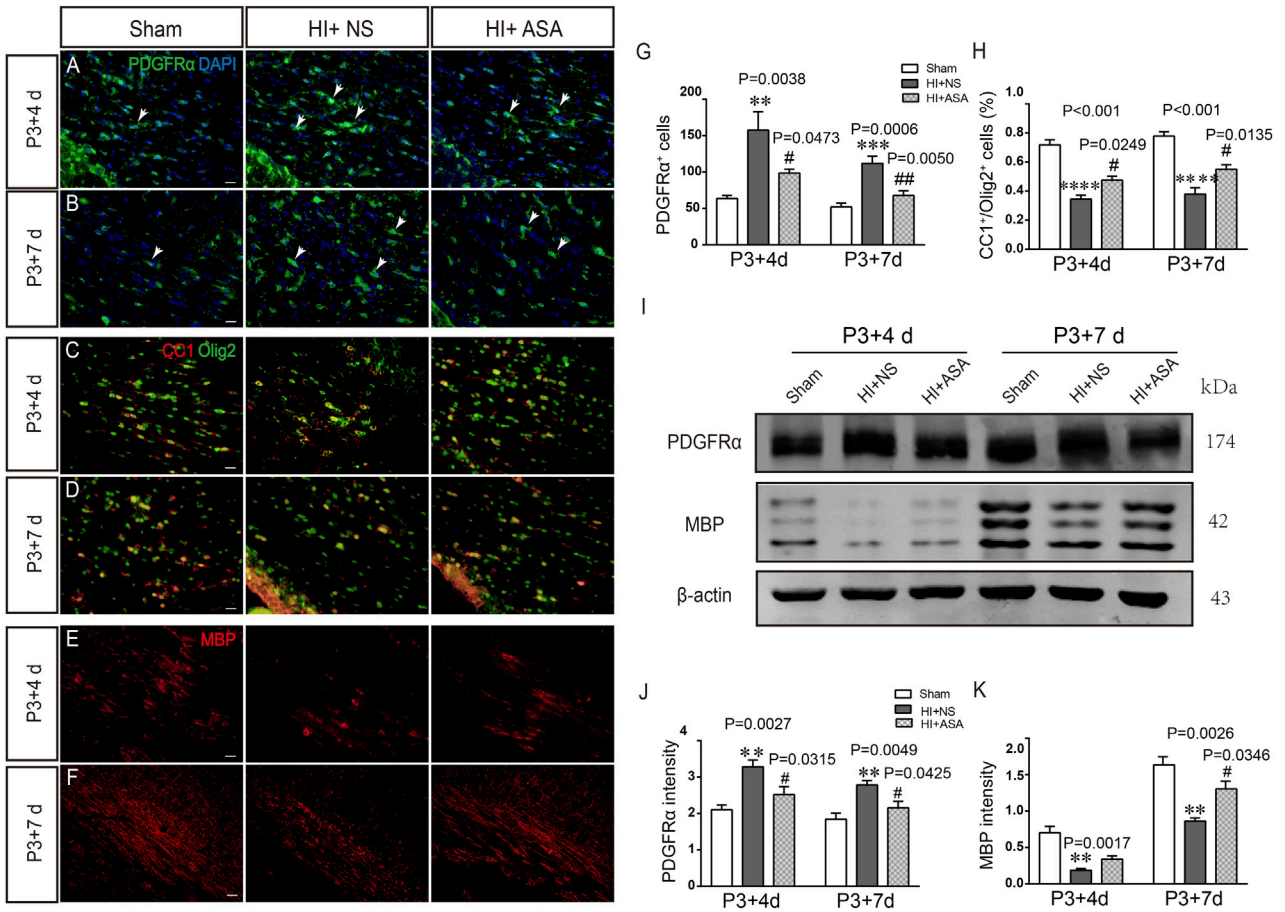

FIGURE 2 | α-Asaronol improves OPC differentiation and relieves dysmyelination in PWMI models. Representative immunofluorescence images for PDGFRα-labeled OPCs. **(A,B)** CC1-labeled mature oligodendrocyte and Olig2-labeled oligodendrocyte lineage **(C,D)** and MBP-labeled myelin sheath **(E,F)** in the corpus callosum at P3 + 4 d and P3 + 7 d after HI. Scale bar, 20 μm. **(G,H)** Quantification of the number of PDGFRα$^+$ cells and the percentage of CC1+/Olig2+ cells. **(I,K)** Western blotting was performed to analyze PDGFRα and MBP protein levels. All data are expressed as the mean ± SEM. $^{**}p < 0.01$, $^{***}p < 0.001$, $^{****}p < 0.001$ vs. sham group. $^{\#}p < 0.05$, $^{\#\#}p < 0.01$ vs. HI + NS group. $N = 4$ for each group.

for docking was obtained from the Protein Data Bank (PDB, http://www.rcsb.org; PDB ID, 5Y2T). The cocrystalized ligand and water molecules were removed from the structure, while H atoms were added and side chains were fixed during protein preparation. The 3D structure of α-asaronol was constructed and energy-minimized using the MM2 molecular mechanics method with Chem3D Pro 14.0 (Cambridge Soft Co., United States). Before docking, PPARγ and α-asaronol were energetically minimized by the CHARMm force field. After preparation, the Surflex-Dock (SFXC) docking mode was performed using the default settings. Surflex-Dock was employed for the molecular docking study. Surflex-Dock scores (total scores) represent binding affinities.

Statistical Analysis

All statistical analyses were performed with GraphPad Prism 7.0 (GraphPad Software; CA, United States), and the data were analyzed by an investigator blinded to the procedure using one-way analysis of variation (ANOVA) followed by either the Newman–Keuls or Tukey's honestly significant difference post hoc test for comparisons among multiple groups. The data were expressed as the mean ± standard error of the mean (SEM). $p < 0.05$ was considered as significant.

RESULTS

α-Asaronol Improves Oligodendrocyte Precursor Cell Differentiation and Relieves Dysmyelination in Preterm White Matter Injury Rats

Overactivation of glutamate receptors causes calcium overload and is a major factor in OPC differentiation inhibition and cell death. To observe the effect of α-asaronol on OPC differentiation and myelination in a PWMI rat model, we designed an *in vivo* experiment. A schematic diagram of the experiment and the molecular structure formula of α-asaronol are shown in **Figure 1**.

TABLE 1 | The glutamate concentration was determined by HPLC in the ipsilateral hemisphere at different time points after HI. Establishment of a standard curve of the glutamate standard. The linear range is from 1 to 200 μg/ml. Correlation coefficient: $r = 0.9996$. All data are expressed as the mean ± SEM. $^{***}p < 0.001$ vs. sham. $^{\#}p < 0.05$, $^{\#\#}p < 0.01$, $^{\#\#\#}p < 0.001$ vs. HI + NS. $N = 3–5$ for each group.

Group	Sham	HI + NS	HI + α-asaronol		
Data			25 mg/kg	50 mg/kg	100 mg/kg
P3 + 12 h	0.198 ± 0.019	0.341 ± 0.029***	0.296 ± 0.016	0.265 ± 0.020	0.259 ± 0.031
P3 + 4 d	0.176 ± 0.014	0.402 ± 0.076***	0.268 ± 0.012#	0.246 ± 0.017##	0.205 ± 0.015###
P3 + 7 d	0.174 ± 0.019	0.364 ± 0.007***	0.244 ± 0.016#	0.215 ± 0.013##	0.204 ± 0.004##

All data are expressed as the mean ± SEM. N = *3–5.* ***p < *0.001 vs. sham.* #p < *0.05,* ##p < *0.01,* ###p < *0.001 vs. HI + NS.*

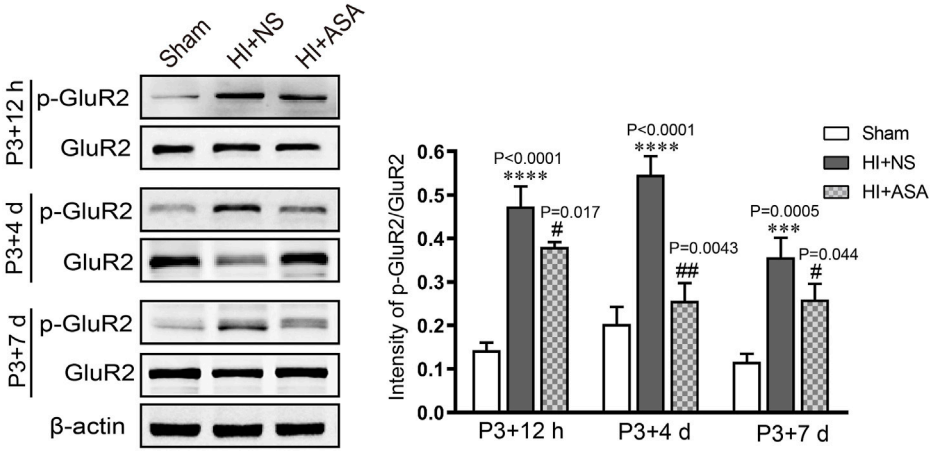

FIGURE 3 | α-Asaronol inhibits HI-induced activation of the ionotropic glutamate receptor AMPAR. The protein level of p-GluR2 (subunit 2 of AMPAR) was detected by western blot at P3 + 12 h, P3 + 4 d, and P3 + 7 d after HI. HI induced an obvious increase in p-GluR2 (Tyr876), and α-asaronol (50 mg/kg) treatment decreased the level of p-GluR2. All data are expressed as the mean ± SEM. $^{***}p < 0.001$, $^{****}p < 0.0001$ vs. sham. $^{\#}p < 0.05$, $^{\#\#}p < 0.01$ vs. HI + NS. $N = 4$ for each group.

Immunofluorescence staining and quantitative analysis revealed that the number of PDGFRα$^+$ OPCs in the corpus callosum in the NS group was much higher than that in the sham group, while α-asaronol significantly decreased the PDGFRα$^+$ cell number at P3 + 4 d and P3 + 7 d (**Figures 2A,B,G**). In contrast, MBP-labeled myelin density and the ratio of CC1-labeled mature oligodendrocytes to Olig2-labeled OPCs/oligodendrocytes in the NS group were significantly lower than those in the sham group, but α-asaronol treatment obviously enhanced the ratio of CC1$^+$/Olig2$^+$ cells (**Figures 2C,D,H**) and MBP$^+$ myelin density (**Figures 2E,F**). Protein analysis also showed that α-asaronol decreased PDGFRα levels and enhanced MBP levels (**Figures 2I–K**).

α-Asaronol Decreases Glutamate Levels in the Brains of Preterm White Matter Injury Rats

In order to investigate the effect of α-asaronol on glutamate levels, the samples were collected from the acute to chronic phase after HI, and the concentration of glutamate was detected by HPLC. The standard curve of glutamate was established. The linear range was from 1 μg/ml to 200 μg/ml, and the value of the correlation coefficient (r) was 0.9996. The glutamate concentration was substantially increased in the NS group at P3 + 12 h (0,341 ± 0.029 μg/mg), P3 + 4 d (0.402 ± 0.076 μg/mg), and P3 + 7 d (0.364 ± 0.007 μg/mg) compared with the sham group (0.198 ± 0.019 μg/mg for P3 + 12 h, 0.176 ± 0.014 μg/mg for P3 + 4 d; 0.174 ± 0.019 μg/mg for P3 + 7 d). The glutamate concentration was significantly decreased at P3 + 4 d and P3 + 7 d in a dose-dependent manner in the α-asaronol-treated rats compared with the NS-treated rats; however, there was no obvious change in glutamate concentration at P3 + 12 h (**Table 1**). Meanwhile, HI-induced activation of the ionotropic glutamate receptor AMPA receptor (AMPAR) was confirmed by a p-GluR2 (Tyr876) increase, and α-asaronol treatment decreased the level of p-GluR2 at P3 + 12 h, P3 + 4 d, and P3 + 7 d (**Figure 3**).

α-Asaronol Increases the Expression of GLT-1 and PPARγ in Astrocytes of Preterm White Matter Injury Rats

Astrocytic GLT-1 is mainly responsible for the clearance of glutamate. We explored whether the decreased concentration of glutamate in PWMI rats treated with α-asaronol is mediated by GLT-1. The location of GLT-1 on astrocytes was confirmed by GLT-1/GFAP double labeling (**Figure 4A**). Data from the western blot and RT-qPCR revealed that GLT-1 levels were mildly increased at P3 + 12 h but significantly decreased at P3

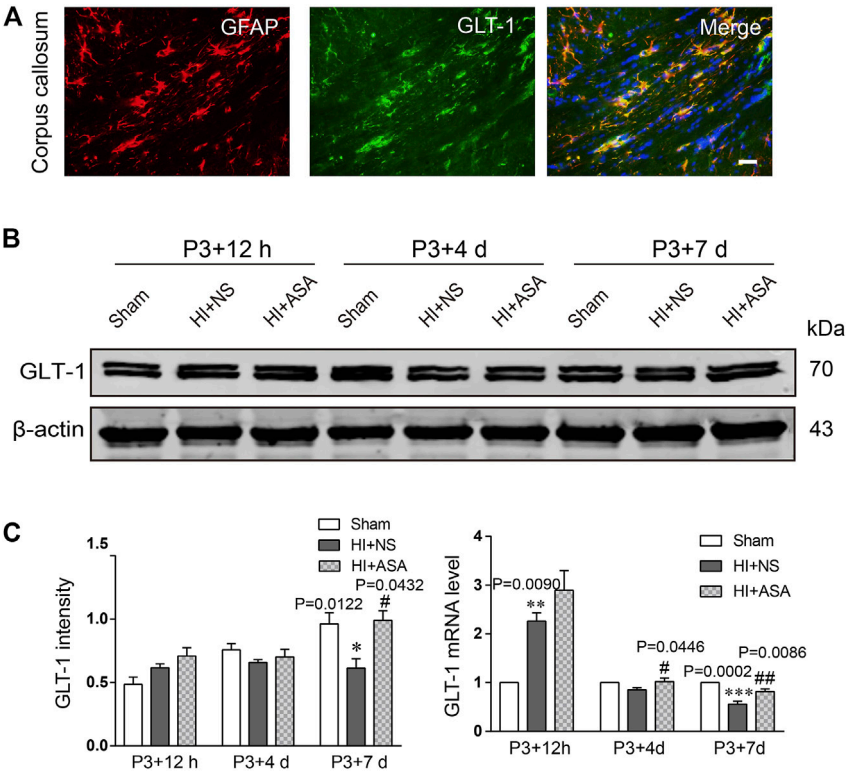

FIGURE 4 | α-Asaronol increases the expression of GLT-1 in the PWMI rat model. **(A)** GLT-1 protein expression was detected by western blotting at P3 + 12 h, P3 + 4 d, and P3 + 7 d. **(B)** GLT-1 was quantified and normalized against β-actin. **(C)** The mRNA level of GLT-1 was quantified by qPCR. All data are represented as the mean ± SEM. $^{*}p < 0.05$, $^{**}p < 0.01$, $^{***}p < 0.001$ vs. sham group, $^{\#}p < 0.05$, $^{\#\#}p < 0.01$ vs. HI + NS group. $N = 4$ for each group.

+ 7 d in the NS group compared with the sham group. α-Asaronol treatment obviously increased GLT-1 protein and mRNA levels at P3 + 7 d (**Figures 4B,C**).

As one of the target genes of PPARγ, GLT-1 is regulated by PPARγ during the acquisition of brain ischemic tolerance (Romera et al., 2007) and is involved in neuroprotection by increasing glutamate uptake in ischemic preconditioning rats (Zhao et al., 2019). Our previous study also found that α-asaronol could promote the mRNA expression of PPARγ in zebrafish (Jin et al., 2020). Thus, we speculated that α-asaronol upregulates the expression of GLT-1, which may be dependent on PPARγ activation. As expected, we identified highly upregulated PPARγ protein and mRNA levels at P3 + 7 d in PWMI rats treated with α-asaronol (**Figures 5A–C**).

In addition, because the transport function of GLT-1 relies on transmembrane Na^+/K^+ gradients, we further examined the expression of ATP1α1, the alpha-1 subunit of a protein pump known as a Na^+/K^+ ATPase. At P3 + 12 h after HI, the fluorescence intensity of ATP1α1 was much weaker in the NS group than in the sham group. Although the α-asaronol treatment did not alter the expression of ATP1α1 at P3 + 12 h, ATP1α1 expression gradually returned to basal levels in PWMI rats treated with α-asaronol at P3 + 4 d and P3 + 7 d (**Figure 5D**).

A molecular docking simulation was performed to investigate the potential binding of α-asaronol and PPARγ. The Surflex-Dock molecular docking program was used to evaluate the results through various scoring functions, and the total score was calculated by valuing the polarity, hydrophobicity, enthalpy, and salvation. The higher the score, the more stable the docking complex. In the docking with PPARγ, the total score of α-asaronol was 5.523. As shown in **Figure 5E**, the α-asaronol molecule entered the binding pocket of PPARγ. α-Asaronol combined with the PPARγ residues LYS295, PHE264, MET348, CYS285, ILE341, ILE281, ARG288, GLY284, and HIS266 *via* van der Waals interactions. Furthermore, the hydroxyl group at the C12 position interacts with LYS265 and HIS266 on PPARγ to form hydrogen bonds. The methoxyl groups at the C1, C2, and C4 sites interact with PPARγ to form hydrophobic interactions and play a role in localization. The ethyl side chain at the C5 position extends into the hydrophobic cavity composed of PHE264 and GLY284 (**Figure 5F**). These results suggested that α-asaronol may activate PPARγ through physical interaction.

α-Asaronol Increases the Expression of Glutamate Transporter 1 in Astrocytes Under Oxygen and Glucose Deprivation Conditions

Astrocytes were subjected to OGD for 3, 6, or 9 h and then reoxygenated for 12 h. Quantification of the western blot data

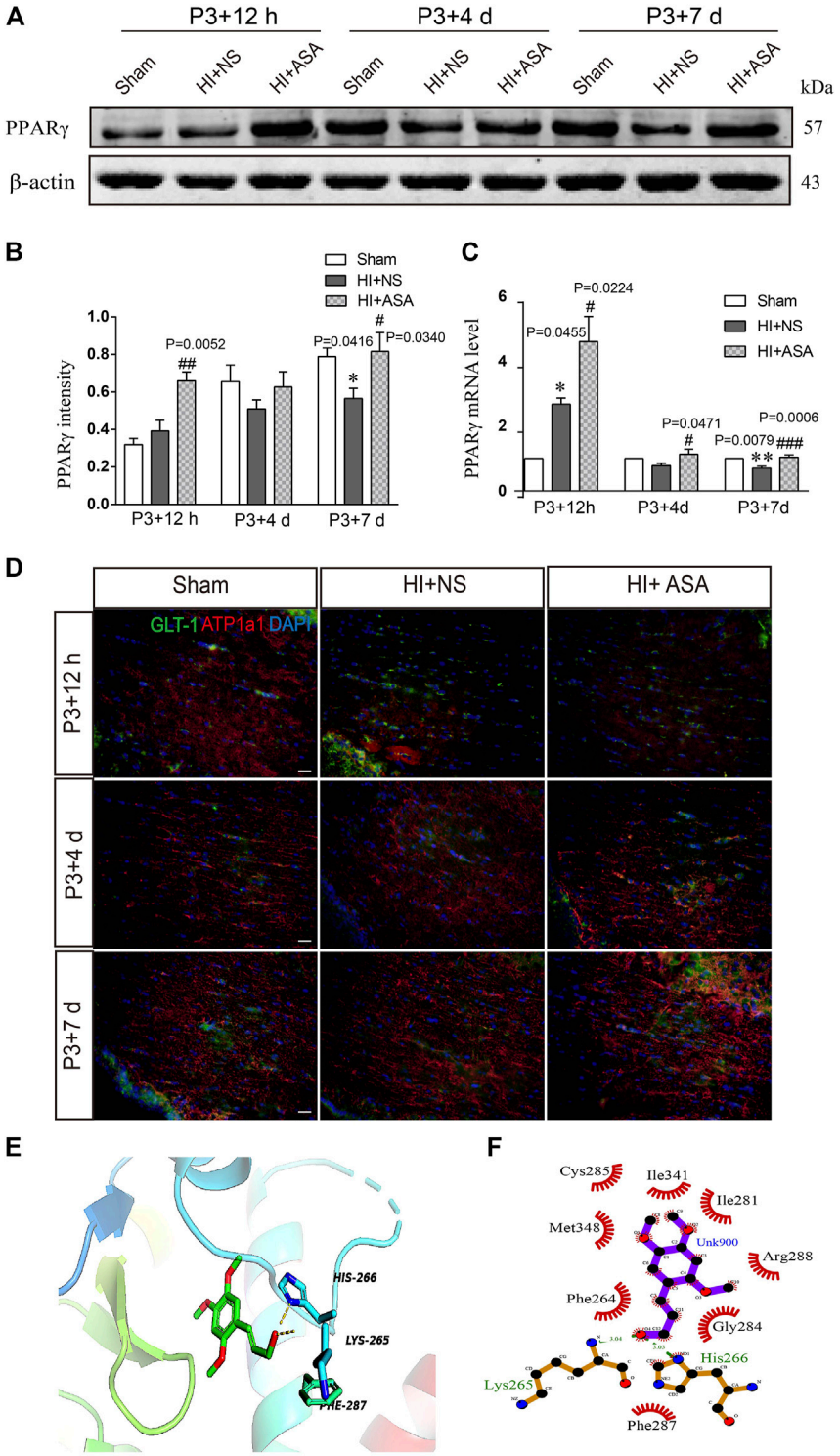

FIGURE 5 | α-Asaronol increases the expression of PPARγ in PWMI models. **(A)** Expression of PPARγ was detected at P3 + 12 h, P3 + 4 d, and P3 + 7 d after HI. **(B)** PPARγ was quantified and normalized against *β*-actin. **(C)** The mRNA level of PPARγ was quantified by qPCR. **(D,E)** Representative immunofluorescence images for GLT-1 and ATP1A1 double staining in the corpus callosum. Scale bar, 20 μm. **(F,G)** Molecular docking simulation of α-asaronol and PPARγ. All data are represented as the mean ± SEM. $^{*}p < 0.05$, $^{**}p < 0.01$ vs. sham group, $^{\#}p < 0.05$, $^{\#\#\#}p < 0.001$ vs. HI + NS group. $N = 4$ for each group.

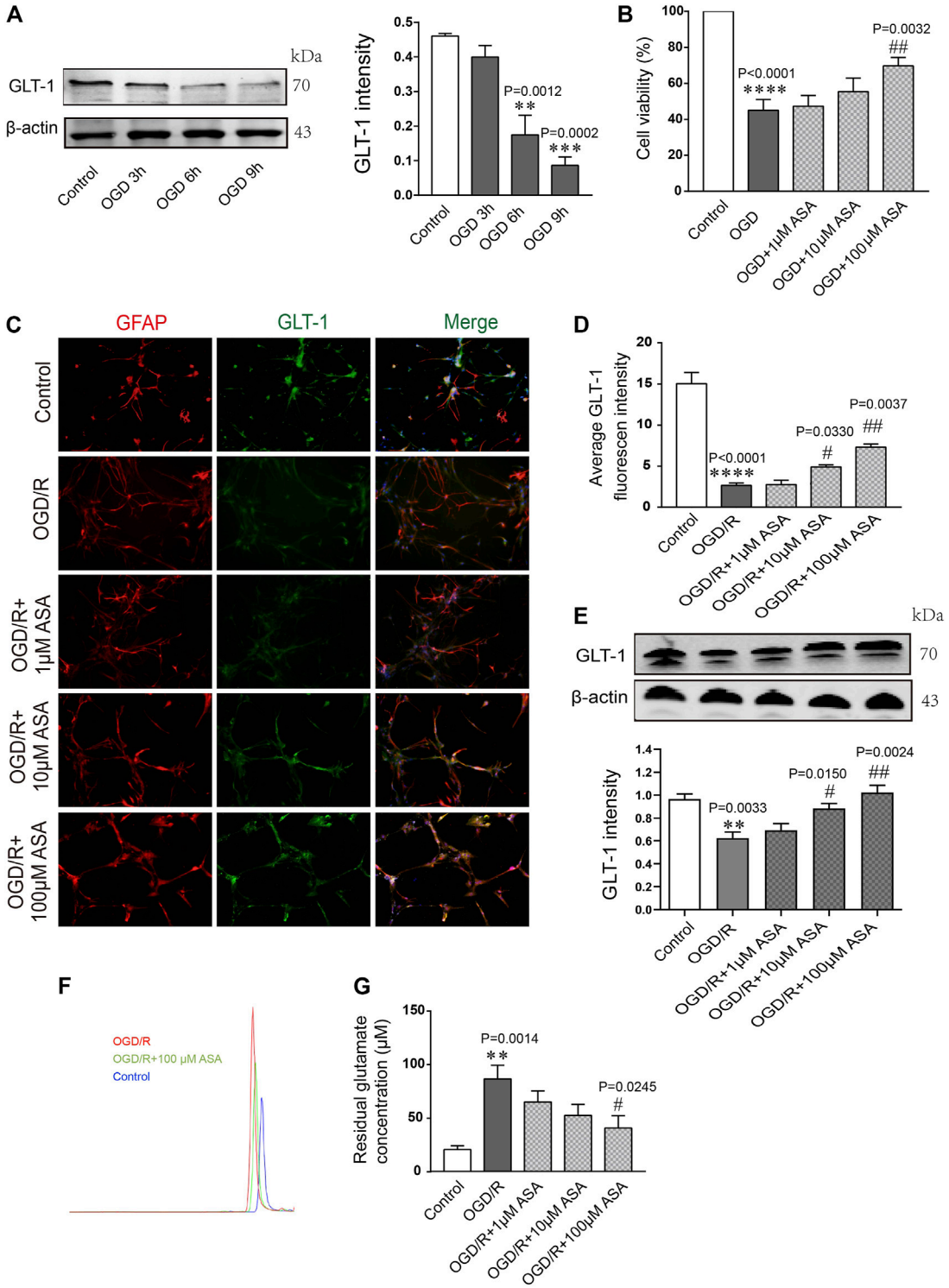

FIGURE 6 | α-Asaronol increases the expression of astrocytic GLT-1 under OGD/R conditions. **(A)** Gradient OGD/R conditions of astrocytes. **(B)** Cell viability of astrocytes. **(C)** Representative immunofluorescence images for GFAP and GLT-1 staining in the corpus callosum for all groups. Scale bar, 20 μm. **(D)** Statistical analysis of GLT-1 mean fluorescence intensity. **(E)** The expression of GLT-1 was detected and quantified. **(F,G)** Chromatographs of glutamate and quantitative analysis of glutamate concentration in the medium for all groups were performed. All data are represented as the mean ± SEM. $^{**}p < 0.01$, $^{****}p < 0.0001$ vs. the control group, $^{\#}p < 0.05$, $^{\#\#}p < 0.01$ vs. the OGD/R group. $N = 4$ for each group.

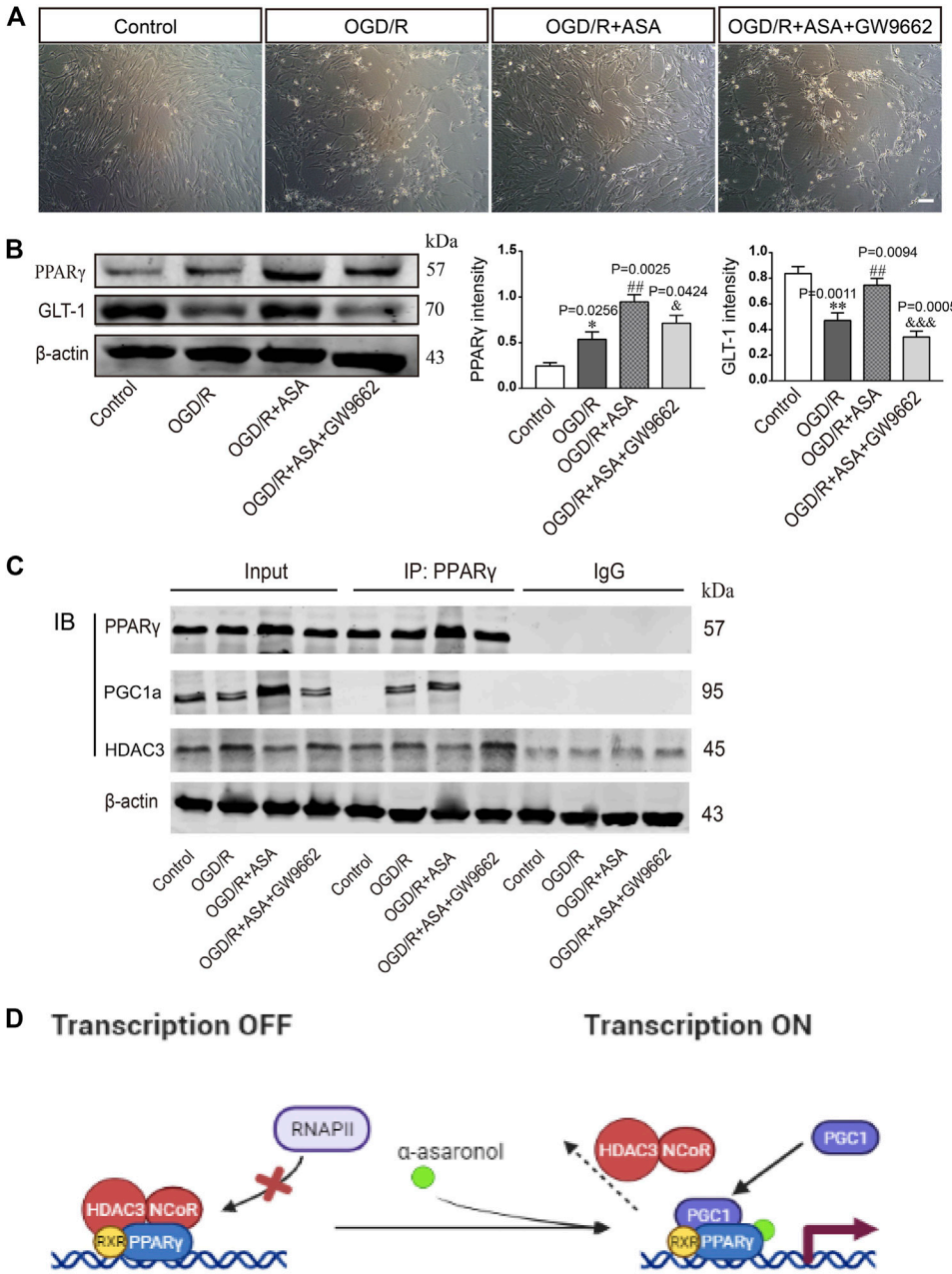

FIGURE 7 | α-Asaronol upregulated GLT-1 expression in astrocytes by activating PPARγ. **(A)** The morphology of astrocytes under the bright field. Scale bar, 50 μm. **(B)** The expression of PPARγ and GLT-1 was detected by western blotting. PPARγ and GLT-1 were quantified and normalized against β-actin. **(C)** Co-IP was used to examine the interaction of PPARγ and PGC1a or PPARγ and HDAC3. **(D)** Graphical image representing the ligand-independent repression and α-asaronol-dependent transactivation of PPARγ. All data are represented as the mean ± SEM. $^{*}p < 0.05$, $^{**}p < 0.01$ vs. control group, $^{\#\#}p < 0.01$ *vs.* OGD/R group, $^{\&}p < 0.05$, $^{\&\&\&}p < 0.001$ vs. OGD/R + ASA group. $N = 4$ for each group.

showed that the level of GLT-1 was obviously reduced at OGD 6 h compared with the control and OGD 3 h; thus, OGD 6 h was chosen for the following research experiments (**Figure 6A**). Astrocytes were pretreated with different doses of α-asaronol and then subjected to OGD for 6 h and reoxygenation for 12 h. CCK-8 data showed that 100 μM α-asaronol improved astrocyte viability (**Figure 6B**). In addition, 100 μM α-asaronol also significantly enhanced the average fluorescence intensity of GLT-1 (**Figures 6C,D**) and the protein level (**Figure 6E**). More interestingly, the glutamate concentration in the medium was lower in the 100 μM α-asaronol group than in the OGD group, as determined by HPLC (**Figures 6F,G**).

α-Asaronol Upregulated Glutamate Transporter 1 Expression in Astrocytes by Activating PPARγ

The PPARγ selective antagonist GW9662 was used to study whether α-asaronol upregulates astrocyte GLT-1 by activating PPARγ. First, we noticed that OGD/R led to some of the astrocytes detaching from the culture dish and clustering, and α-asaronol treatment alleviated the morphological changes of astrocytes. However, the effect of α-asaronol on astrocyte morphology was reversed by GW9662 treatment (**Figure 7A**). Second, GW9662 also inhibited the increase in GLT-1 induced by α-asaronol (**Figure 7B**). Finally, we identified that OGD induced the interaction of PGC-1a and the PPARγ heterodimer, while GW9662 weakened the interaction by decreasing the level of PGC-1a, suggesting that OGD and α-asaronol treatment activated PPARγ signaling (**Figures 7C,D**).

Conditioned Medium From α-Asaronol-Treated Astrocytes Promotes Oligodendrocyte Precursor Cell Differentiation Without Influencing Apoptosis

The conditioned medium from astrocytes was collected and used to treat OPCs. Compared with the control group, the percentage of PDGFRα^+ cells was increased, while the percentages of $CC1^+$ and MBP^+ cells were significantly decreased after treatment with conditioned medium from OGD/R astrocytes. In contrast, the conditioned medium from OGD/R and *α*-asaronol cotreated astrocytes reduced the percentage of PDGFRα^+ cells and increased the percentage of $CC1^+$ and MBP^+ cells. However, the conditioned medium from GW9662-treated astrocytes reversed the effects of *α*-asaronol on OPC differentiation (**Figures 8A–D**). The apoptosis rate of OPCs treated with OGD/R-conditioned medium was increased compared with that of the control group, but there were no obvious differences in the apoptosis rate of OPCs among the OGD/R, OGD/R + NS, and OGD/R+*α*-asaronol groups by flow cytometry (**Figures 8E,F**).

DISCUSSION

In the CNS, over-activating glutamate receptors damage OPCs, and the subsequent differentiation disorder has always attracted attention from researchers (Back et al., 2007). In the present study, our data showed that the concentration of glutamate in the brains of PWMI rats was significantly higher than that in the brains of sham rats. Treatment with α-asaronol significantly decreased the concentration of glutamate, increased GLT-1 levels, promoted OPC differentiation, and alleviated dysmyelination. The neuroprotective mechanism of α-asaronol may be related to the increase in glutamate uptake by activating PPARγ-GLT-1 signaling in astrocytes.

Dysmyelination or demyelination is mainly due to failure of OPC differentiation rather than OPC depletion (Billiards et al., 2008; Buser et al., 2012). Studies have reported that the total pool of OPCs increases severalfold within 24 h after HI and continues to increase for a few days. Although numerous OPCs are regenerated in lesions, they fail to differentiate into myelinating oligodendrocytes following established procedures (Segovia et al., 2008; Wright et al., 2010). Consistent with previous studies, we also found that PDGFR*α*-labeled OPCs sharply increased in the acute phase of HI in neonatal rats; however, dysmyelination of the corpus callosum was still obvious at P3 + 4 d and P3 + 7 d. Interestingly, α-asaronol treatment promoted the differentiation of OPCs into myelinating oligodendrocytes and myelination. Studies have indicated that glutamate excitotoxicity is responsible for neuronal death in acute neurological disorders. When neurons from the rat cortex were exposed to different concentrations of glutamate (10–2,000 μM), glutamate induced a concentration-dependent increase in neuronal death. However, astrocytes exhibited a protective function in neuronal damage induced by glutamate (Zhang et al., 2019). Meanwhile, a high concentration of glutamate or activation of the ionotropic glutamate receptor AMPAR also causes oligodendrocyte precursor excitotoxicity (Deng et al., 2006), inhibiting the proliferation and differentiation of OPCs (Fannon et al., 2015). Reducing extracellular glutamate levels obviously improved HI-induced PWMI in neonatal rats (Yeh et al., 2017). Thus, we speculated that the effect of α-asaronol on myelination may be related to the clearance of glutamate.

The pharmacokinetics of *a*-asaronol and its main metabolite in rats were estimated by HPLC in our previous study (Sun et al., 2019). Tissue distribution evaluation showed that α-asaronol is distributed rapidly and widely in various tissues in the order of brain > heart > kidney > spleen > liver > lung and is eliminated quickly. The maximal concentration of α-asaronol in the brain is approximately 1.603 ± 0.221 μg/g at 5 min, and the half-life of α-asaronol is approximately 6 h. Unfortunately, in this study, we did not examine the half-life of α-asaronol in the HI-related part of the brain, which should be taken into consideration and clarified in future studies.

Glutamate transporters play a crucial role in the efficient clearance of glutamate (Magi et al., 2019). EAAT2 (rodent ortholog GLT-1) is the predominant glutamate transporter in the forebrain and carries out more than 95% of glutamate clearance (Zhou et al., 2014). It has been reported that GLT-1 and ATP-α interact within the processes of astrocytes (Rose et al., 2009; Roberts et al., 2014), and the maintenance of low extracellular glutamate levels depends on ATP-α activation and Na^+ homeostasis (Pellerin and Magistretti, 1997). The maternal separation resulted in early disrupted neuron-glia integrity and axon-myelin entities in the rat brain, as evidenced by inhibited myelination, lowered expression of GLT-1 and ATP-α, and increased glutamate (Zeng et al., 2020). In this study, a drastic increase in glutamate concentration was accompanied by a high level of GLT-1 within 12 h after HI; however, the level of ATP1α1 in the model rats was lower than that in the sham rats, suggesting that the glutamate transport function of GLT-1 was poor at the acute phase of HI. At P3 + 4 d and P3 + 7 d, the glutamate concentration was still high, but the expression of GLT-1 was

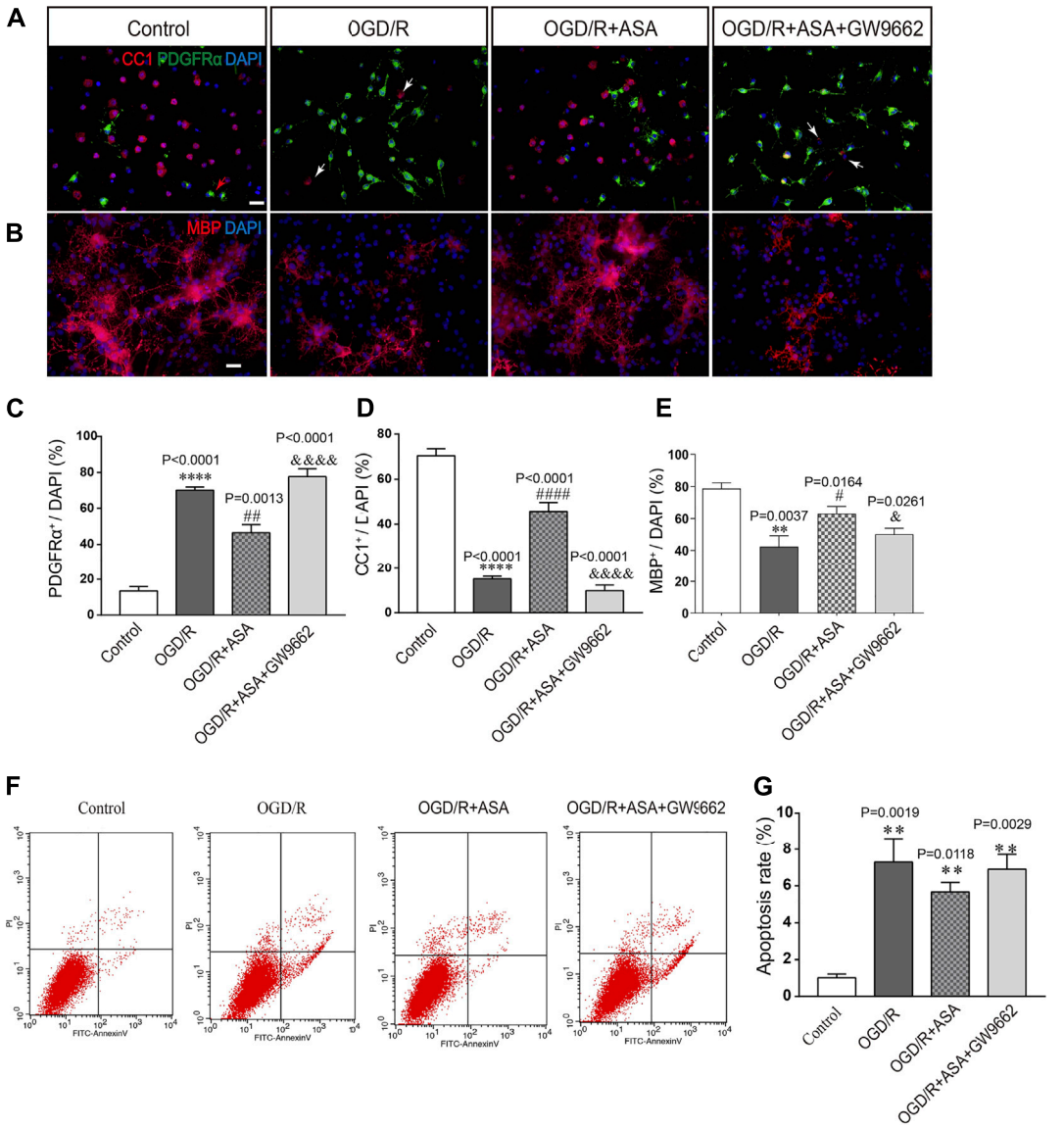

FIGURE 8 | Conditioned medium from α-asaronol-treated astrocytes promotes OPC differentiation without influencing apoptosis. Representative immunofluorescence images for PDGFRα-labeled OPCs and CC1-labeled mature OLs **(A)** and MBP-labeled myelin sheath **(B)**. Scale bar, 20 μm. **(C–E)** Statistical analysis of the numbers of PDGFRα$^+$ cells, CC1$^+$ cells, and MBP$^+$ cells. **(E,F)** Representative flow cytometry images of OPCs and quantitative analysis of the percentage of apoptotic cells for all groups. Scale bar, 20 μm. All data are represented as the mean ± SEM. $^{**}p < 0.01$, $^{****}p < 0.0001$ vs. the control group. $^{\#}p < 0.05$, $^{\#\#}p < 0.01$, $^{\#\#\#\#}p < 0.0001$ vs. the OGD/R group. $^{\&}p < 0.05$, $^{\&\&\&\&}p < 0.001$ vs. the OGD/R + ASA group. $N = 4$ per group.

decreased in PWMI rats, while α-asaronol enhanced the levels of GLT-1 and ATP1α1 and decreased the glutamate concentration, suggesting that α-asaronol promoted glutamate uptake by upregulating GLT-1. *In vitro*, our study showed that GLT-1 protein expression was downregulated gradually after OGD/R in astrocytes, and 100 μM α-asaronol upregulated GLT-1 expression and enhanced glutamate uptake, indicating that the glutamate-scavenging capacity was increased in astrocytes because α-asaronol upregulated the functional expression of astrocytic GLT-1.

As a transcription factor of the nuclear hormone receptor superfamily, PPARγ plays a neuroprotective role in various CNS diseases (Schintu et al., 2009; Zhao et al., 2009; San et al., 2015). It has been reported that the PPARγ agonist rosiglitazone decreases infarct volume and increases GLT-1 expression after cerebral ischemia (Romera et al., 2007). Importantly, our previous research found that α-asaronol attenuated pentylenetetrazol-induced seizures in zebrafish and activated PPARγ (Jin et al., 2020). In the present study, both GLT-1 and PPARγ expression were upregulated in PWMI rats with α-asaronol treatment. To explore the mechanism by which α-asaronol regulates GLT-1 expression, we performed Surflex-Dock molecular docking analyses. The higher total score of α-asaronol docking with PPARγ indicated that α-asaronol and PPARγ could possibly form a stable docking complex.

PPARγ activation is a ligand-dependent process. In the absence of ligands, the PPARγ heterodimer is associated with corepressors, such as nuclear receptor corepressors and HDACs. This complex binds to the peroxisome proliferator response element in the promoter region of target genes and retains the genes in a suppressed state. Following ligand binding, the heterodimer dissociates from corepressors and recruits coactivators such as PGC1a, thereby upregulating target gene transcription (Cai et al., 2018; Bernardo et al., 2021). Here, our results showed that OGD and α-asaronol treatment led to PGC1a being recruited to the PPARγ heterodimer, while HDAC3 dissociated from the heterodimer, suggesting that OGD and α-asaronol treatment activated PPARγ signaling.

In our previous study, we examined the effects of different concentrations of glutamate receptor subunit 3 peptide B antibodies (GluR3B Abs), which can themselves activate GluR3-containing glutamate/AMPAR, on OPC viability. The results showed that a high concentration of GluR3B Ab induced OPC excitotoxicity by causing mitochondrial dysfunction (Liu et al., 2017). In this study, the conditioned medium from α-asaronol-treated astrocytes promoted OPC differentiation, and PPARγ antagonist GW9662 treatment not only reversed the effect of α-asaronol on OPC differentiation but also decreased the expression of GLT-1 and increased the concentration of glutamate, suggesting that PPARγ-GLT-1 mediated the effect of α-asaronol on OPC differentiation and myelination.

CONCLUSION

Taken together, this study proved that α-asaronol can relieve the disorder of OPC differentiation and dysmyelination induced by glutamate excitotoxicity in a PWMI rat model by regulating PPARγ-GLT-1 signaling. Unfortunately, whether α-asaronol binds to PPARγ directly or indirectly was not investigated in this study. In the future, yeast two-hybrid systems, cellular thermal shift assays, or surface plasmon resonance techniques should be used to study α-asaronol and PPARγ interactions.

DATA AVAILABILITY STATEMENT

The original contributions presented in the study are included in the article/Supplementary Material, further inquiries can be directed to the corresponding authors.

ETHICS STATEMENT

The animal study was reviewed and approved by the Institutional Animal Care and Use Committee (IACUC) of Xuzhou Medical University. Written informed consent was obtained from the owners for the participation of their animals in this study.

AUTHOR CONTRIBUTIONS

YG and FZ performed the experiments, collected and analyzed the data, and prepared the manuscript. ZL, ZF, GW, and CZ performed the experiments and collected the data. XW provided experiment design support. YB and XZ provided α-asaronol and technical assistance. RY designed the study, provided financial support, and significantly edited the manuscript. All the authors approved the final manuscript.

FUNDING

This study was supported by the National Natural Science Foundation of China (no. 81771337) and the Project of Key Research and Development Plan of Shaanxi (no. 2017ZDCXL-SF-01-02-01), program for Changjiang Scholars and Innovative Research in University (IRT_15R55).

ACKNOWLEDGMENTS

The experiments were conducted in the Public Experimental Research Center of Xuzhou Medical University.

REFERENCES

Back, S. A., Craig, A., Kayton, R. J., Luo, N. L., Meshul, C. K., Allcock, N., et al. (2007). Hypoxia-ischemia Preferentially Triggers Glutamate Depletion from Oligodendroglia and Axons in Perinatal Cerebral white Matter. *J. Cereb. Blood Flow Metab.* 27 (2), 334–347. doi:10.1038/sj.jcbfm.9600344

Back, S. A., Luo, N. L., Borenstein, N. S., Levine, J. M., Volpe, J. J., and Kinney, H. C. (2001). Late Oligodendrocyte Progenitors Coincide with the Developmental Window of Vulnerability for Human Perinatal white Matter Injury. *J. Neurosci.* 21 (4), 1302–1312. doi:10.1523/jneurosci.21-04-01302.2001

Back, S. A. (2017). White Matter Injury in the Preterm Infant: Pathology and Mechanisms. *Acta Neuropathol.* 134 (3), 331–349. doi:10.1007/s00401-017-1718-6

Bai, Y., He, X., Bai, Y., Sun, Y., Zhao, Z., Chen, X., et al. (2019). Polygala Tenuifolia-Acori Tatarinowii Herbal Pair as an Inspiration for Substituted Cinnamic α-asaronol Esters: Design, Synthesis, Anticonvulsant Activity, and Inhibition of Lactate Dehydrogenase Study. *Eur. J. Med. Chem.* 183, 111650. doi:10.1016/j.ejmech.2019.111650

Bai, Y., Sun, Y., Xie, J., Li, B., Bai, Y., Zhang, D., et al. (2020). The Asarone-Derived Phenylpropanoids from the Rhizome of Acorus calamus Var. Angustatus Besser. *Phytochemistry* 170, 112212. doi:10.1016/j.phytochem.2019.112212

Bernardo, A., Plumitallo, C., De Nuccio, C., Visentin, S., and Minghetti, L. (2021). Curcumin Promotes Oligodendrocyte Differentiation and Their protection against TNF-α through the Activation of the Nuclear Receptor PPAR-γ. *Sci. Rep.* 11 (1), 4952. doi:10.1038/s41598-021-83938-y

Billiards, S. S., Haynes, R. L., Folkerth, R. D., Borenstein, N. S., Trachtenberg, F. L., Rowitch, D. H., et al. (2008). Myelin Abnormalities without Oligodendrocyte Loss in Periventricular Leukomalacia. *Brain Pathol.* 18 (2), 153–163. doi:10.1111/j.1750-3639.2007.00107.x

Buser, J. R., Maire, J., Riddle, A., Gong, X., Nguyen, T., Nelson, K., et al. (2012). Arrested Preoligodendrocyte Maturation Contributes to Myelination Failure in Premature Infants. *Ann. Neurol.* 71 (1), 93–109. doi:10.1002/ana.22627

Cai, W., Yang, T., Liu, H., Han, L., Zhang, K., Hu, X., et al. (2018). Peroxisome Proliferator-Activated Receptor γ (PPARγ): A Master Gatekeeper in CNS Injury and Repair. *Prog. Neurobiol.* 163-164, 27–58. doi:10.1016/j.pneurobio.2017.10.002

Chamorro, G., Salazar, M., Salazar, S., and Mendoza, T. (1993). Pharmacology and Toxicology of Guatteria Gaumeri and Alpha-Asarone. *Rev. Invest. Clin.* 45 (6), 597–604.

Chen, Y., Gao, X., Liu, Q., Zeng, L., Zhang, K., Mu, K., et al. (2020). Alpha-asarone Improves Cognitive Function of Aged Rats by Alleviating Neuronal Excitotoxicity via GABAA Receptors. *Neuropharmacology* 162, 107843. doi:10.1016/j.neuropharm.2019.107843

Deng, W., Yue, Q., Rosenberg, P. A., Volpe, J. J., and Jensen, F. E. (2006). Oligodendrocyte Excitotoxicity Determined by Local Glutamate Accumulation and Mitochondrial Function. *J. Neurochem.* 98 (1), 213–222. doi:10.1111/j.1471-4159.2006.03861.x

Fannon, J., Tarmier, W., and Fulton, D. (2015). Neuronal Activity and AMPA-type Glutamate Receptor Activation Regulates the Morphological Development of Oligodendrocyte Precursor Cells. *Glia* 63 (6), 1021–1035. doi:10.1002/glia.22799

Haugeto, O., Ullensvang, K., Levy, L. M., Chaudhry, F. A., Honoré, T., Nielsen, M., et al. (1996). Brain Glutamate Transporter Proteins Form Homomultimers. *J. Biol. Chem.* 271 (44), 27715–27722. doi:10.1074/jbc.271.44.27715

He, X., Bai, Y., Zeng, M., Zhao, Z., Zhang, Q., Xu, N., et al. (2018). Anticonvulsant Activities of α-asaronol ((E)-3'-hydroxyasarone), an Active Constituent Derived from α-asarone. *Pharmacol. Rep.* 70 (1), 69–74. doi:10.1016/j.pharep.2017.08.004

Huang, C., Li, W. G., Zhang, X. B., Wang, L., Xu, T. L., Wu, D., et al. (2013). α-Asarone from Acorus Gramineus Alleviates Epilepsy by Modulating A-type GABA Receptors. *Neuropharmacology* 65, 1–11. doi:10.1016/j.neuropharm.2012.09.001

Jin, M., Zhang, B., Sun, Y., Zhang, S., Li, X., Sik, A., et al. (2020). Involvement of Peroxisome Proliferator-Activated Receptor γ in Anticonvulsant Activity of α-asaronol against Pentylenetetrazole-Induced Seizures in Zebrafish. *Neuropharmacology* 162, 107760. doi:10.1016/j.neuropharm.2019.107760

Lam, K. Y. C., Yao, P., Wang, H., Duan, R., Dong, T. T. X., and Tsim, K. W. K. (2017). Asarone from Acori Tatarinowii Rhizome Prevents Oxidative Stress-Induced Cell Injury in Cultured Astrocytes: A Signaling Triggered by Akt Activation. *PLoS One* 12 (6), e0179077. doi:10.1371/journal.pone.0179077

Lee, H. J., Ahn, S. M., Pak, M. E., Jung, D. H., Lee, S. Y., Shin, H. K., et al. (2018). Positive Effects of α-asarone on Transplanted Neural Progenitor Cells in a Murine Model of Ischemic Stroke. *Phytomedicine* 51, 151–161. doi:10.1016/j.phymed.2018.09.230

Limón, I. D., Mendieta, L., Diaz, A., Díaz, G., Espinosa, B., Zenteno, E., et al. (2009). Neuroprotective Effect of Alpha-Asarone on Spatial Memory and Nitric Oxide Levels in Rats Injected with Amyloid-Beta((25-35)). *Neurosci. Lett.* 453 (2), 98–103. doi:10.1016/j.neulet.2009.02.011

Liu, Y., Chen, Y., Du, W. T., Wu, X. X., Dong, F. X., Qu, X. B., et al. (2017). GluR3B Ab's Induced Oligodendrocyte Precursor Cells Excitotoxicity via Mitochondrial Dysfunction. *Brain Res. Bull.* 130, 60–66. doi:10.1016/j.brainresbull.2016.12.016

Magi, S., Piccirillo, S., Amoroso, S., and Lariccia, V. (2019). Excitatory Amino Acid Transporters (EAATs): Glutamate Transport and beyond. *Int. J. Mol. Sci.* 20 (22). doi:10.3390/ijms20225674

Marczewska, J., Drozd, E., Anuszewska, E., Chilmonczyk, Z., and Łozowicka, B. (2013). Assessment of the Genotoxic Activity of Alpha-Asarone and its Derivatives in the Comet Assay. *Acta Pol. Pharm.* 70 (2), 349–354.

Murugan, M., Ling, E. A., and Kaur, C. (2013). Dysregulated Glutamate Uptake by Astrocytes Causes Oligodendroglia Death in Hypoxic Perventricular white Matter Damage. *Mol. Cel Neurosci* 56, 342–354. doi:10.1016/j.mcn.2013.07.005

Pages, N., Maurois, P., Delplanque, B., Bac, P., Stables, J. P., Tamariz, J., et al. (2010). Activities of α-asarone in Various Animal Seizure Models and in Biochemical Assays Might Be Essentially Accounted for by Antioxidant Properties. *Neurosci. Res.* 68 (4), 337–344. doi:10.1016/j.neures.2010.08.011

Pellerin, L., and Magistretti, P. J. (1997). Glutamate Uptake Stimulates Na+,K+-ATPase Activity in Astrocytes via Activation of a Distinct Subunit Highly Sensitive to Ouabain. *J. Neurochem.* 69 (5), 2132–2137. doi:10.1046/j.1471-4159.1997.69052132.x

Roberts, R. C., Roche, J. K., and McCullumsmith, R. E. (2014). Localization of Excitatory Amino Acid Transporters EAAT1 and EAAT2 in Human Postmortem Cortex: a Light and Electron Microscopic Study. *Neuroscience* 277, 522–540. doi:10.1016/j.neuroscience.2014.07.019

Romera, C., Hurtado, O., Mallolas, J., Pereira, M. P., Morales, J. R., Romera, A., et al. (2007). Ischemic Preconditioning Reveals that GLT1/EAAT2 Glutamate Transporter Is a Novel PPARgamma Target Gene Involved in Neuroprotection. *J. Cereb. Blood Flow Metab.* 27 (7), 1327–1338. doi:10.1038/sj.jcbfm.9600438

Rose, C. R., Ziemens, D., Untiet, V., and Fahlke, C. (2018). Molecular and Cellular Physiology of Sodium-dependent Glutamate Transporters. *Brain Res. Bull.* 136, 3–16. doi:10.1016/j.brainresbull.2016.12.013

Rose, E. M., Koo, J. C., Antflick, J. E., Ahmed, S. M., Angers, S., and Hampson, D. R. (2009). Glutamate Transporter Coupling to Na,K-ATPase. *J. Neurosci.* 29 (25), 8143–8155. doi:10.1523/JNEUROSCI.1081-09.2009

San, Y. Z., Liu, Y., Zhang, Y., Shi, P. P., and Zhu, Y. L. (2015). Peroxisome Proliferator-Activated Receptor-γ Agonist Inhibits the Mammalian Target of Rapamycin Signaling Pathway and Has a Protective Effect in a Rat Model of Status Epilepticus. *Mol. Med. Rep.* 12 (2), 1877–1883. doi:10.3892/mmr.2015.3641

Schintu, N., Frau, L., Ibba, M., Caboni, P., Garau, A., Carboni, E., et al. (2009). PPAR-Gamma-Mediated Neuroprotection in a Chronic Mouse Model of Parkinson's Disease. *Eur. J. Neurosci.* 29 (5), 954–963. doi:10.1111/j.1460-9568.2009.06657.x

Schmitz, T., Ritter, J., Mueller, S., Felderhoff-Mueser, U., Chew, L. J., and Gallo, V. (2011). Cellular Changes Underlying Hyperoxia-Induced Delay of white Matter Development. *J. Neurosci.* 31 (11), 4327–4344. doi:10.1523/JNEUROSCI.3942-10.2011

Segovia, K. N., McClure, M., Moravec, M., Luo, N. L., Wan, Y., Gong, X., et al. (2008). Arrested Oligodendrocyte Lineage Maturation in Chronic Perinatal white Matter Injury. *Ann. Neurol.* 63 (4), 520–530. doi:10.1002/ana.21359

Sun, Y., Bai, Y., Zeng, M., Chen, X., Xie, J., Li, B., et al. (2019). Pharmacokinetics and Tissue Distribution Evaluation of α-asaronol and its Main Metabolite in Rats by HPLC Method. *J. Pharm. Biomed. Anal.* 172, 349–356. doi:10.1016/j.jpba.2019.05.004

Vannucci, R. C., and Vannucci, S. J. (1997). A Model of Perinatal Hypoxic-Ischemic Brain Damage. *Ann. N. Y Acad. Sci.* 835, 234–249. doi:10.1111/j.1749-6632.1997.tb48634.x

Wright, J., Zhang, G., Yu, T. S., and Kernie, S. G. (2010). Age-related Changes in the Oligodendrocyte Progenitor Pool Influence Brain Remodeling after Injury. *Dev. Neurosci.* 32 (5-6), 499–509. doi:10.1159/000322081

Yeh, C., Yeh, C. M., Yu, T. H., Chang, K. H., Huang, C. C., and Hsu, K. S. (2017). Neonatal Dexamethasone Treatment Exacerbates Hypoxia/Ischemia-Induced White Matter Injury. *Mol. Neurobiol.* 54 (9), 7083–7095. doi:10.1007/s12035-016-0241-4

Younge, N., Goldstein, R. F., Bann, C. M., Hintz, S. R., Patel, R. M., Smith, P. B., et al. (2017). Survival and Neurodevelopmental Outcomes Among Periviable Infants. *N. Engl. J. Med.* 376 (7), 617–628. doi:10.1056/NEJMoa1605566

Zeng, H., Zhang, X., Wang, W., Shen, Z., Dai, Z., Yu, Z., et al. (2020). Maternal Separation with Early Weaning Impairs Neuron-Glia Integrity: Non-invasive Evaluation and Substructure Demonstration. *Sci. Rep.* 10 (1), 19440. doi:10.1038/s41598-020-76640-y

Zhang, L. N., Wang, Q., Xian, X. H., Qi, J., Liu, L. Z., and Li, W. B. (2019). Astrocytes Enhance the Tolerance of Rat Cortical Neurons to Glutamate Excitotoxicity. *Mol. Med. Rep.* 19 (3), 1521–1528. doi:10.3892/mmr.2018.9799

Zhao, C. C., Jiang, M. Y., Zhang, L. Y., Hu, Y. Y., Hu, Z. J., Zhang, M. Y., et al. (2019). Peroxisome Proliferator-Activated Receptor Gamma Participates in the Acquisition of Brain Ischemic Tolerance Induced by Ischemic Preconditioning via Glial Glutamate Transporter 1 *In Vivo* and *In Vitro*. *J. Neurochem.* 151 (5), 608–625. doi:10.1111/jnc.14824

Zhao, X., Strong, R., Zhang, J., Sun, G., Tsien, J. Z., Cui, Z., et al. (2009). Neuronal PPARgamma Deficiency Increases Susceptibility to Brain Damage after Cerebral Ischemia. *J. Neurosci.* 29 (19), 6186–6195. doi:10.1523/JNEUROSCI.5857-08.2009

Zhou, Y., Waanders, L. F., Holmseth, S., Guo, C., Berger, U. V., Li, Y., et al. (2014). Proteome Analysis and Conditional Deletion of the EAAT2 Glutamate Transporter Provide Evidence against a Role of EAAT2 in Pancreatic Insulin Secretion in Mice. *J. Biol. Chem.* 289 (3), 1329–1344. doi:10.1074/jbc.M113.529065

Conflict of Interest: The authors declare that the research was conducted in the absence of any commercial or financial relationships that could be construed as a potential conflict of interest.

Publisher's Note: All claims expressed in this article are solely those of the authors and do not necessarily represent those of their affiliated organizations or those of the publisher, the editors, and the reviewers. Any product that may be evaluated in this article, or claim that may be made by its manufacturer, is not guaranteed or endorsed by the publisher.

frontiers | Frontiers in Pharmacology

STUDY PROTOCOL
published: 11 May 2022
doi: 10.3389/fphar.2022.820447

Potential Treat-to-Target Approach for Methamphetamine Use Disorder: A Pilot Study of Adenosine 2A Receptor Antagonist With Positron Emission Tomography

Kyoji Okita[1,2,3]*, *Toshihiko Matsumoto*[1,2], *Daisuke Funada*[1,2], *Maki Murakami*[1,2], *Koichi Kato*[3], *Yoko Shigemoto*[4], *Noriko Sato*[4] and *Hiroshi Matsuda*[4,5,6]

[1]Department of Psychiatry, Center Hospital, National Center of Neurology and Psychiatry, Tokyo, Japan, [2]Department of Drug Dependence Research, National Institute of Mental Health, National Center of Neurology and Psychiatry, Tokyo, Japan, [3]Integrative Brain Imaging Center, National Center of Neurology and Psychiatry, Tokyo, Japan, [4]Department of Radiology, Center Hospital, National Center of Neurology and Psychiatry, Tokyo, Japan, [5]Drug Discovery and Cyclotron Research Center, Southern TOHOKU Research Institute for Neuroscience, Fukushima, Japan, [6]Department of Biofunctional Imaging, Fukushima Medical University, Fukushima, Japan

OPEN ACCESS

Edited by:
Riham Salah El Dine,
Cairo University, Egypt

Reviewed by:
Mark Gold,
Washington University in St. Louis, United States
Ana Carolina Issy,
University of São Paulo, Brazil
Robert Warren Gould,
Wake Forest School of Medicine, United States

***Correspondence:**
Kyoji Okita
kokita@ncnp.go.jp

Specialty section:
This article was submitted to Neuropharmacology, a section of the journal Frontiers in Pharmacology

Received: 23 November 2021
Accepted: 25 April 2022
Published: 11 May 2022

Citation:
Okita K, Matsumoto T, Funada D, Murakami M, Kato K, Shigemoto Y, Sato N and Matsuda H (2022) Potential Treat-to-Target Approach for Methamphetamine Use Disorder: A Pilot Study of Adenosine 2A Receptor Antagonist With Positron Emission Tomography. Front. Pharmacol. 13:820447. doi: 10.3389/fphar.2022.820447

Introduction: The misuse of stimulant drugs such as methamphetamine is a global public health issue. One important neurochemical mechanism of methamphetamine use disorder may be altered dopaminergic neurotransmission. For instance, previous studies using positron emission tomography (PET) have consistently shown that striatal dopamine D2-type receptor availability (quantified as binding potential; BP_{ND}) is lower in methamphetamine use disorder. Further, methamphetamine use is known to induce chronic neuroinflammation through multiple physiological pathways. Upregulation of D2-type receptor and/or attenuation of neuroinflammation may therefore provide a therapeutic effect for this disorder. *In vitro* studies have shown that blockage of adenosine 2A (A2A) receptors may prevent D2-receptor downregulation and neuroinflammation-related brain damage. However, no study has examined this hypothesis yet.

Methods and Analysis: Using a within-subject design, this trial will assess the effect of the selective A2A receptor antagonist, istradefylline, primarily on D2-type BP_{ND} in the striatum, and secondarily on neuroinflammation in the whole brain in individuals with methamphetamine use disorder. The research hypotheses are that istradefylline will increase striatal D2-type BP_{ND} and attenuate neuroinflammation. Twenty participants with methamphetamine use disorder, aged 20–65, will be recruited to undergo [^{11}C] raclopride PET (for every participant) and [^{11}C]DAA1106 PET (if applicable) once before and once after administration of 40 mg/day istradefylline for 2 weeks. Neuropsychological measurements will be performed on the same days of the PET scans.

Keywords: methamphetamine, addiction, dopamine D2 receptors, adenosine 2A receptor, neuroinflammation, positron emission tomography

INTRODUCTION

Misuse of stimulant drugs such as methamphetamine is a worldwide public health issue. Methamphetamine use is deemed to associate with not only physical harms including HIV transmission (Shoptaw and Reback, 2007), cardiovascular disease (Darke et al., 2017; Kevil et al., 2019), cerebrovascular disease (Lappin et al., 2017) but also psychiatric harms including psychosis, depression, anxiety and suicide In 2019, it is estimated that as much as 0.5% of global population aged between 15 and 64 had used the amphetamine-type stimulants [United Nations Office on Drugs and Crime (UNODC), 2021]. From 2010 to 2018, the prevalence of methamphetamine use within the general population in the United States over the past year has increased by 195% (Paulus and Stewart, 2020), and the number of overdose deaths attributed to psychostimulant use has tripled over the previous 5 years in 2019 (Han et al., 2021). Despite the negative effects of such methamphetamine use on society, current treatments are inadequate, and no pharmacological treatments have been approved for any stimulant use disorders. Understanding the biological basis of methamphetamine use may aid the development of novel therapies for methamphetamine use disorder.

Dopaminergic neurotransmission via actions at D2-type receptors has been suggested to play an important role in addictive disorders (Solinas et al., 2019). For instance, lower striatal dopamine D2-type receptor availability (quantified as binding potential; BP_{ND}) has been consistently observed in individuals with methamphetamine use disorder *vs.* healthy-control subjects in studies using positron emission tomography (PET) [see reviews by (Volkow et al., 2009; Ashok et al., 2017; London, 2020)]. Furthermore, in methamphetamine users, striatal D2-type BP_{ND} is negatively correlated with higher scores on the Barratt Impulsiveness Scale (Lee et al., 2009), a greater choosing of methamphetamine-related images over pleasant images compared to healthy-control subjects in a computer-based picture choice task (Moeller et al., 2018), and even possibly with treatment outcomes (i.e., relapse to methamphetamine use) (Wang et al., 2012).

As such, enhancing neurotransmission through striatal D2-type receptors may create a therapeutic effect for methamphetamine use disorder. D2-type receptor agonists have failed to show a therapeutic effect though (Verrico et al., 2013; Blum et al., 2014), and no pharmacological treatment has been approved for the disorder to date. Importantly, these evidences may suggest that agonistic effects on D2-type receptors are not enough while recovering the function of these receptors (i.e., upregulation of D2-type receptor density) is needed to provide a therapeutic effect.

Adenosine 2A (A2A) receptors, as well as dopamine D2-type receptors, are G protein-coupled receptors (GPCR), and they are expressed on the dendritic spines of striatopallidal GABAergic neurons forming A2A-D2 receptor heteromers in the whole striatum with a higher density than any other brain regions. They functionally interact with each other in the heteromer structure (Ferre et al., 2016). Treatment with selective A2A receptor antagonists attenuates D2 receptor internalization from the membrane into the cell body of cultivated rat striatal neurons (Huang et al., 2013). Thus, A2A receptor antagonism could block internalization of D2 receptors in the human brain and may induce upregulation of these receptors in the individuals with methamphetamine use disorder.

Importantly, methamphetamine use is known to induce chronic neuroinflammation through multiple physiological pathways [see review by (Kim et al., 2020)]. Neuroinflammation is considered to activate microglia, which can be assessed using PET scans with tracers that target the translocator protein 18 kDa (TSPO) *in vivo* (Meyer et al., 2020). Indeed, compared to healthy non-drug-using controls, methamphetamine users who had refrained from methamphetamine use for 6 months–4 years exhibited significantly higher microglial activation in a PET study that used a first generation TSPO tracer [^{11}C]PK11195 (Sekine et al., 2008). Further, compared to healthy controls, methamphetamine users who were abstinent for only 4–7 days also exhibited greater standardized uptake value (SUV) measured with [^{11}C]DAA1106, a second generation TSPO tracer with higher affinity and specificity than [^{11}C]PK11195, although this group differences did not reach significance likely due in part to the small sample size (London et al., 2020).

Previous basic studies have shown evidence that blockade of A2A receptors can have anti-inflammatory and neuroprotective effects in the rodent brain (Pierri et al., 2005; Gołembiowska et al., 2013; Ogawa et al., 2018; Zhou et al., 2019). However, no study has yet attempted to evaluate the effects of A2A receptor antagonism on neuroinflammation in the human brain.

Istradefylline is a selective A2A-receptor antagonist, and it received the drug approval as an add-on treatment to levodopa and/or carbidopa in adult patients with Parkinson's disease in 2013 by Ministry of Health, Labour and Welfare in Japan (Dungo and Deeks, 2013), and in 2019 by the U.S. Food and Drug Administration (Chen and Cunha, 2020). Istradefylline is a structural analog of caffeine and is characterized by long-term safety and high tolerability (Kondo and Mizuno, 2015). When administered in combination with levodopa for patients with Parkinson's disease in a phase I clinical trial, dyskinesia was the most frequently reported side effect (16.9% of participants), although when istradefylline was administered alone to healthy individuals there were no clinically significant adverse events reported (Kirin, 2013). These features would fit for purpose of treating methamphetamine use disorder that requires long term commitment, although the risk of unexpected effect should not be ignored because it is an off-label use and, to our knowledge, this study would be the first trial of istradefylline for methamphetamine use disorder.

The main aim of this study is to evaluate if medium-term treatment with istradefylline can induce D2-type receptor upregulation in striatum in individuals with methamphetamine use disorder (Aim 1). It is hypothesized that this pharmacological intervention will increase D2-type BP_{ND} as measured with [^{11}C] raclopride scan; such increases will be indicated by within-subject differences (i.e., pre- *vs.* post- intervention). The secondary aim is to evaluate the effects of this pharmacological intervention on neuroinflammation (Aim 2). As such, the secondary hypothesis is that whole brain SUV (as quantified by the [^{11}C]DAA1106 scan) will decrease after 2-week administration of istradefylline. Lastly, further aims are to evaluate the extent to which any effects on cognitive performance and/or risk of recurrent methamphetamine use are associated with changes in D2-type receptor (Aim 3) or

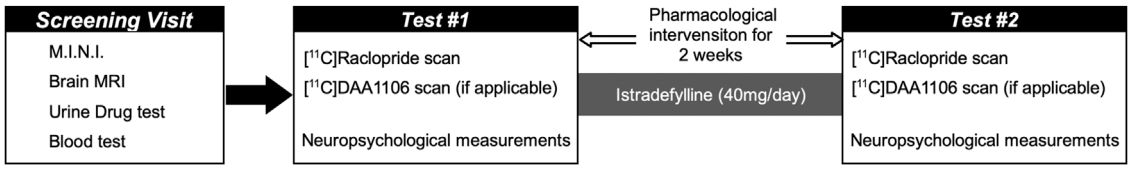

FIGURE 1 | Schematic diagram of the study.

neuroinflammation (Aim 4). The hypotheses pertaining to these aims are that 2-week administration of istradefylline would both improve neurocognitive measures and attenuate the risk of recurrent methamphetamine use as indicated by within-subject pre- *vs*. post-administration difference, and that any effects of the pharmacological intervention on D2-type BP_{ND} measured with [^{11}C]raclopride and/or SUV of [^{11}C]DAA1106 will be associated with such effects on cognitive performance and risk of recurrent use.

METHODS AND ANALYSIS

Research Design

This study will employ a within-subject design and aims to determine the potential effect of istradefylline, a selective A2A receptor antagonist, firstly on striatal D2-type BP_{ND}, and secondarily on neuroinflammation in the whole brain. Participants will receive 40 mg/day of istradefylline for 2 weeks and will undergo two PET scans; one before and one after administration of istradefylline for 2 weeks. All participants will undergo [^{11}C]raclopride PET scans and neurocognitive tests (**Figure 1**). Importantly, if a participant is strongly averse to undergoing a [^{11}C]DAA1106 scan, due to any reason (i.e., if they are anxious about radiation exposure), or if they meet the additional exclusion criterion for a neuroinflammation PET scan (see below for more details), they will not undergo the PET scans.

Participants

Twenty participants with methamphetamine use disorder will be recruited for this study. Inclusion criteria are: being between 20 and 65 years old, being able to comprehend Japanese, and meeting criteria for methamphetamine use disorder, according to the DSM-5. Exclusion criteria include the following: lifetime history or current neurological disorder; past history of psychiatric disorder which precedes initiation of methamphetamine use [confirmed using the Mini International Neuropsychiatric Interview (M.I.N.I.)]; (an) intracranial lesion(s) as observed from the structural magnetic resonance image (MRI); impairment of liver and/or renal function; HIV seropositive; positive urine-sample test for illegal drugs other than methamphetamine at the screening visit; past history of suicidal ideation or attempt; claustrophobia or aichmophobia; metals inside the body incompatible with MRI; use of psychotropic drugs which could interfere D2-type BP_{ND} measurement such as antipsychotics; use of drugs that interact with CYP3A4, a major metabolizing enzyme of istradefylline. Also, individuals will be required to abstain from methamphetamine use during participation in the study; this abstinence will be confirmed with urine sample test on each day of PET scans (**Supplementary Table S1**). Additionally, for those who will undergo the neuroinflammation scan with [^{11}C]DAA1106, the use of anti-inflammatory drugs such as NSAIDs, or current tobacco smoking, which have been proven to influence neuroinflammation (Brody et al., 2017; Brody et al., 2018) will be an exclusion criterion.

Research Ethics and Recruitment

This study will take place at the National Center of Neurology and Psychiatry (NCNP) in Kodaira, Tokyo, Japan. The study procedure has been reviewed and approved by the Certified Review Boards (CRB) of the NCNP. Study participants will be recruited at an outpatient clinic run by Drug Dependence Center at the NCNP. Potential participants will contact the research team by email or phone. After brief screening, those who meet inclusion/exclusion criteria will then be invited to come into the office for an in-person screening. At the initial visit, participants will be given a full description of the study procedure and will be asked to sign the CRB-approved informed consent forms with the PI. Comprehensive baseline assessments including M.I.N.I., urine drug test, blood test and MRI scan (see below for details) then will be performed for rigorous screening. Medical eligibility for the study will be determined by the PI *via* examination of all data acquired at the screening visit and clinical record.

Patient and Public Involvement

Participants will not be involved in the recruitment, conduct of the study and decision of which data and results to report. While, members of the research team may listen to input from participants during the process of deciding what data to report, the final decision as to which findings to report will be made only by the scientists.

Study Medication

Participants will receive 40 mg/day of istradefylline for 2 weeks. This dose was selected because it is the maximum dose approved in clinical practice, and this dose has been shown to be tolerable for healthy individuals in a phase I clinical trial of istradefylline that used a similar administration protocol as our own (i.e., 2-week administration of 20, 40, or 80 mg) (Kyowa Kirin, 2013). Istradefylline (brand name Nourianz®; Kyowa Kirin, Inc., Tokyo, Japan) will be provided by a study pharmacist at the Department of Pharmacology of the NCNP hospital. Participants will receive an email notification from the investigator team every morning to check adherence and potential side effect.

Neuroimaging

Magnetic Resonance Image Scans

Structural MRI scans of the brain for co-registration with PET images and definition of volumes-of-interest (VOIs) will be acquired using Achieva 3.0T TX (Koninklijke Philips N.V., Amsterdam, Netherland). A T1-weighted scan will be acquired using a whole-brain magnetization-prepared rapid acquisition with gradient echo (MPRAGE) (TR = 7.223 ms, TE = 3.468 ms, flip angle = 10, field of view = 384 × 384 × 300, 300 slices, thickness = 0.6 mm).

Positron Emission Tomography Scans

Biograph TruePoint 6 PET/CT (Siemens Healthineers, Erlangen, Germany), which has a resolution full-width at half-maximum (FWHM) of 4.1 mm, and an axial field of view of 162 mm in the 3D mode, will be used for PET data acquisition. Low-dose CT scan for attenuation correction firstly will be performed, then emission data will be collected with a dynamic mode for 60 min after a bolus injection of 10 mCi (±10%; range of 9–11 mCi) [^{11}C]raclopride for measurement of dopamine D2-type receptor availability (Kohler et al., 1985), which has a specific activity of >1 Ci/μmol. For neuroinflammation measurement, emission data collection will start 20 min after injection of 10 mCi (±10%; range of 9–11 mCi, specific activity of >1 Ci/μmol) [^{11}C]DAA1106, a second-generation radiotracer for labeling translocator protein (TSPO) with high affinity (Maeda et al., 2004; Venneti et al., 2008).

Data Processing

Magnetic Resonance Image Data

VOIs will be derived from individual MPRAGE images. For [^{11}C] raclopride scan, striatum VOI, including caudate and putamen, will be created using FSL FIRST (Patenaude et al., 2011). As the reference region (Hall et al., 1994), cerebellum VOI, including the hemispheres but not the vermis, will be manually created in standard space (MNI152 template) and transformed into native space with FSL FNIRT. For [^{11}C]DAA1106 scan, whole brain VOI will be created using FSL BET.

Positron Emission Tomography Data

The PET data reconstruction will use the manufacturer's 3-dimention ordered subset expectation maximization (3D-OSEM) algorithm (Lee et al., 2014). The 60-min [^{11}C]raclopride emission data will be reconstructed into twelve 20-s frames, sixteen 60-s frames, and ten 240-s frames (Kubota et al., 2017), and the 20-min [^{11}C]DAA1106 data will be reconstructed into twelve 60-s frames. Motion correction between the frames will be performed with FSL MCFLIRT (FMRIB Centre, Dept. Clinical Neurology, University of Oxford) (Jenkinson et al., 2002). The images will then be co-registered to the MPRAGE image using a 6-parameter, rigid-body spatial transformation (FSL FLIRT).

BP_{ND} for [^{11}C]raclopride Scan

Time-activity data within striatal and cerebellum VOIs will be extracted from the reconstructed frames of [^{11}C]raclopride scan and imported into PMOD Kinetic Modeling (PKIN) tool (PMOD Technologies Ltd., Zurich, Switzerland). The simplified reference tissue model (SRTM) (Lammertsma and Hume, 1996) will be used to calculate BP_{ND} with time–activity curves from VOIs as follows: $C_T(t) = R1C_R(t) + [k2 - R1k2/(1 + BP_{ND})]\ C_R(t) * \exp[-k2t/(1 + BP_{ND})]$, where $C_T(t)$ is the total radioactivity concentration in the striatum VOI measured by PET, R1 is the ratio of K1 (the influx rate constant for the striatum) to K1' (the influx rate constant for the cerebellum), $C_R(t)$ is the radioactivity concentration in the reference region (cerebellum), and * denotes the convolution integral. The parameters R1, k2, and BP_{ND} in this model are estimated by a nonlinear curve-fitting procedure.

Standardized Uptake Values for [^{11}C]DAA1106 Scan

For measurements of [^{11}C]DAA1106 binding to TSPO in whole brain, standardized uptake values (SUV) will be used as the primary outcome measure because it avoids invasive arterial blood sampling. It will be calculated using the standard definition of SUV = mean tissue activity concentration (Bq/mL)/[(injected dose (Bq)/body weight (g)]. Mean activity in whole brain from 20 to 40 min post-injection was used, based on time-activity curves from our previous study demonstrating stable activity during this time period (Brody et al., 2017; Brody et al., 2018; London et al., 2020).

Neuropsychological Measurements

The following measurements will be administered on each day of [^{11}C]raclopride scan.

- Stimulant Relapse Risk Scale (SRRS): This 30-item self-report questionnaire, which was developed to measure stimulant relapse risk in Japanese language, will be used. The SRRS is composed of five subscales: anxiety and intention to use drugs, emotionality problems, compulsivity for drug use, positive expectancies, lack of control over drug use and lack of negative expectancy for drug use (Ogai et al., 2007).
- Barratt Impulsiveness Scale (BIS): This 30-item self-report questionnaire assesses impulsive personality traits (Patton et al., 1995). The BIS has been shown to be sensitive to changes in impulsivity over time in individuals with methamphetamine use disorder (Ghahremani et al., 2013).
- Stop-Signal Task: Participants will be asked to press a left or right key in response to visual stimuli (left or right-direction arrow) presented on a laptop screen, whilst they will be instructed to withhold pressing the key if a tone (i.e., stop-signal) will be presented after a short delay after the visual stimuli. The primary dependent variable, stop-signal reaction time, indicates individual's capability of response inhibition and it associates with impulsiveness.
- Monetary Choice Questionnaire (MCQ): Participants will be instructed to select between one of two hypothetical options in 27 questions to receive a certain amount of money immediately or a larger amount later. The discrepancies between the monetary amounts and duration of the delay are varied across questions. The primary dependent variable is the indifference point, or total k value, determined from the participant's selections across the task (Kirby et al., 1999).
- Toronto Alexithymia Scale-20 (TAS-20): This self-administered questionnaire will be used to assess emotional self-awareness (Bagby et al., 1994). It a widely used questionnaire including for methamphetamine use disorder (Payer et al., 2011; Okita et al., 2016)Total score is interpreted

as follows: 0–51: no alexithymia; 52–60: possible alexithymia; 61 and above: alexithymia (Taylor et al., 1999).

- Difficulties in Emotion Regulation Scale (DERS): This 36-item self-administered questionnaire will be used to assess emotion dysregulation (Gratz and Roemer, 2004). Total of the questionnaire ranges from 30 to 180 and higher scores represent more difficulties in emotion regulation.
- Beck Depression Inventory (BDI) (Beck et al., 1996) and Beck Anxiety Inventory (BAI) (Beck et al., 1988): The BDI and BAI are self-report inventories to verify depressive and anxiety symptoms respectively. They will be employed to verify exclusion criteria and monitor potential adverse events related to drug administration.

Data Analytic Plan

Power Considerations

A sample size was selected based on a power analysis that was performed in advance. A previous study that showed D2-type receptor upregulation in humans after completion of an exercise intervention revealed a significant increase of striatal D2-type BP_{ND} with a Cohen's dz = 0.97 (Robertson et al., 2016). Test-retest reliability of the [^{11}C]raclopride PET scan has been shown good with a interclass correlation coefficient of 0.8 (Alakurtti et al., 2015). Given those numbers, a sample size of sixteen participants is deemed necessary to provide sufficient power ($\beta > 0.95$) to detect an effect using a critical 2-sided significance of $\alpha = 0.05$. We set a sample size of N = 20 taking into account the potential participant drop-out rate of roughly 20%, which is common based on our previous studies (Moeller et al., 2018; Okita et al., 2018; London et al., 2020).

Statistical Analysis

We will use graphical and numerical summaries to screen the data for outliers and violations of model assumptions. For Aims 1 and 2, the hypotheses will be tested by evaluating the effects of time (pre- *vs*. post-drug administration) on striatal D2-type BP_{ND} and whole brain SUV (which will be the dependent variable) using paired samples *t*-tests. For Aims 3 and 4, the hypotheses will be tested using partial correlation analyses which will examine the associations between A) pre- *vs*. post-drug administration changes in BP_{ND} and SUV and B) changes in neurocognitive measures. These statistical analyses will all be conducted using SPSS IBM 25 (IBM, Armonk, NY, United States).

Adverse Event Reporting

An annual summary of adverse events will be submitted to the Japan Registry of Clinical Trials (jRCT) and the CRB at NCNP. In the event that significant medical problems occur, or in the case that an investigator believes that any aspects of the study may be causing harm to participants' health, the PI will promptly report all severe adverse events to the director of NCNP, the CRB of NCNP, the Pharmaceuticals and Medical Devices Agency, and the Ministry of Health, Labor and Welfare (where appropriate). Significant medical problems are defined as any fatal event, any immediately life-threatening event, any permanent or substantially disabling event, any event that requires or prolongs inpatient hospitalization, any congenital anomaly, or any unexpected adverse drug experiences that have not previously been observed.

Data Monitoring

An independent review board at the Department of Clinical Epidemiology, Translational Medical Center at NCNP will perform regular monitoring over the course of the study. They will oversee the case report forms to verify that all study procedures are in compliance with approved study protocols, and will provide monitoring reports to the PI.

DISCUSSION

Substance use disorders are characterized by impaired dopaminergic neurotransmission. Notably, previous PET studies have repeatedly shown lower striatal D2-type BP_{ND} in individuals with substance use disorders *vs*. healthy control subjects [see reviews (Volkow et al., 2009; Ashok et al., 2017; London, 2020)]. Although the lower striatal D2-type BP_{ND} may reflect intrinsic biological aspect of individuals with substance use disorders, given that the phasic dopamine release in the human brain is induced by acute administration of most addictive substances (Nutt et al., 2015), and that agonism of GPCRs promotes desensitization of these receptors which possibly lead to their downregulation (Ferguson, 2001; Tabor et al., 2017), it seems plausible that chronic substance use could contribute to D2-receptor downregulation (Volkow et al., 2004). Further, *in vitro* studies using cultured cells derived from human neuroblastoma have revealed that coaggregation and co-internalization of A2A receptors and D2 receptors are induced by concurrent agonist stimulation of those receptors (Hillion et al., 2002; Bartlett et al., 2005). We therefore hypothesize that administration of A2A receptor antagonists for methamphetamine use disorder helps to recover from impaired dopaminergic neurotransmission through D2-receptor by producing D2 receptor upregulation.

In a human PET study using [^{11}C]raclopride, which is the same ligand as we will use in this proposed study, a single administration of caffeine increased striatal D2-type BP_{ND} in healthy individuals (Volkow et al., 2015). However, it is unclear if this D2-type BP_{ND} change was a consequence of A2A receptor antagonist-induced D2 receptor internalization as caffeine acts as an antagonist of adenosine 2A receptor subtype as well as other subtypes of adenosine receptors (Ribeiro and Sebastiao, 2010). To eliminate this ambiguity, we are currently running a double-blind, randomized controlled trial assessing the effect of 2-week administration of istradefylline using the same PET scans as planed in this study on healthy individuals, that are not included in this study (Okita et al., 2021). Still, there is also a lack of evidence that A2A receptor antagonism increases D2-type BP_{ND} in addictive disorders, or whether such potential increases are associated with characteristics of addictive disorders such as magnitude of use and level of dependence. Thus, the main aim of this proposed study is to monitor changes in D2-type BP_{ND} in striatum due to istradefylline administration in individuals with methamphetamine use disorder.

As already mentioned, medications that have agonistic effect on dopamine D2-type receptors have failed to show a therapeutic effect (Verrico et al., 2013; Blum et al., 2014). It might be because those agonists are not able to mimic physiological dopaminergic function, in that they simply keep stimulating neurotransmission through D2-type receptors as long as they are in the central nervous system,

regardless of the natural reaction of the dopaminergic system to reward. It has been suggested that the reward system of individuals with substance use disorders predominantly react to the substance addicted more than they react to natural rewards (Koob and Le Moal, 2005; Volkow et al., 2010; Hommer et al., 2011). This malfunctioning of the brain's reward system is thought to be associated with impaired dopaminergic neurotransmission caused by chronic addictive substance use (Volkow et al., 2019). Thus, upregulation of dopamine D2-type receptor density may be beneficial by making the reward systems of methamphetamine-addicted individuals more reactive to other, non-drug-related stimuli, which may in turn provide a therapeutic effect for addictive disorders.

In addition, it has been suggested that the use of methamphetamine can produce neurotoxicity (Miyazaki et al., 2006; Shaerzadeh et al., 2018), which in turn can induce pathological brain changes and possibly cognitive deficits (London et al., 2015). Evidence from basic research has shown methamphetamine causes activation of microglia and astrocytes that produce inflammatory cytokines such as tumor necrosis factor and interleukin (Yamamoto and Raudensky, 2008). Further, higher neuroinflammation levels (represented by microglia activation) have been observed in individuals with methamphetamine use disorder (Sekine et al., 2008; London et al., 2020). Given the presumed important role of neuroinflammation in neuronal damage due to chronic methamphetamine use (Kim et al., 2020) and the suppressing effects of A2A receptor antagonist on neuroinflammation (Pierri et al., 2005; Ogawa et al., 2018; Zhou et al., 2019), it is worth evaluating potential changes in neuroinflammation beside dopamine D2-type receptors.

This study is not without limitations. The randomized placebo-control design would obviously be suitable to assess the medication's effect. We are running another study of healthy individuals, that are not included in this proposed study, using a randomized double-blind placebo-controlled design (Okita et al., 2021). The purpose of the study in progress for healthy individuals is to verify a potential effect of istradefylline on D2-type receptors in human brain. However, the ultimate goal of a series of studies including the study in progress and this proposed study is to develop medication for methamphetamine use disorder. Because the randomized design requires a larger sample size than a study which employs a within-subject design, and because it is difficult to recruit many individuals with methamphetamine use disorder due to many such users failing to satisfy criterion of this D2-type receptor PET study (i.e., not taking antipsychotic medications, HIV negative and can keep abstinence for 2 weeks), we chose to perform a feasibility study due to limited human and budget resources. Despite this fundamental limitation, positive finding of D2-receptor upregulation from this study would have significance for the development of novel treatments for addictive disorders, particularly those that improve the functioning of dopamine D2-type receptors. Also, potential attenuation effect on neuroinflammation of istradefylline would have significance not only for addictive disorders but for neuropsychiatric disorders characterized by neuroinflammation.

ETHICS STATEMENT

The studies involving human participants were reviewed and approved by The Certified Review Boards of National Center of Neurology and Psychiatry. The patients/participants provided their written informed consent to participate in this study.

AUTHOR CONTRIBUTIONS

All authors made a significant contribution to the conception and design of the trial protocol. KO is the PI of the study and made major contributions to the design of this trial, development of the original trial protocol and drafting of the initial manuscript.

FUNDING

This research was funded by following research grants and fellowships: KAKENHI Grant-in-Aid for Young Scientists (grant number: 20K16634).

ACKNOWLEDGMENTS

The authors are grateful to the following contributors: Mitsuru Syakadou, Kaori Takeda, Yumi Saito, Atsushi Yokoyama, Masato Ogura, Satoshi Kanbayashi, Midori Kusama, Kenji Hatano, Kazunori Oih, Ichiko Iizuka, Atsuko Asano, Takami Ishizuka, Komei Shimokawa, and Hirofumi Komaki.

SUPPLEMENTARY MATERIAL

The Supplementary Material for this article can be found online at: https://www.frontiersin.org/articles/10.3389/fphar.2022.820447/full#supplementary-material

REFERENCES

Alakurtti, K., Johansson, J. J., Joutsa, J., Laine, M., Bäckman, L., Nyberg, L., et al. (2015). Long-term Test-Retest Reliability of Striatal and Extrastriatal Dopamine D2/3 Receptor Binding: Study with [(11)C]raclopride and High-Resolution PET. *J. Cereb. Blood Flow. Metab.* 35, 1199–1205. doi:10.1038/jcbfm.2015.53

Ashok, A. H., Mizuno, Y., Volkow, N. D., and Howes, O. D. (2017). Association of Stimulant Use with Dopaminergic Alterations in Users of Cocaine, Amphetamine, or Methamphetamine: A Systematic Review and Meta-Analysis. *JAMA Psychiatry* 74, 511–519. doi:10.1001/jamapsychiatry.2017.0135

Bagby, R. M., Parker, J. D., and Taylor, G. J. (1994). The Twenty-Item Toronto Alexithymia Scale--I. Item Selection and Cross-Validation of the Factor Structure. *J. Psychosom. Res.* 38, 23–32. doi:10.1016/0022-3999(94)90005-1

Bartlett, S. E., Enquist, J., Hopf, F. W., Lee, J. H., Gladher, F., Kharazia, V., et al. (2005). Dopamine Responsiveness Is Regulated by Targeted Sorting of D2 Receptors. *Proc. Natl. Acad. Sci. U. S. A.* 102, 11521–11526. doi:10.1073/pnas.0502418102

Beck, A. T., Epstein, N., Brown, G., and Steer, R. A. (1988). An Inventory for Measuring Clinical Anxiety: Psychometric Properties. *J. Consult Clin. Psychol.* 56, 893–897. doi:10.1037//0022-006x.56.6.893

Beck, A. T., Steer, R. A., Ball, R., and Ranieri, W. (1996). Comparison of Beck Depression Inventories -IA and -II in Psychiatric Outpatients. *J. Pers. Assess.* 67, 588–597. doi:10.1207/s15327752jpa6703_13

Blum, K., Thanos, P. K., and Gold, M. S. (2014). Dopamine and Glucose, Obesity, and Reward Deficiency Syndrome. *Front. Psychol.* 5, 919. doi:10.3389/fpsyg.2014.00919

Brody, A. L., Gehlbach, D., Garcia, L. Y., Enoki, R., Hoh, C., Vera, D., et al. (2018). Effect of Overnight Smoking Abstinence on a Marker for Microglial Activation: a [(11)C]DAA1106 Positron Emission Tomography Study. *Psychopharmacol. Berl.* 235, 3525–3534. doi:10.1007/s00213-018-5077-3

Brody, A. L., Hubert, R., Enoki, R., Garcia, L. Y., Mamoun, M. S., Okita, K., et al. (2017). Effect of Cigarette Smoking on a Marker for Neuroinflammation: A [(11)C]DAA1106 Positron Emission Tomography Study. *Neuropsychopharmacology* 42, 1630–1639. doi:10.1038/npp.2017.48

Chen, J. F., and Cunha, R. A. (2020). The Belated US FDA Approval of the Adenosine A(2A) Receptor Antagonist Istradefylline for Treatment of Parkinson's Disease. *Purinergic Signal* 16, 167–174. doi:10.1007/s11302-020-09694-2

Darke, S., Duflou, J., and Kaye, S. (2017). Prevalence and Nature of Cardiovascular Disease in Methamphetamine-Related Death: A National Study. *Drug Alcohol Depend.* 179, 174–179. doi:10.1016/j.drugalcdep.2017.07.001

Dungo, R., and Deeks, E. D. (2013). Istradefylline: First Global Approval. *Drugs* 73, 875–882. doi:10.1007/s40265-013-0066-7

Ferguson, S. S. (2001). Evolving Concepts in G Protein-Coupled Receptor Endocytosis: the Role in Receptor Desensitization and Signaling. *Pharmacol. Rev.* 53, 1–24.

Ferré, S., Bonaventura, J., Tomasi, D., Navarro, G., Moreno, E., Cortés, A., et al. (2016). Allosteric Mechanisms within the Adenosine A2A-Dopamine D2 Receptor Heterotetramer. *Neuropharmacology* 104, 154–160. doi:10.1016/j.neuropharm.2015.05.028

Ghahremani, D. G., Oh, E. Y., Dean, A. C., Mouzakis, K., Wilson, K. D., and London, E. D. (2013). Effects of the Youth Empowerment Seminar on Impulsive Behavior in Adolescents. *J. Adolesc. Health* 53, 139–141. doi:10.1016/j.jadohealth.2013.02.010

Gołembiowska, K., Wardas, J., Noworyta-Sokołowska, K., Kamińska, K., and Górska, A. (2013). Effects of Adenosine Receptor Antagonists on the *In Vivo* LPS-Induced Inflammation Model of Parkinson's Disease. *Neurotox. Res.* 24, 29–40. doi:10.1007/s12640-012-9372-1

Gratz, K. L., and Roemer, L. (2004). Multidimensional Assessment of Emotion Regulation and Dysregulation: Development, Factor Structure, and Initial Validation of the Difficulties in Emotion Regulation Scale. *J. Psychopathol. Behav. Assess.* 26, 41–54. doi:10.1023/b:joba.0000007455.08539.94

Hall, H., Sedvall, G., Magnusson, O., Kopp, J., Halldin, C., and Farde, L. (1994). Distribution of D1-And D2-Dopamine Receptors, and Dopamine and its Metabolites in the Human Brain. *Neuropsychopharmacology* 11, 245. doi:10.1038/sj.npp.1380111

Han, B., Compton, W. M., Jones, C. M., Einstein, E. B., and Volkow, N. D. (2021). Methamphetamine Use, Methamphetamine Use Disorder, and Associated Overdose Deaths Among US Adults. *JAMA Psychiatry* 78 (12), 1329–1342. doi:10.1001/jamapsychiatry.2021.2588

Hillion, J., Canals, M., Torvinen, M., Casado, V., Scott, R., Terasmaa, A., et al. (2002). Coaggregation, Cointernalization, and Codesensitization of Adenosine A2A Receptors and Dopamine D2 Receptors. *J. Biol. Chem.* 277, 18091–18097. doi:10.1074/jbc.M107731200

Hommer, D. W., Bjork, J. M., and Gilman, J. M. (2011). Imaging Brain Response to Reward in Addictive Disorders. *Ann. N. Y. Acad. Sci.* 1216, 50–61. doi:10.1111/j.1749-6632.2010.05898.x

Huang, L., Wu, D. D., Zhang, L., and Feng, L. Y. (2013). Modulation of A(2)a Receptor Antagonist on D(2) Receptor Internalization and ERK Phosphorylation. *Acta Pharmacol. Sin.* 34, 1292–1300. doi:10.1038/aps.2013.87

Jenkinson, M., Bannister, P., Brady, M., and Smith, S. (2002). Improved Optimization for the Robust and Accurate Linear Registration and Motion Correction of Brain Images. *Neuroimage* 17, 825–841. doi:10.1016/s1053-8119(02)91132-8

Kevil, C. G., Goeders, N. E., Woolard, M. D., Bhuiyan, M. S., Dominic, P., Kolluru, G. K., et al. (2019). Methamphetamine Use and Cardiovascular Disease. *Arterioscler. Thromb. Vasc. Biol.* 39, 1739–1746. doi:10.1161/ATVBAHA.119.312461

Kim, B., Yun, J., and Park, B. (2020). Methamphetamine-Induced Neuronal Damage: Neurotoxicity and Neuroinflammation. *Biomol. Ther. Seoul.* 28, 381–388. doi:10.4062/biomolther.2020.044

Kirby, K. N., Petry, N. M., and Bickel, W. K. (1999). Heroin Addicts Have Higher Discount Rates for Delayed Rewards Than Non-drug-using Controls. *J. Exp. Psychol. Gen.* 128, 78–87. doi:10.1037//0096-3445.128.1.78

Kirin, K. (2013). *Nourianz Tablet 20mg* [Online]. Pharmaceuticals and Medical Devices Agency. Available at: https://www.info.pmda.go.jp/go/pack/1169016F1020_1_06/(Accessed 310 2022, 2022).

Köhler, C., Hall, H., Ogren, S. O., and Gawell, L. (1985). Specific *In Vitro* and *In Vivo* Binding of 3H-Raclopride. A Potent Substituted Benzamide Drug with High Affinity for Dopamine D-2 Receptors in the Rat Brain. *Biochem. Pharmacol.* 34, 2251–2259. doi:10.1016/0006-2952(85)90778-6

Kondo, T., and Mizuno, Y. (2015). A Long-Term Study of Istradefylline Safety and Efficacy in Patients with Parkinson Disease. *Clin. Neuropharmacol.* 38, 41–46. doi:10.1097/WNF.0000000000000073

Koob, G. F., and Le Moal, M. (2005). Plasticity of Reward Neurocircuitry and the 'dark Side' of Drug Addiction. *Nat. Neurosci.* 8, 1442–1444. doi:10.1038/nn1105-1442

Kubota, M., Nagashima, T., Takano, H., Kodaka, F., Fujiwara, H., Takahata, K., et al. (2017). Affinity States of Striatal Dopamine D2 Receptors in Antipsychotic-free Patients with Schizophrenia. *Int. J. Neuropsychopharmacol.* 20, 928–935. doi:10.1093/ijnp/pyx063

Lammertsma, A. A., and Hume, S. P. (1996). Simplified Reference Tissue Model for PET Receptor Studies. *Neuroimage* 4, 153–158. doi:10.1006/nimg.1996.0066

Lappin, J. M., Darke, S., and Farrell, M. (2017). Stroke and Methamphetamine Use in Young Adults: a Review. *J. Neurol. Neurosurg. Psychiatry* 88, 1079–1091. doi:10.1136/jnnp-2017-316071

Lee, B., London, E. D., Poldrack, R. A., Farahi, J., Nacca, A., Monterosso, J. R., et al. (2009). Striatal Dopamine D2/D3 Receptor Availability Is Reduced in Methamphetamine Dependence and Is Linked to Impulsivity. *J. Neurosci.* 29, 14734–14740. doi:10.1523/jneurosci.3765-09.2009

Lee, Y. S., Kim, J. S., Kim, K. M., Kang, J. H., Lim, S. M., and Kim, H. J. (2014). Performance Measurement of PSF Modeling Reconstruction (True X) on Siemens Biograph TruePoint TrueV PET/CT. *Ann. Nucl. Med.* 28, 340–348. doi:10.1007/s12149-014-0815-z

London, E. D. (2020). Human Brain Imaging Links Dopaminergic Systems to Impulsivity. *Curr. Top. Behav. Neurosci.* 47, 53–71. doi:10.1007/7854_2019_125

London, E. D., Kohno, M., Morales, A. M., and Ballard, M. E. (2015). Chronic Methamphetamine Abuse and Corticostriatal Deficits Revealed by Neuroimaging. *Brain Res.* 1628, 174–185. doi:10.1016/j.brainres.2014.10.044

London, E. D., Okita, K., Kinney, K. R., Dean, A. C., Mcclintick, M. N., Rizor, E. J., et al. (2020). No Significant Elevation of Translocator Protein Binding in the Brains of Recently Abstinent Methamphetamine Users. *Drug Alcohol Depend.* 213, 108104. doi:10.1016/j.drugalcdep.2020.108104

Maeda, J., Suhara, T., Zhang, M. R., Okauchi, T., Yasuno, F., Ikoma, Y., et al. (2004). Novel Peripheral Benzodiazepine Receptor Ligand [11C]DAA1106 for PET: an Imaging Tool for Glial Cells in the Brain. *Synapse* 52, 283–291. doi:10.1002/syn.20027

Meyer, J. H., Cervenka, S., Kim, M. J., Kreisl, W. C., Henter, I. D., and Innis, R. B. (2020). Neuroinflammation in Psychiatric Disorders: PET Imaging and Promising New Targets. *Lancet Psychiatry* 7, 1064–1074. doi:10.1016/S2215-0366(20)30255-8

Miyazaki, I., Asanuma, M., Diaz-Corrales, F. J., Fukuda, M., Kitaichi, K., Miyoshi, K., et al. (2006). Methamphetamine-induced Dopaminergic Neurotoxicity Is Regulated by Quinone-Formation-Related Molecules. *Faseb J.* 20, 571–573. doi:10.1096/fj.05-4996fje

Moeller, S. J., Okita, K., Robertson, C. L., Ballard, M. E., Konova, A. B., Goldstein, R. Z., et al. (2018). Low Striatal Dopamine D2-type Receptor Availability Is Linked to Simulated Drug Choice in Methamphetamine Users. *Neuropsychopharmacology* 43, 751–760. doi:10.1038/npp.2017.138

Nutt, D. J., Lingford-Hughes, A., Erritzoe, D., and Stokes, P. R. (2015). The Dopamine Theory of Addiction: 40 Years of Highs and Lows. *Nat. Rev. Neurosci.* 16, 305–312. doi:10.1038/nrn3939

Ogai, Y., Haraguchi, A., Kondo, A., Ishibashi, Y., Umeno, M., Kikumoto, H., et al. (2007). Development and Validation of the Stimulant Relapse Risk Scale for Drug Abusers in Japan. *Drug Alcohol Depend.* 88, 174–181. doi:10.1016/j.drugalcdep.2006.10.005

Ogawa, Y., Furusawa, E., Saitoh, T., Sugimoto, H., Omori, T., Shimizu, S., et al. (2018). Inhibition of Astrocytic Adenosine Receptor A(2A) Attenuates Microglial Activation in a Mouse Model of Sandhoff Disease. *Neurobiol. Dis.* 118, 142–154. doi:10.1016/j.nbd.2018.07.014

Okita, K., Ghahremani, D. G., Payer, D. E., Robertson, C. L., Mandelkern, M. A., and London, E. D. (2016). Relationship of Alexithymia Ratings to Dopamine D2-type Receptors in Anterior Cingulate and Insula of Healthy Control Subjects but Not Methamphetamine-dependent Individuals. *Int. J. Neuropsychopharmacol.* 19, pyv129. doi:10.1093/ijnp/pyv129

Okita, K., Kato, K., Shigemoto, Y., Sato, N., Matsumoto, T., and Matsuda, H. (2021). Effects of an Adenosine A2A Receptor Antagonist on Striatal Dopamine D2-type Receptor Availability: A Randomized Control Study Using Positron Emission Tomography. *Front. Neurosci.* 15, 729153. doi:10.3389/fnins.2021.729153

Okita, K., Morales, A. M., Dean, A. C., Johnson, M. C., Lu, V., Farahi, J., et al. (2018). Striatal Dopamine D1-type Receptor Availability: No Difference from Control but Association with Cortical Thickness in Methamphetamine Users. *Mol. Psychiatry* 23, 1320–1327. doi:10.1038/mp.2017.172

Patenaude, B., Smith, S. M., Kennedy, D. N., and Jenkinson, M. (2011). A Bayesian Model of Shape and Appearance for Subcortical Brain Segmentation. *NeuroImage* 56, 907–922. doi:10.1016/j.neuroimage.2011.02.046

Patton, J. H., Stanford, M. S., and Barratt, E. S. (1995). Factor Structure of the Barratt Impulsiveness Scale. *J. Clin. Psychol.* 51, 768–774. doi:10.1002/1097-4679(199511)51:6<768::aid-jclp2270510607>3.0.co;2-1

Paulus, M. P., and Stewart, J. L. (2020). Neurobiology, Clinical Presentation, and Treatment of Methamphetamine Use Disorder: A Review. *JAMA Psychiatry* 77, 959–966. doi:10.1001/jamapsychiatry.2020.0246

Payer, D. E., Lieberman, M. D., and London, E. D. (2011). Neural Correlates of Affect Processing and Aggression in Methamphetamine Dependence. *Arch. Gen. Psychiatry* 68, 271–282. doi:10.1001/archgenpsychiatry.2010.154

Pierri, M., Vaudano, E., Sager, T., and Englund, U. (2005). KW-6002 Protects from MPTP Induced Dopaminergic Toxicity in the Mouse. *Neuropharmacology* 48, 517–524. doi:10.1016/j.neuropharm.2004.11.009

Ribeiro, J. A., and Sebastião, A. M. (2010). Caffeine and Adenosine. *J. Alzheimers Dis.* 20 (Suppl. 1), S3–S15. doi:10.3233/JAD-2010-1379

Robertson, C. L., Ishibashi, K., Chudzynski, J., Mooney, L. J., Rawson, R. A., Dolezal, B. A., et al. (2016). Effect of Exercise Training on Striatal Dopamine D2/D3 Receptors in Methamphetamine Users during Behavioral Treatment. *Neuropsychopharmacology* 41, 1629–1636. doi:10.1038/npp.2015.331

Sekine, Y., Ouchi, Y., Sugihara, G., Takei, N., Yoshikawa, E., Nakamura, K., et al. (2008). Methamphetamine Causes Microglial Activation in the Brains of Human Abusers. *J. Neurosci.* 28, 5756–5761. doi:10.1523/JNEUROSCI.1179-08.2008

Shaerzadeh, F., Streit, W. J., Heysieattalab, S., and Khoshbouei, H. (2018). Methamphetamine Neurotoxicity, Microglia, and Neuroinflammation. *J. Neuroinflammation* 15, 341. doi:10.1186/s12974-018-1385-0

Shoptaw, S., and Reback, C. J. (2007). Methamphetamine Use and Infectious Disease-Related Behaviors in Men Who Have Sex with Men: Implications for Interventions. *Addiction* 102 (Suppl. 1), 130–135. doi:10.1111/j.1360-0443.2006.01775.x

Solinas, M., Belujon, P., Fernagut, P. O., Jaber, M., and Thiriet, N. (2019). Dopamine and Addiction: what Have We Learned from 40 Years of Research. *J. Neural Transm. (Vienna)* 126, 481–516. doi:10.1007/s00702-018-1957-2

Tabor, A., Möller, D., Hübner, H., Kornhuber, J., and Gmeiner, P. (2017). Visualization of Ligand-Induced Dopamine D2S and D2L Receptor Internalization by TIRF Microscopy. *Sci. Rep.* 7, 10894. doi:10.1038/s41598-017-11436-1

Taylor, G. J., Bagby, R. M., and Parker, J. D. A. (1999). *Disorders of Affect Regulation: Alexithymia in Medical and Psychiatric Illness*. Cambridge: Cambridge University Press.

United Nations Office on Drugs and Crime (Unodc) (2021). World Drug Report 2021. Available at: https://www.unodc.org/unodc/en/data-and-analysis/wdr2021.html (Accessed November 03, 2021).

Venneti, S., Wang, G., Nguyen, J., and Wiley, C. A. (2008). The Positron Emission Tomography Ligand DAA1106 Binds with High Affinity to Activated Microglia in Human Neurological Disorders. *J. Neuropathol. Exp. Neurol.* 67, 1001–1010. doi:10.1097/NEN.0b013e318188b204

Verrico, C. D., Haile, C. N., Newton, T. F., Kosten, T. R., De La Garza, R., 2nd, and De La Garza, R. (2013). Pharmacotherapeutics for Substance-Use Disorders: a Focus on Dopaminergic Medications. *Expert Opin. Investig. Drugs* 22, 1549–1568. doi:10.1517/13543784.2013.836488

Volkow, N. D., Fowler, J. S., Wang, G. J., Baler, R., and Telang, F. (2009). Imaging Dopamine's Role in Drug Abuse and Addiction. *Neuropharmacology* 56 (Suppl. 1), 3–8. doi:10.1016/j.neuropharm.2008.05.022

Volkow, N. D., Fowler, J. S., Wang, G. J., and Swanson, J. M. (2004). Dopamine in Drug Abuse and Addiction: Results from Imaging Studies and Treatment Implications. *Mol. Psychiatry* 9, 557–569. doi:10.1038/sj.mp.4001507

Volkow, N. D., Michaelides, M., and Baler, R. (2019). The Neuroscience of Drug Reward and Addiction. *Physiol. Rev.* 99, 2115–2140. doi:10.1152/physrev.00014.2018

Volkow, N. D., Wang, G. J., Fowler, J. S., Tomasi, D., Telang, F., and Baler, R. (2010). Addiction: Decreased Reward Sensitivity and Increased Expectation Sensitivity Conspire to Overwhelm the Brain's Control Circuit. *Bioessays* 32, 748–755. doi:10.1002/bies.201000042

Volkow, N. D., Wang, G. J., Logan, J., Alexoff, D., Fowler, J. S., Thanos, P. K., et al. (2015). Caffeine Increases Striatal Dopamine D2/D3 Receptor Availability in the Human Brain. *Transl. Psychiatry* 5, e549. doi:10.1038/tp.2015.46

Wang, G. J., Smith, L., Volkow, N. D., Telang, F., Logan, J., Tomasi, D., et al. (2012). Decreased Dopamine Activity Predicts Relapse in Methamphetamine Abusers. *Mol. Psychiatry* 17, 918–925. doi:10.1038/mp.2011.86

Yamamoto, B. K., and Raudensky, J. (2008). The Role of Oxidative Stress, Metabolic Compromise, and Inflammation in Neuronal Injury Produced by Amphetamine-Related Drugs of Abuse. *J. Neuroimmune Pharmacol.* 3, 203–217. doi:10.1007/s11481-008-9121-7

Zhou, Y., Zeng, X., Li, G., Yang, Q., Xu, J., Zhang, M., et al. (2019). Inactivation of Endothelial Adenosine A(2A) Receptors Protects Mice from Cerebral Ischaemia-Induced Brain Injury. *Br. J. Pharmacol.* 176, 2250–2263. doi:10.1111/bph.14673

Conflict of Interest: The authors declare that the research was conducted in the absence of any commercial or financial relationships that could be construed as a potential conflict of interest.

Publisher's Note: All claims expressed in this article are solely those of the authors and do not necessarily represent those of their affiliated organizations, or those of the publisher, the editors and the reviewers. Any product that may be evaluated in this article, or claim that may be made by its manufacturer, is not guaranteed or endorsed by the publisher.

frontiers | Frontiers in Pharmacology

TYPE Systematic Review
PUBLISHED 29 August 2022
DOI 10.3389/fphar.2022.916312

OPEN ACCESS

EDITED BY
Anna Boguszewska-Czubara,
Medical University of Lublin, Poland

REVIEWED BY
Elena Bossi,
University of Insubria, Italy
Clemens Möller,
Hochschule Albstadt-Sigmaringen,
Germany

*CORRESPONDENCE
Luciana E. Drumond de Carvalho,
luianadrumond@ufsj.edu.br

SPECIALTY SECTION
This article was submitted to Neuropharmacology, a section of the journal Frontiers in Pharmacology

RECEIVED 09 April 2022
ACCEPTED 20 July 2022
PUBLISHED 29 August 2022

CITATION
Leite JA, Pôças E, Maia GS, Barbosa L, Quintas LEM, Kawamoto EM, Silva MLCd, Scavone C and de Carvalho LED (2022), Effect of ouabain on calcium signaling in rodent brain: A systematic review of in vitro studies.
Front. Pharmacol. 13:916312.
doi: 10.3389/fphar.2022.916312

Effect of ouabain on calcium signaling in rodent brain: A systematic review of *in vitro* studies

Jacqueline Alves Leite[1], Elisa Pôças[2], Gisele Silva Maia[3], Leandro Barbosa[3], Luis Eduardo M. Quintas[4], Elisa Mitiko Kawamoto[5], Maria Luiza Correia da Silva[5], Cristoforo Scavone[5] and Luciana E. Drumond de Carvalho[3]*

[1]Departamento de Farmacologia, Instituto de Ciências Biológicas, Universidade Federal de Goiás, Goiânia, Brazil, [2]Campus Realengo, Instituto Federal do Rio de Janeiro, Rio de Janeiro, Brazil, [3]Laboratório de Bioquímica Celular, Universidade Federal de São João del Rei, Campus Centro-Oeste Dona Lindu, São Paulo, Brazil, [4]Laboratório de Farmacologia Bioquímica e Molecular, Instituto de Ciências Biomédicas, Universidade Federal do Rio de Janeiro, Rio de Janeiro, Brazil, [5]Departamento de Farmacologia, Instituto de Ciências Biomédicas, Universidade de São Paulo, São Paulo, Brazil

The Na^+/K^+-ATPase is an integral membrane ion pump, essential to maintaining osmotic balance in cells in the presence of cardiotonic steroids; more specifically, ouabain can be an endogenous modulator of the Na^+/K^+-ATPase. Here, we conducted a systematic review of the *in vitro* effects of cardiotonic steroids on Ca^{2+} in the brain of rats and mice. Methods: The review was carried out using the PubMed, Virtual Health Library, and EMBASE databases (between 12 June 2020 and 30 June 2020) and followed the guidelines described in the Preferred Reporting Items for Systematic Reviews and Meta-analyses (PRISMA). Results: in total, 829 references were identified in the electronic databases; however, only 20 articles were considered, on the basis of the inclusion criteria. The studies demonstrated the effects of ouabain on Ca^{2+} signaling in synaptosomes, brain slices, and cultures of rat and mouse cells. In addition to the well-known cytotoxic effects of high doses of ouabain, resulting from indirect stimulation of the reverse mode of the Na^+/Ca^{2+} exchanger and increased intracellular Ca^{2+}, other effects have been reported. Ouabain-mediated Ca^{2+} signaling was able to act increasing cholinergic, noradrenergic and glutamatergic neurotransmission. Furthermore, ouabain significantly increased intracellular signaling molecules such as InsPs, IP3 and cAMP. Moreover treatment with low doses of ouabain stimulated myelin basic protein synthesis. Ouabain-induced intracellular Ca^{2+} increase may promote the activation of important cell signaling pathways involved in cellular homeostasis and function. Thus, the study of the application of ouabain in low doses being promising for application in neurological diseases.

Systematic Review Registration: https://www.crd.york.ac.uk/prospero/display_record.php?ID=CRD42020204498, identifier CRD42020204498.

KEYWORDS

ouabain, Na^+/K^+-ATPase, calcium, signaling, nervous system

Introduction

Na^+/K^+-ATPase, also known as Na^+-K^+ pump, is a plasma membrane transporter essential for cellular homeostasis. It is responsible for the active movement of Na^+ and K^+ against their electrochemical gradients at the expenses of ATP hydrolysis, and supports the maintenance of the cellular osmotic balance, membrane potential and the secondary active transport of substrates and neurotransmitters (Blanco, 2005). Particularly in the brain, which is composed of highly specialized cells (i.e., neurons and glial cells), Na^+/K^+-ATPase is involved in neuronal excitability and astrocyte buffering of extracellular K^+ ions during neuron action potential, in electrolyte balance of the cerebrospinal fluid, and in the secondary transport of molecules across the membrane, playing a fundamental role in the function of the central nervous system (Larsen et al., 2016), (Kinoshita et al., 2020). Therefore, the regulation of Na^+/K^+-ATPase function largely affects cell and system physiology.

This enzyme is composed of three subunits, and two of them are indispensable for enzyme activity (Figure 1). The amino acid sequence of the α subunit, also called the catalytic subunit, comprises more than 1010 residues (around 110 kDa) with 10 transmembrane domains. This subunit harbors the binding sites for ions (Na^+, K^+, Mg^{2+}), ATP, and selective ligands collectively known as cardiotonic steroids, as well as for several other regulators (Blanco, 2005), (Blanco and Mercer, 1998) . All isoforms are encoded by different genes and present a high degree of homology (Clausen et al., 2017). An interesting feature is that Na^+/K^+-ATPase isoforms are expressed in a cell-/tissue-specific fashion (Blanco, 2005), (Cereijido et al., 2012), (Geering, 2008): the α1 isoform is ubiquitously expressed in mammalian tissues and, in rodents, it is 100–1000-fold less sensitive to cardiotonic steroids. In contrast, it has been shown not to be the case for the bufadienolide marinobufagenin (Fedorova and Bagrov, 1997), (Fedorova et al., 2001), although our group reported that it behaves similar to any known cardiotonic steroid (Godinho et al., 2017), (Carvalho et al., 2019); the α_2 isoform is found in striated and smooth muscle, as well as in both astrocytes and neurons in the central nervous system, and adipose tissue; the α_3 isoform is basically found in neurons but not in astrocytes and should be considered a neuronal marker (Dobretsov and Stimers, 2005); the α_4 isoform is specifically found in the midpiece of sperm (Blanco, 2005). The β subunit is a type II glycoprotein of around 300 amino acids, that is, fundamental for a normal pumping activity. Enzyme kinetics modulation, Na^+/K^+-ATPase plasma membrane delivery and assembly, as well as cell adhesion and polarity, are characteristics of this subunit. The third subunit, γ, is a type I protein from the FXYD family (FXYD2) and it comprises around 65 amino acids. FXYD2 is

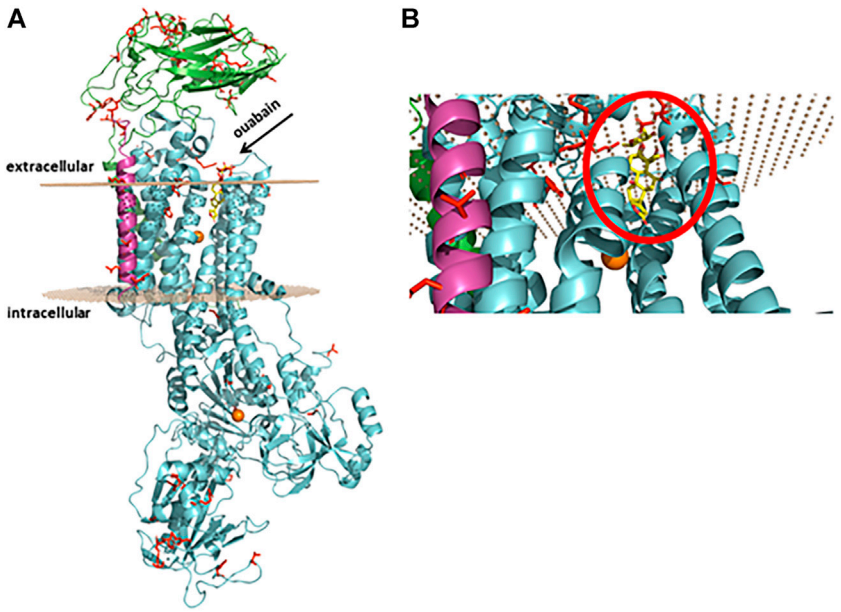

FIGURE 1
Protein representation of rat Na^+/K^+-ATPase α1β1γ isoform subunits. **(A)** In green, α1 subunit, in cyan, β1 subunit, and in pink, γ (FXYD2) subunit. The residues displaying the substitutions present in the rat compared to the human Na^+/K^+-ATPase protein. In orange, magnesium ions. The gray dots represent the Na^+/K^+-ATPase position at the plasma membrane, and the arrow points to the pocket where ouabain (in yellow) interacts. **(B)** Magnification of the binding pocket with ouabain (inside the red circle) seen from the bottom. The protein was constructed by homology using as reference the human crystallographic structure (pdb id:4RET) using the Swiss-model webserver, and for the representation the software PyMOL 7 was used.

not required for enzymatic activity but regulates Na^+/K^+-ATPase affinity for cations (Geering, 2008).

Ouabain is a natural ligand of Na^+/K^+-ATPase and belongs to the cardiotonic steroid class of compounds, i.e., the cardenolide family, originally identified in the African plants *Strophantus gratus* (Ouabain, 1932) and *Acokanthera ouabaio* (also called wabajo or schimperi) (Kupicha, 1982). Its inhibitory capacity was reported in 1953 by Schartzmann (Schatzmamn, 1953); this discovery paved the way for research on the mechanistic pathways of other cardiotonic steroids, such as digoxin, clinically used for decades to treat heart failure (Ziff and Kotecha, 2016). Ouabain selectively binds to Na^+/K^+-ATPase and inhibits its pump activity, increasing intracellular Na^+ and Ca^{2+} concentrations ($[Na^+]i$ and $[Ca^{2+}]i$, respectively), the latter by inducing a lower/reverse activity of the Na^+/Ca^{2+} exchanger that colocalizes with the Na^+/K^+-ATPase (Larsen et al., 2016), (Kinoshita et al., 2020). In the heart, the indirect elevation of sarcoplasmic reticulum Ca^{2+} levels lead to the cardiac inotropism (Akera and Brody, 1977), (Lingrel, 2009). Higher concentrations of ouabain are known to evoke cardiotoxic effects. In other organs, such as the brain, the effects are more complex. Concentrations that induce bulk inhibition of Na^+/K^+-ATPase generate neurotoxic effects (Lees et al., 1990), (Veldhuis et al., 2003). In contrast, ouabain at a low concentration of 10 nm increases the expression of the brain-derived neurotrophic factor (BDNF) mRNA in cerebellar cell culture (de Sá Lima et al., 2013) or after intrahippocampal injection (Tata et al., 2014) and activates the Wnt/β-catenin signaling pathway culminating with the increase of CREB/BDNF and NF-κB levels (Kawamoto et al., 2012a), indicating that the balance between ouabain-induced neuroprotective and neurotoxic effects is concentration-dependent.

Several mechanisms are involved in cellular Ca^{2+} homeostasis. From Ca^{2+}-binding proteins inside cells to proteins that allow Ca^{2+} fluxes across biological membranes, Ca^{2+} concentrations are strictly controlled in cytoplasm and organelles like mitochondria, Golgi apparatus, endoplasmic reticulum and nucleus (Brini et al., 2014). Ca^{2+} Channels (Koh et al., 2017), the high Ca^{2+} affinity but low capacity plasma membrane Ca^{2+}-ATPases and the low Ca^{2+} affinity but high capacity Na^+/Ca^{2+} exchanger (Blaustein et al., 2002), sarco/endoplasmic reticulum Ca^{2+}-ATPases (Valadares et al., 2021), and ryanodine and inositol 1,4,5-triphosphate (IP3) receptors (McGarry and Williams, 1993), (Panizza et al., 2019) are important for Ca^{2+} handling and secondary targets for ouabain action.

Na^+/K^+-ATPase ion pumping is the classical function assigned to this transporter. Nevertheless, around 50 years after the discovery of this mechanism, a new paradigm emerged. A series of works performed by Zijian Xie and Amir Askari's group unveiled that, besides ion transport, Na^+/K^+-ATPase operates as a receptor (Xie and Askari, 2002). The binding of ouabain to Na^+/K^+-ATPase triggers intracellular signaling networks through protein–protein interactions, generating a myriad of effects independent of the impairment of electrochemical gradients (Riganti et al., 2011). In this case, ouabain (and other cardiotonic steroids) would act as an agonist and not as a Na^+/K^+-ATPase inhibitor (Pierre and Xie, 2006). Actually, the assumption is that the agonist or inhibitor function of ouabain is defined depending on which Na^+/K^+-ATPase population ouabain binds with: in the bulk plasma membrane, Na^+/K^+-ATPase is an ion pump and ouabain acts as an inhibitor; in caveolae, which are small lipid raft invaginations of the plasma membrane that function as a platform for signaling cascades, Na^+/K^+-ATPase interacts with several molecules, such as the structural protein caveolin-1 (Quintas et al., 2010) and the nonreceptor tyrosine kinase Src (Tian et al., 2006), and ouabain induces the activation of intracellular signals. Also, Anita Aperia's group revealed that the N-terminus of the α-subunit of the plasma membrane Na^+/K^+-ATPase and of the endoplasmic reticulum IP3 receptor physically interact with each other and ouabain binding to the former may stimulate repetitive cytoplasmic Ca^{2+} transients independent on IP3 (Zhang et al., 2006). Currently, hundreds of proteins are suggested to be involved in ouabain-induced signaling (Panizza et al., 2019). As expected, this discovery opened new horizons for research on the pharmacological effects of ouabain and other cardiotonic steroids.

Different cell functions such as growth, proliferation, differentiation and membrane excitability are regulated by Ca^{2+} (Clapham, 2007), (Capiod, 2016). Calcium signaling in the CNS is a finely regulated process, as alterations in Ca^{2+} homeostasis can alter activity and induce neuronal death seen in neurodegenerative diseases and aging (Bezprozvanny, 2009), (Kumar et al., 2009). Considering the importance of Na^+/K^+-ATPase in brain physiology, the fact that Ca^{2+} ions are involved downstream of Na^+/K^+-ATPase inhibition (or activation), and that cardiotonic steroids, more specifically ouabain, may be endogenous modulators of the Na^+/K^+-ATPase, we conducted a systematic review of the *in vitro* effect of cardiotonic steroids on cytoplasmic Ca^{2+} in rat and mouse brain, which are the most used experimental animal models. Therefore, favoring the perception of the relationship between ouabain-Na^+/K^+-ATPase and homeostasis Ca^{2+} signaling in the CNS in aging and neurodegeneration.

Materials and methods

This study followed the guidelines described in the Preferred Reporting Items for Systematic Reviews and Meta-Analyses (PRISMA), and the protocol was registered on the PROSPERO platform (Reg, No. CRD42020204498). A systematic review was performed by searching PubMed, Virtual Health Library, and EMBASE databases (between 12 June 2020 and 30 June 2020) using the following search

terms: ("cardiotonic steroids" OR "cardiotonic steroid" OR "cardiac glycosides" OR "cardiac glycoside" OR digitalis OR cardenolides OR cardenolide OR bufadienolides OR bufadienolide OR ouabain OR digoxin OR digitoxin) AND (brain OR "central nervous system") AND (calcium OR Ca^{2+}). The following question guided the selection of articles and the development of this review: "What are the effects of cardiotonic steroids on calcium signaling in the central nervous system of rodents?" This question was structured according to the acronym PECO [P: Population; E: Exposure; C: Comparison; O: Outcome] and the eligibility criteria are described in Supplementary Table S1. First, articles were selected by title and abstract. No date restriction was used, however, only publications in Portuguese, English or Spanish were considered. The type of publication was also analyzed and review articles, case reports and papers presented in scientific events were excluded. Four reviewers, working in pairs, performed independent analysis, and included articles considering eligibility criteria. The third reviewer was consulted if there was no consensus on the decision.

We developed a data extraction sheet considering the following information about the included studies: author, date of publication, populations, species, gender, age, concentration of cardiotonic steroids, experimental conditions, calcium effect, and general conclusion of the articles with respect to cardiotonic steroids use. One reviewer performed data extraction from the articles that were included, and a second reviewer checked the information. Again, a third reviewer was consulted in cases of disagreement.

Quality analysis

Most quality features and measures of risk of bias (RoB) do not apply to or are not determined for biochemical studies of the kind here reviewed, and no standard quality assessment tool exists for *in vitro* studies. We based our study on quality/RoB criteria for *in vitro* studies presented by Prueitt et al. (Prueitt et al., 2020). Questions and criteria were modified to be relevant to the evaluation of studies of calcium homeostasis/signaling. The criteria for *in vitro* studies include eight domains which have been divided into three main domains, related to outcome assessment, exposure characterization and control groups. Five other quality/RoB domains that include an analysis of the number of replicates, blinding, complete data, statistical methods, and experimental conditions were also evaluated. The studies were arranged into three levels of quality based on their classification with respect to the evaluated domains. The studies were grouped into three decreasing levels of quality, according to the eight questions addressed in the RoB analysis and identified in Table 1. Tier 1 includes studies presenting a "probably low" or "definitely low" RoB for all key domains relevant to that study type AND a "probably low" or "definitely low" RoB for most (i.e., at least half) of the other domains; Tier 2 includes studies that do not meet the criteria for Tier 1 or Tier 3. Tier 3 includes studies presenting a "probably high" or "definitely high" RoB for all key domains relevant to that study type AND a "probably high " or "definitely high" RoB for most (i.e., at least half) of the other domains. Eight quality/RoB parameters were analyzed. A study may have low RoB in some parameters, but high in others, which classifies it at an intermediate level, Tiers 2. Studies classified as Tier 3 have low quality and high RoB and those classified as Tier 1 have high quality and reliability (Prueitt et al., 2020). The evaluation of the methodological quality of the studies included in this review was done by only one author.

Results

A total of 829 references were identified from electronic databases. Once duplicate entries (125) had been removed, the references were further evaluated for inclusion based on the title and/or abstract. Potentially 59 relevant articles were included in the next stage for full-text evaluation. Of these, it was not possible to gain access to 6 and 3 studies were excluded since they failed to satisfy the inclusion criteria established by the PECO. Finally, 20 studies were included in the analysis (Figure 2).

The publication period of the 20 eligible studies ranged from 1970 to 2020, and they were published in the English language. Most of the studies were conducted in the United States (n = 10; 50%), followed by Germany and Japan (n = 2; 10% each), Brazil, Canada, Denmark, and Hungary (n = 1; 5% each). Two trials were conducted in more than one country (10%).

Quality criteria for *in vitro* studies were applied to each article. In none of the studies experiments were blinded, and no study reported loss of data. Half of the studies did not include statistical analyses of the results. Some did not examine an adequate number of animals and poorly characterized ouabain exposure. These studies were categorized into Tier 2 or Tier 3.

Of the 20 articles, 5 (25%) were categorized into Tier 1, 13 (65%) were categorized into Tier 2, and 2 (10%) were categorized into Tier 3 based on their quality ratings across domains (Table 1). These results indicate that this systematic review presents an intermediary/low risk of bias.

Although no exclusion criteria were applied for the cardiotonic steroid studied in this systematic review, when the PECO criteria were applied, it was observed that all included studies used ouabain.

They employed different methodological strategies: six studies focused on synaptosomes, eight used brain slices, and six employed cell cultures. It was possible to group the 20 articles included in this study, on the basis of their main characteristics, which are summarized in Tables 2–4. Experimental conditions are described in Supplementary Table S2. All 20 articles are described below.

TABLE 1 Study quality/risk of bias ratings.

Study	Article	Key criteria			Other quality criteria					
		Can we be confident in the exposure characterization?	Can we be confident in the outcome assessment?	Were appropriate control groups assessed concurrently?	Did the study have an adequate number of replicates per study group?	Were experimental conditions identical across study groups?	Were research personnel blinded to test group?	Were outcome data complete?	Did the study employ appropriate statistical approaches?	Tier
Cell	Bassetti et al. (2020)	+	++	+	++	++	NR	NR	+	1
	Friess et al. (2016)	+	++	+	-	++	NR	NR	--	2
	Lomeu et al. (2003)	+	++	++	++	++	NR	NR	+	1
	Xiao et al. (2002)	+	++	++	+	++	NR	NR	+	1
	Stelmashook et al. (1999)	NR	-	+	NR	+	NR	NR	+	2
	Mark et al. (1995)	+	++	++	++	++	NR	NR	NR	1
Slices	Bai et al. (2017)	+	++	+	++	++	NR	NR	+	1
	Dietz et al. (2008)	+	++	+	--	++	NR	NR	+	2
	Basarsky et al. (1998)	NR	++	+	-	++	NR	NR	+	2
	Okamoto et al. (1994)	+	-	+	+	++	NR	NR	-	2
	Myles and Fain (1994)	NR	+	+	+	++	NR	NR	NR	2
	Mork and Geisler (1993)	+	-	+	+	+	NR	NR	NR	2
	Balduini and Costa (1990)	+	-	+	+	+	NR	NR	NR	2
	Pincus et al. (1973)	NR	-	+	+	+	NR	NR	NR	2
Synaptosomes	Satoh and Nakazato (1989)	NR	+	+	--	+	NR	NR	NR	2
	Adam-vizi and Ligeti (1986)	+	+	+	--	+	NR	NR	NR	2
	Lin et al. 1982	NR	NR	NR	NR	NR	NR	NR	NR	3
	Goddard and Robinson (1976)	NR	+	+	+	+	NR	NR	--	2
	Swanson et al. (1974)	NR	-	-	--	-	NR	NR	NR	3
	Blaustein et al. (1970)	NR	-	+	--	+	NR	NR	NR	2

++, definitely low risk of bias; +, probably low risk of bias;—or NR (not reported), probably high risk of bias; —, definitely high risk of bias.

10.3389/fphar.2022.916312

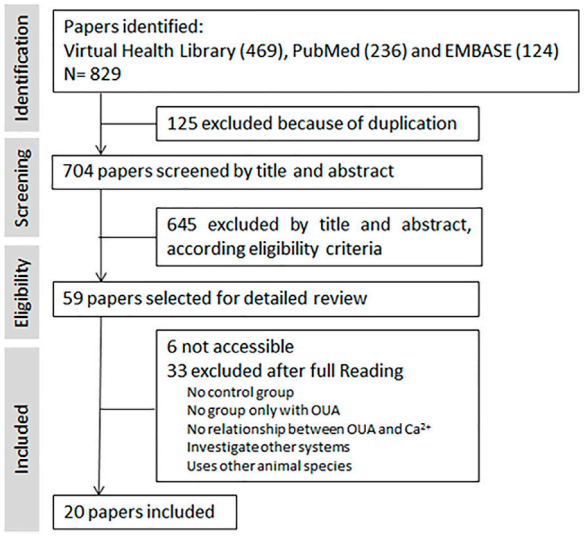

FIGURE 2
Flow diagram of study selection. The search process using the PRISMA flow diagram.

Synaptosome studies

Of six papers—from 1970 to 1982—that used synaptosomes from rodent brain, five directly evaluated Ca^{2+} concentrations (Table 2). One study of the effects of ouabain in Ca^{2+} signaling observed that Ca^{2+}-ATPase activity in intact synaptosomes and in brain subfractions of male ICR (Institute of Cancer Research) mice, was not affected by 1 mm ouabain (Lin and Way, 1982). Except for only one study that reported the use of forebrain, the other articles indicated the nonspecific use of rat brain.

Blaustein and Wiesmann (Blaustein and Wiesmann, 1970) and Swanson et al. (Swanson et al., 1974), observed that Ca^{2+} uptake was enhanced when $1\ M \times 10^{-3}$ M or $1\ M \times 10^{-4}$ M ouabain, respectively, was added to presynaptic synaptosomes, and this effect was directly associated with vesicles' Na^{+} content. Goddard and Robinson (Goddard and Robinson, 1976) noted that $1\ M \times 10^{-4}$ M ouabain augmented Na^{+} uptake as well. The increased uptake of Ca^{2+} induced by ouabain was inhibited by diphenylhydantoin (DPH, well known as phenytoin), tetrodotoxin (TTX), and ruthenium red. Despite being multitarget drugs, the first two agents inhibit voltage-gated Na^{+} channels, and ruthenium red inhibits Ca^{2+} transportation, since it competes for the Ca^{2+} binding site in many proteins (Sasaki et al., 1992). On the other hand, Adam-Vizi and Ligetit, (Adam-Vizi and Ligeti, 1986), when comparing membrane depolarization and Ca^{2+} uptake, did not observe changes in Ca^{2+} uptake in brain cortical synaptosomes using $5\ M \times 10^{-5} - 5\ M \times 10^{-4}$ M ouabain, although membrane potential was significantly affected. Ca^{2+} influx was only detected at higher concentrations (e.g., $1\ M \times 10^{-3}$ M or more).

TABLE 2 Summary of synaptosomes studies.

Article	Population characteristics	[Ouabain]	$[Ca^{2+}]i$ levels, uptake	Major article findings in the domain of ouabain use
Satoh and Nakazato, 1989	• Brain cortex of Sprague-Dawley rats of either sex • 220–350 g	5×10^{-8}-$5x10^{-4}$ M	= $[Ca^{2+}]i$ level (in absence of extracellular Ca^{2+})	Ouabain had no detectable effect on $[Ca^{2+}]i$ in the absence of extracellular Ca^{2+}. However, it induced ACh release from synaptosomes, regardless of the presence or absence of extracellular Ca^{2+}, which release impaired when the protein kinase C (PKC) and ryanodine receptor blocker was coincubated with ouabain
Adam-Vizi and Ligeti (1986)	• Rat brain cortex of CFY rats • 120–150 g • n = 1-3 experiment made in duplicate	5×10^{-5}-$5x10^{-4}$ M	= Ca Uptake and Efflux	Neither Ca^{2+} influx nor Ca^{2+} efflux was changed by ouabain. A slight increase of the uptake was only evoked by ouabain at a high concentration (>1 mM; data not shown)
Goddard and Robinson (1976)	• Rat male brains • 200–300 g • n = 3-6	1×10^{-4} M	↑122.0–185.0% Ca Uptake ↑32.0% $[Ca^{2+}]i$ level ↑32.0% retention	Ouabain leads to an increase in uptake of ^{45}Ca, a high level of total calcium content and effectively prevents ^{45}Ca exit. The increased uptake of ^{45}Ca induced by ouabain was inhibited by voltage-gated sodium channels inhibitor and an inhibitor of intracellular calcium release by ryanodine receptors
Swanson et al. (1974)	• Rat brain • n = 3-4	1×10^{-4} M	↑33.0% Ca Uptake	OUA stimulated Ca uptake by synaptosomes
Blaustein and Wiesmann (1970)	• Rat brain • 200–250 g • n = 3	1×10^{-3} M	↑113.0% Ca Uptake	Calcium influx is increased when the internal sodium concentration is increased by treatment with ouabain

TABLE 3 Summary of brain slices studies.

Article	Population characteristics	[Ouabain]	[Ca^{2+}]i level, transient or uptake	Major article findings in the domain of ouabain use
Bai et al., 2017	• Organotypic brain tissue cultures from somatosensory cortex slices • Sprague-Dawley rats. Postnatal day (P) 1–2	1×10^{-3} M	↑ 250% [Ca^{2+}]i level	The [Ca^{2+}]i increased and reached a maximum around 10 min after the start of ouabain perfusion and then slowly decreased while ouabain was washed out. There was also an increase in cell volume
Dietz et al. (2008)	• Hippocampal slices (350 μm) • Male FVB/N mice 4–6 weeks of age • n = 6	3×10^{-5} M	↑ 2000% [Ca^{2+}]i level	Ouabain produced spreading depression (SD) in hippocampal slices. Before SD the Ca^{2+} signal stays near basal levels. However, after SD, large increase in Ca^{2+} signal was observed
Basarsky et al. (1998)	• Hippocampal or neocortical slices (400 μm) • Sprague-Dawley rats. Postnatal day (P) 15–25 • Dentate gyrus n = 14 Astrocyte n = 4	1×10^{-4} M	↑ 44 % dentate gyrus [Ca^{2+}]i level ↑ 40% astrocytic [Ca^{2+}]i transient	Ouabain induced SD, which started in the CA1 region, propagated across the hippocampal to the dentate gyrus. The Ca^{2+}i signal increased and reached a maximum around 11 and 6 min, for dentate gyrus and astrocyte, respectively, after the start of ouabain perfusion and then decreased
Okamoto et al. (1994)	• Hippocampal slices (350 μm) • Male Wistar rats (100–150 g) • n = 4	1×10^{-5} M	↑ 100% [Ca^{2+}]i levels	Gradual increase in [Ca^{2+}]i, which remained increased for 30 min. Treatment with lithium significantly suppressed the [Ca^{2+}]i increase
Pincus and Lee (1973)	• Temporal lobe slices (200 μm) • Rats • Control n = 4 Experimental n = 6	1×10^{-4} M	↑ 19%^{45}Ca Uptake	Increased$^{45}Ca^{2+}$ uptake and dl-norepinephrine-3H (NE3H) release
Article	**Population characteristics**	**[Ouabain]**	**Ca 2+ signaling proteins**	**Major article findings in the domain of ouabain use**
Balduini and Costa (1990)	• Cerebral córtices slices (350 μm) • Male and female Sprague Dawley rats • n = 3	1×10^{-4} M	↑ 1271% neonatal InsPs	Ouabain induced a dose-dependent accumulation of inositol phosphates (InsPs) which was much higher in neonatal rats than in adult animals
Mørk et al. (1993)	• Cerebral córtices slices (330) μm • Male Wistar rats (180–200 g) • n = 8	1×10^{-4} M	↑ 625,51% cAMP	Ouabain-induced formation of cAMP (dependent on extracellular Ca2+ and blocked by the Ca2+ channel antagonist, verapamil)
Myles and Fain (1994)	• Cerebral córtices slices (350) μm • Male Sprague Dawley rats (125–175 g) • n = 9	1×10^{-4} M	↑ 92,63% IP3	Ouabain elevates IP3 but there is little effect on IP4

Moreover, acetylcholine release was not detected upon ouabain treatment, despite the degree of depolarization being comparable to those of other depolarizing agents that induce neurotransmitter exocytosis. Satoh and Nakazato (Satoh and Nakazato, 1989), showed that ouabain elicited a concentration-dependent (5 M × 10^{-8} −5 M × 10^{-4} M) release of acetylcholine from synaptosomes regardless of the presence or absence of extracellular Ca^{2+}, but such effect was impaired when the protein kinase C (PKC) and ryanodine receptor blocker TMB-8 was coincubated with ouabain, suggesting the importance of intracellular Ca^{2+}.

TABLE 4 Summary of cell culture studies.

Article	Cell characteristics	[Ouabain]	$[Ca^{2+}]i$ level or transient	Major article findings in the domain of ouabain use
Bassetti et al. (2020)	• Primary brain OPCs from C57BL/6N mice	1×10^{-7} M	↑ 23% Ca^{2+} transients' frequency	Increase of $[Ca^{2+}]i$ transient frequency in proximal immature OPC processes
Friess et al. (2016)	• Primary brain oligodendrocyte precursor cells (OPCs) from C57BL/6N mice • Postnatal day (P) 8–9	5×10^{-7} M	↑ 87% $[Ca^{2+}]i$ levels	Significant increase $[Ca^{2+}]i$ in OPCs and stimulated Myelin Basic Protein) synthesis
Lomeo et al. (2003)	• SN56 cells (hybrid of septal neuronal cells from mice with the N18TG2 neuroblastoma) • n > 15	2×10^{-4} M	↑ 250% $[Ca^{2+}]i$ level in the presence and no increase in the absence of $CaCl_2$	Great increase in $[Ca^{2+}]i$ in the SN56 cholinergic cells and this increase was concentrated in the cell soma. The effect was a function of time and the maximum increase of $[Ca^{2+}]i$ in the cells was reached at 20 min. Causes a calcium-independent exocytotic release of ACh that is inhibited by blockers of intracellular calcium stores
Xiao et al. (2002)	• Primary cortical cultures • Fetal mice 15–17 d gestation • n = 13-23 cells	1×10^{-4} M	↑ 124% $[Ca^{2+}]i$ level	The $[Ca^{2+}]i$ level increased continuously, starting at ~ 30 min after exposure, until the maximal rise in ~90 min. This increase was largely blocked by 1M nifedipine and OUA (80 uM) exposure of 20 h induced DNA fragmentation
Stelmashook et al. (1999)	• Primary cerebellar cultures (neuro-glial) from Wistar rats • Postnatal day (P) 7–8 • n = ND	1×10^{-3} M	↑ 936% (20 min) ↑ 2544% (35 min) $[Ca^{2+}]i$ level	The $[Ca^{2+}]i$ level increased continuously, starting at ~10 min after exposure, until the maximal rise in ~35 min. The supplement of a solution with an antagonist of NMDA (1034 M, APH) together with OUA prevented cells from swelling, mitochondrial deenergization, neuronal death and increase of [Ca2+]i
Mark et al. (1995)	• Primary hippocampal cell cultures • Embryonic rats 18 d gestation • n = 9-16 cells	2×10^{-3} M	↑ 169% $[Ca^{2+}]i$ level	Increase in $[Ca^{2+}]i$, which preceded neuronal degeneration

ND, non-determined.

Brain slices studies

Of eight papers—from 1973 to 2017—that used slices from rodent brain, five directly evaluated Ca^{2+} concentrations, and all observed an increase of it (Table 3). Furthermore, three studies evaluated proteins that contribute to the control of Ca^{2+} signaling and homeostasis. These studies, using 1 M × 10^{-4} M ouabain and rat brain cortical slices, demonstrated that ouabain increased IP3 levels but had minimal effects on inositol 1,3,4,5-tetrakisphosphate (IP4) accumulation (Myles and Fain, 1994). Ouabain induced the formation of cAMP, dependently on extracellular Ca^{2+}, and this process was blocked by verapamil, an inhibitor of L-type voltage-gated Ca^{2+}-channels, also known as dihydropyridine receptors, that are responsible for Ca^{2+} entry during the potential action (Mørk et al., 1993). In addition, ouabain induced a concentration-dependent accumulation of inositol phosphates (InsPs), which was much higher in neonatal rat brain than in adult brain. Furthermore, the accumulation of InsPs induced by ouabain was dependent on extracellular Ca^{2+} and was blocked by EGTA (Balduini and Costa, 1990).

A large range of ouabain concentrations, from 1×10^{-5} to 1×10^{-3} M, was demonstrated to increase the $[Ca^{2+}]i$ in different rodent brain slices. Using 1 M × 10^{-5} M ouabain, Okamoto et al. (Okamoto et al., 1995) showed a progressive elevation of $[Ca^{2+}]i$ in hippocampal slices, and this was significantly suppressed with the coadministration of Li^{+}, since lithium appears to antagonize the ouabain Na^{+}/K^{+}-ATPase inhibition, enhancing the extrusion of intracellular Ca^{2+} by Na^{+}/Ca^{2+} exchanger as a consequence. Also, enhanced

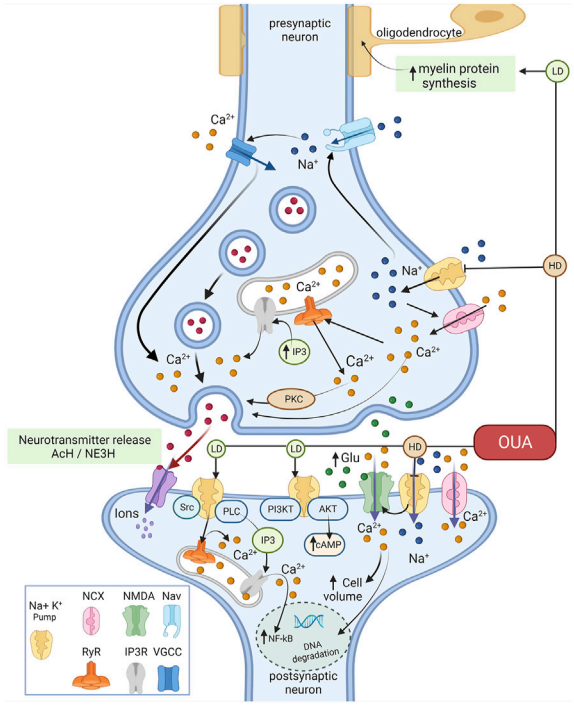

FIGURE 3
Representative schedule of the effects of ouabain on Ca^{2+} signaling. Ouabain in high concentrations selectively binds to Na^+/K^+-ATPase, inhibiting its pump activity, leading to increased intracellular Na^+ and Ca^{2+} concentrations. The latter by inducing a lower/reverse action of the Na^+–Ca^{2+} exchanger (NCX) colocalizes with the Na^+/K^+-ATPase. Ouabain effects on intracellular Ca^{2+} influence the release of acetylcholine (Ach) and norepinephrine (NE3H) and glutamate (Glu). Binding of ouabain to Na^+/K^+-ATPase triggers intracellular signaling networks in the glutamate signaling cascade through protein-protein interactions, generating many effects independent of the impairment of electrochemical gradients. In this case, ouabain (and other cardiotonic steroids) would act as an agonist, stimulating these pathways, acting in a different way observed as Na^+/K^+-ATPase inhibitor. In low concentrations ouabain can stimulate changes in Na^+/K^+-ATPase that triggers signaling complexes such PI3K-AKT pathways, increasing cAMP. Also, ouabain modulates Ca^{2+} intracellular oscillation through activation of ryanodine receptor (RyR) and IP3 receptor (IP3R) that provoke the increasing of NF-κB and activation of PKC. LD- Low Dose and HD- High dose (Figure were created with BioRender.com).

Ca^{2+} uptake was demonstrated using 1 M × 10^{-4} M ouabain, with a subsequent release of norepinephrine (Pincus and Lee, 1973). Ouabain at 1 M × 10^{-3} M increased the [Ca^{2+}]i, reduced transmembrane water flux, and raised the mean neuron and glial cell volume (Bai et al., 2018).

In addition, concentrations of ouabain, 1 M × 10^{-4} M and 3 M × 10^{-5} M, generated *in vitro* spreading depression (SD) in freshly prepared hippocampal and neocortical slices. Interestingly, although ouabain produced a significant elevation of in [Ca^{2+}]i, Ca^{2+} by itself was shown not to be responsible for SD (Basarsky et al., 1998), (Dietz et al., 2008).

Cell culture studies

Of six papers—from 1995 to 2020—that used cell culture from rodent brain, all directly evaluated the Ca^{2+} concentration, and observed an increase of it (Table 4). Of the six articles, five carried out studies focused on primary cell culture. Two studies used cultures of primary brain oligodendrocyte precursor cells (OPCs), one used cortical culture, one cerebellar culture, and one hippocampal cell cultures. Only one article investigated the effects of ouabain on immortalized cells (SN56 cells). The largest increase in the Ca^{2+} level was observed at the highest ouabain concentration (1 M × 10^{-3} M) (Stelmashook et al., 1999), and the smallest increase at the lowest ouabain concentration (1 M × 10^{-4} M) (Bassetti et al., 2020). It is interesting to note that studies from the 1990s used higher concentrations of ouabain in their investigations, whereas more recent studies utilized lower concentrations. In addition to the concentration-dependent increase of the [Ca^{2+}]i induced by ouabain, some articles also observed a time-dependent variation in [Ca^{2+}]i (Stelmashook et al., 1999)- (Xiao et al., 2002).

In primary cerebellar culture, Stelmashook et al. (1999) showed that addition of 1 M × 10^{-3} M ouabain had a toxic effect leading to death 62 ± 3% of the total amount of granule cells against 3 % in control. This effect was abolished when the antagonist of NMDA receptors APH (0.1 mm) was added to the incubation medium together with ouabain. APH also prevented cells from swelling, mitochondrial deenergization, neuronal death. Furthermore, in primary cortical cultures, the neuronal apoptotic and necrotic death associated with Na^+/K^+-ATPase inhibition, caused by the application of 1 M × 10^{-4} M ouabain, was consistent with the intracellular depletion of K^+ and the accumulation of Ca^{2+} and Na^+, In addition, exposure for 20 h to ouabain induced DNA fragmentation (Xiao et al., 2002). In the same way, Mark et al. (1995) using primary hippocampal cell culture using calcium indicator dye Fura-2 showed that 30 min incubation with 2 M × 10^{-3} M ouabain leads to an increase in [Ca^{2+}]i levels and neuronal degeneration. They also demonstrated that the addition of ouabain promotes a decrease in neuron survival in a concentration dependent manner. Moreover, the use of Hoescht dye and ethidium bromide homodimer also revealed nuclear condensation and DNA fragmentation induced by ouabain (Mark et al., 1995).

Using SN56 cells Lomeo at al (2003) showed that ouabain (2 M × 10^{-4} M) had a calcium dependent effect on [Ca^{2+}]i levels, leading to enhanced acetylcholine release. This effect of ouabain on acetylcholine release was dose and time dependent, achieving the maximum value after 30 min and was not inhibited by the addition of 1 μM tetrodotoxin (TTX). However, the effect of ouabain was suppressed with the addition of BAPTA-AM (Lomeo et al., 2003).

Interestingly, studies using cultures of oligodendrocyte precursor cells have shown that a long incubation of oligodendrocyte precursor cells (OPC) cultures with ouabain

(5 M × 10^{-7} M, 24 h) failed to significantly change [Na^+]i levels, but ouabain treatment significantly increased [Ca^{2+}]i and stimulated myelin basic protein synthesis (Friess et al., 2016).

Figure 3 is a schematic summary of the finding of this study.

Discussion

The most studied effects of cardiotonic steroids refer to their action on the cardiovascular system. Here in this systematic review, we demonstrated the effects of ouabain on Ca^{2+} oscillation and signaling in the nervous system of rodents, indicating that the balance between ouabain-induced neuroprotective and neurotoxic effects is concentration-dependent. Furthermore, the action of ouabain is broad, acting not only on neurons but also on glial cells.

Ca^{2+} homeostasis plays a crucial role in the maintenance of different cellular functions. Ca^{2+} has been described as an important second messenger, regulating many different cellular processes, including cell division, proliferation differentiation, apoptosis, necrosis, neurotransmission and synaptic plasticity (Arundine and Tymianski, 2003), (Berridge et al., 2003). The concentration of this free ion in the cytosol is kept about 10,000 times below the extracellular concentration (Nicotera and Orrenius, 1998). This high electrochemical Ca^{2+} gradient between the intra and extracellular compartments enables the transduction of biochemical signals into cells (Berridge et al., 2003).

Regarding neurotransmission modulated by ouabain, Ca^{2+} triggers synaptic vesicle exocytosis, thereby releasing the neurotransmitters contained in the vesicles and initiating synaptic transmission (Katz and Miledi, 1967). Whereas ouabain selectively binds to Na^+/K^+-ATPase and inhibits its ion pump activity, increasing intracellular Na^+ and Ca^{2+} concentrations, the latter by inducing a lower/reverse activity of the Na^+/Ca^{2+} exchanger that colocalizes with the Na^+/K^+-ATPase (Larsen et al., 2016), (Kinoshita et al., 2020), it is expected that it can modulate neurotransmission. Inhibition of the Na^+/K^+-ATPase could lead to depolarization of the neuron, followed by Ca^{2+} influx and transmitter release by exocytosis (Banks, 1967). It could also lead indirectly to a rise in intracellular Ca^{2+}, through mobilization of intracellular Ca^{2+} stores (Baker and Crawford, 1975). The results collected in this study represents the literature. In fact, ouabain is capable of interfering with different neurotransmission systems, such as cholinergic (Satoh and Nakazato, 1989), (v Blasi et al., 1988), noradrenergic (Pincus and Lee, 1973), (Yamazaki et al., 2007) and glutamatergic (Jacobson et al., 1986), (Stelmashook et al., 1999). Moreover, other studies have demonstrated that ouabain also interferes with the release of dopamine in animal models (Sui et al., 1199).

The toxic effect of high concentrations of ouabain has been widely described in the literature, as well as the involvement of high levels of Ca^{2+} influx, promoting neuronal excitotoxicity (Veldhuis et al., 2003). This effect was observed in synaptosomes as well as in brain slices.

Excitotoxicity is a term used to indicate the death of nerve cells by glutamate (Glu) as well as other amino acids, resulting in neurodegenerative diseases (Lewerenz and Maher, 2015), (Olney, 1986), increased release of Glu that occurs under neurological disorders may be a result of metabolic changes and reduced Na^+,K^+-ATPase activity (Shi et al., 2019), (Beal et al., 1993). The findings indicate that NMDA receptors are involved in ouabain effects on [Ca^{2+}]i and cell toxicity. It is known that Na^+/K^+-ATPase inhibition leads to a decrease in Glu uptake in cortical astrocytes cell cultures (Volterra et al., 1994), interfering with GluT transport in astrocytes (Nguyen et al., 2010), favoring the neurotoxic effects of high doses of ouabain. This suggesting that Na^+/K^+-ATPase inhibition by ouabain led to Glu accumulation of extracellular Glu, hyperstimulation of glutamate receptors, and higher Ca^{2+} and Na^+ influxes into the cells through N-methyl-d-aspartate (NMDA) receptors in neuro–glial cell cultures of the cerebellum (Stelmashook et al., 1999). These authors associated the exposure of high ouabain concentrations with a toxic effect on cerebellar and hippocampal cells.

Interestingly, ouabain in nanomolar concentration consistently reduces the Ca^{2+} response to NMDA. Downregulation of the NMDA response is not associated with internalization of the receptor or with alterations in its state of Src phosphorylation (Akkuratov et al., 2020). It has been observed that ouabain activates NF-κB by an NMDA–Src–Ras-like protein through MAPK pathways in cultured cerebellar cells (de Sá Lima et al., 2013). In addition, the intra-hippocampal administration of ouabain in a low concentration that did not alter the activity of Na^+/K^+-ATPase promoted the activation of NF-κB, leading to increased brain-derived neurotrophic factor (BDNF) levels, similar to NMDA treatment, which was reversed by the NMDA antagonist MK-801 (Kawamoto et al., 2012b). Moreover, intrahippocampal injection of ouabain 10 nM activated the Wnt/β-catenin signaling pathway and to increase CREB/BDNF and NFκB levels. These effects contribute to important changes in the cellular microenvironment, resulting in enhanced levels of dendritic branching in hippocampal neurons, in association with an improvement in spatial reference memory and the inhibition of long-term memory extinction (Orellana et al., 2018).

Altered levels of acetylcholine, as well as its receptors, have been observed in neurodegenerative and neuropsychiatric diseases (Tata et al., 2014). In order to obtain a concentration-dependent curve of [^{3}H] acetylcholine release, Satoh and Nakazato (Satoh and Nakazato, 1989) utilized 5 × 10^{-8}-5x10^{-4} M ouabain, possibly inhibiting initially the α_2/α_3 isoforms—which are, in rodents, much more sensitive to cardiotonic steroids—and subsequently the ouabain-resistant α_1 (O'brien et al., 1994), (Lopez et al., 2002). Interestingly Lomeo at al (2003) using SN56 cells showed that ouabain had

a Ca^{2+} dependent effect on $[Ca^{2+}]$i levels, leading to enhanced acetylcholine release. This effect of ouabain on acetylcholine release was dose and time dependent, achieving the maximum value after 30 min. This effect was not inhibited by the addition of 1 μM tetrodotoxin (TTX), discarding the involvement of TTX-sensitive Na^+ channels. However, the effect of ouabain was suppressed with the addition of BAPTA-AM, suggesting the involvement of intracellular calcium stores. The authors suggested that in cholinergic neurons the ouabain induced increase in $[Na^+]_i$ results in intracellular calcium alterations inducing an increase in $[Ca^{2+}]_i$, causing a release of acetylcholine independent of Ca^{2+} (Lomeo et al., 2003). Despite the effect of high doses of ouabain on cholinergic neurotransmission, no studies were found on the role of lower doses of this cardiotonic on the cholinergic system.

Another phenomenon observed on the effect of the micromolar application of ouabain was the Spreading depression (SD), which is a wave of profound depolarization that propagates throughout the brain tissue after traumatic or vascular brain insults (Somjen, 2001). Interestingly, it was observed that the spreading depression is not only caused by the increase of in $[Ca^{2+}]$i, but also the partition of Zn^{2+} and mitochondrial stress, since it was observed that selective chelation of Zn^{2+} with N,N,N,N-tetrakis (2-pyridylmethyl) ethylenediamine (TPEN) eliminated ouabain-SD, implying that Zn^{2+} entry and mitochondrial dysfunction may play a critical role in the Ouabain-induced SD mechanism (Dietz et al., 2008). Thus, this is a useful model for studying the pathways involved in this phenomenon and that can lead to the search for more efficient treatments.

Different studies have demonstrated that neuronal activity promotes an elevation in extracellular $[K^+]$, stimulating an increase in intracellular Ca^{2+}transient in oligodendrocytes, due to the reversion of the Na^+/Ca^{2+} exchanger, which led to increased synthesis of myelin basic protein (MBP) (Belachew et al., 2000), (Chen et al., 2007). Interestingly, using primary brain OPCs cultures, Friess et al. (Friess et al., 2016) showed that incubation with $5\ M \times 10^{-7}$ M ouabain increased the intracellular Ca^{2+} levels and stimulated MBP synthesis, and this effect of ouabain on Ca^{2+} transients was eliminated by the addition to the incubation medium of 1 μMKB-R734 9, a Na^+/Ca^{2+} exchanger inhibitor. In addition, it was observed that the activity of the Na^+/K^+-ATPase α_2 isoform, present in oligodendrocyte lineage cell (OLCs), changed the Na^+/Ca^{2+} exchanger-mediated $[Ca^{2+}]$i, modulating MBP synthesis in OLCs (Hammann et al., 2018). Using the same experimental model of primary OPCs cultures, Basseti et al. (Bassetti et al., 2020) demonstrated that lower concentrations of ouabain ($1\ M \times 10^{-7}$ M) also increased Ca^{2+} transient frequency. Additionally, this work showed that the inhibition of ryanodine receptor type 3 with 10 μM ryanodine also blocked Ca^{2+} transient.

The process of myelination of neuronal axons through oligodendrocyte activity is a process controlled by the release of neurotransmitters and changes in ionic concentrations (Butt and Bay, 2011). Among the important proteins in the myelination process, there is myelin basic protein (MBP), and failures in its production result in CNS hypomyelination processes (Readhead and Hood, 1990), (Wiecien et al., 1998). Interestingly, studies using cultures of oligodendrocyte precursor cells (OPC) have shown that a long incubation (24 h) of these cells with nanomolar concentrations of ouabain failed to significantly change $[Na^+]$i levels, but ouabain treatment significantly increased $[Ca^{2+}]$i and stimulated MPB synthesis (Friess et al., 2016). The same group further suggested that the crosstalk among ryanodine receptors, $Na^+/–Ca^{2+}$ exchangers, and possibly Na^+/K^+-ATPase may evoke Ca^{2+} transients for the development of isolated oligodendrocytes (Bassetti et al., 2020), thus demonstrating the importance of Na^+,K^+-ATPase in the synthesis of axonal myelin by oligodendrocytes.

Interestingly, in addition to the existence of a Na^+/Ca^{2+} exchanger colocalized with Na^+/K^+-ATPase, the discovery of ancillary signaling pathways, involving protein–protein interactions, revealed that the physical association between Na^+/K^+-ATPase and IP3 receptors allows intracellular Ca^{2+} oscillations evoked by ouabain (Fontana et al., 2013), (Miyakawa-Naito et al., 2003). Moreover, Src kinase activation would promote the stimulation of phospholipase C and PKC independently of ion modulation (Mohammadi et al., 2001), (Yuan et al., 2005).

One study in brain slices demonstrated that ouabain caused the stimulation of PtdIns hydrolysis, causing an accumulation of InsPs in the cytoplasm, which may be related to cell signaling modulated by Na^+/K^+-ATPase inhibition, activation of Na^+/Ca^{2+} exchanger, mobilization of Ca^{2+} and PKC (Balduini and Costa, 1990). Interestingly, there was no direct correlation between the stimulus leading to PtdIns hydrolysis and the binding of radioactive ouabain (number of Na^+/K^+-pumps) or strophantidin effect (an equipotent inhibitor), and this may suggest that this outcome is modulated by cell signaling mechanisms besides the classic inhibitory effect. A similar effect was found in the study by Myles et al. (Myles and Fain, 1994), where $1\ M \times 10^{-4}$ M ouabain stimulated an 82% increase in intracellular IP3 levels but had a minimal effect on IP4 accumulation. Moreover, in addition to InsPs, treatment with $1\ M \times 10^{-4}$ M ouabain in brain slices also increased intracellular cAMP (Mørk et al., 1993). Since only few studies utilized slices, it is not possible to say whether accumulation of cytosolic Ca^{2+} found in these studies is an effect modulated only by the regulation of the Na^+/Ca^{2+} exchanger, which is the classic effect of cardiotonic steroids. It is well known that Ca^{2+} mobilization and influx is linked to the activation of cellular signaling pathways, especially those associated with G proteins, with the involvement of cAMP and IP3 (Satoh and Nakazato, 1989), (Liu et al., 2007).

In addition, studies that include the nervous system and others demonstrate that Na^+/K^+-ATPase acts as a receptor and a signal transducer, involving many pathways such as that dependent on the membrane-associated nonreceptor tyrosine kinase Src (Tian et al., 2006) the Ras/Raf/ERK1/2 pathway (Eckert et al., 2008), the phosphate inositol 3-kinase (PI3K) pathway, the PI3K-dependent protein kinase B pathway, phospholipase C signaling, $[Ca^{2+}]i$ oscillations (Liu et al., 2007), (Schoner and Scheiner-Bobis, 2007), (Aperia et al., 2015), and gene transcription (Li et al., 2006). These pathways are also triggered by the interaction of ouabain with Na^+/K^+-ATPase. Na^+/K^+- ATPase inhibition or activation is dependent on ouabain concentration. It has been shown that inhibition of pump activity requires micromolar concentrations of ouabain (Fontana et al., 2013), (Blaustein and Hamlyn, 2020), while activation of Na^+/K^+-ATPase signaling pathways occurs in the presence of nanomolar concentrations of ouabain (Fontana et al., 2013).

As discussed above, several studies using different models have shown that the effects of ouabain at low concentrations are due to the activation of cell signaling pathways. Studies have shown that in renal epithelial cells, as well as in astrocytes, ouabain, at low concentrations, binds with Na^+/K^+-ATPase directly activating the IP3 receptors (physical interaction), and triggering slow Ca^{2+} oscillations and the activation of NF-kB; this ultimately leads to the proliferation of these cells (Liu et al., 2007), (Li et al., 2006), (Aizman et al., 2001). Furthermore, studies in cardiomyocytes have observed that low ouabain concentrations promote $[Ca^{2+}]i$ oscillations due to the activation of Src kinase followed by the stimulation of the Ras/Raf/MEK/MAPK cascade regulating cell hypertrophic growth (Yuan et al., 2005), (Zhu et al., 1996). It is important to note that in such signaling conditions, Ca^{2+} is a key factor, and positive feedback may occur.

The therapeutic range for the use of ouabain and other cardiac steroids is very narrow. Added to this problem of narrow therapeutic index, we have the majority use of this drug by elderly patients, contributing to toxicity problems (Whayne, 12018). This reality caused mistrust and disuse of cardiac steroids in clinical practice. Thus, in addition to expanding knowledge about signaling pathways and neuroprotective effects of low doses of ouabain and other cardiotonic, a strategy for the safe therapeutic use of cardiotonic steroids for neuroprotection would be the chemical modification of their structure to increase the therapeutic index of this class. Gamma-benzylidene digoxin derivatives are digoxin-derived molecules that have demonstrated low toxicity to cells (de Oliveira et al., 2021) and have already demonstrated neuroprotection for chemical ischemia (de Souza Gonçalves et al., 2019) and increased α3 activity and increased antioxidant defenses such as GSH, desired drug characteristics of neuroprotection (Parreira et al., 2021).

Conclusion

Ca^{2+} mobilization is a canonical effect of cardiotonic steroids such as ouabain. In all models studied - synaptosomes, brain slices or cell cultures—an increase in $[Ca^{2+}]i$ was observed. In addition to the well known cytotoxic effects of ouabain, resulting from stimulation of the Na^+/Ca^{2+} exchanger reverse mode and increased Ca^{2+}, other effects have been reported, since Ca^{2+} may play a role in major cellular effects, mainly by activating signaling pathways. Ouabain-induced Ca^{2+} signaling was able to increment cholinergic, noradrenergic and glutamatergic neurotransmission. Treatment with ouabain stimulated MBP synthesis and significantly increased biological second messengers such as InsPs, IP3 and cAMP. This review deepens the knowledge about the effects and signaling mediated by cardiotonic steroids (ouabain) in the nervous system, which has been shown to be concentration dependent. Structural modifications of cardiotonic steroids may be useful for the generation of new agents that are less toxic and with neuroprotective action.

Data availability statement

The raw data supporting the conclusions of this article will be made available by the authors, without undue reservation.

Author contributions

AL, EP, GSM, LB, LEMQ, MLCS, CS, and LEDC. Performed the selection of the studies and the extraction of the data JAL, EP, GSM, MLCS, and LEDC. Performed the quality analysis of the studies LEDC. Write and elaborate the figures and tables of the manuscript: JAL, EP, GSM, LB, LEMQ, MLCS, and LEDC. Reviewed topics and discussed concepts in the manuscript: JAL, EP, GSM, LB, LEMQ, EMK, MLCS, CS, and LEDC.

Funding

ML is supported by a master fellowship from National Council for Scientific and Technological Development (CNPq). CS, EK, LB, and LQ are research fellows of the National Council for Scientific and Technological Development (CNPq). This publication was made possible by grants from São Paulo Research Foundation (FAPESP) to CS (2016/07427-8); CNPq 405089/2018-0; CAPES—STINT program 88887.125409/2016-00 (Joint Brazilian-Swedish Research Collaboration) and USP Neuroscience Research Support Centres (NAPNA) to CS; CNPq Universal #409436/2016-0 and Fundação de Amparo à Pesquisa do Rio de Janeiro (FAPERJ APQ1 # 210.379/2019) to LEMQ. Fundação de Amparo

à Pesquisa do Estado de Minas Gerais (FAPEMIG APQ#01176-16) to LEDC and UFSJ support.

Acknowledgments

We thank BioRender.com and Larissa de Sá Lima for technical support. The authors also thank MSc. Pedro Azalim Neto for building the rat Na^+/K^+-ATPase protein structure.

Conflict of interest

The authors declare that the research was conducted in the absence of any commercial or financial relationships that could be construed as a potential conflict of interest.

Publisher's note

All claims expressed in this article are solely those of the authors and do not necessarily represent those of their affiliated organizations, or those of the publisher, the editors and the reviewers. Any product that may be evaluated in this article, or claim that may be made by its manufacturer, is not guaranteed or endorsed by the publisher.

Supplementary material

The Supplementary Material for this article can be found online at: https://www.frontiersin.org/articles/10.3389/fphar.2022.916312/full#supplementary-material

References

Adam-Vizi, V., and Ligeti, E. (1986). Calcium uptake of rat brain synaptosomes as a function of membrane potential under different depolarizing conditions. *J. Physiol.* 372 (1), 363–377. doi:10.1113/jphysiol.1986.sp016013

Aizman, O., Uhlén, P., Lal, M., Brismar, H., and Aperia, A. (2001). Ouabain, a steroid hormone that signals with slow calcium oscillations. *Proc. Natl. Acad. Sci. U. S. A.* 98 (23), 13420–13424. doi:10.1073/pnas.221315298

Akera, T., and Brody, T. M. (1977). The role of Na+, K+-ATPase in the inotropic action of digitalis. *Pharmacol. Rev.* 29 (3), 187–220.

Akkuratov, E. E., Westin, L., Vazquez-Juarez, E., de Marothy, M., Melnikova, A. K., Blom, H., et al. (40302020). Ouabain modulates the functional interaction between Na, K-ATPase and NMDA receptor. *Mol. Neurobiol.* 57 (10), 4018–4030. doi:10.1007/s12035-020-01984-5

Aperia, A., Akkuratov, E. E., Fontana, J. M., and Brismar, H. (2015). Hugh davson distinguished lectureship of the cell and molecular physiology sectionNa+-k+-ATPase, a new class of plasma membrane receptors. *Am. J. Physiol. Cell Physiol.* 310 (7), C491–C495. doi:10.1152/ajpcell.00359.2015

Arundine, M., and Tymianski, M. (2003). Molecular mechanisms of calcium-dependent neurodegeneration in excitotoxicity. *Cell Calcium* 34 (4–5), 325–337. doi:10.1016/S0143-4160(03)00141-6

Bai, R., Springer, C. S., Plenz, D., and Basser, P. J. (2018). Fast, Na+/K+ pump driven, steady-state transcytolemmal water exchange in neuronal tissue: A study of rat brain cortical cultures. *Magn. Reson. Med.* 79 (6), 3207–3217. doi:10.1002/mrm.26980

Baker, P. F., and Crawford, A. C. (1975). A note of the mechanism by which inhibitors of the sodium pump accelerate spontaneous release of transmitter from motor nerve terminals. *J. Physiol.* 247 (1), 209–226. doi:10.1113/jphysiol.1975.sp010928

Balduini, W., and Costa, L. G. (1990). Characterization of ouabain-induced phosphoinositide hydrolysis in brain slices of the neonatal rat. *Neurochem. Res.* 15 (10), 1023–1029. doi:10.1007/BF00965749

Banks, P. (1967). The effect of ouabain on the secretion of catecholamines and on the intracellular concentration of potassium. *J. Physiol.* 193 (3), 631–637. doi:10.1113/jphysiol.1967.sp008383

Basarsky, T. A., Duffy, S. N., Andrew, R. D., and MacVicar, B. A. (1998). Imaging spreading depression and associated intracellular calcium waves in brain slices. *J. Neurosci.* 18 (18), 7189–7199. doi:10.1523/jneurosci.18-18-07189.1998

Bassetti, D., Hammann, J., Luhmann, H. J., White, R., and Kirischuk, S. (2020). Ryanodine receptor- and sodium-calcium exchanger-mediated spontaneous calcium activity in immature oligodendrocytes in cultures. *Neurosci. Lett.* 732. doi:10.1016/j.neulet.2020.134913

Beal, M. F., Hyman, B. T., and Koroshetz, W. (1993). Do defects in mitochondrial energy metabolism underlie the pathology of neurodegenerative diseases? *Trends Neurosci.* 16 (4), 125–131. doi:10.1016/0166-2236(93)90117-5

Belachew, S., Malgrange, B., Rigo, J. M., Rogister, B., LePrince, P., Hans, G., et al. (2000). Glycine triggers an intracellular calcium influx in oligodendrocyte progenitor cells which is mediated by the activation of both the ionotropic glycine receptor and Na+-dependent transporters. *Eur. J. Neurosci.* 12 (6), 1924–1930. doi:10.1046/j.1460-9568.2000.00085.x

Berridge, M. J., Bootman, M. D., and Roderick, H. L. (2003). Calcium signalling: Dynamics, homeostasis and remodelling. *Nat. Rev. Mol. Cell Biol.* 4 (7), 517–529. doi:10.1038/nrm1155

Bezprozvanny, I. (2009). Calcium signaling and neurodegenerative diseases. *Trends Mol. Med.* 15 (3), 89–100. doi:10.1016/j.molmed.2009.01.001

Blanco, G., and Mercer, R. W. (1998). *Isozymes of the Na-K-ATPase: Heterogeneity in structure, diversity in function*. The American Physiological Society, 245–247. doi:10.1177/153857449803200307

Blanco, G. (2005). Na, K-ATPase subunit heterogeneity as a mechanism for tissue-specific ion regulation. *Semin. Nephrol.* 25 (5), 292–303. doi:10.1016/j.semnephrol.2005.03.004

Blaustein, M. P., and Hamlyn, J. M. (2020). Ouabain, endogenous ouabain and ouabain-like factors: The Na+ pump/ouabain receptor, its linkage to NCX, and its myriad functions. *Cell Calcium* 86, 102159. doi:10.1016/j.ceca.2020.102159

Blaustein, M. P., Juhaszova, M., Golovina, V. A., Church, P. J., and Stanley, E. F. (2002). Na/Ca exchanger and PMCA localization in neurons and astrocytes: Functional implications. *Ann. N. Y. Acad. Sci.* 976, 356–366. doi:10.1111/j.1749-6632.2002.tb04762.x

Blaustein, M. P., and Wiesmann, W. P. (1970). Effect of sodium ions on calcium movements in isolated synaptic terminals. *Proc. Natl. Acad. Sci. U. S. A.* 66 (3), 664–671. doi:10.1073/pnas.66.3.664

Brini, M., Calì, T., Ottolini, D., and Carafoli, E. (2014). Neuronal calcium signaling: Function and dysfunction. *Cell. Mol. Life Sci.* 71 (15), 2787–2814. doi:10.1007/s00018-013-1550-7

Butt, A. M., and Bay, V. (2011). Axon-glial interactions in the central nervous system. *J. Anat.* 219 (1), 1. doi:10.1111/j.1469-7580.2011.01401.x

Capiod, T. (2016). Extracellular calcium has multiple targets to control cell proliferation. *Adv. Exp. Med. Biol.* 898, 133–156. doi:10.1007/978-3-319-26974-0_7

Carvalho, D. C. M., Cavalcante-Silva, L. H. A., Lima, E. d. A., Galvao, J. G. F. M., Alves, A. K. d. A., Feijo, P. R. O., et al. (2019). Marinobufagenin inhibits neutrophil migration and proinflammatory cytokines. *J. Immunol. Res.* 2019, 1094520. doi:10.1155/2019/1094520

Cereijido, M., Contreras, R. G., Shoshani, L., and Larre, I. (2012). The Na +-K +-ATPase as self-adhesion molecule and hormone receptor. *Am. J. Physiol. Cell Physiol.* 302 (3), C473–C481. doi:10.1152/ajpcell.00083.2011

Chen, H., Kintner, D. B., Jones, M., Matsuda, T., Baba, A., Kiedrowski, L., et al. (2007). AMPA-mediated excitotoxicity in oligodendrocytes: Role for Na +-K+-Cl-co-transport and reversal of Na +/Ca2+ exchanger. *J. Neurochem.* 102 (6), 1783–1795. doi:10.1111/j.1471-4159.2007.04638.x

Clapham, D. E. (2007). Calcium signaling. *Cell* 131 (6), 1047–1058. doi:10.1016/j.cell.2007.11.028

Clausen, M. v., Hilbers, F., and Poulsen, H. (2017). The structure and function of the Na, K-ATPase isoforms in health and disease. *Front. Physiol.* 8 (JUN), 371–416. doi:10.3389/fphys.2017.00371

de Oliveira, G. C., Rocha, S. C., da Silva Lopes, M. A., Paixão, N., Alves, S. L. G., Pessoa, M. T. C., et al. (2021). Implications of synthetic modifications of the cardiotonic steroid lactone ring on cytotoxicity. *J. Membr. Biol.* 254 (5–6), 487–497. doi:10.1007/s00232-021-00186-x

de Sá Lima, L., Kawamoto, E. M., Munhoz, C. D., Kinoshita, P. F., Orellana, A. M., Curi, R., et al. (2013). Ouabain activates NFκB through an NMDA signaling pathway in cultured cerebellar cells. *Neuropharmacology* 73, 327–336. doi:10.1016/j.neuropharm.2013.06.006

de Souza Gonçalves, B., de Moura Valadares, J. M., Alves, S. L. G., Silva, S. C., Rangel, L. P., Cortes, V. F., et al. (2019). Evaluation of neuroprotective activity of digoxin and semisynthetic derivatives against partial chemical ischemia. *J. Cell. Biochem.* 120 (10), 17108–17122. doi:10.1002/jcb.28971

Dietz, R. M., Weiss, J. H., and Shuttleworth, C. W. (2008). Zn2+ influx is critical for some forms of spreading depression in brain slices. *J. Neurosci.* 28 (32), 8014–8024. doi:10.1523/JNEUROSCI.0765-08.2008

Dobretsov, M., and Stimers, J. R. (2005). Neuronal function and alpha3 isoform of the Na/K-ATPase. *Front. Biosci.* 10 (1–3), 2373–2396. doi:10.2741/1704

Eckert, A., Tagscherer, K. E., Haas, T. L., Grund, K., Sykora, J., et al. (2008). The PEA-15/PED protein protects glioblastoma cells from glucose deprivation-induced apoptosis via the ERK/MAP kinase pathway. *Oncogene* 27 (8), 1155–1166. doi:10.1038/sj.onc.1210732

Fedorova, O. v., and Bagrov, A. Y. (1997). Inhibition of Na/K ATPase from rat aorta by two Na/K pump inhibitors, ouabain and marinobufagenin: Evidence of interaction with different α- subunit isoforms. *Am. J. Hypertens.* 10 (8), 929–935. doi:10.1016/S0895-7061(97)00096-4

Fedorova, O. v., Kolodkin, N. I., Agalakova, N. I., Lakatta, E. G., and Bagrov, A. Y. (2001). Marinobufagenin, an endogenous alpha-1 sodium pump ligand, in hypertensive Dahl salt-sensitive rats. *Hypertension* 37 (2 II), 462–466. doi:10.1161/01.hyp.37.2.462

Fontana, J. M., Burlaka, I., Khodus, G., Brismar, H., and Aperia, A. (2013). Calcium oscillations triggered by cardiotonic steroids. *FEBS J.* 280 (21), 5450–5455. doi:10.1111/febs.12448

Friess, M., Hammann, J., Unichenko, P., Luhmann, H. J., White, R., and Kirischuk, S. (2016). Intracellular ion signaling influences myelin basic protein synthesis in oligodendrocyte precursor cells. *Cell Calcium* 60 (5), 322–330. doi:10.1016/j.ceca.2016.06.009

Geering, K. (2008). Functional roles of Na, K-ATPase subunits. *Curr. Opin. Nephrol. Hypertens.* 17 (5), 526–532. doi:10.1097/MNH.0b013e3283036cbf

Goddard, G. A., and Robinson, J. D. (1976). Uptake and release of calcium by rat brain synaptosomes. *Brain Res.* 110 (2), 331–350. doi:10.1016/0006-8993(76)90406-6

Godinho, A. N., Costa, G. T., Oliveira, N. O., Cardi, B. A., Uchoa, D. E. A., Silveira, E. R., et al. (2017). Effects of cardiotonic steroids on isolated perfused kidney and NHE3 activity in renal proximal tubules. *Biochim. Biophys. Acta. Gen. Subj.* 1861 (8), 1943–1950. doi:10.1016/j.bbagen.2017.05.012

Hammann, J., Bassetti, D., White, R., Luhmann, H. J., and Kirischuk, S. (2018). α2 isoform of Na + , K + -ATPase via Na + , Ca 2+ exchanger modulates myelin basic protein synthesis in oligodendrocyte lineage cells *in vitro*. *Cell Calcium* 73, 1–10. doi:10.1016/j.ceca.2018.03.003

Jacobson, I., Hagberg, H., Sandberg, M., and Hamberger, A. (1986). Ouabain-induced changes in extracellular aspartate, glutamate and GABA levels in the rabbit olfactory bulb *in vivo*. *Neurosci. Lett.* 64 (2), 211–215. doi:10.1016/0304-3940(86)90102-3

Katz, B., and Miledi, R. (1967). Ionic requirements of synaptic transmitter release. *Nature* 215 (5101), 651. doi:10.1038/215651a0

Kawamoto, E. M., Lima, L. S., Munhoz, C. D., Yshii, L. M., Kinoshita, P. F., Amara, F. G., et al. (2012). Influence of N-methyl-D-aspartate receptors on ouabain activation of nuclear factor-κB in the rat hippocampus. *J. Neurosci. Res.* 90 (1), 213–228. doi:10.1002/jnr.22745

Kawamoto, S., Tran, T. H., Maruya, M., Suzuki, K., Doi, Y., Tsutsui, Y., et al. (2012). The inhibitory receptor PD-1 regulates IgA selection and bacterial composition in the gut. *Science* 821, 485–489. doi:10.1126/science.1217718

Kinoshita, P. F., Orellana, A. M. M., Nakao, V. W., de Souza Port's, N. M., Quintas, L. E. M., Kawamoto, E. M., et al. (2020). The Janus face of ouabain in Na+/K+-ATPase and calcium signalling in neurons. *Br. J. Pharmacol.* 179, 1512–1524. doi:10.1111/bph.15419

Koh, C. H., Wu, J., Chung, Y. Y., Liu, Z., Zhang, R. R., Chong, K., et al. (2017). Identification of Na+/K+-ATPase inhibition-independent proarrhythmic ionic mechanisms of cardiac glycosides. *Sci. Rep.* 7 (1), 2465. doi:10.1038/s41598-017-02496-4

Kumar, A., Bodhinathan, K., and Foster, T. C. (2009). Susceptibility to calcium dysregulation during brain aging. *Front. Aging Neurosci.* 1 (NOV), 2–13. doi:10.3389/neuro.24.002.2009

Kupicha, F. K. (1982). Studies on african apocynaceae: The genus Acokanthera. *Kew Bull.* 37 (1), 41. doi:10.2307/4114719

Larsen, B. R., Stoica, A., and MacAulay, N. (2016). Managing brain extracellular K+ during neuronal activity: The physiological role of the Na+/K+-ATPase subunit isoforms. *Front. Physiol.* 7 (APR), 141–210. doi:10.3389/fphys.2016.00141

Lees, G. J., Lehmann, A., Sandberg, M., and Hamberger, A. (1990). The neurotoxicity of ouabain, a sodium-potassium ATPase inhibitor, in the rat hippocampus. *Neurosci. Lett.* 120 (2), 159–162. doi:10.1016/0304-3940(90)90027-7

Lewerenz, J., and Maher, P. (2015). Chronic glutamate toxicity in neurodegenerative diseases-What is the evidence? *Front. Neurosci.* 9 (DEC), 469–520. doi:10.3389/fnins.2015.00469

Li, J., Zelenin, S., Aperia, A., and Aizman, O. (2006). Low doses of ouabain protect from serum deprivation-triggered apoptosis and stimulate kidney cell proliferation via activation of NF-kappaB. *J. Am. Soc. Nephrol.* 17 (7), 1848–1857. doi:10.1681/ASN.2005080894

Lin, S. C., and Way, E. L. (1982). Calcium-activated ATPases in presynaptic nerve endings. *J. Neurochem.* 39 (6), 1641–1651. doi:10.1111/j.1471-4159.1982.tb07998.x

Lingrel, J. B. (2009). The physiological significance of the cardiotonic steroid/ouabain-binding site of the Na, K-ATPase. *Annu. Rev. Physiol.* 72, 395–412. doi:10.1146/annurev-physiol-021909-135725

Liu, X. L., Miyakawa, A., Aperia, A., and Krieger, P. (2007). Na, K-ATPase generates calcium oscillations in hippocampal astrocytes. *NeuroReport* 18 (6), 597–600. doi:10.1097/WNR.0b013e3280b07bc9

Lomeo, R. S., Gomez, R. S., Prado, M. A. M., Romano-Silva, M. A., Massensini, A. R., and Gomez, M. v. (2003). Exocytotic release of [3H]-Acetylcholine by ouabain involves intracellular Ca2+ stores in rat brain cortical slices. *Cell. Mol. Neurobiol.* 23 (6), 917–927. doi:10.1023/B:CEMN.0000005320.06215.80

Lopez, L. B., Eduardo Quintas, L. M., and Noel, F. U. (2002). Influence of development on Na(+)/K(+)-ATPase expression: Isoform- and tissue-dependency. *Comp. Biochem. Physiol. A Mol. Integr. Physiol.* 131 (2), 323–333. doi:10.1016/s1095-6433(01)00482-2

Mark, R. J., Hensley, K., Butterfield, D. A., and Mattson, M. P. (1995). Amyloid β-peptide impairs ion-motive ATPase activities: Evidence for a role in loss of neuronal Ca2+ homeostasis and cell death. *J. Neurosci.* 15 (9), 6239–6249. doi:10.1523/jneurosci.15-09-06239.1995

McGarry, S. J., and Williams, A. J. (1993). Digoxin activates sarcoplasmic reticulum Ca2+-release channels: A possible role in cardiac inotropy. *Br. J. Pharmacol.* 108 (4), 1043–1050. doi:10.1111/j.1476-5381.1993.tb13503.x

Miyakawa-Naito, A., Uhlen, P., Lal, M., Aizman, O., Mikoshiba, K., Brismar, H., et al. (2003). Cell signaling microdomain with Na, K-ATPase and inositol 1, 4, 5-trisphosphate receptor generates calcium oscillations. *J. Biol. Chem.* 278 (50), 50355–50361. doi:10.1074/jbc.M305378200

Mohammadi, K., Kometiani, P., Xie, Z., and Askari, A. (2001). Role of protein kinase C in the signal pathways that link Na +/K+-ATPase to ERK1/2. *J. Biol. Chem.* 276 (45), 42050–42056. doi:10.1074/jbc.M107892200

Mørk, A., Geisler, A., and Mork, A. (1993). Effects of minocycline on accumulation of cyclic AMP in cerebral cortex of rat. A comparison with lithium. *Neuropharmacology* 32 (8), 793–798. doi:10.1016/0028-3908(93)90188-9

Myles, M. E., and Fain, J. N. (1994). Carbachol, but not norepinephrine, NMDA, ionomycin, ouabain, or phorbol myristate acetate, increases inositol 1, 3, 4, 5-tetrakisphosphate accumulation in rat brain cortical slices. *J. Neurochem.* 62 (6), 2333–2339. doi:10.1046/j.1471-4159.1994.62062333.x

Nguyen, K. T., Buljan, V., Else, P. L., Pow, D. V., and Balcar, V. J. (2010). Cardiac glycosides ouabain and digoxin interfere with the regulation of glutamate transporter GLAST in astrocytes cultured from neonatal rat brain. *Neurochem. Res.* 35 (12), 2062–2069. doi:10.1007/s11064-010-0274-4

Nicotera, P., and Orrenius, S. (1998). The role of calcium in apoptosis. *Biometals.* 11 (4), 375–382. doi:10.1023/A:1009226316146

O'brien, W. J., Lingrel, J. B., and Wallick, E. T. (1994). Ouabain binding kinetics of the rat alpha two and alpha three isoforms of the sodium-potassium adenosine triphosphate. *Arch. Biochem. Biophys.* 310 (1), 32–39. doi:10.1006/abbi.1994.1136

Okamoto, Y., Kagaya, A., Motohashi, N., and Yamawaki, S. (1995). Inhibitory effects of lithium ion on intracellular Ca2+ mobilization in the rat hippocampal slices. *Neurochem. Int.* 26 (3), 233–238. doi:10.1016/0197-0186(94)00130-M

Olney, J. W. (1986). Inciting excitotoxic cytocide among central neurons. *Adv. Exp. Med. Biol.* 203, 631–645. doi:10.1007/978-1-4684-7971-3_48

Orellana, A. M., Leite, J. A., Kinoshita, P. F., Vasconcelos, A. R., Andreotti, D. Z., de Sa Lima, L., et al. (2018). Ouabain increases neuronal branching in hippocampus and improves spatial memory. *Neuropharmacology* 140, 260–274. doi:10.1016/j.neuropharm.2018.08.008

Ouabain (1932). Ouabain. *Nat. Publ. Group* 129, 88. doi:10.1038/129088e0

Panizza, E., Zhang, L., Fontana, J. M., Hamada, K., Svensson, D., Akkuratov, E. E., et al. (2019). Ouabain-regulated phosphoproteome reveals molecular mechanisms for Na+, K+-ATPase control of cell adhesion, proliferation, and survival. *FASEB J.* 33 (9), 10193–10206. doi:10.1096/fj.201900445R

Parreira, G. M., Faria, J. A., Marques, S. M. S., Garcia, I. J. P., Silva, I. F., De Carvalho, L. E. D., et al. (2021). The γ-benzylidene digoxin derivative BD-15 increases the α3-Na, K-ATPase activity in rat Hippocampus and prefrontal cortex and no change on heart. *J. Membr. Biol.* 254 (2), 189–199. doi:10.1007/s00232-021-00173-2

Pierre, S. v., and Xie, Z. (2006). The Na, K-ATPase receptor complex: Its organization and membership. *Cell biochem. Biophys.* 46 (3), 303–316. doi:10.1385/CBB:46:3:303

Pincus, J. H., and Lee, S. (1973). Diphenylhydantoin and calcium. Relation to norepinephrine release from brain slices. *Arch. Neurol.* 29 (4), 239–244. doi:10.1001/archneur.1973.00490280051007

Prueitt, R. L., Li, W., Chang, Y. C., Boffetta, P., and Goodman, J. E. (2020). Systematic review of the potential respiratory carcinogenicity of metallic nickel in humans. *Crit. Rev. Toxicol.* 50 (7), 605–639. doi:10.1080/10408444.2020.1803792

Quintas, L. E. M., Pierre, S. v., Liu, L., Bai, Y., Liu, X., and Xie, Z. J. (2010). Alterations of Na+/K+-ATPase function in caveolin-1 knockout cardiac fibroblasts. *J. Mol. Cell. Cardiol.* 49 (3), 525–531. doi:10.1016/j.yjmcc.2010.04.015

Readhead, C., and Hood, L. (1990). The dysmyelinating mouse mutations shiverer (shi) and myelin deficient (shimld). *Behav. Genet.* 20 (2), 213–234. doi:10.1007/BF01067791

Riganti, C., Campia, I., Kopecka, J., Gazzano, E., Doublier, S., Aldieri, E., et al. (2011). Pleiotropic effects of cardioactive glycosides. *Curr. Med. Chem.* 18 (6), 872–885. doi:10.2174/092986711794927685

Sasaki, T., Naka, M., Nakamura, F., and Tanaka, T. (1992). Ruthenium red inhibits the binding of calcium to calmodulin required for enzyme activation. *J. Biol. Chem.* 267 (30), 21518–21523. doi:10.1016/s0021-9258(19)36640-2

Satoh, E., and Nakazato, Y. (1989). [3H]acetylcholine release and the change in cytosolic free calcium level induced by high K+ and ouabain in rat brain synaptosomes. *Neurosci. Lett.* 107 (1–3), 284–288. doi:10.1016/0304-3940(89)90832-X

Schatzmamn, H. J. (1953). Cardiac glycosides as inhibitors of active potassium and sodium transport by erythrocyte membrane. *Helv. Physiol. Pharmacol. Acta* 11 (4), 346–354. doi:10.1038/cddis.2013.140

Schoner, W., and Scheiner-Bobis, G. (2007). Endogenous and exogenous cardiac glycosides: Their roles in hypertension, salt metabolism, and cell growth. *Am. J. Physiol. Cell Physiol.* 293 (2), C509–C536. doi:10.1152/ajpcell.00098.2007

Shi, M., Cao, L., Cao, X., Zhu, M., Zhang, X., Wu, Z., et al. (2019). DR-region of Na +/K + ATPase is a target to treat excitotoxicity and stroke. *Cell Death Dis.* 10 (1), 6. doi:10.1038/s41419-018-1230-5

Somjen, G. G. (2001). Mechanisms of spreading depression and hypoxic spreading depression-like depolarization. *Physiol. Rev.* 81 (3), 1065–1096. doi:10.1152/physrev.2001.81.3.1065

Stelmashook, E. v., Weih, M., Zorov, D., Victorov, I., Dirnagl, U., and Isaev, N. (1999). Short-term block of Na+/K+-ATPase in neuro-glial cell cultures of cerebellum induces glutamate dependent damage of granule cells. *FEBS Lett.* 456 (1), 41–44. doi:10.1016/S0014-5793(99)00922-9

Sui, L., Song, X. J., Ren, J., Ju, L. H., and Wang, Y. (11992013). Intracerebroventricular administration of ouabain alters synaptic plasticity and dopamine release in rat medial prefrontal cortex. *J. Neural Transm.* 120 (8), 1191–1199. doi:10.1007/s00702-013-0973-5

Swanson, P. D., Anderson, L., and Stahl, W. L. (1974). Uptake of calcium ions by synaptosomes from rat brain. *Biochim. Biophys. Acta* 356 (2), 174–183. doi:10.1016/0005-2736(74)90281-8

Tata, A., Velluto, L., D'Angelo, C., and Reale, M. (2014). Cholinergic system dysfunction and neurodegenerative diseases: Cause or effect? *CNS Neurol. Disord. Drug Targets* 13 (7), 1294–1303. doi:10.2174/18715273136661409171211 32

Tian, J., Cai, T., Yuan, Z., Wang, H., Liu, L., Haas, M., et al. (2006). Binding of Src to Na +/K + -ATPase forms a functional signaling complex. *Mol. Biol. Cell* 17 (1), 317–326. doi:10.1091/mbc.e05-08-0735

v Blasi, J. M., Cefia, V., Gonzfilez-Garcia, C., Marsal, J., and Solsona, C. (1988). Ouabain induces acetylcholine release from pure cholinergic synaptosomes independently of extracellular calcium concentration. *Neurochem. Res.* 13 (11), 1035–1041. doi:10.1007/BF00973147

Valadares, J. M. de M., Bajaj, S. O., Li, H., Wang, H. L., Silva, S. C., Garcia, I. J. P., et al. (2021). Cytotoxic effect of carbohydrate derivatives of digitoxigenin involves modulation of plasma membrane Ca2+-ATPase. *J. Cell. Biochem.* 122 (12), 1903–1914. doi:10.1002/jcb.30150

Veldhuis, W. B., van der Stelt, M., Delmas, F., Gillet, B., Veldink, G. A., Vliegenthart, J. F., et al. (2003). *In vivo* excitotoxicity induced by ouabain, a Na+/K+-ATPase inhibitor. *J. Cereb. Blood Flow. Metab.* 23 (1), 62–74. doi:10.1097/01.WCB.0000039287.37737.50

Volterra, A., Trotti, D., Tromba, C., Floridi, S., and Racagni, G. (1994). Glutamate uptake inhibition by oxygen free radicals in rat cortical astrocytes. *J. Neurosci.* 14 (1), 2924–2932. doi:10.1523/JNEUROSCI.14-05-02924.1994

Whayne, T. F. (0120). "Clinical use of digitalis: A state of the art review," in *American journal of cardiovascular drugs* (Springer International Publishing), 18, 427–440. doi:10.1007/s40256-018-0292-1

Wiecien, D. K. J. M., O'connor, O'connor, L. T., Goetz, B. D., Delaney, K. H., and Duncan, I. D. (1998). Morphological and morphometric studies of the dysmyelinating mutant, the Long Evans shaker rat. *J. Neurocytol.* 27 (8), 581–591. doi:10.1023/a:1006922227791

Xiao, A. Y., Wei, L., Xia, S., Rothman, S., and Yu, S. P. (2002). Ionic mechanism of ouabain-induced concurrent apoptosis and necrosis in individual cultured cortical neurons. *J. Neurosci.* 22 (4), 1350–1362. doi:10.1523/jneurosci.22-04-01350.2002

Xie, Z., and Askari, A. (2002). Na+/K+-ATPase as a signal transducer. *Eur. J. Biochem.* 269 (10), 2434–2439. doi:10.1046/j.1432-1033.2002.02910.x

Yamazaki, T., Akiyama, T., Kitagawa, H., KomakiF., Mori, H., Kawada, T., et al. (2007). Characterization of ouabain-induced noradrenaline and acetylcholine release from *in situ* cardiac autonomic nerve endings. *Acta Physiol.* 191 (4), 275–284. doi:10.1111/j.1748-1716.2007.01749.x

Yuan, Z., Cai, T., Tian, J., v Ivanov, A., Giovannucci, D. R., and Xie, Z. (2005). Na/K-ATPase tethers phospholipase C and IP3 receptor into a calcium-regulatory complex. *Mol. Biol. Cell* 16, 4034–4045. doi:10.1091/mbc.e05-04-0295

Zhang, S., Malmersjö, S., Li, J., Ando, H., Aizman, O., Uhlén, P., et al. (2006). Distinct role of the N-terminal tail of the Na, K-ATPase catalytic subunit as a signal transducer. *J. Biol. Chem.* 281 (31), 21954–21962. doi:10.1074/jbc.M601578200

Zhu, Z., Tepel, M., Neusser, M., and Zidek, W. (1996). Low concentrations of ouabain increase cytosolic free calcium concentration in rat vascular smooth muscle cells. *Clin. Sci.* 90 (1), 9–12. doi:10.1042/cs0900009

Ziff, O. J., and Kotecha, D. (2016). Digoxin: The good and the bad. *Trends cardiovasc. Med.* 26 (7), 585–595. doi:10.1016/j.tcm.2016.03.011

frontiers | Frontiers in Pharmacology

TYPE Original Research
PUBLISHED 30 August 2022
DOI 10.3389/fphar.2022.927419

OPEN ACCESS

EDITED BY
Riham Salah El Dine,
Cairo University, Egypt

REVIEWED BY
Fabiola Paciello,
Catholic University of the Sacred Heart, Italy
Ming Fang,
Guangdong Academy of Medical Sciences, China

*CORRESPONDENCE
Jinqiang Zhang,
552450374@qq.com
Tao Zhou,
taozhou88@163.com

SPECIALTY SECTION
This article was submitted to Neuropharmacology, a section of the journal Frontiers in Pharmacology

RECEIVED 24 April 2022
ACCEPTED 09 August 2022
PUBLISHED 30 August 2022

CITATION
Liu Q, Zhang J, Xiao C, Su D, Li L, Yang C, Zhao Z, Jiang W, You Z and Zhou T (2022), Akebia saponin D protects hippocampal neurogenesis from microglia-mediated inflammation and ameliorates depressive-like behaviors and cognitive impairment in mice through the PI3K-Akt pathway. *Front. Pharmacol.* 13:927419. doi: 10.3389/fphar.2022.927419

Akebia saponin D protects hippocampal neurogenesis from microglia-mediated inflammation and ameliorates depressive-like behaviors and cognitive impairment in mice through the PI3K-Akt pathway

Qin Liu[1], Jinqiang Zhang[1]*, Chenghong Xiao[1], Dapeng Su[1], Liangyuan Li[1], Changgui Yang[1], Zhihuang Zhao[1], Weike Jiang[1], Zili You[2] and Tao Zhou[1]*

[1]Resource Institute for Chinese & Ethnic Materia Medica, Guizhou University of Traditional Chinese Medicine, Guiyang, China, [2]School of Life Science and Technology, University of Electronic Science and Technology of China, Chengdu, China

Given the ability of akebia saponin D (ASD) to protect various types of stem cells, in the present study, we hypothesized that ASD could promote the proliferation, differentiation, and survival of neural stem/precursor cells (NSPCs), even in a microglia-mediated inflammatory environment, thereby mitigating inflammation-related neuropsychopathology. We established a mouse model of chronic neuroinflammation by exposing animals to low-dose lipopolysaccharide (LPS, 0.25 mg/kg/d) for 14 days. The results showed that chronic exposure to LPS strikingly reduced hippocampal levels of PI3K and pAkt and neurogenesis in mice. In the presen of a microglia-mediated inflammatory niche, the PI3K-Akt signaling in cultured NSPCs was inhibited, promoting their apoptosis and differentiation into astrocytes, while decreasing neurogenesis. Conversely, ASD strongly increased the levels of PI3K and pAkt and stimulated NSPC proliferation, survival and neuronal differentiation in the microglia-mediated inflammatory niche *in vitro* and *in vivo*. ASD also restored the synaptic function of hippocampal neurons and ameliorated depressive- and anxiety-like behaviors and cognitive impairment in mice chronically exposed to LPS. The results from network pharmacology analysis showed that the PI3K-AKT pathway is one of the targets of ASD to against major depressive disorder

Abbreviations: AD, Alzheimer's disease; ASD, Akebia saponin D; BDNF, brain-derived neurotrophic factor; BrdU, 5′-bromo-2′deoxyuridine; DAPI, 4′,6-diamidino-2-phenylindole; DCX, doublecortin; DG, dentate gyrus; GCL, granular cell layer; GFAP, glial fibrillary acidic protein; Iba1, ionized calcium binding adapter molecule 1; MAP2, Microtubule-associated protein 2; MDD, major depressive disorder; NeuN, neuron-specific nucleoprotein; NSPC, neural stem/progenitor cell; PBS, phosphate-buffered saline; PI3K/AKT, phosphatidylinositol 3 kinase/serine-threonine kinase; LPS, lipopolysaccharide; SGZ, subgranular zone.

(MDD), anxiety and Alzheimer's disease (AD). And the results from molecular docking based on computer modeling showed that ASD is bound to the interaction interface of the PI3K and AKT. The PI3K-Akt inhibitor LY294002 blocked the therapeutic effects of ASD *in vitro* and *in vivo*. These results suggested that ASD protects NSPCs from the microglia-mediated inflammatory niche, promoting their proliferation, survival and neuronal differentiation, as well as ameliorating depressive- and anxiety-like behaviors and cognitive impairment by activating the PI3K-AKT pathway. Our work suggests the potential of ASD for treating Alzheimer's disease, depression and other cognitive disorders involving impaired neurogenesis by microglia-mediated inflammation.

KEYWORDS

neuroinflammation, akebia saponin D, cognitive impairment, depression, neurogenesis, microglia, neural stem/precursor cell, PI3K-Akt signaling pathway

Highlights

1) ASD protects NSPCs from the microglia-mediated inflammatory niche and stimulates NSPC proliferation and neuronal differentiation.
2) The PI3K-Akt pathway helps mediate the neuroprotective effects of ASD.
3) ASD shows preclinical potential for treatment of disorders involving impaired neurogenesis

1 Introduction

Hippocampal neurogenesis plays an important role in structural plasticity and network maintenance in adults (Cope & Gould, 2019; Gage, 2021). Perturbation of adult neurogenesis contributes to several human diseases, including depression, anxiety, cognitive impairment and neurodegenerative diseases (Snyder et al., 2011; Anacker & Hen, 2017; Zhang J. et al., 2021; Terreros-Roncal et al., 2021). During aging, hippocampal neurogenesis declines, reducing stress resistance and increasing the risk of mood disorders and progression of cognitive impairment (Deng et al., 2010; Snyder et al., 2011; Mehdipour et al., 2021). For example, as mice age, the rate at which new granular cells form in the subgranular zone (SGZ) decreases around 40-fold (Morgenstern et al., 2008).

Neurogenesis in the adult brain can mitigate the effects of aging and neurodegeneration involving amyloid-β (Cameron & Glover, 2015; Bonafina et al., 2019). This implies that promoting neurogenesis in the adult hippocampus may be an effective treatment against Alzheimer's disease and major depressive disorder (Berger et al., 2020).

Adult hippocampal neurogenesis is supported by the proliferation and differentiation of neural stem/precursor cells (NSPCs), which can differentiate into neurons, oligodendrocytes, and astrocytes, thereby counteracting the loss of neurons during aging (Bhattarai et al., 2016; Hattiangady et al., 2020). Such neurogenesis occurs mainly in the SGZ of the dentate gyrus (DG) and in the subventricular zone (SVZ) adjacent to the lateral ventricles (Drew et al., 2013; Jurkowski et al., 2020). Therefore, targeting the proliferation, differentiation, and survival of NSPCs in these zones may alleviate Alzheimer's disease and major depressive disorder.

A challenge to maintaining NSPC proliferation and differentiation is the microglia-mediated neuroinflammatory niche (Sato, 2015). As innate immune cells, microglia can be activated by amyloid-β, cell debris, myelin, and other harmful substances, which enhance their phagocytic activity and thereby maintain brain homeostasis (Pap et al., 2021). However, microglia appear to be hyperactivated in patients and animal models of Alzheimer's disease and major depressive disorder (Qiao et al., 2021). Microglia-mediated inflammation inhibits neurogenesis in the hippocampus of such patients (Santos et al., 2016; Hanslik & Ulland, 2020; Perea et al., 2020) by inhibiting NSPC proliferation and differentiation (Araki et al., 2021).

Researchers have found that akebia saponin D (ASD), a triterpenoid saponin extracted from Dipsacus asper Wall, a traditional Chinese medicine, induces the proliferation and differentiation of various types of stem cells as well as angiogenesis under inflammatory conditions (Ding et al., 2019; Gu et al., 2020; Niu et al., 2021; Chen et al., 2022). Several studies have shown that ASD can cross the blood-brain barrier to improve AD pathology and Aβ-induced cognitive deficits, as well as inflammation-induced depression (Yu et al., 2012; Wang et al., 2018; Zhang et al., 2020c; Stepnik, 2021). However, the molecular mechanisms by which ASD exerts these effects remain elusive. Based on the protective and promoting effects of ASD on the function of various stem cells, we wondered whether ASD might promote NSPC proliferation and differentiation, even in a microglia-mediated inflammatory environment. This led us to wonder whether ASD might exert its neurotherapeutic effects by robustly stimulating NPSCs in the hippocampus.

Therefore we evaluated the effects of ASD on hippocampal neurogenesis and behavior in a mouse model of chronic neuroinflammation. We also evaluated the effects of ASD on NSPC proliferation, differentiation, and survival in a microglia-mediated inflammatory niche *in vitro*. Our studies provide a mechanistic rationale for deepening the exploration of ASD as a promising treatment against Alzheimer's disease, depression and other cognitive disorders involving impaired neurogenesis.

2 Material and methods

2.1 Network pharmacology analysis

To screen the pathways which ASD targets for major depressive disorder (MDD), anxiety and Alzheimer's disease (AD), the network pharmacology analysis was performed based on previous studies (Zhang et al., 2021). In brief, potential MDD-, anxiety- and AD-related targets were retrieved from the Human Gene Database (GeneCards, https://www.genecards. org/) and the DisGeNET Database (https://www.disgenet.org/home/). Targets of ASD were obtained from the TCMSP and SwissTargetPrediction databases (http://www.Swisstargetprediction.ch). Then, the targets were standardized in the UniProt (https://www.uniprot.org) database with status set as 'reviewed' and species set as 'human'. After removing duplicates, a database of ASD and their targets was constructed. Screened targets of the ASD and potential MDD-, anxiety- and AD-related targets were imported into a Venn diagram webtool (http://bioinformatics.psb.ugent.be/webtools/Venn/) for analysis, and common targets were extracted for further Kyoto Encyclopedia of Genes and Genomes (KEGG) pathway enrichment analysis using R software, a free software environment for statistical computing and graphics. The KEGG pathway analyses were screened for $p < 0.05$. The top 20 items of KEGG analysis identified from R software were mapped as bubble plots.

2.2 Molecular docking

The Surflex-Dock module of Sybyl-X2.1 software (Tripos Associates Inc., S.H.R.; St. Louis, MO 631444, USA) was used for molecular docking to predict the binding mode of ASD with the Pi3k and AKT based on previous studies (Yu et al., 2022).

2.3 Animals

Male C57BL/6J mice (7–8 weeks old) were purchased from Changsha Tianqin Biotechnology (Changsha, China) and caged individually. The mice were habituated to their new environment for 1 week. The mice were then habituated to a 1% sucrose solution for 48 h. Sucrose preference was tested before the experiment began, defined as day 0, and this preference as well as the animal body weight served as the baseline. The mice were then divided into seven groups as described in sections 2.4. All experiments were approved by the Institutional Animal Care and Use Committee of the Guizhou University of Traditional Chinese Medicine.

2.4 Pharmacological treatments *in vivo*

ASD (99.92% pure) was purchased from Chengdu Alfa Biotechnology (Chengdu, China). Lipopolysaccharide (LPS; Sigma-Aldrich, MO, USA) or ASD was dissolved in 0.9% saline at a concentration of 4 mg/ml. Minocycline hydrochloride (MedChemExpress, WeVoice, USA) or LY294002 (MedChemExpress) was dissolved to a concentration of 2.5 g/ml in 0.9% saline containing 5% dimethyl sulfoxide (DMSO). Mice were habituated to 1% sucrose solution for 1 week, then allocated into seven groups such that baseline sucrose preference and body weight did not differ significantly across the groups. The seven groups were as follows: control + vehicle (Ctrl), 0.25 mg/kg/d LPS + vehicle (LPS), LPS +10 mg/kg/d ASD [LPS + ASD (10 mg)], LPS +50 mg/kg/d ASD [LPS + ASD (50 mg)], LPS +100 mg/kg/d ASD [LPS + ASD (100 mg)], LPS +50 mg/kg/d minocycline hydrochloride (LPS + Mino), and LPS +100 mg/kg/d ASD +6 μg LY294002 (LPS + ASD + LY294002).

Mice were intraperitoneally administered vehicle, ASD, minocycline hydrochloride or LY294002 once daily (at 10: 00 h). The animals were also intraperitoneally administered saline or LPS once daily (at 16:00 h) for 14 days. The doses of ASD, LPS, minocycline and LY294002 were chosen based on previous studies (Guo et al., 2019; Zhang et al., 2020c; Bassett et al., 2021; Silva et al., 2021).

2.5 Behavioral testing

2.5.1 Sucrose preference test (SPT)

The SPT was performed as described (Zhang J. et al., 2021). Briefly, mice were individually housed, deprived of food and water for 12 h, and then given access to 1% sucrose solution (A) and water (B) for 2 h. The bottle positions were switched daily to avoid a side bias. The sucrose preference was calculated each week for each mouse using the formula: 100 × [VolA/(VolA + VolB)]. The sucrose consumption was normalized to body weight for each mouse.

2.5.2 Forced swimming test (FST)

The FST was performed as described (Zhang J. et al., 2021). Briefly, at 24 h before the test, each mouse was individually placed in a glass cylinder (height: 25 cm, diameter: 15 cm)

filled with 26 °C water to a depth of 15 cm for 15 min. The next day, the mice were placed once again in the same situation for 6 min. The entire process was recorded with a high-definition camera. An observer blinded to animal group recorded the time spent immobile during the last 4 min.

2.5.3 Elevated plus maze test (EPMT)

The elevated plus maze contained two open arms (35 × 5 cm) and two closed arms (35 × 5 cm), connected by a central area (5 × 5 cm). The apparatus was lifted 50 cm above the floor. Tests were carried out in a quiet, dimly lit environment. The apparatus was wiped clean with 75% ethanol between tests. Mice were introduced to the maze at 1 h after the end of open field test. Mice were gently placed in the central area such that they faced one of the open arms. Spontaneous activity was monitored during 5 min. The number of entries into open arms as well as the total time spent in open arms were determined using EMP100 software (Taimeng Tech, Chengdu, China).

2.5.4 Novel object recognition test (NORT)

The novel object recognition test was performed as described (Zhang et al., 2021). Mice were individually placed for 5 min in a Plexiglass arena measuring 40 × 60 cm with walls 30 cm high, and exploration was quantified using OFT100 video tracking software (Taimeng Tech, Chengdu, China). Subsequently, mice were subjected to three habituation sessions in which two objects identical in shape, color, and odor were introduced into the arena for 3 min at a 2-min interval between trials. Before the last session, one of the objects was replaced with a novel object. The time spent exploring each object was scored during each session.

2.5.5 Morris water maze (MWM)

Spatial learning and memory were assessed in a Morris water maze. Experiments were carried out in a blue circular pool (diameter, 150 cm; height, 60 cm) filled to a depth of 30 cm with water rendered opaque by addition of 500 g milk powder and 30 ml blue food coloring. The area of the pool was divided into four virtual quadrants (NW, SW, SE, NE).

The experimental protocol consisted of four training days and an additional probe trial day. On training days, a platform was placed in the center of the SW quadrant, and the mice had to learn the location of the hidden platform with the help of visual cues placed around the maze. All animals had to perform four trials per training day. In each trial, the mice were placed into different quadrants (varied in a clockwise direction) and allowed to search for the hidden platform for 2 min. During the trials, the escape latency (time until the platform was found), the swimming path length to the platform and the swimming speed of the animals were measured and analyzed using Ethovision XT10 software (Noldus, Wageningen, Netherlands). If the platform was not found during the trial, rats were put on the platform for 10 s, and the escape latency was recorded as 2 min. The performance of the animals on the first training day was used to evaluate their short-term memory performance.

2.6 Primary culture of microglia and treatments

Primary microglia were isolated from brains of neonatal C57BL/6J mice (P0–P3) as described (Zhang et al., 2020b). After removing the meninges and blood vessels, brains were minced and centrifuged at 800 g for 5 min. The pellet was dissociated in 0.0125% trypsin (Gibco, CA, USA) for 10 min. The suspension was passed through a 70-μm cell strainer (Koch Membrane Systems, KS, USA). Cell pellets were harvested, washed, and cultured at 37°C in DMED–F12 medium containing 10% fetal bovine serum (FBS; Gibco). This procedure gave rise to mixed cultures in which microglia grew loosely atop a layer of tightly adhering astrocytes. Microglia were harvested by mechanical shaking, then transferred to new culture dishes. The purity of microglia was verified using immunofluorescence based on labeling with anti-Iba1 antibodies to identify microglia and with DAPI to identify nuclei. Cultures in which >98% of cells were Iba1+ were used in subsequent experiments.

2.7 Culture of adult NSPCs

Adult NSPCs were obtained from the subventricular zone of eight-week-old male C57BL/6J mice. The entire subventricular zone was dissected, and the lateral wall of the lateral ventricles was carefully removed from the surrounding brain tissue and collected in phosphate-buffered saline (PBS; BOSTER, Wuhan, China). These tissues were chopped into 1-mm cubes and digested in 0.125% trypsin (Gibco) for 5 min, then the digestion was stopped with soybean trypsin inhibitor. Cells were resuspended in complete DMEM/F12 medium (Gibco) containing 20 ng/ml recombinant murine fibroblast growth factor (FGF; PeproTech, NJ, USA), 20 ng/ml recombinant murine epidermal growth factor (EGF; PeproTech), 1% N-2 supplement (Gibco), and 2% B-27 supplement (Gibco). After culture for 7 days, neurospheres were isolated by centrifugation (600 g for 3 min), enzymatically dissociated into a single-cell suspension using 0.125% pancreatin (Sigma-Aldrich), and plated at a density of 5 × 104 cells/cm2 in proliferation medium. To permit serial cell passaging, this pancreatin dissociation process was repeated every 3–4 days.

2.8 Culture of NSPCs with conditioned medium from LPS-treated microglia

Microglia were plated at a density of 5 × 105 cells/cm2 and treated with either LPS or PBS for 24 h, washed twice with PBS,

then cultured in DMEM-F12 + GlutaMax medium (Gibco) for another 24 h. The microglial medium was collected and used as conditioned medium to stimulate NSPC differentiation and proliferation. NSPCs were cultured in conditioned media from microglia treated with LPS (LPS-M-CM) or PBS (PBS-M-CM). These NSPCs were treated with 0, 10, 50 or 100 μM ASD, 50 ng/ml recombinant mouse brain-derived neurotrophic factor (BDNF; AmyJet, Wuhan, China) or 5 μM LY294002 (MedChemExpress). NSPC proliferation, differentiation, and survival were evaluated by immunofluorescence staining as described in sections 2.12.

2.9 Analysis of NSPC proliferation *in vitro* and *in vivo*

NSPCs were cultured in proliferation medium (97% DMEM/F12 + 20 ng/ml FGF +20 ng/ml EGF +1% N-2 supplement +2% B-27 supplement) and treated with different concentrations of ASD (10, 50, or 100 μM) or 50 ng/ml BDNF in the presence of PBS-M-CM or LPS-M-CM. The number and size of neurospheres were assessed after 4 days of culture.

To examine NSPC proliferation in the brain, mice received intraperitoneal injections of 5′-bromo-2′deoxyuridine (BrdU; Sigma-Aldrich) at a daily dose of 50 mg/kg for 3 days. Mice were euthanized at 24 h after the last injection, and proliferating cells in the hippocampus were labeled with anti-BrdU antibody as described below. The number of BrdU + cells was quantified.

2.10 Analysis of NSPC differentiation *in vitro* and *in vivo*

NSPCs were cultured in differentiation medium (93% DMEM/F12 + 1% N-2 supplement +2% B-27 supplement +5% FBS) and treated with different concentrations of ASD (10, 50, or 100 μM) or 50 ng/ml BDNF in the presence of PBS-M-CM or LPS-M-CM. After 5 days in culture, the rates of NSPC differentiation into neurons or astrocytes were determined by quantifying the percentages of DCX + or GFAP + or NG2+ cells as described in section 2.12.

To examine NSPC differentiation in the brain, mice received intraperitoneal injections of BrdU at a daily dose of 50 mg/kg for 3 days. Mice were euthanized at 7 days after the last injection. Using immunocytochemistry of hippocampal sections as described below, we identified neurons that differentiated from progenitor cells based on double labeling with anti-BrdU and anti-DCX antibodies, and we identified astrocytes that differentiated from progenitor cells based on double labeling with anti-BrdU and anti-GFAP antibodies. Differentiation of hippocampal NSPCs was assessed by quantifying the number and percentage of BrdU + -DCX + cells or BrdU + -GFAP + cells.

2.11 Analysis of NSPC survival and newborn neuron maturation *in vitro* and *in vivo*

NSPCs were cultured in proliferation medium for 24 h, then treated with BrdU for another 12 h. The culture medium was replaced with PBS-M-CM or LPS-M-C, to which were added different concentrations of ASD (10, 50, or 100 μM) or 50 ng/ml BDNF. After 7 days in differentiation culture, the rate of NSPC survival was determined by quantifying the percentage of BrdU + cells as described below.

To evaluate NSPC survival and newborn neuron maturation in the brain, mice received intraperitoneal injections of BrdU at a daily dose of 50 mg/kg for 3 days, after which animals were administered LPS, ASD, minocycline or LY294002 as described in sections 2.4. Mice were euthanized at 14 days after the last injection. The rate of NSPC survival was determined by quantifying the number of BrdU + cells as described below. Mature neurons derived from progenitor cells were identified based on double labeling with anti-BrdU and anti-NeuN antibodies.

2.12 Immunocytochemistry

Brain tissue was prepared and stained as described (Zhang et al., 2020b). Differentiated NSPCs were plated at a density of 105 cells/cm2 and fixed with 4% paraformaldehyde (pH 7.2) for 30 min. Hippocampal tissue or primary cells in culture were permeabilized with 0.5% Triton X-100 in PBS for 15 min, blocked in 10% donkey serum for 2 h, then incubated overnight at 4 °C with the following primary antibodies: goat anti-Iba1 (1:400, Abcam, Cambridge, United Kingdom), goat anti-Doublecortin (DCX; 1:400, Santa Cruz Biotechnology, CA, USA), mouse anti-BrdU (1:400, Cell Signaling Technology, MA, USA), and rabbit anti-GFAP (1:400, Cell Signaling Technology).

Tissue or cells were then incubated for 2 h at room temperature with DyLight 549-conjugated donkey anti-goat or DyLight 488-conjugated donkey anti-mouse secondary antibodies (both 1:300, Jackson ImmunoResearch, PA, USA). Finally, cells were incubated with DAPI (1:10,000, Roche, Basel, Switzerland) for 5 min and imaged using a fluorescence microscope (IX73, Olympus, Tokyo, Japan). Cell numbers were quantified using GraphPad Prism 5.0 (version 8.0, SPSS Inc., Chicago, USA).

2.13 Enzyme-linked immunosorbent assay (ELISA)

The dentate gyrus was dissociated from slices containing the hippocampus, flash-frozen in liquid nitrogen, and homogenized.

Samples were centrifuged at 1,000 g for 30 min. The concentration of total protein was determined using the BCA kit (BOSTER, Wuhan, China). After each sample was diluted to 1 g/ml, supernatants were assayed for interleukin (IL)-1β using an ELISA kit (BOSTER) according to the manufacturer's protocols, and IL-1β concentration per g of total protein was calculated. The manufacturer-specified detection limit was 4 pg/ml.

2.14 Western blotting

Western blotting was used to assess levels of phosphatidylinositol 3 kinase/serine-threonine kinase (PI3K/Akt) signaling in hippocampus and in NSPCs. Mice were perfused with PBS, hippocampi were isolated and homogenized. Hippocampi or primary cultures of NSPCs were sonicated in RIPA buffer containing protease and phosphorylase kinase inhibitors (Solarbio, Beijing, China). Protein lysate was centrifuged at 1,000 g for 30 min, then the supernatant was fractionated on 12% Tris-glycine SDS-PAGE gels, transferred to PVDF membranes (0.2 or 0.45 μm), and incubated with antibodies against PI3K (1:600, Cell Signaling Technology), AKT (1:400, Abcam), or phospho-AKT (pAKT; 1:600, Abcam). Membranes were incubated with the primary antibody overnight at 4 °C, washed with PBS (BOSTER), then incubated with secondary antibodies (1:10,000, Abcam) for 2 h at room temperature. Fluorescence was developed using the ECL-Plus kit (Millipore, MA, USA) and quantified using ImageJ software (version 1.45J; National Institutes of Health, Bethesda, MD, USA).

2.15 Statistical analysis

GraphPad Prism software (version 6.0; GraphPad Software, Chicago, USA) was used for all statistical analyses. Data were presented as the mean ± standard error of the mean (SEM). Pairwise comparisons were assessed for significance using Student's two-tailed *t* test, and comparisons of three or more values were assessed using one- or two-way ANOVA and Tukey's multiple-comparisons test. Differences were considered statistically significant if $p < 0.05$.

3 Results

3.1 ASD protects NSPCs from the microglia-mediated inflammatory niche, promoting their proliferation, survival and neuronal differentiation *in vitro* by activating the PI3K-Akt pathway

To confirm that ASD directly regulates NSPCs, we examined the effects of ASD on NSPC proliferation, survival and neuronal differentiation *in vitro*. To simulate the microglia-mediated inflammatory niche, primary cells or neurospheres were cultured in conditioned medium from primary microglial cultures (Figure 1A). Like BDNF, 100 μM ASD increased the diameter of neurospheres in PBS-M-CM. LPS-M-CM decreased the diameter of the neurospheres, which ASD reversed at concentrations of 50 or 100 μM, but not 10 μM (Figure 1B).

To confirm that ASD promotes NSPC differentiation, NSPCs were allowed to differentiate for 7 days in differentiation medium in the presence or absence of ASD. Then, we analyzed the percentages of cells that were developmentally committed to becoming neurons (DCX + cells) or astrocytes (GFAP + cells). LPS-M-CM reduced the neuronal differentiation of NSPCs, while either BDNF or ASD (50 or 100 μM) promoted it in the presence or absence of LPS-M-CM (Figure 1C).

To confirm that ASD promotes NSPC survival, we used BrdU to label proliferating NSPCs, then these cells were allowed to differentiate for 7 days in differentiation medium. Exposing NSPCs to LPS-M-CM decreased the percentage of BrdU + cells, which 50 or 100 μM ASD partially reversed (Figure 1D).

Next, we confirmed in this *in vitro* system that the PI3K-Akt pathway mediates the effects of ASD on NSPC proliferation, survival and neuronal differentiation. Conditioned medium from microglia treated only with LPS reduced levels of PI3K, Akt, and pAkt in primary cultures of NSPCs, while ASD (100 μM) strongly increased those levels in the presence or absence of LPS-M-CM (Figure 2A). In addition, the PI3K-Akt pathway inhibitor LY294002 blocked the effects of ASD on NSPC proliferation and neuronal differentiation in the presence or absence of LPS-M-CM (Figures 2B–D).

These results suggest that ASD protects NSPCs from the microglia-mediated inflammatory niche and promotes their proliferation and neurogenesis by activating the PI3K-Akt pathway.

3.2 ASD protects hippocampal neurogenesis from the chronic LPS-induced inflammatory niche *in vivo* by activating the PI3K-Akt pathway

Given the neuroprotective effects of ASD, we evaluated its effects on hippocampal neurogenesis and behavior in a mouse model of chronic neuroinflammation, induced by chronic exposure to LPS (Figure 3A). Given the role of PI3K-Akt signaling in regulation of stem cell function and improvement of cognitive deficits (Yu et al., 2012; Ke et al., 2016), we first examined the effects of ASD on PI3K-Akt signaling in the hippocampus. We found that chronic LPS exposure caused a striking reduction in the levels of PI3K and pAkt in hippocampus, which ASD reversed in a dose-dependent manner (Figures 3B,C).

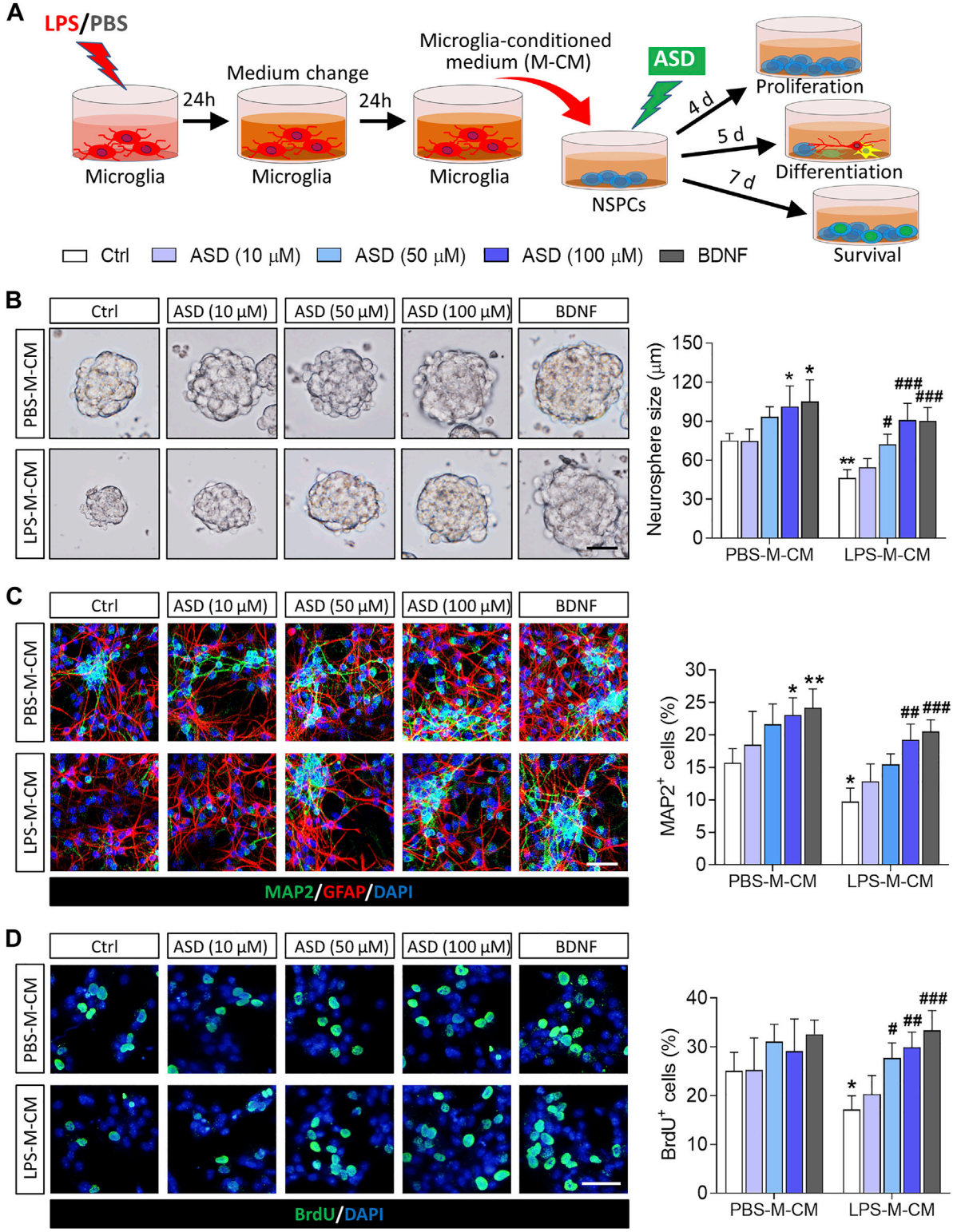

FIGURE 1
Effects of ASD on NSPC proliferation, survival and neuronal differentiation in the presence or absence of a microglia-mediated inflammatory niche. **(A)**, Scheme describing the experimental evaluation of the effects of akebia saponin D (ASD) on survival of neurospheres in the presence or absence of an inflammatory niche. Microglia were treated with phosphate-buffered saline (PBS) or lipopolysaccharide (LPS) for 24 h, and the microglia-conditioned medium (M-CM) was collected. Neural stem/precursor cells (NSPCs) were treated with different concentrations of ASD

(*Continued*)

FIGURE 1
(0, 10, 50, or 100 μM) in the presence of PBS-M-CM or LPS-M-CM. Brain-derived neurotrophic factor (BDNF) at 50 ng/ml was used as control. NSPC proliferation was measured after 4 days in culture; differentiation, after 5 days; and survival, after 7 days. **(B)**, Micrographs and quantification of neurosphere size under different treatment conditions. Scale bar, 100 μm. **(C)**, Micrographs and quantification of pleiotropic NSPC differentiation under different treatment conditions. Astrocytes were labeled with antibody against GFAP (green); neurons, with antibody against microtubule-associated protein 2 (MAP2) (red). Scale bar, 50 μm. **(D)**, Micrographs and quantification of NSPC survival under different treatment conditions. Surviving NSPCs were labeled with BrdU (green). Scale bar, 20 μm. Results for each group were averaged from 5 micrographs (40×) from each of 4-6 slides. Data are mean ± standard error of the mean (SEM). $*p < 0.05$, $**p < 0.01$ vs. control microglia conditioned medium (PBS-M-CM), $\#p < 0.05$, $\#\#p < 0.01$, $\#\#\#p < 0.001$ vs. LPS-treated microglia conditioned medium (LPS-M-CM) by two-way ANOVA with Tukey's multiple-comparisons test.

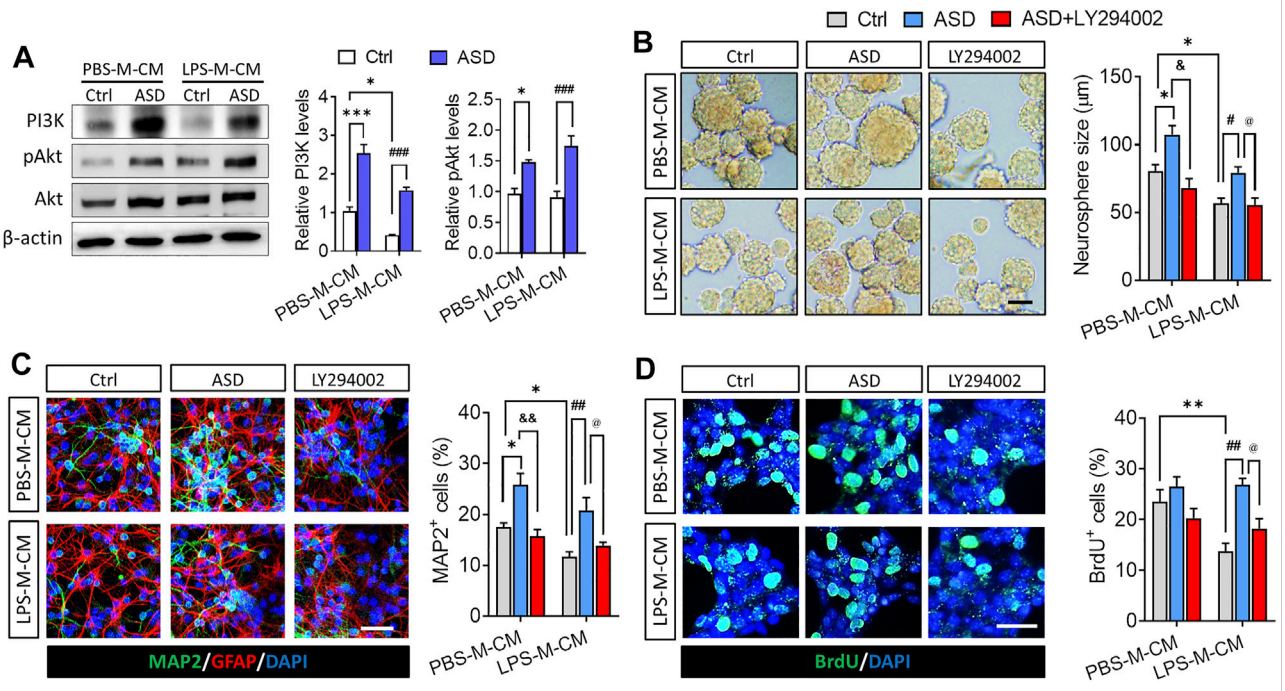

FIGURE 2
ASD protects NSPCs from the microglia-mediated inflammatory niche by activating the PI3K-AKT pathway. **(A)**, Western blotting showing activation of the PI3K-AKT pathway in NSPCs after ASD treatment (100 μM) in the presence of PBS-M-CM or LPS-M-CM. Levels of PI3K and AKT were normalized to those of β-actin, and levels of phospho-AKT (p-AKT) were normalized to those of AKT. Ctrl, control without ASD. **(B)**, Micrographs and quantification of neurosphere size, showing that the PI3K-AKT pathway inhibitor LY294002 blocked the effects of ASD on neurosphere proliferation in the presence of PBS-M-CM or LPS-M-CM. Scale bar, 100 μm. **(C)**, Micrographs and quantification of the percentage of MAP2+ cells, showing that LY294002 also blocked the effects of ASD on neurogenesis in the presence of PBS-M-CM or LPS-M-CM. Astrocytes were labeled with antibody against GFAP (green); neurons, with antibody against MAP2 (red). Scale bar, 50 μm. **(D)**, Micrographs and quantification of the percentage of BrdU + cells, showing that LY294002 blocked the effects of ASD on NSPC survival in the presence of LPS-M-CM. Surviving NSPCs were labeled with BrdU (green). Scale bar, 20 μm. Results for each group were averaged from 5 micrographs (40×) from each of 4-6 slides. Data are mean ± standard error of the mean (SEM), $*p < 0.05$, $**p < 0.01$, $***p < 0.001$ vs. control microglia conditioned medium (PBS-M-CM), $\#p < 0.05$, $\#\#p < 0.01$, $\#\#\#p < 0.001$ vs. LPS-treated microglia conditioned medium (LPS-M-CM), $\&p < 0.05$, $\&\&p < 0.01$ vs. ASD + PBS-treated microglia conditioned medium (ASD + PBS-M-CM), $@p < 0.05$ vs. ASD + LPS-treated microglia conditioned medium (ASD + LPS-M-CM) by two-way ANOVA with Tukey's multiple-comparisons test.

LPS-induced microglial hyperactivation should supress neurogenesis (Littlefield et al., 2015; Bassett et al., 2021), which we confirmed by showing that LPS strongly reduced the numbers of BrdU + cells (proliferating cells) (Figures 4A,B), BrdU + -DCX + cells (newborn neurons) (Figures 4C–E) and BrdU + -NeuN + cells (mature neurons) (Figures 5A–D) in hippocampus, while increasing the number of GFAP + -BrdU + cells in the SGZ of the hippocampus (Figures 4F–H). Like minocycline, ASD at 100 mg/kg/d for 14 days strongly reversed these LPS effects, while the effects of ASD were blocked by the PI3K-Akt signaling inhibitor LY294002 (Figures 4A–H, 5A–D). We also found that ASD at 100 mg/kg/d for 14 days promoted the proliferation of neural stem cells in normal mice, but did not affect hippocampal neurogenesis and the maturation of newborn neurons (Supplementary Figure S1).

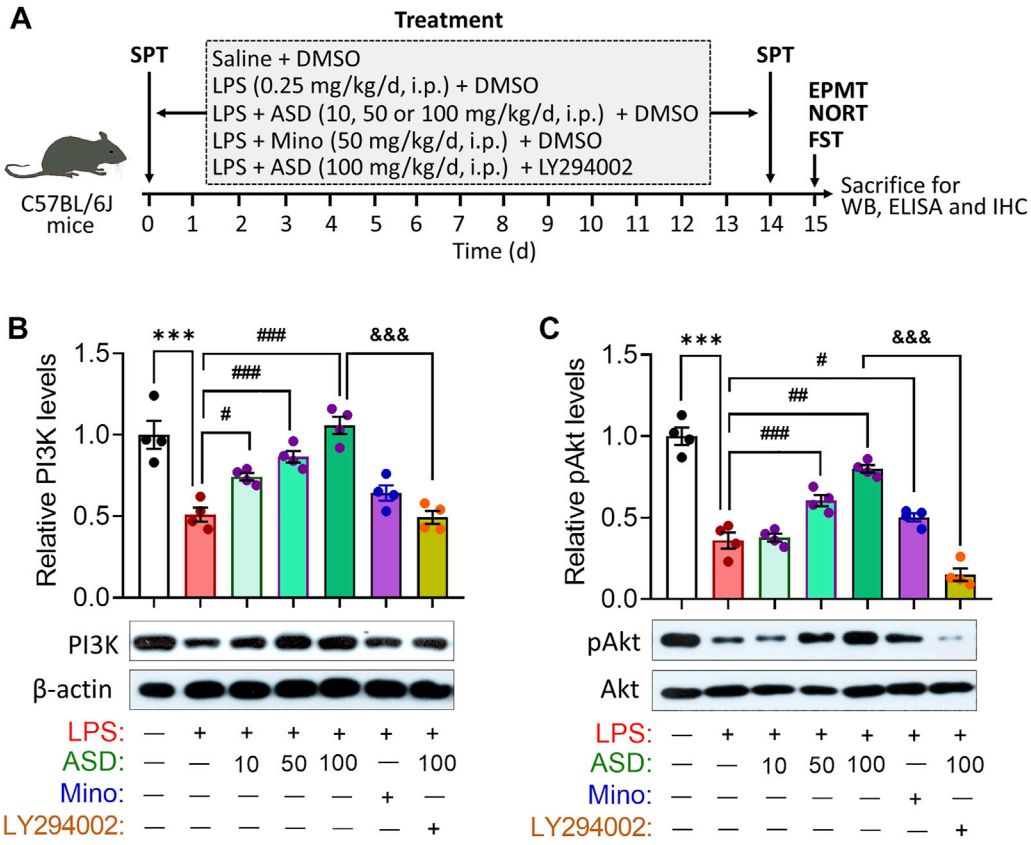

FIGURE 3
ASD activates the PI3K-Akt pathway in hippocampus of mice chronically exposed to LPS. **(A)**, Scheme of the experimental procedure. ASD, akebia saponin D; DMSO, dimethyl sulphoxide; ELISA, enzyme-linked immunosorbent assay; EPMT, elevated plus maze test; FST, forced swimming test; IHC, immunocytochemistry; LPS, lipopolysaccharide; Mino, minocycline; NORT, novel object recognition test; SPT, sucrose preference test; WB, western blotting. **(B,C)**, Western blotting shows the levels of PI3K and pAkt in the hippocampus of mice treated with saline (Ctrl) or lipopolysaccharide (LPS), then with akebia saponin D (ASD), minocycline (Mino) or PI3K-Akt inhibitor (LY294002). Levels of PI3K were normalized to those of β-actin, and levels of pAkt were normalized to those of Akt. Data are mean ± standard error of the mean (SEM) (n = 4), ***$p < 0.001$ vs. Ctrl group, #$p < 0.05$, ##$p < 0.01$, ###$p < 0.001$ vs. LPS group, &&&$p < 0.001$ vs. ASD (100 mg/kg) + LPS group based on one-way ANOVA with Tukey's multiple-comparisons test.

Abnormal neurogenesis in hippocampus will lead to synaptic dysfunction which link to depression- and anxiety-related symptoms aand cognitive function. Indeed, our results showed that chronic LPS exposure decreased the hippocampal levels of glutamate receptor 1 (GluA1) and 2 (GluA2) subunits of the *a*-amino-3-hydroxy-5-methyl-4-isoxazole-propionicacid (AMPA), which mediated rapid excitatory synaptic transmission in the central nervous system. These changes in synaptic function-related markers were partially reversed by ASD, while the effects of ASD were blocked by the PI3K-Akt signaling inhibitor LY294002 (Figures 6A,B).

Given the observed improvement in hippocampal neurogenesis of LPS-administrated mice that were treated with ASD, we determined whether ASD inhibits microglial activation or acts directly on neural stem cells in neurogenic niche of mice exposed LPS stimulation. We found that LPS induced increases in the area of Iba1+ cells in hippocampus and in the level of IL-1β in hippocampus or hippocampal CA1, CA3 and dentate gyrus (Figures 7A–G), reflecting proliferation of microglia and their activation to secrete pro-inflammatory cytokines. Minocycline and ASD at 100 mg, but not 10 mg or 50 mg, reversed these effects of LPS in hippocampal CA1, CA3 (Figures 7A–G). However, even the 100 mg of ASD did not completely reverse the LPS-induce changes in morphology and number of microglia and the increase in IL-1β in hippocampal dentate gyrus (Figures 7A–G). These results suggest that ASD maybe directly activate PI3K-Akt signaling of hippocampal NSPC to promote neurognegesis rather than inhibition of microglial activation in dentate gyrus of LPS-exposed mice.

These experiments indicate that 100 mg/kg/d ASD activated the PI3K-Akt pathway to restore hippocampal NSPC

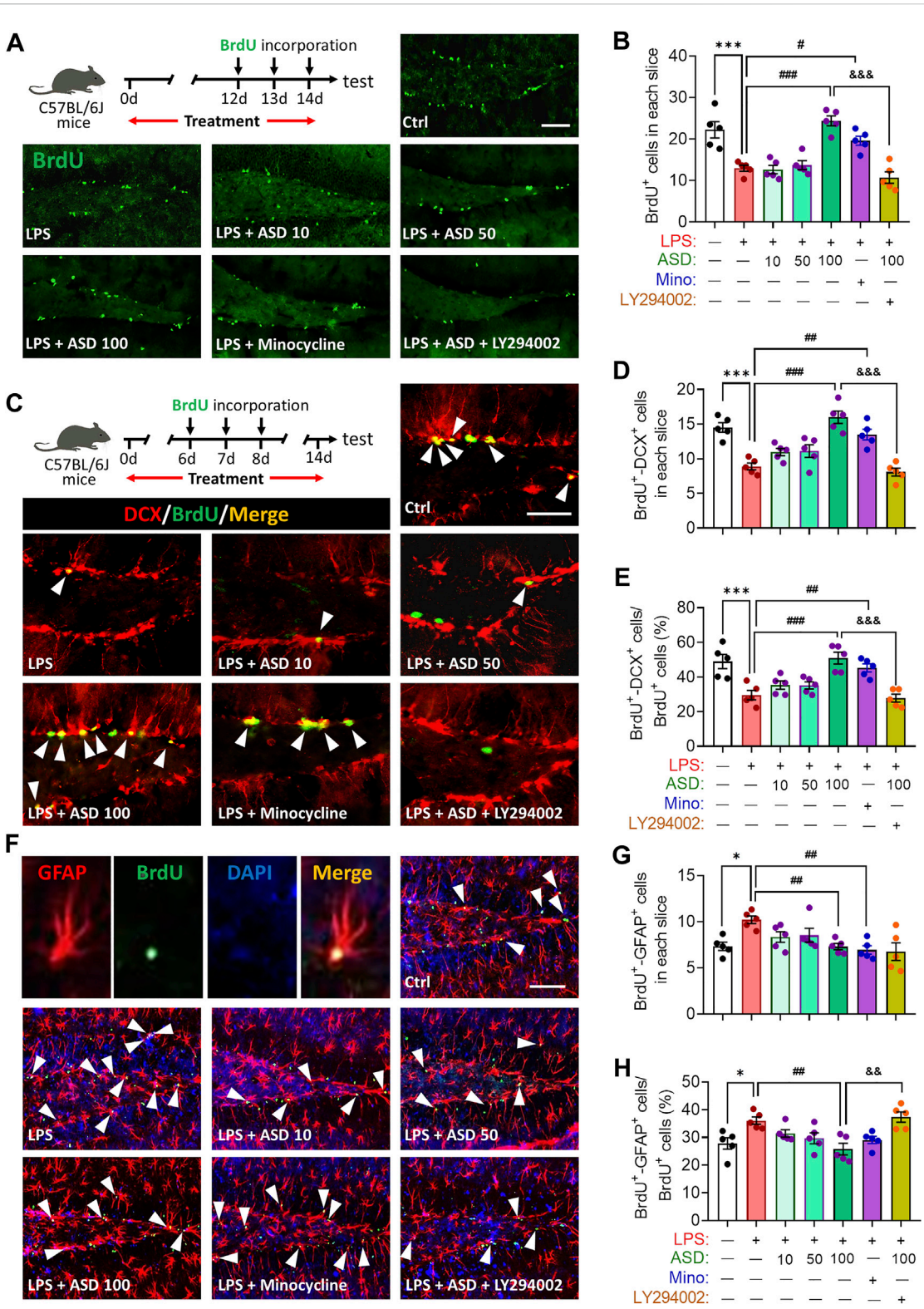

FIGURE 4
Effects of ASD on NSPC proliferation and differentiation in dentate gyrus of mice chronically exposed to LPS. **(A)**, Timeline for detecting proliferation of neural stem/progenitor cells (NSPCs) based on immunofluorescence micrographs of BrdU + cells in dentate gyrus (DG) of mice. Proliferating NSPCs were labeled using 5′-bromo-2′deoxyuridine (BrdU) (green). Scale bar, 100 μm. **(B)**, Quantification of hippocampal BrdU + cells. Five mice from each group were examined, and five hippocampal micrographs (40×) from each animal were quantified. **(C)**, Timeline for

(*Continued*)

FIGURE 4
evaluating NSPC differentiation based on immunofluorescence micrographs of BrdU + -DCX + cells in dentate gyrus (DG) of mice. Proliferating NSPCs were labelled with BrdU (green); immature neurons, with antibody against doublecortin (DCX); and newborn neurons differentiated from NSPCs, with both BrdU and anti-DCX antibody (white arrowheads). Scale bar, 100 μm. **(D)**, Quantification of the hippocampal BrdU + -DCX + cells in each slice. **(E)**, Quantification of the percentage of total BrdU + cells in the DG that were BrdU + -DCX+. **(F)**, Immunofluorescence micrographs of BrdU + -GFAP + cells in the DG. Proliferating NSPCs were labelled with BrdU (green); astrocytes, with antibody against GFAP; and newborn astrocytes differentiated from NSPCs, with BrdU and anti-GFAP antibody (white arrowheads). Scale bar, 100 μm. **(G)**, Quantification of hippocampal BrdU + -GFAP + cells in each slice. **(H)**, Quantification of the percentage of total BrdU + cells in the DG that were BrdU + -GFAP+. Five mice from each group were examined, and five hippocampal micrographs (40×) from each animal were quantified. Each dot in the bar graph represents the average of all micrographs for each mouse. Data are mean ± standard error of the mean (SEM) (n = 5), $*p < 0.05$, $***p < 0.001$ vs. Ctrl group, $\#p < 0.05$, $\#\#p < 0.01$, $\#\#\#p < 0.001$ vs. LPS group, $\&\&p < 0.01$, $\&\&\&p < 0.001$ vs. ASD (100 mg/kg) + LPS group by one-way ANOVA with Tukey's multiple-comparisons test. Each dot in the bar graph represents the average of all micrographs for each mouse.

proliferation, survival and neuronal differentiation, as well as the synaptic function of hippocampal neurons in a microenvironment of chronic neuroinflammation.

3.3 ASD ameliorates depressive- and anxiety-like behaviors and cognitive impairment in a mouse model of chronic neuroinflammation

In healthy individuals, a steady stream of new neurons in the DG can project into the cerebral cortex to regulate emotional and cognitive functions (Zhang et al., 2021), but this steady stream is likely compromised in patients with Alzheimer's disease or depression, who suffer hippocampal atrophy. The impaired neurogenesis likely contributes to depression, anxiety and cognitive impairments. Given our observations above that ASD can promote NSPC proliferation and neuronal differentiation *in vitro* and *in vivo*, even in a chronically inflammatory microenvironment, we wanted to examine whether these effects of ASD could mitigate depression, anxiety and cognitive impairment due to chronic inflammation.

Depressive-like behaviors of mice were evaluated using the SPT, which evaluates anhedonia, and the FST, which assesses behavioral despair. Chronic exposure to LPS decreased the sucrose preference of mice, which ASD (at a daily dose of at least 100 mg/kg) or minocycline reversed (Figures 8A,B). Chronic exposure to LPS shortened the latency time and prolonged immobility time in the FST, which ASD reversed (Figures 8C–E).

Anxiety-like behaviors of mice were evaluated using the elevated plus maze test (Figure 9A). Chronic exposure to LPS reduced the number of open-arm entries and time spent in open arms, which ASD (at a daily dose of at least 100 mg/kg) or minocycline reversed (Figures 9B,C).

Cognition was tested through the novel object recognition test (Figure 10A). No preference was shown for the novel item, regardless of whether it replaced the familiar object on the right or left (Figure 10B). Chronic exposure to LPS induced a significant cognitive defect (Figure 10C), which ASD (at 10–100 mg/kg/d) or minocycline ameliorated (Figures 10A–C).

Learning and memory were assessed using a Morris water maze (Figure 10D). Chronic exposure to LPS prolonged latency time in the maze, which ASD (at a dose of at least 50 mg/kg/d) or minocycline reversed (Figure 10E).

To further expound the pharmacological mechanisms of ASD against disorders involving impaired neurogenesis, we performed network pharmacology-based analysis of ASD for the treatment of major depressive disorder (MDD), anxiety and Alzheimer's disease (AD). We identified 4795 MDD-related targets, 2663 AD-related targets, 4097 AD-related targets, 2,663 anxiety-related targets (Supplementary Figure S2). A total of 1,386 targets involving MDD, AD and anxiety were identified, of which 84 were ASD targets (Figure 11A). These common targets were extracted for further Kyoto Encyclopedia of Genes and Genomes (KEGG) pathway enrichment analysis using R software. The results showed that the PI3K-Akt pathway ranks fourth in KEGG pathway enrichment (Figure 11B).

To probe the possible binding mode of ASD with the PI3K/Akt, molecular docking was performed. ASD is bound to the interaction interface of the PI3K and AKT (Figures 11C,D). Upon calculation of the MM/GBSA binding energy, the ligand ASD bound to the PI3K with a stability of −7.81 ± 0.32 kJ/mol (Figure 11C); and the ligand ASD bound to the AKT with a stability of −7.34 ± 0.44 kJ/mol (Figure 11D).

In support of PI3K-Akt signaling as mediator of the neuroprotective effects of ASD, PI3K-Akt inhibitor LY294002 blocked the compound's ability to reverse the LPS-induced defects on all these behavioral tests (Figures 8A,10E). These results suggested that PI3K-Akt pathway is one of the targets of ASD to against the disorders involving impaired neurogenesis.

4 Discussion

Neurogenesis plays a fundamental role in the postnatal brain, where it is required for neuronal plasticity (Puderbaugh & Emmady, 2022). Promoting neurogenesis in the adult brain may be an effective strategy for treating major depressive disorder and Alzheimer's disease, and the compound ASD

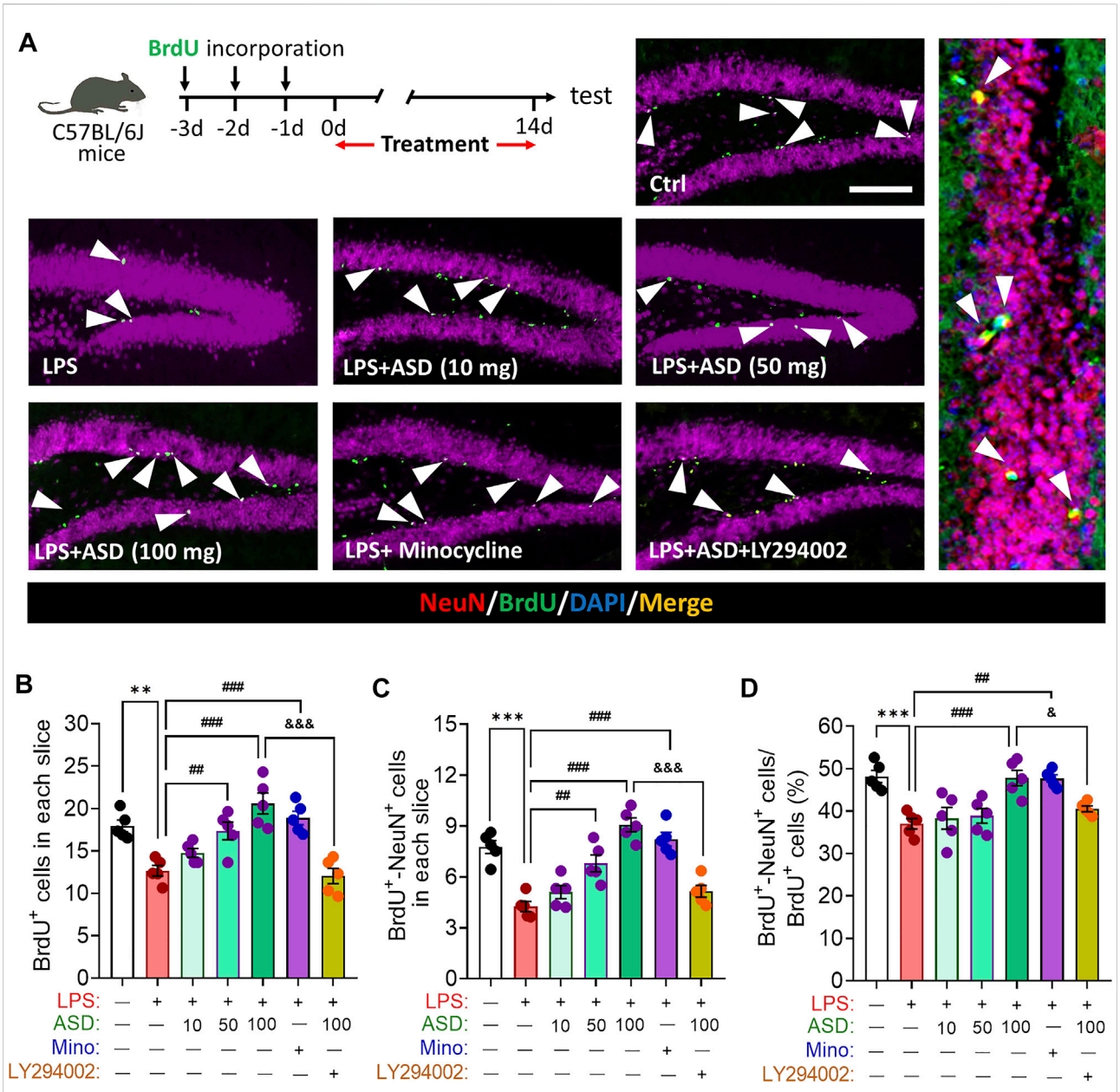

FIGURE 5
Effects of ASD on survival and maturation of newborn neurons in dentate gyrus of mice chronically exposed to LPS. **(A)**, Timeline for evaluating newborn neuron survival and maturation based on immunofluorescence micrographs of BrdU + -NeuN + cells in the dentate gyrus of mice. Surviving cells were labelled with BrdU (green); mature neurons, with antibody against neuron-specific nucleoprotein (NeuN); and mature neurons differentiated from NSPCs, with both BrdU and anti-NeuN antibody (white arrowheads). Scale bar, 100 μm. **(B)**, Quantification of hippocampal BrdU + cells in each slice. **(C)**, Quantification of hippocampal BrdU + -NeuN + cells in each slice. **(D)**, Quantification of the percentage of total BrdU + cells in DG that were BrdU + -NeuN+. Five mice from each group were examined, and five hippocampal micrographs (40×) from each animal were quantified. Each dot in the bar graph represents the average of all micrographs for each mouse. Data are mean ± standard error of the mean (SEM) (n = 5), $^{**}p < 0.01$, $^{***}p < 0.001$ vs. Ctrl group, $\#\#p < 0.01$, $\#\#\#p < 0.001$ vs. LPS group, $\&p < 0.05$, $\&\&\&p < 0.001$ vs. ASD (100 mg/kg) + LPS group by one-way ANOVA with Tukey's multiple-comparisons test.

from traditional Chinese medicine has shown promise in this regard. In the present work, we found that ASD can promote NSPC proliferation, survival and neuronal differentiation *in vitro* and *in vivo*, even in a microglia-mediated inflammatory niche. These effects correlate with milder behavioral symptoms of depression, anxiety and cognitive impairment due to chronic neuroinflammation. Finally, we provide evidence that the therapeutic effects of ASD involve activation of the PI3K-AKT

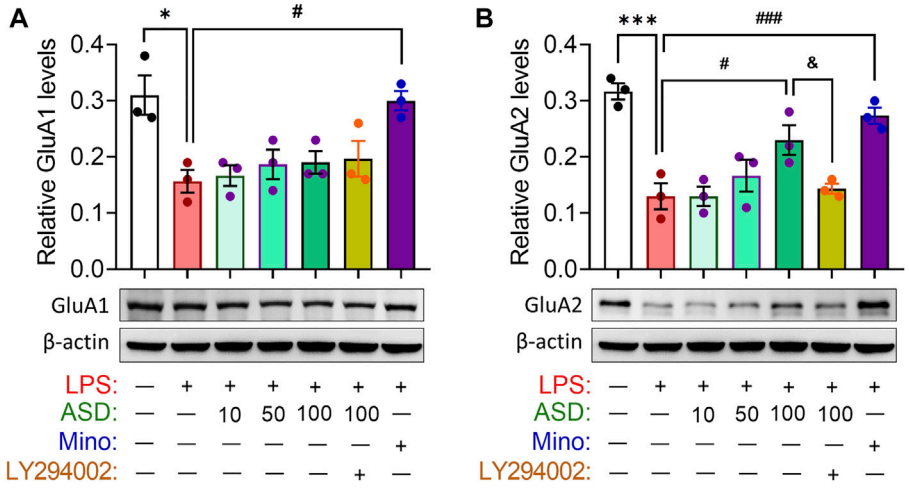

FIGURE 6
Effects of ASD on synaptic function in hippocampus of mice chronically exposed to LPS. **(A,B)**, Western blotting shows the levels of GluA1 and GluA2 in the hippocampus of mice treated with saline (Ctrl) or lipopolysaccharide (LPS), then with akebia saponin D (ASD), minocycline (Mino) or PI3K-Akt inhibitor (LY294002). Levels of GluA1 and GluA2 were normalized to those of β-actin. Figures 6A,B share the same β-actin. Data are mean ± standard error of the mean (SEM) (n = 4), $*p < 0.05$, $***p < 0.001$ vs. Ctrl group, $\#p < 0.05$, $\#\#\#p < 0.001$ vs. LPS group, $\&p < 0.05$ vs. ASD (100 mg/kg) + LPS group based on one-way ANOVA with Tukey's multiple-comparisons test.

pathway. To our knowledge, this study is the first to report the direct regulation of ASD on adult hippocampal NSPCs.

The hippocampus, a brain area critical for learning, memory and emotion, is especially vulnerable to damage in early stages of AD, chronic stress or inflammation, when neurogenesis in the adult hippocampus is altered (Zonis et al., 2015; Chesnokova et al., 2016; Babcock et al., 2021; Du Preez et al., 2021). Various key molecules involved in the pathogenesis of major depression disorder or AD have been linked to the inhibition of neurogenesis (Berger et al., 2020; Babcock et al., 2021; Walgrave et al., 2021). Brain imaging and postmortem studies of patients with either of these disorders indicate reduction in hippocampal volume perhaps due to reduced neurogenesis and loss of mature neurons (Frimodt-Møller et al., 2019; Zarate-Garza et al., 2021).

This reduced neurogenesis seems to be at least partly the fault of microglia. These immune cells create an inflammatory microenvironment that inhibits NSPC proliferation and differentiation (Xiong et al., 2016; Zhang et al., 2020b). In a variety of neurodegenerative settings, microglia alter their transcriptional profile, morphology, and function to exert negative effects in disease models (Mattei et al., 2017; Wolf et al., 2017). Activation of microglia results in phagocytosis and production of pro-inflammatory cytokines, reactive oxygen species, and inducible NO synthase (iNOS), which can alter the hippocampal neurogenic niche, reducing NSPC proliferation, survival and neuronal differentiation. These injuries can contribute to cognitive dysfunction and depression (Snyder et al., 2011; Berger et al., 2020; Zhang et al., 2020b; Zhang J. et al., 2021; Mizuno et al., 2021). In the present study, we found that mice chronically exposed to LPS exhibited obvious depressive- and anxiety-like behaviors and cognitive impairment, which were accompanied by microglial overactivation and inhibition of hippocampal neurogenesis. These results support the idea that microglia-mediated neuroinflammation inhibits hippocampal neurogenesis, with diverse behavioral consequences related to depression, anxiety and cognitive impairment.

Adult hippocampal neurogenesis is supported by NSPC proliferation and neuronal differentiation, as well as maturation and survival of the resulting newborn neurons (Deierborg et al., 2010; Pilz et al., 2018). These processes are strongly dependent on a supportive hippocampal neurogenic niche, which activated microglia antagonize by creating an inflammatory microenvironment (Toda et al., 2019; Zhang et al., 2020b). Consistent with this, we found that chronic LPS exposure reduced the numbers of BrdU + cells, BrdU + -DCX + cells and BrdU + -NeuN + cells in mouse hippocampus. Indeed, conditioned medium from microglia treated with LPS was sufficient to induce NSPC apoptosis and suppress their proliferation and neuronal differentiation.

Several studies have shown that inhibitors of microglial activation such as minocycline can suppress pro-inflammatory cytokine expression and restore hippocampal neurogenesis, as well as ameliorate depressive-like behaviors and cognitive impairment (Zhang et al., 2020b; Alavi et al., 2021; Bassett et al., 2021). Our results are consistent with the observation that variations in the relatively small number of new neurons in adult brains of humans and rodents is strongly linked to the

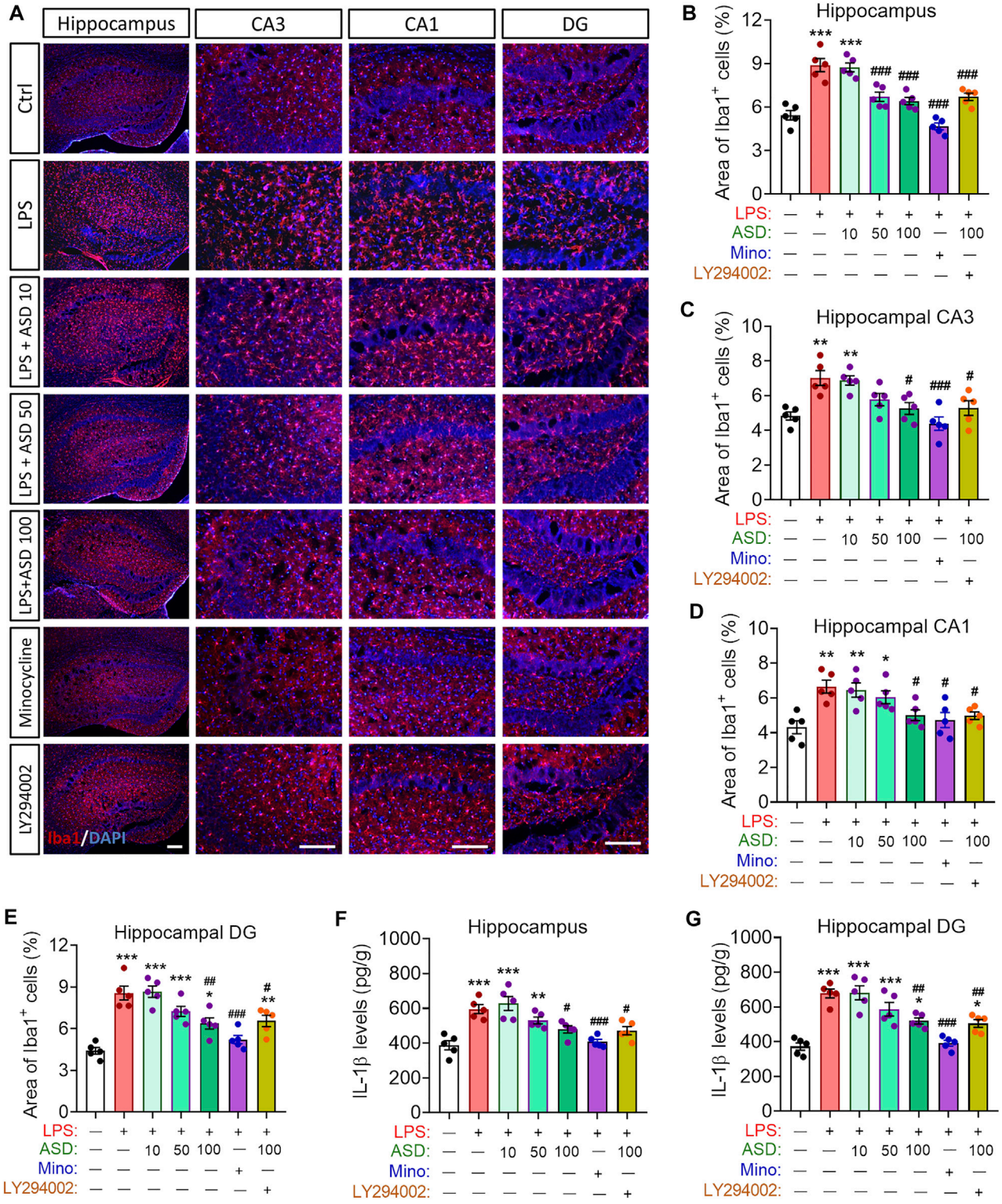

FIGURE 7
Effects of ASD on microglia, astrocyte numbers and IL-1β levels in neurogenic niche of mice chronically exposed to LPS. **(A)**, Representative fluorescence micrographs showing the morphology and density of microglia in the hippocampus of mice treated with saline (Ctrl) or lipopolysaccharide (LPS), followed by akebia saponin D (ASD) or minocycline. Microglia were labeled with antibody against ionized calcium binding adapter molecule 1 (Iba1) (red) and nuclei, with 4′,6-diamidino-2-phenylindole (DAPI) (blue). Scale bar, 100 μm. **(B–E)**, Quantification of the percentages of total area containing Iba1+ cells in hippocampal CA3 (C), CA1 (D) and dentate gyrus (DG) (E) for evaluating changes in the morphology
(*Continued*)

FIGURE 7
and density of microglia. Five mice from each group were examined, and five hippocampal micrographs (40×) from each animal were quantified. Each dot in the bar graph represents the average of all micrographs for each mouse. **(F,G)**, Quantification of the concentration of IL-1β in hippocampus and hippocampal DG as an index of neuroinflammation. Data are mean ± standard error of the mean (SEM) (n = 5), *$p < 0.05$, **$p < 0.01$, ***$p < 0.001$ vs. Ctrl group, #$p < 0.05$, ##$p < 0.01$, ###$p < 0.001$ vs. LPS group by one-way ANOVA with Tukey's multiple-comparisons test.

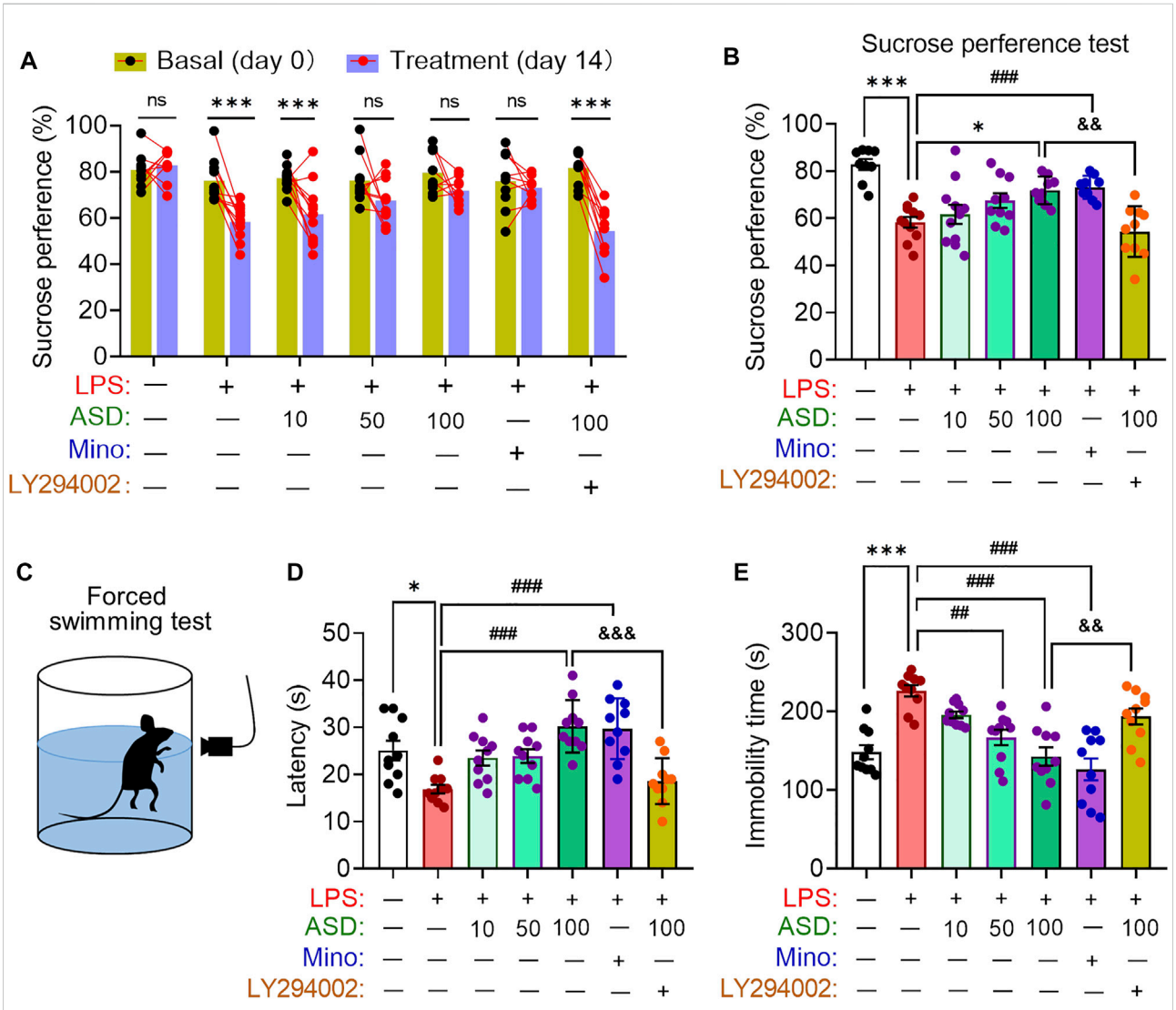

FIGURE 8
Effects of ASD on depressive-like behaviors of mice chronically exposed to LPS in the presence or absence of PI3K-Akt inhibitor. **(A)**, Changes in sucrose preference of individual saline-treated (Ctrl) or lipopolysaccharide (LPS)-treated mice, before treatment (day 0) and afterward (day 14). **(B)**, Changes in sucrose preference following treatment with akebia saponin D (ASD), minocycline (Mino) or PI3K-Akt inhibitor (LY294002) for 14 days. **(C–E)**, Effects of ASD on immobility time and latency in the forced swimming test. Data are mean ± standard error of the mean (SEM) (n = 8-11). Panel (A): ***$p < 0.001$ vs. basal (0-days) by a paired Student's t test for. Panels (B), (D) and (E): *$p < 0.05$, ***$p < 0.001$ vs. Ctrl group, ##$p < 0.01$, ###$p < 0.001$ vs. LPS group, &&$p < 0.01$, &&&$p < 0.001$ vs. ASD (100 mg/kg) + LPS group by one-way ANOVA with Tukey's multiple-comparisons test.

pathogenesis and remission of neuropsychiatric disorders (Grace et al., 2021). We show here that ASD exerted therapeutic effects similar to those of minocycline, yet it did not reverse the LPS-induced increase in the area of Iba1+ cells or IL-1β level. Thus, it appears that ASD restores hippocampal NSPC proliferation, survival and neuronal differentiation, as well as the synaptic

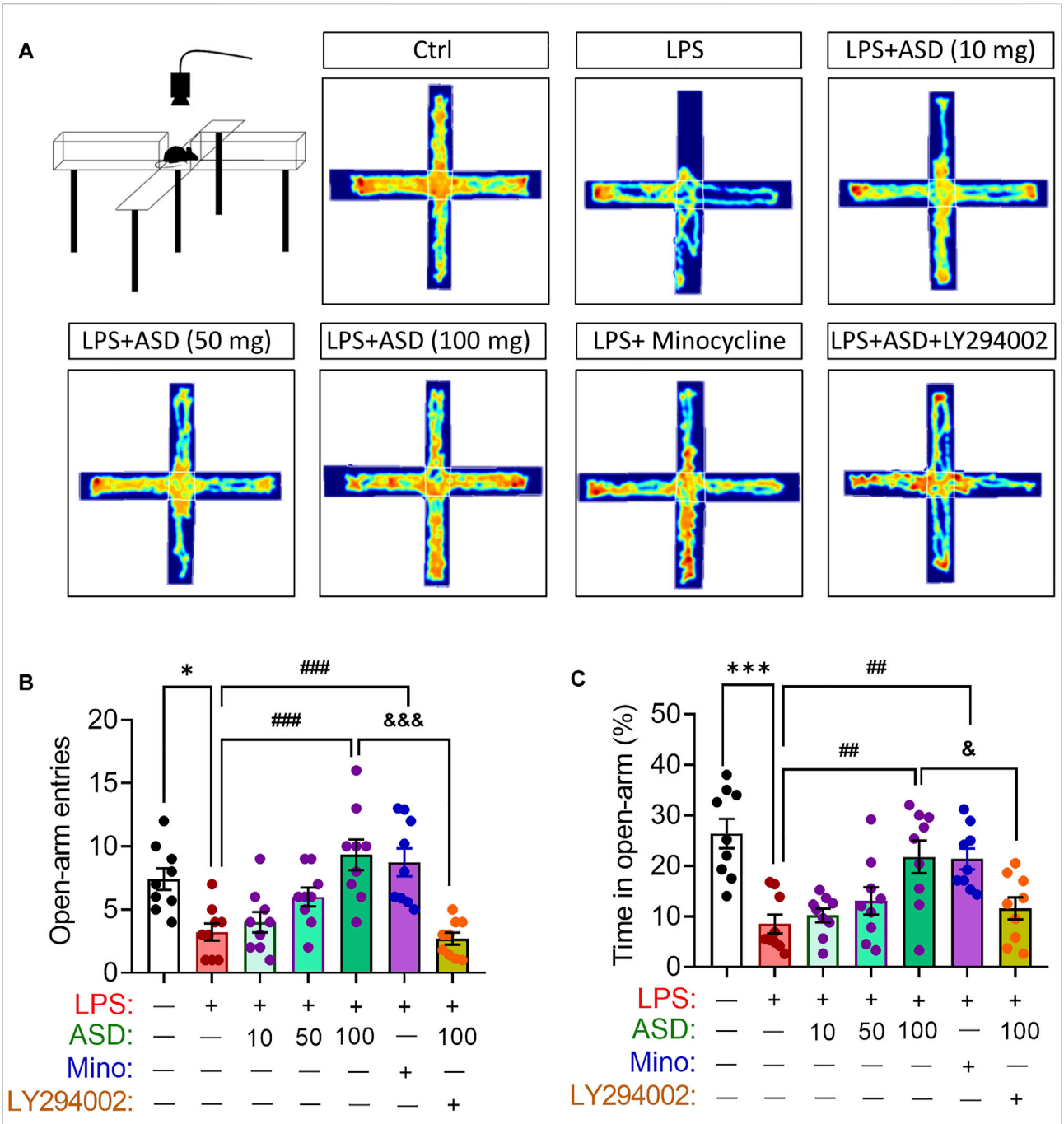

FIGURE 9
Effects of ASD on anxiety-like behaviors of mice chronically exposed to LPS in the presence or absence of PI3K-Akt inhibitor. **(A)**, Scheme describing the experimental evaluation of anxiety-like behaviors of mice using the elevated plus maze test, and the heatmap of mouse behavior in this test. **(B,C)**, Changes in open-arm entries and time in open-arms in mice treated with saline (Ctrl) or lipopolysaccharide (LPS), followed by akebia saponin D (ASD), minocycline (Mino) or PI3K-Akt inhibitor (LY294002) for 14 days. Data are mean ± standard error of the mean (SEM) (n = 8-11). $^{*}p < 0.05$, $^{***}p < 0.001$ vs. Ctrl group, $^{\#\#}p < 0.01$, $^{\#\#\#}p < 0.001$ vs. LPS group, $^{\&}p < 0.05$, $^{\&\&\&}p < 0.001$ vs. ASD (100 mg/kg) + LPS group by one-way ANOVA with Tukey's multiple-comparisons test.

function of hippocampal neurons in a microenvironment of chronic neuroinflammation. However, different from what we found in chronic mild stress model mice (Jiang et al., 2022), ASD does not appear to completely inhibit microglia-mediated inflammation in hippocampus of chronic LPS-treated mice as minocycline does. Instead, ASD acts directly on NSPCs to promote their proliferation, survival and neuronal differentiation. It is interesting that ASD at 100 mg/kg/d for

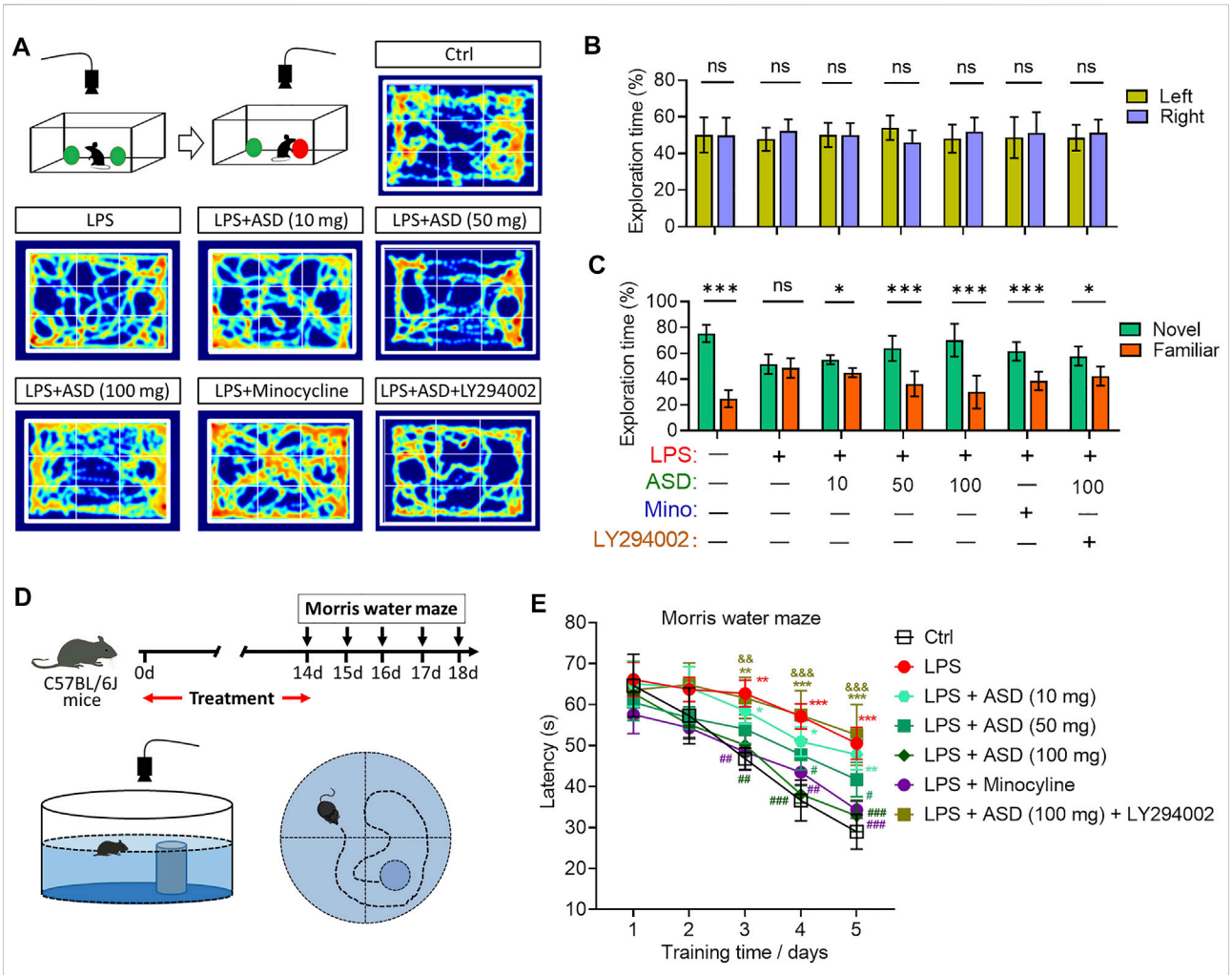

FIGURE 10
Effects of ASD on cognitive impairment of mice chronically exposed to LPS in the presence or absence of PI3K-Akt inhibitor. **(A)**, Scheme describing the experimental evaluation of mice using the novel object recognition test, and heatmap of mouse behavior in this test. **(B)**, Mice showed a preference for the novel item, regardless of whether it replaced the familiar object on the right or left. **(C)**, Comparison of preference for the novel or familiar object. **(D)**, Scheme describing the experimental evaluation of learning and memory using the Morris water maze test. **(E)**, Morris water maze latency of mice treated with saline (Ctrl) or lipopolysaccharide (LPS), followed by akebia saponin D (ASD), minocycline or PI3K-Akt inhibitor (LY294002). Data are mean ± standard error of the mean (SEM) (n = 8-11). Panels (B) and (C): $*p < 0.05$, $***p < 0.001$ vs. left (B) or novel (C) by a paired Student's t-test. Panel (E): $*p < 0.05$, $**p < 0.01$, $***p < 0.001$ vs. Ctrl group, $\#p < 0.05$, $\#\#p < 0.01$, $\#\#\#p < 0.001$ vs. LPS group, $\&\&p < 0.01$, $\&\&\&p < 0.001$ vs. ASD (100 mg/kg) + LPS group by one-way ANOVA with Tukey's multiple-comparisons test.

14 days promoted the proliferation of NSPCs in normal mice, but did not affect hippocampal neurogenesis and the maturation of newborn neurons. It may be that the healthy body itself monitors neurogenesis and limits the number of newborn neurons by inducing apoptosis of excess immature neurons.

Inhibited neurogenesis may exacerbate neuronal vulnerability to Alzheimer's disease, stress or immune challenge, leading to memory impairment, anxiety or depression; under these conditions, enhanced neurogenesis may be a compensatory response to repair and protect the brain (Bassani et al., 2018; Moreno-Jiménez et al., 2019; Tobin et al., 2019). Adult neurogenesis in the hippocampus subgranular zone (SGZ) is associated with the etiology and efficacy of treatments against Alzheimer's disease and major depressive disorder (Anacker & Hen, 2017; Babcock et al., 2021; Zhang J. et al., 2021). Adult hippocampal neurogenesis appears to occur in humans as well as in rodents, although this idea is still controversial (Spalding et al., 2013; Kempermann et al., 2018; Moreno-Jiménez et al., 2021). In this study, we isolated NSPCs from the hippocampal subgranular zone of adult mice and induced their proliferation and differentiation, suggesting that NSPCs do indeed exist in the adult hippocampus of rodents.

The PI3K/Akt signaling pathway is the classical anti-apoptotic and pro-survival signal transduction pathway (Gabbouj et al., 2019; Xie et al., 2019). When PI3K binds to growth factor receptors such as the epidermal growth factor

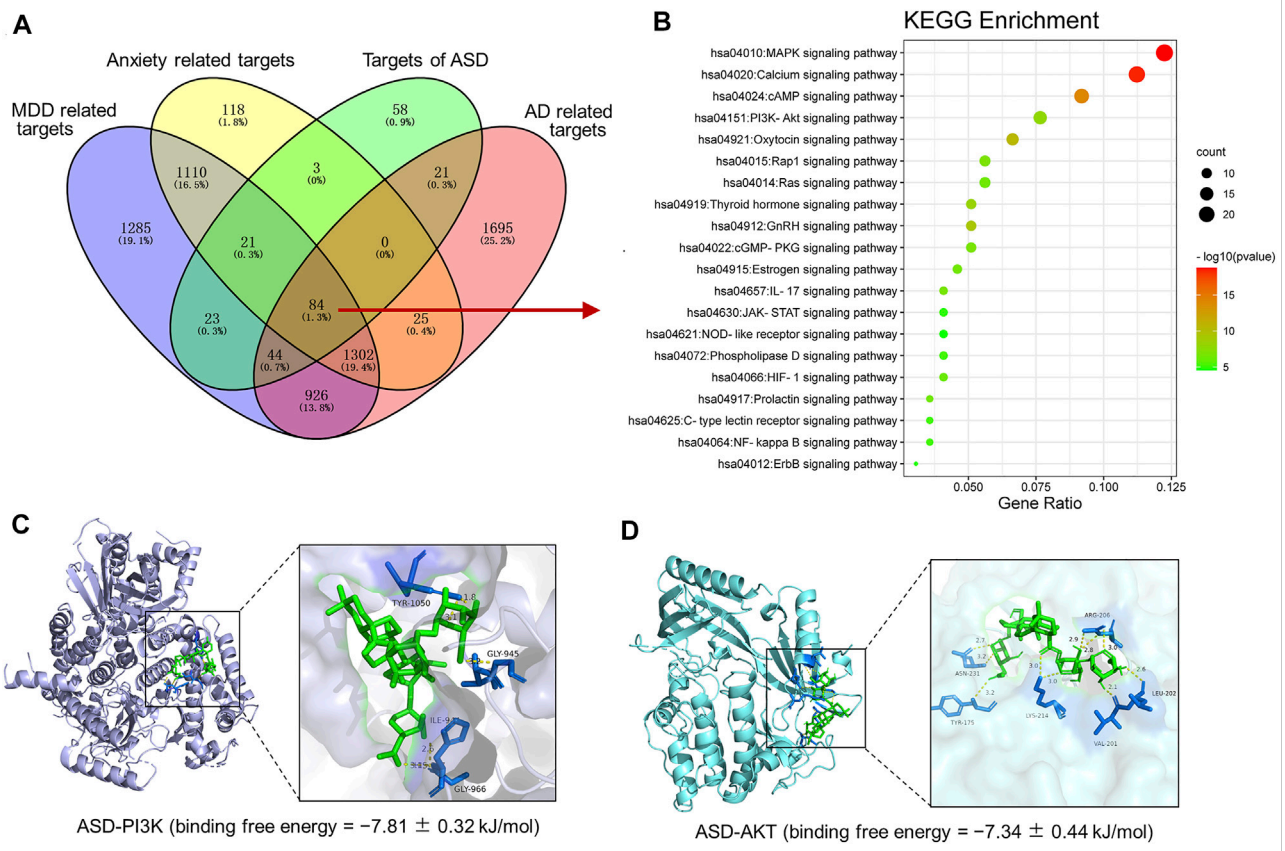

FIGURE 11
Pharmacological mechanisms of ASD against disorders involving impaired neurogenesis. **(A)**, Venn diagram summarizing the intersection targets of the akebia saponin D (ASD), major depressive disorder (MDD), anxiety and Alzheimer's disease (AD). **(B)**, KEGG analysis of key targets of ASD in treatment of MDD, anxiety and AD. Bubble plot of top 20 KEGG pathways. **(C,D)**, Molecular docking diagram of ASD (green) to target PI3K (C) and Akt (D). The yellow lines represent the hydrogen bond interaction force, which is the main force promoting molecule binding with the active site. The blue positions indicate the amino acid residues of the receptors (PI3K/AKT).

receptor, Akt becomes activated, leading to the activation or inhibition of downstream substrates such as the apoptotic proteins Bad and Caspase-9 (Jeong et al., 2008). These substrates go on to regulate cell proliferation, differentiation, apoptosis, migration, and other processes (Darici et al., 2020). Base on the network pharmacology analysis and molecular docking, we found PI3K-Akt pathway is one of the targets of ASD to against the disorders involving impaired neurogenesis, such as Alzheimer's disease, major depressive disorder and anxiety disorder. In our mouse model of chronic neuroinflammation, levels of PI3K and pAkt were strikingly reduced in hippocampus, and this was associated with reduced NSPC proliferation and differentiation. The PI3K-Akt signaling pathway in adult NSPCs is strongly inhibited in an environment of neuroinflammation mediated by microglia, leading to increased apoptosis and differentiation into astrocytes. Conversely, ASD strongly increased levels of PI3K, Akt, and pAkt proteins, even in the presence of LPS-M-CM. These results suggest that the PI3K-Akt pathway mediates the effects of ASD on NSPC proliferation, survival and neuronal differentiation. Consistent with this, we found that LY294002, an inhibitor of the PI3K/Akt pathway, blocked the effects of ASD on NSPC apoptosis, proliferation and neuronal differentiation in the presence or absence of LPS-M-CM. LY294002 treatment also blocked the effects of ASD on hippocampal neurogenesis and depressive- and anxiety-like behaviors and cognitive impairment. Our results add to the number of cellular contexts in which ASD activates PI3K/Akt signaling with therapeutic effects, including bone regeneration (Ke et al., 2016) as well as Alzheimer's disease (Zheng et al., 2017; Razani et al., 2021), anxiety (Qiao et al., 2018) and depression (Guo et al., 2019; Shan et al., 2020). This growing literature argues for activating PI3K/Akt signaling as a strategy against neurological disorders involving impaired neurogenesis.

Our results provide strong evidence that ASD protects NSPCs from the microglia-mediated inflammatory niche and promotes their proliferation, survival and neuronal differentiation by activating the PI3K-Akt pathway (Figure 12). Our results support further evaluation of ASD for

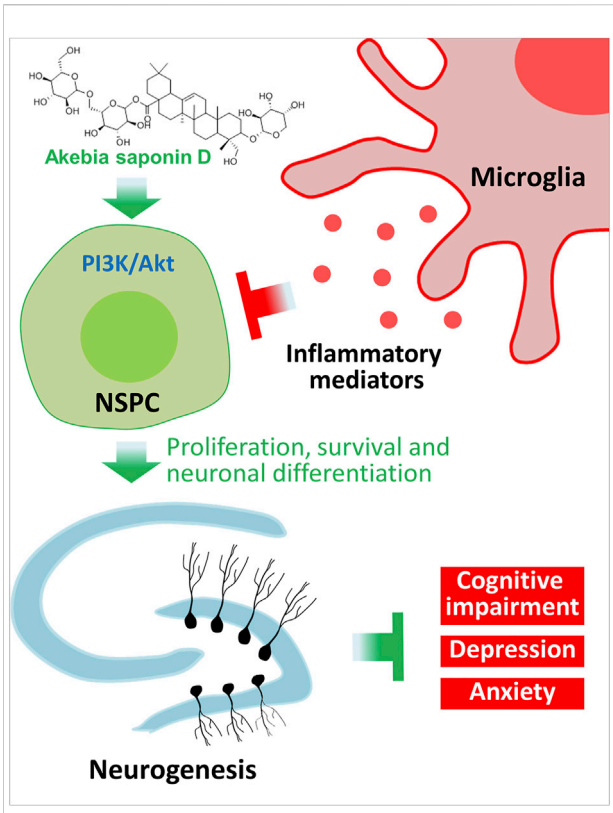

FIGURE 12
Schematic diagram of how akebia saponin D may protect hippocampal neurogenesis. Akebia saponin D activates the PI3K-Akt pathway to protect NSPCs from the microglia-mediated inflammatory niche, promoting their proliferation, survival and neuronal differentiation, as well as ameliorating depressive- and anxiety-like behaviors and cognitive impairment.

the treatment of Alzheimer's disease, major depressive disorder and other conditions associated with impaired neurogenesis.

Data availability statement

The original contributions presented in the study are included in the article/Supplementary Material, further inquiries can be directed to the corresponding authors.

Ethics statement

The animal study was reviewed and approved by Institutional Animal Care and Use Committee of the Guizhou University of Traditional Chinese Medicine.

Author contributions

JZ and TZ conceived and designed the study. JZ and QL wrote the manuscript, which was reviewed by TZ and ZY, and approved by all the authors. CX and CY performed behavioral and immunofluorescence studies. WJ and LL cultured NSPCs and microglia. DS and ZZ performed statistical analysis of the data.

Funding

This work was supported by the National Natural Science Foundation of China (82060726, 81860675), the Department of Science and Technology of Guizhou High-level Innovative Talents (20185638-2), Sichuan Science and Technology Program (2020YJ0225) and Guizhou Science and Technology Plan Project (20195611).

Acknowledgments

We are grateful to Creaducate Consulting GmbH for help in editing the manuscript.

Conflict of interest

The authors declare that the research was conducted in the absence of any commercial or financial relationships that could be construed as a potential conflict of interest.

Publisher's note

Supplementary material

The Supplementary Material for this article can be found online at: https://www.frontiersin.org/articles/10.3389/fphar.2022.927419/full#supplementary-material

References

Alavi, S., Darharaj, M., Bilehsavar, S. H., Amini, M., Zafarghandi, M. B. S., Berenji, V., et al. (2021). Successful use of minocycline for the treatment of methamphetamine-induced psychosis and cognitive impairments: An open-label case series. *Clin. Neuropharmacol.* 44, 126–131. doi:10.1097/WNF.0000000000000460

Anacker, C., and Hen, R. (2017). Adult hippocampal neurogenesis and cognitive flexibility - linking memory and mood. *Nat. Rev. Neurosci.* 18, 335–346. doi:10.1038/nrn.2017.45

Araki, T., Ikegaya, Y., and Koyama, R. (2021). The effects of microglia- and astrocyte-derived factors on neurogenesis in health and disease. *Eur. J. Neurosci.* 54, 5880–5901. doi:10.1111/ejn.14969

Babcock, K. R., Page, J. S., Fallon, J. R., and Webb, A. E. (2021). Adult hippocampal neurogenesis in aging and Alzheimer's disease. *Stem Cell. Rep.* 16, 681–693. doi:10.1016/j.stemcr.2021.01.019

Bassani, T. B., Bonato, J. M., Machado, M. M. F., Cóppola-Segovia, V., Moura, E. L. R., Zanata, S. M., et al. (2018). Decrease in adult neurogenesis and neuroinflammation are involved in spatial memory impairment in the streptozotocin-induced model of sporadic Alzheimer's disease in rats. *Mol. Neurobiol.* 55, 4280–4296. doi:10.1007/s12035-017-0645-9

Bassett, B., Subramaniyam, S., Fan, Y., Varney, S., Pan, H., Carneiro, A. M. D., et al. (2021). Minocycline alleviates depression-like symptoms by rescuing decrease in neurogenesis in dorsal hippocampus via blocking microglia activation/phagocytosis. *Brain Behav. Immun.* 91, 519–530. doi:10.1016/j.bbi.2020.11.009

Berger, T., Lee, H., Young, A. H., Aarsland, D., and Thuret, S. (2020). Adult hippocampal neurogenesis in major depressive disorder and Alzheimer's disease. *Trends Mol. Med.* 26, 803–818. doi:10.1016/j.molmed.2020.03.010

Bhattarai, P., Thomas, A. K., Cosacak, M. I., Papadimitriou, C., Mashkaryan, V., Froc, C., et al. (2016). IL4/STAT6 signaling activates neural stem cell proliferation and neurogenesis upon amyloid-β42 aggregation in adult zebrafish brain. *Cell. Rep.* 17, 941–948. doi:10.1016/j.celrep.2016.09.075

Bonafina, A., Trinchero, M. F., Ríos, A. S., Bekinschtein, P., Schinder, A. F., Paratcha, G., et al. (2019). GDNF and GFRα1 are required for proper integration of adult-born hippocampal neurons. *Cell. Rep.* 29, 4308–4319.e4. e4. doi:10.1016/j.celrep.2019.11.100

Cameron, H. A., and Glover, L. R. (2015). Adult neurogenesis: Beyond learning and memory. *Annu. Rev. Psychol.* 66, 53–81. doi:10.1146/annurev-psych-010814-015006

Chen, F., Liang, Q., Mao, L., Yin, Y., Zhang, L., Li, C., et al. (2022). Synergy effects of Asperosaponin VI and bioactive factor BMP-2 on osteogenesis and anti-osteoclastogenesis. *Bioact. Mat.* 10, 335–344. doi:10.1016/j.bioactmat.2021.09.001

Chesnokova, V., Pechnick, R. N., and Wawrowsky, K. (2016). Chronic peripheral inflammation, hippocampal neurogenesis, and behavior. *Brain Behav. Immun.* 58, 1–8. doi:10.1016/j.bbi.2016.01.017

Cope, E. C., and Gould, E. (2019). Adult neurogenesis, glia, and the extracellular matrix. *Cell. stem Cell.* 24, 690–705. doi:10.1016/j.stem.2019.03.023

Darici, S., Alkhaldi, H., Horne, G., Jørgensen, H. G., Marmiroli, S., and Huang, X. (2020). Targeting PI3K/Akt/mTOR in AML: Rationale and clinical evidence. *J. Clin. Med.* 9, E2934. doi:10.3390/jcm9092934

Deierborg, T., Roybon, L., Inacio, A. R., Pesic, J., and Brundin, P. (2010). Brain injury activates microglia that induce neural stem cell proliferation *ex vivo* and promote differentiation of neurosphere-derived cells into neurons and oligodendrocytes. *Neuroscience* 171, 1386–1396. doi:10.1016/j.neuroscience.2010.09.045

Deng, W., Aimone, J. B., and Gage, F. H. (2010). New neurons and new memories: How does adult hippocampal neurogenesis affect learning and memory? *Nat. Rev. Neurosci.* 11, 339–350. doi:10.1038/nrn2822

Ding, X., Li, W., Chen, D., Zhang, C., Wang, L., Zhang, H., et al. (2019). Asperosaponin VI stimulates osteogenic differentiation of rat adipose-derived stem cells. *Regen. Ther.* 11, 17–24. doi:10.1016/j.reth.2019.03.007

Drew, L. J., Fusi, S., and Hen, R. (2013). Adult neurogenesis in the mammalian hippocampus: Why the dentate gyrus? *Learn. Mem.* 20, 710–729. doi:10.1101/lm.026542.112

Du Preez, A., Onorato, D., Eiben, I., Musaelyan, K., Egeland, M., Zunszain, P. A., et al. (2021). Chronic stress followed by social isolation promotes depressive-like behaviour, alters microglial and astrocyte biology and reduces hippocampal neurogenesis in male mice. *Brain Behav. Immun.* 91, 24–47. doi:10.1016/j.bbi.2020.07.015

Frimodt-Møller, K. E., Møllegaard Jepsen, J. R., Feldt-Rasmussen, U., and Krogh, J. (2019). Hippocampal volume, cognitive functions, depression, anxiety, and quality of life in patients with cushing syndrome. *J. Clin. Endocrinol. Metab.* 104, 4563–4577. doi:10.1210/jc.2019-00749

Gabbouj, S., Ryhänen, S., Marttinen, M., Wittrahm, R., Takalo, M., Kemppainen, S., et al. (2019). Altered insulin signaling in Alzheimer's disease brain - special emphasis on PI3K-Akt pathway. *Front. Neurosci.* 13, 629. doi:10.3389/fnins.2019.00629

Gage, F. H. (2021). Adult neurogenesis in neurological diseases. *Science* 374, 1049–1050. doi:10.1126/science.abm7468

Grace, P. M., Tawfik, V. L., Svensson, C. I., Burton, M. D., Loggia, M. L., and Hutchinson, M. R. (2021). The neuroimmunology of chronic pain: From rodents to humans. *J. Neurosci.* 41, 855–865. doi:10.1523/JNEUROSCI.1650-20.2020

Gu, M., Jin, J., Ren, C., Chen, X., Gao, W., Wang, X., et al. (2020). Akebia Saponin D suppresses inflammation in chondrocytes via the NRF2/HO-1/NF-κB axis and ameliorates osteoarthritis in mice. *Food Funct.* 11, 10852–10863. doi:10.1039/d0fo01909g

Guo, L. T., Wang, S. Q., Su, J., Xu, L. X., Ji, Z. Y., Zhang, R. Y., et al. (2019). Baicalin ameliorates neuroinflammation-induced depressive-like behavior through inhibition of toll-like receptor 4 expression via the PI3K/AKT/FoxO1 pathway. *J. Neuroinflammation* 16, 95. doi:10.1186/s12974-019-1474-8

Hanslik, K. L., and Ulland, T. K. (2020). The role of microglia and the Nlrp3 inflammasome in alzheimer's disease. *Front. Neurol.* 11, 570711. doi:10.3389/fneur.2020.570711

Hattiangady, B., Kuruba, R., Shuai, B., Grier, R., and Shetty, A. K. (2020). Hippocampal neural stem cell grafting after status epilepticus alleviates chronic epilepsy and abnormal plasticity, and maintains better memory and mood function. *Aging Dis.* 11, 1374–1394. doi:10.14336/AD.2020.1020

Jeong, S. J., Dasgupta, A., Jung, K. J., Um, J. H., Burke, A., Park, H. U., et al. (2008). PI3K/AKT inhibition induces caspase-dependent apoptosis in HTLV-1-transformed cells. *Virology* 370, 264–272. doi:10.1016/j.virol.2007.09.003

Jiang, X., Yi, S., Liu, Q., Su, D., Li, L., Xiao, C., et al. (2022). Asperosaponin VI ameliorates the CMS-induced depressive-like behaviors by inducing a neuroprotective microglial phenotype in hippocampus via PPAR-gamma pathway. *J. Neuroinflammation* 19, 115. doi:10.1186/s12974-022-02478-y

Jurkowski, M. P., Bettio, L., Woo, K. E, Patten, A., Yau, S. Y., and Gil-Mohapel, J. (2020). Beyond the Hippocampus and the SVZ: Adult neurogenesis throughout the brain. *Front. Cell. Neurosci.* 14, 576444. doi:10.3389/fncel.2020.576444

Ke, K., Li, Q., Yang, X., Xie, Z., Wang, Y., Shi, J., et al. (2016). Asperosaponin VI promotes bone marrow stromal cell osteogenic differentiation through the PI3K/AKT signaling pathway in an osteoporosis model. *Sci. Rep.* 6, 35233. doi:10.1038/srep35233

Kempermann, G., Gage, F. H., Aigner, L., Song, H., Curtis, M. A., Thuret, S., et al. (2018). Human adult neurogenesis: Evidence and remaining questions. *Cell. stem Cell.* 23, 25–30. doi:10.1016/j.stem.2018.04.004

Littlefield, A. M., Setti, S. E., Priester, C., and Kohman, R. A. (2015). Voluntary exercise attenuates LPS-induced reductions in neurogenesis and increases microglia expression of a proneurogenic phenotype in aged mice. *J. Neuroinflammation* 12, 138. doi:10.1186/s12974-015-0362-0

Mattei, D., Ivanov, A., Ferrai, C., Jordan, P., Guneykaya, D., Buonfiglioli, A., et al. (2017). Maternal immune activation results in complex microglial transcriptome signature in the adult offspring that is reversed by minocycline treatment. *Transl. Psychiatry* 7, e1120. doi:10.1038/tp.2017.80

Mehdipour, M., Mehdipour, T., Skinner, C. M., Wong, N., Liu, C., Chen, C. C., et al. (2021). Plasma dilution improves cognition and attenuates neuroinflammation in old mice. *GeroScience* 43, 1–18. doi:10.1007/s11357-020-00297-8

Mizuno, Y., Abolhassani, N., Mazzei, G., Sakumi, K., Saito, T., Saido, T. C., et al. (2021). MUTYH actively contributes to microglial activation and impaired neurogenesis in the pathogenesis of Alzheimer's disease. *Oxid. Med. Cell. Longev.* 2021, 8635088. doi:10.1155/2021/8635088

Moreno-Jiménez, E. P., Flor-García, M., Terreros-Roncal, J., Rábano, A., Cafini, F., Pallas-Bazarra, N., et al. (2019). Adult hippocampal neurogenesis is abundant in neurologically healthy subjects and drops sharply in patients with Alzheimer's disease. *Nat. Med.* 25, 554–560. doi:10.1038/s41591-019-0375-9

Moreno-Jiménez, E. P., Terreros-Roncal, J., Flor-García, M., Rábano, A., and Llorens-Martín, M. (2021). Evidences for adult hippocampal neurogenesis in humans. *J. Neurosci.* 41, 2541–2553. doi:10.1523/JNEUROSCI.0675-20.2020

Morgenstern, N. A., Lombardi, G., and Schinder, A. F. (2008). Newborn granule cells in the ageing dentate gyrus. *J. physiology* 586, 3751–3757. doi:10.1113/jphysiol.2008.154807

Niu, Y. T., Xie, L., Deng, R. R., and Zhang, X. Y. (2021). In the presence of TGF-β1, Asperosaponin VI promotes human mesenchymal stem cell differentiation into nucleus pulposus like- cells. *BMC Complement. Med. Ther.* 21, 32. doi:10.1186/s12906-020-03169-y

Pap, R., Pandur, E., Jánosa, G., Sipos, K., Agócs, A., and Deli, J. (2021). *Lutein exerts antioxidant and anti-Inflammatory effects and influences iron utilization of BV-2 microglia*, 10.*Antioxidants (Basel)*

Perea, J. R., Bolós, M., and Avila, J. (2020). Microglia in alzheimer's disease in the context of tau pathology. *Biomolecules* 10, 1439. doi:10.3390/biom10101439

Pilz, G. A., Bottes, S., Betizeau, M., Jörg, D. J., Carta, S., Simons, B. D., et al. (2018). Live imaging of neurogenesis in the adult mouse hippocampus. *Science* 359, 658–662. doi:10.1126/science.aao5056

Puderbaugh, M., and Emmady, P. D. (2022). "Neuroplasticity," in *StatPearls, (FL): StatPearls publishing copyright © 2022* (Treasure Island: StatPearls Publishing LLC.).

Qiao, O., Ji, H., Zhang, Y., Zhang, X., Zhang, X., Liu, N., et al. (2021). New insights in drug development for Alzheimer's disease based on microglia function. *Biomed. Pharmacother.* 140, 111703. doi:10.1016/j.biopha.2021.111703

Qiao, X., Gai, H., Su, R., Deji, C., Cui, J., Lai, J., et al. (2018). PI3K-AKT-GSK3β-CREB signaling pathway regulates anxiety-like behavior in rats following alcohol withdrawal. *J. Affect. Disord.* 235, 96–104. doi:10.1016/j.jad.2018.04.039

Razani, E., Pourbagheri-Sigaroodi, A., Safaroghli-Azar, A., Zoghi, A., Shanaki-Bavarsad, M., and Bashash, D. (2021). The PI3K/Akt signaling axis in alzheimer's disease: A valuable target to stimulate or suppress? *Cell. Stress Chaperones* 26, 871–887. doi:10.1007/s12192-021-01231-3

Santos, L. E., Beckman, D., and Ferreira, S. T. (2016). Microglial dysfunction connects depression and Alzheimer's disease. *Brain Behav. Immun.* 55, 151–165. doi:10.1016/j.bbi.2015.11.011

Sato, K. (2015). Effects of microglia on neurogenesis. *Glia* 63, 1394–1405. doi:10.1002/glia.22858

Shan, X., Chen, J., Dai, S., Wang, J., Huang, Z., Lv, Z., et al. (2020). Cyanidin-related antidepressant-like efficacy requires PI3K/AKT/FoxG1/FGF-2 pathway modulated enhancement of neuronal differentiation and dendritic maturation. *Phytomedicine.* 76, 153269. doi:10.1016/j.phymed.2020.153269

Silva, S. P., Zago, A. M., Carvalho, F. B., Germann, L., Colombo, G. M., Rahmeier, F. L., et al. (2021). Neuroprotective effect of taurine against cell death, glial changes, and neuronal loss in the cerebellum of rats exposed to chronic-recurrent neuroinflammation induced by LPS. *J. Immunol. Res.* 2021, 7497185. doi:10.1155/2021/7497185

Snyder, J. S., Soumier, A., Brewer, M., Pickel, J., and Cameron, H. A. (2011). Adult hippocampal neurogenesis buffers stress responses and depressive behaviour. *Nature* 476, 458–461. doi:10.1038/nature10287

Spalding, K. L., Bergmann, O., Alkass, K., Bernard, S., Salehpour, M., Huttner, H. B., et al. (2013). Dynamics of hippocampal neurogenesis in adult humans. *Cell.* 153, 1219–1227. doi:10.1016/j.cell.2013.05.002

Stepnik, K. (2021). Biomimetic chromatographic studies combined with the computational approach to investigate the ability of triterpenoid saponins of plant origin to cross the blood-brain barrier. *Int. J. Mol. Sci.* 22, 3573. doi:10.3390/ijms22073573

Terreros-Roncal, J., Moreno-Jiménez, E. P., Flor-García, M., Rodríguez-Moreno, C. B., Trinchero, M. F., Cafini, F., et al. (2021). Impact of neurodegenerative diseases on human adult hippocampal neurogenesis. *Science* 374, 1106–1113. doi:10.1126/science.abl5163

Tobin, M. K., Musaraca, K., Disouky, A., Shetti, A., Bheri, A., Honer, W. G., et al. (2019). Human hippocampal neurogenesis persists in aged adults and Alzheimer's disease patients. *Cell. stem Cell.* 24, 974–982.e3. e3. doi:10.1016/j.stem.2019.05.003

Toda, T., Parylak, S. L., Linker, S. B., and Gage, F. H. (2019). The role of adult hippocampal neurogenesis in brain health and disease. *Mol. Psychiatry* 24, 67–87. doi:10.1038/s41380-018-0036-2

Walgrave, H., Balusu, S., Snoeck, S., Vanden Eynden, E., Craessaerts, K., Thrupp, N., et al. (2021). Restoring miR-132 expression rescues adult hippocampal neurogenesis and memory deficits in Alzheimer's disease. *Cell. stem Cell.* 28, 1805–1821.e8. e8. doi:10.1016/j.stem.2021.05.001

Wang, Y., Shen, J., Yang, X., Jin, Y., Yang, Z., Wang, R., et al. (2018). Akebia saponin D reverses corticosterone hypersecretion in an Alzheimer's disease rat model. *Biomed. Pharmacother.* 107, 219–225. doi:10.1016/j.biopha.2018.07.149

Wolf, S. A., Boddeke, H. W., and Kettenmann, H. (2017). Microglia in physiology and disease. *Annu. Rev. Physiol.* 79, 619–643. doi:10.1146/annurev-physiol-022516-034406

Xie, Y., Shi, X., Sheng, K., Han, G., Li, W., Zhao, Q., et al. (2019). PI3K/Akt signaling transduction pathway, erythropoiesis and glycolysis in hypoxia (Review). *Mol. Med. Rep.* 19, 783–791. doi:10.3892/mmr.2018.9713

Xiong, X. Y., Liu, L., and Yang, Q. W. (2016). Functions and mechanisms of microglia/macrophages in neuroinflammation and neurogenesis after stroke. *Prog. Neurobiol.* 142, 23–44. doi:10.1016/j.pneurobio.2016.05.001

Yu, X., Wang, L. N., Du, Q. M., Ma, L., Chen, L., You, R., et al. (2012). Akebia saponin D attenuates amyloid β-induced cognitive deficits and inflammatory response in rats: Involvement of Akt/NF-κB pathway. *Behav. Brain Res.* 235, 200–209. doi:10.1016/j.bbr.2012.07.045

Yu, Z., Gao, J., Zhang, X., Peng, Y., Wei, W., Xu, J., et al. (2022). Characterization of a small-molecule inhibitor targeting NEMO/IKKβ to suppress colorectal cancer growth. *Signal Transduct. Target. Ther.* 7, 71. doi:10.1038/s41392-022-00888-1

Zarate-Garza, P. P., Ortega-Balderas, J. A., Ontiveros-Sanchez de la Barquera, J. A., Lugo-Guillen, R. A., Marfil-Rivera, A., Quiroga-Garza, A., et al. (2021). Hippocampal volume as treatment predictor in antidepressant naïve patients with major depressive disorder. *J. Psychiatr. Res.* 140, 323–328. doi:10.1016/j.jpsychires.2021.06.008

Zhang, H., Yao, S., Zhang, Z., Zhou, C., Fu, F., Bian, Y., et al. (2021). Network pharmacology and experimental validation to reveal the pharmacological mechanisms of liuwei dihuang decoction against intervertebral disc degeneration. *Drug Des. devel. Ther.* 15, 4911–4924. doi:10.2147/DDDT.S338439

Zhang, J., He, H., Qiao, Y., Zhou, T., He, H., Yi, S., et al. (2020b). Priming of microglia with IFN-gamma impairs adult hippocampal neurogenesis and leads to depression-like behaviors and cognitive defects. *Glia* 68, 2674–2692. doi:10.1002/glia.23878

Zhang, J., Rong, P., Zhang, L., He, H., Zhou, T., Fan, Y., et al. (2021b). IL4-driven microglia modulate stress resilience through BDNF-dependent neurogenesis. *Sci. Adv.* 7, eabb9888. doi:10.1126/sciadv.abb9888

Zhang, J., Yi, S., Li, Y., Xiao, C., Liu, C., Jiang, W., et al. (2020c). The antidepressant effects of asperosaponin VI are mediated by the suppression of microglial activation and reduction of TLR4/NF-κB-induced Ido expression. *Psychopharmacology* 237, 2531–2545. doi:10.1007/s00213-020-05553-5

Zheng, R., Zhang, Z. H., Chen, C., Chen, Y., Jia, S. Z., Liu, Q., et al. (2017). Selenomethionine promoted hippocampal neurogenesis via the PI3K-Akt-GSK3β-Wnt pathway in a mouse model of Alzheimer's disease. *Biochem. Biophys. Res. Commun.* 485, 6–15. doi:10.1016/j.bbrc.2017.01.069

Zonis, S., Pechnick, R. N., Ljubimov, V. A., Mahgerefteh, M., Wawrowsky, K., Michelsen, K. S., et al. (2015). Chronic intestinal inflammation alters hippocampal neurogenesis. *J. Neuroinflammation* 12, 65. doi:10.1186/s12974-015-0281-0

frontiers | Frontiers in Pharmacology

TYPE Original Research
PUBLISHED 06 September 2022
DOI 10.3389/fphar.2022.921394

OPEN ACCESS

EDITED BY
Anna Boguszewska-Czubara,
Medical University of Lublin, Poland

REVIEWED BY
Inmaculada Posadas,
University of Castilla-La Mancha, Spain
Sadaf Jahan,
Majmaah University, Saudi Arabia

*CORRESPONDENCE
Chengye Yao,
yao_cheng_ye@163.com
Yun Lin,
franklinyun@hust.edu.cn

†These authors have contributed equally to this work

SPECIALTY SECTION
This article was submitted to Neuropharmacology, a section of the journal Frontiers in Pharmacology

RECEIVED 15 April 2022
ACCEPTED 09 August 2022
PUBLISHED 06 September 2022

CITATION
Wang L, Dai M, Ge Y, Chen J, Wang C, Yao C and Lin Y (2022), EGCG protects the mouse brain against cerebral ischemia/reperfusion injury by suppressing autophagy via the AKT/AMPK/mTOR phosphorylation pathway. *Front. Pharmacol.* 13:921394. doi: 10.3389/fphar.2022.921394

EGCG protects the mouse brain against cerebral ischemia/reperfusion injury by suppressing autophagy *via* the AKT/AMPK/mTOR phosphorylation pathway

Li Wang[1†], Maosha Dai[1†], Yangyang Ge[1†], Jiayi Chen[1], Chenchen Wang[1], Chengye Yao[2*] and Yun Lin[1*]

[1]Department of Anesthesiology, Union Hospital, Tongji Medical College, Huazhong University of Science and Technology, Wuhan, China, [2]Department of Neurology, Union Hospital, Tongji Medical College, Huazhong University of Science and Technology, Wuhan, China

Stroke remains one of the leading reasons of mortality and physical disability worldwide. The treatment of cerebral ischemic stroke faces challenges, partly due to a lack of effective treatments. In this study, we demonstrated that autophagy was stimulated by transient middle cerebral artery occlusion/reperfusion (MCAO/R) and oxygen-glucose deprivation/reoxygenation (OGD/R). Treatment with (–)-epigallocatechin-3-gallate (EGCG), a bioactive ingredient in green tea, was able to mitigate cerebral ischemia/reperfusion injury (CIRI), given the evidence that EGCG administration could reduce the infarct volume and protect poststroke neuronal loss in MCAO/R mice *in vivo* and attenuate cell loss in OGD/R-challenged HT22 cells *in vitro* through suppressing autophagy activity. Mechanistically, EGCG inhibited autophagy *via* modulating the AKT/AMPK/mTOR phosphorylation pathway both *in vivo* and *in vitro* models of stroke, which was further confirmed by the results that the administration of GSK690693, an AKT/AMPK inhibitor, and rapamycin, an inhibitor of mTOR, reversed aforementioned changes in autophagy and AKT/AMPK/mTOR signaling pathway. Overall, the application of EGCG relieved CIRI by suppressing autophagy *via* the AKT/AMPK/mTOR phosphorylation pathway.

KEYWORDS

(–)-epigallocatechin-3-gallate (EGCG), autophagy, cerebral ischemia/reperfusion injury (CIRI), middle cerebral artery occlusion/reperfusion (MCAO/R), oxygen-glucose deprivation/reoxygenation (OGD/R), HT22 cell, AKT/AMPK/mTOR pathway

Introduction

The world is facing an epidemic of stroke. Of all strokes, cerebral ischemic stroke (CIS) accounts for almost 87% (Virani et al., 2021) with a high risk of mortality and severe long-term disability, placing an increasing economic burden on family and society (Feigin et al., 2018). Tissue plasminogen activator (tPA) is the only supported pharmacological thrombolytic medicine because of its ability to recanalize arteries and improve clinical

outcomes (National Institute of Neurological Disorders and Stroke rt-PA Stroke Study Group, 1995). Restoration of the blood supply into the ischemic stroke region may also induce cerebral ischemia/reperfusion injury (CIRI) (Lim et al., 2021). Moreover, only a shortage of patients with CIS benefits from tPA treatment due to the narrow therapeutic time window, tendency to transform into a hemorrhage, and other side effects (Bansal et al., 2013; Yeo et al., 2013; Bhaskar et al., 2018). Thus, there is a compelling need to explore more effective therapies to promote ischemic tissue recovery and ameliorate patient prognosis after stroke.

In the pathophysiological process of stroke, several types of neuronal death can be triggered, involving autophagy, apoptosis, necrosis, necroptosis, and pyroptosis (He et al., 2020). Among them, autophagy has been extensively studied in CIRI over the past decades. As a regulated intracellular degradation process, autophagy is demonstrated to maintain normal cellular functions and cellular homeostasis and is involved in some neurodegenerative diseases by degrading and recycling dysfunctional or damaged organelles or proteins (Srivastava et al., 2017; Wang P. et al., 2018; Zhang et al., 2019). Basal autophagic activity exists in cells under physiological conditions, while the process turns more active induced by various stress events including CIRI and plays complex roles (Wirawan et al., 2012). Some studies demonstrated that the activation of autophagy ameliorated CIRI (Sun et al., 2020b; Xu et al., 2020; Zhang B. et al., 2020; Chen et al., 2021; Jin et al., 2021; Yihao et al., 2021; Zha et al., 2021), while more research supported that the inhibition of autophagy activation exerted a neuroprotective effect in brain stroke (Sun et al., 2020a; Zhang et al., 2020b; Li and Huang, 2020; Mei et al., 2020; Shi et al., 2020; Wang L. et al., 2020; Gu et al., 2021; Liu N. et al., 2021; Shao et al., 2021; Wang C. et al., 2021; Xu et al., 2021; Yao et al., 2021; Zhang et al., 2021; Zhao et al., 2021). Obviously, the controversial dual role of the induction of autophagy in the ischemic brain is still a hot topic in research and remains to be further investigated.

There is a growing focus on treating stroke with natural medicines (Jahan et al., 2018), which could assist the body to regain and retain internal balance by providing external stimuli (Tao et al., 2020). Green tea is a celebrated traditional herbal medicine and is popular in the world, with many potentially beneficial effects on human health for its anti-cancer and anti-inflammatory properties (Saeed et al., 2017; Musial et al., 2020). (−)-Epigallocatechin-3-gallate (EGCG) is the most abundant and active polyphenol, accounting for 50%–80% of all catechins, and is believed to make a major contribution to the various benefits of green tea (Prasanth et al., 2019). Accumulating evidence suggested that EGCG conferred a neuroprotective effect in the acute and delayed states of stroke (Han et al., 2014; Zhang et al., 2015; You, 2016; Bai et al., 2017; Wang and You, 2017; Zhang et al., 2017; Park et al., 2020). The effect of EGCG on autophagy has been described in myocardial ischemia/reperfusion injury (MIRI) (Xuan and Jian, 2016; Zhang C. et al., 2020; Liu P. et al., 2021) and some other diseases (Musial et al., 2021; Du et al., 2022; Wang et al., 2022). However, it is not clear whether EGCG ameliorates CIRI through modulating autophagy, which needs to be elucidated. Moreover, there is a long way to go to translate the success of EGCG in animal research to humans. Thus, more consideration should be taken to further elucidate the detailed mechanisms by which EGCG exerts a neuroprotective effect on stroke.

Herein, we investigated the potential effect of EGCG on neuronal injury and autophagy activation. The present results indicated that EGCG exerted a protective effect on ischemic injury through the suppression of autophagy, which was induced by MCAO/R models of mice *in vivo* and OGD/R models of HT22 cells *in vitro*. In addition, the AKT/AMPK/mTOR phosphorylation pathway might be related to the inhibitory influence of EGCG on autophagy activation, which remains to be elucidated.

Materials and methods

Reagents

EGCG, anti-LC3B antibody, and anti-NeuN antibody were purchased from Sigma-Aldrich (USA). Donkey anti-mouse IgG secondary antibody was obtained from Life Technologies (Thermo Fisher Scientific, United States). Phosphor-AKT (p-AKT), AKT, p-AMPK, AMPK, p-mTOR, mTOR, beclin1, β-actin, and GAPDH were obtained from ABclonal Technology Co., Ltd. (China). P62/SQSTM1 polyclonal antibody was obtained from Proteintech (China). Horseradish peroxidase (HRP)-conjugated secondary antibody was obtained from Cell Signaling Technology (United States). GSK690693, rapamycin, and LY294002 were obtained from MedChemExpress (United States). Fetal bovine serum (FBS) and 4′,6-diamidino-2-phenylindole (DAPI) were purchased from Gibco (Thermo Fisher Scientific, United States). The antifade mounting medium was obtained from Solarbio (China). RIPA lysis buffer was obtained from Beyotime (China). Protease and phosphatase inhibitor cocktails and NcmBlot blocking buffer were obtained from New Cell and Molecular Biotech (China). BCA protein assay kit was obtained from CWBIO (China). Cell Counting Kit-8 (CCK8) and ECL chemiluminescent HRP substrate A&B were obtained from Antgene (China). All other reagents, unless stated otherwise, were obtained from Biosharp (China).

Experimental animals and treatments

Adult male wild-type (WT) C57BL/6 mice were obtained from Beijing Weitong Lihua Experimental Animal Technical Co.,

Ltd., China. Throughout the experiment, the mice were kept in the SPF conditions in the Laboratory Animal Center, having food and water freely and avoiding sound and light stimulation. MCAO/R model was established as our previous protocols (Ge et al., 2022). After anesthetizing intraperitoneally (i.p.) in mice (8–12 weeks old, 23–26 g), a 6–0 silicone-coated nylon monofilament was used to obstruct the origin of the MCA to induce focal cerebral ischemia and establish MCAO model. Reperfusion was achieved by gently withdrawing the monofilament after 1 h of occlusion. Body temperature was sustained at 37 ± 0.5°C with an electric blanket until the mice had recovered from surgery. After waking from anesthesia, mice were housed in their cages with conditions as before. Sham group mice underwent the same surgical procedures as MCAO/R models without the obstruction of MCA. The experiment was approved by the Institutional Animal Care and Use Committee at Tongji Medical College, Huazhong University of Science and Technology.

Experimental groups were distributed randomly. Reagents were injected slowly (0.1 μl/min) into the right ventricle (1.5 mm laterally, 0.6 mm posteriorly, 3.1 mm deep from the anterior fontanelle). Mice were randomly divided into seven groups: 1) Sham group: mice received a surgical operation without MCAO/R; 2) MCAO/R group: mice received MCAO/R; 3) MCAO/R + vehicle group: mice were subjected to MCAO/R followed by vehicle (4 μl) injection 1 h later; 4) MCAO/R + EGCG group: mice were subjected to MCAO/R followed by EGCG (1 μg/μl, 4 μl) injection 1 h later; 5) vehicle + MCAO/R + EGCG group: the vehicle (4 μl) was injected 10 min before MCAO/R, followed by EGCG (1 μg/μl, 4 μl) injection 1 h later; 6) GSK690693 + MCAO/R + EGCG group: GSK690693 (10 μM, 4 μl) was injected 10 min before MCAO/R, followed by EGCG (1 μg/μl, 4 μl) injection 1 h later; and 7) rapamycin + MCAO/R + EGCG group: rapamycin (10 μM, 4 μl) was injected 10 min before MCAO/R, followed by EGCG (1 μg/μl, 4 μl) injection 1 h later.

Cell culture and treatments

HT22 cells were cultured in Dulbecco's modified Eagle's medium (DMEM) with glucose, added with 10% FBS and 1% penicillin–streptomycin solution at 37°C in 95% air and 5% CO_2. To simulate CIS *in vitro*, HT22 cells were challenged by OGD/R. In brief, HT22 cells were cultured in DMEM with no glucose and FBS at 37°C in 1% O_2, 5% CO_2, and 94% N_2 for 12 h and then reoxygenated in the aforementioned normal growth environment. Vehicle and EGCG (20 μM) were added to HT22 cells at the time of reoxygenation and incubated for 2 and 4 h. LY294002 (25 μM), GSK690693 (25 μM), and rapamycin (25 μM) were added into HT22 cells at 0.5 h before the administration of EGCG and incubated for 2 h.

2, 3, 5-Triphenyltetrazolium chloride (TTC) staining

On post-surgery day (PSD) 1, infarct volume was assessed by TTC staining. Mice were anesthetized and then killed by the cervical dislocation method. The brains were dissected carefully and rapidly and refrigerated for 20 min at −20°C. After that, each brain was cut coronally into 2-mm-thick thin slices. And slices were put into a 6-well plate and immersed in 2% TTC for 15 min at 37°C. Gentle stirring ensured even staining exposure. Viable brain tissue was stained into deep red by TTC staining, while infarcted tissues kept the original pale color. Slices were fixed in 4% paraformaldehyde in phosphate buffer overnight and then recorded with pictures. An ImageJ analysis system (Version: 2.1.0) was used to quantify the infarct volume and total brain volume. The cerebral infarct volume was calculated as the percentage of the infarcted tissue volume to the total brain tissue volume.

Immunofluorescence staining

On PSD 1, total brain tissues were firstly perfused with saline solution, and then replaced the saline with 4% paraformaldehyde in phosphate buffer and continued perfusing. Afterward, the brains were dissected quickly and then fixed in 4% paraformaldehyde overnight at 4°C. Going through dehydration, transparency, waxing, and embedding successively, the fixed brains were then sliced into 4-μm-thick coronal slices. After dewaxed and antigen repaired at high temperature and high pressure, the sections were incubated in 10% donkey serum at room temperature for 20 min; next, the sections were incubated with primary antibodies, light chain 3 (LC3) antibody (1:200), and NeuN antibody (1:100), overnight at 4°C. After washing with phosphate-buffered saline (PBS) three times, slices were treated with donkey anti-mouse IgG secondary antibody (1:400) at room temperature in a dark place for 30 min, and next washed with PBS three times. DAPI was used to counterstain nuclei. The sections were finally observed and pictured under fluorescence photography and then analyzed by utilizing ImageJ software.

Western blotting assay

The Western blotting assay was completed as our previous protocols (Ge et al., 2022). After the homogenization of the ischemic brain tissue, the BCA Protein Assay Kit was used to quantify the protein concentration of samples and then adjusted the protein concentration to 2 μg/μl with the RIPA lysis buffer. Proteins were analyzed by sodium dodecyl sulfate-polyacrylamide gel electrophoresis (SDS-PAGE) and turned

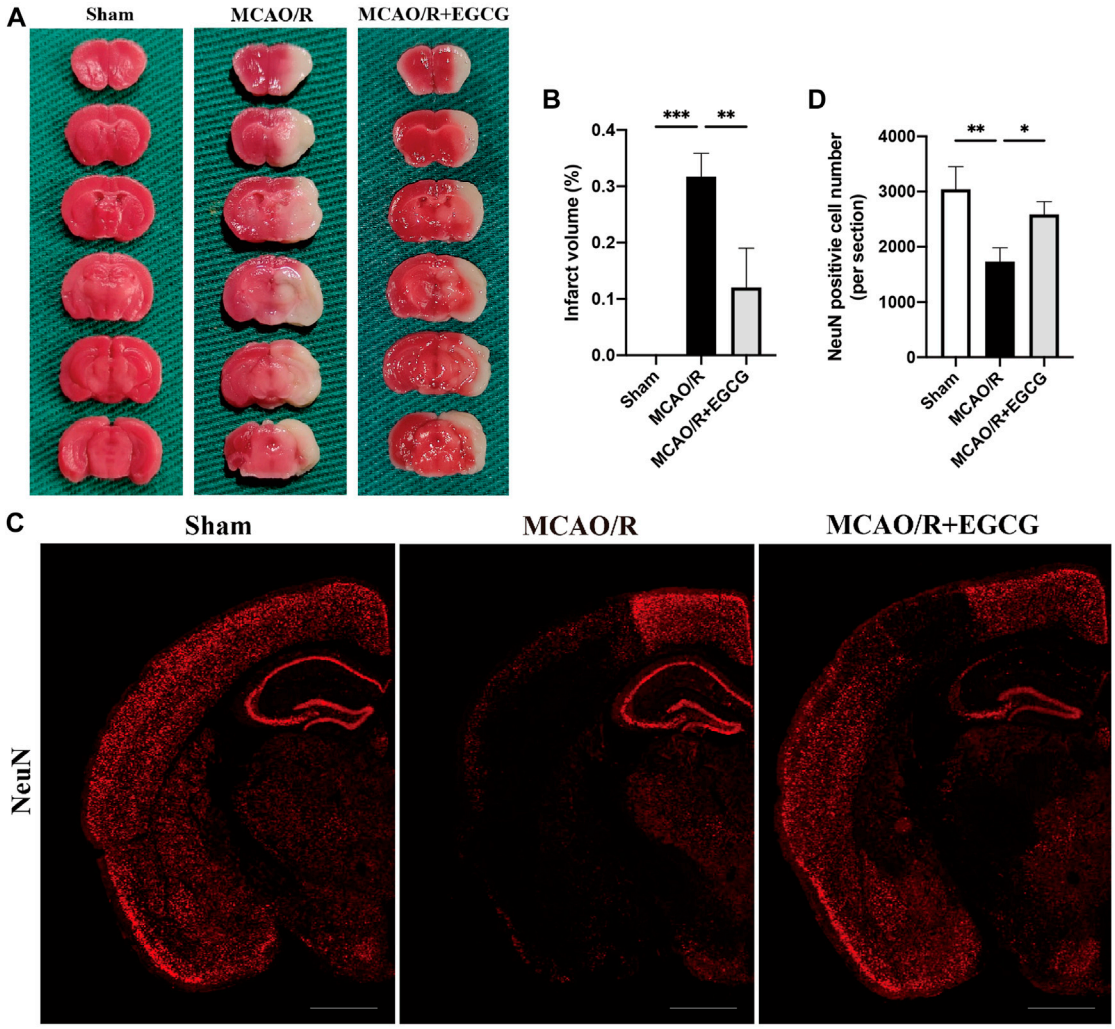

FIGURE 1
EGCG treatment mitigated cerebral ischemia/reperfusion injury (CIRI) in the mice model of middle cerebral artery occlusion/reperfusion (MCAO/R). **(A,B)** 2, 3, 5-Triphenyltetrazolium chloride (TTC) staining assay was performed to evaluate the infarct volume. **(C,D)** Immunofluorescent staining for NeuN. Data were shown in the semi-brain from the ipsilateral side of surgery on post-surgery day (PSD) 1 (scale bar = 1,000 μm). Each experimental datum was presented as mean ± standard deviation (n = 3 animals per group). *p < 0.05, **p < 0.01, ***p < 0.001 versus the specified group.

onto PVDF membranes. After blocking with an NcmBlot blocking buffer for 20 min, the membranes are incubated with primary antibodies, phosphor-AKT (p-AKT) (1:1,000), AKT (1:1,000), p-AMPK (1:1,000), AMPK (1:1,000), p-mTOR (1:1,000), mTOR (1:1,000), p62 (1:1,000), LC3 (1:1,000), beclin1 (1:1,500) β-actin (1:5,000), and GAPDH (1:5,000) overnight at 4°C. After washing, the membranes were incubated with the corresponding horseradish peroxidase (HRP)-conjugated secondary antibody (1:5,000) for 1.5 h at room temperature. Chemiluminescence detection was carried out with ECL chemiluminescent HRP substrate A&B and captured through an imager machine. Band optical intensity was quantified with ImageJ software.

Cell viability assay

The cell viability of HT22 cells was assessed with a cell counting kit (CCK-8) by the manufacturer's protocols.

Statistical analysis

Multiple comparisons were performed by a one-way analysis of variance (ANOVA) followed by Tukey's multiple comparison tests for multiple comparisons (GraphPad Prism statistics software version 9.0.2, La Jolla, CA, United States). A p-value of <0.05 was considered statistically significant.

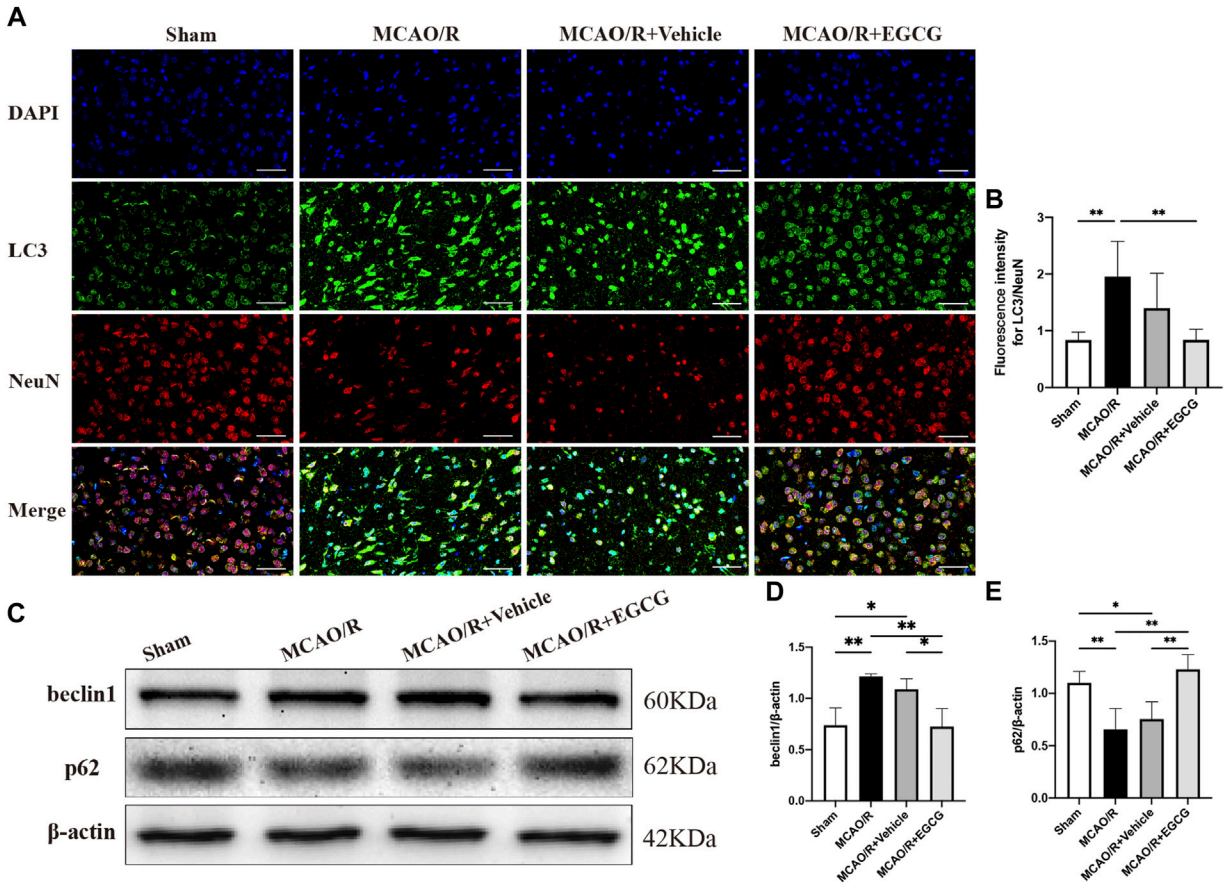

FIGURE 2
EGCG inhibited middle cerebral artery occlusion/reperfusion (MCAO/R)-induced autophagy. **(A,B)** The expression of LC3 was detected by immunofluorescent staining assay. Data were shown in the cortical penumbra area from the ipsilateral side of surgery on post-surgery day (PSD) 1 (scale bar = 20 μm). **(C)** The expression of beclin1 **(D)** and p62 **(E)** was assessed by western blotting assay. Each experimental datum was presented as mean ± standard deviation (n = 3 animals per group). *$p < 0.05$, **$p < 0.01$ versus the specified group.

Results

EGCG mitigated CIRI in MCAO/R mice

To determine the neuroprotective capacity of EGCG in stroke, TTC staining was conducted to evaluate the volume of infarction on PSD 1. TTC staining results showed that, compared with the sham group, the volume of infarction in the MCAO/R group was larger obviously, suggesting a severe brain ischemia injury, whereas administration with EGCG 1 h after reperfusion evidently decreased the infarct volume of MCAO/R mice (Figures 1A,B), indicating that treatment with EGCG relieved brain stroke injury in mice, which was similar to the previous research (Choi et al., 2004; Han et al., 2014; Zhang et al., 2015; Park et al., 2020).

In addition, to further verify the neuroprotective role of EGCG in stroke, immunofluorescent staining for the level of NeuN was conducted to evaluate neuron loss on PSD 1 (Wang H.-K. et al., 2021). As presented in Figures 1C,D, a semi-brain section screening was used, and the results showed that ischemia intrusion distinctly reduced the number of cells with immunoreactive NeuN, and this result was prevented by EGCG administration, indicating that EGCG treatment protected poststroke neuronal loss, which was consistent with the TTC results (Figures 1A,B). Thus, these data suggested that EGCG owned a neuroprotective potential in mice challenged with MCAO/R.

EGCG mitigated CIRI through attenuating autophagy

After confirming the protective potential of EGCG in MCAO/R mice, the autophagic activity after stroke and the effect of EGCG on MCAO/R-induced autophagy were then examined by

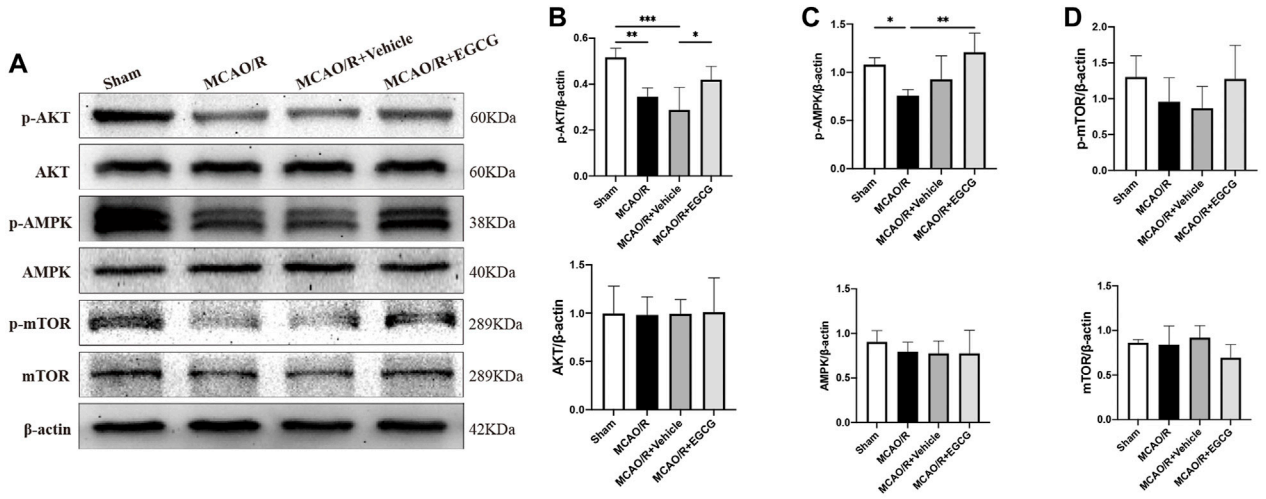

FIGURE 3
EGCG modulated the AKT/AMPK/mTOR phosphorylation pathway in middle cerebral artery occlusion/reperfusion (MCAO/R) mice. **(A)** The expression of p-AKT and AKT **(B)**, p-AMPK and AMPK **(C)**, p-mTOR and mTOR **(D)** was assessed by Western blotting assay. Each experimental datum was presented as mean ± standard deviation (n = 3 animals per group). *p < 0.05, **p < 0.01, ***p < 0.001 versus the specified group.

evaluating the expression of autophagy-associated proteins, LC3, beclin1, and p62. The expression of LC3, a specific marker for autophagy, was measured by immunofluorescent staining. As shown in Figures 2A,B, in comparison with the sham group, the expression of LC3 protein in the cortical penumbra area markedly increased after stroke, while EGCG administration considerably attenuated MCAO/R-induced increase in the LC3 level. Meanwhile, beclin1 and p62 protein levels were evaluated by Western blotting assay. As illustrated in Figures 2C–E, compared with the sham group, the expression level of beclin1 significantly increased on PSD 1, while the elevated expression of beclin1 induced by MCAO/R was prevented by EGCG treatment. In addition, the p62 level decreased after stroke, and the MCAO/R-induced down-regulated expression of p62 was also prevented by EGCG administration. The above results indicated that autophagy was activated by stroke, and EGCG was able to counteract the activation of poststroke autophagy to exert a neuroprotective effect.

EGCG modulated the AKT/AMPK/mTOR phosphorylation pathway in CIRI

To explore the potential molecular mechanisms of EGCG in stroke, we determined the effect of EGCG on AKT, p-AKT, AMPK, p-AMPK, mTOR, and p-mTOR in the ischemic hemisphere brain tissue by Western blotting assay. As shown in Figure 3, in comparison with the sham group, the expression of p-AKT, p-AMPK, and p-mTOR was remarkably reduced on PSD 1, whereas treatment with EGCG prevented MCAO/R caused the reduced level of p-AKT, p-AMPK, and p-mTOR. And AKT, AMPK, and mTOR had no change. These findings suggested that the AKT/AMPK/mTOR phosphorylation pathway was involved in the underlying mechanisms of EGCG to exert a neuroprotective effect in stroke.

GSK690693 and rapamycin reversed the effect of EGCG on ischemic brain tissue

GSK690693, an AKT/AMPK inhibitor (Rhodes et al., 2008; Levy et al., 2009; Altomare et al., 2010), and rapamycin, the inhibitor of mTOR (Edwards and Wandless, 2007), were used to further confirm that phosphorylated AKT, AMPK, and mTOR participated in the anti-autophagy effect of EGCG to protect against ischemic brain damage. As illustrated in Figures 4A–D and Supplementary Figure S1, administration with GSK690693 and rapamycin prevented EGCG-induced elevated levels of p-AKT, p-AMPK, and p-mTOR in MCAO/R mice. And AKT, AMPK, and mTOR had no change. These data verified the reversing effect of GSK690693 on p-AKT, p-AMPK, and rapamycin on p-mTOR in MCAO/R models applicated with EGCG.

After p-AKT, p-AMPK, and p-mTOR were blocked by inhibitors in MCAO/R mice treated with EGCG, autophagy-related proteins were measured. LC3 was measured by immunofluorescence staining. As presented in Figures 4E,G, the EGCG treatment-induced down-regulated expression of LC3 level in MCAO/R mice was prevented by rapamycin

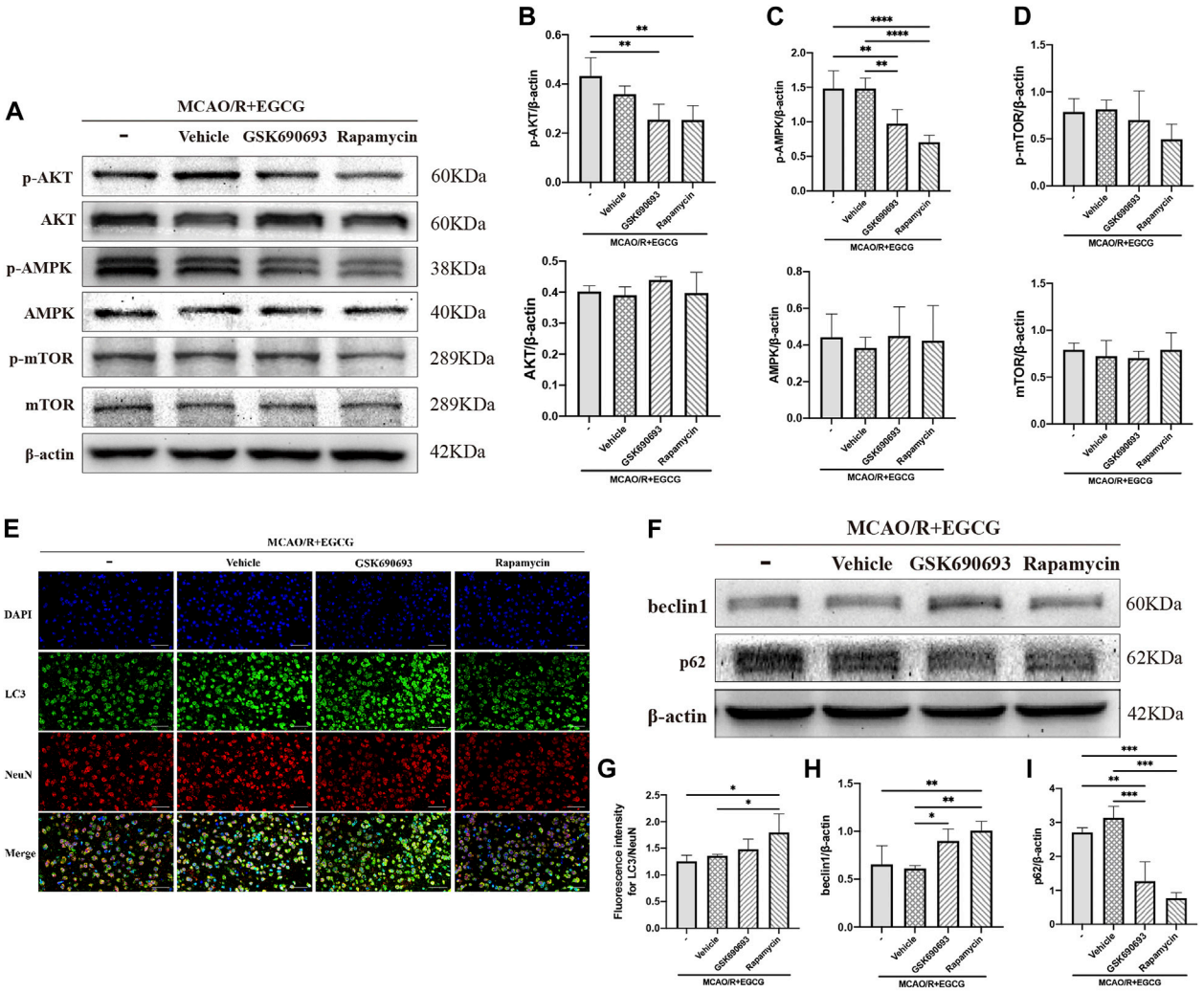

FIGURE 4
GSK690693 and rapamycin reversed the effect of EGCG in the ischemic brains of middle cerebral artery occlusion/reperfusion (MCAO/R) mice. **(A)** The expression of p-AKT and AKT **(B)**, p-AMPK and AMPK **(C)**, p-mTOR and mTOR **(D)** was assessed by Western blotting assay. **(E,G)** The expression of LC3 was detected by immunofluorescent staining assay. Data were shown in the cortical penumbra area from the ipsilateral side of surgery on post-surgery day (PSD) 1. **(F)** The expression of beclin1 **(H)** and p62 **(I)** was assessed by Western blotting assay (scale bar = 20 μm). Each experimental datum was presented as mean ± standard deviation (n = 3 animals per group). *p < 0.05, **p < 0.01, ***p < 0.001, ****p < 0.0001 versus the specified group.

and GSK690693 precondition. In addition, beclin1 and p62 were measured by Western blotting assay. As illustrated in Figures 4F,H,I and Supplementary Figure S1, both GSK690693 and rapamycin precondition were able to prevent the EGCG-induced decreased expression of beclin1 and the increased expression of p62 level in MCAO/R models. Accordingly, these data favored the point that autophagy-related proteins could be influenced after the AKT/AMPK/mTOR phosphorylation pathway was inhibited, further indicating that EGCG inhibited MCAO/R-induced autophagy in the AKT/AMPK/mTOR phosphorylation-dependent manner.

EGCG protected HT22 cells from OGD/R-challenged damage

After OGD/R invasion, immunofluorescent staining for NeuN was examined to confirm the protective role of EGCG on HT22 cells challenged by OGD/R. As presented in Figures 5A,C, the OGD/R challenge markedly reduced the number of HT22 cells with immunoreactive NeuN, but this effect was prevented by EGCG treatment, and the number of HT22 cells with immunoreactive NeuN was more in 4 h than in 2 h of EGCG incubation. Figures 5B,D show the cell pictures in different groups, and the number of HT22 cells was assessed by ImageJ software. And Figures 5B,D also

10.3389/fphar.2022.921394

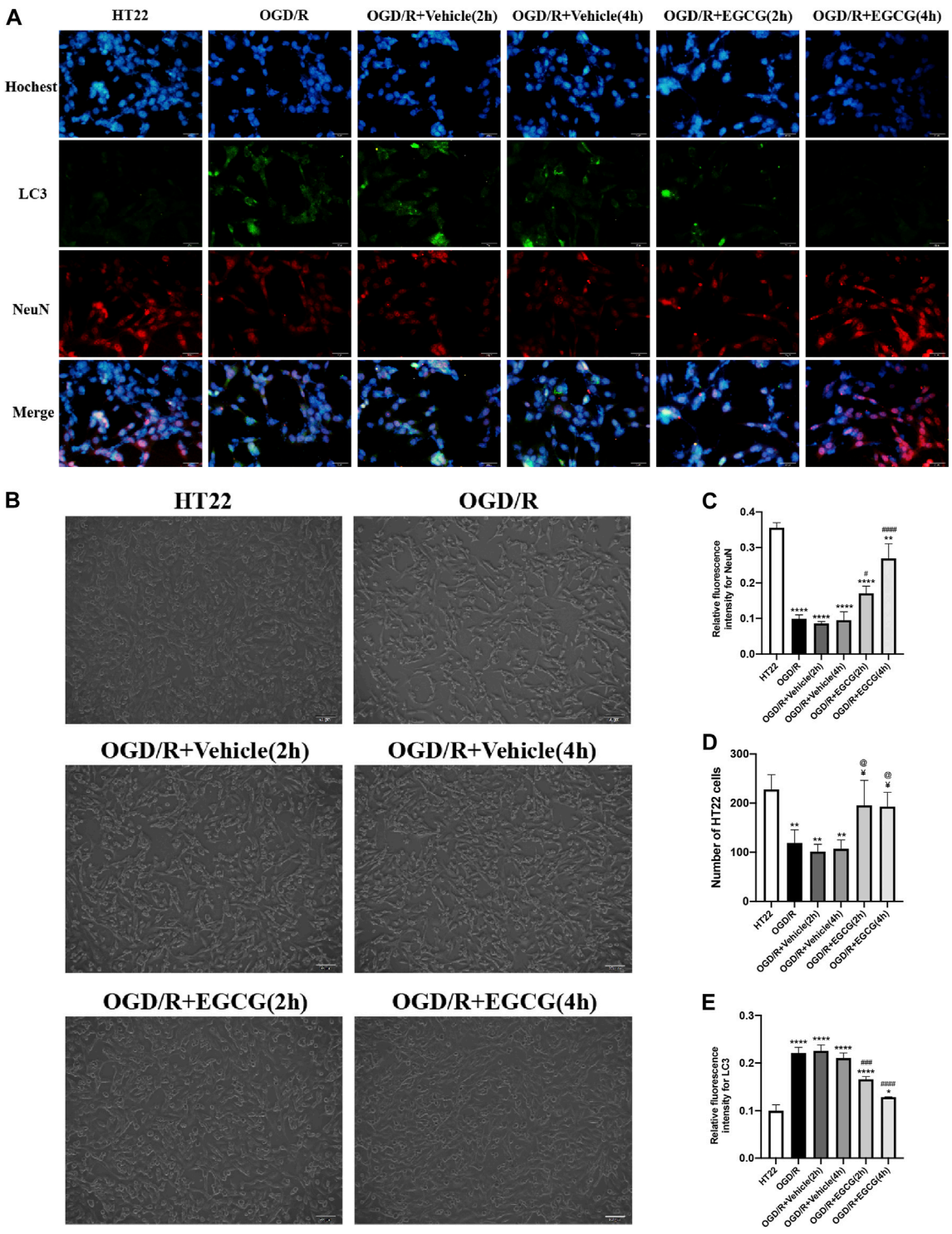

FIGURE 5
EGCG protected HT22 cells from oxygen-glucose deprivation/reoxygenation (OGD/R) damage. **(A)** Immunofluorescent staining for NeuN **(C)** and LC3 **(E)** (scale bar = 50 μm). **(B,D)** The number of HT22 cells in different groups. Each experimental datum was presented as mean ± standard deviation (n = 3 per group). *p < 0.05, **p < 0.01, ****p < 0.0001 versus HT22 group, #p < 0.05, ###p < 0.001, ####p < 0.0001 versus OGD/R group, ¥ p < 0.05 versus OGD/R + Vehicle (2 h) group, @p < 0.05 versus OGD/R + vehicle (4 h) group.

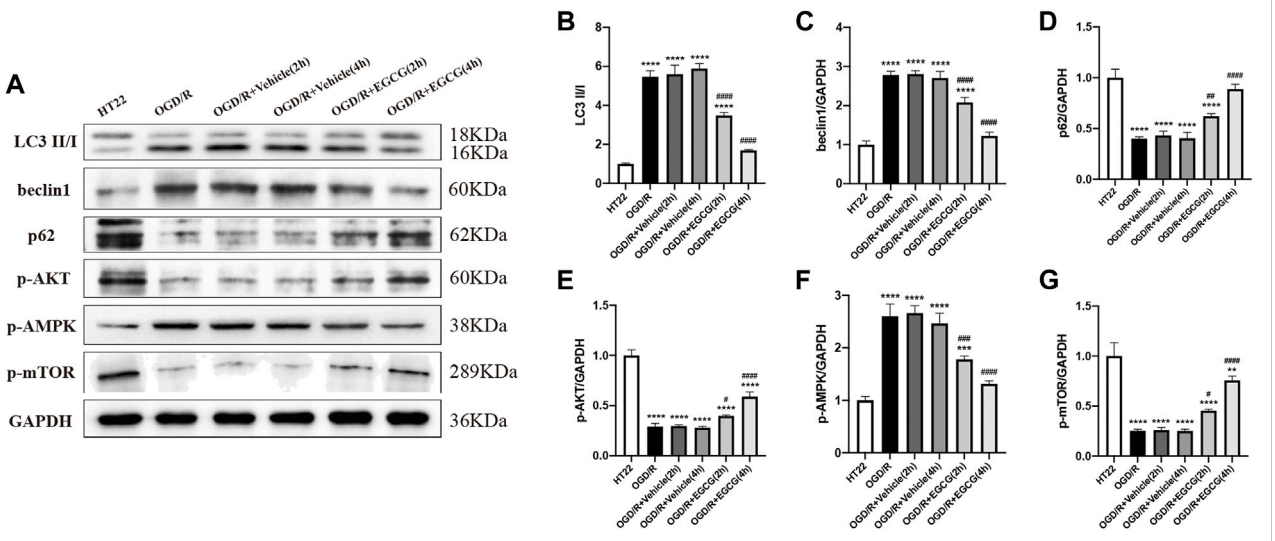

FIGURE 6
EGCG suppressed autophagy and modulated the AKT/AMPK/mTOR phosphorylation pathway in oxygen-glucose deprivation/reperfusion (OGD/R)-challenged HT22 cells. **(A)** The expression of LC3 II/I **(B)**, beclin1 **(C)**, p62 **(D)**, p-AKT **(E)**, p-AMPK **(F)**, and p-mTOR **(G)** was assessed by Western blotting assay. Each experimental datum was presented as mean ± standard deviation (n = 3 per group). $^{**}p < 0.01$, $^{***}p < 0.001$, $^{****}p < 0.0001$ versus HT22 group, $\#p < 0.05$, $\#\#p < 0.01$, $\#\#\#p < 0.001$, $\#\#\#\#p < 0.0001$ versus OGD/R group.

support the protective effect of EGCG on HT22 cells, which is in accordance with Figures 5A,C. Thus, these results supported the ability of EGCG in protecting HT22 cells from the OGD/R challenge, which was consistent with the results *in vivo* (Figures 1C,D), and the efficacy of EGCG might be positively related to the time of incubation.

EGCG suppressed OGD/R-induced autophagy to protect HT22 cells

Autophagy-related proteins were examined to investigate the autophagic activity after OGD/R and the role of EGCG on OGD/R-induced autophagy in HT22 cells. As shown in Figures 5A,E, 6A–D, the LC3 level and beclin1 level increased and p62 level decreased after OGD/R, suggesting that OGD/R led to autophagic activation in HT22 cells. In addition, the OGD/R invasion-induced up-regulated expression of LC3 and beclin1 and down-regulated expression of p62 were prevented by EGCG treatment, which was in accordance with the results *in vivo* (Figures 2A–E). Moreover, the preventing effects of EGCG on these autophagic proteins were more evident in 4 h than in 2 h of incubation time. Accordingly, these results suggested that EGCG substantially inhibited the autophagic activity to protect HT22 cells against OGD/R damage.

EGCG regulated the AKT/AMPK/mTOR phosphorylation pathway in OGD/R-challenged HT22 cells

To confirm the molecular mechanisms by which EGCG exerted a protective effect on OGD/R-damaged HT22 cells, p-AKT, p-AMPK, and p-mTOR were determined by Western blotting assay. As presented in Figures 6A,E–G, the expressions of p-AKT level and p-mTOR level were remarkably reduced after OGD/R, and treatment with EGCG prevented the OGD/R-induced down-regulated expression of p-AKT and p-mTOR, which were consistent with animal results (Figures 3A,B,D). In comparison, after OGD/R invasion, p-AMPK was considerably increased, and EGCG treatment prevented the elevated expression of p-AMPK induced by OGD/R, which was inconsistent with animal results (Figures 3A,C). And the preventing effects of EGCG on these proteins of the pathway were more evident in 4 h than in 2 h of incubation time. Therefore, the above data indicated that the underlying mechanisms by which EGCG protected HT22 cells from OGD/R were related to the AKT/AMPK/mTOR phosphorylation pathway.

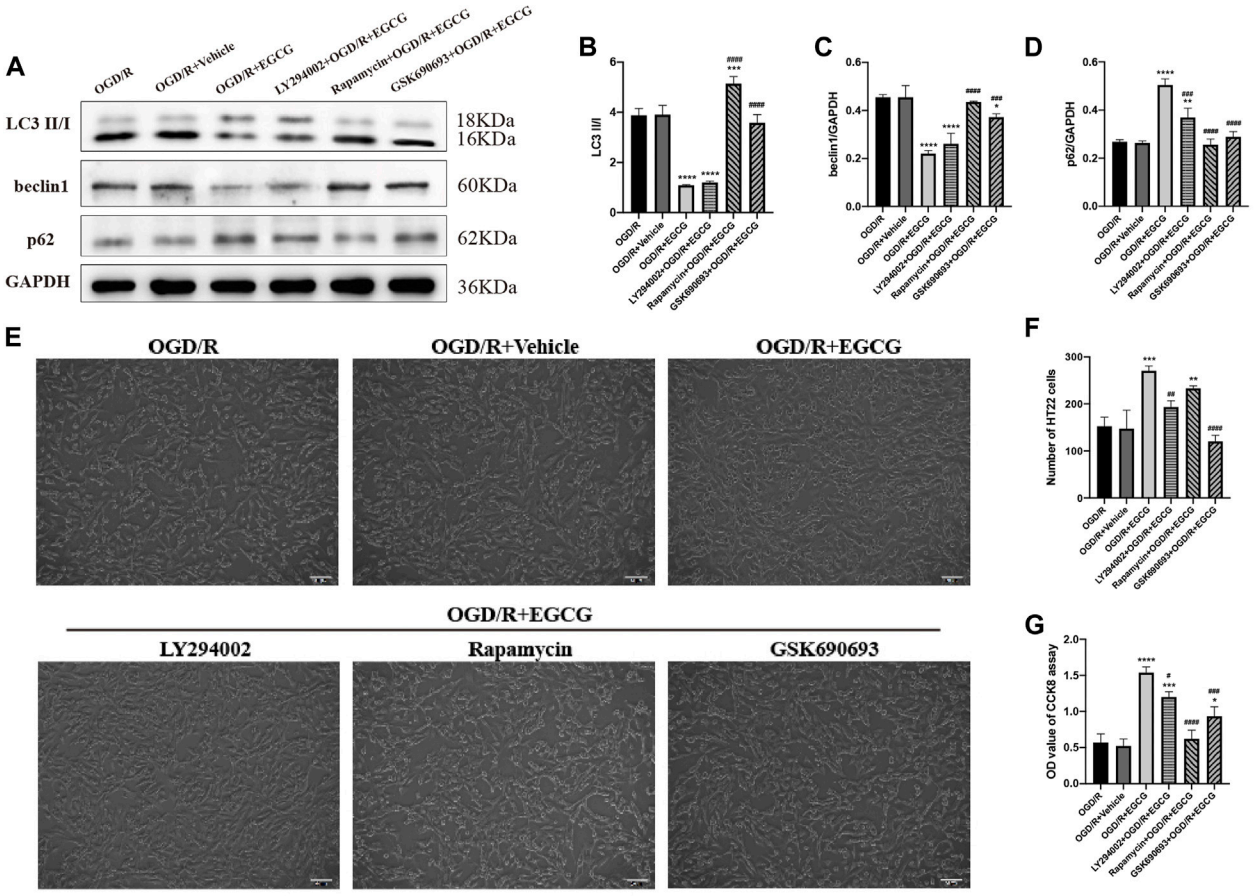

FIGURE 7
LY294002, GSK690693, and rapamycin reversed the effect of EGCG in HT22 cells challenged by oxygen-glucose deprivation/reperfusion (OGD/R). **(A)** The expression of LC3 II/I **(B)**, beclin1 **(C)**, and p62 **(D)** was assessed by Western blotting assay. **(E)** The number **(F)** and cell viability **(G)** of HT22 cells in different groups. Each experimental datum was presented as mean ± standard deviation (n = 3 per group). *p < 0.05, **p < 0.01, ***p < 0.001, ****p < 0.0001 versus OGD/R group, #p < 0.05, ##p < 0.01, ###p < 0.001, ####p < 0.0001 versus OGD/R + EGCG group.

GSK690693 and rapamycin reversed the effect of EGCG on OGD/R-challenged HT22 cells

To further confirm that the phosphorylated AKT, AMPK, and mTOR were required for the anti-autophagy effect of EGCG to exert the protective effect in OGD/R models, we added LY294002, GSK690693, and rapamycin to OGD/R-challenged HT22 cells, respectively, followed by treatment with EGCG. Autophagy-associated proteins were then examined by Western blotting assay. As shown in Figures 7A–D, the EGCG treatment-induced down-regulated expression of LC3 and beclin1 and the up-regulated expression of p62 in OGD/R models were prevented by GSK690693 and rapamycin precondition. In addition, the LY294002 precondition was able to prevent the EGCG treatment-induced increased expression of p62 in OGD/R models, while the effect of LY294002 on LC3 and beclin1 was not statistically significant. Figures 7E–G also show that the protective effect of EGCG on OGD/R-challenged HT22 cells can be weakened by LY294002, GSK690693, and rapamycin precondition. Accordingly, these data suggested that autophagy-related proteins could be influenced after the AKT/AMPK/mTOR phosphorylation pathway was inhibited, which was in accordance with animal experiments (Figures 4E–I), further indicating that EGCG inhibited the OGD/R-induced autophagy of HT22 cells in an AKT/AMPK/mTOR phosphorylation-dependent manner.

Discussion

Stroke is largely related to disability and death all around the world. Neuron destruction is usually found in stroke, involving autophagy. Herein, we examined the role of EGCG on ischemic

injury in MCAO/R models of mice and OGD/R models of HT22 cells. The results supported the point that EGCG protected neurons against ischemic injury both *in vivo* and *in vitro*. Furthermore, the neuroprotective effect of EGCG to ameliorate stroke was associated with the suppression of autophagic activation. In terms of molecular mechanisms, EGCG modulated autophagic activity via the AKT/AMPK/mTOR phosphorylation pathway. In summary, EGCG exerted a neuroprotective effect by suppressing autophagy in an AKT/AMPK/mTOR phosphorylation-dependent manner.

Autophagy is a highly regulated process, participating in multiple pathophysiological processes of many diseases (Wirawan et al., 2012). Mounting evidence has suggested that autophagy activation participated in ischemic stroke closely and exerted divergent roles in stroke's pathological and physiological changes (Sheng and Qin, 2015). The research by Sun et al. (2020b) indicated that eugenol, an active ingredient extracted from traditional herbal medicine, played a neuroprotective role by the enhancement of autophagy flux. Besides, Ginkgo biloba leaf extract (EGb-761), also the extraction of a traditional Chinese herb, was reported to elicit neuroprotection against ischemic brain injury through enhancing autophagy (Yihao et al., 2021). The above studies suggested that enhancing autophagy activation exerted a protective role on the ischemic injury. However, another voice cannot be ignored for the harmful role of autophagy activation in CIRI. Wang L. et al. (2020) demonstrated that Tanshinone IIA (TSA), the major component extracted from traditional medicine, protected brain tissues from ischemic injury by suppressing autophagy. The research by Zhang et al. (2020b) showed that deltonin, an effective ingredient obtained from a type of Chinese medicine, reduced autophagy activity to play a beneficial role in brain stroke. These studies supported the point that the reduction of autophagy activity was beneficial for stroke. Different types of animals, different disease models, and intensity and duration time of ischemia were possibly the reasons for the different roles of autophagy on CIRI (Zhang et al., 2019; Sun et al., 2020b). In the present study, we revealed that autophagy activation was deleterious in the acute phase of CIS, and EGCG mitigated CIRI via inhibition of autophagy activation, given the evidence that EGCG postcondition could suppress autophagic activity and further reduce the volume of infarction and protect poststroke neuronal loss.

Multiple autophagy-related proteins are involved in the process of autophagy. Beclin1, a central component in the autophagy complex, can bind to ligands and thereby initiate autophagosome formation and play a central role in the process of the movement of autophagy-associated proteins to a pre-autophagosome structure (Kang et al., 2011; Wu et al., 2017). During autophagy, LC3 is cleaved into LC3 I by autophagy-related (Atg) genes four proteases and then connected with phosphatidylethanolamine (PE) to produce LC3 II through the activation of Atg7, Atg3, and Atg12 complex in order. And LC3 II exerts a central role in the biogenesis/maturation of autophagosome membrane. Thus, LC3 II is associated with the amount of the formation of autophagosomes, and LC3 II is served as the biological marker to detect autophagy (Lee and Lee, 2016). P62, a cargo protein of ubiquitination substrates, is reported to participate in the degradation process of autophagy (Jiang et al., 2015). It can combine with LC3 directly and be selectively delivered into autophagosomes, and the amount of p62 within the cell is negatively correlated with the intensity of autophagy (Hou et al., 2021). In brief, when autophagy occurs, beclin1 is required for the construction of autophagosomes, and LC3 is cleaved into LC3 I and LC3 II and combines into autophagosomes simultaneously. And p62 is one of the proteins that are sequestered and degraded by the process of autophagy to supply energy to retain metabolic balance within cells. According to our results, EGCG treatment prevented ischemia and reperfusion invasion-mediated upregulation of the expression of beclin1 and LC3 and downregulation of the expression of p62, in both MCAO/R models of mice and OGD/R models of HT22 cells, indicating that the suppression of poststroke autophagy activity was related to the role of EGCG treatment to ameliorate ischemic brain injury.

Thereafter, the potential molecular mechanisms by which EGCG modulated autophagy were then explored. So far, the mammalian target of rapamycin (mTOR) is believed to be the main regulator of autophagy in the mammalian system (Abdul et al., 2020). It is reported that mTOR is critical for autophagosome formation and maturation, and its inactivation is required for the process of autophagy (Hou et al., 2021). A multitude of signals is integrated into the mTOR pathway. AKT is the upstream of mTOR and modulates mTOR activation (Heras-Sandoval et al., 2014). AMP-activated protein kinase (AMPK) plays an important role in keeping the balance of metabolic processes and is reported to be linked with the regulation of autophagy (Heras-Sandoval et al., 2014). Some studies suggested that ischemia postcondition mitigated ischemic stroke by suppressing autophagy *via* promoting the phosphorylation of AKT and mTOR (Yang et al., 2019; Wang H. et al., 2020; Wang M. M. et al., 2020; Meng et al., 2021), while others revealed that the poststroke treatment ameliorated CIRI through inhibiting autophagy via suppressing the phosphorylation of AKT, AMPK, and mTOR (Wang J. F. et al., 2018; Zhang et al., 2020a; Ma et al., 2020; Liu N. et al., 2021; Yang et al., 2021; Zhang et al., 2022). Therefore, the interaction between the phosphorylation of AKT, AMPK, and mTOR and poststroke treatment-induced autophagy suppression is complicated and remains to be further elucidated. In the present study, in MCAO/R models of mice, we revealed that promoting the phosphorylation of AKT, AMPK, and mTOR was involved in the protective mechanisms of EGCG administration. Moreover, after the phosphorylation of AKT, AMPK, and mTOR was blocked by GSK690693 and rapamycin, we found that EGCG treatment-induced autophagy suppression could be prevented. In addition, we obtained similar results in OGD/R models of HT22 cells. EGCG treatment could inactivate autophagy and promote the phosphorylation of AKT and mTOR while inhibiting the phosphorylation of AMPK. And the inhibition of autophagy

caused by EGCG administration could be prevented by the blocking effect of GSK690693 and rapamycin on the phosphorylation of AKT, AMPK, and mTOR. The difference in the phosphorylated AMPK in MCAO/R mice and OGD/R-challenged HT22 cells might be contributed to different pathophysiological environments *in vivo* and *in vitro*. Collectively, these results indicated that EGCG inhibited ischemia-induced autophagy in an AKT/AMPK/mTOR phosphorylation-dependent manner to exert a neuroprotective effect.

Certainly, there remain some limitations in this article. Aging is the prime culprit for most neurodegenerative events (Uddin et al., 2020), including stroke; thus, modeling with older mice may be a better option. Besides, glial and endothelial cells are also important parts of brain tissues, whether the protective effect of EGCG on glial and endothelial cells is similar to that of neurons remains to be further verified. In addition, other types of cell death—necrosis, necroptosis, and apoptosis—do exist in the pathological process of stroke, the effect and mechanisms of EGCG on these ways of cell death, and the crosstalk between these ways of cell death are waiting to be elucidated. Of course, EGCG can never replace tPA as a specific drug, but it can become an indispensable adjuvant drug for the treatment of stroke. Thus, more precise mechanisms of the curative effect of EGCG in stroke still need to be improved to provide a solid foundation for its clinical application in the future.

Conclusion

Taken together, our results indicated that the neuroprotective role of EGCG against CIRI was associated with the suppression of autophagy through the AKT/AMPK/mTOR phosphorylation pathway. The findings provide new insights into the potential mechanisms of the role of EGCG on autophagy and cerebral ischemic injury and may help design therapeutic strategies with more efficacy for stroke.

Data availability statement

The original contributions presented in the study are included in the article/Supplementary Material; further inquiries can be directed to the corresponding authors.

Ethics statement

The animal study was reviewed and approved by The Institutional Animal Care and Use Committee at Tongji Medical College, Huazhong University of Science and Technology.

Author contributions

Study concepts and design: YL and YG. Experimental studies: LW, MD, and YG. Reagents, materials, and analysis tools: MD, JC and CW. Writing the article: LW and CY. Review and editing the article: CY and YL.

Funding

This work was supported by grants from the National Natural Science Foundation of China (Grant No. 81571138) and the National Natural Science Foundation of China (Grant No. 82071485).

Conflict of interest

The authors declare that the research was conducted in the absence of any commercial or financial relationships that could be construed as a potential conflict of interest.

Publisher's note

All claims expressed in this article are solely those of the authors and do not necessarily represent those of their affiliated organizations, or those of the publisher, the editors, and the reviewers. Any product that may be evaluated in this article, or claim that may be made by its manufacturer, is not guaranteed or endorsed by the publisher.

Supplementary material

The Supplementary Material for this article can be found online at: https://www.frontiersin.org/articles/10.3389/fphar.2022.921394/full#supplementary-material

References

Abdul, M., Al-Bari, A., and Xu, P. (2020). Molecular regulation of autophagy machinery by mTOR-dependent and-independent pathways. *Ann. N. Y. Acad. Sci.* 1467, 3–20. doi:10.1111/nyas.14305

Altomare, D. A., Zhang, L., Deng, J., Cristofano, A., Klein-Szanto, A. J., Kumar, R., et al. (2010). GSK690693 delays tumor onset and progression in genetically defined mouse models expressing activated Akt. *Clin. Cancer Res.* 16, 486–496. doi:10.1158/1078-0432.CCR-09-1026

Bai, Q., Lyu, Z., Pan, Z., Lou, J., and Dong, T. (2017). Epigallocatechin-3-gallate promotes angiogenesis via up-regulation of Nfr2 signaling pathway in a mouse model of ischemic stroke. *Behav. Brain Res.* 321, 79–86. doi:10.1016/J.BBR.2016.12.037

Bansal, S., Sangha, K. S., and Khatri, P. (2013). Drug treatment of acute ischemic stroke. *Am. J. Cardiovasc. Drugs* 13 (1 13), 57–69. doi:10.1007/S40256-013-0007-6

Bhaskar, S., Stanwell, P., Cordato, D., Attia, J., and Levi, C. (2018). Reperfusion therapy in acute ischemic stroke: Dawn of a new era? *BMC Neurol.* 18, 8. doi:10.1186/S12883-017-1007-Y

Chen, D., Zheng, K., Wu, H., Zhang, X., Ye, W., Tan, X., et al. (2021). Lin28a attenuates cerebral ischemia/reperfusion injury through regulating Sirt3-induced autophagy. *Brain Res. Bull.* 170, 39–48. doi:10.1016/J.BRAINRESBULL.2021.01.022

Choi, Y. bin, Kim, Y. I., Lee, K. S., Kim, B. S., and Kim, D. J. (2004). Protective effect of epigallocatechin gallate on brain damage after transient middle cerebral artery occlusion in rats. *Brain Res.* 1019, 47–54. doi:10.1016/J.BRAINRES.2004.05.079

Du, B.-X., Lin, P., and Lin, J. (2022). EGCG and ECG induce apoptosis and decrease autophagy via the AMPK/mTOR and PI3K/AKT/mTOR pathway in human melanoma cells. *Chin. J. Nat. Med.* 20, 290–300. doi:10.1016/S1875-5364(22)60166-3

Edwards, S. R., and Wandless, T. J. (2007). The rapamycin-binding domain of the protein kinase mammalian target of rapamycin is a destabilizing domain. *J. Biol. Chem.* 282, 13395–13401. doi:10.1074/JBC.M700498200

Feigin, V. L., Nguyen, G., Cercy, K., Johnson, C. O., Alam, T., Parmar, P. G., et al. (2018). Global, regional, and country-specific lifetime risks of stroke, 1990 and 2016. *N. Engl. J. Med.* 379, 2429–2437. doi:10.1056/NEJMOA1804492

Ge, Y., Wang, L., Wang, C., Chen, J., Dai, M., Yao, S., et al. (2022). CX3CL1 inhibits NLRP3 inflammasome-induced microglial pyroptosis and improves neuronal function in mice with experimentally-induced ischemic stroke. *Life Sci.* 300, 120564. doi:10.1016/J.LFS.2022.120564

Gu, C., Yang, J., Luo, Y., Ran, D., Tan, X., Xiang, P., et al. (2021). ZNRF2 attenuates focal cerebral ischemia/reperfusion injury in rats by inhibiting mTORC1-mediated autophagy. *Exp. Neurol.* 342, 113759. doi:10.1016/J.EXPNEUROL.2021.113759

Han, J., Wang, M., Jing, X., Shi, H., Ren, M., and Lou, H. (2014). (-)-Epigallocatechin gallate protects against cerebral ischemia-induced oxidative stress via Nrf2/ARE signaling. *Neurochem. Res.* 39, 1292–1299. doi:10.1007/S11064-014-1311-5

He, Z., Ning, N., Zhou, Q., Khoshnam, S. E., and Farzaneh, M. (2020). Mitochondria as a therapeutic target for ischemic stroke. *Free Radic. Biol. Med.* 146, 45–58. doi:10.1016/j.freeradbiomed.2019.11.005

Heras-Sandoval, D., Pérez-Rojas, J. M., Hernández-Damián, J., and Pedraza-Chaverri, J. (2014). The role of PI3K/AKT/mTOR pathway in the modulation of autophagy and the clearance of protein aggregates in neurodegeneration. *Cell. Signal.* 26, 2694–2701. doi:10.1016/j.cellsig.2014.08.019

Hou, J., Zhao, L., Tang, H., He, X., Ye, G., Shi, F., et al. (2021). Silver nanoparticles induced oxidative stress and mitochondrial injuries mediated autophagy in HC11 cells through akt/AMPK/mTOR pathway. *Biol. Trace Elem. Res.* 199 (3), 1062–1073. doi:10.1007/s12011-020-02212-w

Jahan, S., Kumar, D., Singh, S., Kumar, V., Srivastava, A., Pandey, A., et al. (2018). Resveratrol prevents the cellular damages induced by monocrotophos via PI3K signaling pathway in human cord blood mesenchymal stem cells. *Mol. Neurobiol.* 55, 8278–8292. doi:10.1007/S12035-018-0986-Z

Jiang, T., Harder, B., Rojo De La Vega, M., Wong, P. K., Chapman, E., and Zhang, D. D. (2015). p62 links autophagy and Nrf2 signaling. *Free Radic. Biol. Med.* 88, 199–204. doi:10.1016/J.FREERADBIOMED.2015.06.014

Jin, L., Mo, Y., Yue, E. L., Liu, Y., and Liu, K. Y. (2021). Ibrutinib ameliorates cerebral ischemia/reperfusion injury through autophagy activation and PI3K/Akt/mTOR signaling pathway in diabetic mice. *Bioengineered* 12, 7432–7445. doi:10.1080/21655979.2021.1974810

Kang, R., Zeh, H. J., Lotze, M. T., and Tang, D. (2011). The Beclin 1 network regulates autophagy and apoptosis. *Cell Death Differ.* 18, 571–580. doi:10.1038/cdd.2010.191

Lee, Y.-K., and Lee, J.-A. (2016). Role of the mammalian ATG8/LC3 family in autophagy: Differential and compensatory roles in the spatiotemporal regulation of autophagy. *BMB Rep.* 49, 424–430. doi:10.5483/bmbrep.2016.49.8.081

Levy, D. S., Kahana, J. A., and Kumar, R. (2009). AKT inhibitor, GSK690693, induces growth inhibition and apoptosis in acute lymphoblastic leukemia cell lines. *Blood* 113, 1723–1729. doi:10.1182/BLOOD-2008-02-137737

Li, L., and Huang, J. (2020). Rapamycin pretreatment alleviates cerebral ischemia/reperfusion injury in dose-response manner through inhibition of the autophagy and NFκB pathways in rats. *Dose. Response.* 18, 1559325820946194. doi:10.1177/1559325820946194

Lim, S., Kim, T. J., Kim, Y. J., Kim, C., Ko, S. B., and Kim, B. S. (2021). Senolytic therapy for cerebral ischemia-reperfusion injury. *Int. J. Mol. Sci.* 22, 11967. doi:10.3390/IJMS222111967

Liu, N., Peng, A., Sun, H., Zhuang, Y., Yu, M., Wang, Q., et al. (2021). LncRNA AC136007.2 alleviates cerebral ischemic-reperfusion injury by suppressing autophagy. *Aging* 13, 19587–19597. doi:10.18632/AGING.203369

Liu, P., Huang, J., Mei, W., Zeng, X., Wang, C., Wen, C., et al. (2021). Epigallocatechin-3-gallate protects cardiomyocytes from hypoxia-reoxygenation damage via raising autophagy related 4C expression. *Bioengineered* 12, 9496–9506. doi:10.1080/21655979.2021.1996018

Ma, H. X., Hou, F., Chen, A. L., Li, T. T., Zhu, Y. F., and Zhao, Q. P. (2020). Mu-Xiang-You-Fang protects PC12 cells against OGD/R-induced autophagy via the AMPK/mTOR signaling pathway. *J. Ethnopharmacol.* 252, 112583. doi:10.1016/J.JEP.2020.112583

Mei, Z. G., Huang, Y. G., Feng, Z. T., Luo, Y. N., Yang, S. B., Du, L. P., et al. (2020). Electroacupuncture ameliorates cerebral ischemia/reperfusion injury by suppressing autophagy via the SIRT1-FOXO1 signaling pathway. *Aging* 12, 13187–13205. doi:10.18632/AGING.103420

Meng, J., Ma, H., Zhu, Y., and Zhao, Q. (2021). Dehydrocostuslactone attenuated oxygen and glucose deprivation/reperfusion-induced PC12 cell injury through inhibition of apoptosis and autophagy by activating the PI3K/AKT/mTOR pathway. *Eur. J. Pharmacol.* 911, 174554. doi:10.1016/J.EJPHAR.2021.174554

Musial, C., Kuban-Jankowska, A., and Gorska-Ponikowska, M. (2020). Molecular Sciences beneficial properties of green tea catechins. *Int. J. Mol. Sci.* 21 (5), 1744. doi:10.3390/ijms21051744

Musial, C., Siedlecka-Kroplewska, K., Kmiec, Z., and Gorska-Ponikowska, M. (2021). Modulation of autophagy in cancer cells by dietary polyphenols. *Antioxidants* 10, 123. doi:10.3390/antiox10010123

National Institute of Neurological Disorders and Stroke rt-PA Stroke Study Group (1995). Tissue plasminogen activator for acute ischemic stroke. *N. Engl. J. Med.* 333, 1581–1587. doi:10.1056/NEJM199512143332401

Park, D. J., Kang, J. B., and Koh, P. O. (2020). Epigallocatechin gallate alleviates neuronal cell damage against focal cerebral ischemia in rats. *J. Vet. Med. Sci.* 82, 639–645. doi:10.1292/JVMS.19-0703

Prasanth, M. I., Sivamaruthi, B. S., Chaiyasut, C., and Tencomnao, T. (2019). A review of the role of green tea (camellia sinensis) in antiphotoaging, stress resistance, neuroprotection, and autophagy. *Nutrients* 11, E474. doi:10.3390/NU11020474

Rhodes, N., Heerding, D. A., Duckett, D. R., Eberwein, D. J., Knick, V. B., Lansing, T. J., et al. (2008). Characterization of an Akt kinase inhibitor with potent pharmacodynamic and antitumor activity. *Cancer Res.* 68, 2366–2374. doi:10.1158/0008-5472.CAN-07-5783

Saeed, M., Naveed, M., Arif, M., Kakar, M. U., Manzoor, R., Abd El-Hack, M. E., et al. (2017). Green tea (Camellia sinensis) and l-theanine: Medicinal values and beneficial applications in humans-A comprehensive review. *Biomed. Pharmacother. = Biomedecine Pharmacother.* 95, 1260–1275. doi:10.1016/J.BIOPHA.2017.09.024

Shao, Z. Q., Dou, S. S., Zhu, J. G., Wang, H. Q., Wang, C. M., Cheng, B. H., et al. (2021). Apelin-13 inhibits apoptosis and excessive autophagy in cerebral ischemia/reperfusion injury. *Neural Regen. Res.* 16, 1044–1051. doi:10.4103/1673-5374.300725

Sheng, R., and Qin, Z. H. (2015). The divergent roles of autophagy in ischemia and preconditioning. *Acta Pharmacol. Sin.* 36, 411–420. doi:10.1038/APS.2014.151

Shi, C. X., Jin, J., Wang, X. Q., Song, T., Li, G. H., Li, K. Z., et al. (2020). Sevoflurane attenuates brain damage through inhibiting autophagy and apoptosis in cerebral ischemia-reperfusion rats. *Mol. Med. Rep.* 21, 123–130. doi:10.3892/MMR.2019.10832

Srivastava, A., Kumar, V., Pandey, A., Jahan, S., Kumar, D., Rajpurohit, C. S., et al. (2017). Adoptive autophagy activation: A much-needed remedy against chemical induced neurotoxicity/developmental neurotoxicity. *Mol. Neurobiol.* 54, 1797–1807. doi:10.1007/S12035-016-9778-5

Sun, X., Liu, H., Sun, Z., Zhang, B., Wang, X., Liu, T., et al. (2020a). Acupuncture protects against cerebral ischemia-reperfusion injury via suppressing endoplasmic reticulum stress-mediated autophagy and apoptosis. *Mol. Med.* 26, 105. doi:10.1186/S10020-020-00236-5

Sun, X., Wang, D., Zhang, T., Lu, X., Duan, F., Ju, L., et al. (2020b). Eugenol attenuates cerebral ischemia-reperfusion injury by enhancing autophagy via AMPK-mTOR-P70S6K pathway. *Front. Pharmacol.* 11, 84. doi:10.3389/fphar.2020.00084

Tao, T., Liu, M., Chen, M., Luo, Y., Wang, C., Xu, T., et al. (2020). Natural medicine in neuroprotection for ischemic stroke: Challenges and prospective. *Pharmacol. Ther.* 216, 107695. doi:10.1016/J.PHARMTHERA.2020.107695

Uddin, M. S., Hossain, M. F., Mamun, A. al, Shah, M. A., Hasana, S., Bulbul, I. J., et al. (2020). Exploring the multimodal role of phytochemicals in the modulation of cellular signaling pathways to combat age-related neurodegeneration. *Sci. Total Environ.* 725, 138313. doi:10.1016/J.SCITOTENV.2020.138313

Virani, S. S., Alonso, A., Aparicio, H. J., Benjamin, E. J., Bittencourt, M. S., Callaway, C. W., et al. (2021). Heart disease and stroke statistics-2021 update: A

report from the American heart association. *Circulation* 143, E254–E743. doi:10.1161/CIR.0000000000000950

Wang, C., Niu, F., Ren, N., Wang, X., Zhong, H., Zhu, J., et al. (2021). Hyperbaric oxygen improves cerebral ischemia/reperfusion injury in rats probably via inhibition of autophagy triggered by the downregulation of hypoxia-inducing factor-1 alpha. *Biomed. Res. Int.* 2021, 6615685. doi:10.1155/2021/6615685

Wang, H.-K., Chen, J.-S., Hsu, C.-Y., Su, Y.-T., Sung, T.-C., Liang, C.-L., et al. (2021). A novel NGF receptor agonist B355252 ameliorates neuronal loss and inflammatory responses in a rat model of cerebral ischemia. *J. Inflamm. Res.* 14, 2363–2376. doi:10.2147/jir.s303833

Wang, H., Liu, Q., and Zhang, X. (2020). C1q/tumor necrosis factor-related protein-1 attenuates microglia autophagy and inflammatory response by regulating the Akt/mTOR pathway. *Life Sci.* 256, 117992. doi:10.1016/J.LFS.2020.117992

Wang, J. F., Mei, Z. G., Fu, Y., Yang, S. B., Zhang, S. Z., Huang, W. F., et al. (2018). Puerarin protects rat brain against ischemia/reperfusion injury by suppressing autophagy via the AMPK-mTOR-ULK1 signaling pathway. *Neural Regen. Res.* 13, 989–998. doi:10.4103/1673-5374.233441

Wang, L., Xiong, X., Zhang, X., Ye, Y., Jian, Z., Gao, W., et al. (2020). Sodium Tanshinone IIA sulfonate protects against cerebral ischemia-reperfusion injury by inhibiting autophagy and inflammation. *Neuroscience* 441, 46–57. doi:10.1016/J.NEUROSCIENCE.2020.05.054

Wang, L., Zhu, T., Feng, D., Li, R., and Zhang, C. (2022). Polyphenols from Chinese herbal medicine: Molecular mechanisms and therapeutic targets in pulmonary fibrosis. *Am. J. Chin. Med.* 50, 1063–1094. doi:10.1142/S0192415X22500434

Wang, P., Shao, B. Z., Deng, Z., Chen, S., Yue, Z., and Miao, C. Y. (2018). Autophagy in ischemic stroke. *Prog. Neurobiol.* 163–164, 98–117. doi:10.1016/J.PNEUROBIO.2018.01.001

Wang, X. H., and You, Y. P. (2017). Epigallocatechin gallate extends therapeutic window of recombinant tissue plasminogen activator treatment for brain ischemic stroke: A randomized double-blind and placebo-controlled trial. *Clin. Neuropharmacol.* 40, 24–28. doi:10.1097/WNF.0000000000000197

Wang, M. M., M. M., Zhang, M., Feng, Y. S., Xing, Y., Tan, Z. X., Li, W. bin, et al. (2020). Electroacupuncture inhibits neuronal autophagy and apoptosis via the PI3K/AKT pathway following ischemic stroke. *Front. Cell. Neurosci.* 14, 134. doi:10.3389/fncel.2020.00134

Wirawan, E., Vanden Berghe, T., Lippens, S., Agostinis, P., and Vandenabeele, P. (2012). Autophagy: For better or for worse. *Cell Res.* 22, 43–61. doi:10.1038/cr.2011.152

Wu, Z. Z., Zhang, J. J., Gao, C. C., Zhao, M., Liu, S. Y., Gao, G. M., et al. (2017). Expression of autophagy related genes mToR, Becline-1, LC3 and p62 in the peripheral blood mononuclear cells of systemic lupus erythematosus. *Am. J. Clin. Exp. Immunol.* 6, 1–8.

Xu, D., Kong, T., Zhang, S., Cheng, B., Chen, J., and Wang, C. (2021). Orexin-A protects against cerebral ischemia-reperfusion injury by inhibiting excessive autophagy through OX1R-mediated MAPK/ERK/mTOR pathway. *Cell. Signal.* 79, 109839. doi:10.1016/J.CELLSIG.2020.109839

Xu, S. Y., Lv, H. Q., Li, W. Q., Hong, H., Peng, Y. J., and Zhu, B. M. (2020). Electroacupuncture alleviates cerebral ischemia/reperfusion injury in rats by histone H4 lysine 16 acetylation-mediated autophagy. *Front. Psychiatry* 11, 576539. doi:10.3389/fpsyt.2020.576539

Xuan, F., and Jian, J. (2016). Epigallocatechin gallate exerts protective effects against myocardial ischemia/reperfusion injury through the PI3K/Akt pathway-mediated inhibition of apoptosis and the restoration of the autophagic flux. *Int. J. Mol. Med.* 38, 328–336. doi:10.3892/ijmm.2016.2615

Yang, G., Zeng, X., Li, J., Leung, C. K., Zhang, D., Hong, S., et al. (2019). Protective effect of gastrodin against methamphetamine-induced autophagy in human dopaminergic neuroblastoma SH-SY5Y cells via the AKT/mTOR signaling pathway. *Neurosci. Lett.* 707, 134287. doi:10.1016/J.NEULET.2019.134287

Yang, Y., Gao, H., Liu, W., Liu, X., Jiang, X., Li, X., et al. (2021). Arctium lappa L. roots ameliorates cerebral ischemia through inhibiting neuronal apoptosis and suppressing AMPK/mTOR-mediated autophagy. *Phytomedicine.* 85, 153526. doi:10.1016/J.PHYMED.2021.153526

Yao, Y., Ji, Y., Ren, J., Liu, H., Khanna, R., and Sun, L. (2021). Inhibition of autophagy by CRMP2-derived peptide ST2-104 (R9-CBD3) via a CaMKKβ/AMPK/mTOR pathway contributes to ischemic postconditioning-induced neuroprotection against cerebral ischemia-reperfusion injury. *Mol. Brain* 14, 123. doi:10.1186/S13041-021-00836-0

Yeo, L. L. L., Paliwal, P., Teoh, H. L., Seet, R. C., Chan, B. P. L., Liang, S., et al. (2013). Timing of recanalization after intravenous thrombolysis and functional outcomes after acute ischemic stroke. *JAMA Neurol.* 70, 353–358. doi:10.1001/2013.JAMANEUROL.547

Yihao, D., Tao, G., Zhiyuan, W., Xiaoming, Z., Lingling, D., and Hongyun, H. (2021). Ginkgo biloba leaf extract (EGb-761) elicits neuroprotection against cerebral ischemia/reperfusion injury by enhancement of autophagy flux in neurons in the penumbra. *Iran. J. Basic Med. Sci.* 24, 1138–1145. doi:10.22038/IJBMS.2021.46318.10694

You, Y. P. (2016). Epigallocatechin gallate extends the therapeutic window of recombinant tissue plasminogen activator treatment in ischemic rats. *J. Stroke Cerebrovasc. Dis.* 25, 990–997. doi:10.1016/J.JSTROKECEREBROVASDIS.2016.01.014

Zha, H., Fan, Y., Yang, L., Yin, M., Miao, W., He, J., et al. (2021). Autophagy protects against cerebral ischemic reperfusion injury by inhibiting neuroinflammation. *Am. J. Transl. Res.* 13, 4726–4737. Available at: https://pubmed.ncbi.nlm.nih.gov/34150053/(Accessed May 26, 2022).

Zhang, B., Deng, F., Zhou, C., and Fang, S. (2020). ClC-3 induction protects against cerebral ischemia/reperfusion injury through promoting Beclin1/Vps34-mediated autophagy. *Hum. Cell* 33, 1046–1055. doi:10.1007/S13577-020-00406-X

Zhang, D. M., Zhang, T., Wang, M. M., Wang, X. X., Qin, Y. Y., Wu, J., et al. (2019). TIGAR alleviates ischemia/reperfusion-induced autophagy and ischemic brain injury. *Free Radic. Biol. Med.* 137, 13–23. doi:10.1016/J.FREERADBIOMED.2019.04.002

Zhang, F. J., Li, N., Jiang, L. L., Chen, L. H., and Huang, M. T. (2015). Neuroprotective effects of (-)-Epigallocatechin-3-Gallate against focal cerebral ischemia/reperfusion injury in rats through attenuation of inflammation. *Neurochem. Res.* 40, 1691–1698. doi:10.1007/S11064-015-1647-5

Zhang, J. C., Xu, H., Yuan, Y., Chen, J. Y., Zhang, Y. J., Lin, Y., et al. (2017). Delayed treatment with green tea polyphenol EGCG promotes neurogenesis after ischemic stroke in adult mice. *Mol. Neurobiol.* 54, 3652–3664. doi:10.1007/S12035-016-9924-0

Zhang, L. N., Zhang, X. W., Li, C. Q., Guo, J., Chen, Y. P., and Chen, S. L. (2021). Vagal nerve stimulation protects against cerebral ischemia-reperfusion injury in rats by inhibiting autophagy and apoptosis. *Neuropsychiatr. Dis. Treat.* 17, 905–913. doi:10.2147/NDT.S300535

Zhang, Y., He, Q., Yang, M., Hua, S., Ma, Q., Guo, L., et al. (2020a). Dichloromethane extraction from Piper nigrum L. and P. longum L. to mitigate ischemic stroke by activating the AKT/mTOR signaling pathway to suppress autophagy. *Brain Res.* 1749, 147047. doi:10.1016/J.BRAINRES.2020.147047

Zhang, Y., Tian, Z., Wan, H., Liu, W., Kong, F., and Ma, G. (2020b). Deltonin ameliorates cerebral ischemia/reperfusion injury in correlation with modulation of autophagy and inflammation. *Neuropsychiatr. Dis. Treat.* 16, 871–879. doi:10.2147/NDT.S227988

Zhang, Y., Yang, M., Yuan, Q., He, Q., Ping, H., Yang, J., et al. (2022). Piperine ameliorates ischemic stroke-induced brain injury in rats by regulating the PI3K/AKT/mTOR pathway. *J. Ethnopharmacol.* 295, 115309. doi:10.1016/J.JEP.2022.115309

Zhang, C., C., Gan, X., Liang, R., and Jian, J. (2020). Exosomes derived from epigallocatechin gallate-treated cardiomyocytes attenuated acute myocardial infarction by modulating MicroRNA-30a. *Front. Pharmacol.* 11, 126. doi:10.3389/fphar.2020.00126

Zhao, Y., Ma, X., Yu, W., Zhang, Z., Wang, W., Zhou, X., et al. (2021). Protective effect of buyang huanwu decoction on cerebral ischemia reperfusion injury by alleviating autophagy in the ischemic penumbra. *Evid. Based. Complement. Altern. Med.* 2021, 9937264. doi:10.1155/2021/9937264

frontiers | Frontiers in Neuroscience

TYPE Systematic Review
PUBLISHED 07 September 2022
DOI 10.3389/fnins.2022.968791

OPEN ACCESS

EDITED BY
Nesrine Salah El Dine El Sayed,
Cairo University, Egypt

REVIEWED BY
Masahiro Nishibori,
Okayama University, Japan
Timothy Joseph Kopper,
University of Colorado, United States

*CORRESPONDENCE
Lin Sun
sunlin_9999@163.com

SPECIALTY SECTION
This article was submitted to Neuropharmacology, a section of the journal Frontiers in Neuroscience

RECEIVED 14 June 2022
ACCEPTED 18 August 2022
PUBLISHED 07 September 2022

CITATION
Deng C, Deng L, Lv J and Sun L (2022) Therapeutic effects and long-term outcomes of HMGB1-targeted therapy in rats and mice with traumatic spinal cord injury: A systematic review and meta-analysis.
Front. Neurosci. 16:968791.
doi: 10.3389/fnins.2022.968791

Therapeutic effects and long-term outcomes of HMGB1-targeted therapy in rats and mice with traumatic spinal cord injury: A systematic review and meta-analysis

Chen Deng, Li Deng, Junqiao Lv and Lin Sun*

Third Hospital of Shanxi Medical University, Shanxi Bethune Hospital, Tongji Shanxi Hospital, Shanxi Academy of Medical Sciences, Taiyuan, China

Background: To date, the clinical need for therapeutic methods to prevent traumatic spinal cord injury (TSCI) progression and improve functional recovery has not been met. High mobility group box-1 (HMGB1) is released by necrotic neurons or secreted by glial cells after TSCI and plays an important role in pathophysiology.

Objective: The purpose of this study was to evaluate the effects of HMGB1-targeted therapy on locomotor function recovery, inflammation reduction, edema attenuation, and apoptosis reduction in rat and mouse models of TSCI.

Methods: We reviewed the literature on HMGB1-targeted therapy in the treatment and prognosis of TSCI. Twelve articles were identified and analyzed from four online databases (PubMed, Web of Science, Cochrane Library and Embase) based on the Preferred Reporting Items for Systematic Reviews and Meta-Analyses (PRISMA) guidelines and strict inclusion criteria.

Results: The methodological quality of the 12 articles was poor. The results of the meta-analysis showed that compared with the SCI group, the treatment group had significantly increased locomotor function scores after SCI [$n = 159$, standardized mean difference (SMD) = 2.31, 95% confidence interval (CI) (1.52, 3.10), $P < 0.00001$], and the change in locomotor function scores was significantly increased in both the drug and anti-HMGB1 Ab groups ($P < 0.000001$ and $P < 0.000001$). A subgroup analysis showed significant differences ($P > 0.05$) between the drug group [(SMD) = 1.95, 95% CI (0.95, 2.94), $P = 0.0001$] and the anti-HMGB1 Ab group [(SMD) = 2.89, 95% CI (1.66, 4.13), $P < 0.00001$]. Compared with the SCI group, HMGB1 expression was significantly diminished [$n = 76$, SMD = −2.31, 95% CI (−3.71, −0.91), $P = 0.001$], TNF-α levels were significantly reduced [$n = 76$, SMD = −2.52, 95% CI (−3.77, −1.27), $P < 0.0001$], water content was significantly reduced [$n = 44$, SMD = −3.94, 95% CI (−6.28, −1.61), $P = 0.0009$], and the number of apoptotic cells was significantly diminished [$n = 36$, SMD = −3.31, 95% CI (−6.40, −0.22), $P = 0.04$] in the spinal cord of the treatment group.

Conclusion: HMGB1-targeted therapy improves locomotor function, reduces inflammation, attenuates edema, and reduces apoptosis in rats and mice with TSCI. Intrathecal injection of anti-HMGB1 Ab 0-3 h after SCI may be the most efficacious treatment.

Systematic review registration: PROSPERO, identifier: CRD42022326114.

KEYWORDS

spinal cord injury, high mobility group box-1 (HMGB1), targeted therapy, inflammation, edema, apoptosis, functional recovery

Introduction

Spinal cord injury (SCI), as one of the most serious diseases with clinical symptoms, often leads to severe sensory and locomotor dysfunction. In recent years, its incidence has increased year by year (James, 2019), ranging from 13.1 to 163.4 per million people in developed countries and from 13.0 to 220.0 per million people in developing countries (van den Berg et al., 2010; Kang et al., 2017). Such a broad range may because of the various sampling methods and the scopes of research. Among them, non-traumatic spinal cord injury (NTSCI) accounts for a part of the proportion. Traumatic spinal cord injury (TSCI) can be divided into primary injury and secondary injury according to pathogenesis. Primary injury causes delayed damage and death to surviving adjacent cells around the lesion. Secondary injury occurs after the primary injury and is characterized by a series of biochemical events leading to further tissue loss and dysfunction through self-destructive changes in intact tissue surrounding the primary injury (Quadri et al., 2020). Secondary damage starts a few minutes after the primary injury and lasts for weeks or months, including vascular damage, inflammation, edema, apoptosis, and free radical formation, ultimately leading to the formation of cystic cavities and the maturation of glial scars (Alizadeh et al., 2019). Currently, experimental treatments for secondary injury include reducing edema and inhibiting inflammation in the acute phase of spinal cord injury; inhibiting apoptosis and glial scar evolution around the injury site in the subacute phase; regulating the formation of glial scars and matrix remodeling; and promoting the growth of axons in the chronic phase. As one of the most important therapeutic methods, regulation of the inflammatory microenvironment in the early stage of spinal cord injury has been widely studied (Hellenbrand et al., 2021).

High mobility group box-1 (HMGB1) is a highly conserved non-histone DNA binding protein. Intracellular HMGB1 plays a key role in the immune response by increasing autophagy, regulating mitochondrial function and inhibiting apoptosis (Huebener et al., 2014). Extracellular HMGB1 shows cytokine activity and acts as a typical danger-associated molecular pattern (DAMP) molecule (Wang and Zhang, 2020). After SCI, HMGB1 can be actively secreted by microglia and astrocytes or passively released by necrotic neurons (Papatheodorou et al., 2017; Yang et al., 2020). Once released, HMGB1 interacts with cell surface receptors, such as the receptor for advanced glycation end products (RAGE) and Toll-like receptors 2/4/9 (TLR-2/4/9) (Paudel et al., 2019; Sun et al., 2019), and mediates a variety of cellular responses, including promoting microglial and macrophage migration and the release of proinflammatory cytokines. It has been reported that extracellular HMGB1 can regulate the production of inflammatory factors such as interleukin-1α (IL-1α), IL-1β, IL-6, and tumor necrosis factor-α (TNF-α) and alter the expression and function of effector proteins in target cells (Man et al., 2015). In addition, inhibition of HMGB1 can reduce early edema and aquaporin-4 protein (AQP-4) expression after spinal cord injury in rats (Sun et al., 2019); AQP-4 is the main aquaporin of the central nervous system (CNS) and plays a key role in the development of edema (Halsey et al., 2018; Kitchen et al., 2020; Masterman and Ahmed, 2021).

To date, no pharmacological interventions for spinal cord injury have been approved for clinical use; however, multiple approaches to regulate HMGB1 expression have been used in preclinical animal models, such as drug intervention and anti-HMGB1 neutralizing antibody (Ab). Most of them achieved good efficacy, but some studies reported different results (Kigerl et al., 2018). The purpose of this study was to investigate the effects of HMGB1-targeted therapy on the treatment and prognosis of TSCI in rat and mouse models and to evaluate the feasibility of various therapeutic approaches.

Materials and methods

A systematic review of the literature was conducted based on guidelines developed by the Preferred Reporting Items for Systematic Reviews and Meta-Analyses (PRISMA) (Moher et al., 2009). The study was conducted by two independent reviewers, and disagreements were resolved by discussion with a third reviewer.

Literature search

Published papers analyzing the therapeutic and prognostic effects of HMGB1 in rat and mouse spinal cord injury models were identified through a search of the PubMed, Web of Science Cochrane Library and Embase electronic databases. Key words included "spinal cord injury," "SCI," "high mobility group box protein 1" and "HMGB1." As an example, the details of the PUBMED database search strategy are as follows: '{"Spinal Cord Injuries"(MeSH Terms) OR ["SCI"(Title/Abstract) OR "spinal cord injury"(Title/Abstract)]} AND ["HMGB1 Protein"(MeSH Terms) OR "HMGB1"(Title/Abstract) OR "high mobility group box protein 1"(Title/Abstract)]'. Studies were screened by title and abstract according to the inclusion and exclusion criteria listed, and duplicated studies were removed. The shortlisted studies were independently reviewed again, and the full text was read to select the final research choice for subsequent analysis.

Inclusion and exclusion criteria

Inclusion criteria

(1) Population: experimental rat or mouse studies involving traumatic SCI of any age or sex, including contusion, crush and compression injury;

(2) Intervention: HMGB1 intervention with no limitations on the method of administration, formulation or dosage;

(3) Comparator: any type of placebo control group, such as DMSO (dimethyl sulfoxide), physiological saline, PBS, IgG2a antibodies (isotype control) or no treatment;

(4) Outcome: (a)locomotor functional evaluation: the Basso, Beattie, and Bresnahan (BBB) rating scale or the Basso Mice Scale (BMS) rating scale; (b) biochemical examinations: HMGB1 expression, TNF-α levels, spinal cord water content and apoptotic cell count;

(5) Study design: controlled studies assessing the *in vivo* administration of HMGB1-targeted therapy to rats or mice with SCI; original study published in English; no publication date or publication status restrictions were imposed.

Exclusion criteria

(1) Studies that were not controlled studies, such as reviews, systematic reviews, case reports or meetings.

(2) Substandard animal models (chronic constriction injury model; spinal cord ischemia–reperfusion injury model; models other than in rats or mice).

(3) Clinical and *in vitro* studies.

(4) No relevant outcomes reported.

(5) Repeated publications.

Assessment of risk of bias in included studies

The risk of bias for the included studies was assessed using the Systematic Review Center for Laboratory Animal Experimentation (SYRCLE) risk of bias tool for animal studies, which was adapted from Cochrane's risk of bias tool (Hooijmans et al., 2014). The risks of bias were assessed by two independent reviewers (CD and LD) for each study. The risk of bias was assessed as a low or high risk of bias, and "unclear risk" indicated that the risk of bias was not clear.

Data extraction

Two reviewers independently extracted details from the studies included in the meta-analysis. It included the first author, date of publication, animal strain, weight, sex, number of animals in each group, method used to induce SCI, SCI level, type of intervention, timing of intervention, daily dose of intervention, follow-up time frame after SCI, and outcomes of significance to SCI. The mean standard deviation (SD) of experimental results and the number of animals in the treatment group and SCI group were extracted from these data for meta-analysis. According to the observation, the first analysis of locomotor function is usually performed within 48 h, which may be the reason for the score of 0; in this case, the measurement is not considered to be the first time. If locomotor function was evaluated more than once, SD changes were used for a meta-analysis. If the biochemical examinations were performed at different times, the last outcome indicators that were measured after SCI were adopted. The last measurements were taken no later than 14 days post-SCI. If there were any controversies, we settled the problem by discussion and with the help of a third reviewer.

All studies included the SCI group and treatment groups. However, some of the results were presented in the form of a graph rather than an exact report of the raw data they obtained, which meant that the actual numbers had to be estimated from the data extracted from the graph. GetData Graph Digitizer 2.24 software was used to estimate numerical values from the graphs, and the study was excluded if the required data were not presented or obtainable.

Data synthesis

The data were then synthesized through a meta-analysis. The main objective is to provide a more accurate estimate of the effect size of the treatment. According to different treatment methods, 12 studies including locomotor function recovery data were divided into the following two groups for subgroup analysis: anti-HMGB1 Ab group and drug group. We also performed a

meta-analysis on the reduction of HMGB1 and TNF-α levels, the attenuation of edema, and the reduction of apoptosis after the various treatments.

Outcome measures

The main outcome measures were locomotor functional evaluation (the BBB rating scale and the BMS rating scale) and biochemical examinations, including HMGB1 expression, TNF-α level, spinal cord water content and apoptotic cell count.

Statistical analysis

Meta-analysis was performed using Review Manager version 5.3 (Cochrane Collaboration). Data from the treatment group were compared with those from the spinal cord injury group. Data were pooled if at least three studies reported results, and continuous variables were expressed as the mean difference (MD) or standardized mean difference (SMD), both with 95% CI. If the unit of measurement was consistent, MD was used to evaluate the effect size; SMD was used to evaluate the effect size when the measurement units were different. A chi-square test was used for heterogeneity: $P < 0.1$ represents heterogeneity, and $P > 0.1$ indicates no heterogeneity. I2 statistics were also used to assess heterogeneity: $0\% \leq I2 < 25\%$ indicated no heterogeneity; $25\% \leq I2 < 50\%$ indicated low heterogeneity; $50\% \leq I2 < 75\%$ showed moderate heterogeneity; and $75\% \leq$ I2 revealed high heterogeneity. When heterogeneity between studies was low, the fixed effects model was used to estimate the combined effect size; otherwise, the random effects model was used. $P<0.05$ was considered statistically significant, and publication bias was determined by funnel plot.

Results

Study selection

A total of 264 results were retrieved from four databases: PubMed, Web of Science, Cochrane Library and EMBASE. After deleting duplicate versions, 170 articles were initially screened. According to previously defined inclusion and exclusion criteria, 149 studies were deleted through titles and abstracts, leaving only 21 studies eligible for study and requiring full reading. After full-text screening, 9 studies were excluded because there was no intervention on HMGB1, so 12 studies were included for further analysis. One article included two treatment groups compared with the same control group, and both studies were included in this study. Therefore, 13 studies were included in this study, which contained 12 articles. The process of the literature identification and ranking strategy is shown in the PRISMA diagram (Figure 1).

Study characteristics

The characteristics of the studies included in this systematic review are shown in Table 1. Most of the 12 articles that met the inclusion criteria were from China, while the remaining three were from Japan (Uezono et al., 2018; Nakajo et al., 2019; Zhu et al., 2021) and one was from the US (Kigerl et al., 2018). All of the studies were randomized controlled trials. Seven studies used SD rats with weights ranging from 180 to 270 g; four studies used C57BL/6J mice ranging in weight from 18 to 25 g; and only one study (Uezono et al., 2018) used non-obese diabetic severe combined immunodeficient (NOD-SCID) mice. The total sample size of the study ranged from 15 to 296, with an average sample size of 79. Four studies used male animals, six used female animals, and the other studies did not report gender information. Eleven studies used contusion injury, and two other studies (Fan et al., 2020; Wu et al., 2021) used compression injury. In all of the studies, SCI was performed at T10 except one study at T8 (Fan et al., 2020) and another at T9 (Kigerl et al., 2018).

In terms of treatment, inhibiting the role of HMGB1 *in vivo* was chosen by all studies. Five of the studies used an anti-HMGB1 Ab (Kigerl et al., 2018; Uezono et al., 2018; Nakajo et al., 2019; Chen et al., 2021; Zhu et al., 2021), most of which was injected within 0-6 hours after injury at a dose of 8 mg/kg, which significantly improved locomotor function recovery. However, in one study (Kigerl et al., 2018), a dose of 50 μg per day injected 1 day before injury and last 7 days had no significant therapeutic effect. In two studies (Yang et al., 2013; Kang et al., 2015), hyperbaric oxygen (HBO) was used to downregulate HMGB1 expression, with an oxygen flow rate of 8-10 L/min and an oxygen concentration of 95%, once a day for 1 h. Three studies (Sun et al., 2019; Fan et al., 2020; Wu et al., 2021) used glycyrrhizin (GL) at doses of 10 or 100 mg/kg, injected immediately after injury, once daily; other studies used shinkonin (Bi et al., 2017) (100 mg/kg), ethyl pyruvate (Sun et al., 2019) (EP) (50 mg/kg) or higenamine (Zhang et al., 2014) (HG) (10 mg/kg), which significantly inhibited HMGB1 expression after spinal cord injury.

Most studies reported results using locomotor function assessment and biochemical analysis. BBB scores were used to assess locomotor function 12 h-42 days after injury in rats. BMS scores were used to assess locomotor function 1-12 weeks after injury in mice. Most studies have examined the expression of inflammatory mediators such as HMGB1 and TNF-α after spinal cord injury. Some studies have also reported the degree of spinal edema and the number of apoptotic cells to detect the characteristics of spinal cord injury. In addition, electrophysiological examination (Uezono et al., 2018) and Evans blue dye extravasation (Uezono et al., 2018; Nakajo et al., 2019) were reported in some studies, which were not included in the meta-analysis due to the small number of studies.

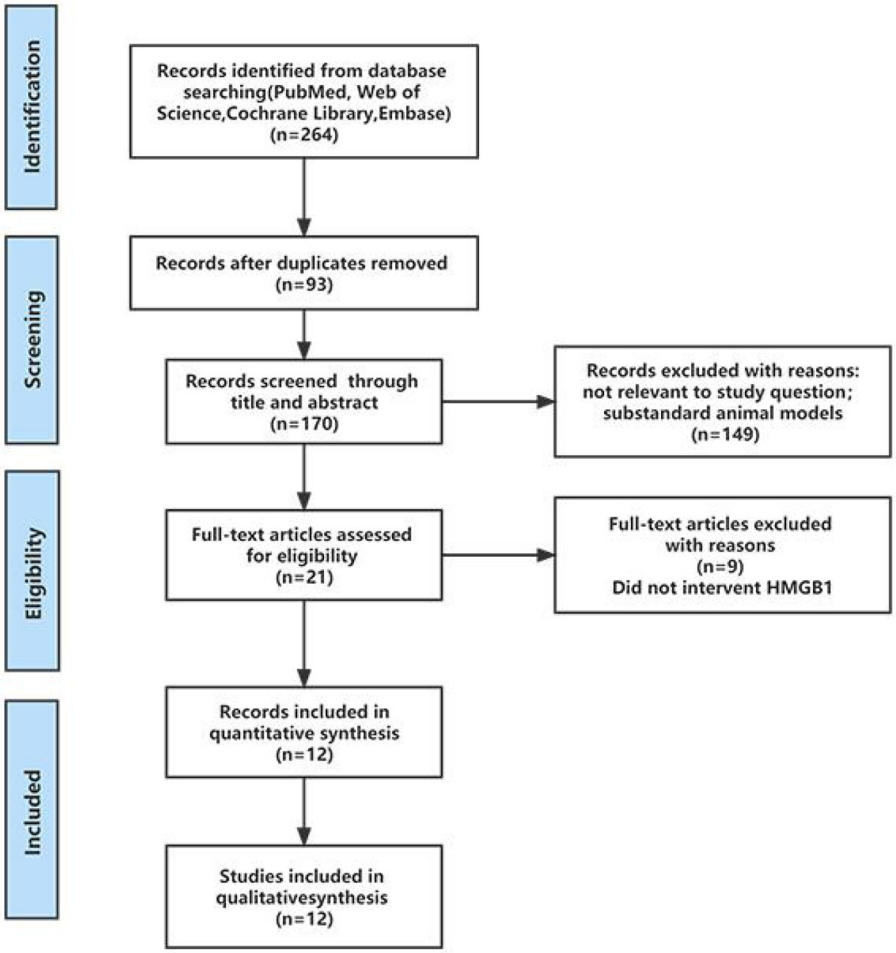

FIGURE 1
PRISMA flow diagram to demonstrate the screening process for included studies in this systematic review.

Bias analysis of included studies

The risks of bias for all 13 studies included in the 12 articles are shown in Figure 2. The process assessed studies across 10 areas, and from the information provided, they were classified as low risk, high risk or unclear risk. Overall, the methodological quality of the included studies was not high. No study described baseline characteristics, allocation concealment, random housing, blinding of participants and personnel, incomplete outcome data, selective reporting or other bias. Nine studies described blinding of outcome assessment. Random outcome assessments were reported in four studies. Only one study (Yang, et al., 2013) reported random sequence generation using the randomization table method.3.4 Meta-analysis.

Assessment of locomotor function improvement by inhibiting HMGB1

A meta-analysis of locomotor function score data from 11 studies showed that inhibiting the role of HMGB1 *in vivo* significantly promoted locomotor function recovery. Inhibiting the role of HMGB1 *in vivo* significantly increased locomotor function scores [11 studies, $n = 159$, SMD = 2.31, 95% CI (1.52–3.10), $P < 0.00001$; Figure 3] in a random-effects model because of the moderate heterogeneity ($I2 = 66\%$, $P = 0.001$).

Then, we performed a subgroup analysis. Seven studies (Yang et al., 2013; Zhang et al., 2014; Kang et al., 2015; Bi et al., 2017; Sun et al., 2019; Fan et al., 2020) used different drug interventions in the drug group and found that the change in locomotor function scores in the treatment group was significantly higher than that in the SCI group using a

TABLE 1 Characteristics of the included studies.

Study ID	Country	Animals	Level of SCI	Injury	Group design	Therpay	Follow up time after SCI	Outcome measures
Rat								
Yang et al. (2013)	China	Adult Sprague-Dawley rats (250–300 g)	T10	Allen's Weight-Dropping method (10 g*25 mm)	Sham (40) sham+HBO (40) SCI (40) SCI +HBO (40)	HBO(1 h,8∼10 L/min, 95%,once daily)	1d, 3d, 7d, 14d	HMGB1, NF-κB expression WB/RT-PCR/IHC; locomotor function.
Kang et al. (2015)	China	Adult Sprague-Dawley rats (250–300 g)	T10	Allen's Weight-Dropping method (10 g*25 mm)	Sham (30) sham+HBO (30) SCI (30) SCI +HBO (30)	HBO(1 h,8∼10 L/min, 95%,once daily)	1d, 2d, 3d, 7d, 14d	HMGB1, TLR4 expression WB/RT-PCR/IHC; HMGB1, NF-κB, IL-1β, TNF-α level ELISA; locomotor function.
Bi et al. (2017)	China	Adult male Sprague-Dawley rats (180–220 g)	T10	Modified Allen's Weight-Dropping method (8 g*40 mm)	Sham (8) SCI (8) SCI+MPSS (8) SCI+Shi(100) (8)	MPSS(100 mg/kg, Immediately); Shinkonin (100 mg/kg, Immediately)	1d, 2d, 3d	HMGB1, TLR4, NF-κB expression WB/RT-PCR; HE staining; IL-1β,IL-6,TNF-α level ELISA; water content; Tunel staining; caspase-3 expression WB; locomotor function.
Sun et al. (2019)	China	Adult female Sprague-Dawley rats	T10	Modified Allen's Weight-Dropping method (10 g*25 mm)	Sham (66) SCI (66) SCI+EP (66) SCI+GL (66)	EP (50 mg/kg, once daily) GL(100 mg/kg, once daily)	12h, 1d, 3d, 7d, 10d, 14d	HMGB1, GFAP, AQP-4, expression WB/IHC; HMGB1 level ELISA; TLR4/MyD88 pathway activation; water content; oedema via MRI; locomotor function.
Fan et al. (2020)	China	Adult male Sprague- Dawley rats (250 g)	T8	Modified Tetzlaff spinal cord lateral crush model (Last 20 s)	Sham (37) SCI (37) SCI+GL (37) SCI+ FPS-ZM1 (37)	GL (10 mg/kg, immediately,14 days after SCI) FPS-ZM1 (1 mg/kg, immediately,14 days after SCI)	1d, 3d, 7d, 10d, 14d, 21d	iNOS, IL-12, CD86, TNF-α expression RT-PCR; rage iNOS iba-1expression IF; Nissl staining; lesion area; neuronal survival; behavioral evaluation
Chen et al. (2021)	China	Adult female Sprague-Dawley rats (270 g)	T10	Contusion injury using a weight drop device (10 g*12.5 mm)	Control (8) Anti-HMGB1 (8)	anti-HMGB1 Ab (50 ng/μl, 1 μl, Immediately)	1w, 2w, 3w, 4w, 5w, 6w	TNF-α IFN-γ IL-1α IL-6 IL-17 level LiquiChip assay; HE staining; Nissl staining; microglia polarization; locomotor function
Wu et al. (2021)	China	Adult male Sprague-Dawley rats (200–220 g)	T10	Compression injury using an aneurysm clip (Last 10 s)	Sham (18) SCI (18) SCI+GA (18)	GA (100 mg/kg, once daily)	3d	HMGB1, TNF-a, IL-1b, IL-6 expression WB/RT-PCR/IHC; HE staining; microglia expression; p38/JNK pathway activation

(Continued)

10.3389/fnins.2022.968791

TABLE 1 (Continued)

Study ID	Country	Animals	Level of SCI	Injury	Group design	Therpay	Follow up time after SCI	Outcome measures
Mice								
Zhang et al. (2014)	China	Male C57BL/6J mice (20–25 g)	T10	Contusion injury using a Infinite Horizons Impactor (60 kydn)	Sham(6) Control(6) HG(6) ZnPPIX(6)	Higenamine (HG,10 mg/kg, immediately), ZnPPIX (10 mg/kg, immediately)	1d, 3d, 7d, 14d, 28d, 42d	HMGB1, IFN-γ, TNF-α, IL-4, IL-10 expression WB; macrophages expression; GAP-43, NF-H IHC; HMGB1 ELISA; locomotor function.
Kigerl et al. (2018)	US	Female C57BL/6 mice	T9	Contusion injury using a Infinite Horizons injury device (70 kydn)	Sham (6) Control (6) anti-HMGB1 mAb (6)	anti-HMGB1 mAb (50 μg/day, 1 day prior to SCI,7 days)	1d, 3d, 7d, 14d, 21d, 28d, 35d, 42d	HMGB1 expression WB/RT-PCR/IF; microglia/macrophages expression; lesion area; locomotor function
Uezono et al. (2018)	Japan	female (NOD-SCID) mice (18–22 g)	T10	Contusion injury using a Infinite Horizon Impactor (70 kydn)	Non-treatment (16) Transplantation alone (16) anti-HMGB1 mAb alone (12)	anti-HMGB1 mAb (8 mg/kg, 5 min and 6 h after SCI) hiPSC-NSCs ($2.5*10^5 \mu l^{-1}$,2μl,7d after SCI)	1d, 3d, 7d, 14d, 28d, 42d	HMGB1, IFN-γ, TNF-α, IL-4, IL-10 expression WB; GFAP IHC; tunel staining; lesion area; neuronal survival; behavioral analysis electrophysiology; Evans Blue dye extravasation; water content
Nakajo et al. (2019)	Japan	Female C57BL/6J mice (18–22 g)	T10	Contusion injury using a Infinite Horizon Impactor (70 kydn)	Sham (5) Control (5) anti-HMGB1 mAb (5)	anti-HMGB1 mAb (8 mg/kg, 0 or 3 or 6 or 9 or 12 h after SCI.)	1w, 2w, 3w, 4w, 5w, 6w—12w	TNF-a, IL-1b, IL-6, MMP-2/9 expression RT-PCR; tunel staining; lesion area; neuronal survival; behavioral analysis; Evans Blue dye extravasation; water content
Zhu et al. (2021)	Japan	Female C57BL/6J mice (18–22 g)	T10	Contusion injury using a Infinite Horizon Impactor (70 kydn)	Control (10) Epo B (10) anti-HMGB1 mAb (10) Combination (10)	anti-HMGB1 mAb (8 mg/kg, 5 min after SCI) Epo B (3 mg/kg, 1d, 15d after SCI)	0d, 7d, 14d, 28d, 42d, 49d, 56d	GFAP expression IF; glial scar formation; neuronal survival; behavioral analysis

NF-κB, nuclear factor-kappa B; GFAP, glial fibrillary acidic protein; GAP-43, growth-associated protein-43; NF-H, neurofilament-H; MyD88, myeloid differentiation primary response 88; RT-PCR, real-time polymerase chain reaction; WB, Western blot; HE, haematoxylin–eosin; IF, immunofluorescence; IHC, immunohistochemistry.

10.3389/fnins.2022.968791

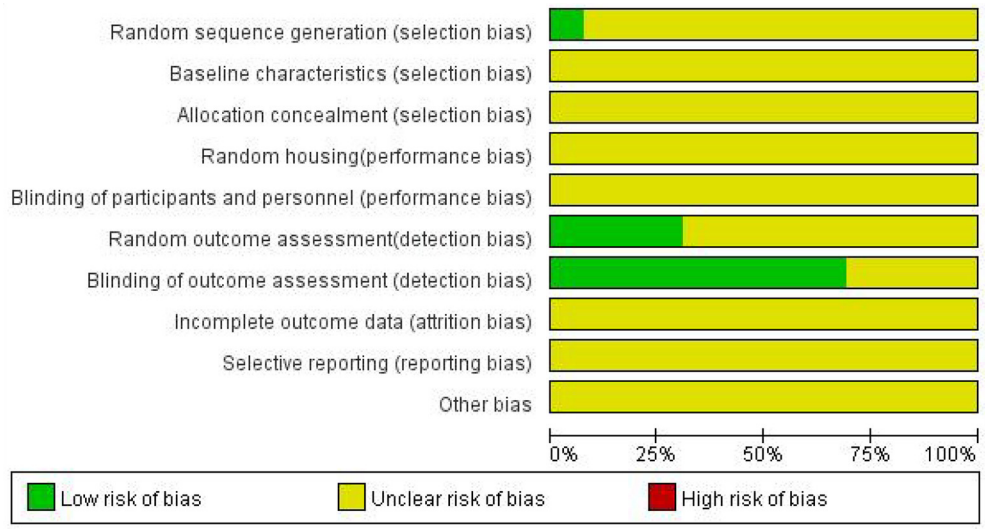

FIGURE 2
Risk of bias.

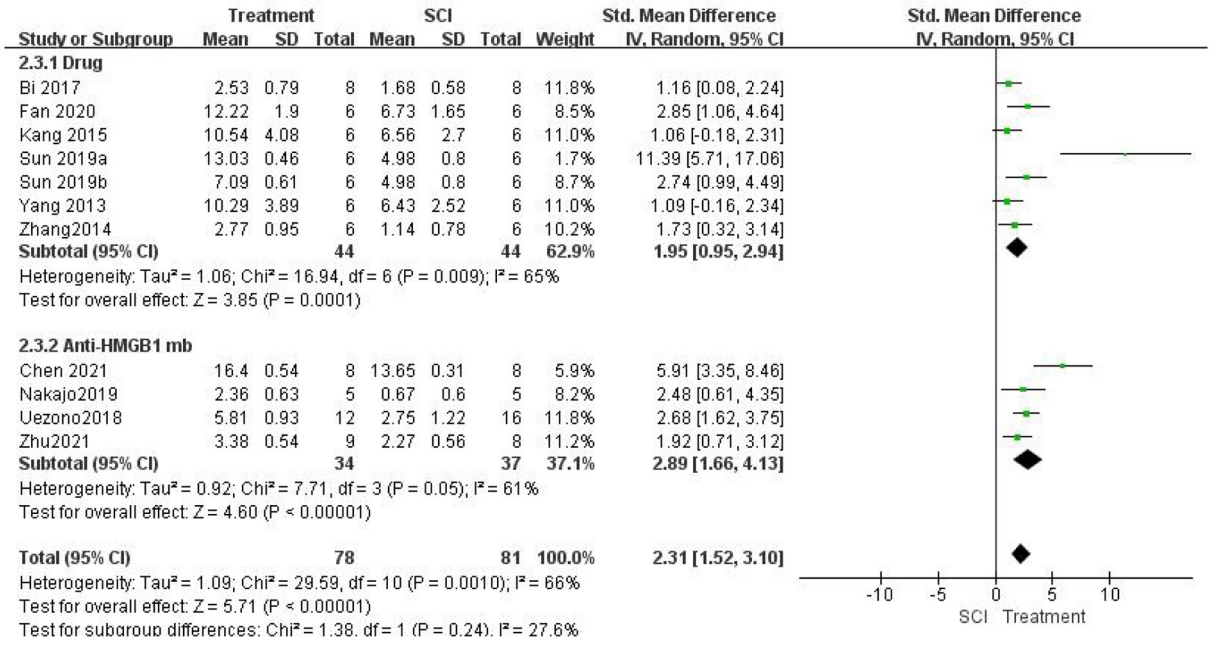

FIGURE 3
Forest plot for the effects of HMGB1 intervention on locomotor function scores in SCI (random-effects model). Green dots indicate weighted effect sizes for 11 treatment regimens and error bars indicate 95% confidence intervals for each outcome. Heterogeneity of the study is indicated by the I2 statistic. $p < 0.001$ indicates statistical significance.

random-effects model [seven studies, $n = 88$, SMD = 1.95, 95% CI (0.95–2.94), $P = 0.0001$; Figure 3]. There was moderate heterogeneity in this group of studies (I2 = 65%, $P = 0.009$). Four studies (Uezono et al., 2018; Nakajo et al., 2019; Chen et al., 2021; Zhu et al., 2021) used anti-HMGB1 Ab and found that the locomotor function scores in the treatment group were significantly higher than those in the SCI group using a random-effects model [four studies, $n = 71$, SMD = 2.89, 95% CI (1.66–4.13), $P < 0.00001$; Figure 3]. The heterogeneity was moderate in this group of studies (I2 = 61%, $P = 0.05$). In addition, there were significant differences between subgroups (I2 = 27.6%, $P = 0.24$).

Locomotor function recovery was measured in one study (Kigerl et al., 2018) with BMS scores, and no differences were found between the control groups and SCI mice treated with anti-HMGB1 Ab ($P > 0.05$). One study (Sun et al., 2019) also measured locomotor function recovery using the inclined plane score. Significant increases in the mean inclined plane test results were found compared with the SCI group ($P < 0.05$). Another study (Fan et al., 2020) used the rump height index (RHI) assay to assess improvement in locomotor function. The results indicated that the RHI value increased significantly compared with that of the SCI group ($P < 0.05$).

Assessment of the anti-inflammatory effect of inhibiting HMGB1

First, we evaluated whether the treatment in this study significantly inhibited the role of HMGB1 *in vivo*. Five studies (Kigerl et al., 2018; Uezono et al., 2018; Nakajo et al., 2019; Chen et al., 2021; Zhu et al., 2021) used HMGB1 neutralizing Abs and did not examine HMGB1 expression. Seven studies (Yang et al., 2013; Zhang et al., 2014; Kang et al., 2015; Bi et al., 2017; Sun et al., 2019; Wu et al., 2021) measured HMGB1 expression levels after SCI. HMGB1 levels were significantly lower in the treatment group than in the SCI groups using a random-effects model [seven studies, $n = 88$, SMD $= -2.67$, 95% CI (-3.96 to -1.38), $P < 0.0001$; Figure 4]. Heterogeneity was significantly high in this group of studies ($I2 = 75\%$, $P = 0.0006$).

Seven studies (Zhang et al., 2014; Kang et al., 2015; Bi et al., 2017; Nakajo et al., 2019; Fan et al., 2020; Chen et al., 2021; Wu et al., 2021) measured TNF-α levels after SCI and found that TNF-α levels were significantly lower in the treatment group than in the SCI groups using a random-effects model [seven studies, $n = 76$, SMD $= -2.65$, 95% CI (-3.90 to -1.41), $P < 0.0001$; Figure 5]. Heterogeneity was moderate in this group of studies ($I2 = 65\%$, $P = 0.0009$).

Assessment of the attenuation of edema by inhibiting HMGB1

Five studies (Bi et al., 2017; Uezono et al., 2018; Nakajo et al., 2019; Sun et al., 2019) examined spinal cord water content. A meta-analysis showed that inhibiting the role of HMGB1 *in vivo* could significantly reduce spinal cord edema. Water content was significantly lower in the treatment group than in the SCI groups [five studies, $n = 56$, SMD $= -4.86$, 95% CI (-7.38 to -2.33), $P = 0.0002$; Figure 6] using a random-effects model because the degree of heterogeneity was high ($I2 = 76\%$, $P = 0.002$).

Assessment of the reduction in apoptosis after inhibiting HMGB1

Three studies (Bi et al., 2017; Uezono et al., 2018; Nakajo et al., 2019) measured the number of apoptotic cells after SCI and found that the number of apoptotic cells was significantly lower in the treatment group than in the SCI groups using a random-effects model (three studies, $n = 36$, SMD $= -3.31$, 95% CI (-6.40– -0.22), $P = 0.04$; Figure 7]. Heterogeneity was significantly high in this group of studies ($I2 = 85\%$, $P = 0.001$).

Publication bias

Funnel plots of publication bias for locomotor function scores were assessed (Figure 8). The asymmetries found in the funnel plots indicated the possibility of publication bias.

Discussion

Summary of evidence

In this study, we first systematically reviewed the recently published literature on the therapeutic and prognostic role of HMGB1-targeted therapy in TSCI. The search identified 170 studies, which were eventually narrowed down to 12 by applying our inclusion/exclusion criteria. After reading the full text, the outcome characteristics were extracted and analyzed, and finally, a meta-analysis was conducted to calculate an accurate estimate of the effect size for each treatment.

All studies investigated the efficacy of targeting HMGB1 in SCI treatment. Seven studies (Yang et al., 2013; Zhang et al., 2014; Kang et al., 2015; Bi et al., 2017; Sun et al., 2019; Wu et al., 2021) selected different drugs to inhibit HMGB1 expression. Moreover, there were variations of the timing and protocol of the intervention in the above studies (Table 1).

Glycyrrhizin (GL) is a natural anti-inflammatory found in licorice root that is able to inhibit HGMB1 and its cytokine-like signaling, ethyl pyruvate (EP) has also been shown to be a neuroprotective therapeutic agent, inhibiting neuroinflammation and promoting spinal cord repair. Sun et al. (Sun et al., 2019) used EP or GL *via* an intraperitoneal injection to inhibit HMGB1. Rats received a 50 mg/kg dose of EP (diluted in 0.9% saline) or a 100 mg/kg dose of GL (diluted in 0.9% saline) *via* an intraperitoneal injection (i.p.) immediately after SCI, and then continued to receive this injection daily after the injury. The results showed that EP and GL inhibited HMGB1 expression in the spinal cord and HMGB1 levels in the serum of SCI rats. Inhibition of HMGB1 can improve locomotor function and reduce spinal water content and AQP-4 overexpression in rats with spinal cord injury. Furthermore, HMGB1 inhibition also repressed the activation of the TLR-4/myeloid differentiation primary response gene 88 (Myd 88)/nuclear factor-kappa B (NF-κB) signaling pathway. Two other studies (Fan et al., 2020; Wu et al., 2021) also used GL, and both of them significantly reduced the expression levels of HMGB1 and inflammatory factors. Fan et al. (2020)

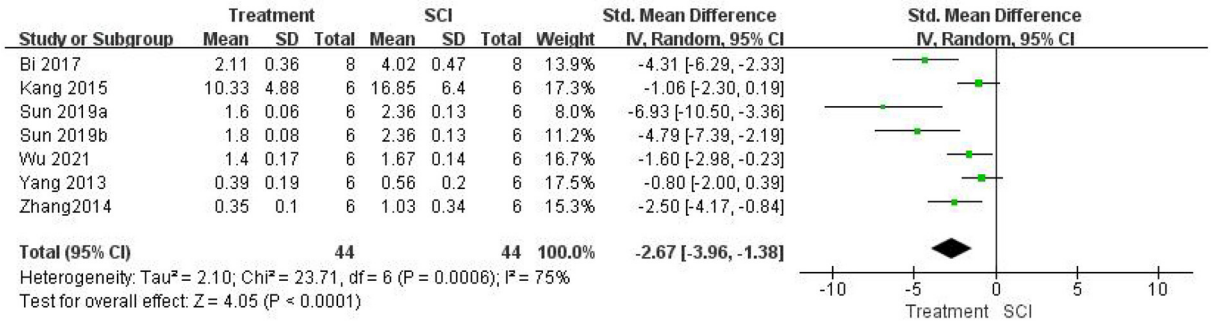

FIGURE 4
Forest plot for the effects of HMGB1 intervention on HMGB1 expression in SCI (random-effects model).

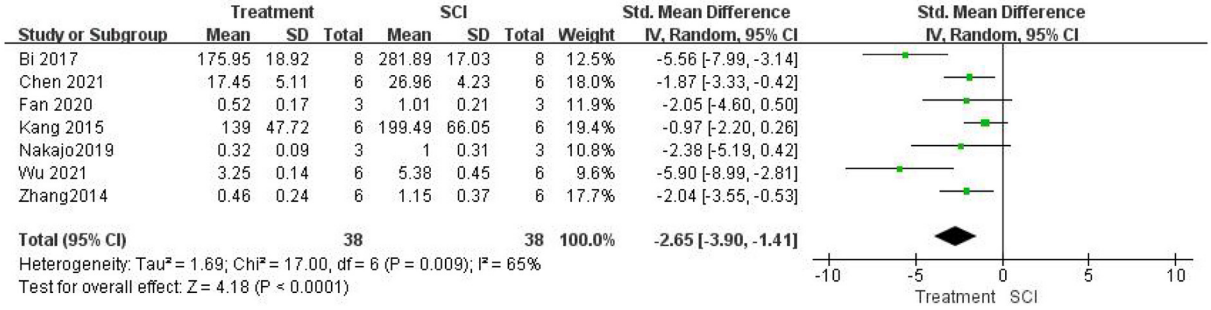

FIGURE 5
Forest plot for the effects of HMGB1 intervention on TNF-α levels in SCI (random-effects model).

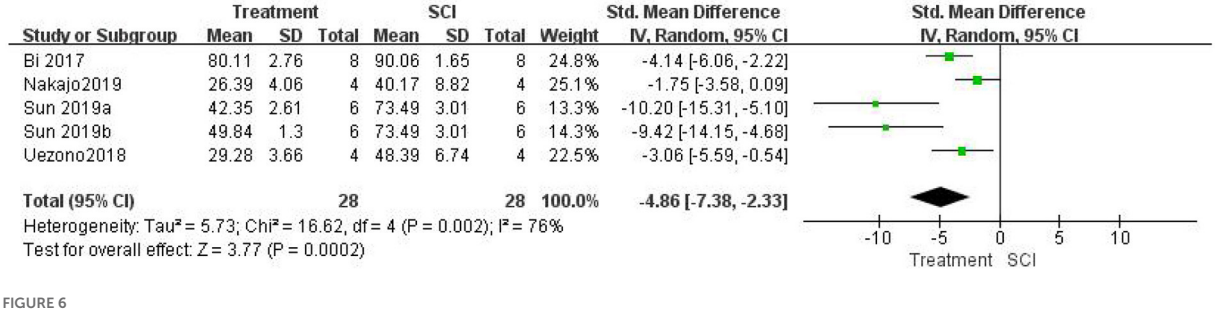

FIGURE 6
Forest plot for the effects of HMGB1 intervention on spinal cord water content in SCI (random-effects model).

showed that a 10 mg/kg dose of GL in saline administered daily *via* i.p. for 14 days after SCI and the first injection immediately after SCI inhibited HMGB1 expression, decreased the number of proinflammatory macrophages/microglia after SCI through the RAGE/NF-κB pathway, reduced neuronal loss and demyelination and improved functional recovery. However, Wu et al. (2021) used different doses. In this study, GL was diluted in dimethyl sulfoxide and 20% sulfobutylether-b-cyclodextrin in 0.9% saline. Rats received 100 mg/kg GL by i.p. immediately after injury, and then daily for 3 days. The results demonstrated that GL could inhibit HMGB1 expression through the P38/Jun N-terminal kinase (JNK) pathway, thus alleviating the inflammatory response after SCI.

Shikonin is the major bioactive component extracted from the roots of Lithospermum erythrorhizon. Recent studies have shown that shikonin is an effective inhibitor of protein–protein interactions with multiple targets in both the intracellular and extracellular compartments, and exhibits a variety of

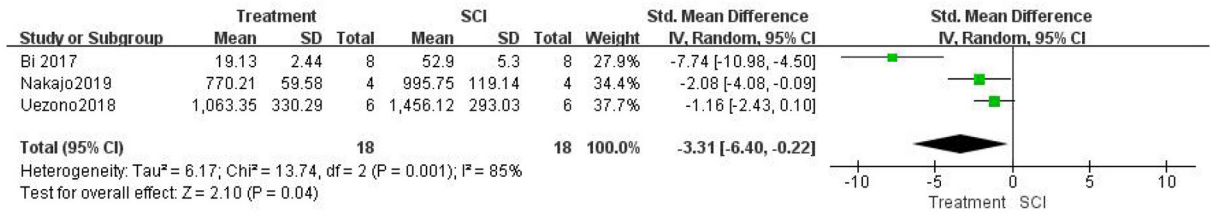

FIGURE 7
Forest plot for the effects of HMGB1 intervention on apoptosis in SCI (random-effects model).

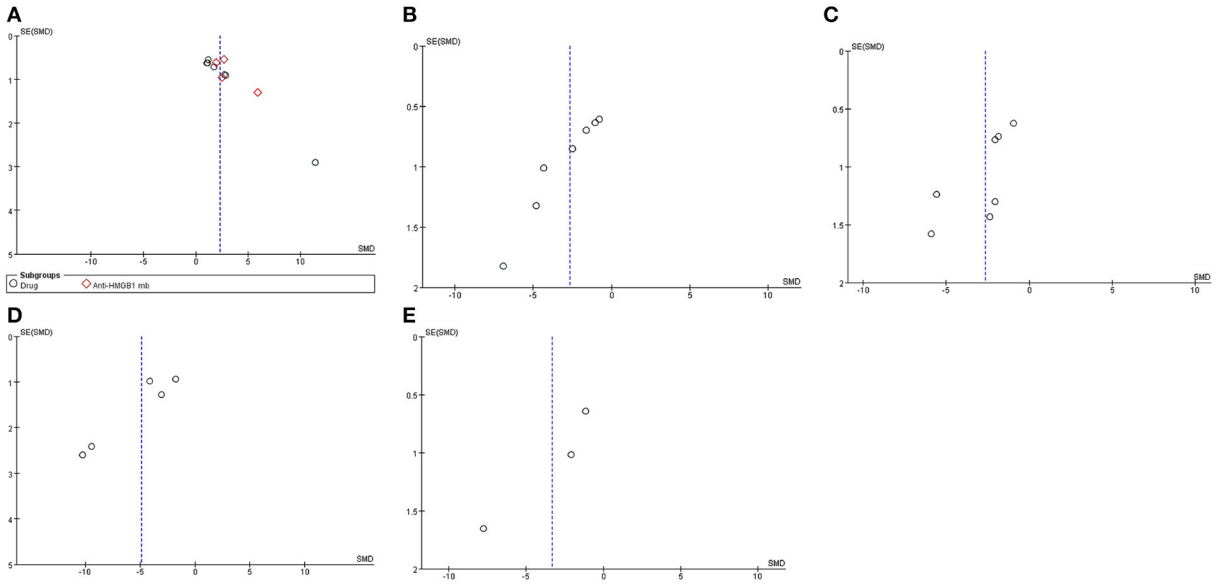

FIGURE 8
Asymmetries found in the funnel plots indicated the possibility of publication bias. Funnel plots of publication bias for locomotor function score **(A)**, HMGB1 levels **(B)**, TNF-α levels **(C)**, water content **(D)**, and apoptosis **(E)**.

biological activities related to cancer treatment, inflammation and wound healing (Chen et al., 2002; Guo et al., 2019a). Its anti-inflammatory effect may be related to the downregulation of HMGB1 expression (Yang et al., 2014; Bi et al., 2017). One study (Bi et al., 2017) used 100 mg/kg shikonin administered by intraperitoneal injection 30 min after SCI to downregulate HMGB1 levels and showed that shikonin could promote the recovery of locomotor function, suppress apoptosis and inhibit spinal cord edema *via* inactivation of the HMGB1/TLR4/NF-κB signaling pathway in an SCI model in rats.

HG, an active ingredient of Aconiti Lateralis Radix Praeparata, has been traditionally used as an anti-inflammatory agent in oriental countries (Zhang et al., 2017). A study has shown that HG plays protective roles in brain injury by inducing the upregulation of HO-1 to reduce the level of HMGB1 (Ha et al., 2012). Among the seven studies, one study (Zhang et al., 2014) used HG as an anti-inflammatory agent. The results showed that 10 mg/kg HG *via i.*p. just after SCI increased the expression of IL-4 and IL-10 and promoted M2 macrophage activation, reduced HMGB1 expression dependent on HO-1 induction and then promoted locomotor function after SCI.

In recent years, HBO therapy has received increasing attention in reducing the inflammatory response and apoptosis in SCI (Meng et al., 2019; Ying et al., 2019; Zhou et al., 2019b). HBO intervention was used in two studies (Yang et al., 2013; Kang et al., 2015) with the same timing and protocol. During HBO intervention, continuous ventilation was maintained for 1 h with oxygen flow of 8–10 L/min and chamber oxygen concentration exceeding 95%. The intervention was managed once daily. The results demonstrated that HBO

intervention could reduce the secondary damage of SCI caused by inflammatory responses by decreasing the expression of HMGB1 and TNF-α and promoting the recovery of locomotor function by downregulating HMGB1/TLR4/NF-KB pathway.

Five studies (Kigerl et al., 2018; Uezono et al., 2018; Nakajo et al., 2019; Chen et al., 2021; Zhu et al., 2021) using anti-HMGB1 Ab were included in this study. Three of the studies (Uezono et al., 2018; Nakajo et al., 2019; Zhu et al., 2021) improved the recovery of locomotor function with intraperitoneal injections of anti-HMGB1 monoclonal antibody (mAb) (IgG2a subclass, 8 mg/kg). The mAb recognition epitopes were identified by using synthetic overlapping peptides of 15 amino acids in length derived from the human HMGB1 sequence. The clone (#10–22, subclass IgG2a) recognizing the C-terminal sequence of the HMGB1 molecule (DEDEEEE) was used for the experiments (Liu et al., 2007). Moreover, it is important to note that the timing of mAb injection varies. Uezono et al. (2018) opted two injections 5 min and 6 h after injury. Zhu et al. (2021) selected a single injection 5 min after spinal cord injury. The results showed that both interventions significantly improved motor function recovery after SCI in rats, but two injections improved locomotor function better than a single injection (2.68>1.92, Figure 3). However, from the perspective of clinical application, 5 min after spinal cord injury is not practical. Nakajo et al. (2019) chosed to inject mAb at 0 h, 3 h, 6 h, 9 h and 12 h after SCI to test the therapeutic time window of mAb administration. The results showed that there was no significant difference in functional recovery between the 0 h and 3 h administered groups, while injection at 6 h had a poor effect, and injection at 9 and 12 h had no therapeutic effect.

Kigerl et al. (2018) also received i.p. of anti-HMGB1 mAb, but the improvement in locomotor function was not statistically significant. There are several possible reasons. First, the mAb recognition epitopes were different. Overlapping 18–amino acid peptides covering the entire HMGB1 sequence were synthesized for epitope mapping. Clone 1 bound to a region between amino acids 53 and 63 and clone 2 bound to amino acids 67–78 of the protein, both in the A box region of HMGB1 (Qin et al., 2006). Second, the timing and protocol of the injection are different. Ab was injected daily *via* i.p. injection (50 μg/day) starting 1 day prior to SCI and continuing for 7 days. Under this administration, intraperitoneal route of administration (50 μg/day) may not allow sufficient concentration of blocking antibodies to accumulate in tissue at the site of injury and adjacent to the intact spinal cord. Interestingly, in another study (Chen et al., 2021), although they used polyclonal antibodies, which are less specific than mAb, at a dose of 1 μl (50 ng/μl), intrathecal injection of anti-HMGB1 Ab immediately after SCI improved locomotor function more significantly than i.p. (5.91 > 2.68, Figure 3). Therefore, a more direct route of delivery may improve access and binding efficiency. Intrathecal injections are a better option, bypassing the blood–spinal barrier and ensuring sufficient concentrations of antibodies can accumulate at the site of spinal cord injury. In addition, subgroup analysis showed that there was a greater improvement in locomotor function in the anti-HMGB1 Ab group than in the drug group (2.89 > 1.95, I2 = 27.6%, $P = 0.24$); thus, immediate intrathecal injection after SCI may be a more efficacious treatment. It has been reported that neuroprotective factors have a longer treatment window for spinal cord injury in primate models than in rodent models (Nishimura et al., 2014). From the perspective of clinical application, 0–3 hours after spinal cord injury may be a more practical choice.

Possible mechanism of the effect of HMGB1-targeted therapy in TSCI

We found that HMGB1-targeted therapy can improve functional recovery after spinal cord injury in a variety of ways (Nishibori et al., 2019; Zhou et al., 2019a; Chen et al., 2021). This is mostly through the following three key modalities: reduce the release of inflammatory factors and inhibit inflammation in the early stage of spinal cord injury; reduce the expression of AQP-4 and attenuate spinal cord edema; and inhibit cell apoptosis.

Traumatic spinal cord injury (TSCI) can lead to a systemic inflammatory response, that is, an increase in immune cells and proinflammatory mediators, resulting in the persistence of an inflammatory microenvironment that ultimately leads to organ dysfunction (Sun et al., 2016). The local inflammatory microenvironment in the injured spinal cord includes necrotic neurons, damaged endothelial cells, and activated glial cells. This microenvironment produces various proinflammatory mediators (Hasturk et al., 2009), such as HMGB1, TNF-α, IL-1β, and IL-6. As HMGB1 plays an active role in the inflammatory response as an endogenous alarm, many studies have focused on HMGB1 as a cytokine that can exert therapeutic potential by inhibiting its gene expression or extracellular activity (Kikuchi et al., 2011; Andersson et al., 2018). In this study, 7 studies (Yang et al., 2013; Zhang et al., 2014; Kang et al., 2015; Bi et al., 2017; Sun et al., 2019; Wu et al., 2021) inhibited the expression of HMGB1 to varying degrees by five methods, including GL, EP, SHI, HG and HBO, among which EP, perhaps the most effective method, significantly reduced HMGB1 expression on the first day after SCI compared with the control group. Shi, GL and HG downregulated the expression of HMGB1 to varying degrees, but the overall effect was inferior to that of EP. In addition, HBO is not as effective as the other methods mentioned above, but it can also effectively inhibit HMGB1 expression. In sterile inflammation, such as traumatic spinal cord injury and ischemia–reperfusion injury, HMGB1 is considered to be an early mediator of inflammation (Chen et al., 2011). HMGB1 translocates from the nucleus to the cytoplasm after SCI, and its expression increases earlier than that of pro-inflammatory cytokines such as TNF-α, IL-1β, and IL-6. By inhibiting HMGB1

expression after spinal cord injury, its role as a proinflammatory mediator is also blocked. Therefore, in seven studies measuring TNF-α levels (Zhang et al., 2014; Kang et al., 2015; Bi et al., 2017; Nakajo et al., 2019; Fan et al., 2020; Chen et al., 2021; Wu et al., 2021), five different methods, including anti-HMGB1 Ab, GL, SHI, HG, and HBO, significantly reduced TNF-α levels. Early intervention with HMGB1 may have a positive effect on reducing the proinflammatory cascade in the early stages of SCI.

Spinal cord edema, a hallmark of spinal cord injury, aggravates primary injury by increasing intrathecal pressure, leading to bleeding and BSCB destruction and causing further injury, which triggers further cell necrosis (Ahuja et al., 2017; Quadri et al., 2020). It is mainly due to inflammation after SCI. HMGB1 is an inflammatory cytokine that is closely related to spinal cord edema after SCI (Sun et al., 2019). Studies have shown that anti-HMGB1 treatment can attenuate CNS edema and reduce the inflammatory response induced by HMGB1 (Nosaka et al., 2018; Xia et al., 2020). In five studies (Bi et al., 2017; Uezono et al., 2018; Nakajo et al., 2019; Sun et al., 2019), HMGB1 was inhibited by Shi, anti-HMGB1 Ab, EP and GL, and spinal cord water content was measured. The results showed that inhibition of HMGB1 expression reduced spinal cord water content to varying degrees. In the spinal cord, inhibition or downregulation of AQP4 overexpression leads to an attenuation in spinal cord edema after spinal cord injury (Ge et al., 2013; Hu et al., 2015). Sun et al. (2019) reported that AQP-4 expression was also significantly downregulated after inhibition of HMGB1, suggesting that inhibition of HMGB1 expression and further inhibition of edema may play a role by reducing AQP-4 overexpression.

Apoptosis is a naturally occurring physiological process and plays a key role in secondary spinal cord injury (Beattie et al., 2000; Shi et al., 2021). Finding a method to inhibit apoptosis after spinal cord injury may have important clinical significance for further treatment. HMGB1 can be passively released by necrotic neurons or damaged cells after SCI. It has been reported that the ability of Hmgb1(-/-) necrotic cells to promote inflammation was greatly reduced, which proved that the release of Hmgb1 can signal the demise of a cell to neighboring cells (Scaffidi et al., 2002). In recent years, an increasing number of studies have reported that HMGB1 plays an important role in the process of CNS apoptosis (Guo et al., 2019b; Wang and Zhang, 2020). Three studies (Bi et al., 2017; Uezono et al., 2018; Nakajo et al., 2019) in this study investigated the effect of inhibiting HMGB1 expression on apoptosis after SCI. The results showed that inhibition of HMGB1 expression by Shi and anti-HMGB1 Ab could significantly reduce the number of apoptotic cells.

NF-κB is an important inflammatory transcription factor in the CNS, that regulates many genes and signaling pathways involved in inflammation (Ma and Hottiger, 2016). Previous reports have shown that NF-κB upregulates proinflammatory cytokines, including TNF-α, IL-1β, and IL-6 in SCI (Sun et al., 2017; Liu et al., 2019). Extracellular HMGB1 activates inflammatory cells by activating the receptor for RAGE, TLR-2 and TLR-4 (van Beijnum et al., 2008; Paudel et al., 2018). Activation of any of these receptors enhances the NF-κB mediated transcription of inflammatory mediators (Kawai and Akira, 2007; Tóbon-Velasco et al., 2014). Seven studies (Yang et al., 2013; Kang et al., 2015; Bi et al., 2017; Sun et al., 2019; Fan et al., 2020; Chen et al., 2021) demonstrated that HMGB1-targeted therapy alleviated secondary injury via the NF-κB signaling pathway, including four studies (Kang et al., 2015; Bi et al., 2017; Sun et al., 2019) via the HMGB1/TLR-4/NF-κB pathway and one study (Fan et al., 2020) via the HMGB1/RAGE/NF-κB pathway. However, only one (Chen et al., 2021) of these seven studies used anti-HMGB1 Ab, so whether anti-HMGB1 Ab plays a role through the NF-κB signaling pathway needs further research.

Anti-HMGB1 therapy can jointly alleviate secondary injury after SCI through different mechanisms, and different therapeutic methods have different effects.Anti-HMGB1 Ab has been reported to be beneficial in animal models for the treatment of various types of inflammatory diseases, particularly in the CNS (Vijayakumar et al., 2019). In this study, considering the above effects of HMGB1 in rat or mouse models of TSCI, HMGB1-targeted therapy may be an effective treatment strategy after TSCI, and it improves locomotor function recovery, reduces inflammation, attenuates edema, and reduces apoptosis after TSCI. Intrathecal injection of anti-HMGB1 Ab 0-3 h after TSCI may be the most efficacious treatment. In addition, some novel therapies, such as the combination of anti-HMGB1 antibodies with other therapies, may generate more significant therapeutic effects. With the application of new therapeutic methods, we can expect the prospect of HMGB1-targeted therapy in the treatment of TSCI to improve.

Limitations

This systematic review has several limitations. First, among the 12 articles included, only 4 articles were from Japan and the US, and the rest were all from China. The limited number of articles was also a major limitation of this review. Moreover, given the existence of publication bias, the conclusions drawn thus far may also be overestimated. In addition, according to the information reported in articles, we were unable to assess whether all baseline features were balanced among groups, and the animal models and species used in the study were different, as well as simple data integration, which also contributed to the high heterogeneity of this meta-analysis. Sex as a biological variable is an important reference factor. Male and female animals respond differently to injury. However, sex was not reported comprehensively in the included studies, and sex characteristics were not reported in the two studies, which also leads to bias. The wide variety of drug or anti-HMGB1 Ab doses, different treatment initiation times, different routes of

administration, and varied methodological quality of studies could also bring confounding factors. The BBB scale or BMS scale is the most common method used to assess locomotor function recovery effects after SCI. However, it depends on the judgment and interpretation of the observer and is prone to bias.

Moreover, although all animal studies in this systematic review evaluated models of spinal cord injury in the chest, 50% of human spinal cord injuries affect the neck region, with C5 being the most commonly affected region (Alizadeh et al., 2019). There are significant anatomical differences in the spinal cord between the neck and thoracic vertebrae that affect the degree of injury and recovery.

Conclusion

HMGB1-targeted therapy improves locomotor function recovery, reduces inflammation, attenuates edema, and reduces apoptosis in rat and mouse models of TSCI. Intrathecal injection of anti-HMGB1 Ab 0-3 h after SCI may be the most efficacious treatment. The use of this meta-analysis was limited by the poor methodological quality of the included studies. Therefore, more high-quality studies and objective evidence are needed to support preclinical HMGB1-targeted therapy for SCI.

Data availability statement

The original contributions presented in the study are included in the article/supplementary material, further inquiries can be directed to the corresponding author.

Author contributions

CD and LS conceived the review. CD and LD performed the literature searches, study selection, data extraction, quality assessment, and undertook the review analyses with JL. LS checked as third advisers and critically revised the manuscript. CD wrote the initial draft. All authors approved the final version of the paper.

Funding

This study was supported by grants from the National Natural Science Foundation of China (No. 81870976) and Shanxi Provincial Health Commission Key Projects to Tackle Key Problems (No. 2020XM27).

Conflict of interest

The authors declare that the research was conducted in the absence of any commercial or financial relationships that could be construed as a potential conflict of interest.

Publisher's note

References

Ahuja, C. S., Wilson, J. R., Nori, S., Kotter, M. R. N., Druschel, C., Curt, A., et al. (2017). Traumatic spinal cord injury. *Nat. Rev. Dis. Primers* 3, 17018. doi: 10.1038/nrdp.2017.18

Alizadeh, A., Dyck, S. M., and Karimi-Abdolrezaee, S. (2019). Traumatic spinal cord injury: an overview of pathophysiology, models and acute injury mechanisms. *Front. Neurol.* 10, 282. doi: 10.3389/fneur.2019.00282

Andersson, U., Yang, H., and Harris, H. (2018). Extracellular HMGB1 as a therapeutic target in inflammatory diseases. *Expert Opin. Ther. Targets* 22, 263–277. doi: 10.1080/14728222.2018.1439924

Beattie, M. S., Farooqui, A. A., and Bresnahan, J. C. (2000). Review of current evidence for apoptosis after spinal cord injury. *J. Neurotrauma* 17, 915–925. doi: 10.1089/neu.2000.17.915

Bi, Y., Zhu, Y., Zhang, M., Zhang, K., Hua, X., Fang, Z., et al. (2017). Effect of shikonin on spinal cord injury in rats via regulation of HMGB1/TLR4/NF-κB signaling pathway. *Cell. Physiol. Biochem.* 43, 481–491. doi: 10.1159/000480474

Chen, K. B., Chang, M. M., Wang, S. L., Li, Y. X., Wang, Y. X., Xu, Z. G., et al. (2021). High mobility group box-1 serves a pathogenic role in spinal cord injury via the promotion of pro-inflammatory cytokines. *J. Leukoc. Biol.* 110, 1131–1142. doi: 10.1002/JLB.3MA0721-007R

Chen, K. B., Uchida, K., Nakajima, H., Yayama, T., Hirai, T., Rodriguez Guerrero, A., et al. (2011). High-mobility group box-1 and its receptors contribute to proinflammatory response in the acute phase of spinal cord injury in rats. *Spine* 36, 2122–2129. doi: 10.1097/BRS.0b013e318203941c

Chen, X., Yang, L., Oppenheim, J. J., and Howard, M. Z. (2002). Cellular pharmacology studies of shikonin derivatives. *Phytother. Res.* 16, 199–209. doi: 10.1002/ptr.1100

Fan, H., Tang, H. B., Chen, Z., Wang, H. Q., Zhang, L., Jiang, Y., et al. (2020). Inhibiting HMGB1-RAGE axis prevents pro-inflammatory macrophages/microglia polarization and affords neuroprotection after spinal cord injury. *J. Neuroinflammation* 17, 295. doi: 10.1186/s12974-020-01973-4

Ge, R., Zhu, Y., Diao, Y., Tao, L., Yuan, W., and Xiong, X. C. (2013). Anti-edema effect of epigallocatechin gallate on spinal cord injury in rats. *Brain Res.* 1527, 40–46. doi: 10.1016/j.brainres.2013.06.009

Guo, C., He, J., Song, X., Tan, L., Wang, M., Jiang, P., et al. (2019a). Pharmacological properties and derivatives of shikonin-a review in recent years. *Pharmacol. Res.* 149, 104463. doi: 10.1016/j.phrs.2019.104463

Guo, X., Shi, Y., Du, P., Wang, J., Han, Y., Sun, B., et al. (2019b). HMGB1/TLR4 promotes apoptosis and reduces autophagy of hippocampal neurons in diabetes combined with OSA. *Life Sci.* 239, 117020. doi: 10.1016/j.lfs.2019.117020

Ha, Y. M., Kim, M. Y., Park, M. K., Lee, Y. S., Kim, Y. M., Kim, H. J., et al. (2012). Higenamine reduces HMGB1 during hypoxia-induced brain injury by induction of heme oxygenase-1 through PI3K/Akt/Nrf-2 signal pathways. *Apoptosis* 17, 463–474. doi: 10.1007/s10495-011-0688-8

Halsey, A. M., Conner, A. C., Bill, R. M., Logan, A., and Ahmed, Z. (2018). Aquaporins and their regulation after spinal cord injury. *Cells* 7, 174. doi: 10.3390/cells7100174

Hasturk, A., Atalay, B., Calisaneller, T., Ozdemir, O., Oruckaptan, H., and Altinors, N. (2009). Analysis of serum pro-inflammatory cytokine levels after rat spinal cord ischemia/reperfusion injury and correlation with tissue damage. *Turk. Neurosurg.* 19, 353–359. Available online at: https://www.researchgate.net/publication/38028502_Analysis_of_serum_pro-inflammatory_cytokine_levels_after_rat_spinal_cord_ischemiareperfusion_injury_and_correlation_with_tissue_damage

Hellenbrand, D. J., Quinn, C. M., Piper, Z. J., Morehouse, C. N., Fixel, J. A., and Hanna, A. S. (2021). Inflammation after spinal cord injury: a review of the critical timeline of signaling cues and cellular infiltration. *J. Neuroinflammation* 18, 284. doi: 10.1186/s12974-021-02337-2

Hooijmans, C. R., Rovers, M. M., de Vries, R. B., Leenaars, M., Ritskes-Hoitinga, M., and Langendam, M. W. (2014). SYRCLE's risk of bias tool for animal studies. *BMC Med. Res. Methodol.* 14, 43. doi: 10.1186/1471-2288-14-43

Hu, A. M., Li, J. J., Sun, W., Yang, D. G., Yang, M. L., Du, L. J., et al. (2015). Myelotomy reduces spinal cord edema and inhibits aquaporin-4 and aquaporin-9 expression in rats with spinal cord injury. *Spinal Cord* 53, 98–102. doi: 10.1038/sc.2014.209

Huebener, P., Gwak, G. Y., Pradere, J. P., Quinzii, C. M., Friedman, R., Lin, C. S., et al. (2014). High-mobility group box 1 is dispensable for autophagy, mitochondrial quality control, and organ function *in vivo*. *Cell Metab.* 19, 539–547. doi: 10.1016/j.cmet.2014.01.014

James, S. L. (2019). Global, regional, and national burden of traumatic brain injury and spinal cord injury, 1990-2016: a systematic analysis for the global burden of disease study 2016. *Lancet Neurol.* 18, 56–87. doi: 10.1016/S1474-4422(18)30415-0

Kang, N., Hai, Y., Yang, J., Liang, F., and Gao, C. J. (2015). Hyperbaric oxygen intervention reduces secondary spinal cord injury in rats via regulation of HMGB1/TLR4/NF-kappa B signaling pathway. *Int. J. Clin. Exp. Pathol.* 8, 1141–1153.

Kang, Y., Ding, H., Zhou, H., Wei, Z., Liu, L., Pan, D., et al. (2017). Epidemiology of worldwide spinal cord injury: a literature review. *J. Neurorestoratology*. 6, 1–9. doi: 10.2147/JN.S143236

Kawai, T., and Akira, S. (2007). Signaling to NF-kappaB by toll-like receptors. *Trends Mol. Med.* 13, 460–469. doi: 10.1016/j.molmed.2007.09.002

Kigerl, K. A., Lai, W., Wallace, L. M., Yang, H., and Popovich, P. G. (2018). High mobility group box-1 (HMGB1) is increased in injured mouse spinal cord and can elicit neurotoxic inflammation. *Brain Behav. Immun.* 72, 22–33. doi: 10.1016/j.bbi.2017.11.018

Kikuchi, K., Uchikado, H., Miura, N., Morimoto, Y., Ito, T., Tancharoen, S., et al. (2011). HMGB1 as a therapeutic target in spinal cord injury: a hypothesis for novel therapy development. *Exp. Ther. Med.* 2, 767–770. doi: 10.3892/etm.2011.310

Kitchen, P., Salman, M. M., Halsey, A. M., Clarke-Bland, C., MacDonald, J. A., Ishida, H., et al. (2020). Targeting aquaporin-4 subcellular localization to treat central nervous system edema. *Cell* 181, 784–799.e719. doi: 10.1016/j.cell.2020.03.037

Liu, J., Zhang, S., Fan, X., Yuan, F., Dai, J., and Hu, J. (2019). Dexmedetomidine preconditioning ameliorates inflammation and blood-spinal cord barrier damage after spinal cord ischemia-reperfusion injury by down-regulation high mobility group box 1-toll-like receptor 4-nuclear factor κB signaling pathway. *Spine* 44, E74–e81. doi: 10.1097/BRS.0000000000002772

Liu, K., Mori, S., Takahashi, H. K., Tomono, Y., Wake, H., Kanke, T., et al. (2007). Anti-high mobility group box 1 monoclonal antibody ameliorates brain infarction induced by transient ischemia in rats. *FASEB J.* 21, 3904–3916. doi: 10.1096/fj.07-8770com

Ma, B., and Hottiger, M. O. (2016). Crosstalk between Wnt/β-catenin and NF-κB signaling pathway during inflammation. *Front. Immunol.* 7, 378. doi: 10.3389/fimmu.2016.00378

Man, L. L., Liu, F., Wang, Y. J., Song, H. H., Xu, H. B., Zhu, Z. W., et al. (2015). The HMGB1 signaling pathway activates the inflammatory response in Schwann cells. *Neural. Regen. Res.* 10, 1706–1712. doi: 10.4103/1673-5374.167773

Masterman, E., and Ahmed, Z. (2021). Experimental treatments for oedema in spinal cord injury: a systematic review and meta-analysis. *Cells* 10, 2682. doi: 10.3390/cells10102682

Meng, X. L., Hai, Y., Zhang, X. N., Wang, Y. S., Liu, X. H., Ma, L. L., et al. (2019). Hyperbaric oxygen improves functional recovery of rats after spinal cord injury via activating stromal cell-derived factor-1/CXC chemokine receptor 4 axis and promoting brain-derived neurothrophic factor expression. *Chin. Med. J.* 132, 699–706. doi: 10.1097/CM9.0000000000000115

Moher, D., Liberati, A., Tetzlaff, J., Altman, D. G., and Group, P. (2009). Preferred reporting items for systematic reviews and meta-analyses: the PRISMA statement. *PLoS Med.* 6, e1000097. doi: 10.1371/journal.pmed.1000097

Nakajo, M., Uezono, N., Nakashima, H., Wake, H., Komiya, S., Nishibori, M., et al. (2019). Therapeutic time window of anti-high mobility group box-1 antibody administration in mouse model of spinal cord injury. *Neurosci. Res.* 141, 63–70. doi: 10.1016/j.neures.2018.03.004

Nishibori, M., Mori, S., and Takahashi, H. K. (2019). Anti-HMGB1 monoclonal antibody therapy for a wide range of CNS and PNS diseases. *J. Pharmacol. Sci.* 140, 94–101. doi: 10.1016/j.jphs.2019.04.006

Nishimura, S., Sasaki, T., Shimizu, A., Yoshida, K., Iwai, H., Koya, I., et al. (2014). Global gene expression analysis following spinal cord injury in non-human primates. *Exp. Neurol.* 261, 171–179. doi: 10.1016/j.expneurol.2014.05.021

Nosaka, N., Hatayama, K., Yamada, M., Fujii, Y., Yashiro, M., Wake, H., et al. (2018). Anti-high mobility group box-1 monoclonal antibody treatment of brain edema induced by influenza infection and lipopolysaccharide. *J. Med. Virol.* 90, 1192–1198. doi: 10.1002/jmv.25076

Papatheodorou, A., Stein, A., Bank, M., Sison, C. P., Gibbs, K., Davies, P., et al. (2017). High-mobility group box 1 (HMGB1) is elevated systemically in persons with acute or chronic traumatic spinal cord injury. *J. Neurotrauma* 34, 746–754. doi: 10.1089/neu.2016.4596

Paudel, Y. N., Angelopoulou, E., Piperi, C., Balasubramaniam, V., Othman, I., and Shaikh, M. F. (2019). Enlightening the role of high mobility group box 1 (HMGB1) in inflammation: updates on receptor signalling. *Eur. J. Pharmacol.* 858, 172487. doi: 10.1016/j.ejphar.2019.172487

Paudel, Y. N., Shaikh, M. F., Chakraborti, A., Kumari, Y., Aledo-Serrano, Á., Aleksovska, K., et al. (2018). HMGB1: a common biomarker and potential target for TBI, neuroinflammation, epilepsy, and cognitive dysfunction. *Front. Neurosci.* 12, 628. doi: 10.3389/fnins.2018.00628

Qin, S., Wang, H., Yuan, R., Li, H., Ochani, M., Ochani, K., et al. (2006). Role of HMGB1 in apoptosis-mediated sepsis lethality. *J. Exp. Med.* 203, 1637–1642. doi: 10.1084/jem.20052203

Quadri, S. A., Farooqui, M., Ikram, A., Zafar, A., Khan, M. A., Suriya, S. S., et al. (2020). Recent update on basic mechanisms of spinal cord injury. *Neurosurg. Rev.* 43, 425–441. doi: 10.1007/s10143-018-1008-3

Scaffidi, P., Misteli, T., and Bianchi, M. E. (2002). Release of chromatin protein HMGB1 by necrotic cells triggers inflammation. *Nature* 418, 191–195. doi: 10.1038/nature00858

Shi, Z., Yuan, S., Shi, L., Li, J., Ning, G., Kong, X., et al. (2021). Programmed cell death in spinal cord injury pathogenesis and therapy. *Cell Prolif.* 54, e12992. doi: 10.1111/cpr.12992

Sun, L., Li, M., Ma, X., Feng, H., Song, J., Lv, C., et al. (2017). Inhibition of HMGB1 reduces rat spinal cord astrocytic swelling and AQP4 expression after oxygen-glucose deprivation and reoxygenation via TLR4 and NF-kappaB signaling in an IL-6-dependent manner. *J. Neuroinflammation* 14, 231. doi: 10.1186/s12974-017-1008-1

Sun, L., Li, M., Ma, X., Zhang, L., Song, J., Lv, C., et al. (2019). Inhibiting high mobility group box-1 reduces early spinal cord edema and attenuates astrocyte activation and aquaporin-4 expression after spinal cord injury in rats. *J. Neurotrauma* 36, 421–435. doi: 10.1089/neu.2018.5642

Sun, X., Jones, Z. B., Chen, X. M., Zhou, L., So, K. F., and Ren, Y. (2016). Multiple organ dysfunction and systemic inflammation after spinal cord injury: a complex relationship. *J. Neuroinflammation* 13, 260. doi: 10.1186/s12974-016-0736-y

Tóbon-Velasco, J. C., Cuevas, E., and Torres-Ramos, M. A. (2014). Receptor for AGEs (RAGE) as mediator of NF-kB pathway activation in neuroinflammation and oxidative stress. *CNS Neurol. Disord. Drug Targets* 13, 1615–1626. doi: 10.2174/1871527313666140806144831

Uezono, N., Zhu, Y., Fujimoto, Y., Yasui, T., Matsuda, T., Nakajo, M., et al. (2018). Prior treatment with anti-high mobility group box-1 antibody boosts human neural stem cell transplantation-mediated functional recovery after spinal cord injury. *Stem Cells* 36, 737–750. doi: 10.1002/stem.2802

van Beijnum, J. R., Buurman, W. A., and Griffioen, A. W. (2008). Convergence and amplification of toll-like receptor (TLR) and receptor for advanced glycation end products (RAGE) signaling pathways via high mobility group B1 (HMGB1). *Angiogenesis* 11, 91–99. doi: 10.1007/s10456-008-9093-5

van den Berg, M. E., Castellote, J. M., Mahillo-Fernandez, I., and de Pedro-Cuesta, J. (2010). Incidence of spinal cord injury worldwide: a systematic

review. *Neuroepidemiology* 34, 184–192; discussion 192. doi: 10.1159/000279335

Vijayakumar, E. C., Bhatt, L. K., and Prabhavalkar, K. S. (2019). High mobility group box-1 (HMGB1): a potential target in therapeutics. *Curr. Drug Targets* 20, 1474–1485. doi: 10.2174/1389450120666190618125100

Wang, S., and Zhang, Y. (2020). HMGB1 in inflammation and cancer. *J. Hematol. Oncol.* 13, 116. doi: 10.1186/s13045-020-00950-x

Wu, Z., Wang, Z., Xie, Z., Zhu, H., Li, C., Xie, S., et al. (2021). Glycyrrhizic acid attenuates the inflammatory response after spinal cord injury by inhibiting high mobility group box-1 protein through the p38/Jun N-terminal kinase signaling pathway. *World Neurosurg.* 158, e856–e864. doi: 10.1016/j.wneu.2021.11.085

Xia, H., Wang, D., Guo, X., Wu, K., Huang, F., and Feng, Y. (2020). Catalpol protects against spinal cord injury in mice through regulating microRNA-142-mediated HMGB1/TLR4/NF-κB signaling pathway. *Front. Pharmacol.* 11, 630222. doi: 10.3389/fphar.2020.630222

Yang, H., Wang, H., and Andersson, U. (2020). Targeting inflammation driven by HMGB1. *Front. Immunol.* 11, 484. doi: 10.3389/fimmu.2020.00484

Yang, J., Liu, X., Zhou, Y., Wang, G., Gao, C., and Su, Q. (2013). Hyperbaric oxygen alleviates experimental (spinal cord) injury by downregulating HMGB1/NF-κB expression. *Spine* 38, E1641–E1648. doi: 10.1097/BRS.0000000000000005

Yang, Y., Wang, J., Yang, Q., Wu, S., Yang, Z., Zhu, H., et al. (2014). Shikonin inhibits the lipopolysaccharide-induced release of HMGB1 in RAW264.7 cellsvia IFN and NF-κB signaling pathways. *Int. Immunopharmacol.* 19, 81–87. doi: 10.1016/j.intimp.2014.01.003

Ying, X., Tu, W., Li, S., Wu, Q., Chen, X., Zhou, Y., et al. (2019). Hyperbaric oxygen therapy reduces apoptosis and dendritic/synaptic degeneration via the BDNF/TrkB signaling pathways in SCI rats. *Life Sci.* 229, 187–199. doi: 10.1016/j.lfs.2019.05.029

Zhang, N., Lian, Z., Peng, X., Li, Z., and Zhu, H. (2017). Applications of higenamine in pharmacology and medicine. *J. Ethnopharmacol.* 196, 242–252. doi: 10.1016/j.jep.2016.12.033

Zhang, Z., Li, M., Wang, Y., Wu, J., and Li, J. (2014). Higenamine promotes M2 macrophage activation and reduces Hmgb1 production through HO-1 induction in a murine model of spinal cord injury. *Int. Immunopharmacol.* 23, 681–687. doi: 10.1016/j.intimp.2014.10.022

Zhou, J., Shuang, O., Li, J., Cai, Z., Wu, C., and Wang, W. (2019a). miR-34a alleviates spinal cord injury via TLR4 signaling by inhibiting HMGB-1. *Exp. Ther. Med.* 17, 1912–1918. doi: 10.3892/etm.2018.7102

Zhou, Y., Dong, Q., Pan, Z., Song, Y., Su, P., Niu, Y., et al. (2019b). Hyperbaric oxygen improves functional recovery of the injured spinal cord by inhibiting inflammation and glial scar formation. *Am. J. Phys. Med. Rehabil.* 98, 914–920. doi: 10.1097/PHM.0000000000001225

Zhu, Y., Uezono, N., Yasui, T., Nakajo, M., Nagai, T., Wang, D., et al. (2021). Combinatrial treatment of anti-High Mobility Group Box-1 monoclonal antibody and epothilone B improves functional recovery after spinal cord contusion injury. *Neurosci. Res.* 172, 13–25. doi: 10.1016/j.neures.2021.04.002

frontiers | Frontiers in Neuroscience

TYPE Review
PUBLISHED 16 September 2022
DOI 10.3389/fnins.2022.947295

OPEN ACCESS

EDITED BY
Barbara Budzynska,
Medical University of Lublin, Poland

REVIEWED BY
Raghunath Singh,
University of Toronto, Canada
Bérengère Coupé,
Vaiomer, France

*CORRESPONDENCE
Meng He
menghe@whut.edu.cn
Guanbin Gao
gbgao@whut.edu.cn
Taolei Sun
suntl@whut.edu.cn

†These authors have contributed equally to this work

SPECIALTY SECTION
This article was submitted to Neuropharmacology, a section of the journal Frontiers in Neuroscience

RECEIVED 18 May 2022
ACCEPTED 29 August 2022
PUBLISHED 16 September 2022

CITATION
Zhou R, He M, Fan J, Li R, Zuo Y, Li B, Gao G and Sun T (2022) The role of hypothalamic endoplasmic reticulum stress in schizophrenia and antipsychotic-induced weight gain: A narrative review. *Front. Neurosci.* 16:947295. doi: 10.3389/fnins.2022.947295

The role of hypothalamic endoplasmic reticulum stress in schizophrenia and antipsychotic-induced weight gain: A narrative review

Ruqin Zhou[1†], Meng He[1*†], Jun Fan[1], Ruoxi Li[2], Yufeng Zuo[1], Benben Li[1], Guanbin Gao[3*] and Taolei Sun[1*]

[1]School of Chemistry, Chemical Engineering and Life Sciences, Wuhan University of Technology, Wuhan, China, [2]School of Public Health, Tongji Medical College, Huazhong University of Science and Technology, Wuhan, China, [3]State Key Laboratory of Advanced Technology for Materials Synthesis and Processing, Wuhan University of Technology, Wuhan, China

Schizophrenia (SCZ) is a serious mental illness that affects 1% of people worldwide. SCZ is associated with a higher risk of developing metabolic disorders such as obesity. Antipsychotics are the main treatment for SCZ, but their side effects include significant weight gain/obesity. Despite extensive research, the underlying mechanisms by which SCZ and antipsychotic treatment induce weight gain/obesity remain unclear. Hypothalamic endoplasmic reticulum (ER) stress is one of the most important pathways that modulates inflammation, neuronal function, and energy balance. This review aimed to investigate the role of hypothalamic ER stress in SCZ and antipsychotic-induced weight gain/obesity. Preliminary evidence indicates that SCZ is associated with reduced dopamine D2 receptor (DRD2) signaling, which significantly regulates the ER stress pathway, suggesting the importance of ER stress in SCZ and its related metabolic disorders. Antipsychotics such as olanzapine activate ER stress in hypothalamic neurons. These effects may induce decreased proopiomelanocortin (POMC) processing, increased neuropeptide Y (NPY) and agouti-related protein (AgRP) expression, autophagy, and leptin and insulin resistance, resulting in hyperphagia, decreased energy expenditure, and central inflammation, thereby causing weight gain. By activating ER stress, antipsychotics such as olanzapine activate hypothalamic astrocytes and Toll-like receptor 4 signaling, thereby causing inflammation and weight gain/obesity. Moreover, evidence suggests that antipsychotic-induced ER stress may be related to their antagonistic effects on neurotransmitter receptors such as DRD2 and the histamine H1 receptor. Taken together, ER stress inhibitors could be a potential effective intervention against SCZ and antipsychotic-induced weight gain and inflammation.

KEYWORDS

antipsychotics, schizophrenia, ER stress, obesity, inflammation, astrocytes

Introduction

Schizophrenia (SCZ) is a severe mental disorder that affects approximately 1% of people worldwide. This disease is characterized by positive symptoms (e.g., hallucinations, delusion, thought disturbances, and disorganized speech and behavior); negative symptoms (e.g., poverty of speech, anhedonia, and apathy); and cognitive impairment associated with memory, attention, and executive function (McCutcheon et al., 2020). These symptoms impair social and occupational functioning and increase the risk for suicide, substantially reducing the lifespan of patients with SCZ. A body of evidence has revealed that dysregulation of neurotransmission pathways such as dopaminergic, glutamatergic, gamma-aminobutyric acid (GABA)-ergic, serotonergic, opioid, and cholinergic plays an important role in the pathogenesis of SCZ (McCutcheon et al., 2020). However, the etiology of SCZ remains elusive and new therapeutic strategies are urgently needed. Additionally, clinical evidence has consistently demonstrated that patients with SCZ have a higher risk of developing metabolic disorders such as obesity, glucose metabolic disorders, dyslipidemia, and hyperinsulinemia (Harris et al., 2013). Numerous studies have demonstrated that these metabolic side effects are mainly caused by antipsychotic drug treatment. However, growing evidence has revealed that patients with SCZ have an intrinsic metabolic risk (Freyberg et al., 2017). Researchers have reported that drug-naïve patients or patients from the pre-medication era have metabolic disorders such as a higher body mass index (BMI), waist circumference, and low-density lipoprotein (LDL) levels; hyperinsulinemia; and abnormalities in insulin secretion (Harris et al., 2013; Freyberg et al., 2017). There have been similar findings in youth (12–17 years old) compared with controls. Drug-naïve patients experiencing their first psychotic episode have a larger waist circumference and LDL levels (Jensen et al., 2017). However, the mechanisms underlying these abnormalities are not clear. The hypothalamus is well known to control a variety of body functions such as hunger, energy expenditure, the sleep/wake cycle, stress response, and reproduction, among others. Research suggests that the hypothalamus also mediates cognitive performance and psychosocial health (Burdakov and Peleg-Raibstein, 2020). Accumulated evidence indicates that patients with SCZ have abnormalities in gross anatomic regions (hypothalamus, the third ventricle, and the hypothalamic subregions such as the paraventricular nucleus [PVN]) as well as changes at the cellular level (reduction of PVN neurons, peptides, and neurotransmitters) (Bernstein et al., 2021). A recent clinical study reported a reduction in hypothalamic dopamine D2/D3 receptor (DRD2/DRD3) availability (examined by ^{18}F-fluorodeoxyglucose and ^{18}F-fallypride positron emission tomography [PET] imaging) in unmedicated patients with SCZ (Mitelman et al., 2020), suggesting the involvement of hypothalamic DRD2/DRD3 signaling in SCZ. Reduced DRD2 signaling in the hypothalamus is known to increase food intake, body weight, and regulate glucose metabolism (Ikeda et al., 2020), suggesting that the reduced DRD2 signaling may also be related to SCZ-related metabolic disorders such as increased BMI and abnormalities in glucose metabolism. However, the mechanisms are currently incompletely understood.

Antipsychotics are the mainstay of treatment for SCZ. However, almost all antipsychotics are associated with varying degrees of weight gain and even obesity (Barton et al., 2020). Clinical studies have reported weight gain ranging from 0.09 to 12.4 kg in patients taking antipsychotics such as olanzapine, clozapine, quetiapine, ziprasidone, risperidone, and haloperidol for 6 weeks to 1 year (Nasrallah, 2008; Barton et al., 2020). The weight gain liability of antipsychotics is clozapine ≈ olanzapine > zotepine > quetiapine > risperidone > ziprasidone > aripiprazole (Nasrallah, 2008; Stogios et al., 2022). Olanzapine is one of the most obesogenic antipsychotics. Previous studies have shown that approximately 67–90% of patients taking olanzapine gain at least 3.3–12 kg of body weight after 8 weeks to 12 months of olanzapine treatment (Eder et al., 2001; Nasrallah, 2008). Antipsychotic-induced weight gain/obesity is an important risk factor for type II diabetes, cardiovascular disease, stroke, and patient noncompliance, and leads to decreased life expectancy and increased mortality in patients with SCZ.

Significant efforts have been made to uncover the underlying mechanisms of antipsychotic-induced weight gain/obesity. Several neurotransmitter receptors that regulate food intake and energy expenditure are involved in antipsychotic-induced weight gain including the histamine H1 receptor (H1R), the serotonin 2C receptor (5-HT2CR), DRD2, the α2 adrenergic receptor, the muscarinic M3 receptor (M3R), the cannabinoid type 1 receptor (CB1R), the GABA type A receptor, and the melanocortin 4 receptor (MC4R) (Nasrallah, 2008). It has been reported that olanzapine, clozapine, risperidone, or quetiapine could block hypothalamic H1R or 5-HT2CR, thereby activating adenosine 5′-monophosphate (AMP)-activated protein kinase (AMPK) signaling and increasing neuropeptide Y (NPY) expression, which in turn leads to increased food intake, weight gain, and glucose intolerance (Ikegami et al., 2013; He et al., 2014; Wan et al., 2020). Another study reported that acute olanzapine and clozapine treatment tends but does not significantly induce AMPK activation in the hypothalamus (Fernø et al., 2011). However, pharmacological studies have shown that H1R agonists such as 2-((3-trifluoromethyl)phenyl) histamine dimaleate (FMPH) cannot pass through the brain-blood barrier (BBB) (Malmberg-Aiello et al., 1998), which has limited the use of H1R agonists in reducing antipsychotic-induced weight gain. Activation of hypothalamic H1R by using betahistine, an H1R agonist/H3R antagonist, partially inhibits olanzapine-induced weight gain in patients (Poyurovsky et al., 2013) and rodents (Deng et al., 2012). Our recent study reported that gold nanoclusters (AuNCs) could eliminate

olanzapine-induced food intake and obesity in rats partly *via* affecting H1R-AMPK signaling (He et al., 2022b). Moreover, a 5-HT2CR-specific agonist, lorcaserin, decreases risperidone- and olanzapine-induced overeating and weight gain in rats (Lord et al., 2017; Wan et al., 2020). Co-treatment with cevimeline, an M3R agonist, attenuates olanzapine-induced weight gain *via* M3R-AMPK signaling in female rats (Han et al., 2022). Olanzapine treatment also decreases CB1R expression in the dorsal vagal complex (DVC) and the hypothalamus (Weston-Green et al., 2012; Lazzari et al., 2017). Co-treatment with a neutral CB1R antagonist and an inverse agonist, rimonabant and NESS06SM, respectively, significantly reduces olanzapine-induced weight gain in rats (Lazzari et al., 2017).

Antipsychotic-induced weight gain/obesity is also associated with several neuropeptides or hormones that regulate energy balance and neuroendocrine function such as proopiomelanocortin (POMC), NPY, AgRP, insulin, leptin, and ghrelin (Ballon et al., 2014). Olanzapine, clozapine, and risperidone treatment in rodents has been associated with increased expression of NPY and AgRP or decreased expression of POMC in the hypothalamus (Kirk et al., 2006; Fernø et al., 2011; Lian et al., 2015). Infusing an MC4R agonist, setmelanotide, reduces hyperphagia in risperidone-fed mice (Li L. et al., 2021). In rats, olanzapine treatment upregulates the messenger RNA (mRNA) and protein expression of growth hormone secretagogue receptor 1a (GHS-R1a), a receptor of ghrelin in the hypothalamus (Zhang et al., 2014). Cerebroventricular injection of a GHS-R1a antagonist, D-Lys3-GHRP-6, suppresses olanzapine-induced hyperphagia in rats, suggesting the involvement of ghrelin signaling in antipsychotic-induced weight gain (Zhang et al., 2014). A recent study reported that olanzapine activates hypothalamic NPY-AMPK signaling by disrupting the GHSR-H1R interaction, and this effect contributes to olanzapine-induced weigh gain (Chen et al., 2020). Antipsychotic-induced weight gain is associated with glucose metabolism disorders (Zhang et al., 2017a). Olanzapine, clozapine, risperidone, and quetiapine treatment has been associated with weight gain and abnormal blood glucose and leptin levels in patients (Doane et al., 2022) and rodents (Cope et al., 2005; Kirk et al., 2009). Anti-diabetic drugs such as metformin partially reduce olanzapine- or clozapine-induced weight gain in patients (Ellul et al., 2018) and rodents (Hu et al., 2014). Interestingly, evidence suggests that gut microbiome alterations are largely associated with the pathophysiology of SCZ as well as antipsychotic-induced obesity (Singh et al., 2022). Indeed, obesogenic antipsychotic treatment causes gut microbiota imbalance in both rodents and humans (Singh et al., 2022). Co-administration of the prebiotic Bimuno galacto-oligosaccharides (B-GOS®) alleviates olanzapine-induced weight gain in rats (Kao et al., 2018). Despite significant progress on the underlying mechanisms of antipsychotic-induced weight gain, there is still a lack of effective drugs for the treatment of antipsychotic-induced obesity.

Endoplasmic reticulum (ER) stress refers to physiological or pathological states in which proteins are over unfolded or misfolded in the ER. Hypothalamic ER stress plays a critical role in mediating neuroinflammation and neuronal injury (Yi et al., 2019), as well as regulating food intake, energy expenditure, and body weight (Ramírez and Claret, 2015). Several studies have investigated the association between ER stress and SCZ and have reported that genotypes of ER stress-related genes, including X-box-binding protein 1 (XBP-1) 116C/G and 197C/G, are causative factors of SCZ (Chen et al., 2004; Kakiuchi et al., 2004). An ER stress inhibitor 4-phenylbutyric acid (4-PBA) has been suggested as an important therapy to treat SCZ-related manifestations (Patel et al., 2017). The alterations of ER stress in the hypothalamus of patients with SCZ are not clear. SCZ has been reported to be accompanied by reduced hypothalamic DRD2 signaling (Mitelman et al., 2020), which is largely implicated in ER stress (Song et al., 2017), suggesting that hypothalamic ER stress may be involved in SCZ pathology and its associated metabolic disturbances. Moreover, the most widely used but obesogenic antipsychotics such as olanzapine induce activation of hypothalamic ER stress in rodents (He et al., 2019). Inhibition of ER stress suppresses olanzapine-induced hyperphagia and weight gain (He et al., 2019). These findings suggest the importance of hypothalamic ER stress in obesity induced by antipsychotics such as olanzapine. This review systematically elucidates the association between hypothalamic ER stress in SCZ and antipsychotic-induced weight gain/obesity, discussing the possible underlying molecular mechanisms and providing insights into the search for targets that could alleviate SCZ and antipsychotic-induced obesity.

The role of hypothalamic endoplasmic reticulum stress in body weight control

The hypothalamus is an indispensable "headquarters" for regulating energy homeostasis (Tran et al., 2022). It contains a number of nuclei such as the arcuate nucleus (ARC), the PVN, the ventromedial hypothalamus (VMH), the dorsomedial hypothalamus (DMH), and the lateral hypothalamus (LH) to respond to hormones and nutrients and to regulate food intake and energy expenditure. The ARC which contains two major populations of "first-order" neurons with opposing effects on energy homeostasis: POMC neurons that express the anorexigenic peptides POMC and cocaine- and amphetamine-regulated transcript, and NPY/AgRP neurons that express the orexigenic peptides NPY and AgRP (Vohra et al., 2022). NPY/AgRP and POMC neurons send projections to

"second-order" neurons in other hypothalamic regions such as the VMH, PVN, and LH, regulating body weight and glucose homeostasis (Vohra et al., 2022). Leptin and insulin are two important hormones that inhibit food intake and body weight by acting on the hypothalamus. Insulin and leptin receptors are expressed on POMC and AgRP neurons (Shin et al., 2017; Üner et al., 2019). By binding to their receptors, insulin and leptin directly stimulate anorexigenic POMC neurons and inhibit orexigenic NPY/AgRP neurons in the ARC to suppress food intake and to increase energy expenditure. Treatment with leptin or insulin increases POMC expression but decreases the release of AgRP (Breen et al., 2005). Mechanically, leptin and insulin reduce food intake and stimulate energy expenditure partly through AMPK, phosphoinositide 3-kinase (PI3K), suppressor of cytokine signaling 3 (SOCS3), protein tyrosine phosphatase 1B (PTP1B), and mammalian target of rapamycin (mTOR) signaling in the hypothalamus (Thon et al., 2016), and these effects play an essential role in leptin- and insulin-derived AgRP and POMC expression. Furthermore, other neurons such as dopaminergic and histaminergic neurons in the hypothalamus play an important role in regulating food intake and weight gain (Panula et al., 2000; Yonemochi et al., 2019). Hypothalamic dopamine suppresses food intake and weight gain by acting on postsynaptic DRD2 (Meguid et al., 2000). Hypothalamic histamine inhibits food intake and weight gain by activating H1R in the ARC and PVN (Panula et al., 2000). It has been reported that leptin and insulin regulate food intake and body weight partly by communicating with the hypothalamic DRD2 (Kleinridders and Pothos, 2019) and H1R pathways (Yoshimatsu et al., 1999).

In addition to neurons, growing evidence indicates that hypothalamic glia cells such as the astrocytes and microglia have a critical role in body weight regulation. Hypothalamic astrocytes and microglia accumulate and are activated in response to high-fat diet (HFD) (Zhang et al., 2017b; Valdearcos et al., 2019). Pharmacological deletion of astrocytes and microglia or reducing their capability for activating inflammation in the hypothalamus reduces food intake and weight gain and enhances leptin signaling in HFD-fed rodents (Valdearcos et al., 2019; Varela et al., 2021). Reactive astrocytes and microglia activate inflammatory signals such as inhibitor of nuclear factor kappa-B kinase subunit beta (IKKβ)/nuclear factor κB (NF-κB) signaling and produce inflammatory cytokines during HFD feeding (Valdearcos et al., 2019; Sa et al., 2022). Moreover, hypothalamic astrocytes reduce ghrelin-induced food intake by affecting AgRP neurons (Yang L. et al., 2015). Deletion of angiopoietin-like 4 in astrocytes increases the excitability and insulin sensitivity of POMC neurons and alleviates HFD-induced weight gain in mice (Varela et al., 2021). These findings suggest that astrocytes may partly regulate food intake and body weight by interacting with POMC and AgRP neurons.

Hypothalamic neuronal endoplasmic reticulum stress and weight gain

Endoplasmic reticulum stress is an adaptive mechanism that refers to the pathophysiological process in which ER function is disturbed under conditions of hypoxia, oxidative stress, nutritional imbalance, or calcium homeostasis dysfunction (Schönthal, 2012). Mechanically, ER stress is mediated by protein kinase R-like ER kinase (PERK), activating transcription factor 6 (ATF6), and inositol requiring enzyme 1 (IRE1) (Cnop et al., 2012). Under unstressed conditions, these proteins bind to the chaperone BiP, also known GRP78 (Cnop et al., 2012). When ER stress is activated, GRP78 dissociates from PERK, IRE1, and ATF6. PERK is subsequently activated by phosphorylation. PERK phosphorylates the downstream eukaryotic initiation factor 2α (eIF2α) to increase the translation of activating transcription factor 4 (ATF4). Upon ER stress, ATF6 relocated to the Golgi apparatus and is processed by site 1 and 2 proteases; these changes form active ATF6 (p50), which is then transported to the nucleus to activate gene transcription (Matos et al., 2015). IRE1 could be activated by phosphorylation. Phospho-IRE1 cleaves 26 nucleotides from the mRNA of XBP1 and produces an active spliced form of XBP1 (Park et al., 2021). Then, these proteins activate comprehensive transcriptional and translational signaling, resulting in up- or downregulation of their downstream expression of signaling pathways (Kroeger et al., 2019; **Figure 1**).

Hypothalamic ER stress plays a crucial role in the development of obesity (**Table 1**). Mice with diet-induced obesity (DIO) have increased expression of hypothalamic ER stress markers, including phospho-PERK (p-PERK), phospho-eukaryotic initiation factor-2α (p-eIF2α), and phospho-IRE1 (p-IRE1) (Won et al., 2009; Cakir et al., 2013). Overnutrition activates hypothalamic PERK and promotes leptin resistance during obesity development in mice (Zhang et al., 2008). Pharmacologic activation of hypothalamic ER stress in rats results in hyperphagia and weight gain, and promotes leptin resistance (Ozcan et al., 2009). On the contrary, suppression of hypothalamic ER stress with ER stress inhibitors including tauroursodeoxycholic acid (TUDCA) or 4-PBA suppresses food intake in DIO mice (Ozcan et al., 2006). The mechanisms by which ER stress mediates feeding and body weight are not fully understood. Previous studies suggest that hypothalamic POMC neurons may be important response neurons. Diet-induced ER stress obstructs post-translational processing of POMC in mice (Cakir et al., 2013). Deletion of ATF4 from hypothalamic POMC neurons protects mice from obesity, glucose intolerance, and leptin resistance during HFD feeding (Xiao et al., 2017b). ATF4 also impairs hypothalamic α-melanocyte-stimulating hormone (α-MSH) production (Xiao et al., 2017a). Hypothalamic induction of ER stress attenuates POMC processing and decreases α-MSH levels by decreasing pro-converting enzyme 2 (Cakir et al., 2013). Hypothalamic ER stress could favor

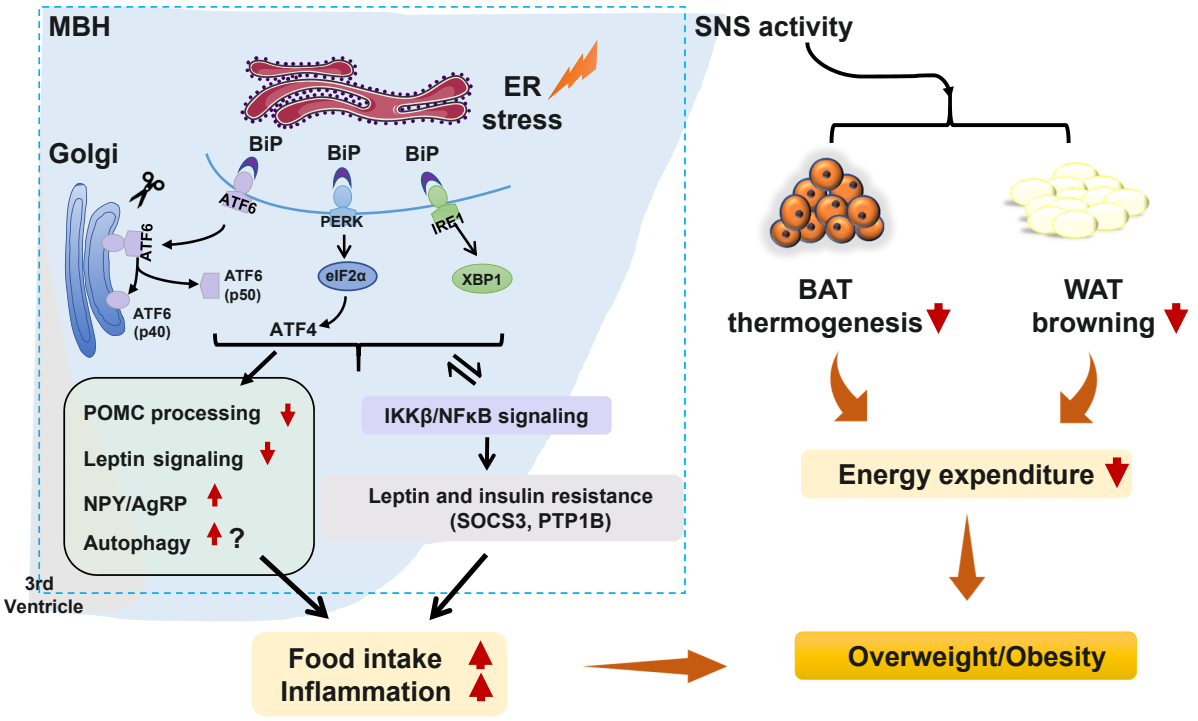

FIGURE 1
Potential role of hypothalamic endoplasmic reticulum (ER) stress in obesity and inflammation. Under certain stimuli, such as high-fat diet (HFD) feeding, drug treatment, or infection, ER stress is activated, and binding immunoglobulin protein (BiP) dissociates from protein kinase R-like ER kinase (PERK), inositol requiring enzyme 1 (IRE1), and activating transcription factor 6 (ATF6), resulting in the release of those three proteins. PERK is then activated by phosphorylation and p-PERK phosphorylates eukaryotic initiation factor 2α (eIF2α) and increases the translation of ATF4. ATF6 relocates to the Golgi apparatus and is processed by site 1 and 2 proteases, resulting in ATF6 activation. IRE1 is activated by phosphorylation. pIRE1 catalyzes X-box-binding protein 1 (XBP1) mRNA splicing, resulting in increased production of active spliced XBP1. These effects could (1) activate the hypothalamic autophagy signaling, impede proopiomelanocortin (POMC) processing, attenuate leptin signaling, and possibly increase neuropeptide Y (NPY), and agouti-related peptide (AgRP) expression, leading to increased food intake, decreased energy expenditure, inflammation, and weight gain; (2) decrease white adipose tissue (WAT) browning and brown adipose tissue (BAT) thermogenesis by affecting sympathetic nervous system (SNS) activity, resulting in lower energy expenditure and weight gain; and (3) trigger activation of the inhibitor of nuclear factor kappa-B kinase subunit beta (IKKβ)/nuclear factor κB (NF-κB) signaling pathway, resulting in hypothalamic leptin and insulin resistance (by affecting suppressor of cytokine signaling 3 [SOCS3] and protein tyrosine phosphatase 1B [PTP1B]). These effects could increase food intake, decrease energy expenditure, and promote inflammation, thus resulting in weight gain. Furthermore, activated IKKβ/NF-κB signaling could lead to ER stress in the hypothalamus and worsen hypothalamic inflammation.

a positive energy balance by attenuating its response to an anorectic hormone leptin, whose receptors are expressed on POMC neurons (Cakir and Nillni, 2019). Activation of ER stress inhibits acute leptin signaling in arcuate POMC neurons (Williams et al., 2014). Constitutive expression of a dominant XBP1s form in POMC neurons protects mice from gaining weight by increasing energy expenditure and leptin sensitivity (Williams et al., 2014). Moreover, a recent study reported that genetic deletion of autophagy in POMC neurons of *ob*/*ob* mice worsens hyperphagia and reduces POMC neuronal projections to the PVN, characterized by less dense α-MSH-immunoreactive fibers (Park et al., 2020). The mechanisms by which autophagy reduces POMC neurons appear to involve inhibition of mTOR signaling, which is important for regulating cell growth and proliferation (Jaboin et al., 2007). Reduced POMC neuron projections would result in decreased expression of POMC and POMC-derived peptides such as α-MSH, leading to leptin resistance, hyperphagia, and weight gain (Oh et al., 2016). Neonatal TUDCA treatment ameliorates loss of autophagy-induced hyperphagia, weight gain, and the reduction in POMC neuronal projections is ameliorated (Park et al., 2020), suggesting that the ER stress-autophagy pathway in POMC neurons controls hypothalamic development and energy balance (**Figure 1**). Therefore, hypothalamic ER stress could mediate food intake and body weight by reducing POMC processing, activating autophagy, and inhibiting leptin signaling (**Figure 1**). Furthermore, ER stress could regulate food intake by affecting NPY/AgRP expression and neuronal function. NPY and AgRP are expressed in particular hypothalamic neurons that play an important role in feeding control (Morton and Schwartz, 2001). Induction of ER stress by tunicamycin significantly increases NPY and AgRP mRNA in the mouse hypothalamus (Ozcan et al., 2009). In AgRP neurons, RNA-seq revealed that ER-stress-related genes such as BiP and ATF6 are significantly

activated during food deprivation (Henry et al., 2015). ATF4 knockout in AgRP neurons protects mice from weight gain by decreasing food intake and increasing energy expenditure (Deng et al., 2017). Additionally, in rodents fed a HFD, inhibition of ER stress reduces orexigenic NPY gene expression in the amygdala, suggesting a role for brain ER stress-NPY in regulating feeding (Areias and Prada, 2015). These findings suggest that ER stress could also regulate food intake *via* affecting AgRP and NPY.

The role of ER stress in other hypothalamic neuronal systems involved in metabolism and body weight regulation have not been studied extensively. The available evidence suggests that ER stress is related to several neurotransmitter receptors that play essential roles in regulating food intake and body weight such as DRD2, H1R, and CB1R. One study reported that the DRD2 agonist (bromocriptine) decreases the expression of GRP78/BiP in cultured cells, indicating that ER stress could be inhibited by DRD2 activation (Henderson et al., 2021). A study also reported that H1R antagonism induces ER stress in cultured cells (Jakhar et al., 2016). The CB1R agonist arachidonyl-2′-chloroethylamide (ACEA) attenuates ER stress and inflammation in Neuro-2a neuroblastoma cells (Vrechi et al., 2018). These findings suggest that the ER stress could be the downstream effect of DRD2, H1R, and CB1R signaling. Future studies should investigate whether hypothalamic ER stress could be mediated by altering hypothalamic DRD2, H1R, and CB1R signaling and its potential role in food intake and body weight regulation.

Hypothalamic ER stress also drives obesity by reducing energy expenditure (**Table 1**). Pharmacological activation of ER stress in the hypothalamus by ceramides effectively reduces brown adipose tissue (BAT) thermogenesis, resulting in weight gain (Contreras et al., 2014). Genetic overexpression of GRP78 in the VMH reduces ceramide-induced ER stress and increases BAT thermogenesis, resulting in weight loss in rats (Contreras et al., 2014). In HFD-induced obese rats, overexpression of GRP78 in the VMH attenuates ER stress, increases BAT thermogenesis, and stimulates white adipose tissue (WAT) browning, ultimately attenuating HFD-induced obesity (Contreras et al., 2017). Moreover, the study revealed that ER stress in the VMH decreases sympathetic nervous system (SNS) activity to inhibit BAT function and increases WAT browning, and these effects could be independent of feeding and leptin (Contreras et al., 2017). Treatment with TUDCA, an ER stress inhibitor, reduces food intake and tends to increase oxygen consumption in DIO mice (Cakir et al., 2013). Intracerebroventricular (ICV) administration of TUDCA induces weight loss, decreases hypothalamic ER stress, and elevates BAT temperature in rats (González-García et al., 2018). Furthermore, hypothalamic POMC neuron-specific ATF4 knockout protects DIO mice from obesity by increasing BAT thermogenesis and increasing oxygen consumption (Xiao et al., 2017b). ATF4 knockout in AgRP neurons promotes mouse fat loss mainly by increasing energy expenditure (Deng et al., 2017). Induction of XBP1s in POMC neurons significantly increases the metabolic rate to mediate thermogenesis in both BAT and inguinal WAT (Williams et al., 2014), therefore protecting mice against DIO. These findings suggest that hypothalamic ER-stress-induced reductions in energy expenditure may be at least partially related to the hypothalamic POMC and AgRP (**Figure 1**).

In the pathogenesis of obesity, hypothalamic ER stress is significantly linked to inflammation. Activation of hypothalamic inflammation leads to central metabolic dysregulations, uncoupling of food intake and energy expenditure, and weight gain (Jais and Brüning, 2017; Le Thuc et al., 2017). ER stress markers including PERK, ATF6, and IRE1 participate in activating the inflammatory processes (Garg et al., 2012). In the progression of obesity, a HFD could induce hypothalamic ER stress, and this effect could promote hypothalamic inflammation in mice (Zhang et al., 2008) and rats (Ropelle et al., 2010). Activation of hypothalamic ER stress *via* overnutrition activates IKKβ-NF-κB signaling, whereas inhibition of ER stress *via* intraventricular injection of TUDCA suppresses hypothalamic IKKβ-NF-κB signaling, reduces food intake, and induces weight loss in DIO mice (Zhang et al., 2008). This study also revealed that activation of IKKβ-NF-κB signaling by ER stress induces leptin and insulin resistance by affecting SOCS3, and these effects cause energy imbalance and weight gain (Zhang et al., 2008). Interestingly, ER stress is also regulated by inflammation. A study revealed that administration of a small molecule inhibitor of NF-κB, withaferin A (WA), reduces the expression of ER stress hallmarkers including PERK, XBP1, and ATF6 in the mouse pancreas (Kanak et al., 2017). An intraperitoneal injection of active IKKβ ($IKK\beta^{CA}$) lentivirus increases phosphorylation of PERK and eIF2α (Zhang et al., 2008). In rats, a single intraperitoneal injection of tumor necrosis factor alpha (TNF-α) increases expression of p-PERK, IRE1α, and GRP78 in the hypothalamus (Denis et al., 2010). Palmitate and TNF-α treatment upregulate NF-κB expression and ER stress-related gene expression in hypothalamic appetite-stimulating NPY/AgRP neurons (Dalvi et al., 2017). Therefore, ER stress and NF-κB signaling positively regulate each other during HFD feeding, and these effects induce a positive energy balance and cause obesity (Zhang et al., 2008; **Figure 1**).

Hypothalamic astrocytic endoplasmic reticulum stress and weight gain

In addition to ER stress in hypothalamic neurons, ER stress in hypothalamic astrocytes has recently gained attention for its important role in the development of obesity and inflammation (**Figure 2**). Astrocytes are the most abundant glial cells in the central nervous system (CNS). Numerous studies have

TABLE 1 Findings highlighting role of hypothalamic ER stress-related proteins in mediating appetite and weight gain and their modifications by antipsychotic drugs.

References	Study design	ER stress-related markers	Physiological role	Alteration in schizophrenia	Alteration during antipsychotic treatment
Won et al., 2009	1. Mice were injected with leptin after pretreatment with tunicamycin in the third ventricle. 2. Mice fed a HFD were co-treated with 4-PBA. 3. WB and PCR were used to detect the expression of STAT3 related with leptin and insulin signaling and ER stress markers in the hypothalamus.	PERK ↑ eIF2α ↑ IRE1 ↑ XBP-1 ↑ CHOP ↑ GRP78 ↑	ER stress induced central leptin and insulin resistance and increased food intake and weight gain.	NR	NR
Cakir et al., 2013	1. Rats fed a HFD were co-treated with TUDCA after central injection of leptin. 2. N43/5 cells were treated with tunicamycin or thapsigargin after pretreated with 4-PBA or salubrinal. 3. RT-qPCR, RIA, and WB were used to detect the expression of POMC-processing-related proteins and ER stress markers in the ARC and PVN of rats, and in N43/5 cells.	p-PERK ↑ p-eIF2α ↑	ER stress obstructed the post-translational processing of POMC, and induced leptin resistance, therefore regulating feeding.	NR	NR
Ozcan et al., 2009	1. Mice with specific knockout of XBP1 in neurons fed with HFD and *ob/ob* mice pretreated with 4-PBA and leptin were used to examine the effect of XBP1 in leptin signaling. 2. GTT and ITT were used to detect glucose metabolism and insulin function. WB was used to analyze ER stress markers and LepRB and STAT3 in hypothalamus.	PERK ↑ IRE-1α ↑ XBP1 ↑ CHOP ↑	Hypothalamic ER stress induced leptin resistance and impaired glucose homeostasis, resulting in weight gain.	NR	NR
Contreras et al., 2014	1. Rats were centrally injected with ceramide to induce ER stress. 2. Then, an adenovirus encoding GRP78 wild-type was injected into the VMH of these rats and obese Zucker rats with higher ceramide C16 and C18. 3. RT-PCR, WB and IHC were used to detect expression of ER stress markers in the MBH and VMH, UCP1 and FABP3 in BAT, and leptin and insulin signaling in the VMH.	GRP78 ↑ p-IRE1 ↑ p-PERK ↑ p-eIF2α ↑ ATF6α ↑ CHOP ↑	1. Hypothalamic ER stress decreased BAT thermogenesis. 2. GRP78 overexpression in the VMH improved leptin and insulin resistance, increased BAT thermogenesis, causing weight loss.	NR	NR
Contreras et al., 2017	1. Rats were fed a HFD to induce hypothalamic ER stress, then the rats were treated with TUDCA. 2. GRP78 adenovirus was injected into the VMH of rats. 3. GTT and ITT were used to detect insulin function and glucose metabolism. RT-PCR, WB, and IHC were used to detect expression of ER stress markers, BAT thermogenesis markers, and key proteins of leptin signaling in the VMH.	GRP78 ↑ p-IRE1 ↑ p-PERK ↑ p-eIF2α ↑ ATF6α ↑ CHOP ↑	1. Hypothalamic ER stress inhibited BAT thermogenesis and WAT browning, and induced leptin and insulin resistance. 2. GRP78 overexpression in the VMH improved leptin and insulin resistance, and increased BAT thermogenesis and WAT browning, causing weight loss.	NR	NR
Henry et al., 2015	1. AgRP and POMC neurons were dissociated from transgenic mice with food deprived. 2. RNA-seq was used to detect the expression of ER stress markers in AgRP and POMC neurons.	BiP ↑ IRE1 ↑ XBP1 ↑ ATF6 ↑	XBP1 in AgRP and POMC neurons regulated food intake.	NR	NR

(Continued)

10.3389/fnins.2022.947295

TABLE 1 (Continued)

References	Study design	ER stress-related markers	Physiological role	Alteration in schizophrenia	Alteration during antipsychotic treatment
Park et al., 2020	1. *Ob/ob* mice from P4 to P16 postnatal were treated with TUDCA and leptin. 2. *Ob/ob* mice exposed to insulin and glucose were treated with TUDCA. 3. *Ob/ob-POMC*-Cre-*ATG7*$^{loxP/loxP}$ mice stimulated by glucose were treated with TUDCA. 4. GTT and ITT were used to detect insulin function and glucose metabolism. Using WB, RT-qPCR, IHC and M-FISH to examine ER stress markers and POMC projections in the hypothalamus.	ATF4 ↑ ATF6 ↑ GRP78 ↑ XBP1 ↑ CHOP ↑	ER stress inhibited leptin and insulin sensitivity, impaired glucose homeostasis and worsened POMC neuronal projections in the PVN, resulting in increased food intake and weight gain.	NR	NR
Deng et al., 2017	1. AgRP-ATF4 KO mice fed with HFD or injected with leptin were used to examine metabolic-related alteration. 2. AgRP-ATF4 KO mice were under cold exposure to detect thermogenic response. 3. GTT and ITT were used to detect insulin function and glucose metabolism. Using a rectal probe attached to a digital thermometer to measure rectal temperature in mice.	NR	AgRP ATF4 reduced insulin sensitivity, and decreased BAT thermogenesis and WAT browning.	NR	NR
Zhang et al., 2008	1. Normal chow-fed mice were injected with tunicamycin to induce ER stress. 2. Mice fed a HFD were injected with TUDCA. 3. IKKβ^{CA} was delivered bilaterally into the MBH of HFD mice, followed by insulin injection. 4. AgRP/IKKβ$^{lox/lox}$ mice were fed with HFD. 5. Immunostaining and WB were used to examine the effects of IKKβ^{CA} on leptin and insulin signaling in the MBH. IP and WB were used to examine ER stress markers in the hypothalamus, and GTT was used to detect glucose metabolism.	p-PERK ↑ p-eIF2α ↑	Hypothalamic ER stress activated IKKβ/NF-κB signaling, causing inflammation, glucose intolerance and central insulin and leptin resistance.	NR	NR
Wang et al., 2021	1. Rat primary astrocytes were pretreated with high glucose for 48 h, and then these cells were incubated with metformin for 1 h. 2. Rat primary astrocytes were treated with high glucose for 48 h after pretreatment with the AMPK activator AICAR for 1 h. 3. ELISA, co-IP, and WB were used to detect the ER stress markers and inflammatory cytokines in astrocytes.	p-PERK ↑ p-IRE1α ↑ ATF6 ↑	Astrocytic ER stress induced inflammation by mediating AMPK.	NR	NR

(Continued)

10.3389/fnins.2022.947295

CENTRAL NERVOUS SYSTEM ACTING DRUGS – MOLECULAR MECHANISMS OF NEUROPROTECTION AND NEURODEGENERATION

Topic Editors:
Nesrine Salah El Dine El Sayed, Cairo University, Egypt
Riham Salah El Dine, Cairo University, Egypt
Jolanta Kotlinska, Medical University of Lublin, Poland
Barbara Budzynska, Medical University of Lublin, Poland
Anna Boguszewska-Czubara, Medical University of Lublin, Poland

Citation: El Dine El Sayed, N. S., El Dine, R. S., Kotlinska, J., Budzynska, B., Boguszewska-Czubara, A., eds. (2022). Central Nervous System Acting Drugs – Molecular Mechanisms of Neuroprotection and Neurodegeneration. Lausanne: Frontiers Media SA. doi: 10.3389/978-2-83250-661-5

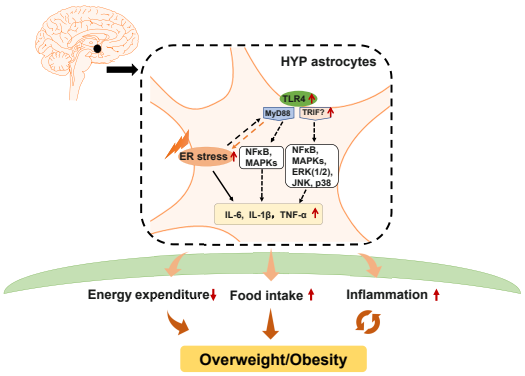

FIGURE 2
Potential role of astrocytic endoplasmic reticulum (ER) stress and Toll-like receptor 4 (TLR4) signaling in obesity and inflammation. In hypothalamic astrocytes, ER stress may activate TLR4 that then activates myeloid differentiation primary response 88 (MyD88)-independent and MyD88-dependent signaling, which increases the expression of nuclear factor κB (NF-κB), mitogen-activated protein kinases (MAPKs), extracellular signal-regulated kinase 1/2 (ERK1/2), c-Jun N-terminal kinase (JNK), and p38. These effects upregulate pro-inflammatory cytokines such as interleukin 6 (IL-6), IL-1β, and tumor necrosis factor alpha (TNF-α), and causing central inflammation. Activated astrocytic TLR4 signaling could also lead to decreased energy expenditure and promote ER stress activation, which increases food intake, eventually leading to obesity.

demonstrated the importance of hypothalamic astrocytes in regulating feeding (Kim J. G. et al., 2014), energy expenditure (Manaserh et al., 2020), and inflammation (Douglass et al., 2017). For example, fasting activates hypothalamic astrocytes (Chen et al., 2016). Astrocyte insulin receptor deletion in mice reduces energy expenditure and temperature (Manaserh et al., 2020). Researchers have reported that chronic and acute (single) HFD exposure in rodents induce inflammation and astrocytes activation in the hypothalamus (Zhang et al., 2017b; Cansell et al., 2021). Mice fed a HFD for 28 days had increased TNF-α mRNA expression in hypothalamic astrocytes (Sugiyama et al., 2020).

Previous studies have reported that in astrocytes, TLR4 signaling plays an essential role in obesity pathogenesis and inflammation (**Figure 2**). TLR4 is expressed by activated astrocytes (Shen et al., 2016). Growing evidence suggests that astrocytic TLR4 could be activated in response to natural ligands and existing compounds, such as tenascin C, damage-associated molecular patterns (DAMPS), lipopolysaccharide (LPS), and saturated fatty acids (SFA), which are well known to promote inflammation or induce weight gain. For example, tenascin C, an endogenous activator of TLR4, induces IL-6 expression in primary cortical astrocytes (Krasovska and Doering, 2018). LPS, which induces hypothalamic inflammation (Rorato et al., 2017), acts on the TLR4-myeloid differentiation factor 2 (MD2) complex (the binding site of LPS) to activate TLR4 and enhances IL-1β, IL-6, and TNF-α expression (Wu et al., 2012). DAMPs such as the high mobility group box protein 1 (HMGB-1) has been reported to activate TLR4 in mixed cultures of astrocytes and microglia, thereby inducing NF-κB activation (Rosciszewski et al., 2019). SFA, which is known to cause hypothalamic inflammation and obesity, activates TLR4 to induce an inflammatory response (Milanski et al., 2009). Moreover, a clinical study reported that obese patients have increased tenascin C and TLR4 levels in visceral adipose tissue (Catalán et al., 2012). LPS, total free fatty acid levels, and TLR4 mRNA are significantly increased in the plasma of patients with nonalcoholic steatohepatitis (Sharifnia et al., 2015). Serum from obese patients shows TLR4/NF-κB signaling activation in THP-1 monocytes (Yao et al., 2010). SFA induces pro-inflammatory cytokines secretion including TNF-α, IL-6, and IL-8 in human placental cells *via* activating TLR4 signaling (Yang X. et al., 2015). These findings suggest the importance of TLR4 in the pathogenesis of inflammation and obesity in humans. However, the role of hypothalamic astrocyte TLR4 signaling in inflammation and obesity is not clear in humans.

Toll-like receptor 4 has a cytoplasmic Toll/interleukin-1 receptor/resistance protein (TIR) domain and interacts with two adaptor molecules, namely myeloid differentiation primary response 88 (MyD88) (Medzhitov et al., 1998) and TIR domain-containing adapter protein-inducing interferon-β (TRIF) (Zuany-Amorim et al., 2002). In the MyD88-dependent pathway, TLR4 activation induces early recruitment of MyD88 and rapidly activates NF-κB and mitogen-activated protein kinases (MAPKs), therefore inducing inflammatory factors expression such as TNF-α and interleukin (IL)-1β, IL-6, and IL-15 (Gorina et al., 2011). In the MyD88-independent pathway, TLR4 interacts with TRIF and activates interferon regulatory factor 3 (IRF3), NF-κB, and MAPKs, including extracellular signal-regulated kinase 1/2 (ERK1/2), c-Jun N-terminal kinase (JNK), and p38, among others, thereby inducing the secretion of inflammatory factors such as TNF-α, IL-1β, and IL-6. Pharmacologic inhibition of TLR4, TLR4 knockout, TLR4-interactor knockdown, or hypothalamic ARC-restricted TLR4 knockdown reduces food intake, increases whole-body energy expenditure, reduces hypothalamic inflammation, and protects rodents from HFD-induced obesity (Milanski et al., 2009; Camandola and Mattson, 2017; Zhao et al., 2017; de Vicente et al., 2021). MyD88 deficiency in the mouse CNS (MyD88$^{\Delta CNS}$) or astrocyte-specific MyD88 knockout protects mice from chronic HFD-induced obesity, and mice exhibit ameliorated hypothalamic reactive gliosis and inflammation (Jin et al., 2020). *Trif* deficient (*Trif*$^{-/-}$) mice show increased food intake and weight gain (Yang and Fukuchi, 2020). However, the role of hypothalamic TRIF signaling in food intake and weight gain is unclear. Moreover, activation of astrocytic IKKβ-NF-κB signaling increases fat mass and causes weight gain (Zhang et al., 2017b). Astrocytic IKKβ-NF-κB loss of function counteracts DIO in mice (Zhang et al., 2017b).

Astrocyte-specific deletion of IKKβ in mice after 6 weeks of HFD feeding decreases hypothalamic inflammation and astrocytosis in the hypothalamic ARC, therefore reducing food intake and increased energy expenditure (Douglass et al., 2017). These findings suggest that astrocytes may regulate food intake, energy expenditure and inflammation development at least partly *via* TLR4 signaling, which involves the participation of MyD88, TRIF, and IKKβ-NF-κB signaling (**Figure 2**).

It is worth noting that TLR4 activation is associated with ER stress. TLR4 activation in HFD-induced obese mice could precede hypothalamic ER stress (Milanski et al., 2009). Inhibition of TLR4 signaling by anti-TLR4 antibodies (Milanski et al., 2009) or TLR4 knockout (Pierre et al., 2013) attenuates ER stress and reduces HFD-induced ER stress. Downstream molecules of TLR4 including MAPK and NF-κB, and the expression of inflammatory factors such as IL-1β and IL-6, could be activated by ER stress (Darling and Cook, 2014; Kim S. et al., 2014). Moreover, ER stress could mediate inflammation *via* TLR4 signaling during the development of obesity (Li, 2018). HFD-induced obese mice show significantly increased mRNA and protein expression of TLR4, TNF-α, and IL-6 in adipose tissue, while these changes are suppressed by treatment with the ER stress inhibitor 4-PBA (Li, 2018). TUDCA inhibits NF-κB activation in astrocytes induced by combined stimulation of LPS and interferon-γ (IFN-γ) (Yanguas-Casás et al., 2014), suggesting that inhibition of ER stress decreases astrocyte inflammation. These studies clarify the important relationship between ER stress and TLR4 signaling (**Figure 2**). In conclusion, hypothalamic ER stress in neurons and astrocytes has an important role in the regulation of body weight and inflammatory responses.

While it is known that ER stress induces inflammation in neurons and astrocytes, are these effects dependent or independent? Studies in cultured neurons have revealed that ER stress activates NF-κB signaling and increases expression of pro-inflammatory cytokines, and these effects could be inhibited by co-treatment with ER stress inhibitors such as 4-PBA (Wang et al., 2016; He et al., 2019). Studies in astrocytes have shown the same results: Activation of ER stress triggers an inflammatory response, which is inhibited by co-treatment with ER stress inhibitors (Yanguas-Casás et al., 2014; He et al., 2021). These findings suggest that ER-stress-induced inflammation in neurons and astrocytes could be independent. However, astrocytes and neurons are known to communicate with each other (Paixão and Klein, 2010). Research has proved that ER stress is transmissible between astrocytes and neurons (Sprenkle et al., 2019). ER stress in astrocytes/neurons could regulate inflammatory and ER stress in other astrocytes/neurons (Sprenkle et al., 2019). In astrocytes, ER stress activation augments inflammatory signaling and increases the expression and secretion of pro-inflammatory cytokines such as IL-6 and IL-1β (Wang et al., 2018). The receptors for IL-1β, and TNF-α are expressed on neurons (Friedman, 2001; Chadwick et al., 2008). It is possible that pro-inflammatory cytokines secreted by astrocytes can act on their receptors on neurons to stimulate neuronal ER stress, triggering neuronal inflammatory responses. It has been suggested that overnutrition/HFD activates astrocytes and microglia to release cytokines, and these cytokines then mediate inflammation in POMC and AgRP neurons and cause leptin and insulin resistance, resulting in impaired metabolism and weight gain (Ullah et al., 2021). Furthermore, the receptors for the above pro-inflammatory cytokines are also expressed on astrocytes (Friedman, 2001; Bobbo et al., 2021). Therefore, pro-inflammatory cytokines including IL-6, IL-1β, and TNF-α secreted by neurons may also activate ER stress in astrocytes to induce an inflammatory response. Taken together, during obesity development, hypothalamic inflammation could be a combined effects of ER stress activation in both neurons and astrocytes, and they could both trigger each other.

Besides astrocytes, other glia cells such as microglia, hypothalamic neural stem cells, and NG2 cells play a role in metabolic inflammation. Obesity activates microglia and inflammation in the hypothalamus (Mendes et al., 2018), whereas deletion of hypothalamic microglia abrogates inflammation in rodents (Valdearcos et al., 2014). NG2 glia cells, which express inflammatory cytokines such as IL-1β (Galichet et al., 2021), are increased in the brain of HFD-fed mice (Xiao et al., 2018). Neural stem cells, which express IL-6, IL-1β, and TNF-α (Chang and Kong, 2019), are reduced by HFD exposure *via* IKKβ/NF-κB signaling (Livesey, 2012). The role of ER stress in mediating inflammation in microglia, N2 glia, and neural stem cells has not been fully studied; and the available information is inconsistent. Increased ER stress in microglia contributes to neuroinflammation induced by paraquat (an herbicide) (Yang et al., 2020). Inhibition of ER stress *via* TUDCA reduces activation of microglial NF-κB induced by LPS and IFN-γ (Yanguas-Casás et al., 2014). However, LPS-induced increased IL-1β, IL-6, and TNF-α expression in microglia are partially reversed by tunicamycin (an ER stress inducer) (Wang et al., 2017). Inhibition of ER stress by 4-PBA promotes LPS-induced inflammation in cultured microglia (Wang et al., 2017). Furthermore, whether ER stress in hypothalamic microglia, N2 glia, and neural stem cells plays a role in metabolic inflammation and obesity remains to be uncovered. How antipsychotics affect ER stress in these glia cells and its potential role in antipsychotic-related inflammation is unknown. Astrocytes, which make up the largest glial population, are related to ER stress signaling in inflammatory regulation (Martin-Jiménez et al., 2017). Obesogenic antipsychotics such as olanzapine activate astrocytic ER stress, leading to weight gain (He et al., 2021). Therefore,

the next section focuses on the role of astrocytic ER stress in antipsychotic-related inflammation and weight gain.

The role of hypothalamic endoplasmic reticulum stress in schizophrenia and antipsychotic-induced weight gain

There are numerous studies reporting that SCZ is associated with metabolic disorders. Almost all antipsychotics cause weight gain/obesity, and this effect is the main cause of metabolic disorders in SCZ patients. Hypothalamic ER stress is well known in regulating food intake, energy expenditure, inflammation, and insulin and leptin signaling (Cakir and Nillni, 2019). In this section, we discuss the relationship between ER stress and SCZ and antipsychotic-induced weight gain.

Insights from clinical studies on endoplasmic reticulum stress in schizophrenia and antipsychotic-induced weight gain

Several studies have investigated the relationship between ER stress and SCZ (**Table 2**). A study in B lymphocytes from patients with bipolar disorder reported that XBP1 and CHOP are upregulated upon treatment with ER stress inducers (thapsigargin and tunicamycin) (So et al., 2007), suggesting the ER stress could occur in patients with psychiatric disorders. XBP1 polymorphisms are associated with psychiatric disorders including SCZ, depression, and bipolar disorder in patients with or without antipsychotic treatment (**Table 2**). GRP78/BiP is an essential HSP70 resident protein in the ER. HSP70 is overexpressed in patients with SCZ and is suggested to be involved in the pathology of the disease (**Table 2**). Another study in a Korean population showed that HSP70-2 gene polymorphism might be related to the pathogenesis of SCZ (**Table 2**). Moreover, an autopsy study reported that in the dorsolateral prefrontal cortex of antipsychotic-treated SCZ patients, expression of GRP78/BiP and sXbp1/uXbp1 were increased (**Table 2**). These findings suggest that brain ER stress may play an important role in the pathophysiology of SCZ. However, in these studies certain subjects had been treated with antipsychotics; therefore, antipsychotics could have affected these results. Currently, there is a lack of direct clinical evidence regarding whether hypothalamic ER stress is related to the pathophysiology of SCZ. It has been reported that DRD2/DRD3 availability is significantly decreased in the hypothalamus of SCZ patients not receiving antipsychotic treatment (Mitelman et al., 2020). In mice lacking the dysbindin-1 gene, an animal model of SCZ, there are reduced dopamine levels in the hypothalamus (Hattori et al., 2008). These findings suggest that SCZ reduces DRD2/DRD3 signaling in the hypothalamus. Given that ER stress could work downstream of DRD2 (Song et al., 2017), it is possible that DRD2-ER stress pathway mediates SCZ. Moreover, it is currently unclear that how antipsychotics affect the hypothalamic ER stress in SCZ patients and whether it is involved in antipsychotic-induced obesity. The most widely used antipsychotics such as olanzapine, quetiapine and risperidone are known DRD2 antagonists. Therefore, it is possible that antipscyhotics may mediate the hypothalamic ER stress in SCZ patients. Furthermore, there is no clinical evidence of how hypothalamic astrocytes would be affected in patients with SCZ. The role of astrocytic ER stress in this population is currently not clear.

A possible role of hypothalamic endoplasmic reticulum stress in schizophrenia-associated metabolic disorder?

Hypothalamic DRD2 signaling plays an essential role in the regulation of food intake, body weight, and glucose metabolism (Yonemochi et al., 2019; Ikeda et al., 2020). Several studies have proved that a decline in central dopaminergic activity significantly influences metabolic parameters such as BMI, glucose, and lipid metabolism in humans (Brunerova et al., 2013). Treatment with a DRD2 antagonist (L-741) but not a DRD3 antagonist could increase food intake and body weight of mice during anorexia (Klenotich et al., 2015). Mice with insulin receptors knocked out in the brain show reduced dopamine signaling, leading to behavioral disturbances (Kleinridders et al., 2015). Mice with *Drd2* gene knocked out exhibit impaired insulin secretion and glucose intolerance (García-Tornadú et al., 2010). Moreover, it has been proved that ER stress is involved in the dopaminergic neuronal function. In the substantia nigra pars compacta (SNpc) of *Drd2*-knockout mice, increased phospho-eIF2α was observed, showing that DRD2 inhibition may activate ER stress eIF2α signaling (Tinsley et al., 2009). Researchers reported that the DRD2 antagonist haloperidol increases PERK expression in a hepatocyte cell model (Lauressergues et al., 2012). On the contrary, activating DRD2 by levodopa attenuated α-syn-induced increased ER stress markers including ATF4, C/EBP homologous protein expression (CHOP), GRP78/BiP and XBP1 in SH-SY5Y neuronal cells (Song et al., 2017). These evidences suggested that reduced DRD2 signaling induced ER stress and these effects could be inhibited by DRD2 activation. Due to the importance of ER stress in regulating food intake, body weight and insulin secretion (Kim et al., 2012; Ajoolabady et al., 2022), it is suggested that in SCZ, reduced DRD2 signaling may lead to induction of ER stress, and these effects may largely contribute

TABLE 2 Clinical studies of ER stress proteins in schizophrenia patients treated with or without antipsychotics.

References	Study location	Study design	ER stress-related protein/genes	Findings	Antipsychotic treatment
Kim et al., 2021	United States	UPR protein expression in the DLPFC of 22 matched pairs of elderly control subjects and subjects with SCZ was analyzed by WB and RT-qPCR.	sXBP1/uXBP1 ↑ GRP78/BiP ↑	1. In SCZ, BiP expression was increased, p-IRE1α expression was decreased, and PERK expression positively related to age was decreased. 2. There were decreased p-JNK2 and increased sXBP1, and IRE1α increased XBP1 mRNA splicing and drove upregulation of sXBP1 protein expression.	YES
Kakiuchi et al., 2004	Japan	The *XBP1*-116C/G polymorphism in 234 unrelated patients was genotyped by PCR, and Fisher's exact test was used to examine the differences in genotype and allele frequencies.	*XBP1*-116C/C ↓	1. The *XBP1*-116C/C genotype, a protective factor for bipolar disorder and schizophrenia, is decreased in patients with SCZ.	NO
Cheng et al., 2014	Asia	The *XBP1*-116C/G polymorphism was analyzed in different databases for case-control studies up to July 31, 2014.	*XBP1*-116C/G ↑	The *XBP1*-116C/G polymorphism is associated with an increased risk of psychiatric illness including bipolar disorder in the Asian population.	NM
Chen et al., 2004	China	The *XBP1*-197C/G polymorphism in unrelated patients (374 cases and 371 controls) was genotyped by PCR.	*XBP1*-197C/G ↑	1. *XBP1*-197C/G was significantly associated with SCZ, and the GG genotype frequency was higher than controls. 2. The G allele was significantly higher in the SCZ male groups; there were no significant changes in female groups.	NO
Kim et al., 2008	Korea	Five SNPs of *HSP70* in patients with SCZ (294 cases and 288 controls) were genotyped by using pyrosequencing method.	*HSP70*- rs2075799*G/A ↑	1. The rs2075799*G/A genotype was more represented in SCZ. 2. The T-A haplotype of rs2227956 and rs2075799 was significantly associated with SCZ.	NM
Kowalczyk et al., 2014	Poland	Polymorphisms of the *HSP-1* and *HSP-2* genes were genotyped by PCR-RFLP in drug-naïve patients with SCZ (203 cases and 243 controls) to examine the differences in genotype and allele frequencies.	*HSP-1* +190CC ↑	1. The *HSP-1*+190CC genotype and +190C allele were more represented in patients with SCZ. 2. Female patients with the *HSP-1*+190CC genotype have a higher risk of developing paranoid schizophrenia than male patients.	NO
Pae et al., 2005	Korea	Polymorphisms of the *HSP-1* and *HSP-2* were genotyped by PCR-RFLP in inpatients (161cases and 165 controls) to examine the differences in genotype and allele frequencies.	*HSP-2* ↑	1. *HSP-2* polymorphism contributed to the development of schizophrenia in a gene dose–dependent manner. 2. The *HSP-2* polymorphism conferred some susceptibility to schizophrenia in the Korean population.	YES

BiP, binding immunoglobulin protein; DLPFC, dorsolateral prefrontal cortex; GRP78, glucose regulatory protein 78; HSP, heat shock protein; PCR, polymerase chain reaction; PCR-RFLP, polymerase chain reaction-restriction fragment length polymorphism; p-JNK2, phosphorylated-c-Jun N-terminal kinase 2; RT-qPCR, real-time quantitative polymerase chain reaction; SCZ, schizophrenia; sXBP1, spliced X-box binding protein 1; UPR, unfolded protein response; WB, western blotting; XBP1, X-box binding protein 1; NM, not mentioned.

to SCZ-associated metabolic disorders such as increased BMI and glucose metabolic disorders (**Figure 3**).

Although there are controversial results, a meta-analysis suggests that SCZ is associated with the propensity to produce pro-inflammatory cytokines such as TNF-α, IL-6, and IL-1β in the brain (Momtazmanesh et al., 2019). Evidence has shown that DRD2 pathway regulates inflammation, and this effect cause metabolic disorders such as weight gain (Leite and Ribeiro, 2020). *Drd*2 knockout in mice produces a remarkable inflammatory response in the CNS (Shao et al., 2013). The DRD2 antagonist haloperidol increases TNF-α, IL-1β, and IL-6 expression *via* activating NF-κB signaling in SH-SY5Y cells exposed to hypoglycemia and hypoxia (Yang et al., 2022). Quinpirole, a DRD2 agonist, inhibits TLR4/NF-κB signaling and suppresses the expression of pro-inflammatory cytokines including TNF-α, IL-6, and IL-1β in the brain of an allergic rhinitis mouse model (Liu et al., 2021). ER stress *via* the IRE1-XBP1 and PERK pathways promotes inflammatory NF-κB

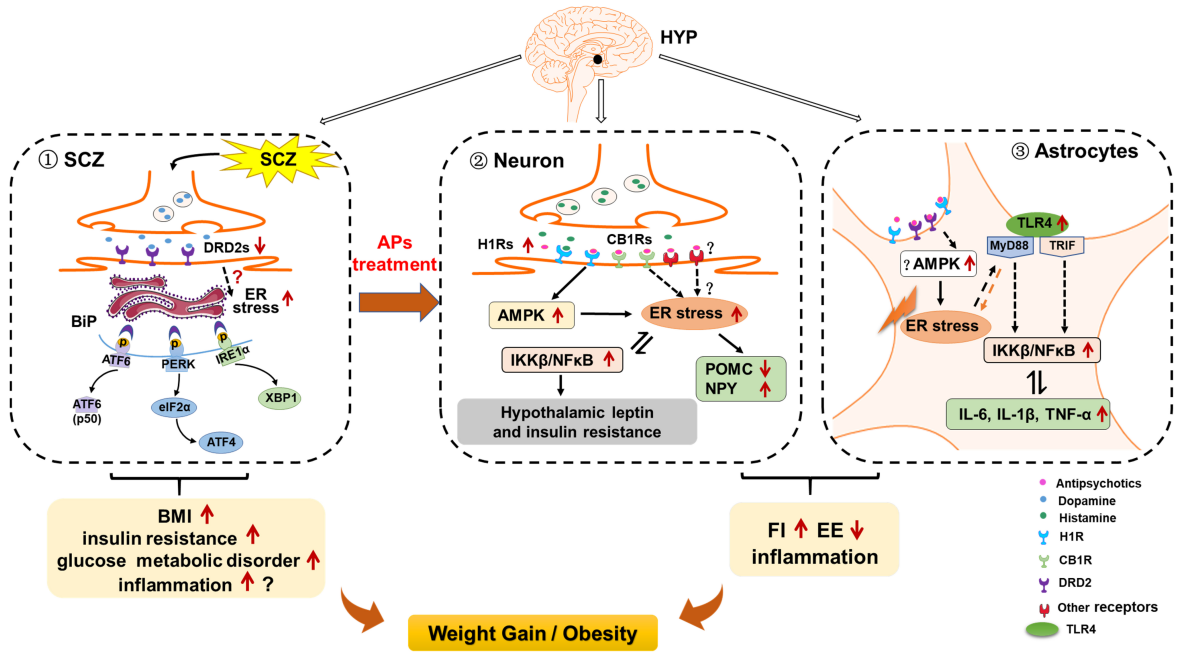

FIGURE 3
Possible role of hypothalamic endoplasmic reticulum (ER) stress in schizophrenia (SCZ)- and antipsychotic-induced weight gain/obesity. **(1)** Hypothalamic ER stress may be activated by decreased dopamine receptor D2 (DRD2) signaling, and these effects may be related to SCZ-related upregulation of body mass index (BMI), insulin resistance, and other metabolic disorders. Activated ER stress may also induce neuroinflammation; these effects may also be related to SCZ and its associated metabolic disorders. **(2)** In hypothalamic neurons, ER stress may contribute to antipsychotic-induced weight gain by inducing hyperphagia, decreasing energy expenditure, and inducing inflammation. Antipsychotics such as olanzapine and clozapine may activate hypothalamic ER stress by affecting H1 receptors (H1R) and CB1 receptors (CB1R), and activating adenosine 5′-monophosphate (AMP)-activated protein kinase (AMPK). On the one hand, activation of ER stress may inhibit proopiomelanocortin (POMC) processing, attenuate leptin signaling, and increase neuropeptide Y (NPY) and agouti-related protein (AgRP) expression, leading to increased food intake; reduced brown adipose tissue (BAT) thermogenesis and white adipose tissue (WAT) browning; increased inflammation; and thus weight gain/obesity Moreover, antipsychotic-induced ER stress activates inhibitor of nuclear factor kappa-B kinase subunit beta (IKKβ)/nuclear factor κB (NF-κB) signaling, leading to insulin and leptin resistance, and increased expression of pro-inflammatory cytokines such as interleukin 6 (IL-6), IL-1β, and tumor necrosis factor alpha (TNF-α). These effects may also contribute to antipsychotic-induced weight gain. **(3)** In hypothalamic astrocytes, antipsychotics such as olanzapine may induce ER stress possibly by acting on H1R, DRD2, and AMPK signaling. These effects may cause hyperphagia and decreased energy expenditure, resulting in weight gain. Antipsychotic-induced ER stress also leads to the increased TLR4 expression and activation of myeloid differentiation primary response 88 (MyD88)-independent/dependent signaling, which could stimulate the downstream IKKβ-NF-κB signaling activation and further causing the increased expression of pro-inflammatory cytokines such as TNF-α, IL-6, and IL-1β. These effects may be important for antipsychotic-induced obesity development.

signaling and increases TNF-α, IL-6, and IL-1β expression (Chipurupalli et al., 2021). Therefore, it is also possible that in SCZ, reduced DRD2 signaling activates ER stress, and these effects could activate inflammatory response and regulate body weight. Additional studies are necessary to evaluate this eventuality.

Hypothalamic neuronal endoplasmic reticulum stress and antipsychotic-induced weight gain

Studies have revealed that treatment with antipsychotic drugs including olanzapine, haloperidol, clozapine, and aripiprazole increases the expression of IRE1 and PERK in human and mouse hepatocytes (Lauressergues et al., 2012; Weston-Green et al., 2018; Forno et al., 2020). Olanzapine or risperidone treatment causes significant ER stress in the pancreatic β-cell line of hamsters (Ozasa et al., 2013). This evidence suggests that antipsychotics activate ER stress. Our previous study showed that in human neuroblastoma SH-SY5Y cells, olanzapine treatment induces ER stress and activation of IKKβ-NF-κB signaling and secretion of the pro-inflammatory cytokines including TNF-α, IL-6, and IL-1β (He et al., 2019). Hence, olanzapine could directly act on neurons to induce ER stress and inflammation (He et al., 2019). The fact that the ER stress inhibitor 4-PBA suppresses olanzapine-induced ER stress and inflammation in SH-SY5Y cells suggests that olanzapine-induced inflammation is at least partly regulated by ER stress (He et al., 2019). In rats, both acute (1 day) and short-term (8 days) olanzapine treatment induce ER stress *via* PERK-eIF2α signaling; activate inflammatory IKKβ-NF-κB

signaling; and augment TNF-α, IL-6, and IL-1β expression in the hypothalamus (He et al., 2019). These results suggest that olanzapine-induced ER stress and inflammation occur before rats are obese and could be a significant contributor rather than a consequence of obesity. Moreover, co-treatment with 4-PBA reduces olanzapine-induced hyperphagia and weight gain and inhibits olanzapine-induced ER stress and inflammation (He et al., 2019; **Table 1**). These findings indicate that olanzapine treatment activates hypothalamic neuronal ER stress and its related inflammatory IKKβ-NF-κB signaling, and these effects could lead to weight gain partly by increasing food intake. Hypothalamic ER stress also plays an important role in modulating energy expenditure. Numerous animal studies have revealed that obesogenic antipsychotics including olanzapine, clozapine, and risperidone reduce energy expenditure by inhibiting BAT thermogenesis, reducing tail artery vasoconstriction, and decreasing oxygen consumption and locomotor activity, all of which promote weight gain (Stefanidis et al., 2009; Bahr et al., 2015; Blessing et al., 2017). A study in humans reported that chronic olanzapine, risperidone, and quetiapine treatment (1, 3, 6, and 12 months) promotes weight gain with a hypometabolic state (Cuerda et al., 2011). Therefore, a reduction in energy expenditure induced by antipsychotics might be related to activation of hypothalamic ER stress. This eventuality should be evaluated in future studies. For example, investigating whether central inhibition of ER stress could reverse the antipsychotic-induced reduction in BAT thermogenesis and suppress the hypometabolic state in rodents would help to understand the role of ER stress in antipsychotic-induced decreased energy expenditure.

Hypothalamic astrocyte endoplasmic reticulum stress and antipsychotic-induced weight gain

We recently found that olanzapine treatment also causes ER stress in cultured astrocytes, and induces activation of astrocytes in the rat hypothalamus (He et al., 2021). Astrocyte activation during olanzapine treatment occurs before weight gain onset, which indicates that astrocytic ER stress may be a contributor to antipsychotic-induced obesity (He et al., 2021). Moreover, we found upregulated expression of p-NF-κB, p-p38 (a MAPK), TLR4, MyD88, and p-ERK1/2 in olanzapine-treated cultured astrocytes. In rats, both short- and long-term olanzapine treatment significantly increase food intake and weight gain, accompanied by activated astrocytes and TLR4 signaling in the hypothalamus. In a pair-fed experiment, we found that olanzapine-treated rats do not exhibit significantly increased weight gain because of their limited access to food. However, the pair-fed olanzapine rats still exhibit activated astrocytes and TLR4 signaling in the hypothalamus, demonstrating that these changes are primarily caused by olanzapine rather than the secondary effects of hyperphagia or weight gain. Moreover, 4-PBA co-treatment inhibits olanzapine-induced hyperphagia, weight gain, astrocyte activation, and TLR4 signaling in the hypothalamus (He et al., 2021). These findings suggest that weight gain induced by olanzapine treatment may also be related to the hypothalamic astrocytes and TLR4 signaling, and these effects are mediated by the hypothalamic ER stress. After olanzapine activates ER stress, the TLR4 signaling pathway may be activated and thereby induce hyperphagia and weight gain (**Figure 2**). It is important to investigate whether astrocytic TLR4 knockout affects the hyperphagic and obesogenic effects of olanzapine in rodents.

The effects of other antipsychotics on astrocytes, ER stress, and TLR4 signaling, as well as their role in antipsychotic-induced obesity, are controversial. It has been reported that both acute (120 min) and short-term (7 days) treatment of clozapine, quetiapine, and brexpiprazole induce astroglial L-glutamate release and connexin 43 expression, suggesting that most second-generation antipsychotics affect astrocyte activity (Fukuyama and Okada, 2021). Clozapine treatment increases intracellular Ca^{2+} concentrations and decreases Ca^{2+} reentry in cultured cortical astrocytes and C6 cells (Kanda et al., 2016). Quetiapine treatment upregulates adenosine triphosphate (ATP) synthesis in astrocytes (Wang et al., 2014). Studies have reported that quetiapine inhibits astrocyte activation in APP/PS1 mice (Zhu et al., 2014) and in streptozotocin-induced diabetic mice (Wang et al., 2019). A previous study reported that chronic exposure to olanzapine (17–27 month period) in macaques significantly reduces the number of astrocytes in parietal gray matter by 20.5% (Dorph-Petersen et al., 2005). Moreover, a study in C6 astroglial cells reported that haloperidol increases extracellular levels of TNF-α and IL-1β and decreases IL-10, while risperidone decreases the release of TNF-α and IL-1β (Bobermin et al., 2018). This evidence suggests that antipsychotic drugs induce variable effects depending on the brain region, treatment period, animal models, and cell lines. Future studies should investigate the effect of antipsychotics such as olanzapine, risperidone and quetiapine on astrocytic ER stress in the hypothalamus and its role in antipsychotic-induced weight gain.

As previously mentioned, microglia also mediate inflammation and obesity development, and there is evidence that antipsychotics interact with microglia. Olanzapine and haloperidol activate microglia in the rat brain (Cotel et al., 2015). Risperidone inhibits microglial activation induced by IFN-γ (Racki et al., 2021). Clozapine reduces microglial activation induced by LPS in neuron-glia cultures (Hu et al., 2012). Clozapine, risperidone, and haloperidol do not affect cytokine expression levels in the absence of external stimuli to microglia (Giridharan et al., 2020). After induction of inflammation in microglia by poly (I:C), clozapine, risperidone, and haloperidol decrease the expression of IL-1α and IL-1β, and risperidone and haloperidol (but not clozapine) increase the

expression of IL-6, IL-10, and TNF-α (Giridharan et al., 2020). Microglial ER stress and TLR4 signaling play a crucial role in the development of inflammation and obesity (Masson et al., 2015; Reis et al., 2015). Modulation of ER stress regulates the production of pro-inflammatory cytokines in microglia (Wang et al., 2017). Activation of TLR4 signaling by LPS induced a pro-inflammatory response in microglia (Zusso et al., 2019). TLR4 neutralization inhibited hypoxia-induced secretion of TNF-α and IL-1β in primary cultured microglia (Yao et al., 2013). However, the effects of antipsychotics on microglial ER stress and TLR4 signaling are currently unknown.

Potential mechanisms in schizophrenia- and antipsychotic-induced endoplasmic reticulum stress during obesity development

As discussed above, hypothalamic ER stress may be activated by reduced DRD2 signaling that is part of the pathogenesis of SCZ and SCZ-related metabolic disorders, but additional studies are needed. The mechanisms by which reduced DRD2 signaling leads to ER stress activation are unknown. It has been suggested that in SCZ, DRD2 controls Ca^{2+} upregulation or release in neurons (Frégeau et al., 2013). Ca^{2+} is an important inducer of cellular ER stress (Krebs et al., 2015). Hence, in SCZ, DRD2 might regulate ER stress by affecting Ca^{2+}. Studies that investigate alterations in hypothalamic ER stress markers and the Ca^{2+} level, DRD2 signaling in SCZ, and whether these effects could be inhibited by ER stress inhibitors are warranted. Moreover, we have reported that antipsychotics such as olanzapine activate hypothalamic ER stress in neurons (He et al., 2019) and astrocytes (He et al., 2021). Antipsychotics largely affect the energy sensor, AMPK, and have affinity for different neurotransmitter receptors such as DRD2 and H1R, which are expressed on both neurons and astrocytes and are related to ER stress. Could antipsychotic-induced ER stress be related to AMPK or these neurotransmitter receptors? In this section, we discuss the mechanisms by which antipsychotics induce ER stress.

The possible mechanisms of antipsychotic-induced endoplasmic reticulum stress in neurons

Growing evidence suggests that AMPK may play a role in antipsychotic-induced ER stress. A previous study showed that ceramide-induced reduction in ER stress is regulated by AMPK in the VMH, but the exact mechanism is unclear (Martinez-Sanchez et al., 2017). Inactivation of AMPK within the VMH reduces ER stress, whereas constitutive activation of AMPK prevents triiodothyronine (T3)-induced inhibition of ER stress (Liu et al., 2020). These results suggest that AMPK could act as an upstream regulator of ER stress in the VMH (Liu et al., 2020). Previous studies have revealed that obesogenic antipsychotics such as olanzapine, clozapine, risperidone, and quetiapine activate hypothalamic AMPK and cause weight gain (Kim et al., 2007; He et al., 2014), but there are currently no data demonstrating that antipsychotics trigger hypothalamic ER stress *via* AMPK signaling. Furthermore, it is unclear which receptors antipsychotics affect to induce ER stress. Antipsychotics including olanzapine, clozapine, and quetiapine induce AMPK activation by blocking H1R (Kim et al., 2007). A previous study reported that H1R antagonism induces ER stress in MCF-7 cells (Jakhar et al., 2016). Therefore, antipsychotic-induced ER stress may be partly related to antagonism of hypothalamic H1R (**Figure 1**). More studies should investigate whether H1R activation could counteract antipsychotic-induced ER stress. Moreover, it has been reported that ACEA, a CB1R agonist, attenuates ER stress and inflammation in Neuro-2a neuroblastoma cells (Vrechi et al., 2018). Olanzapine treatment significantly reduces CB1R expression in the rat hypothalamus (Weston-Green et al., 2012). These findings indicate that ER stress may also be activated by antipsychotics such as olanzapine *via* CB1R pathways. Activation of hypothalamic ER stress leads to decreased POMC processing and disrupts leptin signaling. Previous studies have reported that olanzapine reduced the expression of POMC and leptin receptor as well as increased the expression of NPY and AgRP in the hypothalamus of rats (He et al., 2014; Zhang et al., 2014). Risperidone upregulated the mRNA expression of H1R, NPY, and AgRP in the hypothalamus (Lian et al., 2015). Hence, olanzapine and risperidone may activate ER stress by affecting H1R, CB1R, and AMPK. These effects may result in decreased POMC expression, increased NPY and AgRP expression and disrupted leptin signaling, therefore caused hyperphagia, decreased energy expenditure, weight gain, and inflammation (**Figure 2**). Furthermore, activation of IKKβ-NF-κB signaling through ER stress in the hypothalamus is associated with dysfunction of SOCS3 signaling (Zhang et al., 2008), which means central leptin and insulin resistance. Previous studies have suggested that antipsychotic treatment is associated with leptin resistance and insulin resistance at least partly by activating on H1R and DRD2 (Kim et al., 2007; Hahn et al., 2011); however, the molecular mechanisms are unknown. Antipsychotic-induced leptin and insulin resistance may be related to elevated hypothalamic ER stress. It is well known that leptin and insulin resistance are important contributors to hyperphagia, thermogenesis dysfunction and inflammation. Therefore, antipsychotic-induced ER stress may also cause leptin and insulin resistance, and these effects may worsen obesity and inflammation development during antipsychotic treatment (**Figure 2**).

The potential mechanisms of antipsychotic-induced endoplasmic reticulum stress in astrocytes

The mechanisms by which antipsychotics induce inflammation, including secretion of pro-inflammatory factors and activation of TLR4 signaling in astrocytes, are not fully understood. Previous studies have reported that AMPK subunits such as α2, β2, and β1 are expressed in astrocytes (Turnley et al., 1999). Metformin reduces high-glucose-induced ER stress and inflammation partly by inhibiting AMPK signaling in primary cultured rat astrocytes (Wang et al., 2021). These results suggest that in astrocytes, AMPK may act upstream of ER stress. Therefore, it is possible that in astrocytes, olanzapine-induced ER stress may be related to AMPK during the development of inflammation and obesity (**Figure 3**). Future studies should explore whether inhibition of astrocytic AMPK suppresses antipsychotic-induced ER stress. Moreover, the receptors involved in antipsychotic-induced ER stress in astrocytes are unknown. As described above, in the hypothalamus, antipsychotics (e.g., olanzapine, clozapine, and quetiapine) induce AMPK activation by antagonizing H1R (Kim et al., 2007). A previous study reported that H1R is expressed in astrocytes (Xu et al., 2018). Histamine inhibits the secretion of pro-inflammatory factors including TNF-α and IL-1β, and these effects are completely abolished by co-treatment with the H1R antagonist cetirizine in primary cultured astrocytes (Xu et al., 2018). Hence, antipsychotic-induced activation of the inflammatory pathways and ER stress may be largely associated with the antagonism of astrocytic H1R.

Previous studies have proved that DRD2 inhibition is related to astrocytic inflammation. In LPS-stimulated astrocytes, bromocriptine, a DRD2 agonist, suppresses the expression of caspase-1, IL-1β, and TNF-α, changes that suggest DRD2 activation could reduce astrocytic inflammation (Tanaka et al., 2011; Zhu et al., 2018). In a Parkinson's disease mouse model, the DRD2 agonist LY171555 specifically inhibits astrocytic inflammation by inducing the interaction of β-arrestin 2 and nod-like receptor protein 3 (NLRP3) (Zhu et al., 2018). In contrast, there are marked inflammatory responses in different brain regions of *Drd2*-deficient mice, including the hippocampus, spinal cord, striatum, and ventral midbrain (Shao et al., 2013). Ablation of *Drd2* in astrocytes activates astrocytes in the mouse substantia nigra and increased the mRNA expression of pro-inflammatory factors including IL-1β, IL-6, and cyclooxygenase 2 (COX-2) (Shao et al., 2013). Based on these findings, astrocytic DRD2 might be involved in astrocytic inflammation. Furthermore, in the SNpc of *Drd2*-knockout mice, there is significantly increased p-eIF2α, suggesting that DRD2 inhibition could activate ER stress (Tinsley et al., 2009). On the contrary, in SH-SY5Y cells, the DRD2 agonist bromocriptine reduces the expression of BiP, indicating that ER stress could be inhibited by DRD2 activation (Henderson et al., 2021). Given that olanzapine, haloperidol, risperidone, and ziprasidone block DRD2, antipsychotics may induce ER stress in astrocytes by antagonizing DRD2, resulting in activation of TLR4 and IKKβ-NF-κB signaling, and secretion of pro-inflammatory markers such as IL-6 and IL-1β, ultimately leading to inflammation and weight gain. Moreover, H1R, CB1R, and DRD2 are expressed on microglia (Dong et al., 2014; Huck et al., 2015; De Meij et al., 2021). H1R, CB1R, and DRD2 signaling in microglia mediates the expression of pro-inflammatory cytokines (Dong et al., 2014; Huck et al., 2015; De Meij et al., 2021), although the exact mechanisms are not clear. As has been mentioned, ER stress could work as a downstream of H1R and DRD2 signaling in astrocytes. However, in microglia, whether ER stress plays a role in H1R-, CB1R-, and DRD2-related inflammatory response is unknown. It is possible that antipsychotics affect microglial ER stress by antagonizing H1R, CB1R, and DRD2, therefore affecting the inflammatory response and body weight. Future studies should investigate whether inhibition of ER stress affects inflammatory cytokine expression induced by activation of H1R, CB1R, and DRD2 in microglia, and how ER stress inhibitors affect the effects of antipsychotics on microglial cytokine expression.

It is noteworthy that the reported effects of antipsychotics on inflammation are inconsistent and complex. In patients with SCZ, both stimulatory and inhibitory effects on inflammatory cytokines have been reported from studies on olanzapine, haloperidol, clozapine, and risperidone (Drzyzga et al., 2006). In rodents, clozapine increases the expression of IL-1β in rat serum (Sernoskie et al., 2022). Olanzapine induces the expression of IL-1β, IL-6, and TNF-α in the rat hypothalamus (He et al., 2019). The role of other antipsychotics on hypothalamic inflammation has not been elucidated fully. In astrocytes, olanzapine, risperidone, quetiapine, and haloperidol increase IL-1β (He et al., 2022a). In microglia, as has been reviewed, haloperidol and risperidone reduce IL-1β induced by poly (I:C) treatment, but increase IL-6 and TNF-α (Giridharan et al., 2020). These findings suggest that the effects of antipsychotics on inflammatory markers vary by cell type. The reasons are likely complicated. For example, antipsychotics such as clozapine, olanzapine, and quetiapine have affinity for DRD2 and H1R, which regulate inflammatory pathways in astrocytes and microglia. However, these receptors differentially regulate inflammatory pathways in different cell types. H1R activation decreases TNF-α and IL-1β in astrocytes (Xu et al., 2018), whereas H1R activation increases TNF-α and IL-6 in microglia (Dong et al., 2014). Activation of DRD2 suppresses the upregulation of IL-1β induced by LPS + ATP in primary cultured astrocytes (Zhu et al., 2018), whereas activation of DRD2 increases nitrite production in microglia (Huck et al., 2015). ER stress signaling could be downstream of H1R and DRD2 (Jakhar et al., 2016; Song et al., 2017). Studies suggest that ER stress differentially mediates inflammation in astrocytes and microglia. Inhibition of ER stress in astrocytes

suppresses NF-κB activation induced by LPS and IFN-γ (Yanguas-Casás et al., 2014). However, in microglia, activation of ER stress by tunicamycin suppresses LPS-induced increases in IL-1β, IL-6, and TNF-α, whereas 4-PBA suppresses ER stress and promotes LPS-induced inflammation (Wang et al., 2017). Another study reported that suppression of ER stress by oxytocin inhibits TNF-α and IL-6 in microglia (Inoue et al., 2019). Therefore, the exact role of ER stress in microglia in regulating inflammation requires further investigation. The available evidence suggests that antipsychotics have differential effects on microglial and astrocytic inflammation by affecting H1R and DRD2 and their associated ER stress pathways. This may be an important reason why antipsychotics have been reported to produce pro- and anti-inflammatory effects in different studies. The overall effect of antipsychotics on inflammation in the hypothalamus is a combination of effects on neurons, astrocytes, and microglia. We suggest that ER stress in hypothalamic neurons and astrocytes may be related to antipsychotic-induced inflammation and obesity. Additional studies are needed to unravel how different doses of antipsychotics for different periods of time affect the astrocytic and microglial ER stress-inflammation pathways in the hypothalamus, to understand the mechanisms by which antipsychotics shows pro- or anti-inflammatory effects during different conditions.

Endoplasmic reticulum stress inhibitors as therapeutic alternatives in managing metabolic alterations associated with schizophrenia and antipsychotic treatment

Schizophrenia is accompanied by metabolic disorders such as weight gain/obesity, glucose metabolism disorder, and leptin and insulin resistance. Antipsychotics are the main cause of these side effects. As discussed above, activation of hypothalamic ER stress *via* reduced DRD2 signaling may contribute to SCZ-associated increased BMI and insulin signaling dysfunction. Olanzapine activates ER stress in both neurons and astrocytes in the hypothalamus, and these effects could be related to olanzapine-induced weight gain/obesity (He et al., 2019, 2021). Clozapine, haloperidol, and risperidone activate ER stress, and these effects may involve antipsychotic-induced metabolic side effects (Lauressergues et al., 2012). These findings suggest that ER stress inhibitors are potential effective interventions against SCZ and antipsychotic related metabolic disorders such as weight gain/obesity and insulin signaling dysfunction. Previous studies have demonstrated that inhibition of ER stress by TUDCA or 4-PBA significantly reduces food intake, weight gain, abnormal glucose metabolism, and insulin and leptin resistance in obese rodents (Basseri et al., 2009; Zhou et al., 2016). Of note, 4-PBA and TUDCA have a very good safety profile and are used medications for patients. TUDCA and PBA could improve β-cell function in humans and increase insulin sensitivity in obese women and men (Kars et al., 2010; Sarvani et al., 2017). In antipsychotic-induced obese rodents, 4-PBA reverses olanzapine-induced weight gain and inflammation by inhibiting hypothalamic ER stress (He et al., 2019). Metformin, which suppresses weight gain at least partly by inhibiting ER stress (Li X. et al., 2021), inhibits olanzapine-induced weight gain in patients (Wu et al., 2008) and rodents (Hu et al., 2014). TUDCA inhibits olanzapine-induced insulin secretion (stimulated by glucose) in pancreatic β cells (Grajales et al., 2022). Overall, the ER stress inhibitors may be useful therapeutic alternatives to manage metabolic alterations associated with SCZ and antipsychotic treatment. Future studies should investigate the effects of TUDCA or 4-PBA on clozapine-, risperidone-, and quetiapine-induced weight gain and other metabolic disorders.

As has been reviewed, ER stress may also play an important role in the pathology of SCZ. ER stress inhibitors including 4-PBA and TUDCA are neuroprotective and significantly ameliorate the cognitive disorders in various neuropsychiatric disorders such as Alzheimer's disease (Cuadrado-Tejedor et al., 2011; Dionísio et al., 2015) and cerebral ischemic injury (Qi et al., 2004). Pioglitazone, an antidiabetic agent, is an ER stress inhibitor and has been found to reduce the negative symptoms in patients with SCZ (Iranpour et al., 2016). Morin, an ER stress inhibitor, inhibits the IRE1-sXBP-1 signaling pathway induced by tunicamycin (an ER stress inducer) (Mo et al., 2019) and attenuates LPS + ketamine-induced SCZ-like behaviors in mice (Ben-Azu et al., 2019). The ER stress inhibitor, 4-PBA, could be a potential therapy for SCZ (Patel et al., 2017). These findings suggest that, in addition to managing SCZ-related metabolic disorders, the ER stress inhibitors may also effective in treating SCZ.

Conclusion

The role of ER stress in SCZ and antipsychotic-induced weight gain/obesity has not been explored extensively. Based on evidence from clinical and pre-clinical studies, ER stress may be an important underlying mechanism for SCZ and antipsychotic-induced weight gain/obesity. Patients with SCZ show a reduction in hypothalamic DRD2 signaling, which may lead to activation of ER stress, thereby causing weight gain and dysregulated glucose metabolism. Antipsychotic drugs, in particular olanzapine, induce hypothalamic ER stress, and this effect is associated with inflammation and weight gain. Antipsychotics seems to induce hypothalamic ER stress by (1) obstructing POMC processing, attenuating leptin signaling, and increasing the expression of NPY/AgRP, therefore resulting in hyperphagia; (2) decreasing WAT browning and BAT thermogenesis, which inhibit energy expenditure; and (3)

activating the MyD88-independent and MyD88-dependent pathways in astrocytes, resulting in increased secretion of pro-inflammatory cytokines. Based on the published evidence, antipsychotic-induced ER stress and the resulting inflammation may be related to the antipsychotic antagonism of H1R and DRD2. Taken together, hypothalamic ER stress could be a valuable target for mitigating SCZ and antipsychotic-induced metabolic side effects such as weight gain/obesity.

Author contributions

MH and RZ wrote the manuscript. RZ, JF, RL, YZ, and BL revised the manuscript and figures. MH, GG, and TS provided the funding. All authors have contributed to and have approved the final manuscript.

Funding

This work was supported by the National Natural Science Foundation of China (21975191), the Natural Science Foundation of Hubei Province (2021CFB301 and 2021CFB299), and the State Key Laboratory of Advanced Technology for Materials Synthesis and Processing (WUT) (2022-KF-27).

Conflict of interest

The authors declare that the research was conducted in the absence of any commercial or financial relationships that could be construed as a potential conflict of interest.

Publisher's note

References

Ajoolabady, A., Liu, S., Klionsky, D. J., Lip, G. Y. H., Tuomilehto, J., Kavalakatt, S., et al. (2022). ER stress in obesity pathogenesis and management. *Trends Pharmacol. Sci.* 43, 97–109. doi: 10.1016/j.tips.2021.11.011

Areias, M. F. C., and Prada, P. O. (2015). Mechanisms of insulin resistance in the amygdala: Influences on food intake. *Behav. Brain Res.* 282, 209–217. doi: 10.1016/j.bbr.2015.01.003

Bahr, S. M., Weidemann, B. J., Castro, A. N., Walsh, J. W., deLeon, O., Burnett, C. M., et al. (2015). Risperidone-induced weight gain is mediated through shifts in the gut microbiome and suppression of energy expenditure. *EBioMedicine* 2, 1725–1734. doi: 10.1016/j.ebiom.2015.10.018

Ballon, J. S., Pajvani, U., Freyberg, Z., Leibel, R. L., and Lieberman, J. A. (2014). Molecular pathophysiology of metabolic effects of antipsychotic medications. *Trends Endocrinol. Metab.* 25, 593–600. doi: 10.1016/j.tem.2014.07.004

Barton, B. B., Segger, F., Fischer, K., Obermeier, M., and Musil, R. (2020). Update on weight-gain caused by antipsychotics: A systematic review and meta-analysis. *Expert Opin. Drug Saf.* 19, 295–314. doi: 10.1080/14740338.2020.1713091

Basseri, S., Lhoták, S., Sharma, A. M., and Austin, R. C. (2009). The chemical chaperone 4-phenylbutyrate inhibits adipogenesis by modulating the unfolded protein response. *J. Lipid Res.* 50, 2486–2501. doi: 10.1194/jlr.M900216-JLR200

Ben-Azu, B., Aderibigbe, A. O., Ajayi, A. M., Eneni, A. O., Omogbiya, I. A., Owoeye, O., et al. (2019). Morin decreases cortical pyramidal neuron degeneration via inhibition of neuroinflammation in mouse model of schizophrenia. *Int. Immunopharmacol.* 70, 338–353. doi: 10.1016/j.intimp.2019.02.052

Bernstein, H. G., Keilhoff, G., and Steiner, J. (2021). The implications of hypothalamic abnormalities for schizophrenia. *Handb. Clin. Neurol.* 182, 107–120. doi: 10.1016/b978-0-12-819973-2.00008-3

Blessing, W. W., Blessing, E. M., Mohammed, M., and Ootsuka, Y. (2017). Clozapine, chlorpromazine and risperidone dose-dependently reduce emotional hyperthermia, a biological marker of salience. *Psychopharmacology* 234, 3259–3269. doi: 10.1007/s00213-017-4710-x

Bobbo, V. C., Engel, D. F., Jara, C. P., Mendes, N. F., Haddad-Tovolli, R., Prado, T. P., et al. (2021). Interleukin-6 actions in the hypothalamus protects against obesity and is involved in the regulation of neurogenesis. *J. Neuroinflamm.* 18:192. doi: 10.1186/s12974-021-02242-8

Bobermin, L. D., da Silva, A., Souza, D. O., and Quincozes-Santos, A. (2018). Differential effects of typical and atypical antipsychotics on astroglial cells in vitro. *Int. J. Dev. Neurosci.* 69, 1–9. doi: 10.1016/j.ijdevneu.2018.06.001

Breen, T. L., Conwell, I. M., and Wardlaw, S. L. (2005). Effects of fasting, leptin, and insulin on AGRP and POMC peptide release in the hypothalamus. *Brain Res.* 1032, 141–148. doi: 10.1016/j.brainres.2004.11.008

Brunerova, L., Potockova, J., Horacek, J., Suchy, J., and Andel, M. (2013). Central dopaminergic activity influences metabolic parameters in healthy men. *Neuroendocrinology* 97, 132–138. doi: 10.1159/000338405

Burdakov, D., and Peleg-Raibstein, D. (2020). The hypothalamus as a primary coordinator of memory updating. *Physiol. Behav.* 223:112988. doi: 10.1016/j.physbeh.2020.112988

Cakir, I., and Nillni, E. A. (2019). Endoplasmic reticulum stress, the hypothalamus, and energy balance. *Trends Endocrinol. Metab.* 30, 163–176. doi: 10.1016/j.tem.2019.01.002

Cakir, I., Cyr, N. E., Perello, M., Litvinov, B. P., Romero, A., Stuart, R. C., et al. (2013). Obesity induces hypothalamic endoplasmic reticulum stress and impairs proopiomelanocortin (POMC) post-translational processing. *J. Biol. Chem.* 288, 17675–17688. doi: 10.1074/jbc.M113.475343

Camandola, S., and Mattson, M. P. (2017). Toll-like receptor 4 mediates fat, sugar, and umami taste preference and food intake and body weight regulation. *Obesity* 25, 1237–1245. doi: 10.1002/oby.21871

Cansell, C., Stobbe, K., Sanchez, C., Le Thuc, O., Mosser, C. A., Ben-Fradj, S., et al. (2021). Dietary fat exacerbates postprandial hypothalamic inflammation involving glial fibrillary acidic protein-positive cells and microglia in male mice. *Glia* 69, 42–60. doi: 10.1002/glia.23882

Catalán, V., Gómez-Ambrosi, J., Rodríguez, A., Ramírez, B., Rotellar, F., Valentí, V., et al. (2012). Increased tenascin C and Toll-like receptor 4 levels in visceral adipose tissue as a link between inflammation and extracellular matrix remodeling in obesity. *J. Clin. Endocrinol. Metab.* 97, E1880–E1889. doi: 10.1210/jc.2012-1670

Chadwick, W., Magnus, T., Martin, B., Keselman, A., Mattson, M. P., and Maudsley, S. (2008). Targeting TNF-alpha receptors for neurotherapeutics. *Trends Neurosci.* 31, 504–511. doi: 10.1016/j.tins.2008.07.005

Chang, Y., and Kong, R. (2019). Ganoderic acid A alleviates hypoxia-induced apoptosis, autophagy, and inflammation in rat neural stem cells through the PI3K/AKT/mTOR pathways. *Phytother. Res.* 33, 1448–1456. doi: 10.1002/ptr.6336

Chen, N., Sugihara, H., Kim, J., Fu, Z., Barak, B., Sur, M., et al. (2016). Direct modulation of GFAP-expressing glia in the arcuate nucleus bi-directionally regulates feeding. *Elife* 5:e18716. doi: 10.7554/eLife.18716

Chen, W., Duan, S., Zhou, J., Sun, Y., Zheng, Y., Gu, N., et al. (2004). A case–control study provides evidence of association for a functional polymorphism –197C/G in XBP1 to schizophrenia and suggests a sex-dependent effect. *Biochem. Biophys. Res. Commun.* 319, 866–870. doi: 10.1016/j.bbrc.2004.05.060

Chen, X., Yu, Y., Zheng, P., Jin, T., He, M., Zheng, M., et al. (2020). Olanzapine increases AMPK-NPY orexigenic signaling by disrupting H1R-GHSR1a interaction in the hypothalamic neurons of mice. *Psychoneuroendocrinology* 114:104594. doi: 10.1016/j.psyneuen.2020.104594

Cheng, D., Zhang, K., Zhen, G., and Xue, Z. (2014). The -116c/G polymorphism in Xbp1 gene is associated with psychiatric illness in asian population: A meta-analysis. *Am. J. Med. Genet B Neuropsychiatry Genet.* 165b, 665–672. doi: 10.1002/ajmg.b.32271

Chipurupalli, S., Samavedam, U., and Robinson, N. (2021). Crosstalk between er stress, autophagy and inflammation. *Front. Med.* 8:758311. doi: 10.3389/fmed.2021.758311

Cnop, M., Foufelle, F., and Velloso, L. A. (2012). Endoplasmic reticulum stress, obesity and diabetes. *Trends Mol. Med.* 18, 59–68. doi: 10.1016/j.molmed.2011.07.010

Contreras, C., Gonzalez-Garcia, I., Martinez-Sanchez, N., Seoane-Collazo, P., Jacas, J., Morgan, D. A., et al. (2014). Central ceramide-induced hypothalamic lipotoxicity and ER stress regulate energy balance. *Cell Rep.* 9, 366–377. doi: 10.1016/j.celrep.2014.08.057

Contreras, C., Gonzalez-Garcia, I., Seoane-Collazo, P., Martinez-Sanchez, N., Linares-Pose, L., Rial-Pensado, E., et al. (2017). Reduction of hypothalamic endoplasmic reticulum stress activates browning of white fat and ameliorates obesity. *Diabetes* 66, 87–99. doi: 10.2337/db15-1547

Cope, M. B., Nagy, T. R., Fernández, J. R., Geary, N., Casey, D. E., and Allison, D. B. (2005). Antipsychotic drug-induced weight gain: Development of an animal model. *Int. J. Obes.* 29, 607–614. doi: 10.1038/sj.ijo.0802928

Cotel, M. C., Lenartowicz, E. M., Natesan, S., Modo, M. M., Cooper, J. D., Williams, S. C., et al. (2015). Microglial activation in the rat brain following chronic antipsychotic treatment at clinically relevant doses. *Eur. Neuropsychopharmacol.* 25, 2098–2107. doi: 10.1016/j.euroneuro.2015.08.004

Cuadrado-Tejedor, M., García-Osta, A., Ricobaraza, A., Oyarzabal, J., and Franco, R. (2011). Defining the mechanism of action of 4-phenylbutyrate to develop a small-molecule-based therapy for Alzheimer's disease. *Curr. Med. Chem.* 18, 5545–5553. doi: 10.2174/092986711798347315

Cuerda, C., Merchan-Naranjo, J., Velasco, C., Gutierrez, A., Leiva, M., de Castro, M. J., et al. (2011). Influence of resting energy expenditure on weight gain in adolescents taking second-generation antipsychotics. *Clin. Nutr.* 30, 616–623. doi: 10.1016/j.clnu.2011.03.007

Dalvi, P. S., Chalmers, J. A., Luo, V., Han, D. Y., Wellhauser, L., Liu, Y., et al. (2017). High fat induces acute and chronic inflammation in the hypothalamus: Effect of high-fat diet, palmitate and TNF-α on appetite-regulating NPY neurons. *Int. J. Obes.* 41, 149–158. doi: 10.1038/ijo.2016.183

Darling, N. J., and Cook, S. J. (2014). The role of MAPK signalling pathways in the response to endoplasmic reticulum stress. *Biochim. Biophys. Acta* 1843, 2150–2163. doi: 10.1016/j.bbamcr.2014.01.009

De Meij, J., Alfanek, Z., Morel, L., Decoeur, F., Leyrolle, Q., Picard, K., et al. (2021). Microglial cannabinoid type 1 receptor regulates brain inflammation in a sex-specific manner. *Cannabis Cannabinoid Res.* 6, 488–507. doi: 10.1089/can.2020.0170

de Vicente, L. G., Muñoz, V. R., Pinto, A. P., Rovina, R. L., da Rocha, A. L., Marafon, B. B., et al. (2021). TLR4 deletion increases basal energy expenditure and attenuates heart apoptosis and ER stress but mitigates the training-induced cardiac function and performance improvement. *Life Sci.* 285:119988. doi: 10.1016/j.lfs.2021.119988

Deng, C., Lian, J., Pai, N., and Huang, X. F. (2012). Reducing olanzapine-induced weight gain side effect by using betahistine: A study in the rat model. *J. Psychopharmacol.* 26, 1271–1279. doi: 10.1177/0269881112449396

Deng, J., Yuan, F., Guo, Y., Xiao, Y., Niu, Y., Deng, Y., et al. (2017). Deletion of ATF4 in AgRP neurons promotes fat loss mainly via increasing energy expenditure. *Diabetes* 66, 640–650. doi: 10.2337/db16-0954

Denis, R. G., Arruda, A. P., Romanatto, T., Milanski, M., Coope, A., Solon, C., et al. (2010). TNF-α transiently induces endoplasmic reticulum stress and an incomplete unfolded protein response in the hypothalamus. *Neuroscience* 170, 1035–1044. doi: 10.1016/j.neuroscience.2010.08.013

Dionísio, P. A., Amaral, J. D., Ribeiro, M. F., Lo, A. C., D'Hooge, R., and Rodrigues, C. M. (2015). Amyloid-β pathology is attenuated by tauroursodeoxycholic acid treatment in APP/PS1 mice after disease onset. *Neurobiol. Aging* 36, 228–240. doi: 10.1016/j.neurobiolaging.2014.08.034

Doane, M. J., Bessonova, L., Friedler, H. S., Mortimer, K. M., Cheng, H., Brecht, T., et al. (2022). Weight gain and comorbidities associated with oral second-generation antipsychotics: Analysis of real-world data for patients with schizophrenia or bipolar I disorder. *BMC Psychiatry* 22:114. doi: 10.1186/s12888-022-03758-w

Dong, H., Zhang, W., Zeng, X., Hu, G., Zhang, H., He, S., et al. (2014). Histamine induces upregulated expression of histamine receptors and increases release of inflammatory mediators from microglia. *Mol. Neurobiol.* 49, 1487–1500. doi: 10.1007/s12035-014-8697-6

Dorph-Petersen, K. A., Pierri, J. N., Perel, J. M., Sun, Z., Sampson, A. R., and Lewis, D. A. (2005). The influence of chronic exposure to antipsychotic medications on brain size before and after tissue fixation: A comparison of haloperidol and olanzapine in macaque monkeys. *Neuropsychopharmacology* 30, 1649–1661. doi: 10.1038/sj.npp.1300710

Douglass, J. D., Dorfman, M. D., Fasnacht, R., Shaffer, L. D., and Thaler, J. P. (2017). Astrocyte IKKβ/NF-κB signaling is required for diet-induced obesity and hypothalamic inflammation. *Mol. Metab.* 6, 366–373. doi: 10.1016/j.molmet.2017.01.010

Drzyzga, L., Obuchowicz, E., Marcinowska, A., and Herman, Z. S. (2006). Cytokines in schizophrenia and the effects of antipsychotic drugs. *Brain Behav. Immun.* 20, 532–545. doi: 10.1016/j.bbi.2006.02.002

Eder, U., Mangweth, B., Ebenbichler, C., Weiss, E., Hofer, A., Hummer, M., et al. (2001). Association of olanzapine-induced weight gain with an increase in body fat. *Am. J. Psychiatry* 158, 1719–1722. doi: 10.1176/appi.ajp.158.10.1719

Ellul, P., Delorme, R., and Cortese, S. (2018). Metformin for weight gain associated with second-generation antipsychotics in children and adolescents: A systematic review and meta-analysis. *CNS Drugs* 32, 1103–1112. doi: 10.1007/s40263-018-0571-z

Fernø, J., Varela, L., Skrede, S., Vázquez, M. J., Nogueiras, R., Diéguez, C., et al. (2011). Olanzapine-induced hyperphagia and weight gain associate with orexigenic hypothalamic neuropeptide signaling without concomitant AMPK phosphorylation. *PLoS One* 6:e20571. doi: 10.1371/journal.pone.0020571

Forno, F., Maatuf, Y., Boukeileh, S., Dipta, P., Mahameed, M., Darawshi, O., et al. (2020). Aripiprazole cytotoxicity coincides with activation of the unfolded protein response in human hepatic cells. *J. Pharmacol. Exp. Ther.* 374, 452–461. doi: 10.1124/jpet.119.264481

Frégeau, M. O., Carrier, M., and Guillemette, G. (2013). Mechanism of dopamine D2 receptor-induced Ca(2+) release in PC-12 cells. *Cell Signal.* 25, 2871–2877. doi: 10.1016/j.cellsig.2013.08.021

Freyberg, Z., Aslanoglou, D., Shah, R., and Ballon, J. S. (2017). Intrinsic and antipsychotic drug-induced metabolic dysfunction in schizophrenia. *Front. Neurosci.* 11:432. doi: 10.3389/fnins.2017.00432

Friedman, W. J. (2001). Cytokines regulate expression of the type 1 interleukin-1 receptor in rat hippocampal neurons and glia. *Exp. Neurol.* 168, 23–31. doi: 10.1006/exnr.2000.7595

Fukuyama, K., and Okada, M. (2021). Effects of atypical antipsychotics, clozapine, quetiapine and brexpiprazole on astroglial transmission associated with connexin43. *Int. J. Mol. Sci.* 22:5623. doi: 10.3390/ijms22115623

Galichet, C., Clayton, R. W., and Lovell-Badge, R. (2021). Novel tools and investigative approaches for the study of oligodendrocyte precursor cells (NG2-Glia) in CNS development and disease. *Front. Cell. Neurosci.* 15:673132. doi: 10.3389/fncel.2021.673132

García-Tornadú, I., Ornstein, A. M., Chamson-Reig, A., Wheeler, M. B., Hill, D. J., Arany, E., et al. (2010). Disruption of the dopamine d2 receptor impairs insulin secretion and causes glucose intolerance. *Endocrinology* 151, 1441–1450. doi: 10.1210/en.2009-0996

Garg, A. D., Kaczmarek, A., Krysko, O., Vandenabeele, P., Krysko, D. V., and Agostinis, P. (2012). ER stress-induced inflammation: Does it aid or impede disease progression? *Trends Mol. Med.* 18, 589–598. doi: 10.1016/j.molmed.2012.06.010

Giridharan, V. V., Scaini, G., Colpo, G. D., Doifode, T., Pinjari, O. F., Teixeira, A. L., et al. (2020). Clozapine prevents poly (I:C) induced inflammation by modulating NLRP3 pathway in microglial cells. *Cells* 9:577. doi: 10.3390/cells9030577

González-García, I., Contreras, C., Estévez-Salguero, Á, Ruíz-Pino, F., Colsh, B., Pensado, I., et al. (2018). Estradiol regulates energy balance by ameliorating hypothalamic ceramide-induced ER stress. *Cell Rep.* 25, 413–423.e5. doi: 10.1016/j.celrep.2018.09.038

Gorina, R., Font-Nieves, M., Marquez-Kisinousky, L., Santalucia, T., and Planas, A. M. (2011). Astrocyte TLR4 activation induces a proinflammatory environment through the interplay between MyD88-dependent NFkappaB signaling, MAPK, and Jak1/Stat1 pathways. *Glia* 59, 242–255. doi: 10.1002/glia.21094

Grajales, D., Vázquez, P., Alén, R., Hitos, A. B., and Valverde, ÁM. (2022). Attenuation of olanzapine-induced endoplasmic reticulum stress improves insulin secretion in pancreatic beta cells. *Metabolites* 12:433. doi: 10.3390/metabo12050443

Hahn, M., Chintoh, A., Giacca, A., Xu, L., Lam, L., Mann, S., et al. (2011). Atypical antipsychotics and effects of muscarinic, serotonergic, dopaminergic and histaminergic receptor binding on insulin secretion in vivo: An animal model. *Schizophr. Res.* 131, 90–95. doi: 10.1016/j.schres.2011.06.004

Han, M., Lian, J., Su, Y., and Deng, C. (2022). Cevimeline co-treatment attenuates olanzapine-induced metabolic disorders via modulating hepatic M3 muscarinic receptor: AMPKα signalling pathway in female rats. *J. Psychopharmacol.* 36, 202–213. doi: 10.1177/02698811211050549

Harris, L. W., Guest, P. C., Wayland, M. T., Umrania, Y., Krishnamurthy, D., Rahmoune, H., et al. (2013). Schizophrenia: Metabolic aspects of aetiology, diagnosis and future treatment strategies. *Psychoneuroendocrinology* 38, 752–766. doi: 10.1016/j.psyneuen.2012.09.009

Hattori, S., Murotani, T., Matsuzaki, S., Ishizuka, T., Kumamoto, N., Takeda, M., et al. (2008). Behavioral abnormalities and dopamine reductions in sdy mutant mice with a deletion in Dtnbp1, a susceptibility gene for schizophrenia. *Biochem. Biophys. Res. Commun.* 373, 298–302. doi: 10.1016/j.bbrc.2008.06.016

He, M., Fan, J., Zhou, R., Gao, G., Li, R., Zuo, Y., et al. (2022a). NLRP3/Caspase-1-mediated pyroptosis of astrocytes induced by antipsychotics is inhibited by a histamine H1 receptor-selective agonist. *Front. Aging Neurosci.* 14:847561. doi: 10.3389/fnagi.2022.847561

He, M., Huang, X. F., Gao, G., Zhou, T., Li, W., Hu, J., et al. (2019). Olanzapine-induced endoplasmic reticulum stress and inflammation in the hypothalamus were inhibited by an ER stress inhibitor 4-phenylbutyrate. *Psychoneuroendocrinology* 104, 286–299. doi: 10.1016/j.psyneuen.2019.03.017

He, M., Qian, K., Zhang, Y., Huang, X.-F., Deng, C., Zhang, B., et al. (2021). Olanzapine-induced activation of hypothalamic astrocytes and toll-like receptor-4 signaling via endoplasmic reticulum stress were related to olanzapine-induced weight gain. *Front. Neurosci.* 14:589650. doi: 10.3389/fnins.2020.589650

He, M., Yao, J., Zhang, Z., Zhang, Y., Chen, R., Gu, Z., et al. (2022b). Gold nanoclusters eliminate obesity induced by antipsychotics. *Sci. Rep.* 12:5502. doi: 10.1038/s41598-022-09541-x

He, M., Zhang, Q., Deng, C., Wang, H., Lian, J., and Huang, X. F. (2014). Hypothalamic histamine H1 receptor-AMPK signaling time-dependently mediates olanzapine-induced hyperphagia and weight gain in female rats. *Psychoneuroendocrinology* 42, 153–164. doi: 10.1016/j.psyneuen.2014.01.018

Henderson, M. J., Trychta, K. A., Yang, S. M., Back, S., Yasgar, A., Wires, E. S., et al. (2021). A target-agnostic screen identifies approved drugs to stabilize the endoplasmic reticulum-resident proteome. *Cell Rep.* 35:109040. doi: 10.1016/j.celrep.2021.109040

Henry, F. E., Sugino, K., Tozer, A., Branco, T., and Sternson, S. M. (2015). Cell type-specific transcriptomics of hypothalamic energy-sensing neuron responses to weight-loss. *Elife* 4:e09800. doi: 10.7554/eLife.09800

Hu, X., Zhou, H., Zhang, D., Yang, S., Qian, L., Wu, H. M., et al. (2012). Clozapine protects dopaminergic neurons from inflammation-induced damage by inhibiting microglial overactivation. *J. Neuroimmune Pharmacol.* 7, 187–201. doi: 10.1007/s11481-011-9309-0

Hu, Y., Young, A. J., Ehli, E. A., Nowotny, D., Davies, P. S., Droke, E. A., et al. (2014). Metformin and berberine prevent olanzapine-induced weight gain in rats. *PLoS One* 9:e93310. doi: 10.1371/journal.pone.0093310

Huck, J. H., Freyer, D., Böttcher, C., Mladinov, M., Muselmann-Genschow, C., Thielke, M., et al. (2015). De novo expression of dopamine D2 receptors on microglia after stroke. *J. Cereb. Blood. Flow. Metab.* 35, 1804–1811. doi: 10.1038/jcbfm.2015.128

Ikeda, H., Yonemochi, N., Mikami, R., Abe, M., Kawamura, M., Natsume, R., et al. (2020). Central dopamine D(2) receptors regulate plasma glucose levels in mice through autonomic nerves. *Sci. Rep.* 10:22347. doi: 10.1038/s41598-020-79292-0

Ikegami, M., Ikeda, H., Ishikawa, Y., Ohsawa, M., Ohashi, T., Kai, M., et al. (2013). Olanzapine induces glucose intolerance through the activation of AMPK in the mouse hypothalamus. *Eur. J. Pharmacol.* 718, 376–382.

Inoue, T., Yamakage, H., Tanaka, M., Kusakabe, T., Shimatsu, A., and Satoh-Asahara, N. (2019). Oxytocin suppresses inflammatory responses induced by lipopolysaccharide through inhibition of the eIF-2-ATF4 pathway in mouse microglia. *Cells* 8:527. doi: 10.3390/cells8060527

Iranpour, N., Zandifar, A., Farokhnia, M., Goguol, A., Yekehtaz, H., Khodaie-Ardakani, M. R., et al. (2016). The effects of pioglitazone adjuvant therapy on negative symptoms of patients with chronic schizophrenia: A double-blind and placebo-controlled trial. *Hum. Psychopharmacol.* 31, 103–112. doi: 10.1002/hup.2517

Jaboin, J. J., Shinohara, E. T., Moretti, L., Yang, E. S., Kaminski, J. M., and Lu, B. (2007). The role of mTOR inhibition in augmenting radiation induced autophagy. *Technol. Cancer Res. Treat.* 6, 443–447. doi: 10.1177/153303460700600510

Jais, A., and Brüning, J. C. (2017). Hypothalamic inflammation in obesity and metabolic disease. *J. Clin. Invest.* 127, 24–32. doi: 10.1172/jci88878

Jakhar, R., Paul, S., Bhardwaj, M., and Kang, S. C. (2016). Astemizole-Histamine induces Beclin-1-independent autophagy by targeting p53-dependent crosstalk between autophagy and apoptosis. *Cancer Lett.* 372, 89–100. doi: 10.1016/j.canlet.2015.12.024

Jensen, K. G., Correll, C. U., Rudå, D., Klauber, D. G., Stentebjerg-Olesen, M., Fagerlund, B., et al. (2017). Pretreatment cardiometabolic status in youth with early-onset psychosis: Baseline results from the TEA trial. *J. Clin. Psychiatry* 78, e1035–e1046. doi: 10.4088/JCP.15m10479

Jin, S., Kim, K. K., Park, B. S., Kim, D. H., Jeong, B., Kang, D., et al. (2020). Function of astrocyte MyD88 in high-fat-diet-induced hypothalamic inflammation. *J. Neuroinflamm.* 17:195. doi: 10.1186/s12974-020-01846-w

Kakiuchi, C., Ishiwata, M., Umekage, T., Tochigi, M., Kohda, K., Sasaki, T., et al. (2004). Association of the XBP1-116C/G polymorphism with schizophrenia in the Japanese population. *Psychiatry. Clin. Neurosci.* 58, 438–440. doi: 10.1111/j.1440-1819.2004.01280.x

Kanak, M. A., Shahbazov, R., Yoshimatsu, G., Levy, M. F., Lawrence, M. C., and Naziruddin, B. (2017). A small molecule inhibitor of NFκB blocks ER stress and the NLRP3 inflammasome and prevents progression of pancreatitis. *J. Gastroenterol.* 52, 352–365. doi: 10.1007/s00535-016-1238-5

Kanda, Y., Okada, M., Ikarashi, R., Morioka, E., Kondo, T., and Ikeda, M. (2016). Bimodal modulation of store-operated Ca(2+) channels by clozapine in astrocytes. *Neurosci. Lett.* 635, 56–60. doi: 10.1016/j.neulet.2016.10.027

Kao, A. C., Spitzer, S., Anthony, D. C., Lennox, B., and Burnet, P. W. J. (2018). Prebiotic attenuation of olanzapine-induced weight gain in rats: Analysis of central and peripheral biomarkers and gut microbiota. *Transl. Psychiatry* 8:66. doi: 10.1038/s41398-018-0116-8

Kars, M., Yang, L., Gregor, M. F., Mohammed, B. S., Pietka, T. A., Finck, B. N., et al. (2010). Tauroursodeoxycholic Acid may improve liver and muscle but not adipose tissue insulin sensitivity in obese men and women. *Diabetes* 59, 1899–1905. doi: 10.2337/db10-0308

Kim, J. G., Suyama, S., Koch, M., Jin, S., Argente-Arizon, P., Argente, J., et al. (2014). Leptin signaling in astrocytes regulates hypothalamic neuronal circuits and feeding. *Nat. Neurosci.* 17, 908–910. doi: 10.1038/nn.3725

Kim, M. K., Kim, H. S., Lee, I. K., and Park, K. G. (2012). Endoplasmic reticulum stress and insulin biosynthesis: A review. *Exp. Diabetes Res.* 2012:509437. doi: 10.1155/2012/509437

Kim, S. F., Huang, A. S., Snowman, A. M., Teuscher, C., and Snyder, S. H. (2007). From the cover: Antipsychotic drug-induced weight gain mediated by histamine H1 receptor-linked activation of hypothalamic AMP-kinase. *Proc. Natl. Acad. Sci. U.S.A.* 104, 3456–3459. doi: 10.1073/pnas.0611417104

Kim, S., Joe, Y., Jeong, S. O., Zheng, M., Back, S. H., Park, S. W., et al. (2014). Endoplasmic reticulum stress is sufficient for the induction of IL-1β production via activation of the NF-κB and inflammasome pathways. *Innate Immun.* 20, 799–815. doi: 10.1177/1753425913508593

Kim, J. J., Mandelli, L., Lim, S., Lim, H. K., Kwon, O. J., Pae, C. U., et al. (2008). Association analysis of heat shock protein 70 gene polymorphisms in schizophrenia. *Eur. Arch. Psychiatry Clin. Neurosci.* 258, 239–244. doi: 10.1007/s00406-007-0791-6

Kim, P., Scott, M. R., and Meador-Woodruff, J. H. (2021). Dysregulation of the unfolded protein response (UPR) in the dorsolateral prefrontal cortex in elderly patients with schizophrenia. *Mol. Psychiatry* 26, 1321–1331. doi: 10.1038/s41380-019-0537-7

Kirk, S. L., Cahir, M., and Reynolds, G. P. (2006). Clozapine, but not haloperidol, increases neuropeptide Y neuronal expression in the rat hypothalamus. *J. Psychopharmacol.* 20, 577–579. doi: 10.1177/0269881106061199

Kirk, S. L., Glazebrook, J., Grayson, B., Neill, J. C., and Reynolds, G. P. (2009). Olanzapine-induced weight gain in the rat: Role of 5-HT2C and histamine H1 receptors. *Psychopharmacology* 207:119. doi: 10.1007/s00213-009-1639-8

Kleinridders, A., and Pothos, E. N. (2019). Impact of brain insulin signaling on dopamine function, food intake, reward, and emotional behavior. *Curr. Nutr. Rep.* 8, 83–91. doi: 10.1007/s13668-019-0276-z

Kleinridders, A., Cai, W., Cappellucci, L., Ghazarian, A., Collins, W. R., Vienberg, S. G., et al. (2015). Insulin resistance in brain alters dopamine turnover and causes behavioral disorders. *Proc. Natl. Acad. Sci. U.S.A.* 112, 3463–3468. doi: 10.1073/pnas.1500877112

Klenotich, S. J., Ho, E. V., McMurray, M. S., Server, C. H., and Dulawa, S. C. (2015). Dopamine D2/3 receptor antagonism reduces activity-based anorexia. *Transl. Psychiatry* 5:e613. doi: 10.1038/tp.2015.109

Kowalczyk, M., Owczarek, A., Suchanek, R., Paul-Samojedny, M., Fila-Danilow, A., Borkowska, P., et al. (2014). Heat shock protein 70 gene polymorphisms are associated with paranoid schizophrenia in the polish population. *Cell Stress Chaperones* 19, 205–215. doi: 10.1007/s12192-013-0446-7

Krasovska, V., and Doering, L. C. (2018). Regulation of IL-6 secretion by astrocytes via TLR4 in the fragile X mouse model. *Front. Mol. Neurosci.* 11:272. doi: 10.3389/fnmol.2018.00272

Krebs, J., Agellon, L. B., and Michalak, M. (2015). Ca(2+) homeostasis and endoplasmic reticulum (ER) stress: An integrated view of calcium signaling. *Biochem. Biophys. Res. Commun.* 460, 114–121. doi: 10.1016/j.bbrc.2015.02.004

Kroeger, H., Chiang, W. C., Felden, J., Nguyen, A., and Lin, J. H. (2019). ER stress and unfolded protein response in ocular health and disease. *FEBS J.* 286, 399–412. doi: 10.1111/febs.14522

Lauressergues, E., Bert, E., Duriez, P., Hum, D., Majd, Z., Staels, B., et al. (2012). Does endoplasmic reticulum stress participate in APD-induced hepatic metabolic dysregulation? *Neuropharmacology* 62, 784–796. doi: 10.1016/j.neuropharm.2011.08.048

Lazzari, P., Serra, V., Marcello, S., Pira, M., and Mastinu, A. (2017). Metabolic side effects induced by olanzapine treatment are neutralized by CB1 receptor antagonist compounds co-administration in female rats. *Eur. Neuropsychopharmacol.* 27, 667–678. doi: 10.1016/j.euroneuro.2017.03.010

Le Thuc, O., Stobbe, K., Cansell, C., Nahon, J. L., Blondeau, N., and Rovère, C. (2017). Hypothalamic inflammation and energy balance disruptions: Spotlight on chemokines. *Front. Endocrinol.* 8:197. doi: 10.3389/fendo.2017.00197

Leite, F., and Ribeiro, L. (2020). Dopaminergic pathways in obesity-associated inflammation. *J. Neuroimmune Pharmacol.* 15, 93–113. doi: 10.1007/s11481-019-09863-0

Li, L., Yoo, E. S., Li, X., Wyler, S. C., Chen, X., Wan, R., et al. (2021). The atypical antipsychotic risperidone targets hypothalamic melanocortin 4 receptors to cause weight gain. *J. Exp. Med.* 218:e20202484. doi: 10.1084/jem.20202484

Li, X. (2018). Endoplasmic reticulum stress regulates inflammation in adipocyte of obese rats via toll-like receptors 4 signaling. *Iran. J. Basic Med. Sci.* 21, 502–507. doi: 10.22038/ijbms.2018.27346.6674

Li, X., Cai, Y., Luo, J., Ding, J., Yao, G., Xiao, X., et al. (2021). Metformin attenuates hypothalamic inflammation via downregulation of RIPK1-independent microglial necroptosis in diet-induced obese mice. *Cell Death Discov.* 7:338. doi: 10.1038/s41420-021-00732-5

Lian, J., De Santis, M., He, M., and Deng, C. (2015). Risperidone-induced weight gain and reduced locomotor activity in juvenile female rats: The role of histaminergic and NPY pathways. *Pharmacol. Res.* 9, 20–26. doi: 10.1016/j.phrs.2015.03.004

Liu, H., Xu, Y., and Hu, F. (2020). AMPK in the ventromedial nucleus of the hypothalamus: A key regulator for thermogenesis. *Front. Endocrinol.* 11:578830. doi: 10.3389/fendo.2020.578830

Liu, P., Qin, D., Lv, H., Fan, W., Zhou, F., Gao, Z., et al. (2021). Activation of dopamine D2 receptor alleviates neuroinflammation in a mouse model of allergic rhinitis with olfactory dysfunction. *Allergy Asthma Immunol. Res.* 13, 882–895. doi: 10.4168/aair.2021.13.6.882

Livesey, F. J. (2012). A potential link between obesity and neural stem cell dysfunction. *Nat. Cell Biol.* 14, 987–989. doi: 10.1038/ncb2599

Lord, C. C., Wyler, S. C., Wan, R., Castorena, C. M., Ahmed, N., Mathew, D., et al. (2017). The atypical antipsychotic olanzapine causes weight gain by targeting serotonin receptor 2C. *J. Clin. Invest.* 127, 3402–3406. doi: 10.1172/JCI93362

Malmberg-Aiello, P., Lamberti, C., Ipponi, A., Bartolini, A., and Schunack, W. (1998). Evidence for hypernociception induction following histamine H1 receptor activation in rodents. *Life Sci.* 63, 463–476. doi: 10.1016/s0024-3205(98)00295-1

Manaserh, I. H., Maly, E., Jahromi, M., Chikkamenahalli, L., Park, J., and Hill, J. (2020). Insulin sensing by astrocytes is critical for normal thermogenesis and body temperature regulation. *J. Endocrinol.* 247, 39–52. doi: 10.1530/joe-20-0052

Martinez-Sanchez, N., Seoane-Collazo, P., Contreras, C., Varela, L., Villarroya, J., Rial-Pensado, E., et al. (2017). Hypothalamic AMPK-ER stress-JNK1 axis mediates the central actions of thyroid hormones on energy balance. *Cell Metab.* 26, 212–229.e12. doi: 10.1016/j.cmet.2017.06.014

Martin-Jiménez, C. A., García-Vega, Á, Cabezas, R., Aliev, G., Echeverria, V., González, J., et al. (2017). Astrocytes and endoplasmic reticulum stress: A bridge between obesity and neurodegenerative diseases. *Prog. Neurobiol.* 158, 45–68. doi: 10.1016/j.pneurobio.2017.08.001

Masson, G. S., Nair, A. R., Dange, R. B., Silva-Soares, P. P., Michelini, L. C., and Francis, J. (2015). Toll-like receptor 4 promotes autonomic dysfunction, inflammation and microglia activation in the hypothalamic paraventricular nucleus: Role of endoplasmic reticulum stress. *PLoS One* 10:e0122850. doi: 10.1371/journal.pone.0122850

Matos, L., Gouveia, A. M., and Almeida, H. (2015). ER stress response in human cellular models of senescence. *J. Gerontol. A Biol. Sci. Med. Sci.* 70, 924–935. doi: 10.1093/gerona/glu129

McCutcheon, R. A., Reis Marques, T., and Howes, O. D. (2020). Schizophrenia-an overview. *JAMA Psychiatry* 77, 201–210. doi: 10.1001/jamapsychiatry.2019.3360

Medzhitov, R., Preston-Hurlburt, P., Kopp, E., Stadlen, A., Chen, C., Ghosh, S., et al. (1998). MyD88 is an adaptor protein in the hToll/IL-1 receptor family signaling pathways. *Mol. Cell* 2, 253–258. doi: 10.1016/s1097-2765(00)80136-7

Meguid, M. M., Fetissov, S. O., Varma, M., Sato, T., Zhang, L., Laviano, A., et al. (2000). Hypothalamic dopamine and serotonin in the regulation of food intake. *Nutrition* 16, 843–857. doi: 10.1016/s0899-9007(00)00449-4

Mendes, N. F., Kim, Y. B., Velloso, L. A., and Araújo, E. P. (2018). Hypothalamic microglial activation in obesity: A mini-review. *Front. Neurosci.* 12:846. doi: 10.3389/fnins.2018.00846

Milanski, M., Degasperi, G., Coope, A., Morari, J., Denis, R., Cintra, D. E., et al. (2009). Saturated fatty acids produce an inflammatory response predominantly through the activation of TLR4 signaling in hypothalamus: Implications for the pathogenesis of obesity. *J. Neurosci.* 29, 359–370. doi: 10.1523/jneurosci.2760-08.2009

Mitelman, S. A., Buchsbaum, M. S., Christian, B. T., Merrill, B. M., Buchsbaum, B. R., Mukherjee, J., et al. (2020). Positive association between cerebral grey matter metabolism and dopamine D(2)/D(3) receptor availability in healthy and schizophrenia subjects: An (18)F-fluorodeoxyglucose and (18)F-fallypride positron emission tomography study. *World J. Biol. Psychiatry* 21, 368–382. doi: 10.1080/15622975.2019.1671609

Mo, J. S., Choi, D., Han, Y. R., Kim, N., and Jeong, H. S. (2019). Morin has protective potential against ER stress induced apoptosis in renal proximal tubular HK-2 cells. *Biomed. Pharmacother.* 112:108659. doi: 10.1016/j.biopha.2019.108659

Momtazmanesh, S., Zare-Shahabadi, A., and Rezaei, N. (2019). Cytokine alterations in schizophrenia: An updated review. *Front. Psychiatry* 10:892. doi: 10.3389/fpsyt.2019.00892

Morton, G. J., and Schwartz, M. W. (2001). The NPY/AgRP neuron and energy homeostasis. *Int. J. Obes.* 25, S56–S62. doi: 10.1038/sj.ijo.0801915

Nasrallah, H. A. (2008). Atypical antipsychotic-induced metabolic side effects: Insights from receptor-binding profiles. *Mol. Psychiatry* 13, 27–35. doi: 10.1038/sj.mp.4002066

Oh, T. S., Cho, H., Cho, J. H., Yu, S. W., and Kim, E. K. (2016). Hypothalamic AMPK-induced autophagy increases food intake by regulating NPY and POMC expression. *Autophagy* 12, 2009–2025. doi: 10.1080/15548627.2016.1215382

Ozasa, R., Okada, T., Nadanaka, S., Nagamine, T., Zyryanova, A., Harding, H., et al. (2013). The antipsychotic olanzapine induces apoptosis in insulin-secreting pancreatic β cells by blocking PERK-mediated translational attenuation. *Cell Struct. Funct.* 38, 183–195. doi: 10.1247/csf.13012

Ozcan, L., Ergin, A. S., Lu, A., Chung, J., Sarkar, S., Nie, D., et al. (2009). Endoplasmic reticulum stress plays a central role in development of leptin resistance. *Cell Metab.* 9, 35–51. doi: 10.1016/j.cmet.2008.12.004

Ozcan, U., Yilmaz, E., Ozcan, L., Furuhashi, M., Vaillancourt, E., Smith, R. O., et al. (2006). Chemical chaperones reduce ER stress and restore glucose homeostasis in a mouse model of type 2 diabetes. *Science* 313, 1137–1140. doi: 10.1126/science.1128294

Pae, C. U., Kim, T. S., Kwon, O. J., Artioli, P., Serretti, A., Lee, C. U., et al. (2005). Polymorphisms of heat shock protein 70 gene (Hspa1a, Hspa1b and Hspa1l) and schizophrenia. *Neurosci. Res.* 53, 8–13. doi: 10.1016/j.neures.2005.05.004

Paixão, S., and Klein, R. (2010). Neuron-astrocyte communication and synaptic plasticity. *Curr. Opin. Neurobiol.* 20, 466–473. doi: 10.1016/j.conb.2010.04.008

Panula, P., Karlstedt, K., Sallmen, T., Peitsaro, N., Kaslin, J., Michelsen, K. A., et al. (2000). The histaminergic system in the brain: Structural characteristics and changes in hibernation. *J. Chem. Neuroanat.* 18, 65–74. doi: 10.1016/s0891-0618(99)00052-6

Park, S. M., Kang, T. I., and So, J. S. (2021). Roles of XBP1s in transcriptional regulation of target genes. *Biomedicines* 9:791. doi: 10.3390/biomedicines9070791

Park, S., Aintablian, A., Coupe, B., and Bouret, S. G. (2020). The endoplasmic reticulum stress-autophagy pathway controls hypothalamic development and energy balance regulation in leptin-deficient neonates. *Nat. Commun.* 11:1914. doi: 10.1038/s41467-020-15624-y

Patel, S., Sharma, D., Kalia, K., and Tiwari, V. (2017). Crosstalk between endoplasmic reticulum stress and oxidative stress in schizophrenia: The dawn of new therapeutic approaches. *Neurosci. Biobehav. Rev.* 83, 589–603. doi: 10.1016/j.neubiorev.2017.08.025

Pierre, N., Deldicque, L., Barbé, C., Naslain, D., Cani, P. D., and Francaux, M. (2013). Toll-like receptor 4 knockout mice are protected against endoplasmic reticulum stress induced by a high-fat diet. *PLoS One* 8:e65061. doi: 10.1371/journal.pone.0065061

Poyurovsky, M., Fuchs, C., Pashinian, A., Levi, A., Weizman, R., and Weizman, A. (2013). Reducing antipsychotic-induced weight gain in schizophrenia: A double-blind placebo-controlled study of reboxetine-betahistine combination. *Psychopharmacology* 226, 615–622. doi: 10.1007/s00213-012-2935-2

Qi, X., Hosoi, T., Okuma, Y., Kaneko, M., and Nomura, Y. (2004). Sodium 4-phenylbutyrate protects against cerebral ischemic injury. *Mol. Pharmacol.* 66, 899–908. doi: 10.1124/mol.104.001339

Racki, V., Marcelic, M., Stimac, I., Petric, D., and Kucic, N. (2021). Effects of haloperidol, risperidone, and aripiprazole on the immunometabolic properties of BV-2 microglial cells. *Int. J. Mol. Sci.* 22:4399. doi: 10.3390/ijms22094399

Ramírez, S., and Claret, M. (2015). Hypothalamic ER stress: A bridge between leptin resistance and obesity. *FEBS Lett.* 589, 1678–1687. doi: 10.1016/j.febslet.2015.04.025

Reis, W. L., Yi, C. X., Gao, Y., Tschöp, M. H., and Stern, J. E. (2015). Brain innate immunity regulates hypothalamic arcuate neuronal activity and feeding behavior. *Endocrinology* 156, 1303–1315. doi: 10.1210/en.2014-1849

Ropelle, E. R., Flores, M. B., Cintra, D. E., Rocha, G. Z., Pauli, J. R., Morari, J., et al. (2010). IL-6 and IL-10 anti-inflammatory activity links exercise to hypothalamic insulin and leptin sensitivity through IKKbeta and ER stress inhibition. *PLoS Biol.* 8:e1000465. doi: 10.1371/journal.pbio.1000465

Rorato, R., Borges, B. C., Uchoa, E. T., Antunes-Rodrigues, J., Elias, C. F., and Elias, L. L. K. (2017). LPS-induced low-grade inflammation increases hypothalamic JNK expression and causes central insulin resistance irrespective of body weight changes. *Int. J. Mol. Sci.* 18:1431. doi: 10.3390/ijms18071431

Rosciszewski, G., Cadena, V., Auzmendi, J., Cieri, M. B., Lukin, J., Rossi, A. R., et al. (2019). Detrimental effects of HMGB-1 require microglial-astroglial interaction: Implications for the status epilepticus -induced neuroinflammation. *Front. Cell. Neurosci.* 13:380. doi: 10.3389/fncel.2019.00380

Sa, M., Park, M. G., and Lee, C. J. (2022). Role of hypothalamic reactive astrocytes in diet-induced obesity. *Mol. Cells* 45, 65–75. doi: 10.14348/molcells.2022.2044

Sarvani, C., Sireesh, D., and Ramkumar, K. M. (2017). Unraveling the role of ER stress inhibitors in the context of metabolic diseases. *Pharmacol. Res.* 119, 412–421. doi: 10.1016/j.phrs.2017.02.018

Schönthal, A. H. (2012). Endoplasmic reticulum stress: Its role in disease and novel prospects for therapy. *Scientifica* 2012:857516. doi: 10.6064/2012/857516

Sernoskie, S. C., Lobach, A. R., Kato, R., Jee, A., Weston, J. K., and Uetrecht, J. (2022). Clozapine induces an acute proinflammatory response that is attenuated by inhibition of inflammasome signaling: Implications for idiosyncratic drug-induced agranulocytosis. *Toxicol. Sci.* 186, 70–82. doi: 10.1093/toxsci/kfab154

Shao, W., Zhang, S. Z., Tang, M., Zhang, X. H., Zhou, Z., Yin, Y. Q., et al. (2013). Suppression of neuroinflammation by astrocytic dopamine D2 receptors via αB-crystallin. *Nature* 494, 90–94. doi: 10.1038/nature11748

Sharifnia, T., Antoun, J., Verriere, T. G., Suarez, G., Wattacheril, J., Wilson, K. T., et al. (2015). Hepatic TLR4 signaling in obese NAFLD. *Am. J. Physiol. Gastrointest. Liver Physiol.* 309, G270–G278. doi: 10.1152/ajpgi.00304.2014

Shen, Y., Qin, H., Chen, J., Mou, L., He, Y., Yan, Y., et al. (2016). Postnatal activation of TLR4 in astrocytes promotes excitatory synaptogenesis in hippocampal neurons. *J. Cell Biol.* 215, 719–734. doi: 10.1083/jcb.201605046

Shin, A. C., Filatova, N., Lindtner, C., Chi, T., Degann, S., Oberlin, D., et al. (2017). Insulin receptor signaling in POMC, but not AgRP, neurons controls adipose tissue insulin action. *Diabetes* 66, 1560–1571. doi: 10.2337/db16-1238

Singh, R., Stogios, N., Smith, E., Lee, J., Maksyutynsk, K., Au, E., et al. (2022). Gut microbiome in schizophrenia and antipsychotic-induced metabolic alterations: A scoping review. *Ther. Adv. Psychopharmacol.* 12:20451253221096525. doi: 10.1177/20451253221096525

So, J., Warsh, J. J., and Li, P. P. (2007). Impaired endoplasmic reticulum stress response in B-lymphoblasts from patients with bipolar-I disorder. *Biol. Psychiatry* 62, 141–147. doi: 10.1016/j.biopsych.2006.10.014

Song, J., Kim, B. C., Nguyen, D. T., Samidurai, M., and Choi, S. M. (2017). Levodopa (L-DOPA) attenuates endoplasmic reticulum stress response and cell death signaling through DRD2 in SH-SY5Y neuronal cells under alpha-synuclein-induced toxicity. *Neuroscience* 358, 336–348. doi: 10.1016/j.neuroscience.2017.06.060

Sprenkle, N. T., Lahiri, A., Simpkins, J. W., and Meares, G. P. (2019). Endoplasmic reticulum stress is transmissible in vitro between cells of the central nervous system. *J. Neurochem.* 148, 516–530. doi: 10.1111/jnc.14642

Stefanidis, A., Verty, A. N., Allen, A. M., Owens, N. C., Cowley, M. A., and Oldfield, B. J. (2009). The role of thermogenesis in antipsychotic drug-induced weight gain. *Obesity* 17, 16–24. doi: 10.1038/oby.2008.468

Stogios, N., Smith, E., Bowden, S., Tran, V., Asgariroozbehani, R., McIntyre, W. B., et al. (2022). Metabolic adverse effects of off-label use of second-generation antipsychotics in the adult population: A systematic review and meta-analysis. *Neuropsychopharmacology* 47, 664–672. doi: 10.1038/s41386-021-01163-7

Sugiyama, M., Banno, R., Yaginuma, H., Taki, K., Mizoguchi, A., Tsunekawa, T., et al. (2020). Hypothalamic glial cells isolated by MACS reveal that microglia and astrocytes induce hypothalamic inflammation via different processes under high-fat diet conditions. *Neurochem. Int.* 136:104733. doi: 10.1016/j.neuint.2020.104733

Tanaka, K., Kanno, T., Yanagisawa, Y., Yasutake, K., Hadano, S., Yoshii, F., et al. (2011). Bromocriptine methylate suppresses glial inflammation and moderates disease progression in a mouse model of amyotrophic lateral sclerosis. *Exp. Neurol.* 232, 41–52. doi: 10.1016/j.expneurol.2011.08.001

Thon, M., Hosoi, T., and Ozawa, K. (2016). Possible integrative actions of leptin and insulin signaling in the hypothalamus targeting energy homeostasis. *Front. Endocrinol.* 7:138. doi: 10.3389/fendo.2016.00138

Tinsley, R. B., Bye, C. R., Parish, C. L., Tziotis-Vais, A., George, S., Culvenor, J. G., et al. (2009). Dopamine D2 receptor knockout mice develop features of Parkinson disease. *Ann. Neurol.* 66, 472–484. doi: 10.1002/ana.21716

Tran, L. T., Park, S., Kim, S. K., Lee, J. S., Kim, K. W., and Kwon, O. (2022). Hypothalamic control of energy expenditure and thermogenesis. *Exp. Mol. Med.* 54, 358–369. doi: 10.1038/s12276-022-00741-z

Turnley, A. M., Stapleton, D., Mann, R. J., Witters, L. A., Kemp, B. E., and Bartlett, P. F. (1999). Cellular distribution and developmental expression of AMP-activated protein kinase isoforms in mouse central nervous system. *J. Neurochem.* 72, 1707–1716. doi: 10.1046/j.1471-4159.1999.721707.x

Ullah, R., Rauf, N., Nabi, G., Yi, S., Yu-Dong, Z., and Fu, J. (2021). Mechanistic insight into high-fat diet-induced metabolic inflammation in the arcuate nucleus of the hypothalamus. *Biomed. Pharmacother.* 142:112012. doi: 10.1016/j.biopha.2021.112012

Üner, A. G., Keçik, O., Quaresma, P. G. F., De Araujo, T. M., Lee, H., Li, W., et al. (2019). Role of POMC and AgRP neuronal activities on glycaemia in mice. *Sci. Rep.* 9:13068. doi: 10.1038/s41598-019-49295-7

Valdearcos, M., Myers, M. G. Jr., and Koliwad, S. K. (2019). Hypothalamic microglia as potential regulators of metabolic physiology. *Nat. Metab.* 1, 314–320. doi: 10.1038/s42255-019-0040-0

Valdearcos, M., Robblee, M. M., Benjamin, D. I., Nomura, D. K., Xu, A. W., and Koliwad, S. K. (2014). Microglia dictate the impact of saturated fat consumption on hypothalamic inflammation and neuronal function. *Cell Rep.* 9, 2124–2138. doi: 10.1016/j.celrep.2014.11.018

Varela, L., Kim, J. G., Fernández-Tussy, P., Aryal, B., Liu, Z. W., Fernández-Hernando, C., et al. (2021). Astrocytic lipid metabolism determines susceptibility to diet-induced obesity. *Sci. Adv.* 7:eabj2814. doi: 10.1126/sciadv.abj2814

Vohra, M. S., Benchoula, K., Serpell, C. J., and Hwa, W. E. (2022). AgRP/NPY and POMC neurons in the arcuate nucleus and their potential role in treatment of obesity. *Eur. J. Pharmacol.* 915:174611. doi: 10.1016/j.ejphar.2021.174611

Vrechi, T. A., Crunfli, F., Costa, A. P., and Torrão, A. S. (2018). Cannabinoid receptor type 1 agonist ACEA protects neurons from death and attenuates endoplasmic reticulum stress-related apoptotic pathway signaling. *Neurotox. Res.* 33, 846–855. doi: 10.1007/s12640-017-9839-1

Wan, X. Q., Zeng, F., Huang, X. F., Yang, H. Q., Wang, L., Shi, Y. C., et al. (2020). Risperidone stimulates food intake and induces body weight gain via the hypothalamic arcuate nucleus 5-HT2c receptor-NPY pathway. *CNS Neurosci. Ther.* 26, 558–566. doi: 10.1111/cns.13281

Wang, G., Cui, W., Chen, S., Shao, Z., Li, Y., Wang, W., et al. (2021). Metformin alleviates high glucose-induced ER stress and inflammation by inhibiting the interaction between caveolin1 and AMPKα in rat astrocytes. *Biochem. Biophys. Res. Commun.* 534, 908–913. doi: 10.1016/j.bbrc.2020.10.075

Wang, J., Zhu, S., Wang, H., He, J., Zhang, Y., Adilijiang, A., et al. (2014). Astrocyte-dependent protective effect of quetiapine on GABAergic neuron is associated with the prevention of anxiety-like behaviors in aging

mice after long-term treatment. *J. Neurochem.* 130, 780–789. doi: 10.1111/jnc.12771

Wang, K., Song, F., Wang, H., Wang, J. H., and Sun, Y. (2019). Quetiapine attenuates the neuroinflammation and executive function deficit in streptozotocin-induced diabetic mice. *Mediators Inflamm.* 2019:1236082. doi: 10.1155/2019/1236082

Wang, Y. W., Zhou, Q., Zhang, X., Qian, Q. Q., Xu, J. W., Ni, P. F., et al. (2017). Mild endoplasmic reticulum stress ameliorates lipopolysaccharide-induced neuroinflammation and cognitive impairment via regulation of microglial polarization. *J. Neuroinflamm.* 14:233. doi: 10.1186/s12974-017-1002-7

Wang, Y., Chen, Y., Zhou, Q., Xu, J., Qian, Q., Ni, P., et al. (2018). Mild endoplasmic reticulum stress protects against lipopolysaccharide-induced astrocytic activation and blood-brain barrier hyperpermeability. *Front. Cell. Neurosci.* 12:222. doi: 10.3389/fncel.2018.00222

Wang, Z., Huang, Y., Cheng, Y., Tan, Y., Wu, F., Wu, J., et al. (2016). Endoplasmic reticulum stress-induced neuronal inflammatory response and apoptosis likely plays a key role in the development of diabetic encephalopathy. *Oncotarget* 7, 78455–78472. doi: 10.18632/oncotarget.12925

Weston-Green, K., Babic, I., de Santis, M., Pan, B., Montgomery, M. K., Mitchell, T., et al. (2018). Disrupted sphingolipid metabolism following acute clozapine and olanzapine administration. *J. Biomed. Sci.* 25:40. doi: 10.1186/s12929-018-0437-1

Weston-Green, K., Huang, X. F., and Deng, C. (2012). Alterations to melanocortinergic, GABAergic and cannabinoid neurotransmission associated with olanzapine-induced weight gain. *PLoS One* 7:e33548. doi: 10.1371/journal.pone.0033548

Williams, K. W., Liu, T., Kong, X., Fukuda, M., Deng, Y., Berglund, E. D., et al. (2014). Xbp1s in Pomc neurons connects ER stress with energy balance and glucose homeostasis. *Cell Metab.* 20, 471–482. doi: 10.1016/j.cmet.2014.06.002

Won, J. C., Jang, P. G., Namkoong, C., Koh, E. H., Kim, S. K., Park, J. Y., et al. (2009). Central administration of an endoplasmic reticulum stress inducer inhibits the anorexigenic effects of leptin and insulin. *Obesity* 17, 1861–1865. doi: 10.1038/oby.2009.194

Wu, R. R., Zhao, J. P., Guo, X. F., He, Y. Q., Fang, M. S., Guo, W. B., et al. (2008). Metformin addition attenuates olanzapine-induced weight gain in drug-naive first-episode schizophrenia patients: A double-blind, placebo-controlled study. *Am. J. Psychiatry* 165, 352–358. doi: 10.1176/appi.ajp.2007.07010079

Wu, Y., Li, W., Zhou, C., Lu, F., Gao, T., Liu, Y., et al. (2012). Ketamine inhibits lipopolysaccharide-induced astrocytes activation by suppressing TLR4/NF-κB pathway. *Cell Physiol. Biochem.* 30, 609–617. doi: 10.1159/000341442

Xiao, G., Burguet, J., Kawaguchi, R., Havton, L., and Hinman, J. (2018). Obesity blocks oligodendrocyte precursor cell differentiation and impedes repair after white matter stroke. *bioRxiv [Preprint]* doi: 10.1101/283184

Xiao, Y., Deng, Y., Yuan, F., Xia, T., Liu, H., Li, Z., et al. (2017a). An ATF4-ATG5 signaling in hypothalamic POMC neurons regulates obesity. *Autophagy* 13, 1088–1089. doi: 10.1080/15548627.2017.1307488

Xiao, Y., Deng, Y., Yuan, F., Xia, T., Liu, H., Li, Z., et al. (2017b). ATF4/ATG5 signaling in hypothalamic proopiomelanocortin neurons regulates fat mass via affecting energy expenditure. *Diabetes* 66, 1146–1158. doi: 10.2337/db16-1546

Xu, J., Zhang, X., Qian, Q., Wang, Y., Dong, H., Li, N., et al. (2018). Histamine upregulates the expression of histamine receptors and increases the neuroprotective effect of astrocytes. *J. Neuroinflamm.* 15:41. doi: 10.1186/s12974-018-1068-x

Yang, J., and Fukuchi, K. I. (2020). TIR-domain-containing adaptor-inducing interferon-β (TRIF) is involved in glucose metabolism in adipose tissue through the insulin/AKT signaling pathway. *Int. J. Endocrinol.* 2020:6942307. doi: 10.1155/2020/6942307

Yang, L., Qi, Y., and Yang, Y. (2015). Astrocytes control food intake by inhibiting AGRP neuron activity via adenosine A1 receptors. *Cell Rep.* 11, 798–807. doi: 10.1016/j.celrep.2015.04.002

Yang, X., Haghiac, M., Glazebrook, P., Minium, J., Catalano, P. M., and Hauguel-de Mouzon, S. (2015). Saturated fatty acids enhance TLR4 immune pathways in human trophoblasts. *Hum. Reprod.* 30, 2152–2159. doi: 10.1093/humrep/dev173

Yang, Y., Song, J., Liu, N., Wei, G., Liu, S., Zhang, S., et al. (2022). Salvianolic acid A relieves cognitive disorder after chronic cerebral ischemia: Involvement of Drd2/Cryab/NF-κB pathway. *Pharmacol. Res.* 175:105989. doi: 10.1016/j.phrs.2021.105989

Yang, Z., Shao, Y., Zhao, Y., Li, Q., Li, R., Xiao, H., et al. (2020). Endoplasmic reticulum stress-related neuroinflammation and neural stem cells decrease in mice exposure to paraquat. *Sci. Rep.* 10:17757. doi: 10.1038/s41598-020-74916-x

Yanguas-Casás, N., Barreda-Manso, M. A., Nieto-Sampedro, M., and Romero-Ramírez, L. (2014). Tauroursodeoxycholic acid reduces glial cell activation in an animal model of acute neuroinflammation. *J. Neuroinflamm.* 11:50. doi: 10.1186/1742-2094-11-50

Yao, L., Kan, E. M., Lu, J., Hao, A., Dheen, S. T., Kaur, C., et al. (2013). Toll-like receptor 4 mediates microglial activation and production of inflammatory mediators in neonatal rat brain following hypoxia: Role of TLR4 in hypoxic microglia. *J. Neuroinflamm.* 10:785. doi: 10.1186/1742-2094-10-23

Yao, L., Xiao, Y., Liu, S. P., Xu, A. M., and Zhou, Z. G. (2010). [Serum of obesity induce the activation of TLR4/NF-κB signaling pathway on THP-1 cell line]. *Zhonghua Yi Xue Za Zhi* 90, 3119–3123.

Yi, S., Chen, K., Zhang, L., Shi, W., Zhang, Y., Niu, S., et al. (2019). Endoplasmic reticulum stress is involved in stress-induced hypothalamic neuronal injury in rats via the PERK-ATF4-CHOP and IRE1-ASK1-JNK pathways. *Front. Cell. Neurosci.* 13:190. doi: 10.3389/fncel.2019.00190

Yonemochi, N., Ardianto, C., Yang, L., Yamamoto, S., Ueda, D., Kamei, J., et al. (2019). Dopaminergic mechanisms in the lateral hypothalamus regulate feeding behavior in association with neuropeptides. *Biochem. Biophys. Res. Commun.* 519, 547–552. doi: 10.1016/j.bbrc.2019.09.037

Yoshimatsu, H., Itateyama, E., Kondou, S., Tajima, D., Himeno, K., Hidaka, S., et al. (1999). Hypothalamic neuronal histamine as a target of leptin in feeding behavior. *Diabetes* 48, 2286–2291. doi: 10.2337/diabetes.48.12.2286

Zhang, Q., He, M., Deng, C., Wang, H., Lian, J., and Huang, X. F. (2014). Hypothalamic ghrelin signalling mediates olanzapine-induced hyperphagia and weight gain in female rats. *Int. J. Neuropsychopharmacol.* 17, 807–818. doi: 10.1017/S1461145713001697

Zhang, X., Zhang, G., Zhang, H., Karin, M., Bai, H., and Cai, D. (2008). Hypothalamic IKKβ/NF-κB and ER stress link overnutrition to energy imbalance and obesity. *Cell* 135, 61–73. doi: 10.1016/j.cell.2008.07.043

Zhang, Y., Liu, Y., Su, Y., You, Y., Ma, Y., Yang, G., et al. (2017a). The metabolic side effects of 12 antipsychotic drugs used for the treatment of schizophrenia on glucose: A network meta-analysis. *BMC Psychiatry* 17:373. doi: 10.1186/s12888-017-1539-0

Zhang, Y., Reichel, J. M., Han, C., Zuniga-Hertz, J. P., and Cai, D. (2017b). Astrocytic process plasticity and IKKbeta/NF-kappaB in central control of blood glucose, blood pressure, and body weight. *Cell Metab.* 25, 1091–1102.e4. doi: 10.1016/j.cmet.2017.04.002

Zhao, Y., Li, G., Li, Y., Wang, Y., and Liu, Z. (2017). Knockdown of Tlr4 in the arcuate nucleus improves obesity related metabolic disorders. *Sci. Rep.* 7:7441. doi: 10.1038/s41598-017-07858-6

Zhou, L., Ding, S., Li, Y., Wang, L., Chen, W., Bo, T., et al. (2016). Endoplasmic reticulum stress may play a pivotal role in lipid metabolic disorders in a novel mouse model of subclinical hypothyroidism. *Sci. Rep.* 6:31381. doi: 10.1038/srep31381

Zhu, J., Hu, Z., Han, X., Wang, D., Jiang, Q., Ding, J., et al. (2018). Dopamine D2 receptor restricts astrocytic NLRP3 inflammasome activation via enhancing the interaction of beta-arrestin2 and NLRP3. *Cell Death Differ.* 25, 2037–2049. doi: 10.1038/s41418-018-0127-2

Zhu, S., Shi, R., Li, V., Wang, J., Zhang, R., Tempier, A., et al. (2014). Quetiapine attenuates glial activation and proinflammatory cytokines in APP/PS1 transgenic mice via inhibition of nuclear factor-κB pathway. *Int. J. Neuropsychopharmacol.* 18:pyu022. doi: 10.1093/ijnp/pyu022

Zuany-Amorim, C., Hastewell, J., and Walker, C. (2002). Toll-like receptors as potential therapeutic targets for multiple diseases. *Nat. Rev. Drug. Discov.* 1, 797–807. doi: 10.1038/nrd914

Zusso, M., Lunardi, V., Franceschini, D., Pagetta, A., Lo, R., Stifani, S., et al. (2019). Ciprofloxacin and levofloxacin attenuate microglia inflammatory response via TLR4/NF-kB pathway. *J. Neuroinflamm.* 16:148. doi: 10.1186/s12974-019-1538-9

Advantages of publishing in Frontiers

OPEN ACCESS
Articles are free to read for greatest visibility and readership

FAST PUBLICATION
Around 90 days from submission to decision

HIGH QUALITY PEER-REVIEW
Rigorous, collaborative, and constructive peer-review

TRANSPARENT PEER-REVIEW
Editors and reviewers acknowledged by name on published articles

Frontiers
Avenue du Tribunal-Fédéral 34
1005 Lausanne | Switzerland

Visit us: www.frontiersin.org
Contact us: frontiersin.org/about/contact

REPRODUCIBILITY OF RESEARCH
Support open data and methods to enhance research reproducibility

DIGITAL PUBLISHING
Articles designed for optimal readership across devices

FOLLOW US
@frontiersin

IMPACT METRICS
Advanced article metrics track visibility across digital media

EXTENSIVE PROMOTION
Marketing and promotion of impactful research

LOOP RESEARCH NETWORK
Our network increases your article's readership